ADVANCED NUMERICAL TECHNIQUES TO SIMULATE SOIL-TOOL INTERFACE PROBLEMS

Mootaz E Aboelnor

Thesis

Presented for the Degree of Doctor of Philosophy

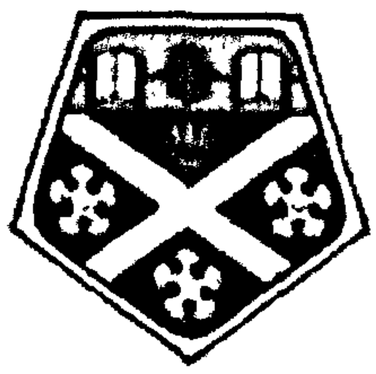

Department of Mechanical Engineering

University of Strathclyde

June 2002

Declaration of Author's Rights

ABSTRACT

In most mine clearing or earth moving equipment such as bulldozers, the working tool is a blade. The blade geometry and operating conditions, such as cutting speed, cutting angle, and cutting depth, have a great effect on overall machine productivity. Most of the published experimental studies confirm these effects. However experimental studies are expensive and their results are highly dependant on the accuracy of measurement devices and the reliability of experimental procedures employed. Numerical techniques have recently shown more promise especially with the current increase in computational power and development of more sophisticated material models. However in order to simulate the soil-tool interface process accurately, careful selection of the appropriate material model for the soil and the interface is required. This should, ideally, be based on a reasonable number of material parameters that have direct physical meaning.

In this study a review of the available constitutive models for soil (particularly sand) and soil-tool interface was carried out. This review study concluded by selecting the so called hypoplastic model as the most appropriate to simulate the sandy soil behavior over a wide range of stresses. Some modifications were carried out on this selected hypoplastic model to optimize it for simulation of the soil-tool interaction process, which is characterized by monotonic loading and high deformation. The modified model was verified numerically and then implemented into the finite element method via an ABAQUS user defined subroutine UMAT. Then the implemented model was verified through analysis of some benchmark problems and results were compared with results from different classical failure criteria. The finite element analysis revealed the high performance of the hypoplastic model in simulating sand behaviour. Finally an analysis of various factors affecting soil-tool interaction was carried out in both two-dimensions and three-dimensions. Results revealed the significant effect of both geometry and operating conditions on blade cutting forces and confirmed the ability of the finite element method to analyze the soil-tool interaction process.

ACKNOWLEDGEMENTS

I would like to thank my supervisors, Prof. Jim Boyle and Dr. Robert Hamilton, for all they have done to assist me during my candidature. They have provided expert advice, support and encouragement in that period.

I am indebted to my country, Egypt, which provided an endless support to this project.

Thanks go to those who have provided advice, information, or publications and papers.

A very special thank you go to my wife and my lovely kids for their patience, and to my mother, uncle and my brother for their endless prayers, encouragement, and support. It may not be possible for me to return their endless love and sacrifice.

Many thanks go to anyone else who has helped me either explicitly or implicitly.

Mootaz E. AboElnor

June 2002

CONTENTS

LIST OF FIGURES

Page

LIST OF TABLES

Page

NOTATION

The following symbols are used in this thesis, and are defined where they first appear in the text. Some symbols have been assigned more than one meaning, but it will be evident from the context.

A	Speed effect coefficient of adhesion	
a	Adhesion stress for a soil-metal interface	
$\hat{a}(\theta)$	Radius of the intersection between the CSS and the π-plane	
C\	Soil-metal adhesion when v = 1m/s	(kPa)
C_c	Compression index	
$\hat{C}_J$	RKF parameters	
$\tilde{C}_J$	RKF parameters	
c	Soil cohesion	
D	Relative density	
d	Cutting depth	
d_1, d_2, d_3	Principal stretching components	
d_{ij}	Stretching measure	
E	Incremental stiffness modulus or Young's modulus	
E_i	Initial tangent elastic or Young's modulus	
E_s	Secant elastic modulus	
E_t	Tangent elastic modulus	
e	Void ratio	
e_o	Initial void ration of a sand sample	
$\dot{e}$	Void ratio change rate	
e_c	Critical void ratio	
e_{co}	Initial value of the critical void ration	
e_d	Lower bound void ratio	
e_{do}	Initial value of the lower bound void ratio	
e_i	Upper bound void ratio	
e_{io}	Initial value of the upper bound void ratio	
e_p	Proportion void ratio at mean skeleton pressure p	
e_{po}	Void ratio at zero pressure	

exp	Exponential function	
$\mathbf{F}$	Deformation gradient	
$\mathbf{F}_o$	Deformation gradient at the beginning of an increment	
f_d	Density function	
f_p	Soil-metal friction stress	(kPa)
f_s	Stiffness function	
$\mathbf{H}$	Tensorial function represent the hypoplastic equation	
h	Sample (soil bin) height	
h_s	Granulate hardness	(kPa)
$\mathbf{I}$	Unit matrix	
I_1, I_2, I_3	Tensor invariants	
k	Generic sub-step number	
$\mathbf{L}(\sigma)$	Linear tonsorial function of stress tensor	
L	Sample (soil bin) length	
L_1	Distance between the blade and the left boundary	
l	Blade flat part length	
ln	Logarithmic function	
M	Critical state line slope in the p-q diagram	
max	Maximum of two values	
min	Minimum of two values	
$\mathbf{N}(\sigma)$	Nonlinear function of stress tensor	
n	Hypoplastic material parameter	
ns	Number of sub-steps	
p	Pressure stress or stress level	
p_s	Mean skeleton pressure	
q	Deviator stress	
$\mathbf{R}$	Rotation tensor	
R	Blade radius of curvature	
r_k	Norm of the difference between two different order RK results	
T_k	Dimensionless time ratio of the generic substep k	
TOL	Error tolerance	

t_n	Time at the beginning of sub-step n	
t_{n+1}	Time at the end of sub-step n	
tr	Matrix trace	
u_i	Displacement function	
V	Soil volume in a specimen	
V_a	Volume of air in a soil specimen	
V_S	Volume of solid particle in a soil specimen	
V_v	Total voids volume in a soil specimen	
V_w	Volume of water in a soil specimen	
υ	Sliding peed	(m/s)
W1	Lateral bound width	
W2	Blade cutting width	
W	Spin tensor	
w_{ij}	Spin tensor measure	
x_i	Position coordinates	
ΔT_{k+1}	Size of $k+1$ sub-step	
ΔT_k	Dimensionless sub-step size	
Δt	Time increment or interval	
$\Delta\varepsilon$	Strain increment	
$\Delta\varepsilon_{n+1}$	Finite strain increment	
$\boldsymbol{\Omega}$	Angular velocity tensor of a material	
α	Hypoplastic material parameter	
β	Hypoplastic material parameter	
β_{dp}	Drucker-Prager material angle of friction	
β_{JI}	Parameters for the RKF	
β_{mc}	Mohr's-coulomb material angle of friction	
γ	Blade cutting angle	
δ	External frictional angle for a soil-tool interface	
$\delta\varepsilon_V$	Volumetric strain increment	
$\delta\gamma_{\max}$	Maximum shear strain increment	
δ_{ij}	Kronecker's symbol	

$\dot{\boldsymbol{\varepsilon}}$	Strain rate tensor
$\boldsymbol{\varepsilon}_o$	Initial strain state tensor
$\varepsilon_1, \varepsilon_2, \varepsilon_3$	Principal strain components
ε_{ij}	Strain measure
ε_r	Lateral (radial) strain
ε_v	Volumetric strain
ε_z	Vertical (axial) strain
ν	Poisson's ratio
ϕ_a	Soil-metal friction angle
φ	Soil internal frictional angle
η	Stress ratio
φ_c	Critical friction angle
θ	Reference angle of the stress point on the deviatoric plane
$\lambda_1, \lambda_2, \lambda_3$	Eigenvalues of the stress tensor
μ	Soil-Tool frictional coefficient
σ	Effective stress
$\dot{\sigma}$	Stress rate
$\boldsymbol{\sigma}^{\circ}$	Jaumann stress rate
$\hat{\boldsymbol{\sigma}}$	Stress ratio
$\hat{\boldsymbol{\sigma}}^*$	Deviatoric stress ratio
$\sigma_1, \sigma_2, \sigma_3$	Principal stresses
σ_a	Axial stress component
$\boldsymbol{\sigma}_o$	Initial stress state
$\boldsymbol{\sigma}_n$	Stress at increment n
σ_n	Normal stress
σ_r	Radial stress component
τ	Tangential stress or shear stress
ψ	Dilatancy angle
ψ_{dp}	Drucker-Prager dilatancy angle
ψ_{mc}	Mohr's-coulomb dilatancy angle
*	Denotes an ABAQUS command or option

ABBREVIATIONS

The following abbreviations are used in this thesis, and are defined where they first appear in the text. Some symbols have been assigned more than one meaning, but it will be evident from the context.

TC	Triaxial compression
TE	Triaxial extension
CTC	Conventional triaxial compression
CTE	Conventional triaxial extension
RTC	Released triaxial compression
RTE	Released triaxial extension
HC	Hydrostatic compression
CSL	Critical state line
CSS	Critical stress surface
RKF	Runge-Kutta Fehlberg integration scheme
ODE	Ordinary differential equations
TOL	Allowable error tolerance for the RKF integration scheme
RK	Runge-Kutta integration scheme
MP	Crank-Nicolson (Mid-Point) integration scheme
EF	Euler-Forward integration scheme
EB	Euler-Backward integration scheme
HKS	ABAQUS/Standard by Hibbitt, Karlsson & Sorensen,
FEM	Finite element method

Chapter 1

INTRODUCTION

Land reclamation is an important step in the development of new or expanding societies. This reclamation may include earth digging and moving, establishing roads, opening irrigation trenches and clearing mines that may be left during a war. This in turn makes new land available and safe for industry, agriculture, housing and other infra-structure development. Mechanical equipment is one of the most important and powerful tools for achieving land reclamation in a productive and efficient manner.

In most mine cleaning and earth moving equipment such as motor graders, scrappers and bulldozers, the working tool is a blade or tillage. Blade geometry and operating conditions, such as cutting speed, cutting angle, and cutting depth, have a great effect on machine productivity. In order to obtain optimum performance with lower power consumption in cutting and digging, an experimental evaluation of the various interaction parameters should be carried out. Experimental results can give some insight into the geometry and operating conditions effects, but this way may be expensive, time consuming and limited. With increasing computing power and development of more sophisticated material models, numerical simulation methods now show more promise in providing new and improved insights. Constitutive stress-strain laws, or models of engineering materials, play a significant role in providing reliable results from any solution procedure. Their importance has been

enhanced significantly with the great increase in development and application of many modern computer-based techniques such as the finite element, finite difference, and boundary integral equation methods. However it has been realized that the advances and sophistication in computational solution techniques have far exceeded our knowledge of the behaviour of materials defined by constitutive laws. As a consequence, very often, results from a numerical procedure that may have used less appropriate constitutive laws can be of limited or doubtful validity. Hence selecting the correct or most appropriate available material model is of prime importance in achieving reasonable results from a numerical simulation.

1.1 AIM OF THE THESIS

It is clear that for both mine clearing and earth moving equipment soil-tool interaction is an important phenomenon. Achieving higher performance of these machines can be done through an investigation of the physical and design factors that affect the soil-tool interaction process. However as stated previously experimental study is expensive, limited by measurement accuracy and time consuming; an alternative way of studying the soil-tool interaction problem is to use numerical simulation in combination with the modern computing power and advanced constitutive stress-strain laws.

The main aim of the thesis is to simulate the soil-tool interaction numerically using the finite element technique, primarily in fully drained sands.

The main aim can be subdivided into further sub-sections:

1. Review of the available models of studying soil-tool interaction.
2. Review of the available constitutive models for simulating sand to select the appropriate model for simulation.
3. Implement the selected model into finite element code.
4. Review of the available simulation software capabilities of simulating the soil-tool interaction process.
5. Investigate the validity of the implemented model and the simulation of the interaction.
6. Studying different factors affecting the soil-tool interface process.

1.2 BACKGROUND

The Middle East is one of the most heavily mined regions in the world. Egypt is one of the countries that have the largest number of landmines. It alone has one quarter of the world's landmines buried in its deserts, most leftover from the Second World War. Figure (1.1) represents the most mine infected areas from the Egyptian western desert.

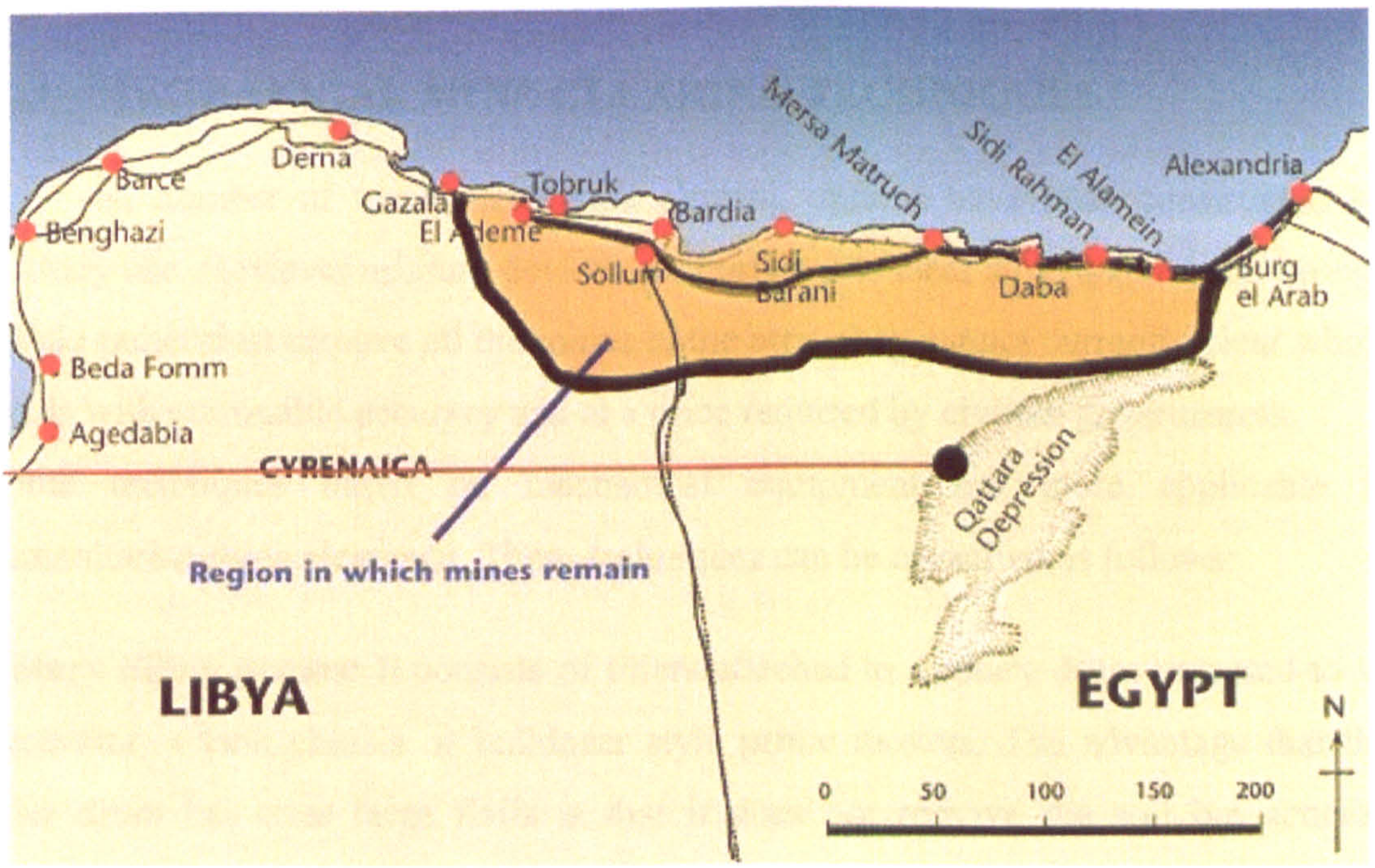

Figure (1.1) The Western Desert area where mines remain from World War II

Over the past decades, the gravity of this problem has unfolded as landmines have caused the death or injury of thousands of people in the Western Desert, Sinai and Suez Canal zones. In addition, landmines have disrupted economic development efforts in these parts of the country. Out of a total of about 110 million landmines planted around the world, Egypt has 23 million, i.e.; 20% of the total number of landmines, spreading horror and the imminent threats of loss of life and property in the east and west parts of the country. Undoubtedly, the presence of this huge number of landmines on the Egyptian territory has resulted in the disruption of various development operations in both Eastern and Western Deserts. Many people are killed or injured, handicapped as a result of the explosion of these mines.

Despite being the most reliable method of mine clearing, hand prodding is dangerous and slow. However, mechanical clearance in support of manual clearance can be cheaper, significantly safer and improve safety for civilize the area. It is also faster than manual demining alone. Hence any improvements in demining techniques or methods of design and analysis have the potential to provide huge benefits to Egypt's economy and population. This then was the motivation to undertake the current study.

1.3 MECHANICAL MINE CLEARING TECHNIQUES

A number of mechanical mine clearing options have been constructed for military use. However military devices are designed to clear a navigable path through a field rather than remove all the mines in the area, they cannot currently clear whole fields with reasonable accuracy and at a price required by civilian governments.
Some techniques based on mechanical equipment are more applicable to humanitarian mine clearance. These techniques can be classified as follows:

Rotary tilling drums: It consists of tillers attached to a rotary drum mounted to an excavator, a tank chassis or bulldozer style prime movers. The advantage that the tiller drum has over large flails is that it does not remove the soil but actually prepares the soil for the next stage of clearance, this being sifting, manual, or other such clearance methods.

Flails: Similar to the mini-tiller, Figure (1.2), can be mounted on to a tank chassis proving very successful for the clearance of anti-tank and anti-personnel mines.

Ploughs: Can be useful in humanitarian demining to provide quick access through mined areas to minimize civilian casualties and allow quick access to critical resources such as food and water. An armored bulldozer with a blade can provide similar capability. The full-width mine plough is moved by a tank or armored bulldozer. It is V shaped and clears ground to a depth of 30 centimeters, pushing earth and mines to the side as shown in Figure (1.3). However it requires great horsepower to push the plough at the required depth. Armored bulldozers are usually commercial types with extra protection for the operator. The bulldozer blade pushes

earth and mines to one side by angling the blade. Both bulldozers and ploughs suffer the disadvantages that the mines will usually still be armed after they have been 'ploughed'.

The rake plough: Specially designed for desert environment, it uses tines, which allow sand to pass through, but not mines, Figure (1.4). It is unsuitable in other terrain.

Sifting: Can be mounted to the front of an armored bulldozer and follows behind the tillers, flails and in some cases ploughs. The sifter lifts and screens the soil so that any mines, or parts thereof, left in the ground are uncovered. After the sifter has processed the ground, the land is ready for final manual clearance or returned to agricultural use etc. The sifter also leaves the ground totally prepared as a seedbed for planting.

Single or double rollers: Are particularly effective for proofing roads which are suspected of mine contamination. Rollers can be most effective in the early stages of humanitarian operations to allow the establishment of supply routes. Smaller rollers can easily be manufactured to achieve low costs and easy repairs. Numerous roller systems exist, but they tend to be heavy and require a powerful prime mover. Rollers are also sensitive to terrain and can be defeated by 'smart' mines, which do not explode on first contact.

In this study a bulldozer blade was considered for its wide range of applications in soil-tool interaction.

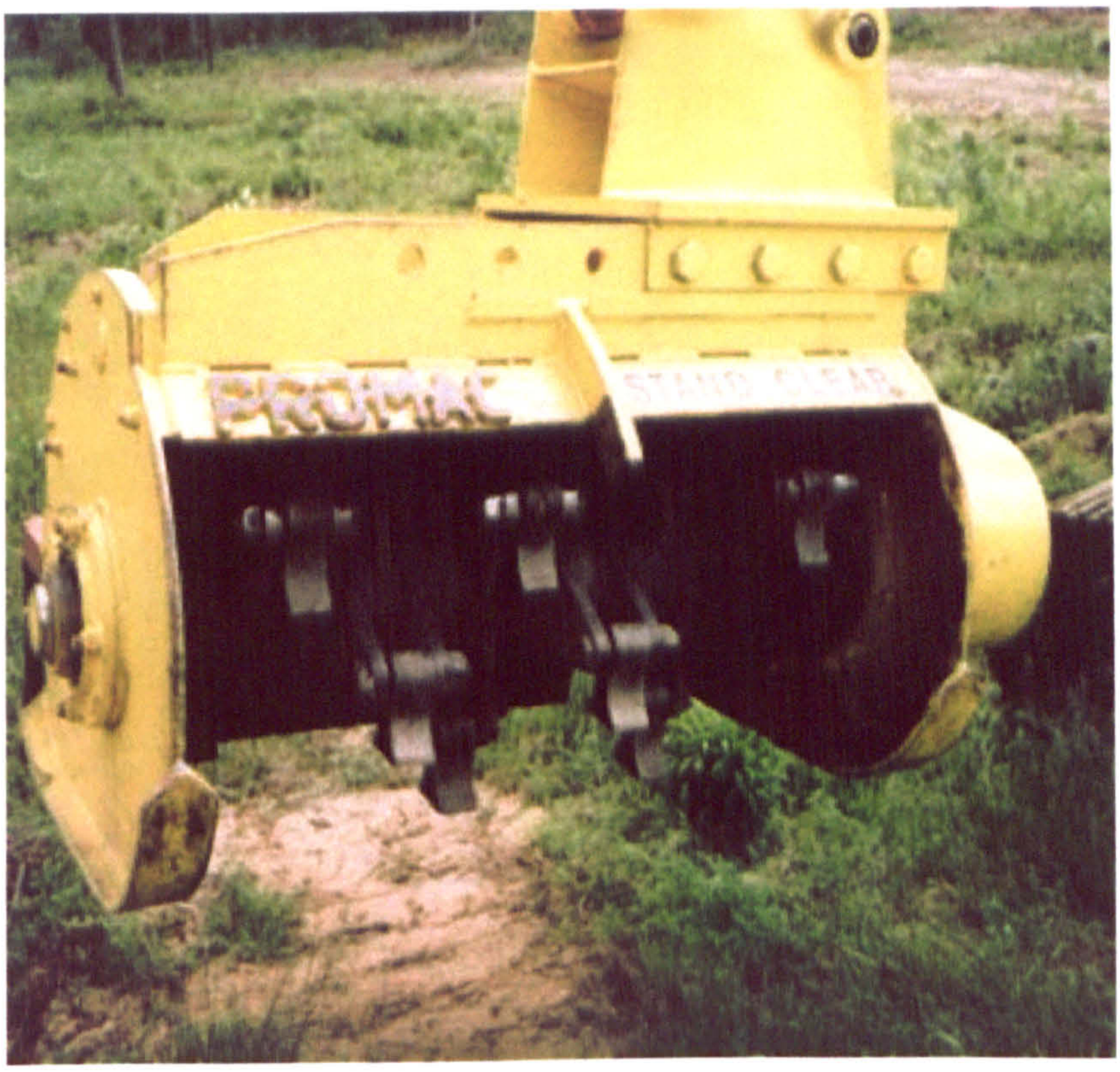

Figure (1.2) Flails mounted on an excavator arm

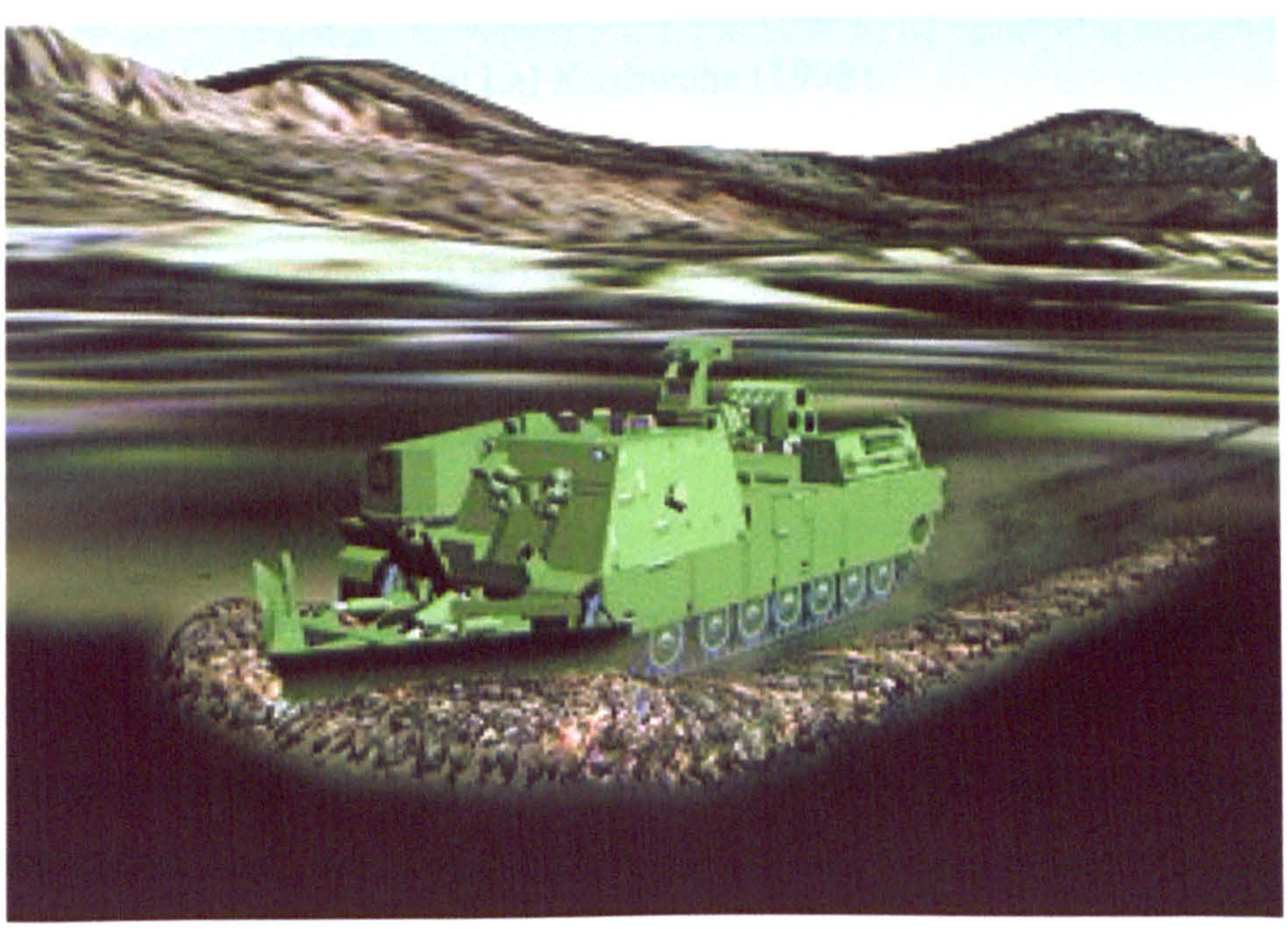

Figure (1.3) Plough with V type dozer blade

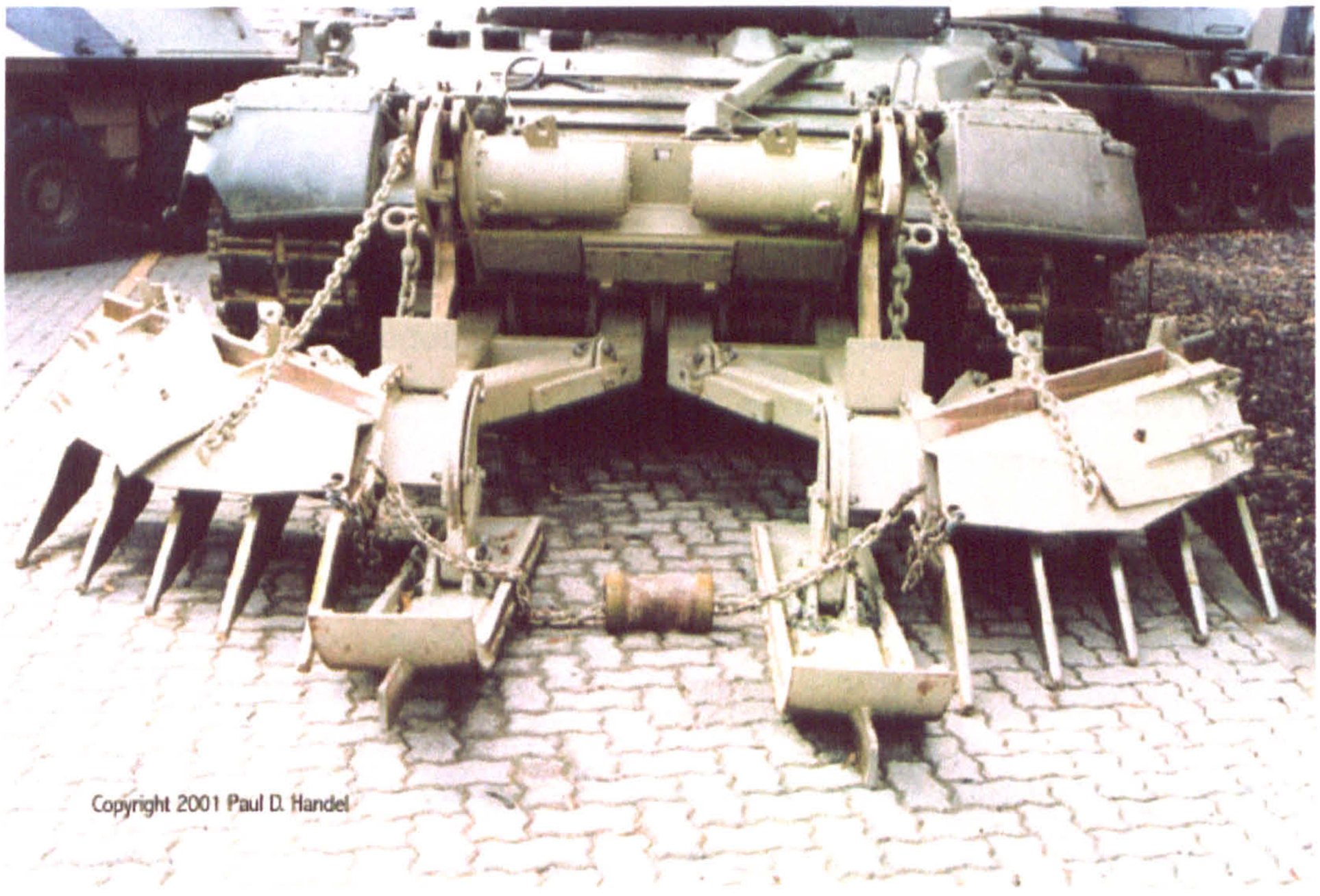

Figure (1.4) Rake plough mounted on a tank

1.4 CLASSIFICATION OF EARTH WORK

A soil-machine system in a broad sense might refer to any of the following systems, by Jie Shen and Radhey Lal Kushwaha (1998):

1. Soil-agricultural machinery

The dynamic response of soil to farm tractors is one main factor in determining their overall interactive performance. The interaction between tillage tools and farm soil is of primary interest to the design and use of these tools for soil manipulation.

2. Soil-military machinery

A variety of military tanks, tracks and other special-purpose vehicles operated on off-road ground are typical components in such a system. Another instance consists of the working tools of machines for laying antitank mines or digging trenches, and the associated ground.

3. Soil-forest machinery

The success of a power-driven tree planter depends upon primarily the interaction between its working tool and the soil during the digging process. The soil

compaction caused by machines in harvesting practices may have a detrimental effect on forest productivity.

4. Soil-mining and construction machinery

Hydraulic excavators and bulldozers are widely accepted for quarrying, mining, earthmoving and construction applications. The performance and efficiency of these machines are dependent upon the interaction between soil and the working tools: shovel or blade.

1.5 FACTORS AFFECTING THE PERFORMANCE OF EARTH WORK MACHINERY

Soil-Tool interface importance appears not only in mine clearing but also in earth moving equipment used for constructing the foundation pits, trenches, earth embankments, dams, leveling work, and roadbeds, where destruction and separation of soil from the ground mass is required. The productivity of mine clearing and earth moving equipment depends on soil properties, operating tool geometry, and operating conditions (cutting speed, cutting angle, and cutting depth).

The performance of earth-moving machines is affected by the following physical and mechanical properties of soil and tool design and operating condition. These are included here to give the reader a feel for the complexity of the modeling required and will be described in more detail in the literature review in Chapter 2.

Physical and mechanical properties of soil

- Granular composition, i.e. percentage by weight of particles of various size
- Volume mass γ, i.e. mass of 1 m^3 of soil, taken in a natural state, together with pores.
- Porosity, defined as the volume of pores filled with water and air, expressed in percent of the total volume of soil.
- Cohesion of soil, which is characterized by the effort required to overcome the adhesion between particles and their relative displacement.

- Plasticity, which is property of soil to change its shape under external forces and to preserve this shape upon removal of the forces.
- Bearing power, which is the property of soil to resist destruction when acted upon by external loads.
- Friability, which is defined as the capacity of soil to increase its volume upon destruction.
- Angle of accumulation of cut soil.
- Angle of internal friction.

Tool design and operating conditions

- Tool width
- Tool curvature
- Cutting edge
- Cutting angle
- Cutting depth
- Cutting speed
- Surface roughness of the cutting tool

1.6 OUTLINE OF THE THESIS

In Chapter 2, a review of the different methods used in studying the soil-tool interaction is presented. In Chapter 3, a description of soil properties and most common experimental tests are presented along with a comparison study of the available constitutive models for sand. In Chapter 4, a review of the proposed constitutive model for simulating sand is carried out then the model is modified to account for monotonic loading. At the end a validation study of various available integration schemes used in the numerical simulation of the modified model is carried out. In Chapter 5, implementation and validation of the implemented model through analysis of some benchmark problems are presented. In Chapter 6, an extensive study of soil-tool interaction in 2-dimensions is presented and then extended to the 3-dimensional study. Chapter 7 represents summary and concluding remarks along with some hints of the expected future work.

Chapter 2

LITERATURE REVIEW

2.1 CHAPTER SYNOPSIS

In this chapter the soil-tool interface process is described and a review of different approaches (experimental, analytical and numerical) previously attempted in the literature in studying soil-tool interaction is presented. A review of the available numerical interface models is also described. A description and review of sand material properties and models is given separately in Chapter 3.

2.2 METHODS OF STUDYING SOIL-TOOL INTERACTION

As mentioned in the introductory chapter, Soil-Tool interaction is affected by several physical, design and operating factors. The methods of studying soil-tool interaction may be classified into three types:

Experimental study: using an indoor soil bin equipped with a blade or cutting tool carrying device and measuring instruments to account for different forces acting on the tool.

Analytical approach: the soil in front of the tool is broken up into several parts each of which is considered as a rigid object. The limit equilibrium method is applied to analyze the force balance in the entire system.

Numerical approach: the soil-tool interaction is analyzed using numerical methods such as finite difference, finite element or boundary element.

Each of these methods has its advantages and limitations as will be shown in the following.

2.2.1 EXPERIMENTAL STUDY

Most of the experimental studies previously done were mainly carried out for the verification of either mathematical or finite element models. In this section a review of the experimental studies in the literature is reported to assess the different factors affecting the soil-tool interaction process.

Yong and Hanna (1977) provided an experimental study of a simple flat straight blade in interface with a clay soil using an indoor soil bin. The study focused on the effect of cutting angle on both draft (horizontal) and vertical forces applied on the cutting blade. The study shows that the cutting angle has a significant effect on blade cutting forces. This conclusion was drawn using a relatively small blade frontal displacement (8 cm).

Spektor and Katz (1985) presented an experimental study on the frontal resistance forces in soil cutting, with emphasis on the dependence on tool displacement during the loading and unloading stages under quasi-static and dynamic regimes. Laboratory tests were conducted on undisturbed sand soil, using specially developed equipment, and showed that:

1. During the loading stage, at pre-limiting levels of the resistance force, the soil undergoes both reversible and residual deformations.
2. At the onset of the unloading stage, the restoring force undergoes a downward jump.
3. The limiting value of the frontal resistance force increases considerably in the cutting velocity interval of 0.1 to 3-5 mm/s; at higher velocity, up to 25mm/s, this force increases slowly.
4. The frontal resistance force is linearly related to the tool width and non-linearly to the depth of cutting.

Mouazen and Nemenyi (1999) used a 25-m long soil bin to study the effect of narrow tillage tool cutting angle on the subsoil. The results also show a significant effect of the tillage tool angle of cutting on cutting forces in both draft and vertical directions. To study the effect of cutting speed, Rosa and Wulfsohn (1999) designed a high-speed monorail system to drive narrow tillage tools through a 9-m long linear soil bin. The monorail system was shown to be capable of driving tools at a maximum draft force of 1.5 kN at a maximum steady speed of 10 m/s over a distance of the order of 1-3 m. The study which was focused only on the effect of cutting speed shows severe changes in cutting forces with relatively low change in cutting speed. A detailed experimental study was carried out, AboElnor, et al. (1998) to investigate the effect of different operating conditions on cutting forces using 5-m long indoor soil bin shown in Figure (2.1).

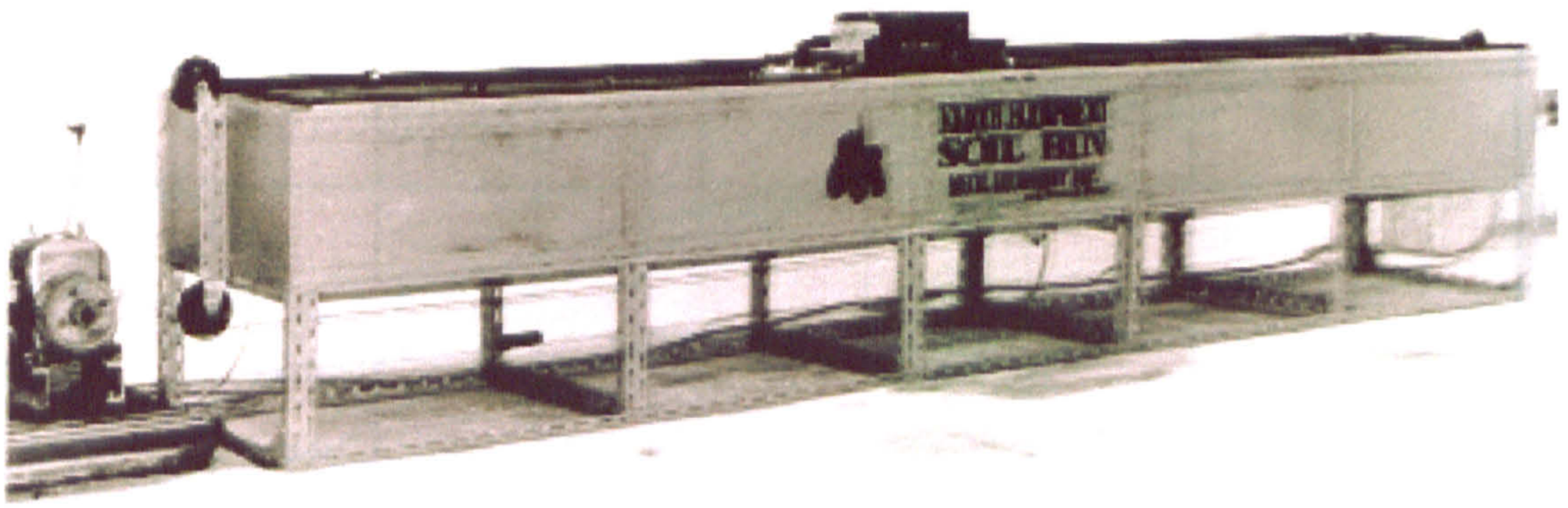

Figure (2.1) Indoor soil bin (after AboElnor, et al. 1998a)

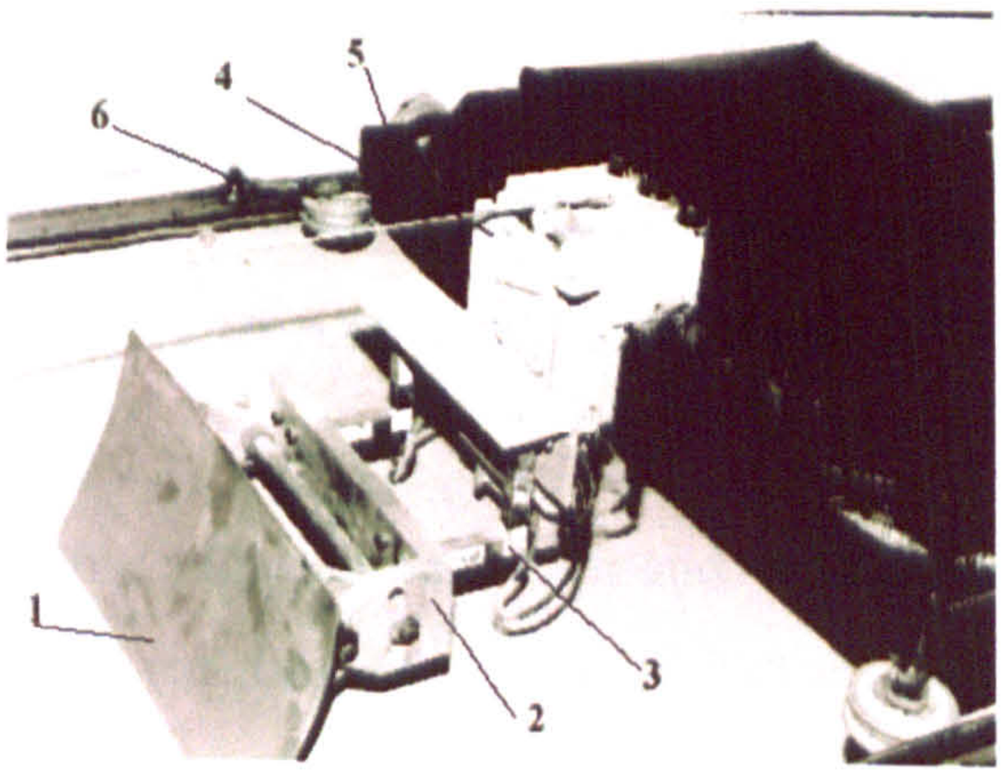

Figure (2.2) Dozer model (after AboElnor, et al. 1998a)

The dozer model arrangement, Figure (2.2) was capable of changing blade cutting angle, depth and speed for different blade geometry and measures both draft and vertical forces acting on the cutting blade through a 4-m travel distance.

Experimental testing of the effect of blade geometry and operating conditions on the cutting forces using loose sand soil type led to the following conclusions:

- ***Effect of cutting speed***

The effect of change of blade cutting edge length "a" on both draft and vertical forces under different cutting speeds is shown in Figure (2.3). The figure reveals that as the cutting speed increases, draft force increases and vertical force decreases. Also blades with long flat cutting edge are better in low speeds.

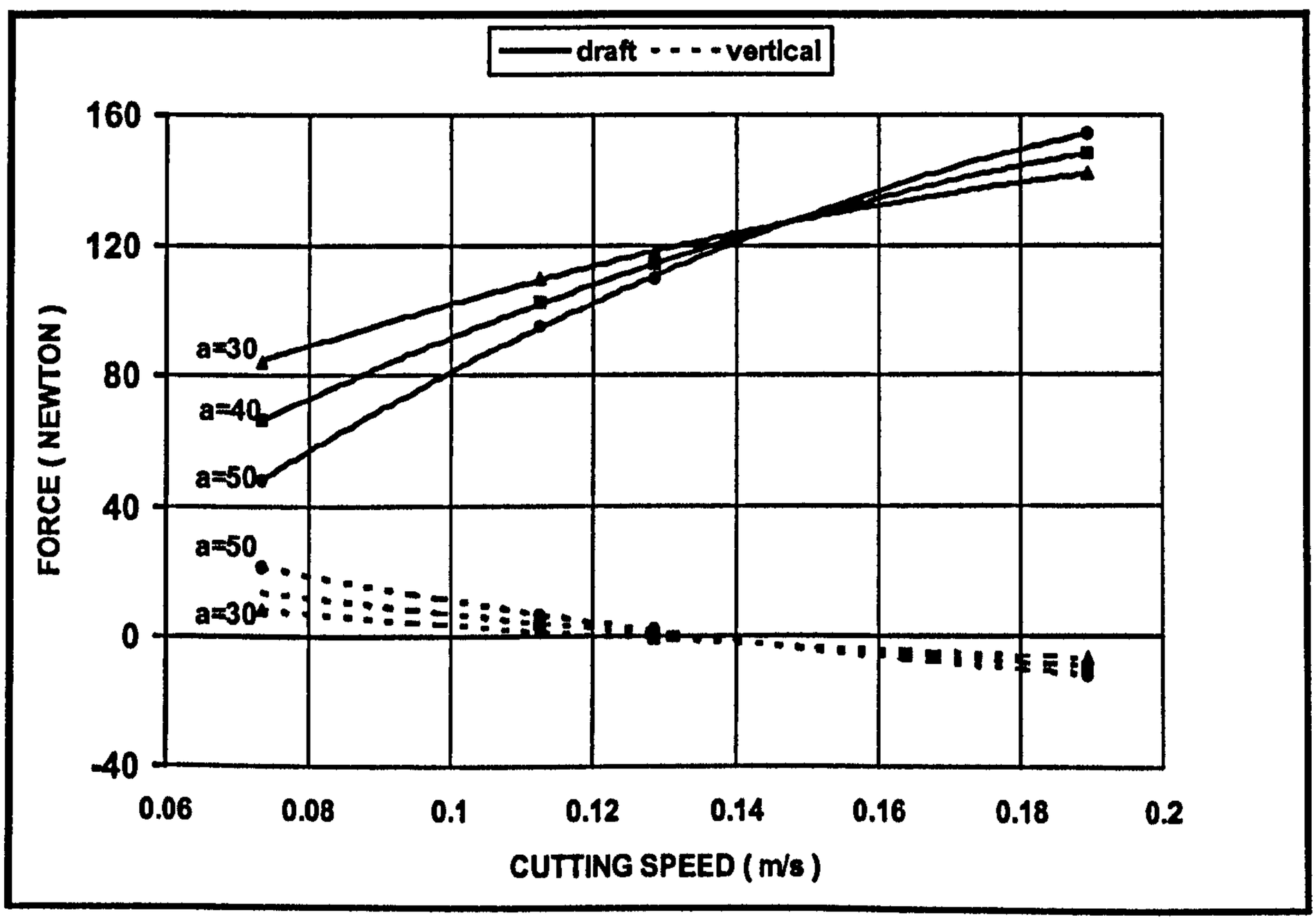

Figure (2.3) Effect of cutting speed (after AboElnor, et al. 1998a)

- ***Effect of cutting angle***

The effect of change of blade cutting angle on both draft and vertical forces for different blade cutting edge length "a" (in mm) is shown in Figure (2.4). As shown in this figure, blades with long flat cutting edge are better whatever the cutting angle.

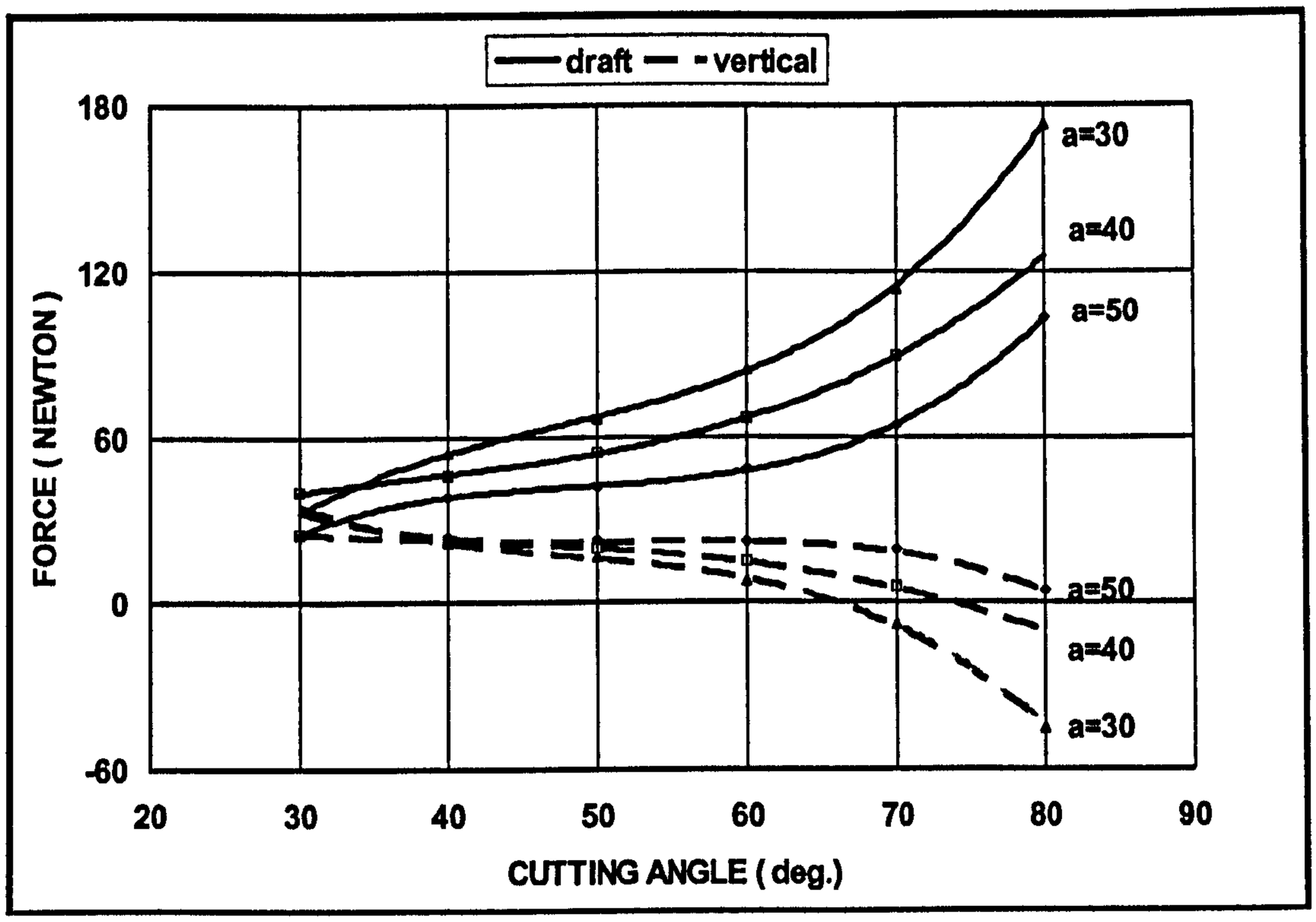

Figure (2.4) Effect of cutting angle (after AboElnor, et al. 1998a)

- ***Effect of cutting depth***

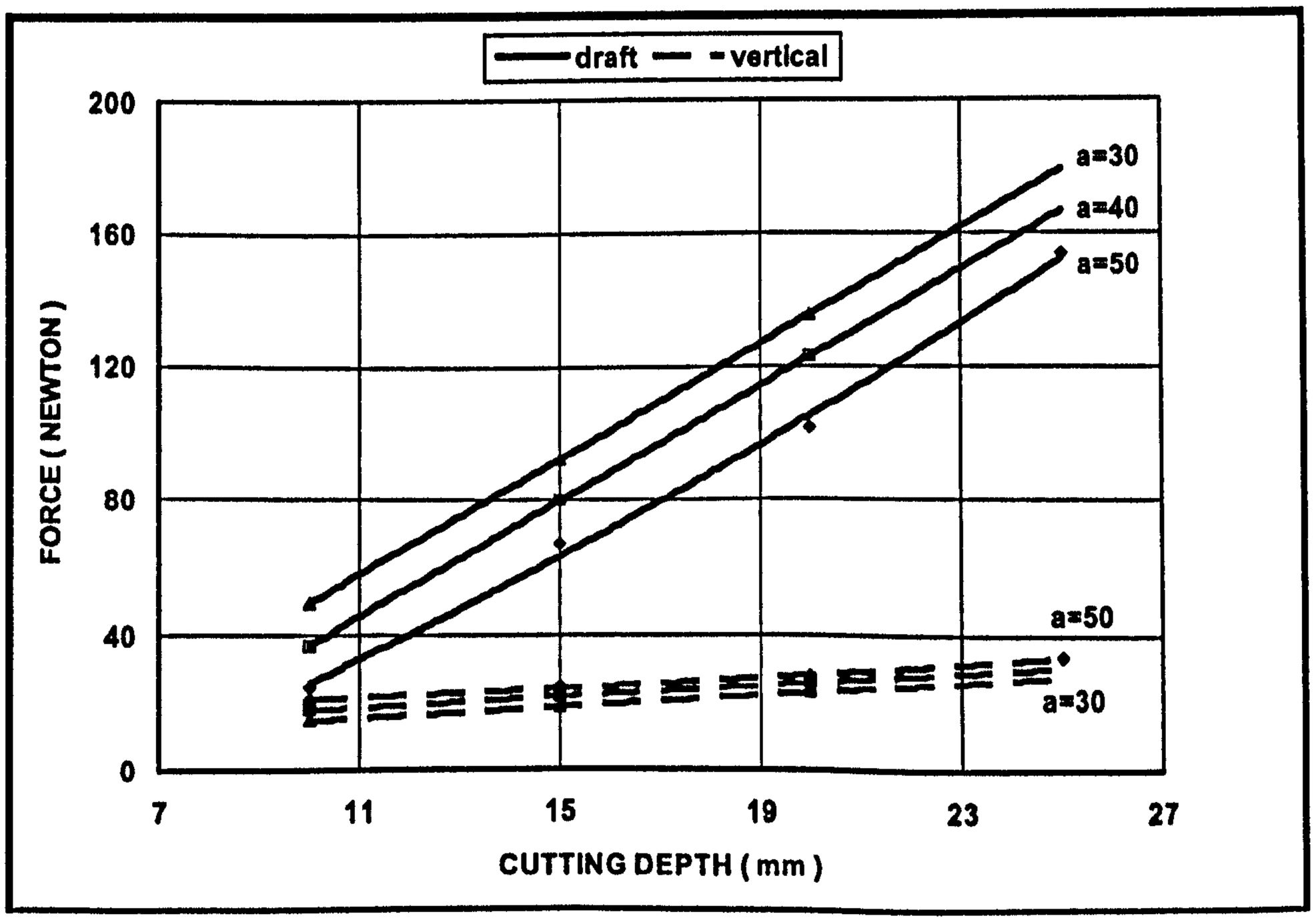

Figure (2.5) Effect of cutting depth (after AboElnor, et al. 1998a)

Figure (2.5) presents the relation between both draft and vertical forces and cutting depth at the blade flat part of length of a = 30, a = 40, and a = 50mm. As shown from the figure, by increasing the cutting depth the draft force and vertical force increase. The rate of increase of the draft force is very high, by about 400 %, compared with the rate of increase of the vertical force, which is about 150 %.

In conclusion, an experimental study is limited by its expense, time and measurement accuracy at high cutting speed and large cutting depth; analytical and numerical approaches are an alternative.

2.2.2 ANALYTICAL APPROACH

A conventional analytical method has been used to develop two- and three-dimensional models based on Terzaghi's concept of passive earth pressure, Atkinson (1993). These models are based on the assumptions that soils are homogenous, isotropic, semi-infinite and ideal plastic.

Limit equilibrium is one of the most important analytical approaches. The basic idea behind it is that the soil and tool (or machine) are considered as a whole. Force equilibrium equations over the entire system are established with soil being in its limit state where its resistance becomes large. From the equilibrium equations, forces acting on a tool or a machine can be obtained. It should be kept in mind that the limit equilibrium method could be used to obtain information about the maximum forces that can be generated inside the soil body without providing much of a clue about how the soil body deforms. This is due to the fundamental assumptions embedded in the limit equilibrium. These assumptions give the method a very simple form but it is quite limited in its ability to analyse the deformation in the system.

In general, the basic assumptions for a limit equilibrium method are:

(a) The soil is considered as a rigid material, that is, it is not deformable.

(b) The soil might fail inside the soil body and/or at a metal-soil interface. For the failure inside the soil body, one or several parts of soil may slide over a potential failure surface; while with the failure at the interface; soil may slide over a metal-soil interface.

(c) The pattern of one or more failure surfaces inside the soil body is assumed or predetermined depending on the application. In fact, different investigators have proposed many possible failure patterns in the past. Each pattern may involve one or more unknown parameters leading to a series of potential failure surfaces. The unknown parameters are determined by performing an optimization to find the most critical failure surface that generates a minimum reaction force in a tool or machine.

(d) The forces interacting on a failure surface in the soil body are determined by the Mohr-Coulomb criterion:

$$\tau = c + \sigma_n \tan\phi$$

where: τ and σ_n = tangential and normal stresses, respectively

c = Cohesion of soil

ϕ = Internal friction angle of soil

(e) The forces interacting on a metal-soil interface are determined by the following criterion:

$$\tau = a + \sigma_n \tan\delta$$

where: a = Adhesion at a soil-tool interface

δ = External frictional angle at a soil-tool interface

On the basis of the above assumptions, the limit equilibrium method can be applied. However the two most important factors in this approach are:

(a) Shape of soil failure surfaces: The shape is normally proposed on the basis of empirical observation or data, and is very crucial to the success in applying the limit equilibrium to an analysis of soil-machine systems.

(b) Equilibrium equations: For two dimensional cases, the equilibrium equations in the horizontal and vertical directions can be established by considering each individual soil block separated by failure surfaces in the soil body or metal-soil interfaces.

For three-dimensional cases, the equilibrium equations are set up in horizontal, sideways and vertical directions. By solving these equations, we can obtain useful

force information in a soil-machine system such as the draft or penetration force of a work tool. In the past three decades, numerous studies have been conducted in applying the limit equilibrium method to the soil-tool interaction problem. The most significant ones are summarized below with a focus on the shape of soil failure surface.

The logarithmic spiral method, which was originally developed for the evaluation of soil loads in civil engineering, Terzaghi (1959) has been used extensively in calculating soil resistance to tillage tools, as shown in Figure (2.6). The soil in front of a tool and above the failure surface is assumed to consist of two parts: (1) a Rankine passive zone and (2) a complex shear zone bounded by part of a logarithmic spiral curve. Equilibrium of surface forces on the boundaries of these two parts, as well as their body forces, can be used to calculate the horizontal and vertical forces on the tool.

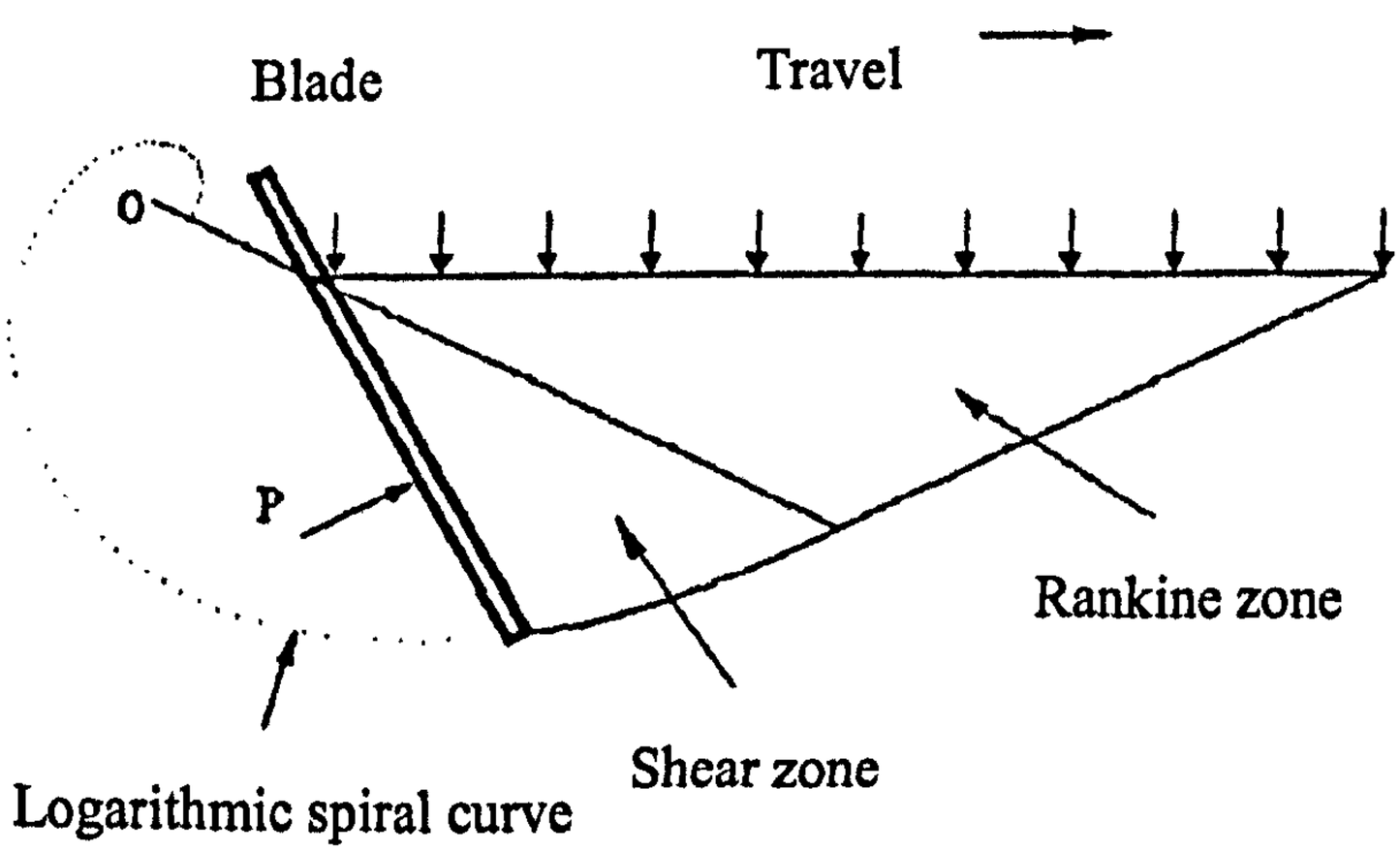

Figure (2.6) Logarithmic spiral failure zone (after Terzaghi 1959)

Swick and Perumpral (1988) developed a mathematical model for predicting the resistance forces acting on narrow blade tillage tools. they used an artificial soil for the test and variable cutting conditions such as cutting speed, cutting depth, and cutting angle. The angle of internal friction, soil-metal friction angle, cohesion, and adhesion were found to be independent of shear rate for artificial soil. The results also showed that the model is acceptable for narrow blades, while for DOZER blades

the problem is more complicated because of the accumulation of cut soil in front of the blade.

Through analysis of the fundamental behavior of soil-metal friction, a non-Newtonian fluid equation has been found to be applicable to describe the mechanics of soil-metal friction, Yusu and Dechao (1990). An expression for the friction stress as a function of sliding speed and normal pressure was established. This expression was verified with laboratory tests under sliding speed ranges between 0.4 - 1.7 m/s and various soil conditions. The developed relation between soil-metal friction and sliding speed is in the form

$$f_p = C' + A \ln \upsilon + \sigma_n \tan \phi_a$$

Where

A	Speed effect coefficient of adhesion	
C'	Soil-metal adhesion when v = 1m/s	(kPa)
f_p	Soil-metal friction stress	(kPa)
υ	Sliding peed	(m/s)
σ_n	Normal pressure	(kPa)
ϕ_a	Soil-metal friction angle	

A model of soil shear strength as a function of shear rate and normal pressure has also been developed by Dechao and Yusu (1991) and verified with a series of laboratory tests under shear rate range of 5 - 30 s^{-1} and in various soil conditions. Experimental results showed that an increase in soil shear strength is intensified by a rise in shear rate. They also showed that the relation between soil shear strength and normal pressure is non linear at high shear rate. This suggested that the Mohr-Coulomb criterion could only be applied under low shear rate conditions and that the shear rate effect is more significant at higher volume weight.

To account for the effect of the shear rate on soil shear strength and soil-metal friction; a dynamic model for soil cutting resistance predicted by blade and tin was developed by Dechao and Yusu (1992). The model was verified with a series of tests in a soil bin with a blade and tin. Unlike most previous models, which were all based

on empirical failure patterns and considered soil as a rigid-plastic body, this model was based on soil flow under cutting. The model was found to be applicable in a wider range of soil types. The relations of cutting resistance to major factors such as cutting depth, cutting width, rake angles and cutting speed were simulated by this model. It was found to be satisfactory as compared with previously reported test results, but the accumulated soil in front of the cutting blade was not considered in this model and, as shown in the verification study, Figure (2.7), there is an error of the order of 20-40% between the predicted and the test results. This error makes the model unreliable.

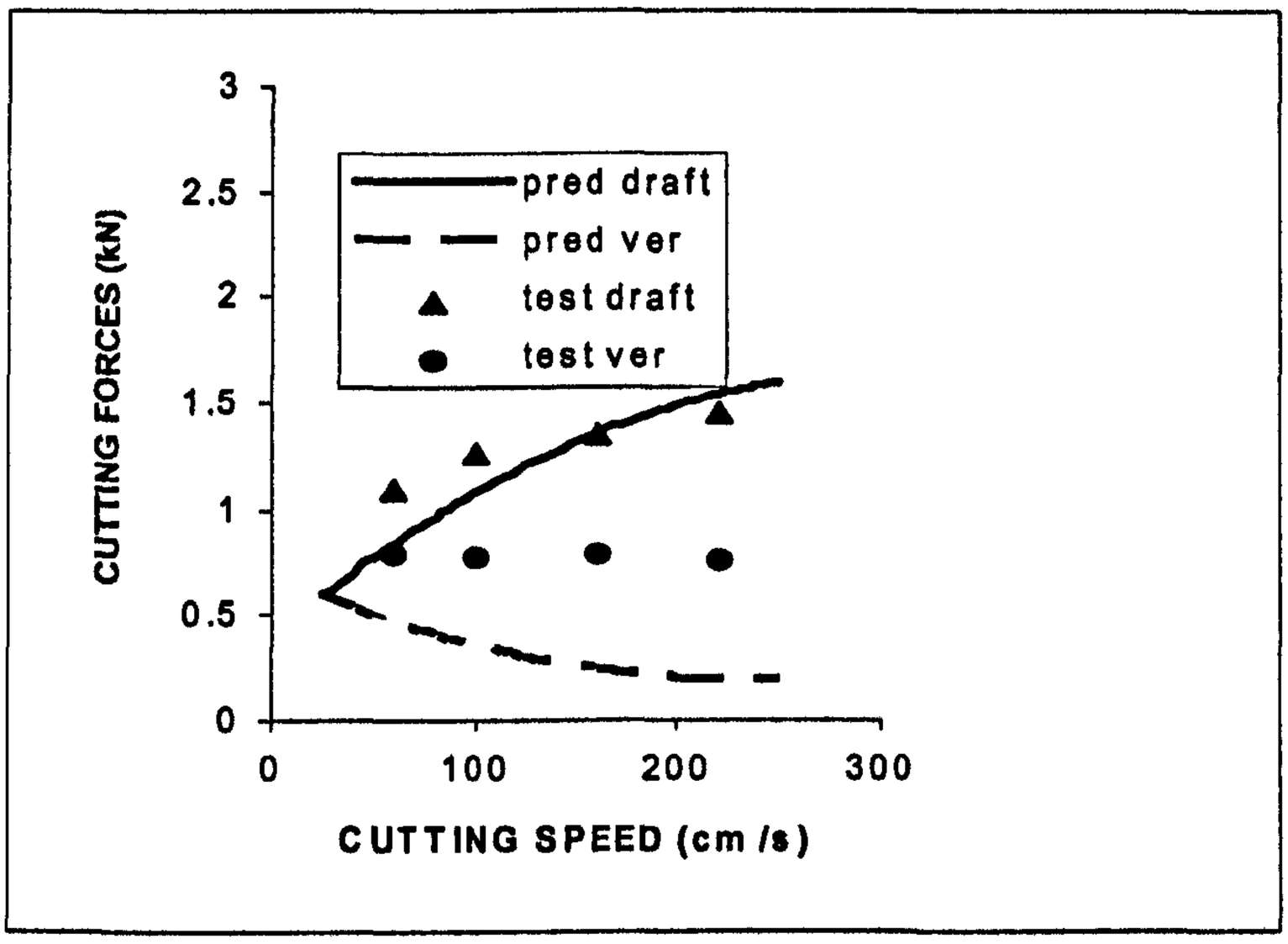

Figure (2.7) Predicted draft and vertical load as compared with test values (after Dechao and Yusu 1992)

Qinsen and Shuren (1994) presented a mathematical model of soil-tool interaction for bulldozer blades. The model was found to be useful for predicting the behavior of slow moving bulldozer blades. It was also found that the soil density and tool depth of the bulldozer blade have a significant effect on the mean and fluctuated amplitude of force on the blade, but at low velocity (less than 20 cm/s) this effect is insignificant. So it is desirable to investigate further velocity and acceleration effects on the blade forces. To this end, a simple mathematical model was developed, AboElnor, et al. (1998b), based on the following assumptions;

1- The soil cut from the ground slides up on the surface of the blade first, and then it falls down from the highest point.
2- The cut soil in front of the blade can only move, but not turn over.
3- The rupture surface is planar.
4- The soil before being cut has cohesion and frictional characteristics, after being cut the soil still has frictional but little cohesion characteristics.
5- Acceleration forces on the blade are zero.

The resulting model based on such an assumed cutting mechanism is shown in Figure (2.8). The cut soil is separated from the groundmass by a wedge-shaped, part (1) in Figure (2.8). Two motions are imparted to the working member: one for penetrating the working member into the ground, which is characterized by the feed rate, and the other for motion during which a part of the ground is separated and characterized by the cutting speed.

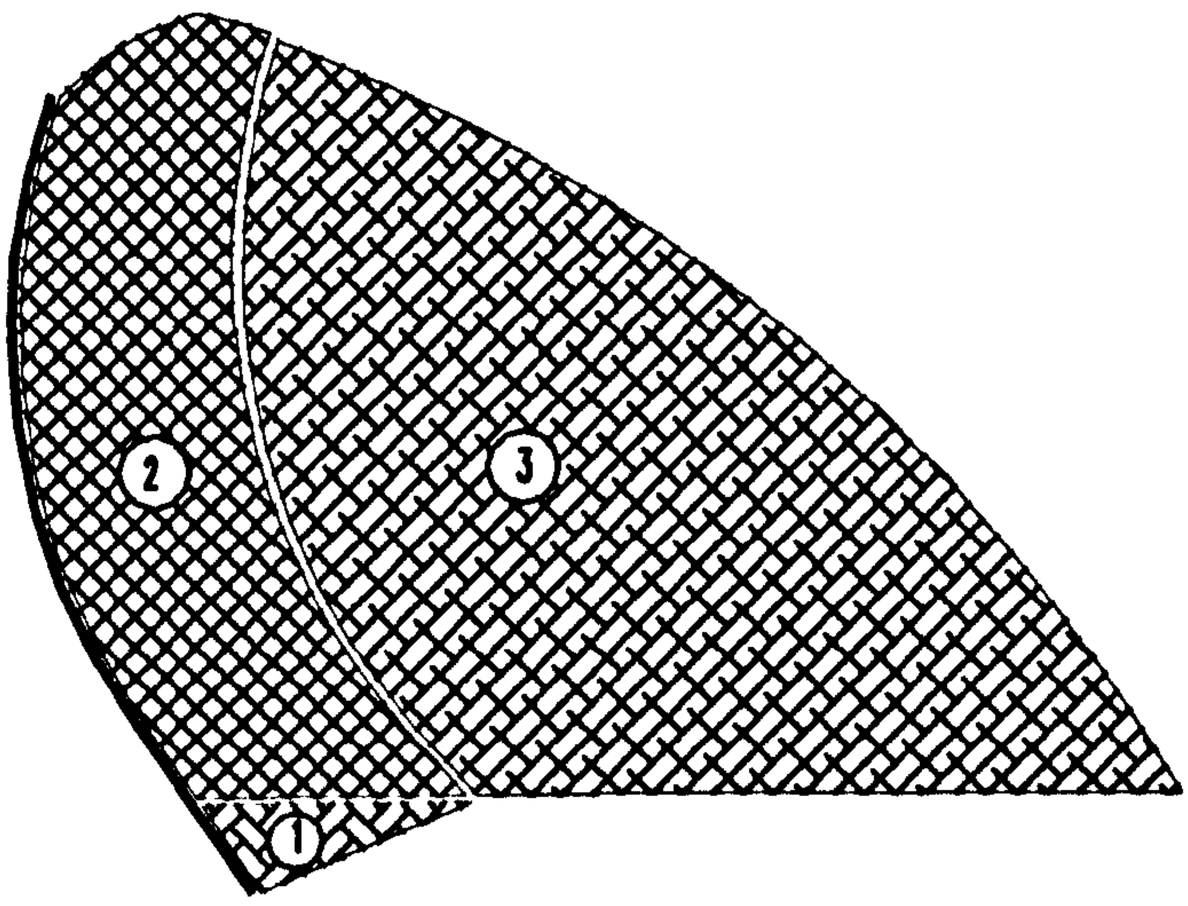

Figure (2.8) Soil failure mechanism

The process involving only separation of soil from the bulk mass is called the *cutting process*. The process of moving the separated soil by the working member (blade, tine and tillage) is referred to as the *digging process*. Then the cut soil, part (2), slides along the blade surface and moves, part (3), in front of the blade. The moving soil in front of the blade depends on the blade width and it is insignificant for the case of tine and tillage tools.

Forces acting on the cutting blade are classified into:

1- Friction force between cut soil on the ground and ground.

2- Friction force between cut slides and cutting blade.

3- Adhesion force between cut soil and cutting blade.

4- Cohesion force between cut soil and ground at rupture plane.

5- Friction force between cut soil and ground at rupture plane.

Model validation revealed its capability of predicting blade-cutting forces within mean standard deviation of 9% at low cutting forces and 20% at high cutting forces (large depth, large cutting angle or high speed). O. Luengo and S. Singh (1998) presented a developed formulation of soil-tool interaction accounted for terrain slope during digging. Further analytical models have been summerized in Shen and Kushwaha (1998).

Although the above analytical based models do serve their purposes to a certain extent, the methodology used in developing these models has the following intrinsic weaknesses:

1. A failure profile is a prerequisite for the limit equilibrium analysis. The choice of the assumed profiles is arbitrary and depends on each particular investigator.
2. Soil mechanical properties are assumed to be uniform without considering the layered characteristics of some farm fields.
3. The mode of soil failure is affected by the tool speed, and it is difficult to define its influence by tracing or describing the failure profile as variant with speed.
4. Soil velocity and acceleration profiles in front of a tillage tool have to be simplified and assumed to follow a simple pattern without a rigorous justification.

Evidently these weaknesses may introduce errors in calculating forces in soil-tool interaction, especially in cases different from the conditions under which the model was developed. Hence, it is important to have a method that can alleviate these weaknesses to a certain extent.

2.2.3 NUMERICAL APPROACH

Soil-tool interaction can be analyzed using numerical methods such as finite difference, finite element or boundary element. Since the finite element method has been the dominant numerical approach during the past three decades it will be used in this study to analyze soil-tool interaction.

2.2.3.1 The finite element method

The finite element method (FEM) is a relatively new and effective numerical method, the advent of which is enhanced by the progress in modern computer architecture, programming languages and algorithms, Rao (1999) and Smith and Griffiths (1997).

In the 1950s, the basic idea of the FEM originated from the matrix analysis of airplane structures in aviation engineering. According to the structure matrix analysis method, an entire structure can be considered as an assembly formed by linking many finite mechanical elements together; the function of each element is similar to the role of a brick in a building.

In 1960, this idea was extended in solving plane stress problems in elastic mechanics and a terminology of FEM "finite element method" was adopted. However, for a continuum medium, which is actually composed of infinite number of elements, the FEM can be used only after the continuum medium is discretized in the following manner:

(a) The continuum medium is divided into a finite number of blocks (or elements) which are linked to each other only at certain specified points, called nodes;

(b) Inside each element, the displacement distribution is approximated using a simple function and the relation between nodal force and nodal displacement is determined by the variation principle.

(c) Assembling the nodal force-displacement relation of all elements yields a set of algebric equations with nodal displacements being unknowns. Solving such a set of equations provides the displacement information at a finite number of

nodes within the continuum medium, i.e., the approximate solution to the problem.

Therefore, if the mechanical properties of each element are obtainable, the continuum medium can be analyzed by the FEM.

The FEM is different from classic analytical methods that in classic analytical methods, the mechanical properties of a micro-block are considered and a continuum medium is assumed to contain an infinite number of micro-blocks. By letting the size of the micro-block tend to be zero, a set of differential equations describing the mechanical properties of the continuum medium may be obtained. Solving such a set of equations leads to an analytical solution that provides the values of unknowns at any point within the continuum medium. However, in most practical problems in engineering with irregular geometric shapes, non-linear and non-uniform material properties, an analytical solution is almost impossible. On the other hand, in the FEM, different elements can be assigned different material parameters to simulate the material non-uniformity. Iterative and incremental methods may be used to solve non-linear problems; arbitrary mesh generation eliminates the difficulty in modeling irregular geometric shapes. Thus, using the FEM may lead to an approximate solution to most problems in engineering.

The main advantages of the FEM include:

(a) It is suited for solving almost all the problems of continuum media and fields. It has been successfully used not only in stress analyses of non-uniform materials, anti-isotropic materials, non-linear stress-strain relations and complex boundary conditions, but also in heat transfer, fluid mechanics and electromagnetic field.

(b) It adopts the expression in matrix forms and thus is suited for computer programming. Once a general computer program is developed, it can be used for solving problems with any geometric shape simply by changing the input data.

2.2.3.2 Soil-tool interface mechanism

It has been noted that the accurate determination or evaluation of soil reaction and deformation fields in the soil mass throughout the cutting (loading) sequence is complicated by a number of factors which need to be addressed in a finite element soil-tool interface model: some of these factors are

1. The interacting system generally consists of two materials, soil and metal, with complex interface geometries as shown in Figure (2.9).
2. The interacting system has a continuously changing topology caused by the movement of the blade in the soil.
3. Constitutive relationships and failure criteria for soil under combined stress states are difficult to specify or obtain.
4. The characteristics of interaction at the soil-metal interface are not well defined and thus contribute to the complexity of the problem.

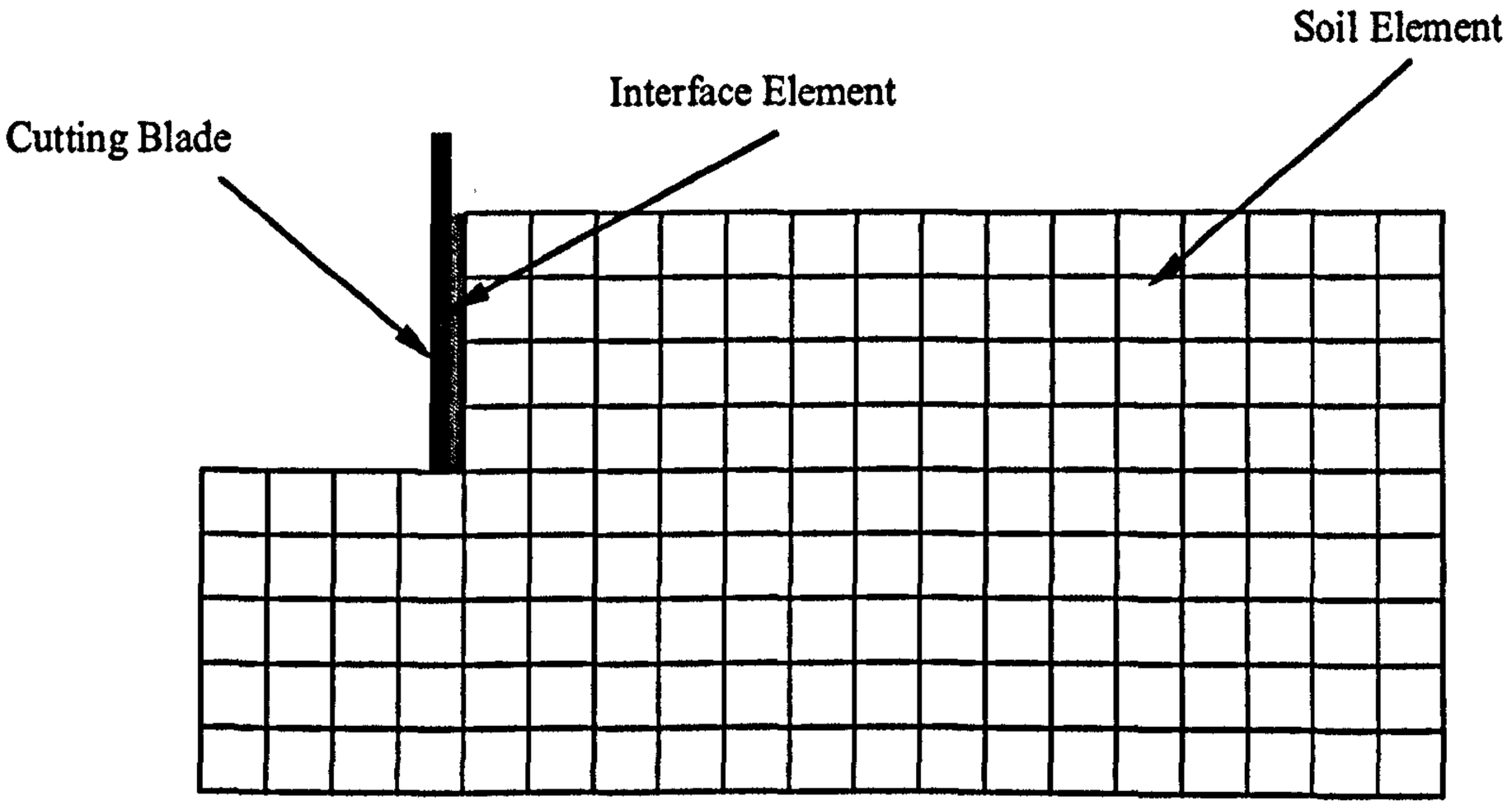

Figure (2.9) Soil-tool interface mechanism

The interface element, Figure (2.10), should be able to represent the soil-tool interaction in the following three cases:

1. Separation state; when the tool element loses contact with the corresponding soil element
2. Stick state; the soil and the tool elements contact each other without any relative movement.

3. Slip state; there is relative movement between the tool and the soil element.

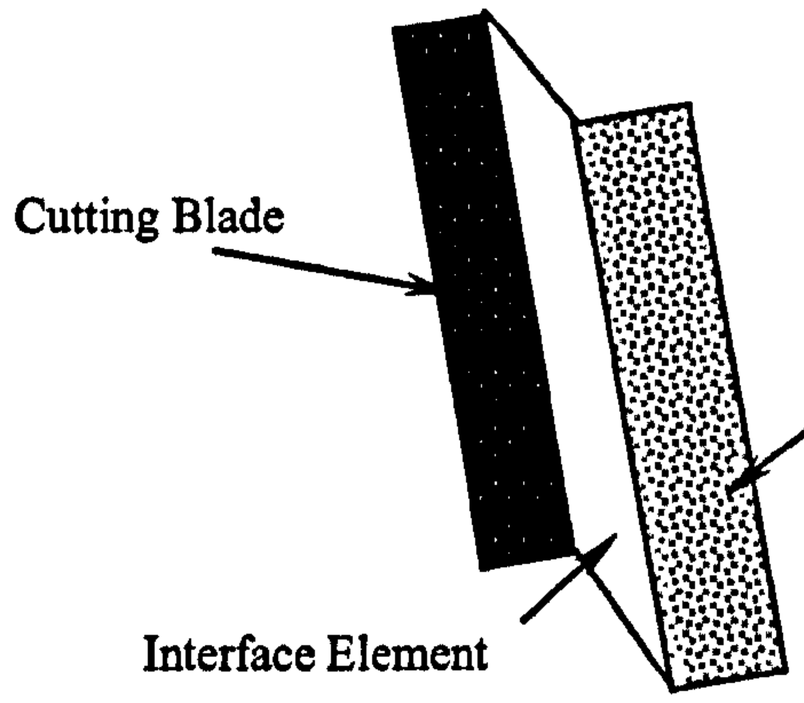

Figure (2.10) Interface element

2.2.3.3 Soil-tool interface models

It is observed that in the construction of a realistic model of soil cutting, the effect of progressive cutting of soil at the tool tip needs to be properly represented. In addition, there should be consideration of the possible development of failure surface in the soil mass where the shear strength of the soil is exceeded.

To accommodate these requirements, several numerical models using the finite element method have been attempted in the literature.

In all interface elements, the constitutive relation of the interface actually means the relationship between stress and displacement. The shear stress–displacement relation can be of one the following forms:

1. Elastic-perfect plastic
2. Hypoelastic
3. Hyperbolic

1. Elastic-perfect plastic interface modeling

In the elastic-perfect plastic models, the shear stress initially increases linearly with the relative displacement before the shear stress reaches its maximum value. After that, perfect plasticity occurs, that is, the shear stress remains constant as the relative displacement increases as shown in Figure (2.11).

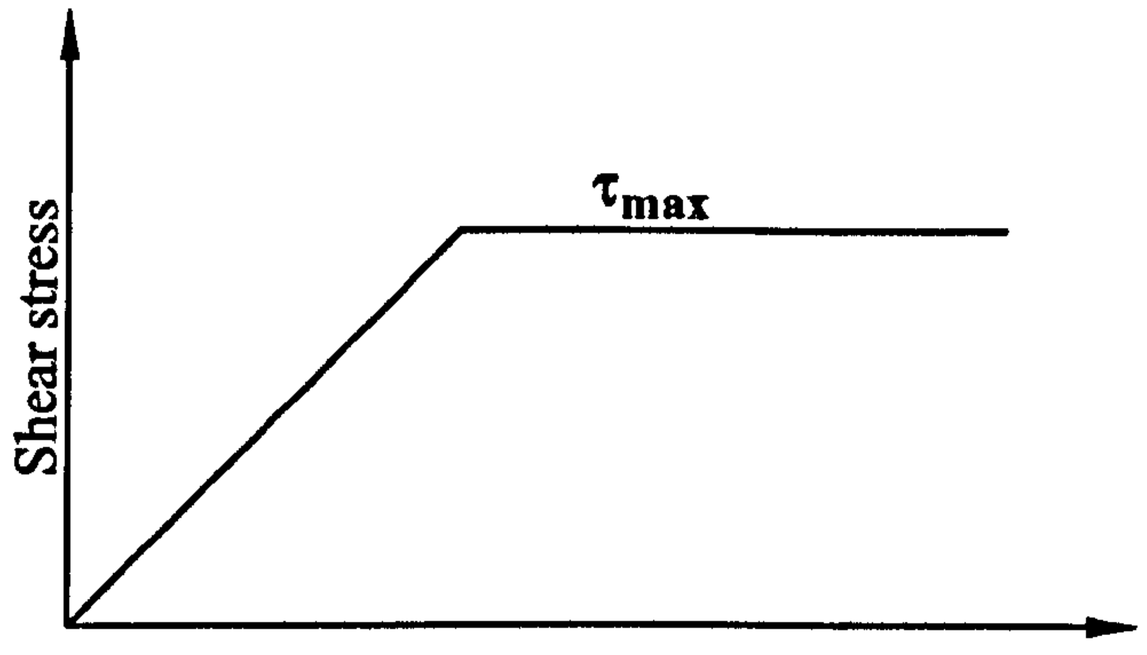

Figure (2.11) Shear stress versus relative displacement (elastic-perfect plastic)

Based on this concept, several researchers have developed FEM models of soil cutting by simple tillage tools. Mouazen and Nemenyi (1999) made an investigation to emphasis that the finite element method (FEM) is a viable technique to model soil cutting processes in non-homogenous soils. This study introduced the development of non-linear three-dimensional FEM model for cutting a layered (non-homogeneous) sandy loam soil with a medium-deep subsoiler having a chisel and shank with different angles and effective cutting widths. The soil material was considered as elastic-perfectly plastic, and the Drucker-Prager elastic-perfectly plastic material model was adopted with plasticity associated flow rule. Soil-tool interaction was simulated, adopting Coulomb's law of friction. A three-dimensional finite element mesh was generated using eight-noded, linear solid elements to represent the soil material and two-noded, gap elements were inserted between each pair of nodes on the soil and front edges of the subsoiler to represent the interface zone. The analysis was performed using commercial finite element software (COSMOS/M1.71). To account for soil separation at the chisel tip level, two-node cutting elements were a priori located along one row in front of the subsoiler tip. The influence of dynamic aspects and soil water pressure on soil cutting process was not considered. Also soil-metal adhesion was ignored for its relatively small value under dry conditions. In order to deal with material non-linearity of the soil, an incremental analysis technique was used. Inside each, the Newton-Raphson iteration method was applied. In order to verify the results calculated by the FEM, a soil bin experiment was carried out. The test soil was sandy loam, finally the study concluded to the

ability of the FEM to simulate the soil cutting processes in non-homogenous soils and to investigate the soil deep loosing (excavation) and subsoiler performance.

2. *Hypoelastic interface modeling*

Quasi-static modeling of soil-tool interaction is acceptable for the low speed range of agricultural operations; however, high speeds cutting operations can produce considerable dynamic effects on soil, so that dynamic components must be incorporated in analytical models. The dynamic effects of high speeds soil cutting can be described using the hypoelastic constitutive model. In a hypoelastic material, the rate of change of stress is defined as a tangent modulus matrix multiplying the rate of change of the elastic strain.

A hypoelastic soil constitutive relationship with variable Young's modulus and Poisson's ratio was developed recently by Rosa and Wulfsohn (1999) to describe the dynamic soil-tool cutting problem. Geometrical non-linearity was incorporated by updating nodal coordinates. This is equivalent to a first order approximation of the updated Lagrangian technique. Incremental load steps were used with constant time steps in the dynamic solution. The Newmark method was adopted (at each incremental load step) due to its stability and effectiveness to solve equilibrium equations. Material nolinearity arises due to the stress history of the material. Material stiffness changes with loading changes and these changes are usually nonlinear for soils. Thus the constitutive matrix is continuously updated, as well as updating the mesh nodal coordinates. The stiffness matrix was recalculated for each incremental step. The modified Newton-Raphson method was used to solve for material nonlinearity. To verify the numerical analysis, a high-speed monorail system was designed and built to drive narrow tillage tools through a 9-m long linear soil bin. Comparison between predicted and experimental data reveals that the hypoelastic model that incorporated both inertial and viscous terms (the latter directly in the stiffness matrix) produced severe numerical oscillations for minute tool displacements. As a result the model was not capable of simulating high speed soil-tool interaction. Finally the authors identified the need to develop appropriate

soil models to improve finite element simulations of dynamic tillage tool cutting with correct representation of soil failure.

3. *Hyperbolic interface modeling*

In the hyperbolic models, the transition behavior between the elastic zone and plastic zone of the elastic-perfect plastic interface modeling is a smooth function instead of the sharp corner as shown in Figure (2.12).

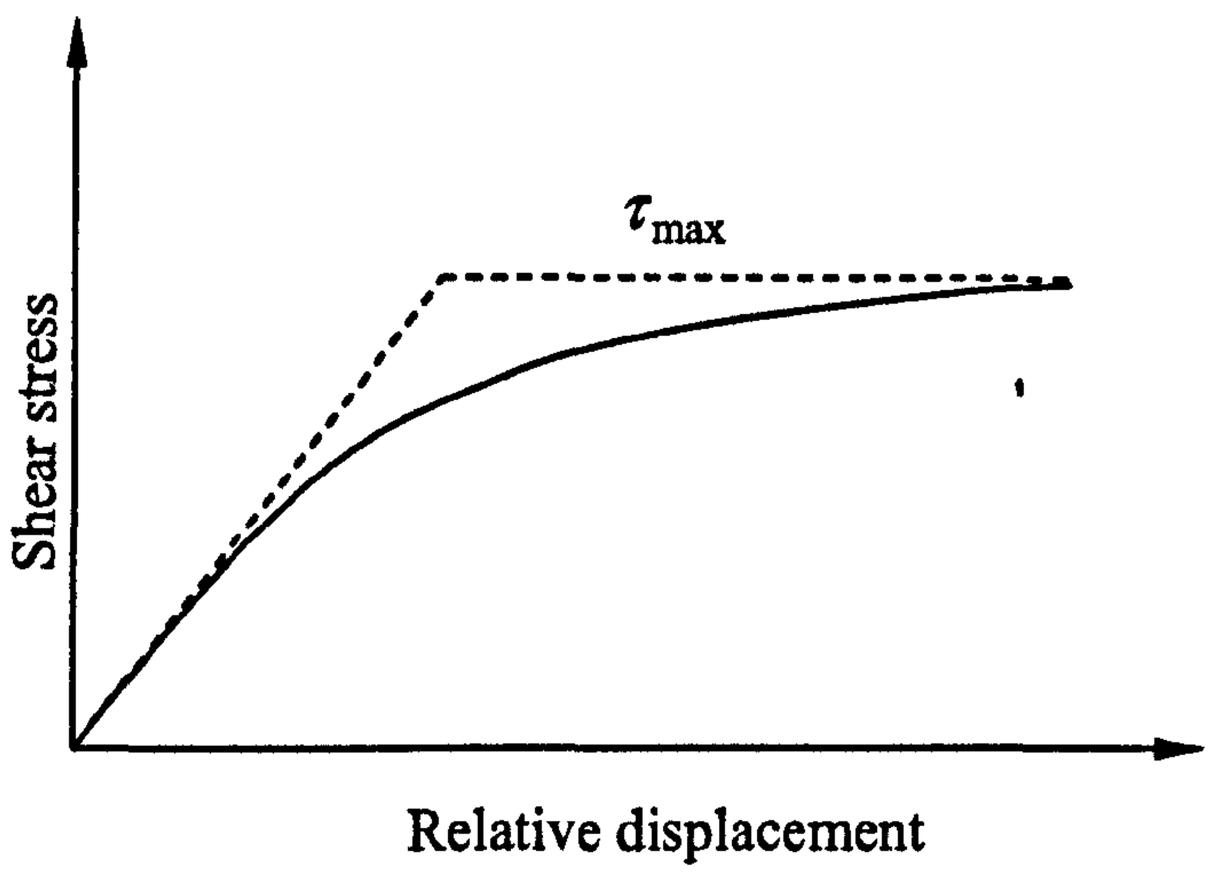

Figure (2.12) Shear stress versus relative displacement (hyperbolic relation)

Based on this concept; a three-dimensional non-linear finite element model for three-dimensional soil cutting under a narrow tillage tool was developed by Chi and Kushwaha (1990), with an anticipation that the finite element analysis will (a) provide the soil force required for cutting,(b) predict the soil failure zone, (c) the displacement field and (d) the stress along the tool surface. The weighted residual method was applied to formulate the finite element model and the Galerkin method was applied to select the approximation incremental displacement and the weighting function. A hyperbolic stress-strain model is used to model both the soil and the interface behavior. An interface element is inserted between the soil and the tool surface in order to account for the adhesion and friction, which always react between soil and blade surface. At each increment, normal stresses, shear stresses and principal stresses were calculated for each element. The stresses of each element were examined by using the Mohr-Coulomb soil failure criterion. Comparison between the draft and vertical force from the finite element model and the results

obtained from the soil bin test shows that the finite element model predicted a relatively accurate draft force.

The friction phenomenon at the soil-tool interface was also analyzed using the finite element method by Kushwaha and Shen (1995a). A modified tangent shear modulus based on a hyperbolic stress-strain relation was used to account for the loading rate effect. The characteristics of the soil-metal interface were studied in a laboratory test with a modified shear box. The distribution of normal force, tangential force and tangential displacement at the soil-tool interface at different travel speeds was studied. The results showed that the proposed hyperbolic model provided a good fit to the test data.

Kushwaha and Shen (1995b) applied the FEM to analyze the soil-tool interaction on a clay soil at high cutting speeds in 2-D. A hyperbolic stress-strain model was adopted in this application using an approximate linear relation between stress and logarithm of strain rate. An incremental method was adopted in order to deal with material nonlinearity and obtain stress and strain information at different steps of a loading process. During each incremental step, the tangential modulus of soil elements was assumed to be constant. The model was used in the evaluation of the dynamic interaction between soil and several kinds of tillage tools.

Jori and Kerenyi (1998) developed a 2-D constitutive model considering the effect of both frictional angle and dilatancy angle. The model was limited to simulation of wide blades in slow motion.

Other models were developed to increase the accuracy of the predicted forces in the soil-tool interaction by considering the effect of the boundary conditions, Tejchman and Wu (1995), Herle and Nubel (1999), and stress path, Fakharian and Evgin (2000), or by determining the stress-strain relation of soil at soil metal contact surface experimentally using a modified triaxial apparatus, Kushwaha and Shen (1996). Predicted forces could be used for optimum design of the cutting tool, S. B. Richey, A. K. Srivastava, et al. (1989).

2.3 SUMMARY

Experimental studies show that both blade geometry and operating conditions have a significant effect on blade resisting forces. Due to the expense and limitation of experimental studies, a review of alternative soil-tool analysis methods was carried out. The finite element method was found to be more suitable for simulating the soil-tool interaction problem. In the finite element modeling of soil-tool interaction, a reasonable simulation of soil-tool interaction is based on a reasonable simulation of the soil behaviour more than the interface modeling and a simple elasto-plastic interface model leads to relatively similar results. Hence an extensive study of soil properties and behaviour is carried on in the next chapter to help select a constitutive model for simulating sand under monotonic loading.

Chapter 3

SOIL PROPERTIES & MODELING

3.1 CHAPTER SYNOPSIS

Proper simulation of soil-tool interaction is based on having an accurate representation for the soil model which is, in our case, a fully drained sand soil as this is the most common soil type in the Egyptian desert that is infected with land mines. In the previous chapter various options for modeling the interface between the soil and the cutting blade were reviewed. However a good understanding of soil properties and behaviour based on experimental observation is also of key importance for reasonable simulation of the soil behaviour and hence for the overall soil-tool interface process. In this chapter a brief description of soil properties and behaviour is presented along with a comparative review of the available constitutive models for soil (particularly sand). The rationale used here is to gain a deep understanding of soil properties and behaviour to enable selection of the most appropriate model for simulating sand in soil-tool interaction analysis.

3.2 NATURE AND COMPOSITION OF SOILS

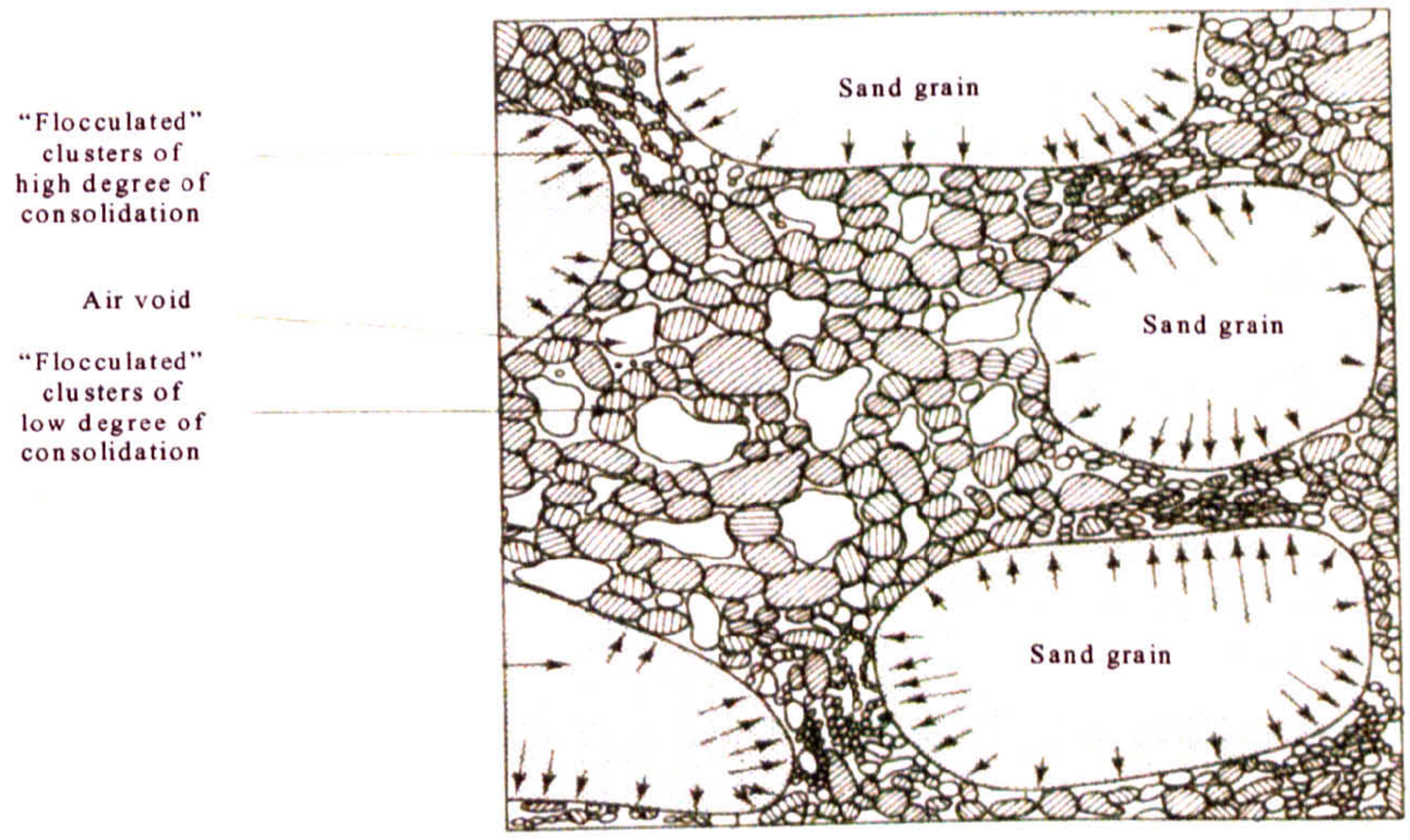

Figure (3.1) Soil skeleton

Soils are formed by the physical and chemical weathering processes of rocks and other organic materials. The discrete particles that make up soils are not strongly bounded together, Figure (3.1), so that they are free to move relatively among themselves. Soils are therefore particulate systems, and this basic fact that distinguishes soil mechanics from solid and fluid mechanics, Desai and Siriwardane (1984). Due to this particulate nature, when soil deforms, the overall deformation is partly the result of deformation and/or crushing of individual particles, and partly the result of relative sliding between particles: this relative sliding provides the most important component of its behaviour, since sliding is a nonlinear and irreversible process; soil behaviour is highly nonlinear and irreversible. In addition it must be realized that the voids or pores between the particles are filled with water and/or air, so that soils are multi-phase materials, their behaviour being influenced by the interaction between solids and fluids.

Because of the particulate nature of soils, most of the parameters used when describing soil behaviour are not physical properties but rather state parameters depending on state variables. This dependency of the parameters on the state variable is basically because these state parameters are obtained via some experimental tests on samples under certain conditions; that samples from the same soil types may lead to different parameters.

3.3 SOIL FABRIC AND STRUCTURE

Composition, structure and properties are the result of the history of a soil deposit. This history includes weathering, transportation, deposition and post-depositional changes. The actual state of homogeneity and anisotropy of any soil deposit is related to this formational history and to subsequent changes. Weathering is the physical and chemical process by which debris is formed. Physical process also includes cracks and joints formed by stress relief due to uplift, erosion, or changes of fluid pressure.

The relative size and shape of particles, plus their distribution, define the soil texture. Sands and gravels, in this respect, are of coarse texture; on the contrary, silts and clays appear as fine-textured soils, because they are composed of particles that are invisible to the naked eye. Soils are divided into coarse-grained and fine-grained soils on the basis of their texture, and the dividing reference size is that which is visible to the naked eye (about 0.05 mm). Gravels and sands are coarse materials, whereas silts and clays are termed fine-grained materials. This distinction also reflects some engineering characteristics of such soils: sand and gravels are cohesionless materials (there is no cohesion force attracts its grains to each other). Their behaviour is not affected by water when the stresses refer to the soil structure (dynamic loading conditions and loose saturated sands are exceptions), and the grain size distribution is a relevant parameter. The influence of grain size distribution is unimportant in silts and clays, while their behaviour depends on the influence of water.

When a soil is analyzed as a continuum, the most significant parameters in such an analysis depend on particle characteristics, on their arrangement and on forces among the particles. The factors that influence soil behaviour, can be summarized as follows:

1. Compositional factors determine the potential range of any soil property:
    - Type of minerals
    - Amount of each mineral
    - Shape and size distribution of particles

- Pore water composition

2. Environmental factors determine the actual value of any soil parameter:
   - Water content
   - Density
   - Confining pressure
   - Temperature

Some of these factors are discussed in greater detail later in this chapter.

3.4 EXPERIMENTAL TEST DEVICES

Laboratory and/or field test have played and continue to play a significant role in the development of constitutive laws of materials. Mathematical basis and development are indeed important; however, unless the parameters in the models are determined from appropriate tests, there will always be a gap between theory and practice. Hence development of appropriate models for the behavior of materials must include realistic tests that can simulate all significant factors that govern the behavior of the intended boundary value problem, Lancellotta (1995). A few of the conventional and recently developed test devices for solid (geological) materials are summarized below.

3.4.1 OEDOMETER TEST

A one-dimensional consolidation process can be simulated in the laboratory by compressing a soil specimen in a special testing apparatus called an Oedometer. Figure (3.2) shows the main components of this apparatus: an undisturbed soil specimen is carefully trimmed and placed into the rigid ring that does not allow any lateral displacement or radial flow during compression. Porous stones at the top and bottom of the sample allow drainage during consolidation. Dry stones should be used in both soft and stiff clays and the sample should be flooded only after a vertical pressure equal to a certain value of the volumetric stress has been reached. It is necessary to flood the soil sample in order to prevent desiccation during the test or to allow the sample to absorb water during swelling. Soil sample dimensions depend on different requirements. In general the sample should be representative of the soil

structural features, a factor which requires large dimensions, but this however prevents the possibility of obtaining good quality specimens from conventional tube samplers, therefore usual diameters are of the order of 50 mm.

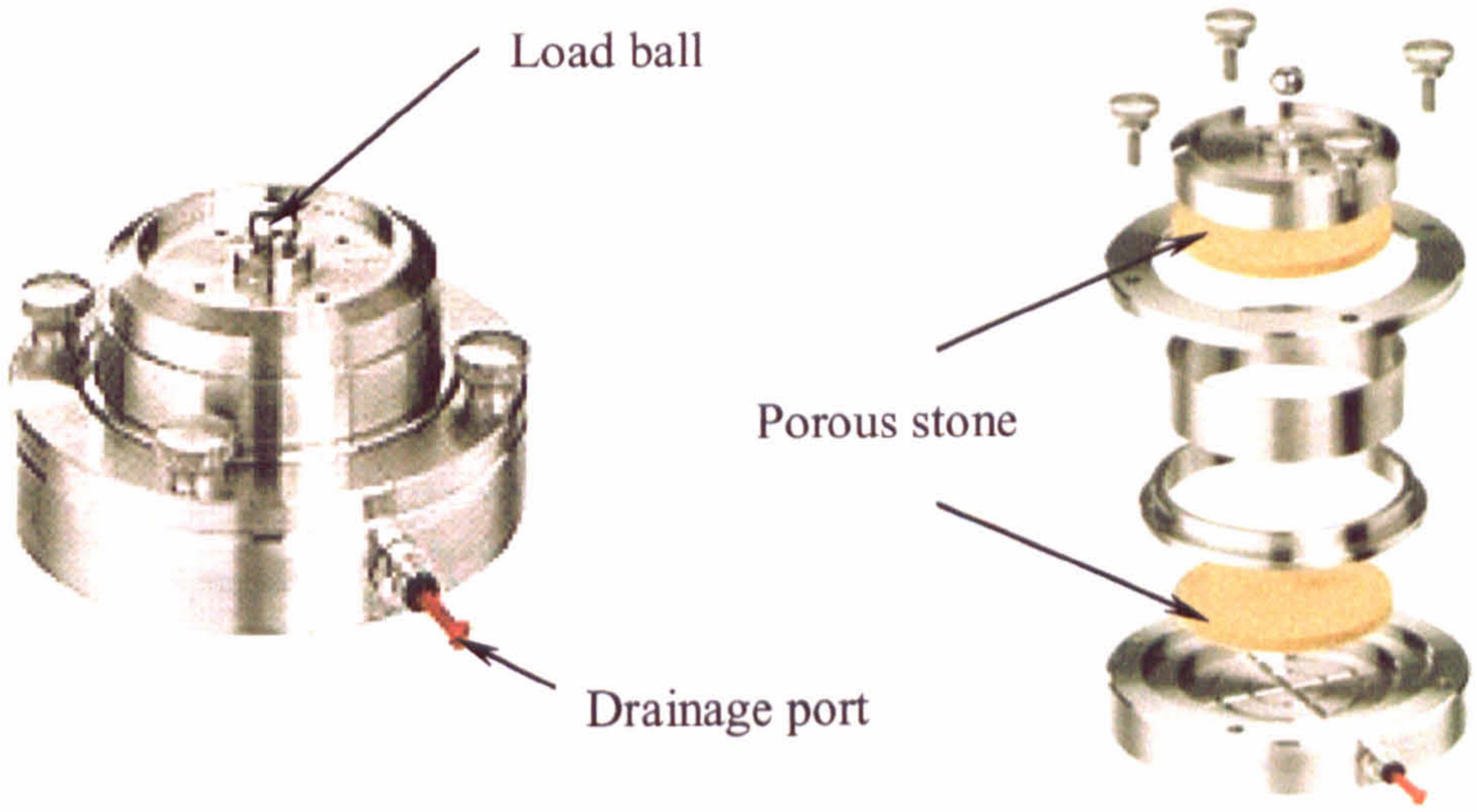

Figure (3.2) Oedometer test apparatus

To reduce the friction along the lateral surface, the ratio of the diameter to the height should be greater than 2.5, but less than 6 to avoid disturbance during trimming. Often, a floating ring apparatus Figure (3.3a) is used for this reason, rather than the more common fixed ring Figure (3.3b).

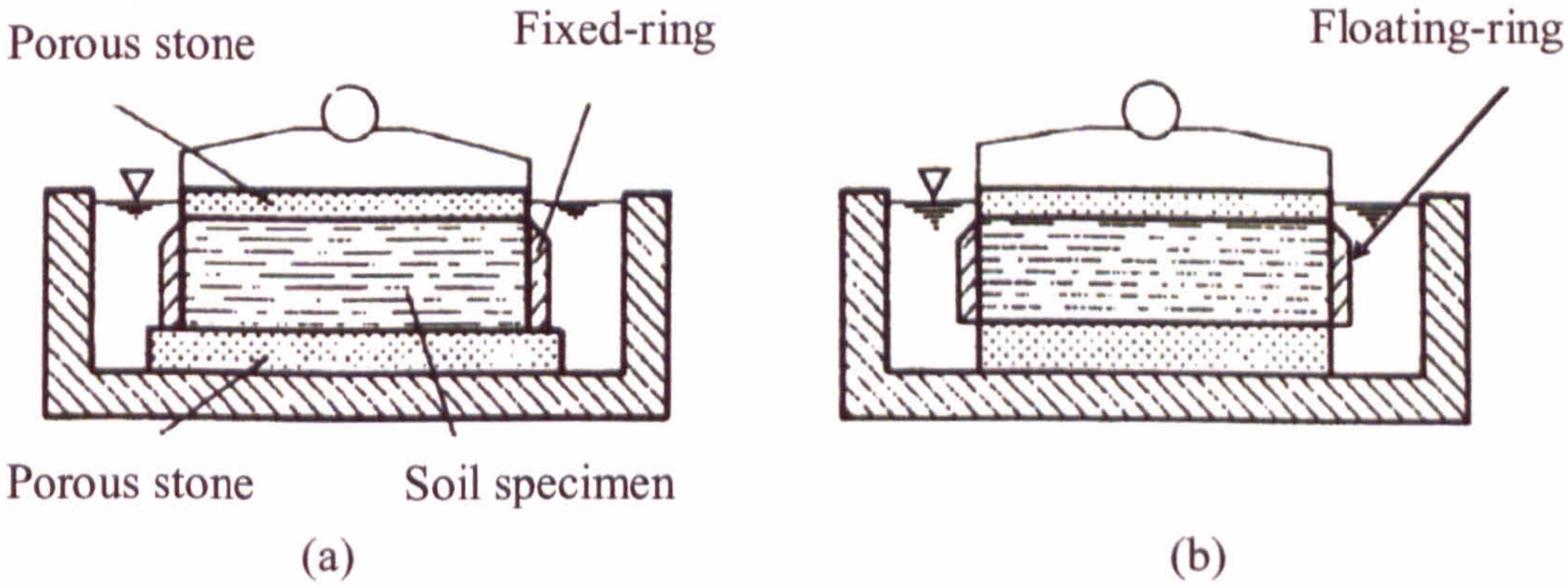

Figure (3.3) Sketch of Oedometer apparatus; (a) fixed-ring and (b) floating-ring

A sequence of vertical loads is applied to the specimen, each of which is usually double the previous value. After each load the sample is allowed to consolidate until the excess pore pressure is equal to zero. The load is usually maintained for 24 hours, and the compression readings are observed at convenient intervals.

3.4.2 CYLINDRICAL TRIAXIAL TEST

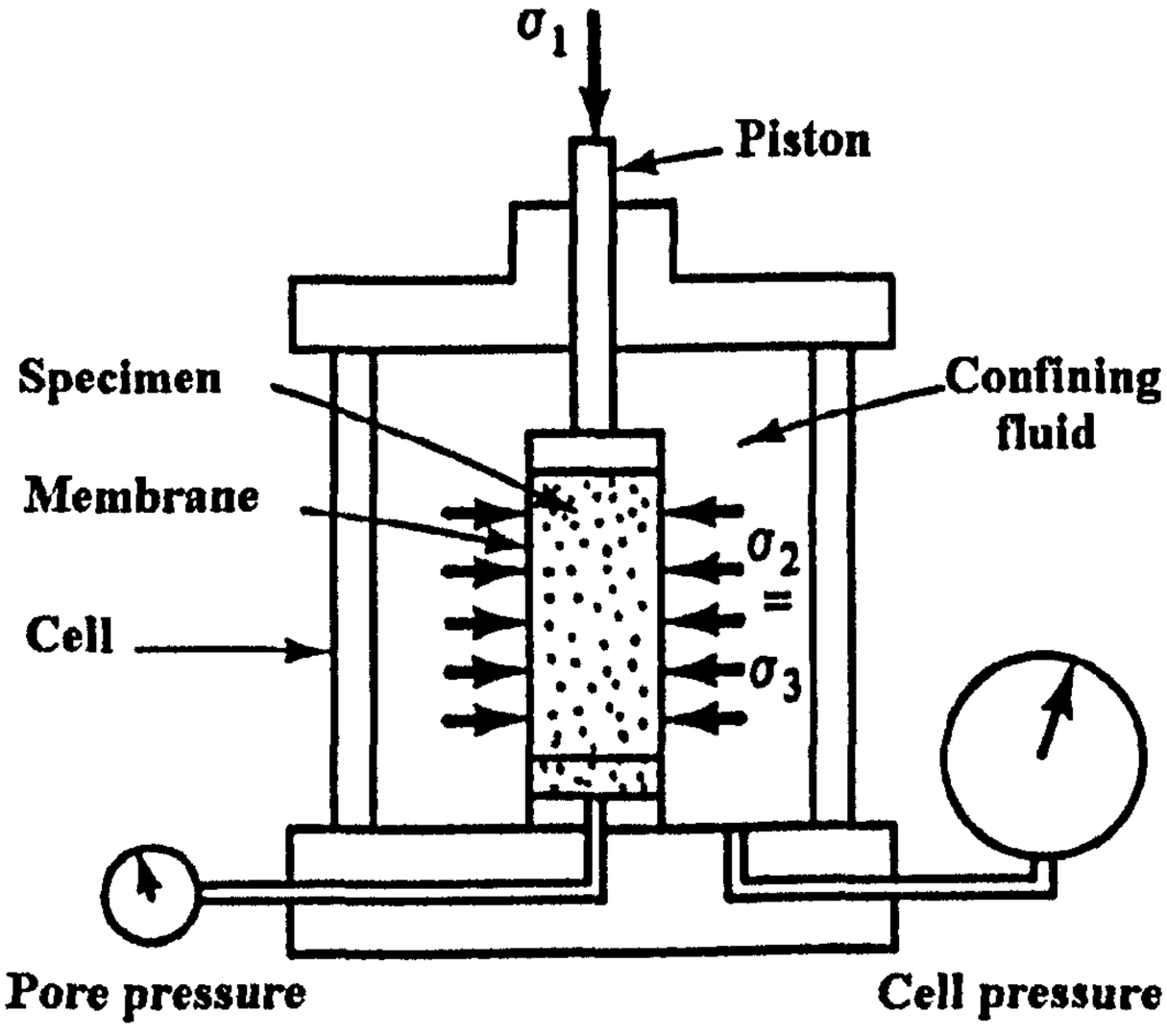

Figure (3.4) Cylindrical triaxial test

This device permits testing of a cylindrical specimen of a material. A confining stress (pressure) equal to σ_3 $(=\sigma_2)$ is applied, usually by using a fluid in the chamber. In the case of geologic media, this confining pressure simulates initial or in site stresses that exist at the site before a load increment is applied, Figure (3.4). The axial (σ_1) or deviator stress, $(\sigma_1 - \sigma_3)$ is then applied, which causes shearing of the sample. Measurements are obtained in terms of the two stresses $(\sigma_1, \sigma_2 = \sigma_3)$, axial deformation (strain), lateral or radial deformation (strain), and in the case of drained tests, by allowing expulsion of fluid from the pores of the medium and measurement of the exiting liquid volume. These measurements allow plotting of results in various forms; typical schematic plots in terms of stress difference $(\sigma_1 - \sigma_3)$ versus axial strain (ε_1) and radial strain (ε_3) versus (ε_1) can be obtained

using the device. In the case of undrained tests, measurements of fluid pressure in the pores are also obtained.

3.4.3 DIRECT SHEAR TEST

This kind of test is quite simple in principle. The soil specimen is encased in a shear box, which has been divided into two halves in order to allow relative movements, Figure (3.5). A normal (axial) load is first applied to the soil specimen; then one half of the box is pushed horizontally, and the other half remains fixed. Measurements are taken of the shear load, the vertical and the horizontal displacements.

The major disadvantage of this test is that it is impossible to control the drainage. As a consequence the test should only be run under completely drained conditions. To accomplish this requirement, it has been suggested to use a rate of relative horizontal displacement of the order of 0.0001 mm/s for clays, and of 0.02 mm/s for sands, Lancellotta (1995). In addition, during the test the specimen is forced to fail on the horizontal plane. Moreover, highly non-uniform strain conditions, due to the constraints at the boundaries, exist within the specimen. Finally, the state of stress cannot be completely determined because the only stresses that are known are the normal and the shear stresses on the horizontal plane.

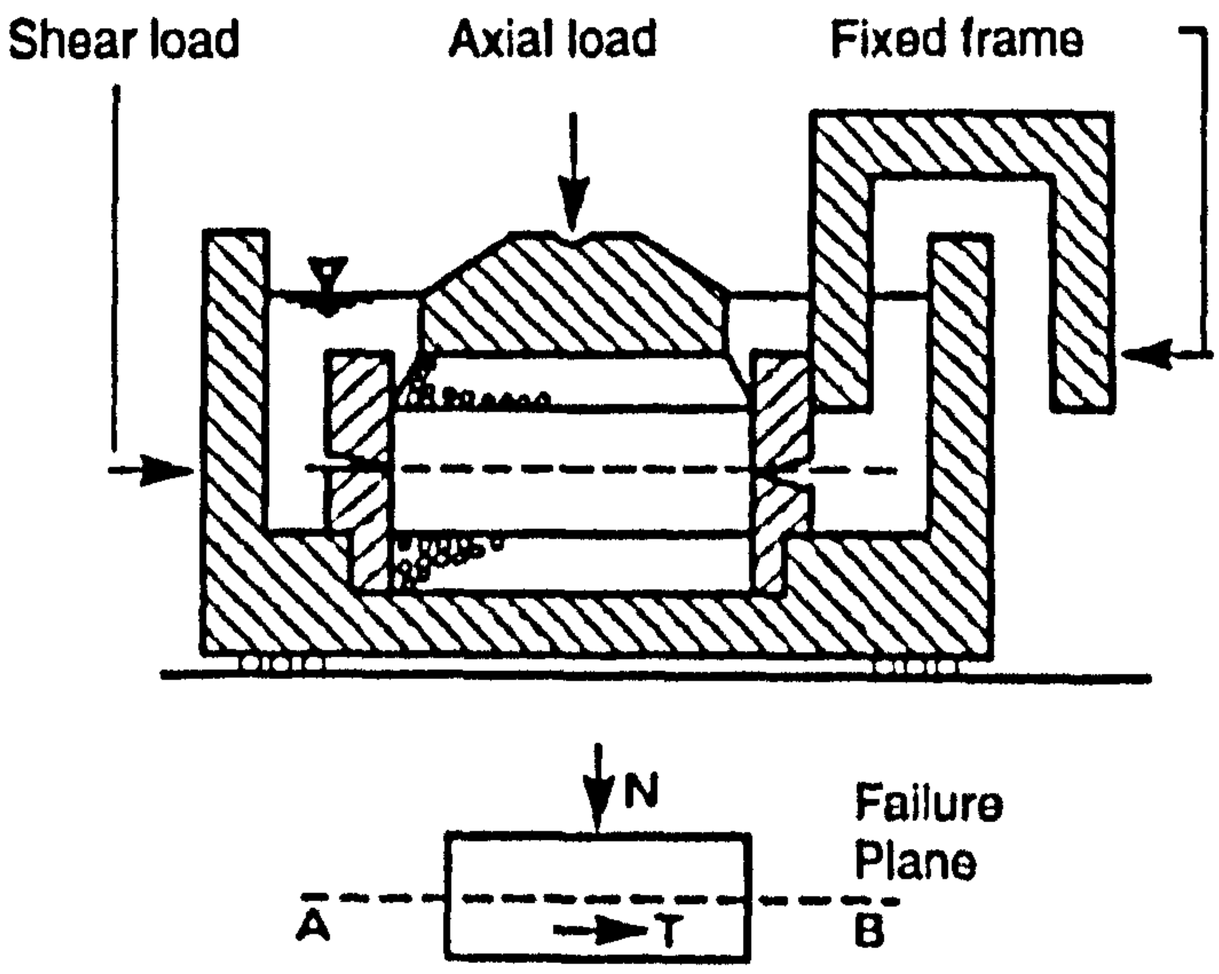

Figure (3.5) Direct shear device

3.4.4 TRULY TRIAXIAL OR MULTIAXIAL TEST

The foregoing testing devices allow application of load and measurement of stress only in limited directions and modes of deformation. In reality, materials are subjected to three-dimensional states of stress and strain. The truly triaxial device Figure (3.6) permits application of three independent (principal) stresses (σ_1, σ_2, and σ_3) on six faces of a cubical specimen of a material. The application of the stresses can be such that any path of loading in the three-dimensional stress space can be followed.

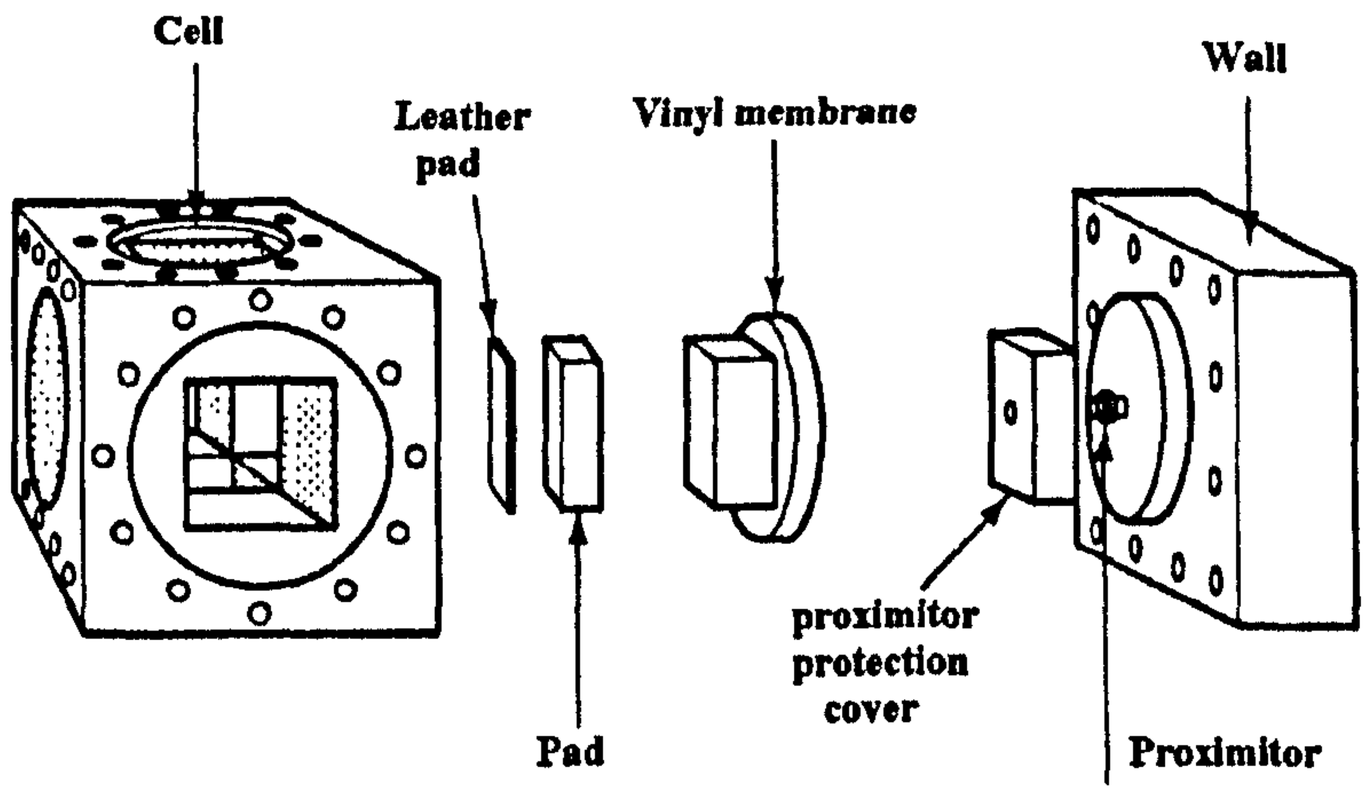

Figure (3.6) Truly triaxial or multiaxial device

Development and use of truly triaxial testing is found to play a significant role in research for development of constitutive laws of engineering materials, Desai and Siriwardane (1984).

3.5 BASIC GRANULAR MATERIAL PARAMETERS

In constitutive modelling of granular materials such as soils, and in particular sand, there are some main and basic parameters, which are obtained from experimental tests. These parameters are essential to describe a state of the material and/or predict its behaviour when subjected to stress. Whatever the basis of description of material behaviour, a constitutive law has to use some of these basic parameters otherwise it will fail to adequately describe the material behaviour.

3.5.1 POISSON'S RATIO

Poisson's ratio is a well known parameter in solid mechanics. In soil mechanics it similarly used to describe the relation between the different strain components. For isotropic material idealization, Poisson's ratio can be obtained from a triaxial shear test from the following relation

$$\nu = \frac{\varepsilon_r}{\varepsilon_z} \tag{3.1}$$

Where

ν Poisson's ratio

ε_r Lateral (radial) strain

ε_z Vertical (axial) strain

3.5.2 YOUNG'S MODULUS

Young's modulus is also a well known parameter in solid mechanics. It is used in geomechanics to describe the elastic behaviour of a material.

Young's modulus describes a linear stress strain relation (for a uniaxial case) in the form

$$\sigma = E * \varepsilon \tag{3.2}$$

Where

σ Stress

ε Strain

E Young's modulus

In soil mechanics this relation is non-linear so it is difficult to obtain a single Young's modulus value for a soil specimen. Estimates of E, if required, can be obtained using the results of an Oedometer test, section (3.4.1), for the stress-strain relation as shown in Figure (3.7).

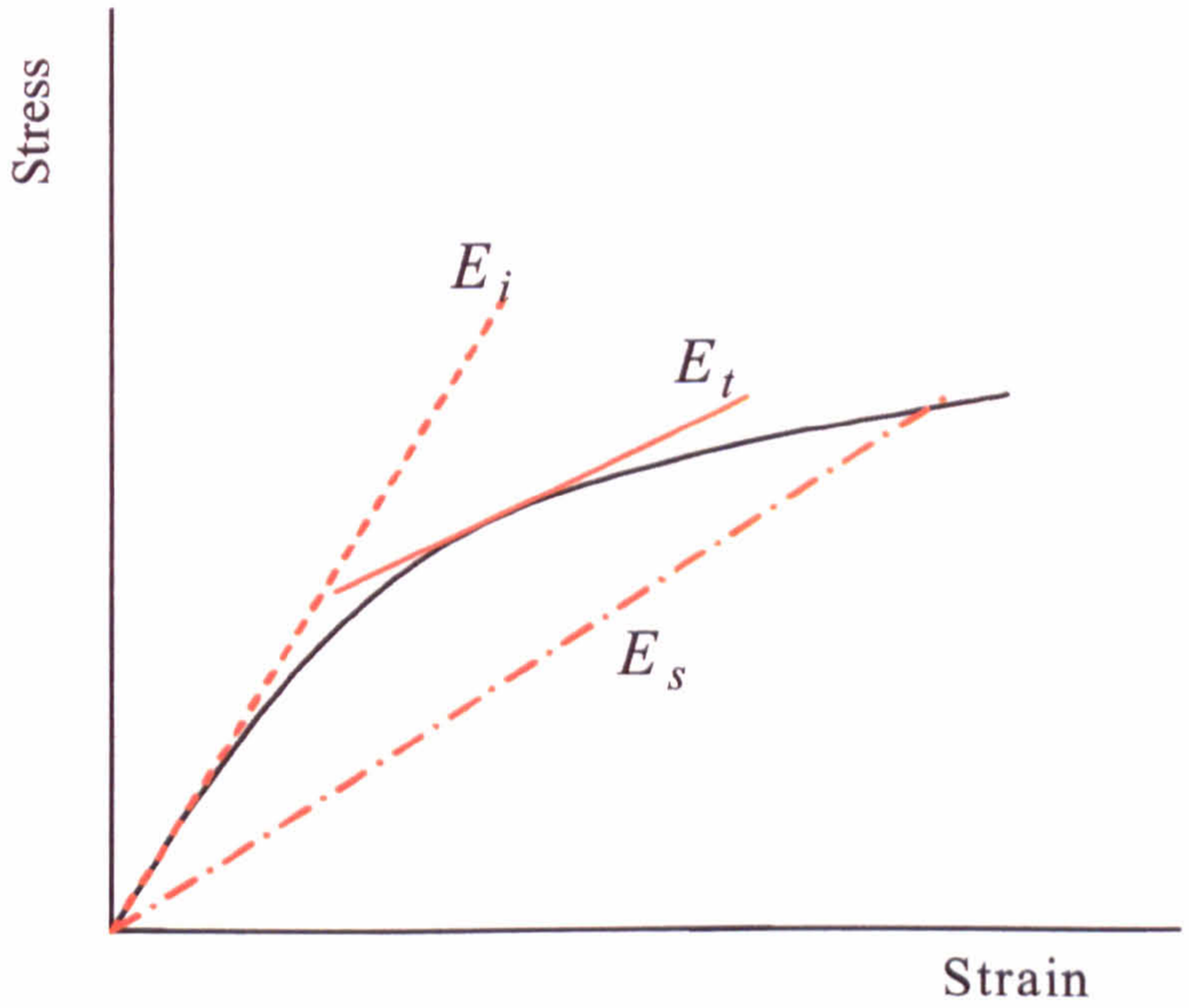

Figure (3.7) Stress-strain relation of soil obtained from Oedometer test

Where

E_i Initial tangent elastic or Young's modulus

E_t Tangent elastic modulus

E_s Secant elastic modulus

All the parameters discussed in this section appear throughout soil mechanics. Their importance will be revealed later when describing the behaviour of soils using various constitutive laws.

3.5.3 GRAIN SIZE

The grain size is useful for granular materials classification; for example sand soil is characterized by a grain size of the range (0.075mm to 4mm). One of the experimental methods used for determining the grain size distribution of a material is

the mechanical sieve analysis, in which particle diameters are determined by passing a known weight of oven-dried specimen through a series of sieves with different mesh openings. The mass of soil retained on each sieve is determined using a balance and then the percent finer (% finer) than each sieve is calculated, Budhu and Budhu (1999). The results are then plotted on a semi-logarithm graph of % finer on the ordinate (arithmetic scale) versus grain size (sieve size opening) on the logarithmic scale as shown in Figure (3.10).

3.5.4 VOID RATIO

Soils consist of an assemblage of particles with different sizes and shapes that form a skeleton whose voids are filled with water and air or gas, Figure (3.8).

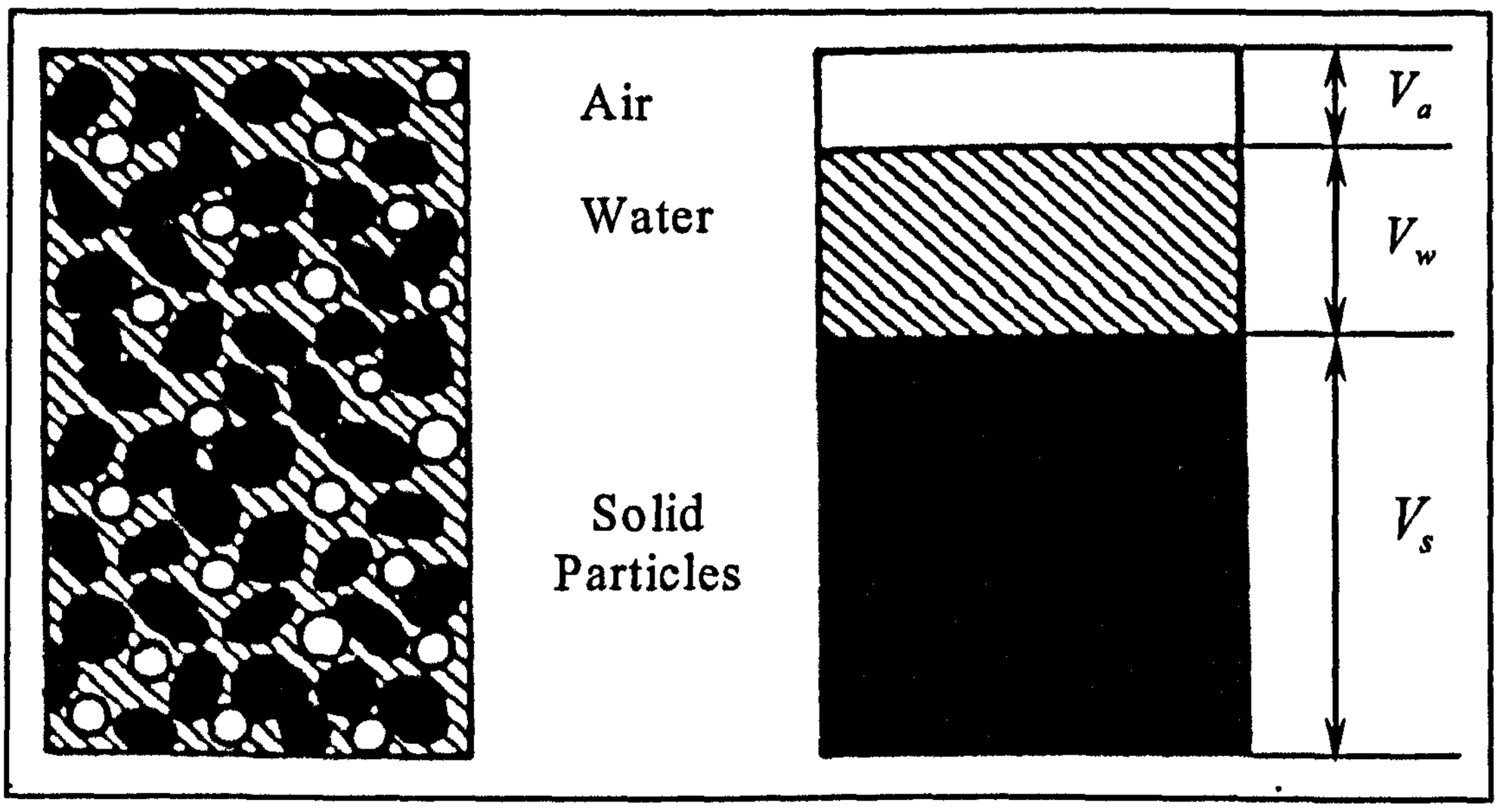

Figure (3.8) Divisions of a volume of soil

For a volume of soil (V) a separation of its contents into solid particles of volume (V_S), water (V_w) and air (V_a) is to be imagined. The total volume of the soil specimen can be written in the form

$$V = V_S + V_w + V_a \tag{3.3}$$

The void ratio can be defined as the ratio of the voids (air + water) volume to the solid volume;

$$e = \frac{V_v}{V_s} \tag{3.4}$$

Where

e *The void ratio*

V_v *Total voids volume*

$$V_v = V_w + V_a$$

It is well known that the void ratio is dependant on the present state of the soil and can be vary from place within for the same type of soil; hence it represents one of the key state-dependant parameters for material simulation

3.5.5 COHESION

Certain soils can exhibit bonding characteristics between its particles; these bonding forces try to keep the particles in contact. This force is called the cohesion stress of the soil. For dry sand the cohesion may be vanish. The cohesion stress is obtained using a direct shear test described in section (3.4.3) by drawing a shear stress / shear strain graph and identifying the peak point which represents the failure. The test is then repeated at different initial stress level (three at least) as shown in Figure (3.9a).

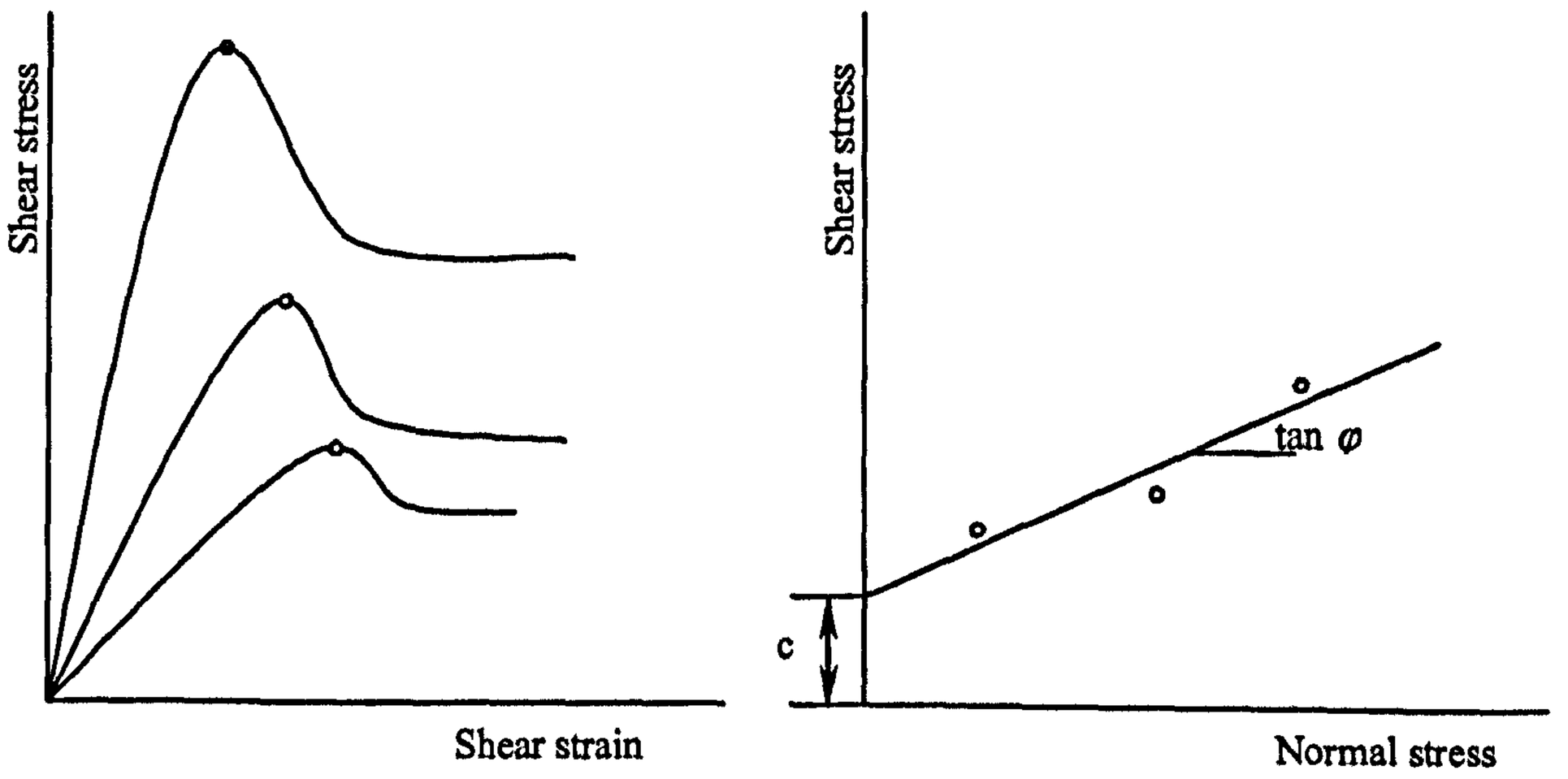

Figure (3.9) Determination of cohesion and internal friction angle

Failure points are then plotted on a shear stress / normal stress diagram, and a straight line fitted as shown in Figure (3.9b). Then the cohesion "c" can be measured on the shear stress axes. The triaxial shear test, described in section (3.4.4), can be used for the same purpose.

3.5.6 ANGLE OF INTERNAL FRICTION

The angle of internal friction φ, in which a soil skeleton is sheared, can be measured from the direct shear or Triaxial tests as shown in Figure (3.9b) following the same procedures of determining the cohesion stress.

3.5.7 ANGLE OF DILATION

The angle of dilation is an indication of the volume changes which occur during shearing of soils, Parry (1995).

$$\sin\psi = -\frac{\delta\varepsilon_v}{\delta\gamma_{max}} \tag{3.5}$$

Where

ψ	Dilatancy angle (angle of dilation)
$\delta\varepsilon_v$	Volumetric strain increment
$\delta\gamma_{max}$	Maximum shear strain increment

3.6 SOIL CLASSIFICATION

Classification methods provide a tool to categorize soils according to their probable behaviour, whereas it is the parameter of the intact material that determines the behaviour of the soil. Therefore any single classification system does not fully eliminate the need for specific investigation and testing, even though it represents a general picture of the possible behaviour.

The Unified Soil Classification System was developed for the U.S. Army Engineering Corps and was adopted in 1969 by the American Society for Testing and Materials as a standard method for classification of soils for engineering purposes, Table [3.1]. According to this Unified system, the coarse-grained soils are divided into gravel (G) and sands (S). Each of these groups is subdivided into four additional groups:

1. Well graded, fairly clean material (W)
2. Poorly graded, fairly clean material (P)
3. Well graded material with clay binder (C)
4. Coarse material containing fines (M)

Fine-grained soils are divided into inorganic silts and very fine sandy soils (M), inorganic clays (C) and organic silts and clays (O). These three groups are subdivided, according to their liquid limit (upper limit of water content within which a clay element exhibits plastic behaviour), into:

1. Fine-grained soils of low to medium compressibility (L), if the liquid limit is lower than 50%.
2. Fine-grained soils of high compressibility (H), for a liquid limit greater than 50%.

Organic soils are placed in a group with the symbol Pt.

Sieve analysis (measure of grain size distribution) of soil type from Egypt is shown in Figure (3.10), by AboElnor (1997). The soil type can be graded according to the Unified Soil Classification System as sandy soil,

Table [3.1] Soil classification, Lancellotta (1995)

Major Divisions			Group Symbols	Typical names	Field identification procedures		
1	2		3	4	5		
Coarse-grained soils More than half material is larger than 75 μm	Gravels More than half material is larger than 4.75 mm	Clean Gravels	GW	Well-Graded gravels, gravel sand mixtures, little or no fines	Wide range in grain sizes and substantial amounts of all intermediate particle sizes		
			GP	Poorly-Graded gravels, gravel sand mixtures, little or no fines	Predominantly one size or a range of sizes with some intermediate sizes missing		
		Gravel with Fines	GM	Silty gravels, gravel-sand-silt mixture	Non-plastic fines or fines with low plasticity		
			GC	Clayey gravels, gravel-sand-clay mixture	Plastic fines		
	Sands More than half material is smaller than 4.75 mm	Clean Sands	SW	Well-Graded sands, gravelly sands, little or no fines	Wide range in grain sizes and substantial amounts of all intermediate particle sizes		
			SP	Poorly-Graded sands, gravelly sands, little or no fines	Predominantly one size or a range of sizes with some intermediate sizes missing		
		Sands with fines	SM	Silty sands, sand-silt mixtures	Non-plastic fines or fines with low plasticity		
			SC	Clayey sands, sand-clay mixtures	Plastic fines		
Fine-grained soils More than half of material is smaller than 75 μm					**Identification Procedures**		
					Dry Strength	Dilatancy	Toughness
	Silts and Clays Liquid limit less than 30		ML	Inorganic silts and very fine sands, rock flour, silty or clayey fine sands or clayey silts with slight plasticity	Non to slight	Quick to slow	None
			CL	Inorganic clays of low to medium plasticity, gravelly clays, sandy clays, silty clays, lean clays	Medium to high	None to very slow	Medium
			OL	Organic silts and organic silty clays of low plasticity	Slight to medium	Slow	Slight
	Silts and Clays Liquid limit greater than 30		MH	Inorganic silts	Slight to medium	Slow to non	Slight to medium
			CH	Inorganic clays of high plasticity, fat clays	High to very high	None	High
			OH	Organic clays of medium to high plasticity, organic silts	Medium to high	None to very slow	Slight to medium
Highly Organic Soils			Pt	Peat and other highly organic soils	Readily identified by color, odor, spongy feel, and frequently by fibrous texture		

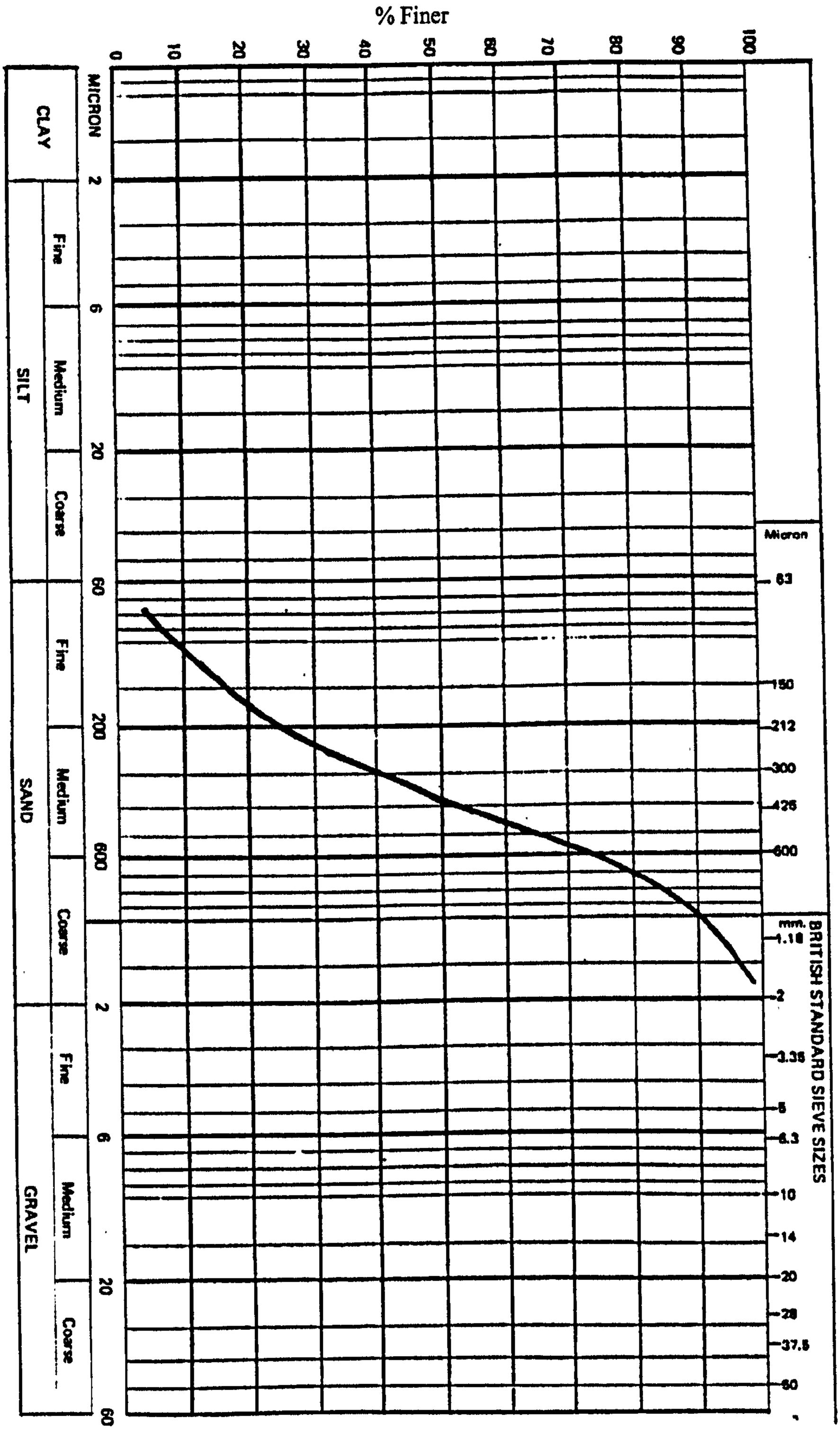

Figure (3.10) Soil grain size distribution for Egyptian sand soil

3.7 MATERIAL PROPERTIES OF GRANULAR MATERIALS

As mentioned before, this study will be focused on a fully drained sand soil, as this soil is the most popular soil type in Egypt. Sand can be classified as a granular material with relatively small grain size. To this point, studying the behavior and properties of granular materials is particularly important for modeling sand.

Granular materials consist of grains in contact and surrounding voids. The micromechanical behavior of granular materials is therefore inherently discontinuous and heterogeneous. The macroscopic (overall or averaged) behavior of granular materials is determined not only by how discrete grains are arranged in space, but also by what kinds of interactions that are operating among them. Even in the mechanics of granular materials, some continuum mechanical concepts such as stress and strain tensors are necessary to formulate a constitutive model describing the behaviour of granular materials. In fact, a good description of granular materials has to include several features:

3.7.1 INTERNAL FRICTION

Internal friction is an essential feature in describing the behaviour of granular materials. As a first approximation, shear stress in a specimen is proportional to the isotropic part of the stress tensor applied. This proportionality can be described by the internal friction angle via the following equation:

$$\tau = \sigma \tan \phi \tag{3.6}$$

Where

τ Shear stress

σ Normal effective stress

ϕ Angle of internal friction

However, this linear dependency of the shear stress on the stress level, equation (3.6), is only an idealization of the behaviour of real material. For practical engineering purposes, the internal friction can be assumed to be dependant only on the void ratio e (or relative density). In reality several factors can affect the internal friction, Oda and Iwashita (1999), which are:

a) The value of the intermediate principal stress (σ_2)

b) Effective confining pressure (or effective mean pressure)

c) Principal stress direction with respect to the bedding plane (anisotropy)

3.7.2 DILATANCY

Granular materials exhibit dilatancy (or contractancy) when subjected to loads. Pure deviatoric stress increments applied to a homogeneous specimen in an elementary test will generally result in volumetric strain increments together with deviatoric ones. Both dilatant and contractant volumetric strains can be observed, depending on the stress level and void ratio. In most conditions, the grain material itself can be considered as incompressible, so the volume change of the granular medium is due to void ratio changes, Tejchman and Wu (1995).

3.7.3 CRITICAL STATE

When subjected to shear and/or large deformation, a fully drained soil sample will reach an ultimate condition where deformation can occur without any further changes of volume or effective stress ratio. This ultimate condition is known as the critical state. The critical state in soil mechanics is represented in a p-q diagram, where p represents the mean pressure ($p=(\sigma_1+2\sigma_3)/3$) and q represents the deviatoric stress ($q=\sigma_1-\sigma_3$) obtained mainly from cylindrical triaxial test.

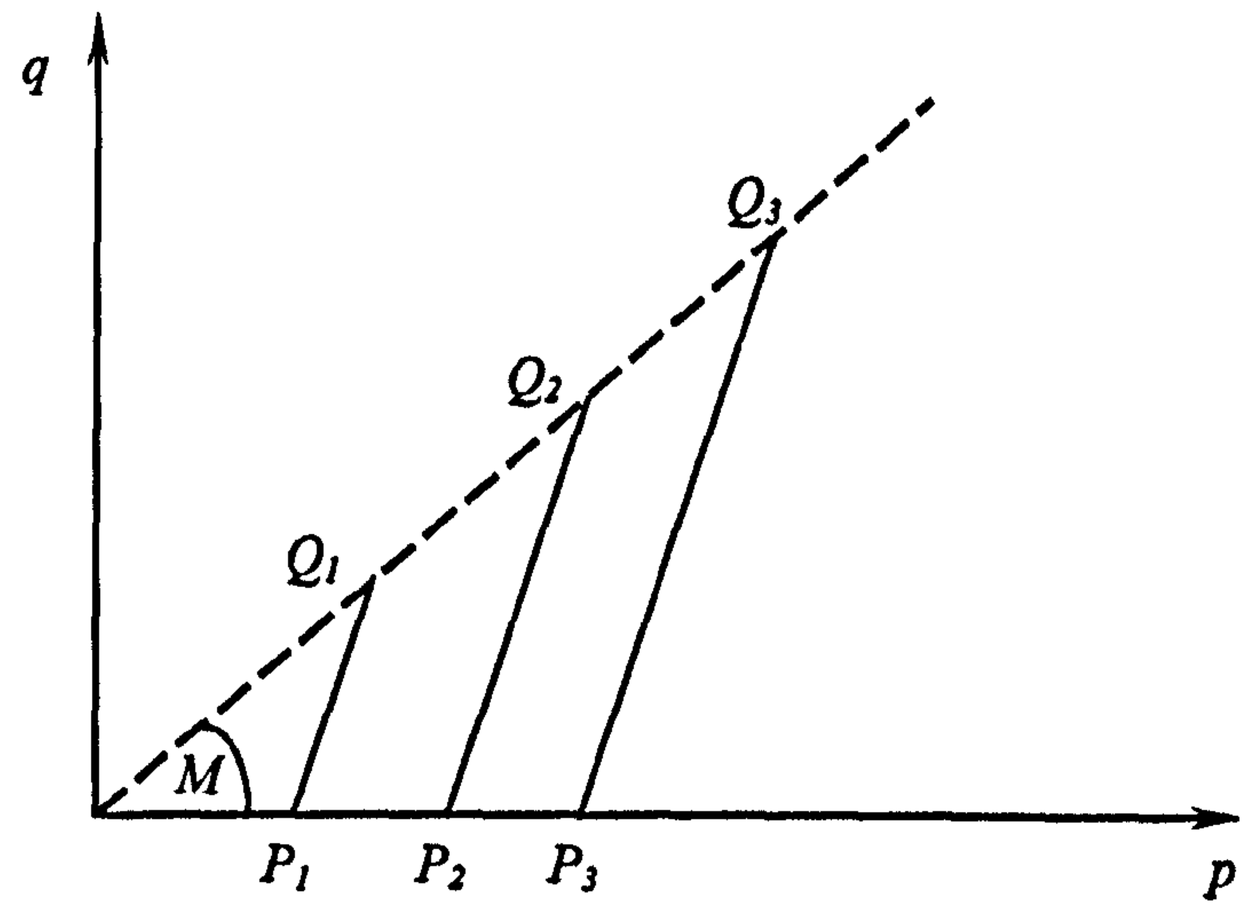

Figure (3.11) Critical state line in p-q space for fully drained sand sample

Figure (3.11) represent a *p-q* plot of deformed samples at different initial stress states p_i and the loci of there critical state points Q_i. As shown from the figure all the critical state points are located on a straight line of slope M which is a material parameter. This line is known as the Critical State Line (CSL), Somerville and Paul (1983).

Particularly for sands, one additional negative feature was that samples at sufficiently different densities were treated as different rather than the same materials. Including the critical state as a state parameter in sand modeling can avoid this negative feature.

3.7.4 LIMIT SURFACE

A main and well-known experimental fact about soil behaviour is the existence of a failure, bound or limit surface in stress space, Chambon and Desrues, et al. (1994); and Wu and Niemunis (1997), as shown in Figure (3.12).

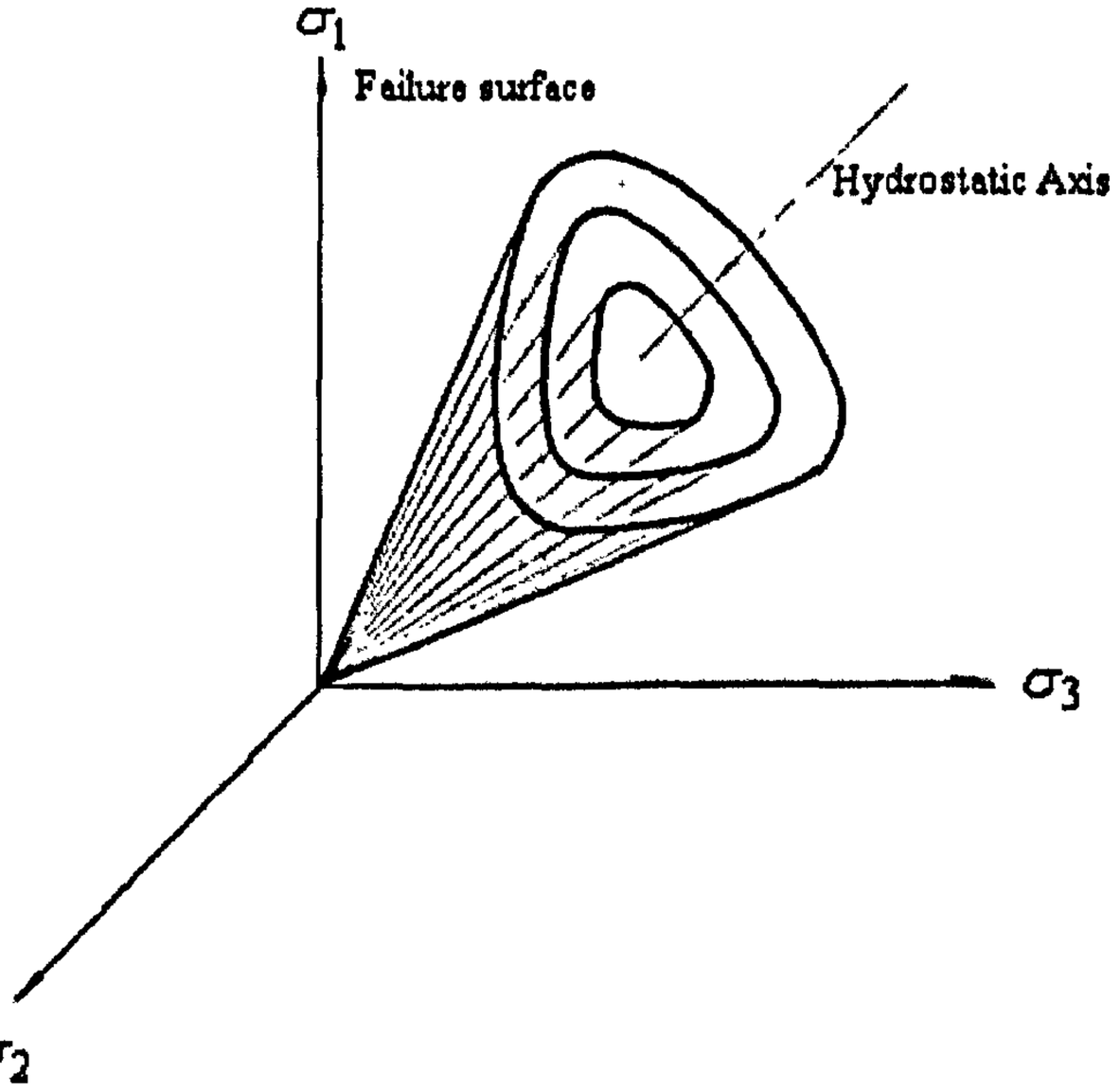

Figure (3.12) Failure surfaces in the stress space

This surface splits the stress space into two sets: the set of admissible stress states and the set of forbidden stress states. It is notable from Figure (3.12) that this limit or failure surface is not fixed in the stress space but it depends on the stress level that it

expands as the stress level increases till a certain limit at which failure will take place. Being defined in this way, this surface can only be approached asymptotically.

3.7.5 IRREVERSIBILITY

Granular materials show strong irreversibility on unloading through a given loading path: this is an illustration of material incremental non-linearity (reverse strain increment does not result in reverse stress increment). More generally, experiments show that any change in the incremental loading direction (in the strain rate, stress rate, or combined space) induces non-proportional material responses: real materials are thoroughly non-linear rather than bi-linear (loading, unloading) or multi linear (multi mechanism plasticity).

3.7.6 CYCLIC LOADING

Reloading after a loading/unloading sequence on a granular specimen will generally produce a response quite different from initial loading. This is conveniently modeled in the framework of classical plasticity by the concept of an elastic domain inside a so-called loading surface in the stress space, the size of which can be controlled by a hardening law. However a continued loading-unloading process on a real specimen (cyclic loading) will produce an accumulation of strain, in both deviatoric and isotropic (hydrostatic) components. This accumulation can be continuing, or vanishing, depending on loading parameters. Such behaviour is not easily modeled; models accounting for cyclic behaviour have to incorporate discrete memory variables, non-isotropic hardening with back stress, or other rather elaborated feature, Chambon et al. (1994).

3.7.7 ROTATION OF PRINCIPAL STRESS DIRECTION

The response of granular materials to principal stress rotation has not been extensively studied up to now. Experimental tests allowing a proper investigation of this response are becoming more common; such as torsional-hollow cylinder tests, Fukushima and Tatsuoka (1982). It is worth noting that principal stress rotation occurs in shear band initiation and development, Tejchman and Bauer (1996), Wu (2000) and Tejchman and Gudehus (2001).

3.7.8 STRAIN LOCALIZATION

This is observed as a final mode of deformation in most of the elementary tests performed on granular materials when rupture is approached. Theoretical studies by researchers have shown that, when considered as a bifurcation phenomenon, strain localization can be predicted on the basis of so-called localization criterion, Chambon et al. (1994).

3.7.9 STRAIN SOFTENING

This behaviour is still a controversial point in experimental characterization of granular material. Different experimental studies have recognized non-homogeneities in the deformation field in theological tests. Improved tests show less pronounced peaks in the stress-strain curves, which induces the idea that experimentally observed softening responses could be an effect of strain localization. It is still considered that at least a part of observed softening is due to some kind of damage process in the granular structure (for example, void ratio inflation in dilatant materials), Chambon et al. (1994).

3.7.10 SHEAR LOCALIZATION

Localization of deformation in the form of narrow zones of intense shearing can develop in granular bodies during processes of flow or penetration of objects with sharp edges, Tejchman, Herle , et al. (1999). Shear localization can occur inside materials as a single shear zone or a regular pattern of zones. It can also appear as a single shear zone along the walls of various stiff structures. Within shear zones, pronounced grain rotations and curvatures connected to couple stresses, large strain gradients, and high void ratios together with material softening are observed. The thickness of a shear zone depends mainly upon the mean grain diameter, the initial density of a granular material, the pressure level and the shear velocity. Experiments and numerical calculations evidently show that shear stresses in shear zones increase with decreasing zone thickness and increasing mean grain diameter. Shear zones occur inside granular bodies whose initial void ratio is smaller than the critical void ratio.

3.7.11 STRESS PATH

In order to develop a constitutive model valid for all (significant) generalized states of loading and deformation, a comprehensive series of tests should be conducted with as many relevant test modes as possible. Here factors such as density, water content, (initial) anisotropy, stress path and type of loading (static, dynamic, and repetitive) can be important depending on the expected use of the model for practical boundary value problems. Hence it becomes necessary to perform appropriate tests on specimens of materials by including and subsequently varying these factors. One of the most significant factors not discussed so far is the stress path.

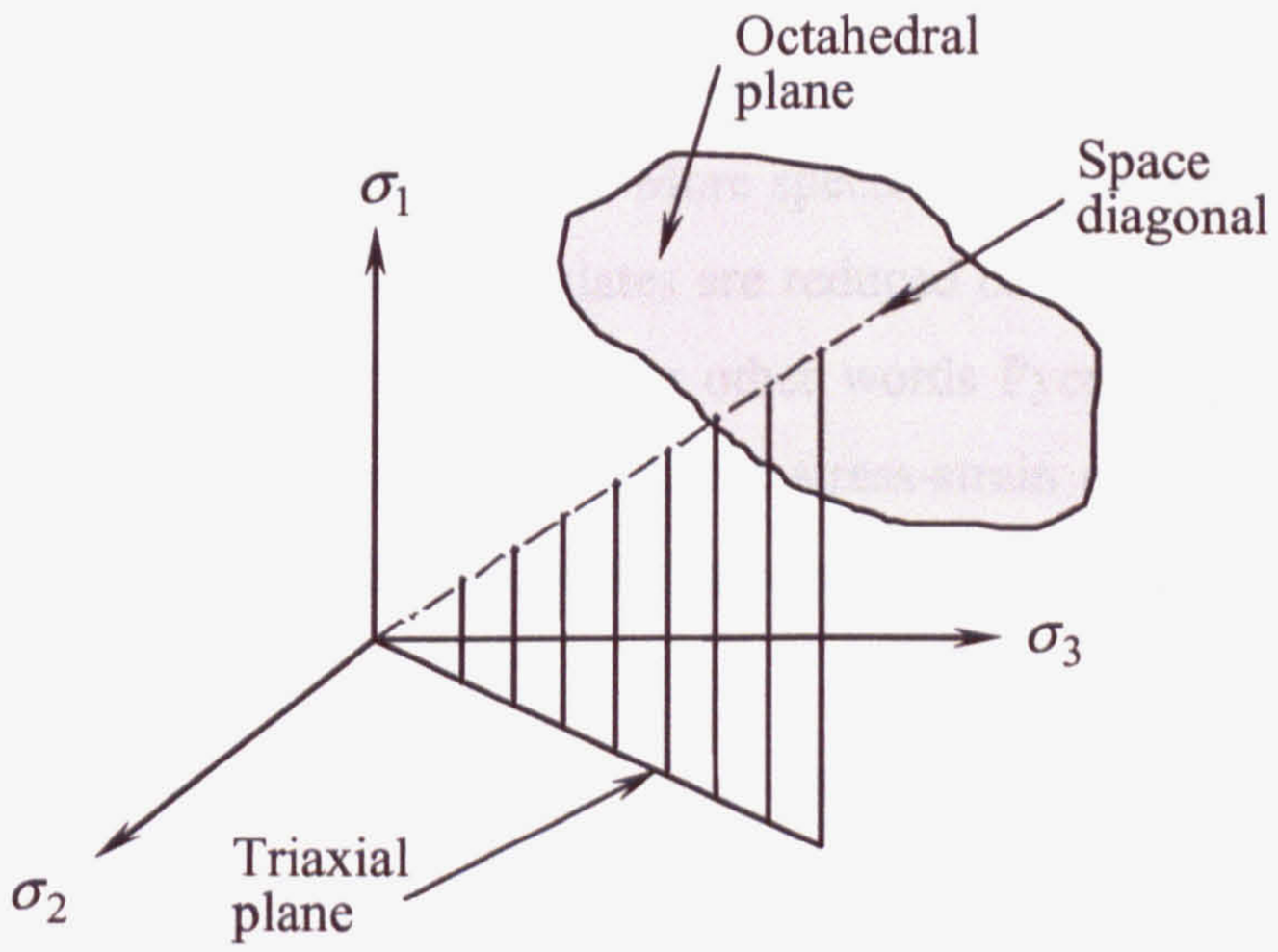

Figure (3.13) Principal stress space

TC	Triaxial compression
TE	Triaxial extension
CTC	Conventional TC
CTE	Conventional TE
RTC	Released TC
RTE	Released TE
HC	Hydrostatic compression

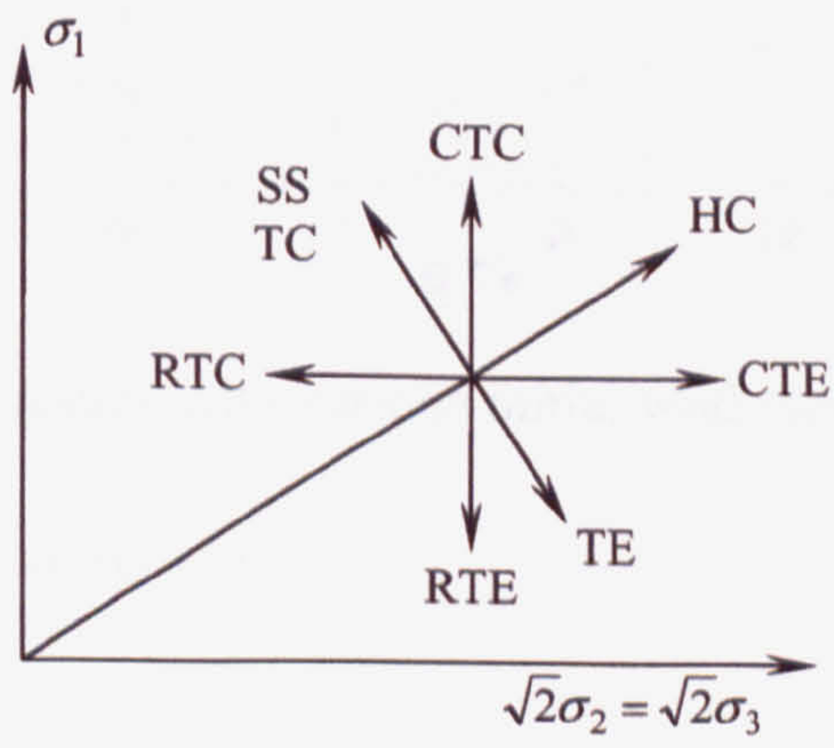

Figure (3.14) Projection of stress space on triaxial plane

In practice, it is customary to use a conventional (cylindrical) triaxial device to study the stress-strain behavior of geologic materials. In this apparatus two of the major principal stresses are always equal: that is $\sigma_2 = \sigma_3$, therefore, all possible stress paths followed in cylindrical triaxial device will fall on a plane in the stress space. This plane is called the triaxial plane and is shown in Figure (3.13). Figure (3.14) shows a schematic representation of various commonly considered stress paths in the principal stress space, they are shown in the triaxial and octahedral planes.

3.7.12 PYCNOTROPY

Among all materials, granulates have the exclusive property that their density (represented by either the void ratio *e* or the relative density *D*) does not depend uniquely on the pressure; i.e. on the hydrostatic stress. Their mechanical behaviour depends markedly on the actual density. More specifically, the stiffness, the friction angle and the dilatancy of loose granulates are reduced compared with denser ones. This phenomenon is called Pycnotropy. In other words Pycnotropy means that the outcomes of deformation experiments (i.e. the stress-strain curves) are not unique, but depend on the initial void ratio of the specimen, Figure (3.15) after Kolymbas (1995).

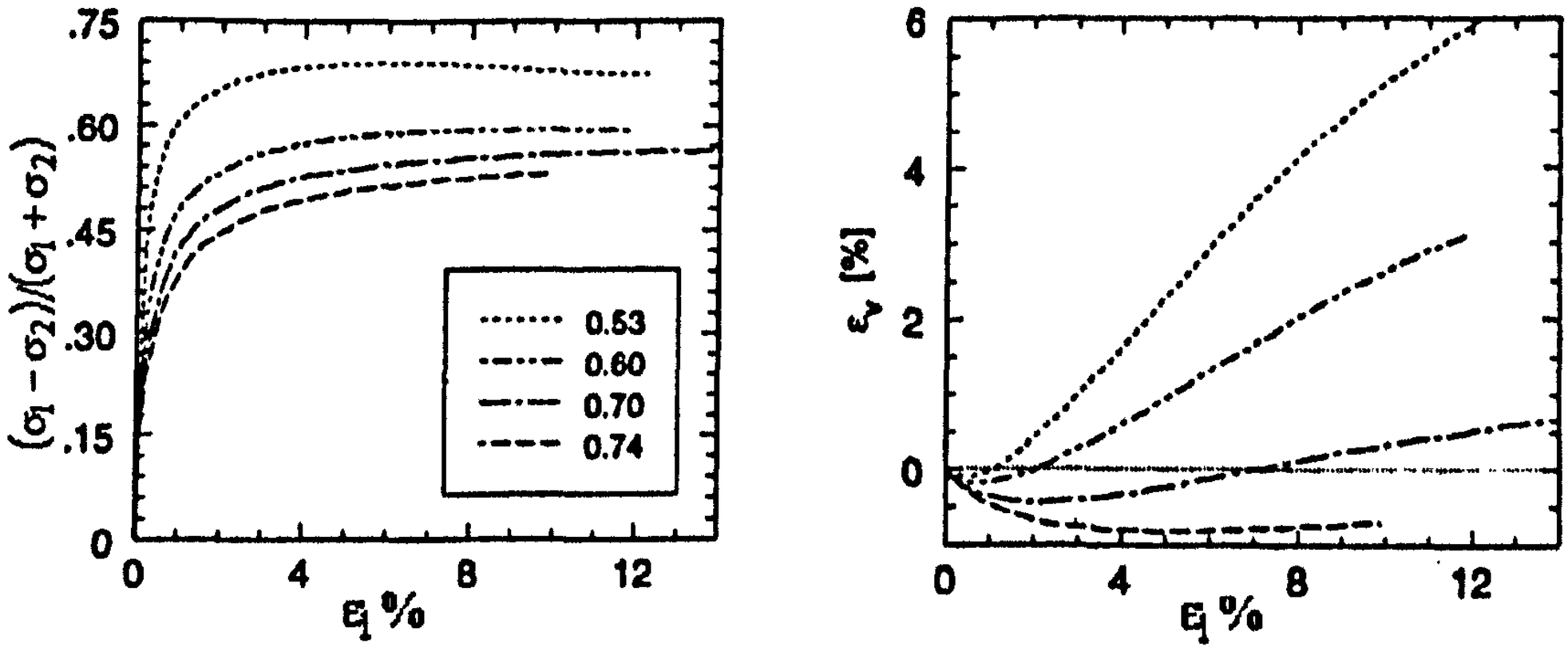

Figure (3.15) Pycnotropy effects (triaxial test results with various initial void ratios)

Where: $(\sigma_1 - \sigma_2)/(\sigma_1 + \sigma_2)$ is the normalized stress and

ε_1 Axial strain

ε_v Volumetric strain, $\varepsilon_v = \varepsilon_1 + \varepsilon_2 + \varepsilon_3$

Soil mechanics generally assumes as a first approximation that normalized stress versus strain plots coincide when tests are conducted under various stress levels. This means that the plots of normalized stress, say σ_1/σ_2, $(\sigma_1-\sigma_2)/\sigma_2$ or $(\sigma_1-\sigma_2)/(\sigma_1+\sigma_2)$ versus strain ε_1 are expected to be coincide for tests performed at various stress levels. This can help in studying the effect of void ratio without considering the effect of stress level as shown in Figure (3.15).

3.7.13 BAROTROPY

The stiffness of a granular body originates from the inter-particle forces acting between the individual grains. Therefore, the stiffness increases with increasing stress level *p*. This property can be discussed more specifically with reference to the conventional triaxial test. Therefore, the lateral stresses $\sigma_2=\sigma_3$ are kept constant during the compression of the specimen. If two tests carried out under different lateral stresses are compared, say $\sigma_2=\sigma_3=a$, and $\sigma_2=\sigma_3=b$ with $|b|>|a|$ then two different stress-strain curves can be obtained, Figure (3.16).

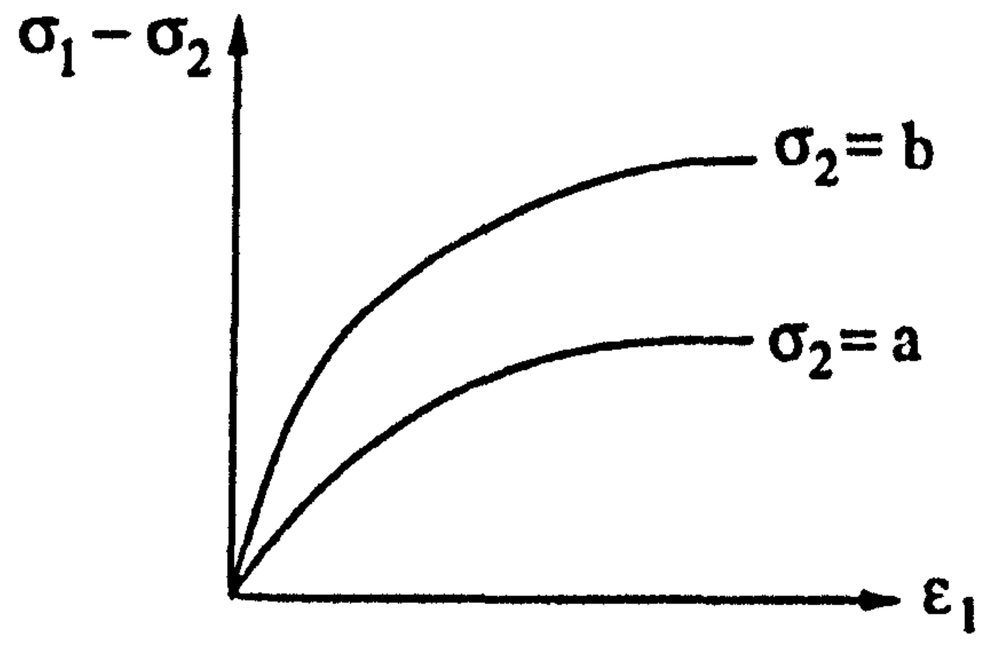

Figure (3.16) Triaxial compression at two different stress levels

3.7.14 STATE VARIABLE

In soil mechanics there are some variables govern the stress-strain relation. These variables can not be considered as a material constant as they depend on the present state of the soil and hence they are considered as state variable. One of these variables is the void ratio.

3.7.15 PORE PRESSURES

It is known that the pores of a soil may be filled with one or more pore fluids, water and air for example. Each of these fluids may be under pressure, and it is probable that if more than one fluid is present, the pressures in the different fluids will be different. Saturated soils contain only one pore fluid, which is usually water or air. There will then be just one pore pressure in the pore water or air that fills the pores of the soil, which may, in general, be assumed to be continuous. If the equilibrium of the pore water is somehow disturbed, then, in some locations, pore pressures will be observed different from datum values. Such non-equilibrium pore pressures are called excess pore pressures. The pore water will flow, as a result of gradients of excess pore water pressure, to reestablish equilibrium.

3.7.16 NONLINEARITY

Non-linearity may be defined as the failure of the magnitude of response to be proportional to the magnitude of excitation. There can be a number of factors that can be contribute to non-linearity, which for engineering bodies is usually manifested through large changes in the geometry and changes in material properties; the first is called geometric non-linearity and the second is called material non-linearity. Often, non-linearity occurs as a mixture of both categories. Both sources of non-linearity are to be expected when a soil is being under external load. The stress-strain relation can describe material non-linearity, but more than one stress-strain coefficient is required to fully represent the mechanical behavior of any material under a general system of changing stresses. These coefficients are Young's modulus and Poisson's ratio. In order to deal with the material non-linearity of soil, an incremental analysis technique may be used.

3.7.17 ANISOTROPY

Natural soils are often deposited in horizontal layers and then subjected to anisotropic stresses leading to preferred orientation of the particles. As a consequence, most natural sand deposits possess an inherently anisotropic structure which causes variation in deformation strength characteristics as the loading direction changes. Conceptually distinction may be made between inherent and

induced anisotropy with the former being caused by deposition and the latter being induced by stressing or straining. While this distinction may make sense for laboratory prepared specimens, for natural soils, however, it is often difficult to differentiate between inherent and induced anisotropy, since natural soils usually experience both inherent and induced anisotropy, Wu (1998). The mode of depositions, the particles shape, among other features, can lead to an inherent anisotropy, moreover, when subjected to a loading process, the material will deform irreversibly and acquire induced anisotropy.

Sands are believed to exhibit two distinct types of anisotropy, inherently anisotropy and induced anisotropy. Inherently anisotropy, in which the anisotropic deformation and strength characteristics are entirely independent of the applied strain, whereas induced anisotropy behaviour is exclusively due to applied strain, Ghaboussi and Momen (1984).

3.7.18 PLASTIC FLOW RULE

When the state of stress reaches the yield criterion represented by a yield function f the material undergoes plastic deformation. The flow rule defines the relationship between the next increment of the plastic strain increment $d\varepsilon_{ij}^{p}$ and the present state of stress σ_{ij} for a yielded element. The direction of the plastic strain increment $d\varepsilon_{ij}^{p}$ is defined by the plastic potential function g in the form $d\varepsilon_{ij}^{p} = d\lambda \frac{\partial g}{\partial \sigma_{ij}}$, where $d\lambda$ is a positive scalar of proportionality dependent on the state of stress and loading history. The direction of the plastic increment vector $d\varepsilon_{ij}^{p}$ is normal to the surface of plastic potential g at the current stress point σ_{ij}. This is known as the '*normality rule*'. If the potential and yield surfaces coincide with each other ($f = g$), the flow rule is called *associated* type, otherwise it is the *non-associated* type. Geologic materials are considered to flow in non-associative flow rule manner.

3.8 SAND BEHAVIOR

The word "soil" implies a mixture of assorted mineral grains with various fluids. Hence, soil in general can be considered as (i) dry soil or (ii) saturated soil or (iii) multiphase (partially saturated soil) material whose state is to be described by the stresses and displacements (velocities) within each phase. There are still great uncertainties on how to deal analytically with partly saturated soils. The stresses carried by the soil skeleton are conventionally called "effective stresses" in the soil mechanics literature and those in the fluid phase are called the "pore fluid pressures".

In a saturated soil, when free drainage conditions prevail, the steady state pore-fluid pressures depend only on the hydraulic conditions and are independent of the soil skeleton response to external loads. Therefore, in that case, a single-phase continuum description of soil behaviour is certainly adequate. Similarly, a single-phase description is also adequate when no drainage (e.g., no flow) conditions prevail. However, in intermediate cases in which some flow can take place, there is an interaction between the skeleton strains and the pore-fluid flow. The solution of these problems requires that soil behaviour be analyzed by incorporating the effects of the transient flow of the pore-fluid through the voids, and therefore requires that a two phase continuum formulation be available for porous media.

During deformations, the solid particles that form the soil skeleton undergo irreversible motions such as slips at grain boundaries, creations of voids by particles coming out of a packed configuration, and combinations of such irreversible motions. When the particulate nature and the microscopic origin on the phenomena involved are not sought, phenomenological equations are used to provide a description of the behaviour of the various phases that form the soil medium. In multiphase theories the conceptual model is thus one in which each phase (or constituent) enters through its averaged properties obtained as if the particles were smeared out in space. In other words, the particulate nature of the constituent is described in terms of phenomenological laws in which the particles behave collectively as a continuum. Soil is thus viewed as consisting of a solid skeleton interacting with the pore fluids.

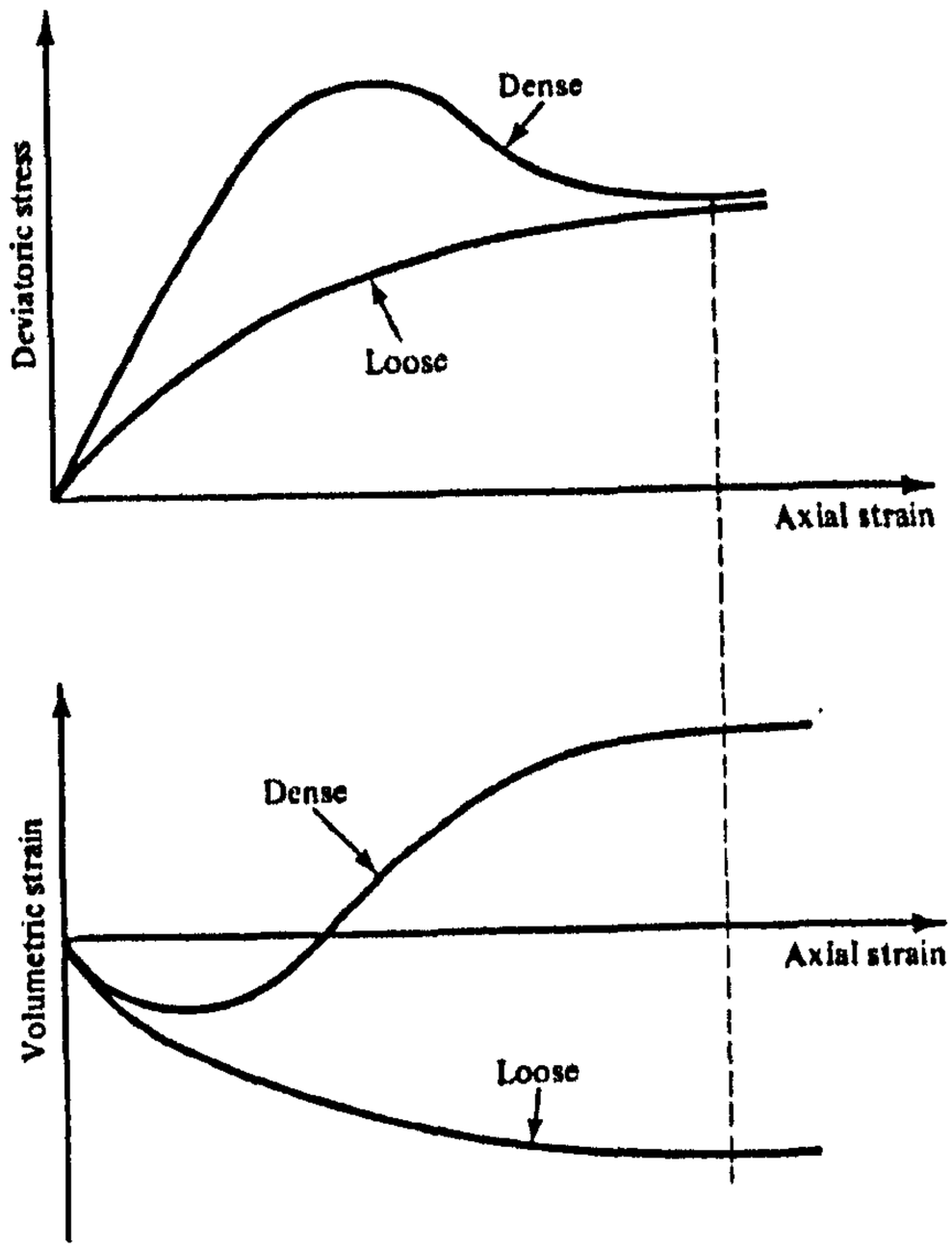

Figure (3.17) Scheme of stress-strain behaviour of sand soil

The stress-strain response of a granular material is dependent on the degree of saturation, the interstitial pore fluid, the void ratio, and the loading history of the material. Void ratio, in particular, reflects the state of compaction of the material, e.g., loose or dense. Loose sand compacts and exhibits ductile-type stress-strain behaviour when subjected to a deviatoric state of stress. Dense sand, on the other hand, dilates and exhibits brittle-type stress-strain behaviour when subjected to a similar stress condition, Figure (3.17). The boundary between the loose and dense states is characterized by the void ratio at which shearing deformation occurs without volume changes. This void ratio is referred to as "critical void ratio" and its magnitude varies inversely with hydrostatic stress. The stress-strain behaviour of the sand is, therefore, highly dependent on the confining pressure or the superimposed hydrostatic state of stress. In the case of saturated sand, the stress-strain behaviour also varies greatly depending on whether during loading the sand is in a drained or an undrained condition. *Here sand in the fully drained condition is considered since dry sand is the most common soil type in the Egyptian desert.*

3.8.1 EFFECT OF STRESS LEVEL AND VOID RATIO ON SAND BEHAVIOR

Experimental evaluation of the effect of the stress level on the critical void ratio has been carried out by Wan and Guo (1998). Figure (3.18) shows that the relationship of the stress level and the void ratio can be modeled through an exponential function.

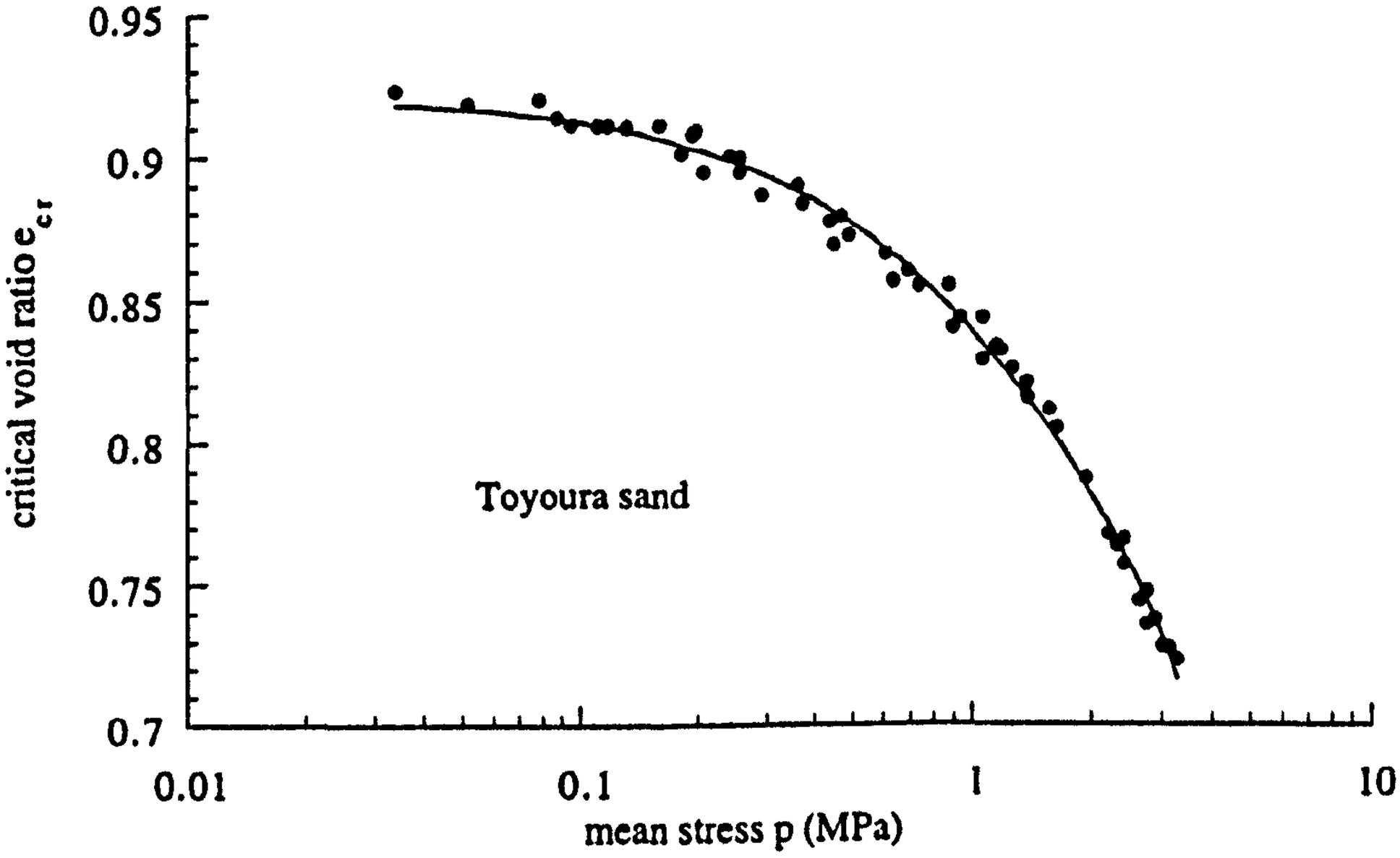

Figure (3.18) Void ratio as a function of stress level, Wan and Guo (1998)

Based on experimental findings, some distinctive features of the effect of void ratio and stress level are briefly summarized:

- For a given initial void ratio the friction angle and the dilatancy decrease as the stress level increases; for a given stress level the friction angle and the dilatancy decrease with increasing void ratio.
- Under low confining pressure, the stress-strain curve of dense sand shows a peak. After the peak, strain softening can be observed, and the dilatants volume change becomes less pronounced. A critical state, characterized by the critical friction angle and the critical void ratio, will be reached asymptotically with progressive deformation.
- Dense specimens under high confining pressure and loose specimens do not show strain softening and the volume change remains constant.

- Dense sand specimens under high confining pressure and loose specimens under low confining pressure show similar behaviour. With increasing confining pressure, the difference between dense and loose packing tends to diminish.
- The void ratio in a critical state depends on the stress level. The critical void ratio decreases with increasing stress level. There exists a unique relation between the critical void ratio and the stress level as shown in Figure (3.19).

p, Confining pressure

$$p = \frac{(\sigma_1 + 2\sigma_3)}{3}$$

q, Deviatoric stress

$$q = \sigma_1 - \sigma_3$$

σ_1 Normal stress

σ_3 Lateral stress

e, Void ratio

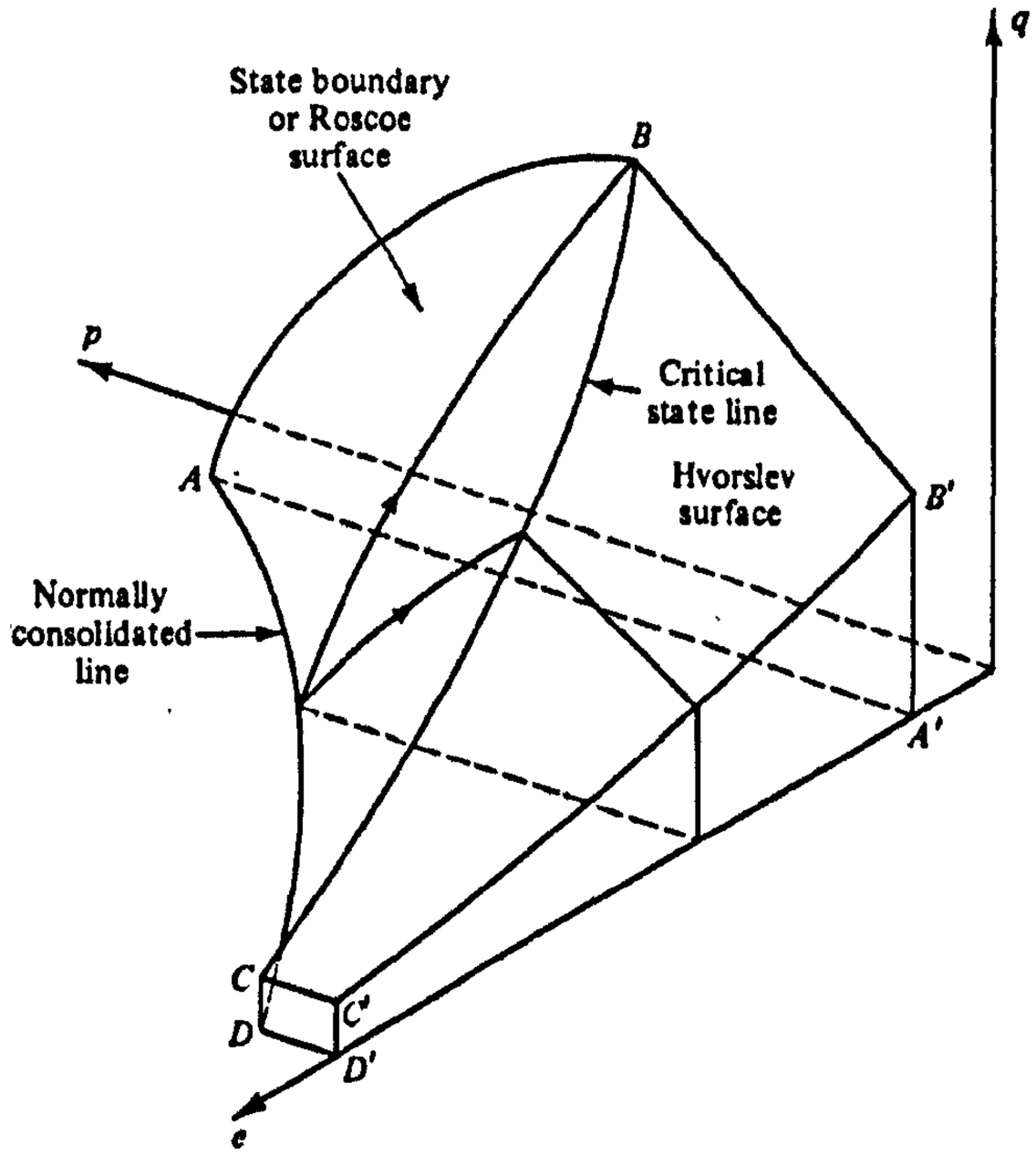

Figure (3.19) Effect of stress level and void ratio

A study of the stress-strain relationship of sand under different types of loads (static and dynamic) has been carried out, Liu (1995). New test equipment was used to determine the bearing capacity of wet sand under unconsolidated un-drained conditions (drain-air conditions for dry sand). The influence of grain size, moisture content and bulk density of the sand, as well as vibration, on its bearing capacity was also studied. The results indicate that the dynamic strength of dry sand is higher than its static strength. For wet sand, on the contrary, dynamic strength is lower than the static strength.

3.9 SAND MODELING

Recent advances in digital computer technology and numerical techniques such as the finite element method have rendered possible, at least in principle, the solution of any properly posed boundary value problems in soil mechanics. With the continuous increase in computational speed and storage capacity of modern computers, the finite element method (FEM) has been feasibly applied in a variety of large-scale design or simulation problems. Even though it originated from structural analyses, the theory upon which it is based is universally applicable. The finite element method has successfully been used in simulating or solving many problems in other engineering fields including the soil-tool interaction in soil-machine systems.

For a long time, soil mechanics has been based on Hooke's law of linear elasticity for stress and deformation analysis for a soil mass under a footing or behind a retaining wall when no failure of the soil is involved. This is known as the elasticity problem in soil mechanics. On the other hand, the theory of perfect plasticity is used to deal with the conditions of ultimate failure of a soil mass. Problems of earth pressure, retaining walls, bearing capacity of foundations, and stability of slopes are all considered in the realm of perfect plasticity. These are called stability problems, long-term settlement problems and consolidation problems; these, are treated in soil mechanics as essentially viscoelastic problems.

Partly for simplicity in practice and partly because of the historical development of the mechanics of solids, the elasticity problems and the stability problems in soil mechanics are treated separately and in unrelated ways. The essential connection between elasticity and stability is known as progressive failure. The progressive failure problems deal with the elastic-plastic transition from the initial linear elastic state to the ultimate state of the soil by plastic flow. The essential set of equations for the solution of progressive failure problems is the constitutive equations of soils, which give a unique relationship of stress and strain for different geotechnical materials.

Further progress in expanding analytical capabilities in geomechanics depends upon consistent mathematical formulations of generally valid and realistic material constitutive relations. An increasing effort has thus been devoted since the 1960's to a more comprehensive description of soil behaviour. Numerous formulations have been proposed in the soil mechanics literature. All rely on a better knowledge and understanding of mechanics in general, and continuum mechanics in particular, than has been common in traditional soil mechanics.

The results and progress in the field of constitutive relations have, until recently, been mostly ignored by the mainstream of soil engineering. However, recent progress and validation exercises have instilled confidence and finally attracted the attention of the practice of such constitutive models. In recent years, the growing interest in constitutive relations has led to a number of conferences devoted exclusively to theoretical, experimental, numerical implementations and application problems associated with this field. For example: "Numerical Models in Geomechanics – NUMOG".

Various methods exist for incorporating the material constitutive models developed for soils and rocks into finite-element computer programs for solving practical geotechnical problems that require nonlinear stress analyses involving both material and geometric nonlinearity. Iterative calculations based on linear incremental formulation can now be treated with comparative ease within the framework of finite element software.

In recent years, the development of more sophisticated material models based on the concept of continuum mechanics has rapidly advanced with the aid of finite element computational work. Although the finite element method has had a profound effect on the rapid development of the analysis based on the nonlinear stress-strain behaviour of geotechnical materials, there are still some analytical and theoretical difficulties associated with the present nonlinear stress analysis in geotechnical engineering problems in particular. These are:

1. *Selection or evaluation of material models*
2. *Selection or evaluation of material constants*

3. *Idealization of ground conditions*
4. *Assessment of analytical results, and*
5. *Evaluation of analytical procedures in the finite-element method*

Although several familiar constitutive models such as the nonlinear elastic models, the classical elastic-plastic models and the advanced strain-hardening models have been widely used in the nonlinear stress analysis of geotechnical materials, the selection of an appropriate model depends on the material characteristics assumed in the analysis, the accuracy required for the analysis and the type of loading condition, e.g. undrained or drained condition. Constitutive models for granular materials like sand are more complex than the classic nonlinear theories.

3.9.1 MICROSTRUCTURAL ASPECTS

The particulate nature of soil materials is directly responsible for their complex overall behavior. Sand consists of an aggregate of particles with different sizes and shapes that interact with each other through contact forces (both normal and tangential) at the points of contact. If the particles are considered as essentially incompressible, deformation of the granular assembly occurs as the particles translate; slip and/or roll and either form or break contacts with neighboring particles to define a new microstructure. The result is an uneven distribution of contact forces and particle densities that manifests in the form of complex overall material. Similarly, clays are composed of plate-shaped particles of clay mineral. Each plate is subject to gravity forces and electrostatic forces at the points of contact, which hold the particles together. Therefore, if one knew all about the particles' geometry (their shapes and contacts) and understood all the physics and mechanics of inter-particle contacts, then in principle one should be able to predict the overall macroscopic response of the assembly. Such studies could lead to a rational explanation of the observed macroscopic behavior, and allow direct correlation between average macroscopic constitutive parameter values and microscopic entities (e.g., relate the overall friction angle to the individual particle-to-particle friction coefficient). A number of studies have been initiated along these lines. Several experimental, analytical and numerical models have been proposed to study the effect of particle-

to-particle interaction on the overall material response, Zervos, Vardoulakis, et al. (2000). Because of oversimplifications, these studies have had, as yet, little or no impact on the relations used in current constitutive models. Eventually, this may change as the models are further refined.

The most popular microstructural numerical models, commonly called Distinct Element or Discrete Element Methods consist of approximating the mechanical constraint of non inter-penetrability of the particles by some close-range steep repulsion law. Each instant two particles are close enough to be viewed as contacting, they are assumed to exert on each other some dissipative forces which mimic friction. Thus, the evolution problem is reduced to the integration of a system of second order differential equations, to which classical methods are applied. The steeper the approximate laws of interaction, the more realistic are the results, at the price of reducing the time-step length to ensure numerical stability. Some researchers have recently advocated the use of semi-implicit procedures to avoid full integration of Newtonian dynamical equations when computing quasi-static responses of granular systems, at the price of having to approximate and/or neglect the complicated intermediate path-dependent phenomena involved when contact and friction occur between particles.

3.9.2 MACROSCOPIC ASPECTS

Although very complex when examined on the micro-scale, soils as many other materials may be idealized at the macro-scale as behaving like continua. At the macro-scale, the various phenomena associated with the discrete soil entities such as sand grains, clay platelets, etc., are integrated and averaged to the level of a homogeneous continuum model. In the macroscopic field, the averaging volume represents and characterizes a physical point. Despite the large differences in the nature and structure of materials such as metals and alloys, polymers and composites, concrete, and soils, there is a great unity displayed in their macroscopic behavior. With different orders of magnitude, terms like elasticity, viscosity, plasticity, hardening, softening, brittleness and ductility can be applied to all these materials. Therefore, while still recognizing the underlying particulate nature of these materials,

instead of studying them as discrete systems, it is more convenient to consider them as continua, and use concepts from continuum mechanics and thermodynamics to analyze and model their behavior. The phenomenological behavior of the material is therefore the standard of reference in this approach, and it is the one adopted in modern soil constitutive theory.

3.9.3 REQUIREMENTS OF A CONSTITUTIVE MODEL FOR SOIL

Considerable attention has been given since the late 1960's to the development of constitutive equations for soil media, but although many different models have been proposed, there is not yet firm agreement among researchers. Further, many of the constitutive models presented seem unnecessarily arbitrary, and at this stage it is important to emphasize that, to be satisfactory, a material model idealization should possess the following *necessary* properties:

1. The model should be *complete*, i.e. able to make statements about the material behavior for all stress and strain paths, and not merely restricted to a single class of paths (e.g., axial symmetry or pure shear);
2. It should be possible to identify the model parameters by means of *a small* number of standard, and relatively simple material tests;
3. The model should be founded on some *physical interpretation* of the ways in which the material is responding to changes in applied stress or strain (e.g., the material should not be modeled as elastic if permanent deformations are observed upon unloading).
4. The fundamental mean stress and density dependencies of the mechanical behaviour of the soils.
5. The smooth transition from the very high initial stiffness in the small strain region, to the large plastic strains near failure, Gajo and Wood (1999).
6. Models that describe anisotropy behavior need to incorporate the memory of the soil for its history, Gajo and Wood (1999).
7. A comprehensive sand model should be able to model the variation of sand behaviour during loading. Most of the earlier models treat sand with different initial densities as different materials. This approach results in multiple sets of parameters for a single material and does not have very good control over

a crucial change in the material state during loading, Li, Dafalias, et al. (1999).

The first property is clearly essential if the model is to be of practical application, and the second property is very desirable. The third property, linked with the first and second one, helps to ensure that the model is based on mechanical and physical observations, and not merely phenomenological, that is an elaborate curve-fitting exercise of limited application. Finally, it must be added that a material model may only be deemed to be satisfactory when it can be used first to determine the stress-strain-strength behavior of the material using one piece of testing equipment (e.g., in triaxial tests), and then to predict the observed behavior of the same material in some other type of testing equipment (e.g., in simple shear tests).

3.9.4 CLASSIFICATION OF CONSTITUTIVE MODELS

It is perhaps a stimulating fact that the number of constitutive models proposed in the literature is continuously increasing in such a way that one can hardly gain an overview of all of them. In this section a classification of the available constitutive models is listed according to the stress-strain response of a material and how it described by the model.

1. Elasticity: Elasticity means that the current stress is a function of the current strain. In other words, the current stress does not depend on the previous deformation path. An elastic medium returns to its initial state after a cycle of loading and unloading.

2. Plasticity: Plasticity in its broadest sense implies that the deformation can be dissipative and the actual stress depends on the deformation path.

3. Elastoplasticity: Elastoplasticity is a combination of elasticity and plasticity. A distinction between response to loading and unloading is established by means of a 'yield surface', and the strains are subdivided into elastic and plastic parts.

4. Hyperelasticity: Hyperelasticity is a special case of elasticity in that a constitutive model is said to be hyperelastic if the stress is recovered after a deformation or strain

cycle. The stress rate and strain rate are also related through an elastic potential. Owing to the existence of the elastic potential there exists a unique relation between stress and strain. The behaviour described by a hyperelastic constitutive equation is path independent.

5. Hypoelasticity: The stress rate and strain rate in a hypoelastic constitutive equation are related through some function that need not be derivable from a potential. The behaviour described by a hypoelastic constitutive equation is, in general, path dependent. The stress is recoverable only on special strain cycles, e.g. with zero enclosed area. Hypoelastic constitutive equations are incrementally linear in the sense that the tangential stiffness depends only on stress.

6. Hyperplasticity: In hyperplasticity, the constitutive models are based on plasticity theory admitting plastic potentials as in hyperelasticty. Usually, two or more equations, representing different branches of the stress-strain behavior for loading and unloading, are employed. As a consequence, switch functions are needed to distinguish between the different branches. The stress at the end of the strain circuit is recovered for the one branch and is not recovered for the other. Hyperplasic constitutive equations are some-times called bilinear or multi-linear models in the sense that the relation between the stress rate and strain rate takes on different linear relations depending on the value of stress or strain

7. Hypoplasticity: As in hypoelasticity no plastic potential is used in the hypoplastic model and the relation between stress rate and strain rate is incrementally non-linear in the sense that no matter how small the strain rate may be the behaviour is always path dependent.

3.9.5 CONCEPTS IN SAND MODELING

Some measure of density (void ratio, relative density, etc.) should be included as a state variable in representing the behaviour of cohesionless soils (like sand), Pestana and Whittle (1999). Also the dependence of sand behaviour on the stress level, Wu, Bauer, et al. (1996), has to be considered. It has been experimentally demonstrated that virgin samples of sand generated by the process of deposition

generally exhibit higher stiffness in the direction of the deposition than along the bedding planes. It is well known that geomaterials (soils, rocks, or concrete) do not obey the normality rule, or other solid mechanics relations. However, it is known that for such materials, a vertex model (accounting for the effect of hydrostatic stress) is necessary for a good model, Chambon, Caillerie, et al. (1999). Experimental research on clay and dense sands suggests that any two samples of a soil will behave in a similar manner regardless of their stress-strain history provided the state variable is the same for each sample, Yu (1998). This is because the state variable does not eliminate the influence of either density or confining pressure on the behaviour of such materials.

Whereas the volume change of loose sand is contracting throughout, dense sand shows an initial contractancy and a subsequent dilatancy. As a consequence, the associated flow rule in elasto-plasticity can not be applied. Liquefaction and cyclic mobility mark further characteristics that are substantially different from that of clay. The existing models for sand are often rather complicated in their formulations and usually involve many material parameters. Geological media, in particular cohesionless soils, do not exhibit associated flow plasticity behaviour, but rather non-associated flow (resulting in separate yield and potential functions), Lade and Nelson (1984).

Section (3.7) reveals some concepts which should be emphasized when modeling sand, which are:

- Strength of sand is generally accepted to be governed by some sort of frictional relationship in which the available shear strength depends on the stress level.
- The peak angle of friction that can be attained by sand is dependent on density (Pycnotropy) and mean stress level (Barotropy).
- At large deformation, sand attains critical states in which shearing can continue with no further changes in stress or density.
- There may be a small region of stress space within which the sand can be described as behaving elastically.

- The shear stiffness decreases steadily during monotonic shearing.
- Sands show volume changes as they are sheared, with the rate and sign (compression or expansion) of the volume change being dependent on the stress ratio (or mobilized friction).

3.9.6 CONSTITUTIVE MODELS FOR SAND

There are many different types of constitutive models available which could simulate soil under monotonic loading. Often soil models based on the concept of yield and potential surfaces have proven to be able to reproduce the complex behaviour of soil reasonably well.

A Review of the literature for the available constitutive models summarizes here as:

- Elasto-plastic models
- Kinematic hardening models
- Bounding surface models
- Rate-type models
- Hypoplastic models

Which are described further below:

3.9.6.1 Elasto-plastic models

One of the main features of soil behaviour, observed in engineering works and in controlled laboratory tests, is the occurrence of irreversible deformation. In many practical problems it is admissible to neglect the more or less pronounced time dependent character of soil deformation and treat soils as rate-independent materials. The most well-known classical theory of elasto-plasticity framework is used to describe soil behaviour as a rate-independent material. Elasto-plasticity is characterized by decomposition of the behaviour into an elastic part and a plastic part as shown in Figure (3.20). The elastic part can be modeled using Cauchy or Green elastic laws, and the plastic part can be modeled using Von-Mises, Extended Von-Mises, Drucker-Prager, Mohr-oulomb, Tresca or Extended Tresca criteria, Desai and Siriwardane (1984).

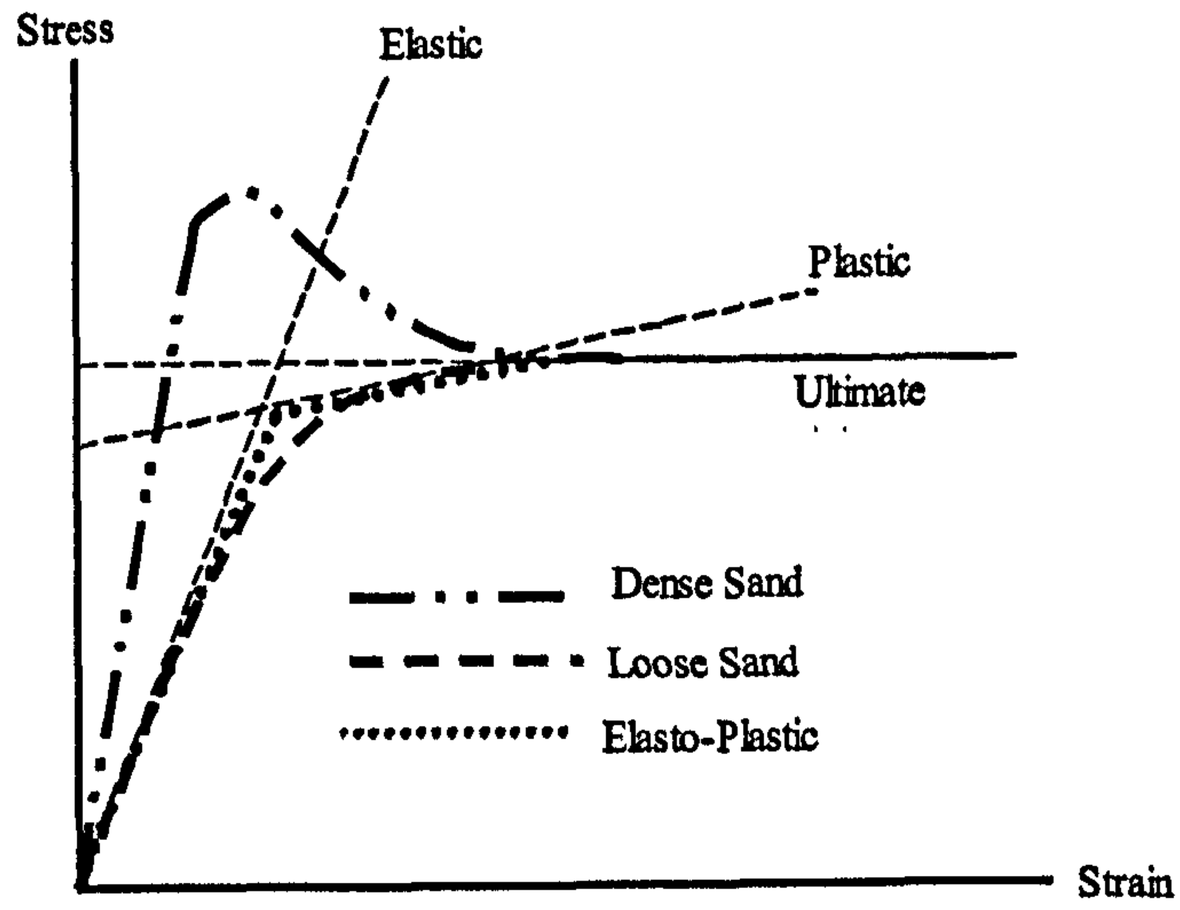

Figure (3.20) Elasto-plastic model description

For sand models to account for the effect of stress level the extended Mohr-Coulomb, Figure (3.21a), or extended Drucker-Prager, Figure (3.21b), may be used. Also to account for the effect of hydrostatic state of stress, a moving cap should be incorporated into the model, Figure (3.21c).

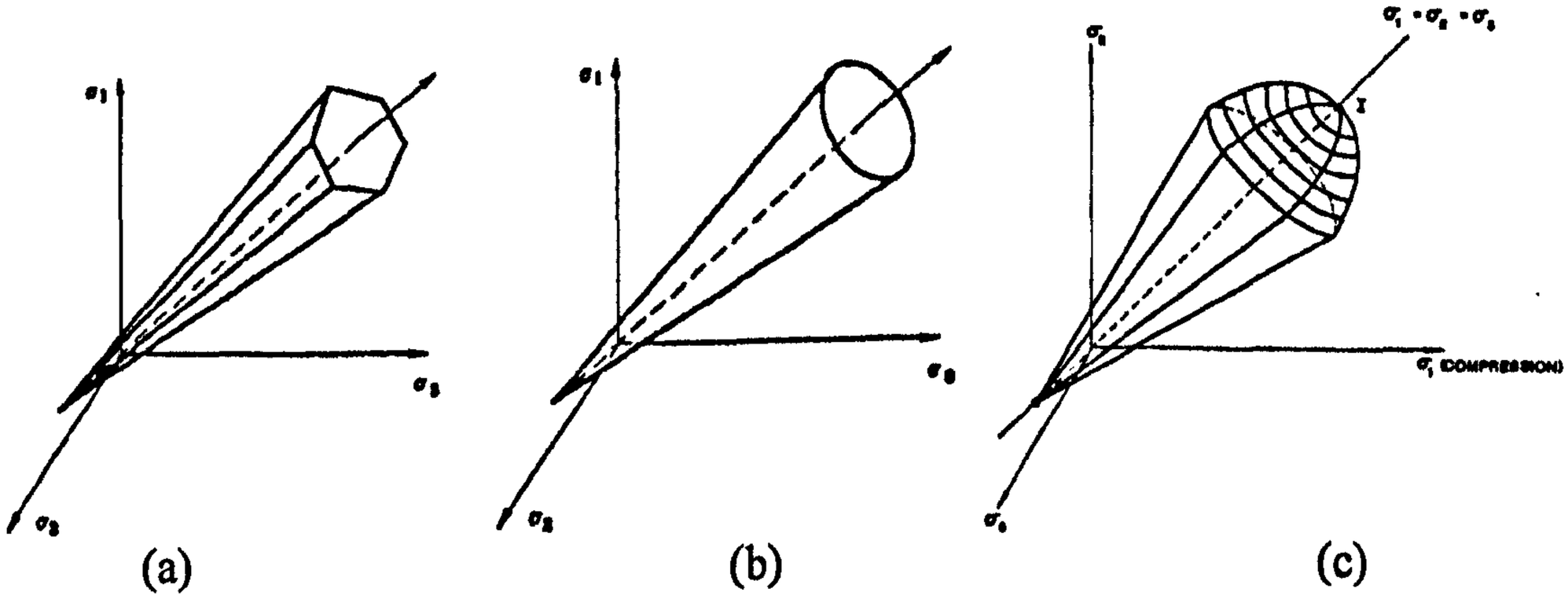

(a) Extended Mohr-Coulomb, (b) Extended Drucker-Prager, (c) Cap model

Figure (3.21) Failure criteria

Elastoplastic based models have been developed with increasing complexity in order to represent soil behaviour. In 1979 Baladi and Rohani presented a development of a three-dimensional isotropic elastic-plastic constitutive model simulating the stress-strain-pore pressure response of saturated granular materials. The model was intended to be used for effective stress analysis in realistically posed boundary value

problems involving fluid-saturated sand. This constitutive model contains seven material constants that can be determined from standard laboratory tests such as triaxial tests. The model is found to be capable of reproducing the hysteretic behaviour of the material under both hydrostatic and deviatoric states of stresses, and accounts for the effect of superimposed hydrostatic stress on the shearing response. In addition, the model accounts for shear-induced volume change and produced negative pore pressure for dilative material and positive pore pressure for contractive material under undrained test conditions. The behaviour of the constitutive model under axisymmetric triaxial test conditions was also examined and correlated with experimental results for fluid-saturated sand at both loose and dense initial states of compaction. *In its present form, this constitutive model was found to be able to only qualitatively simulate the behaviour of the material.* For a quantitative simulation of test data, some parameters would need to be replaced with appropriate functions of stress or strain invariants, or both, as dictated by test results.

The inherent anisotropy in deformation and strength characteristics of sands is due to the preferred orientation of particles and bedding planes generated during the process of deposition. Considering this aspect, a plasticity model has been developed by Ghaboussi and Momen (1984) which is capable of simulating such anisotropy behaviour. The model contains a number of coefficients of anisotropy. Using experimental data, the coefficient of anisotropy was determined for a number of well-known sand types. Stress-dilatancy was modeled by using the `normalized work` and it has been shown that the normalized work is independent of inherent anisotropy. Finally some reasonably close comparisons between experimental results and model simulations showed that the simulated results were in reasonable agreement with the test results. However, this agreement indicates that the material model is capable of simulating test results with a reasonable degree of accuracy for certain values of material parameters, which can still only be determined by trial and error.

A general mathematical procedure for generating incremental elasto-plastic constitutive relations for material modeled by multiple, intersecting yield surfaces to

be employed directly in non-linear matrix computer analysis codes has been presented by Lade and Nelson (1984). Basic concepts from the classical plasticity theory were employed in the derivation of the incremental elasto-plastic stress-strain relationship. The derivation leads to a relatively simple, straightforward procedure for determining the incremental stress-strain relationship (stiffness matrix) required.

An elastoplastic model coupled with an elastic model with damage has been developed by Chazallon and Hicher (1998) in order to model various phenomena that govern the mechanical response of bonded geomaterials under monotonic loadings taking into account both the frictional and cohesive aspects of these materials. The mean confining pressure was introduced in the damage evolution law to account for the brittle-ductile transition. Triaxial test simulation was carried out for different soil types and under different mean confining pressure to illustrate the capabilities of the model to reproduce the mechanical behaviour of bonded geomaterials. Results showed that, for weak bonds, the elasto-plastic part played the predominant role, whereas for strong bonds, the elastic part with damage governed the mechanical behaviour.

The dependencies of granular soil behaviour on void ratio and stress level were modeled by Wan and Guo (1998) within plasticity theory but enhanced by a modified stress-dilatancy law. By using a void ratio dependent factor that measures the deviation of the current void ratio from the critical one, a stress dilatancy equation was introduced. This modification corresponds to a new energy dissipation equation for a granular assembly that sustains kinematical constraints under the action of stresses. The constitutive law predicted, in a very consistent manner, the response of sands in monotonic loading conditions for a large range of initial void ratios and confining pressures without any need for adjusting the modeled material parameters.

Based on elastic-plastic strain hardening (or softening), a unified critical state theory for both clay and sand was developed by Yu (1998) in order to link the plastic behaviour of the soil during shear and consolidation in a rational manner. Like the standard Cam-Clay models, the state parameter theory is a volumetric strain

hardening plasticity model. While the use of both volumetric and deviatoric plastic strain hardening may be able to capture the strong dilation during hardening prior to failure in dense sands, a few more material constants was introduced into the model. A limitation associated with volumetric strain hardening is that no plastic deformation is allowed within the state boundary surface, i.e. it is difficult to represent the tendency of the mean effective stress to decrease a bit before increasing to critical state.

Based on the incrementally linearized theory of rate independent elastoplasticity, a new generalized effective stress-strain model was presented by Pestana and Whittle (1999), referred to as MIT-S1, which is capable of predicting the rate independent, effective stress-strain-strength behaviour of uncemented (sand soil) soils over a wide range of confining pressure and densities within a single framework by introducing the void ratio as an independent state variable. The main conceptual departure from other effective stress models is the explicit inclusion of void ratio as a state variable in the description of the yield function. The model represents the unloading and reloading behaviour through two components: (1) equations to describe the non-linear but reversible response during unloading and reloading at constant stress ratio or constant mean effective stress referred to as 'perfectly hysteretic' response; and (2) development of irrecoverable (plastic) strain for stress paths approaching the yield surface through a bounding surface formulation. Only thirteen input parameters are required by this model in order to characterize clays, while fourteen input parameters are used for freshly deposited sands. Although the model formulation is relatively complex, all of the input parameters for these materials can be determined from standard types of laboratory test.

Limitation of the elasto-plastic models

Most of the existing elasto-plastic models for sands suffer from the following limitations:

1. Although it is generally accepted that some measure of density (void ratio, relative density, etc.) should be included as a state variable in representing the behaviour of cohesionless soils, most existing models have material input parameter that depend on density (and/or confining pressure). This situation

arises in formulations that assume that the yield surface, peak friction angle, and dilatancy rates are functions of the initial density (e.g. loose, dense). As a result, the stress-strain-strength properties of sand samples at two different initial states (confining pressure or density) are characterized as two separate materials with different sets of input parameters.

2. Most constitutive models for sands are based on the assumption of isotropic material behaviour (using isotropic yield functions). However, there is increasing evidence that sands exhibit anisotropic stress-strain properties due to their initial depositional structure and subsequent stress history.
3. Salient behavior of dense sand cannot be modeled
4. Most of the models idealized the flow rule to be associated
5. Models of high accuracy suffers from large number of material parameters

3.9.6.2 Kinematic hardening models

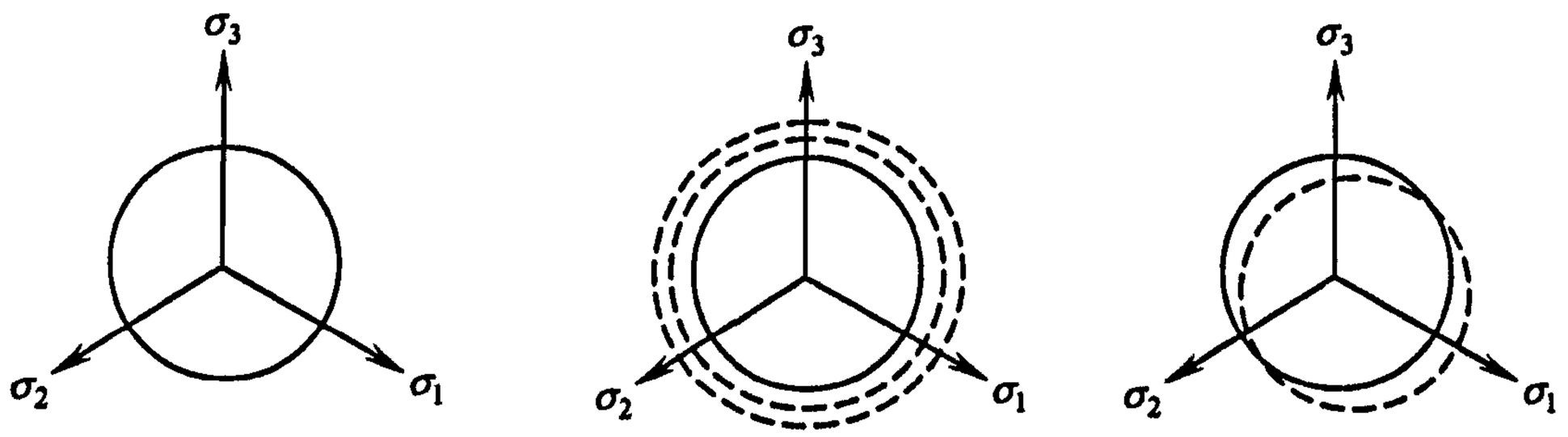

(a) Perfectly plastic (b) Isotropic hardening (c) Kinematic hardening

Figure (3.22) Yield locus for different models

Plastic hardening models are mainly based on the existence of a yield surface, the yield surface can expand in the case of Isotropic hardening, Figure (3.22b), or move in the case of Kinematic hardening, Figure (3.22c). Hardening models can conveniently incorporate the behaviour of non-monotonic loading (including cyclic behaviour), which can reproduce both small elastic stiffness and hysteric energy dissipation associated with the accumulation of plastic strains which are induced by regular or irregular cycles of loading and unloading. As an extension of the axisymmetric *p-q* formulation of the kinematic hardening plasticity, Gajo and Wood

(1999) represent a general multiaxial stress-strain behaviour of granular materials over the full range of void ratios and stress levels (neglecting grain crushing) using a combination of well accepted concepts in the geotechnical engineering community, such as (1) the Mohr-Coulomb strength criterion, (2) critical state, (3) the existence of a small strain elastic region, (4) a hyperbolic relationship for representing global plastic stress-strain behaviour and (5) the dependency of strength on state parameter and flow rules derived from the Cam-Clay model. The general multiaxial stress-strain model analysis showed that yield surface shape has negligible effect and that, in stress-driven tests leading to a more or less radial stress path in the deviatoric plane, the effects are mainly connected to the size of the selected strength surface along the particular radial stress path. Despite the model simplicity, it suffers from some limitations, mainly: neglecting the strain-softening phase for dense sand.

Despite the success in modifying the standard Cam-Clay models over the last twenty years, the following problems still remain, Yu (1998):

1. The yield surfaces adopted in many critical state models significantly overestimate failure stress.
2. Many critical state soil models assume an associated flow rule and therefore are unable to predict the deviatoric stress peak that is commonly observed in undrained tests on loose sand and normally consolidated undistributed clays before approaching the critical state.
3. The critical state concept has been much less successful for modeling granular materials. The main problem lays in the fact that existing Cam-Clay models fail to predict observed softening and dilatancy of dense sands and undrained response of very loose sands.

In 1999 Woodward and Molenkamp carried out an implementation of the non-linear elastic multi-surface plastic kinematic hardening constitutive soil model, referred to as ALTERNAL, into a general uncoupled finite element program called ALTICA. To account for the dissipation of energy due to plastic deformation during alternating loading, multiple yield surfaces expand and translate at the same time (isotropic and kinematic hardening). A new yield surface is generated which can expand and

translate in principal stress space to simulate stress-induced anisotropy. Although the ability of the constitutive model to simulate the monotonic and cyclic behaviour of granular material was clearly demonstrated, the model requires twenty four material parameters, which is relatively very high.

Limitation of the Kinematic hardening models

Despite the capability of the kinematic hardening model to simulate most sand behaviour, it suffers from some limitation from the implementation point of view in that a large number of material parameters are required and further large memory is required to store each yield surface.

3.9.6.3 Bounding surface models

Descended from the Kinematic hardening model, the bounding surface models are characterized by the existence of only two surfaces, one describes the yield surface and the other describes the strength or limit surface, Figure (3.23).

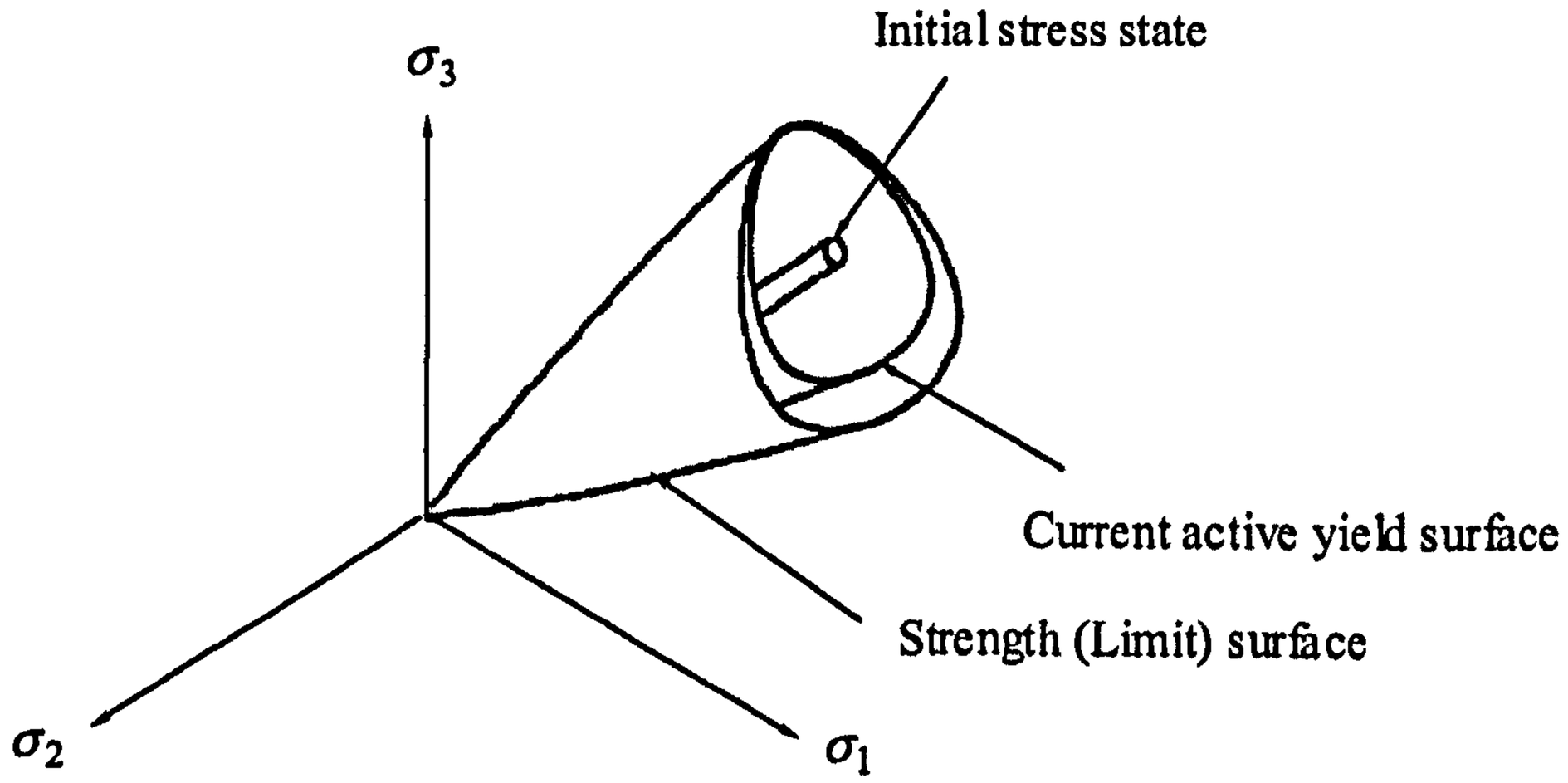

Figure (3.23) Bounding surface layout

The two surfaces are related to each other by some factor less that one; the current active yield surface can expand and shrink between these boundaries. The bounding surface model has an advantage over other models in that it can reliably represent the smooth variation of stiffness during monotonic loading. Bounding surface plasticity allows the transition between elastic and elastoplastic responses to be modeled.

Many models have been developed within the bounding surface framework; Bardet (1986), constructed a constitutive equation to simulate the nonlinear behaviour of loose and dense sands subjected to various types of loadings in a two-dimensional stress space. The critical state, which depends upon the initial void ratio in the case of sand, defines the evolution of the bounding surface during plastic flow. The model describes strain softening and stress-dilatancy with nine material constants calculated from the results of conventional triaxial tests. Comparing experimental and numerical results reveals the model's capability of simulating drained and undrained responses, hysteretic energy dissipation, and accumulation of irreversible strain during cyclic laboratory tests.

Models which account for the effective stress are found to be applicable to the study the engineering problems associated with sand liquefaction. Manzari and Dafalias (1997) developed a comprehensive constitutive model for sands within the critical state soil mechanics frame-work: the two-surface formulation of plasticity is coupled with a state parameter. The operation of the two-surface model takes place in the deviatoric stress-ratio space, and the state variable is used to define the peak and dilatancy stress ratios of sand. The model was based on two main concepts: (1) the concept of a yield/bounding or two-surface plasticity, and (2) the concept of the state parameter, Been and Jefferies (1985), as an essential variable arising in a critical state soil mechanics framework. The model is capable of realistically simulating stress-strain behaviour of sands under monotonic and cyclic, drained and undrained loading conditions. The numerical efficiency of the model is good because only the yield surface must be updated owing to kinematic and isotropic hardening.

The advantages of the bounding surface plasticity theory over conventional plasticity have been discussed here in modeling behaviour during monotonic loading. The existence and direction of the irreversible strain increment, which requires a non-associative flow rule in conventional plasticity in order to be realistically simulated at failure state, can be defined by only one surface in bounding surface plasticity.

3.9.6.4 Rate type models

Besides classical elastoplasticity, other kinds of rate-type constitutive equations, incrementally nonlinear, have been described in the past twenty years for geomaterials. As an alternative to the elastoplastic framework, the rate type models are characterized by the concepts of separation of strain rate into elastic strain rate and plastic strain rate parts, with strain rates deriving from elastic and plastic potentials. These models have proved to be of considerable interest especially when a close reproduction of the experimental complexity of soil behaviour is required. Vardoulakis and Graf (1985) developed a rate type constitutive equation considering the effect of stress state on the frictional angle using the term 'mobilized friction angle'. The model was mainly used to simulate biaxial experimental tests. In 1994 Chambon, Desrues, et al. defined an identification procedure, referred to as CLoE, Using parameters which are essentially familiar to geotechnical data, like friction angle (compression and extension), dilatancy factor and characteristic point (the transition point from contractancy to dilatancy). Finally the CLoE identification procedure outputs a set of numerical parameters, to be used as material parameters by the constitutive model. The latter can be embedded in a finite element code. The concepts of limit surface and of flow rule for perfectly plastic states are linked in a consistency condition. The model is illustrated by some examples show its reasonable representation of sand behaviour in monotonic loading.

A comparison between a classical bi-linear elastoplastic Von Mises model and the incrementally non-linear CLoE model has been given by Chambon, Caillerie, et al. (1999). The classical isotropic hardening elastic-plastic models were compared with the CLoE model, from different perspectives namely: (1) the 'Gudehus' diagram' in which the model is fully described by a mapping between the strain rate space represented by an hyper sphere of unit radius centered at the origin of the strain rate space and the corresponding hyper surface in the stress rate space as shown latter in Figure (3.25). (2) The second-order work; which is interpreted as a property of the tangent moduli tensor for incrementally non-linear models. (3) The localization criterion. Studies show that the CLoE model is similar to classical elastoplastic models and easy to introduce into the finite element method.

A consistent framework with embedded microstructure considerations for stress-dilatancy behaviour of sand was developed by Wan and Guo (1999). The sand stress-strain relationship was described in the model via a second order tensorial function. Incorporating soil fabric (the way of soil forming in the natural) is found to have a significant effect on the accurate description of sand behaviour.

Most of the rate type models are applicable to cyclic loading such as in earthquakes analysis and other foundation stability problems. But they suffer from weak simulation of the sand behaviour under monotonic loading. To avoid these limitations, a Hypoplastic framework has been developed.

3.9.6.5 Hypoplastic models

In geotechnical engineering, failure often occurs in a progressive way. The description of progressive failure requires constitutive models that are capable of representing strain softening at large strain. A perusal of the relevant publications in the literature suggests that there are only a few constitutive models that incorporate strain softening. Moreover, most of these constitutive models have been developed with complex mathematical formulations and involve too many material parameters to be practical.

The hypoplastic constitutive models are an attractive alternative to elasto-plastic formulations for continuum modeling of granular materials. They incorporate the advantages of both bounding surface and rate type frameworks. A comparison study between hypoplastic and elastoplastic models, described by Viggiani and Tamagnini (2000), reveals the high performance of the hypoplastic model in the prediction of specific features of geotechnical materials.

Figure (3.24) represents a comparison of different available failure criteria along with experimental data, the figure reveals the accuracy of the hypoplastic equation in prediction a smooth failure envelope to avoid the well known mathematical singularity problems caused when using the Mohr-Coulomb.

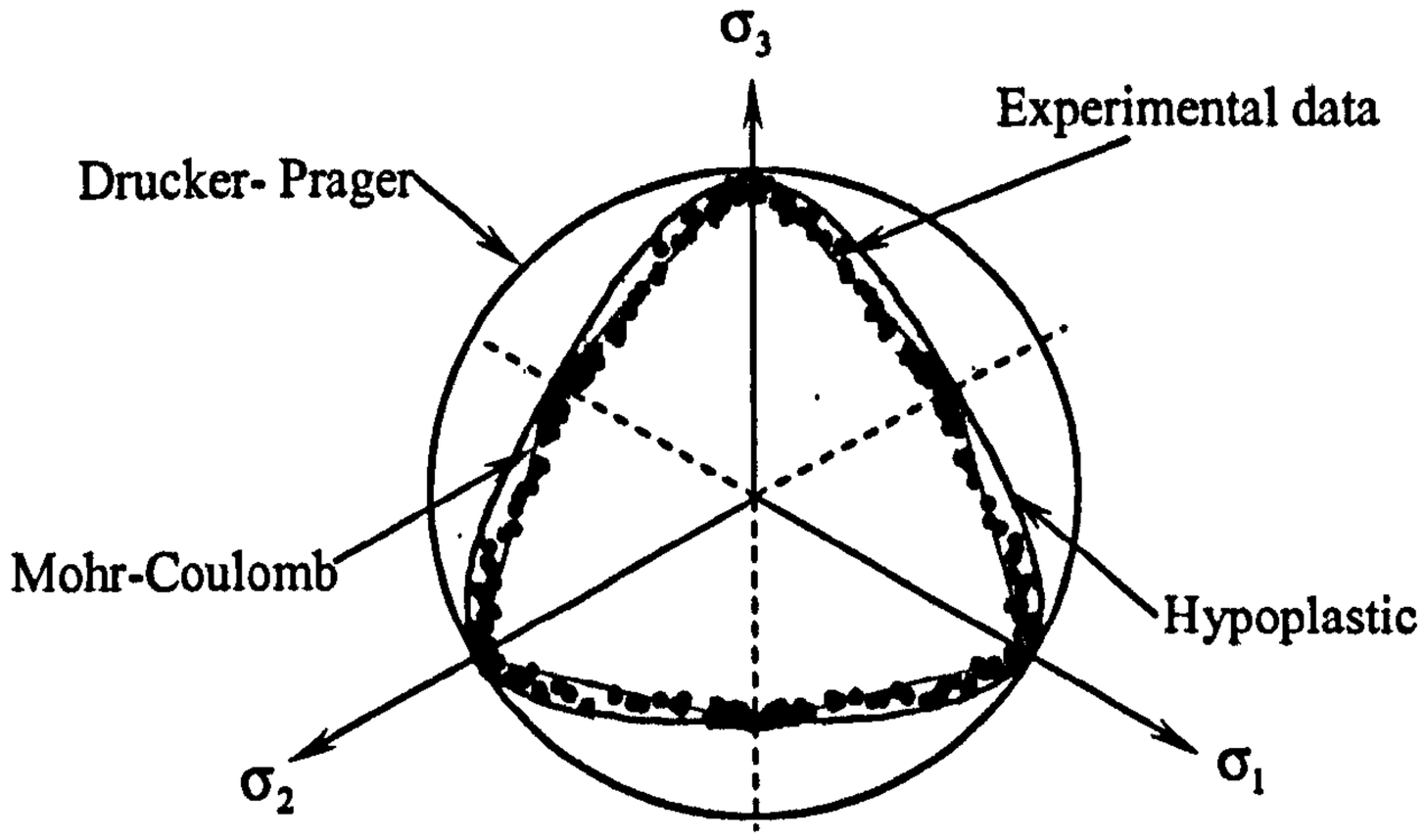

Figure (3.24) Failure surfaces for different failure criteria

A powerful tool to examine a constitutive model performance was introduced by Gudehus (1979) and Royis and Doanh (1998) which called the stress response envelope. For ease description of the stress response envelope, a 2D state is considered. For a unit strain rate $\dot{\varepsilon}$, defined by $\sqrt{\dot{\varepsilon}_1^2 + 2\dot{\varepsilon}_2^2} = 1$ the stress rate $\dot{\sigma}$ is calculated and plotted. Figure (3.25) represents a stress response envelope for the hypoplastic model. The figure shows the continuity of the hypoplastic equation.

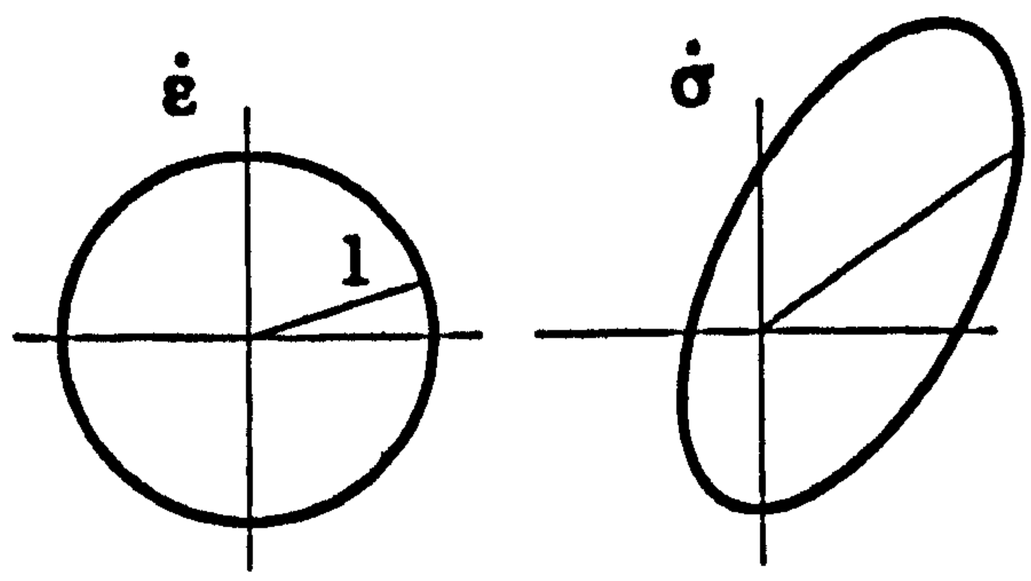

Figure (3.25) Stress response diagram for the rate relation

In contrast to elasto-plastic models, the decomposition of deformation components into elastic and plastic parts is not considered. Consequently yield surface, plastic potential, flow rule and hardening function are also not used, Kolymbas (1991). Moreover, material parameters of recent hypoplastic models are closely related to granular material properties and can be estimated from mean grain diameter, non-uniformity coefficient, grain shape, and grain hardness.

The hypoplastic model describes the mechanical behaviour of the so-called simple grain skeletons assuming that the macroscopic state can be sufficiently characterized by mean values of microscopic state values (e.g. grain contact forces). It describes the material behaviour through non-linear tensorial function of stress rate and strain rate. The following properties of granular materials result from the formulation of hypoplastic models, Tejchman, Herle, et al. (1999):

1. The state is fully defined merely through the effective stress and the void ratio (inherent anisotropy of contact forces between grains is not considered and vanishing principal stresses are not allowed).
2. Deformation results only from grain rearrangement.
3. The grains are permanent (abrasion and crushing of grains are excluded in order to keep the granulometric properties unchanged).
4. There exist pressure-dependent minimum, maximum and critical void ratios.
5. The material manifests an asymptotic behaviour for monotonic and cyclic shearing.
6. The deformation of the grain skeleton is rate independent.
7. Physical-chemical effects (capillary and osmotic pressure) and cementation of grain contacts are not taken into account.

A historical literature review of available models based on the hypoplastic concept is given in the following.

In 1990 Wu and Kolymbas, presented an outline of the so-called hypoplastic constitutive equation and applied a stability criterion to examine its performance. From the analysis of the response envelope, the hypoplastic equation is shown to be stable and applicable.

In 1990 a hypoplastic model was formulated by Bardet (1990) to simulate the nonlinear and irreversible behaviour of loose and dense sands. For the sake of simplification of the mathematical formulation of the constitutive model, that author assumed that the anisotropy of sand behaviour could be neglected; this leads to a formulation in terms of three stress invariants instead of six stress components in the anisotropic case. The incremental stress-strain relationships are inverted and derived

in a format compatible with conventional solution techniques, such as finite element method. The model has twelve material constants calibrated from triaxial tests. Comparison of predicted and experimental results on loose and dense (Sacramento River) sand allowed the capability of the model to predict the drained and undrained behaviour of loose and dense sands to be assessed.

A comprehensive constitutive model for sand was formulated, by Wang, Dafalias, et al. (1990), within the general framework of bounding surface Hypoplasticity. The distinctive feature of this model is the dependence of the loading and plastic strain rate directions on the stress rate direction. The model can simulate different features of sand behaviour under loading conditions, which range from simple monotonic to complex cyclic at different amplitudes and directions. In particular, the successful simulation of the response under "rotational shear" is one of the distinctive properties of the model, and mainly attributable due to its hypoplastic character. From the practical point of view, the model can be a useful tool not only for the analysis of simple loading cases (which can be done with simpler models), but mainly for cases of high loading complexity, involving pronounced features of rotational shear loading, which are recent great interest to the geotechnical engineering community in both onshore and offshore structures. Li, Dafalias , et al. (1999) then modified the model to incorporate the basic premises of critical-state soil mechanics and covered both loose and dense sand behavior.

A three-dimensional non-linear stress-strain and dilatants volume change behaviour of sand in an elegant mathematical formulation with only four material parameters was achieved by Wu and Bauer (1994). To facilitate finite element implementation, explicit expressions in matrix form were provided. The model was validated by a series of tests on Karlsruhe medium sand, which is composed mainly of quartz with sub-rounded grains. The capability of the model to account for the path dependence was demonstrated by simulating the triaxial test on medium dense Erksak sand. Model validation showed that the model is not well suited to complex loading programs involving closed strain cycles. Also the reduction of the shear strength after failure, so-called strain softening, cannot be obtained. Due to the independent of the

friction angle on the stress level, the model is found to be not applicable for studying engineering problems with large variations of the stress level. Despite all these limitations, the model is capable of simulating the great majority of the problems in geotechnical engineering with relatively simple loading programs and with small to moderate change of the stress level.

Triaxial compression tests on sand typically show density-dependent and pressure-dependent response of the stress-strain relationship. Strain softening from a peak stress ratio is a familiar feature of the observed stress-strain relations, and it is important that this should be incorporated into constitutive models that describe sand behaviour. Based on the specific volume of the sand, and the specific volume that the sand would have if brought to a critical state, a state parameter was developed, by Wood, Belkheir, et al. (1994). A simple hypoplastic model for strain softening of sand by integrating the critical state was presented, by Wu, Tejchman, et al. (1994). Kolymbas in 1995 discussed the dependence of the soil stiffness on (i) the density (Pycnotropy) and (ii) the pressure or stress level (Barotropy).

Based on the framework of critical state to incorporate the effect of stress level and void ratio on the stress-strain relation and to avoid previous shortcomings, Wu, Bauer, et al. (1996), extended their previous model, Wu and Bauer (1994). This accounted for the effect of the void ratio and stress level on the behaviour of granular material by integrating the critical state into the constitutive equation. This development added another seven constants to the model giving a total of eleven constants all of which can be obtained from the triaxial test. The model was shown to be applicable to both the initial and fully developed plastic deformation of granular materials. Many well-established concepts in soil mechanics, which would otherwise be modeled entirely independently, can be unified with this constitutive model. Simulations of various elementary tests, including Oedometer, triaxial and simple shear tests show that the model is capable of capturing the salient behaviour of granular materials under monotonic as well as cyclic loading. The model was then extended to predict failure, by Wu and Niemunis (1997), and to account for

transverse anisotropy and was shown to successfully describe various aspects of the behaviour of granular materials, Wu (1998).

A more comprehensive, simpler and physically more appealing, model has been developed, by Gudehus (1996). The model proved to be capable of predicting a wide range of soil properties and deformations in granular bodies caused by changes of boundary conditions, e.g. by static loading, drainage or excavation. The model was extended to simulate the pore water pressure and cohesive or viscous soils. Using the advantages of the factorized function represented the stress level and void ratio as state parameters in Gudehus (1996) and Bauer (1996), Wolffersdorf (1996) improved the mathematical formulation of the hypoplastic model using the results of elasto-plastic theory. The new model is based on the Drucker-Prager model and a limit surface introduced by Matsuko and Nakai (1977). This improved hypoplastic constitutive law has the following advantages with respect to earlier hypoplastic formulations.

1. Realistic friction angles are obtained for deviatoric loading programs rather than conventional triaxial compression, e.g. for biaxial paths and for triaxial extension paths.
2. More realistic results are obtained for critical states, and also for limit states with peak.
3. The developed constitutive relation requires four material constants that allow for a realistic description of granular material behaviour over a wide range of stresses and densities and another four calibration constants.
4. Contrary to elastoplastic models the developed hypoplastic equation can be written as a single tensorial equation.
5. Verification of the model using data from different element tests reveals the capability of the model to simulate granular materials over a wide range of stress level and void ratios.

Experimental and numerical investigations for hypoplastic model calibration (particularly for Wolffersdorf model, Wolffersdorf (1996)) have been carried out by Erich Bauer (1996).

The effect of ratcheting under cyclic loading was incorporated into the Hypoplastic model by, Niemunis and Herle (1997). For easy calibration of the hypoplastic constitutive equation, suitable ways were used to factorize both the linear and non-linear parts of the constitutive equation. Response envelopes were used in order to visualize the qualitative aspects of the factorization. Also the effects of the density and stress level were represented using these response envelopes. With a unified description of the density and stress level effect, the model was shown to be applicable for a wider range of pressures and densities using only one set of constitutive constants. Numerical simulation of element tests (Oedometer, triaxial, biaxial and simple shear tests) showed the capability of the model in reproducing the salient features of granular materials under both drained and undrained conditions.

A study of the relevant experiments in the literature showed that both the stress ratio and the void ratio approach the critical state asymptotically under increasing deformation. According to whether the sand specimen is denser or looser than the critical state the critical void ratio will be approached as an upper or lower bound. Numerical results showed that dense sand at high stress level behaved like loose sand at low stress level. Wu (1999) presented a hypoplastic constitutive model with critical state for three-dimensional non-linear stress-strain and dilatant volume change behaviour of sand. Some of the well-known failure criterion, e.g. Matsuoka-Nakai and Lade-Duncan were incorporated into the model along with incorporating void ratio as a state parameter. Numerical simulation of the triaxial tests shows the capability of the model to simulate the salient behaviour of the granular materials. Despite the wide range of granular material behaviors that can be predicted using WU model, some of the model parameters have no physical meaning.

It is shown, for several sands and gravel, that all parameters of the hypoplastic model are closely related to the granulometric properties of grain assemblies. Herle and Gudehus (1999), showed, in the hypoplastic model proposed by Wolffersdorf (1996), that all the eight constants of the hypoplastic equation could be determined from simple experiments on grain assemblies: angle of repose, minimum and maximum index density, a shear test (triaxial or shear box) on a dense specimen, and

oedometric compressions of an initially loose specimen and a dense specimen. Simple calibration procedures were demonstrated for six different quartzes of sand and one of gravel. Results showed a close relation between the model parameters and the granulometric properties, such as; the mean grain diameter and the non-uniformity coefficient.

The mechanical behavior of granular materials is strongly influenced by the orientation of the tangential planes at grain contacts resulting from the shape and the spatial arrangement of the grains within the grain skeleton. Whenever a preferred spatial orientation exists, the material behaves anisotropically. In order to model such a behavior, a unified description of the interaction between the mean pressure, the current density and the evolution of the anisotropy parameters corresponding to the loading history was carried out, Bauer and Huang (1999). A particular hypoplastic constitutive model by Gudehus (1996) for a cohesionless and initially isotropic material was extended with respect to transverse isotropy. The constitutive equation is of rate-type and based on a nonlinear tensor valued-function depending on the current void ratio, the Cauchy stress, the rate of deformation, and a structure tensor defining the isotropic plane. Transversely isotropic material properties are included with a certain invariant form of a tensor function. The extended model was applied to predict the peak friction angle depending on the bedding plane in triaxial compression for various initial void ratios. For large monotonic shearing, the influence of the initial anisotropy declines. Thus, after the peak, the stress ratio and the volume strain tend towards a stationary state that is independent of the initial state.

Wang and Makdisi, (1999), conducted a study to assess the feasibility of implementing a bounding surface Hypoplasticity model into a two-dimensional computer code (named FLAC) to improve the simulation of variations in effective stress and liquefaction of sands in dynamic analysis of soil structures. The capability of the original model, Wang, Dafalias, et al. (1990), was implemented for plane strain conditions. To simplify numerical implementation of the hypoplastic model, the implemented model was based on some assumptions, which are: (1) eliminating

the strain in the third direction; (2) the use of the "deviatoric normality flow rule" which is a special case of the original model; (3) the use of a conical shape for the bounding surface; (4) the removal of the flat cap, which is used for simulating the consolidation effect of sand in the original model. The incremental stress-strain relation was decomposed into elastic and plastic parts. Eight parameters were required in the effective stress analysis using the bounding surface plasticity model, which could be obtained from cyclic strength data from laboratory or field tests and from consolidation tests. To account for the dilatation and strain softening in the critical state, a critical state parameter, the void ratio, was used in the model. Sand behaviour under shear loading was simulated up to the critical state. Shear-induced dilation and softening under undrained conditions were captured. Generation of pore water pressure, dilation, and liquefaction under cyclic loading were illustrated.

3.10 SUMMARY

Soil modeling in geotechnical engineering has expanded rapidly in the past 40 years as a result of the increasing need for more accurate simulation of material nonlinearity. Recently, many constitutive equations have been proposed for geomaterials. Among all the types of constitutive equations of continuum mechanics, those based on plasticity theory remains the one most commonly applied to sand. Two rules are used to prescribe the evolution of the yield and plastic potential surfaces during plastic flow; (1) the isotropic hardening, which expands surfaces uniformly in every stress-space direction and generate a large elastic domain during the first stress cycles, that making it unable to simulate the accumulation of irreversible strain during subsequent cycles and also the build-up of pore pressure leading to liquefaction during undrained loading (2) the kinematic hardening, which translates surfaces in stress space, preserves a small elastic domain. But the kinematic hardening requires a more complex definition for the surface translation. Most of the constitutive equations have been proposed along the line of elastoplasticity. There are some difficulties in applying elastoplasticity to geomaterials, e.g., decomposition of deformation into elastic and plastic parts and the transition between elastic and plastic parts and the transition between elastic and

plastic deformation. Different investigators attempted alternative approaches to the elastoplastic constitutive equations. In addition to conventional plasticity theory, other types of constitutive equations have been applied to model cyclic behaviour of sands: incremental theory, rate-type law, multiple yield surface plasticity and finally bounding surface plasticity. The bounding surface plasticity theory could be used in modeling behaviour during monotonic loadings (as in case of soil cutting by blade or ripper) which is difficult to model within conventional plasticity. The existence and direction of the irreversible strain increment, which requires non-associative flow rule in conventional plasticity in order to be realistically simulated at failure state, can be defined by only one surface in bounding surface plasticity. The hypoplastic relations are of the rate type bounding surface. Due to the incremental non-linearity with the deformation rate, a hypoplastic model can describe a non-linear, both stress-strain and volumetric behaviour of granular bodies during shearing with only a single tensorial equation.

3.11 CONCLUSION

The hypoplastic model features described in the literature and outlined in this chapter appears to have more promise in simulating sand during monotonic loading. Hence one of the hypoplastic models will be implemented into a finite element code to simulate soil-tool interaction for earth moving and mine clearing equipment. In this study the model developed by Wolffersdorf (1996) has been shown to be more suitable for simulating sand in monotonic loading. Some modifications to this model will be carried out for proper simulation of soil-tool interface problems. This hypoplastic model implementation and verification is discussed in Chapter 4.

Chapter 4

HYPOPLASTIC MODEL,
NUMERICAL INTEGRATION & VERIFICATION

4.1 CHAPTER SYNOPSIS

An overall review of the available constitutive models for sand was given in Chapter 3 which concluded that the hypoplastic model is best suited to simulate sand soil. In this chapter the background framework of hypoplasticity along with a detailed description of a particular hypoplastic model are presented. Then some modification is carried out on the selected hypoplastic model to accommodate it for monotonic cutting and progressive failure simulation. Towards the end of the chapter different numerical techniques of integrating the modified hypoplastic model, required for finite element implementation are discussed along with their verification.

4.2 INTRODUCTION

The mechanical behaviour of granular soils, typically ranging from silt to gravel, can be modeled by various different mathematical perspectives. Hypoplastic theory stems from the framework of Rational Mechanics, Ignatieff (1996). Starting from the principal requirements on the model properties, Chapter 3, a single equation describing many important features of the behaviour of granular soils can be

obtained. Contrary to classical elastoplasticity theory no distinction between elastic and plastic deformation, yield, plastic potential surfaces and hardening rules are required. The behaviour of an inelastic material is formulated by using a single nonlinear tensorial function of the rate-type. Based on the general concept of hypoplasticity various aspects of the mechanical behaviour of granular materials have been investigated in the past few years, e.g. shear banding by Bauer and Huang (1999) and Tejchman and Herle, et al. (1999), rate-dependence and cohesion by Prisco and Imposimato (1996). Critical state has also been incorporated in order to better describe the influence of pressure level and density on the material behaviour, by Wu and Bauer (1993), Wu and Bauer, et al. (1996), Wu (1999), and Tejchman and Herle, et al. (1999). It has been demonstrated in the literature that the hypoplastic model can describe the dependence of material behaviour on the stress level (Barotropy) and on the density (Pycnotropy) with a single set of material constants.

Use of incremental non-linear constitutive models, in particular the hypoplastic model proposed by Wolffersdorf (1996), to simulate the behaviour of soil is an attractive alternative to prevailing plasticity theories. This hypoplastic model is simple in formulation and involves few material parameters, in fact eight in total. The model is formulated using tensor algebra with a non-linear tensorial function based on the Representation Theorem. Some well-known failure criteria, e.g. Drucker-Prager, Matsuoka-Nakai and Lade-Duncan may also be incorporated into the model.

4.3 MATHEMATICAL FRAMEWORK OF HYPOPLASTICITY

Through the mathematical description of the hypoplastic framework the dyadic notation system (represented in bold characters) will be mainly used along with tensor notation system (represented in italic characters), which will be sometimes used to explain some dyadic notations. The hypoplastic equation, being a rate equation, does not use any conventional strain measure ε_{ij}. Instead, the stretching d_{ij} and the spin tensor w_{ij}, are used which in some sense can be interpreted as the rate of strain. However, the equality $d_{ij} = \dot{\varepsilon}_{ij}$ is only correct if ε_{ij} is

an infinitesimal strain tensor or if ε_{ij} is the logarithmic strain tensor for rectilinear extensions. In hypoplasticity the actual configuration always coincides with the reference configuration of the tensors variables involved. Therefore hypoplastic equations can be integrated up to arbitrary large deformations provided the reference configuration is updated. As is usual in continuum mechanics, compressive stresses and strains are negative. Asterisk (*) over the stress σ_{ij} denotes the deviatoric part of a tensor, e.g.

$$\sigma_{ij}^{*} = \sigma_{ij} - \frac{1}{3}\sigma_{kk}\delta_{ij} \tag{4.1}$$

Herein, δ_{ij} stands for Kronecker's symbol, Goodbody (1982). Referring to standard soil mechanics laboratory tests, the logarithmic axial strain ε_1 and the logarithmic volumetric strain ε_v are used for several representations. To be consistent with traditional soil mechanics, the stress deviator $\sigma_1 - \sigma_2$ and the axial strain ε_1 are considered positive in compression for graphical representations, Lancellotta (1995). The stress level (p) denotes the first invariant (or trace "*tr*") of the stress tensor:

$$p = \sigma_{kk}, \qquad k=1, 2, 3 \tag{4.2}$$

$(\sigma_1, \sigma_2, \sigma_3)$, $(\varepsilon_1, \varepsilon_2, \varepsilon_3)$ and (d_1, d_2, d_3) denote the principal components of the corresponding tensors σ_{ij}, ε_{ij} and d_{ij}.

The hypoplastic constitutive equation relates Cauchy stress $\boldsymbol{\sigma}$, the Jaumann derivative of $\boldsymbol{\sigma}$ ($\boldsymbol{\sigma}^{\circ}$) and the stretching $\dot{\boldsymbol{\varepsilon}}$ as:

$$\boldsymbol{\sigma}^{\circ} = \mathbf{H}(\boldsymbol{\sigma}, \dot{\boldsymbol{\varepsilon}}) \tag{4.3}$$

where $\mathbf{H}$ tensorial function

$\boldsymbol{\sigma}^{\circ}$ Jaumann stress rate define as follows

$$\boldsymbol{\sigma}^{\circ} = \dot{\boldsymbol{\sigma}} + \boldsymbol{\sigma}\,\mathbf{w} - \mathbf{w}\boldsymbol{\sigma} \tag{4.4}$$

$\boldsymbol{\sigma}$ Cauchy stress tensor

$\mathbf{w}$ Spin tensor

$$w_{ij} = \frac{1}{2}\left(\frac{\partial \dot{u}_i}{\partial x_j} - \frac{\partial \dot{u}_j}{\partial x_i}\right)$$

$\dot{\boldsymbol{\varepsilon}}$ Stretching or strain rate, Shames (1992)

$$\dot{\boldsymbol{\varepsilon}} = d_{ij} = \frac{1}{2}\left(\frac{\partial \dot{u}_i}{\partial x_j} + \frac{\partial \dot{u}_j}{\partial x_i}\right)$$

u_i Displacement function

x_i Position coordinates

The function $\mathbf{H}(\boldsymbol{\sigma}, \dot{\boldsymbol{\varepsilon}})$ must be isotropic with respect to $\boldsymbol{\sigma}$ and $\dot{\boldsymbol{\varepsilon}}$ to obey the principle of objectivity in rational mechanics, and so, making use of the representation theorem of tensor algebra, Kolymbas (2000), it can be written as:

$$\mathbf{H}(\boldsymbol{\sigma}, \dot{\boldsymbol{\varepsilon}}) = \phi_0 \mathbf{I} + f_1 \boldsymbol{\sigma} + \phi_2 \dot{\boldsymbol{\varepsilon}} + \phi_3 \boldsymbol{\sigma}^2 + \phi_4 \dot{\boldsymbol{\varepsilon}}^2 + \phi_5(\boldsymbol{\sigma}\dot{\boldsymbol{\varepsilon}} + \dot{\boldsymbol{\varepsilon}}\boldsymbol{\sigma}) + \phi_6(\boldsymbol{\sigma}\dot{\boldsymbol{\varepsilon}}^2 + \dot{\boldsymbol{\varepsilon}}^2\boldsymbol{\sigma}) + \phi_7(\boldsymbol{\sigma}^2\dot{\boldsymbol{\varepsilon}} + \dot{\boldsymbol{\varepsilon}}\boldsymbol{\sigma}^2) + \phi_8(\boldsymbol{\sigma}^2\dot{\boldsymbol{\varepsilon}}^2 + \dot{\boldsymbol{\varepsilon}}^2\boldsymbol{\sigma}^2) \quad (4.5)$$

In this ϕ_i are scalar functions of joint invariants of $\boldsymbol{\sigma}$ and $\dot{\boldsymbol{\varepsilon}}$. It is clear that for each particular stress $\boldsymbol{\sigma}$, the relation between $\boldsymbol{\sigma}^\circ$ and $\dot{\boldsymbol{\varepsilon}}$, is non-linear. The constitutive equation can be written in the form:

$$\boldsymbol{\sigma}^\circ = \mathbf{L}(\boldsymbol{\sigma})\,\dot{\boldsymbol{\varepsilon}} + \mathbf{N}(\boldsymbol{\sigma})\,\|\dot{\boldsymbol{\varepsilon}}\| \quad (4.6)$$

where

$\mathbf{L}(\boldsymbol{\sigma})$ Linear function in $\dot{\boldsymbol{\varepsilon}}$

$\mathbf{N}(\boldsymbol{\sigma})$ Non-linear in $\dot{\boldsymbol{\varepsilon}}$

$\|\dot{\boldsymbol{\varepsilon}}\|$ Stands for the norm of the strain rate tensor

The constitutive equation, (4.6), is constructed by choosing items provided by the representation theorem for isotropic tensorial functions and has been employed successfully to describe various aspects of the behaviour of granular materials.

Starting from equation (4.6), several workers have carried out studies in order to find appropriate form for the linear tonsorial function $\mathbf{L}(\boldsymbol{\sigma})$ and the nonlinear one $\mathbf{N}(\boldsymbol{\sigma})$, e.g. Wu and Bauer (1994) & Wu, et al. (1994), Wu and Niemunis (1996), Wu, et al. (1996), Wu (1999), Kolymbas (1995), Gudehus (1996) and Wolffersdorf (1996). The model proposed by Wu was based on parameters which have no physical meaning. However the model proposed by Wolffersdorf (1996) has the following advantages with respect to earlier hypoplastic formulations.

1. Realistic friction angles are obtained for deviatoric loading programs rather than conventional triaxial compression, e.g. for biaxial paths and for triaxial extension paths. More realistic values are obtained for critical states, and also for limit states with peak
2. Most of the model parameters have physical meaning and can be easily obtained from ordinary test devices.

One of the salient features of constitutive equation (4.6) is that the history dependence is reduced to the instantaneous stress state. In other words the stress rate depends on the stress state but not on how this stress state is reached. In order to account for strain softening, constitutive equation (4.3) is extended to include the void ratio as a state variable, Wu (1999).

$$\boldsymbol{\sigma}^{\circ} = \mathbf{H}(\boldsymbol{\sigma}, \dot{\boldsymbol{\varepsilon}}, e) \tag{4.7}$$

where e represents the void ratio

The idea of incorporating void ratio into the model is simple and effective. A study of the relevant experiments in the literature showed that both the stress level and the void ratio approach the critical state asymptotically under increasing deformation, e.g. Gudehus (1996), Tejchman, et al. (1999). According to whether the specimen is denser or looser than the critical state, the critical state characterized by the critical friction angle φ_c and the critical void ratio e_c will be approached as an upper or lower bound. Note that equation (4.6) consists of linear and nonlinear terms. For a given strain rate the linear and the nonlinear terms give rise to an increase and a decrease of the stress rate respectively. In a critical state, defined by $\boldsymbol{\sigma}^{\circ} = 0$ and $tr\,\dot{\boldsymbol{\varepsilon}} = 0$, there is an equilibrium between the linear and the nonlinear terms. The deviation of the nonlinear term away from the critical state can be viewed as an initial disturbance, which will fade when the critical state is approached. For this, equation (4.6) should be augment by multiplying the nonlinear term with a multiplier $f_d(tr\,\boldsymbol{\sigma}, e)$ which is a density function accounting for the density effect, Pycnotropy. Since the constitutive equation (4.6) is homogenous of the first degree in stress, the tangential stiffness is proportional to the stress level. By making use of this feature, the tangential stiffness can be altered by multiplying equation (4.6) as a whole with a

scalar function, $f_s\,(tr\,\boldsymbol{\sigma}\,,\,e)$, called the stiffness function, without changing the critical state. Equation (4.6) will then be in the form

$$\boldsymbol{\sigma}^{\circ} = f_s(tr\boldsymbol{\sigma},e)\left\{\mathbf{L}(\boldsymbol{\sigma})\dot{\boldsymbol{\varepsilon}} + f_d(tr\boldsymbol{\sigma},e)\,\mathbf{N}(\boldsymbol{\sigma})\,\|\,\dot{\boldsymbol{\varepsilon}}\,\|\right\} \tag{4.8}$$

4.4 WOLFFERSDORF MODEL FORMULATION

Many publications have tried to state a constitutive relation that controls the effect of void ratio and stress level, such as Wu (1999), Kolymbas (1995), Tejchman and Herle et al (1999), Wolffersdorf (1996), and Wu et al. (1994). The proposed model by Wolffersdorf (1996), includes these relations by normalizing the stress tensor and using suitable factor functions for Barotropy and Pycnotropy as follows.

$$\boldsymbol{\sigma}^{\circ} = f_s\frac{1}{tr(\hat{\boldsymbol{\sigma}}.\hat{\boldsymbol{\sigma}})}\left\{\mathrm{F}^2\,\dot{\boldsymbol{\varepsilon}} + a^2 tr(\hat{\boldsymbol{\sigma}}\,\dot{\boldsymbol{\varepsilon}})\hat{\boldsymbol{\sigma}} + f_{\mathrm{d}}\,a\,\mathrm{F}\left[\hat{\boldsymbol{\sigma}} + \hat{\boldsymbol{\sigma}}^{*}\right]\|\,\dot{\boldsymbol{\varepsilon}}\,\|\right\} \tag{4.9}$$

where

$\hat{\boldsymbol{\sigma}} = \boldsymbol{\sigma}/tr\boldsymbol{\sigma}$ Stress ratio

$\hat{\boldsymbol{\sigma}}^{*} = \left(\boldsymbol{\sigma} - \frac{1}{3}tr\boldsymbol{\sigma}\;\mathbf{I}\right)\Big/tr\boldsymbol{\sigma}$ or

$\hat{\boldsymbol{\sigma}}^{*} = \hat{\boldsymbol{\sigma}} - \frac{1}{3}\mathbf{I}$ Deviatoric stress ratio

$\mathbf{I}$ Unit matrix

$$a = \frac{\sqrt{3}(3-\sin\varphi_c)}{2\sqrt{2}\,\sin\varphi_c} \tag{4.10}$$

φ_c Critical friction angle, *material parameter*

$$\mathrm{F} = \sqrt{\frac{1}{8}\tan^2\psi + \frac{2-\tan^2\psi}{2+\sqrt{2}(\tan\psi\,\cos 3\theta)}} - \frac{1}{2\sqrt{2}}\tan\psi$$

ψ The angle between the stress point vector and the octahedral axes, Figure (4.1)

$\tan\psi = \sqrt{3}\,\|\,\hat{\boldsymbol{\sigma}}^{*}\,\|$

θ Reference angle of the stress point on the deviatoric plane, Figure (4.1)

$$\cos 3\theta = -\sqrt{6}\frac{tr\left(\hat{\sigma}^{*3}\right)}{\left[tr\left(\hat{\sigma}^{*2}\right)\right]^{3/2}}$$

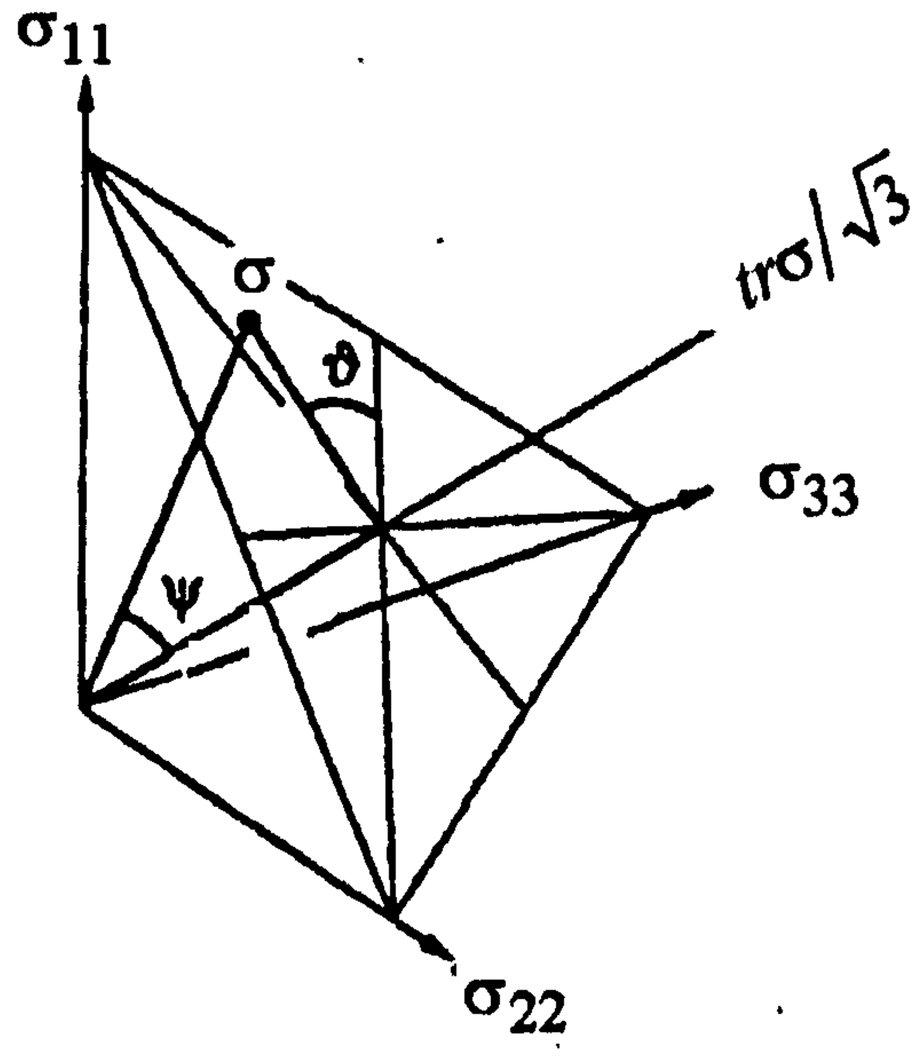

Figure (4.1) Representation of the invariants ψ and θ in the principal stress space, Wolffersdorf (1996)

$$f_s = \frac{h_s}{n}\left(\frac{e_i}{e}\right)^{\beta}\left(\frac{1+e_i}{e_i}\right)\left(\frac{-tr\sigma}{h_s}\right)^{1-n}\left[3+a^2-a\sqrt{3}\left(\frac{e_{io}-e_{do}}{e_{co}-e_{do}}\right)^{\alpha}\right]^{-1} \qquad (4.11)$$

where

h_s Granulate hardness, *material parameter*

n, α, β Material parameters

e_i Upper bound of the void ratios, which decreases with increasing mean skeleton pressure p_s

$$f_d = \left(\frac{e-e_d}{e_c-e_d}\right)^{\alpha} \qquad (4.12)$$

where e_c Critical void ratios, which decreases with increasing mean skeleton pressure p_s

e_d Lower bound of the void ratios

e_{io} Initial value of e_i

e_{co} Initial value e_c

e_{do} Initial value e_d

Referring to equation (4.9) and its components, we have only eight material parameters (identified in italic above) which are φ_c, n, h_s, e_{do}, e_{io}, e_{co}, α, β four of them are independent on σ and e which are h_s, φ_c, e_{co}, e_{do}.

4.4.1 PRESSURE DEPENDENCE OF THE VOID RATIOS

Experimental observation shows that for each granular material there are possible ranges of void ratio values dependent on the stress level, all these values can be plotted as a relation to the stress as shown in Figure (4.2)

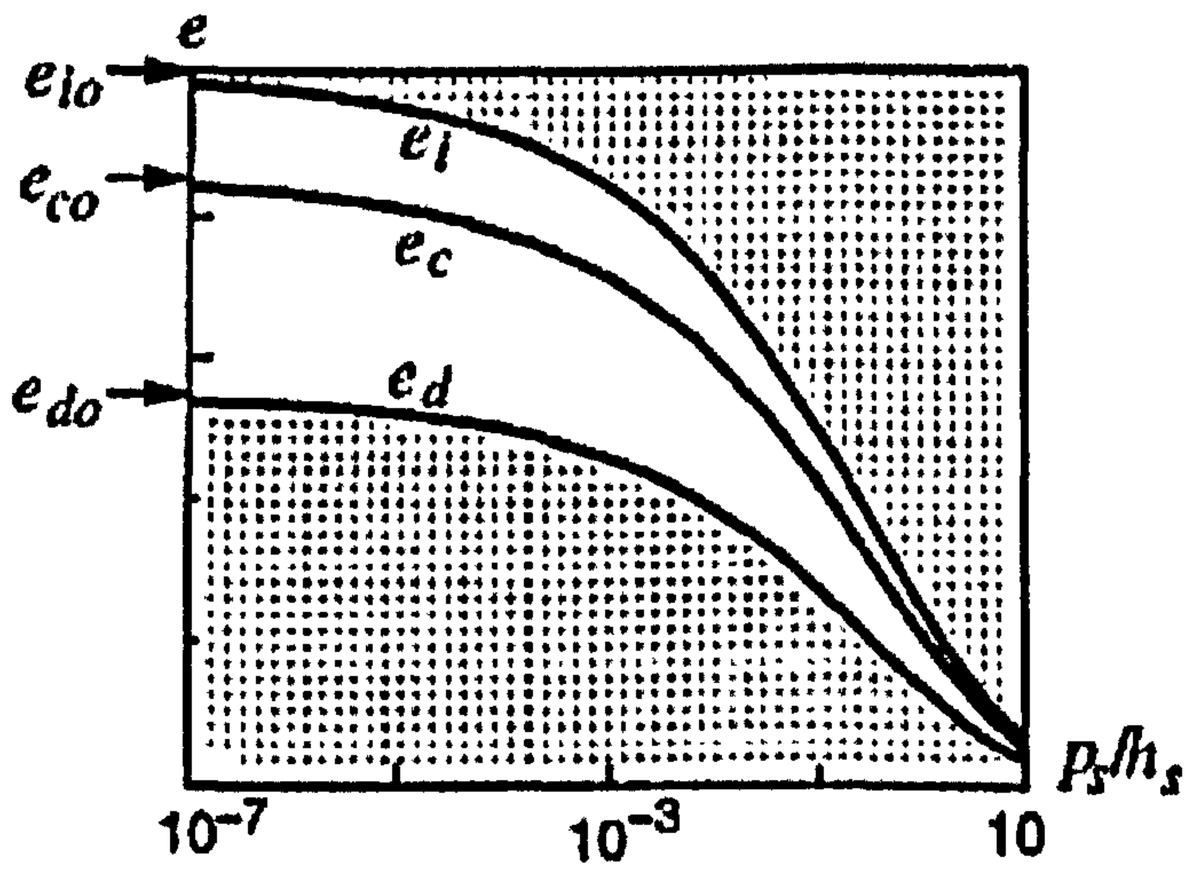

Figure (4.2) Relation between e_i, e_c, e_d and p_s in logarithmic scale, Bauer (1996)

The void ratio bounds shown in Figure (4.2) are; an upper bound of the void ratios (e_i), lower bound of the void ratios (e_d) and critical void ratios (e_c). According to Figure (4.2) e_i, e_c, e_d can be obtained from the characteristic void ratio relation

$$\frac{e_i}{e_{io}} = \frac{e_c}{e_{co}} = \frac{e_d}{e_{do}} = \exp\left[-\left(\frac{-3p_s}{h_s}\right)^n\right], \text{ after Bauer (1996)} \qquad (4.13)$$

where h_s Granulate hardness (kPa)

p_s Mean skeleton pressure (kPa)

$$p_s = \frac{-tr\boldsymbol{\sigma}}{3}$$

During stress increment, the incremental void ratio e can be updated by means of one of the following relations

$$e = e_o \exp\left[-\left(\frac{3p_s}{h_s}\right)^n\right] \qquad \text{If the grains are compressible} \qquad (4.14)$$

$$\dot{e} = (1+e)tr\dot{\boldsymbol{\varepsilon}} \qquad \text{If the grains are incompressible} \qquad (4.15)$$

Substituting p_s then equation (4.13) can be written in the form

$$\frac{e_i}{e_{io}} = \frac{e_c}{e_{co}} = \frac{e_d}{e_{do}} = \exp\left[-\left(\frac{-tr\boldsymbol{\sigma}}{h_s}\right)^n\right] \qquad (4.16)$$

4.4.2 MODEL PARAMETERS IDENTIFICATION

Calibration of the hypoplastic model parameters was carried out by Herle and Gudehus (1999) to insure that all parameters of the hypoplastic model are closely related to the granulometric properties of grain assemblies. An axially symmetric compression case of stress is found to be sufficient to determine the model parameters. I.e.:

$$\boldsymbol{\sigma} = \begin{bmatrix} \sigma_1 & 0 & 0 \\ 0 & \sigma_2 & 0 \\ 0 & 0 & \sigma_2 \end{bmatrix}, \qquad \boldsymbol{\varepsilon} = \begin{bmatrix} \varepsilon_1 & 0 & 0 \\ 0 & \varepsilon_2 & 0 \\ 0 & 0 & \varepsilon_2 \end{bmatrix}$$

where $\sigma_1 = \sigma_a$ represents the axial stress component

$\sigma_2 = \sigma_r$ represents the radial stress component

$\varepsilon_1 = \varepsilon_a$ represents the axial strain component

$\varepsilon_2 = \varepsilon_r$ represents the radial strain component

Hence the tensorial equation, (4.9), is to be reduced into two equations of scalar arguments:

$$\dot{\sigma}_1 = f_s \frac{(\sigma_1 + 2\sigma_2)^2}{\sigma_1^2 + 2\sigma_2^2}\left[\dot{\varepsilon}_1 + a^2 \frac{\sigma_1\dot{\varepsilon}_1 + 2\sigma_2\dot{\varepsilon}_2}{(\sigma_1 + 2\sigma_2)^2}\sigma_1 + f_d \frac{a}{3}\frac{5\sigma_1 - 2\sigma_2}{\sigma_1 + 2\sigma_2}\sqrt{\dot{\varepsilon}_1^2 + 2\dot{\varepsilon}_2^2}\right] \tag{4.17}$$

$$\dot{\sigma}_2 = f_s \frac{(\sigma_1 + 2\sigma_2)^2}{\sigma_1^2 + 2\sigma_2^2}\left[\dot{\varepsilon}_2 + a^2 \frac{\sigma_1\dot{\varepsilon}_1 + 2\sigma_2\dot{\varepsilon}_2}{(\sigma_1 + 2\sigma_2)^2}\sigma_2 + f_d \frac{a}{3}\frac{4\sigma_2 - \sigma_1}{\sigma_1 + 2\sigma_2}\sqrt{\dot{\varepsilon}_1^2 + 2\dot{\varepsilon}_2^2}\right] \tag{4.18}$$

4.4.2.1 CRITICAL FRICTION ANGLE φ_c

The critical friction angle can be determined (simply) from the angle of the repose of dry angular materials, Herle and Gudehus (1999), as shown in Figure (4.3). A small excavation at the toe of the slope is recommended in order to erase the influence of the heap preparation.

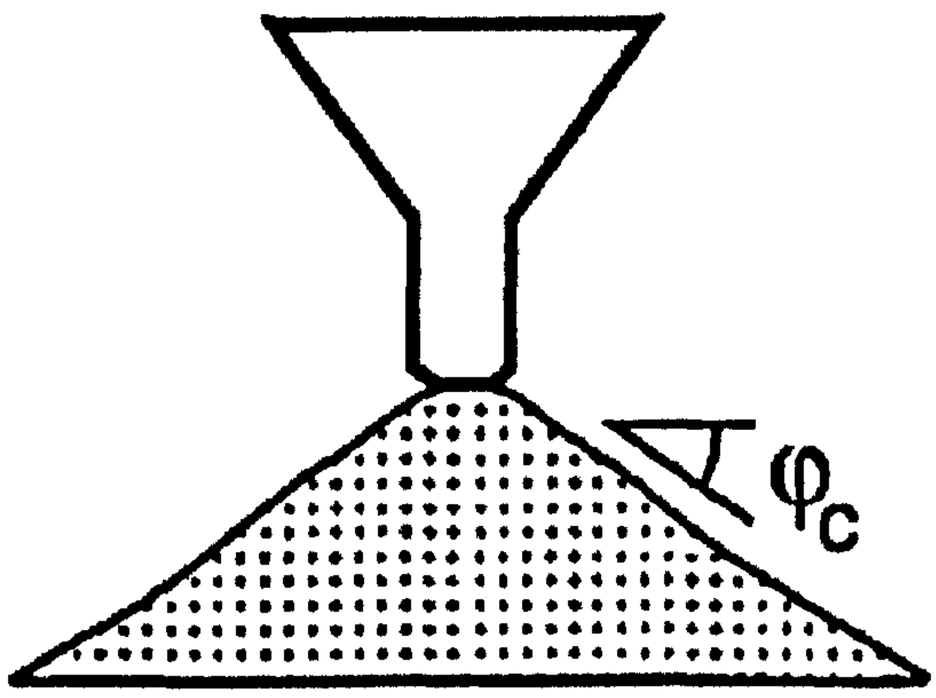

Figure (4.3) Determination of φ_c from the angle of repose

The critical friction angle can be also obtained experimental using cylindrical triaxial test described in section (3.4.2) in Chapter 3. A cylindrical sampled compression is carried out with constant mean stress (i.e. $\dot{\sigma}_1 + 2\dot{\sigma}_2 = 0$) until it reaches the critical state characterized by zero dilatancy (i.e. $\dot{\varepsilon}_1 + 2\dot{\varepsilon}_2 = 0$). At critical state $e = e_c$ and hence, from equation (4.12), $f_d = 1$. Substituting these conditions into equations (4.17) and (4.18) leads to

$$a = \frac{\sqrt{6}}{2}\left(\frac{\sigma_1 + 2\sigma_2}{\sigma_1 - \sigma_2}\right) \tag{4.19}$$

Substitute the value of a in equation (4.10) into equation (4.19) Then φ_c can be obtained from the following relation

$$\sin\varphi_c = \frac{\sigma_1 - \sigma_2}{\sigma_1 + \sigma_2} \tag{4.20}$$

4.4.2.2 EXPONENT n

The exponent n takes into account the pressure-sensitivity of a grain skeleton, thus allowing for a non-proportional increase of the incremental stiffness with increasing mean skeleton pressure (p_s). In order to determine n, a compression test with an initially very loose specimen has to be performed using the Oedometer test or a soft Oedometer device, Kolymbas and Bauer (1993). During a proportional compression, starting from a suitable void ratio e_{p_0} at zero pressure, the characteristic void ratio relation can be used to describe n.

$$e_p = e_{p_0} \exp\left[-\left(\frac{-tr\sigma}{h_s}\right)^n\right] \tag{4.21}$$

The relation between the proportion void ratio e_p and the mean skeleton pressure p_s is as shown in Figure (4.4)

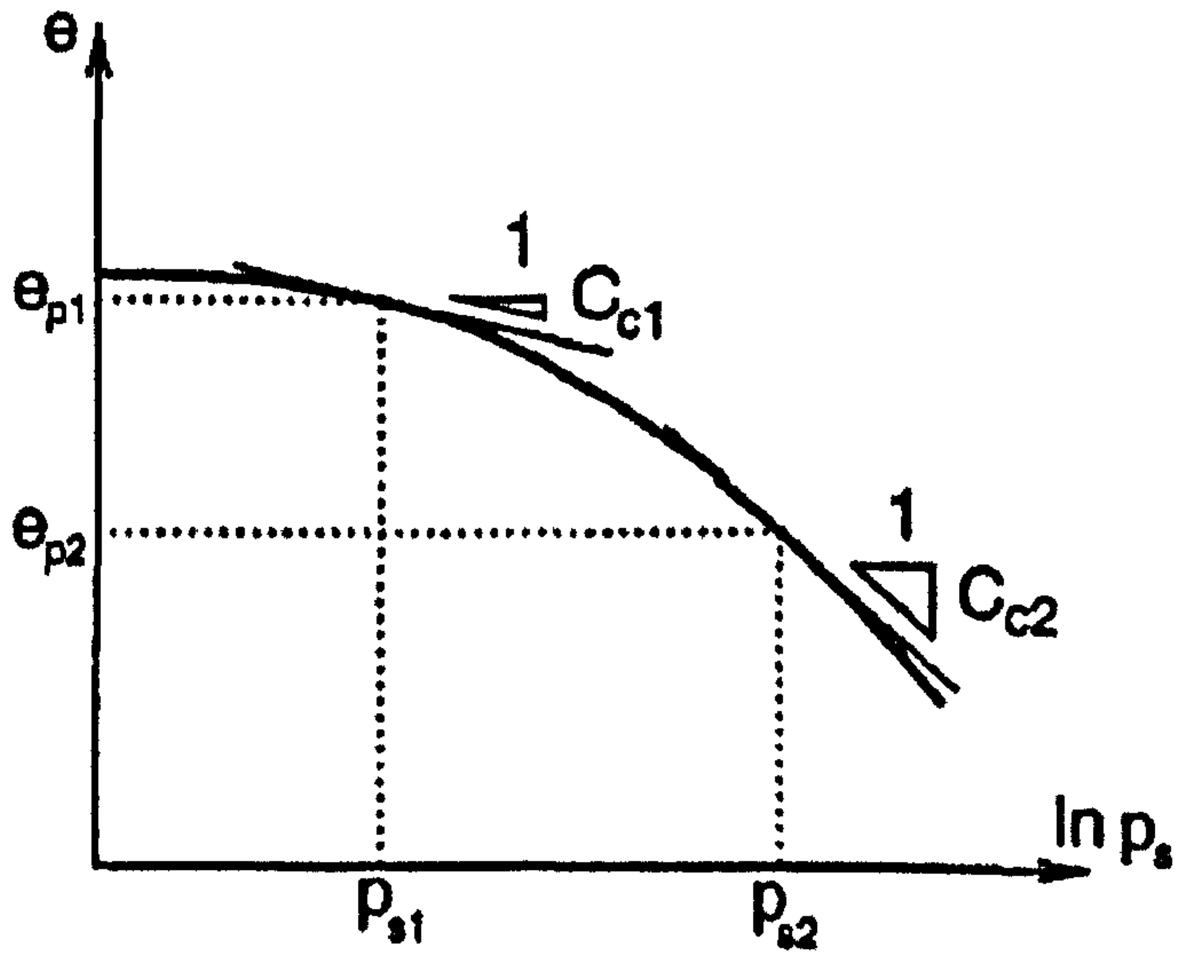

Figure (4.4) Determination of n , Herle and Gudehus (1999)

Considering a range from p_{s1} to p_{s2} with corresponding void ratios e_{p1} and e_{p2} and compression indices C_{c1} and C_{c2} at the boundaries of this pressure range, the value of n can be calculated from the equation

$$n = \frac{\ln\left(e_{p1}\, C_{c2} / e_{p2}\, C_{c1}\right)}{\ln\left(p_{s2} / p_{s1}\right)} \tag{4.22}$$

4.4.2.3 GRANULATE HARDNESS h_s

The granulate hardness h_s is the only hypoplastic material parameter with the units of stress. h_s Is used as a reference pressure and it does not mean the hardness of a single grain. Using the same procedure developed to determine n, h_s can be obtained from the relation

$$h_s = -tr\sigma \left(\frac{n e_p}{C_c}\right)^{1/n} \tag{4.23}$$

Knowing n and for any void ratio e_p, we can get $p_s = -\frac{1}{3} tr\sigma$ and hence C_c from a plot as in Figure (4.4).

4.4.2.4 MINIMUM VOID RATIO e_{do} AT ZERO PRESSURE

The best densification of a granular material can be generally reached by means of cyclic shearing with small amplitude under constant pressure. From the characteristic void ratios, if a single value of e_d is known together with h_s and n, e_{do} can be obtained from the relation

$$e_{do} = e_d \exp\left[\left(\frac{3p_s}{h_s}\right)^n\right] \tag{4.24}$$

with $p_s = -\frac{1}{3} tr\sigma$

4.4.2.5 MAXIMUM VOID RATIO e_{io} AT ZERO PRESSURE

e_{io} is the maximum void ratio of a simple grain skeleton, which is reached during an isotropic consolidation of a grain suspension in a gravity-free space. It is almost impossible to determine e_{io} experimentally but it can be calculated by some idealization using the same procedure of determining e_{do}.

If a single value of e_i is known together with h_s and n, e_{io} can be obtained from the relation

$$e_{io} = e_i \exp\left[\left(\frac{3p_s}{h_s}\right)^n\right] \tag{4.25}$$

4.4.2.6 CRITICAL VOID RATIO e_{co} AT ZERO PRESSURE

e_{co} is the critical void ratio at zero pressure. Like e_{do} and e_{io}, e_{co} can be obtained from the relation

$$e_{co} = e_c \exp\left[\left(\frac{3p_s}{h_s}\right)^n\right] \tag{4.26}$$

4.4.2.7 EXPONENT α

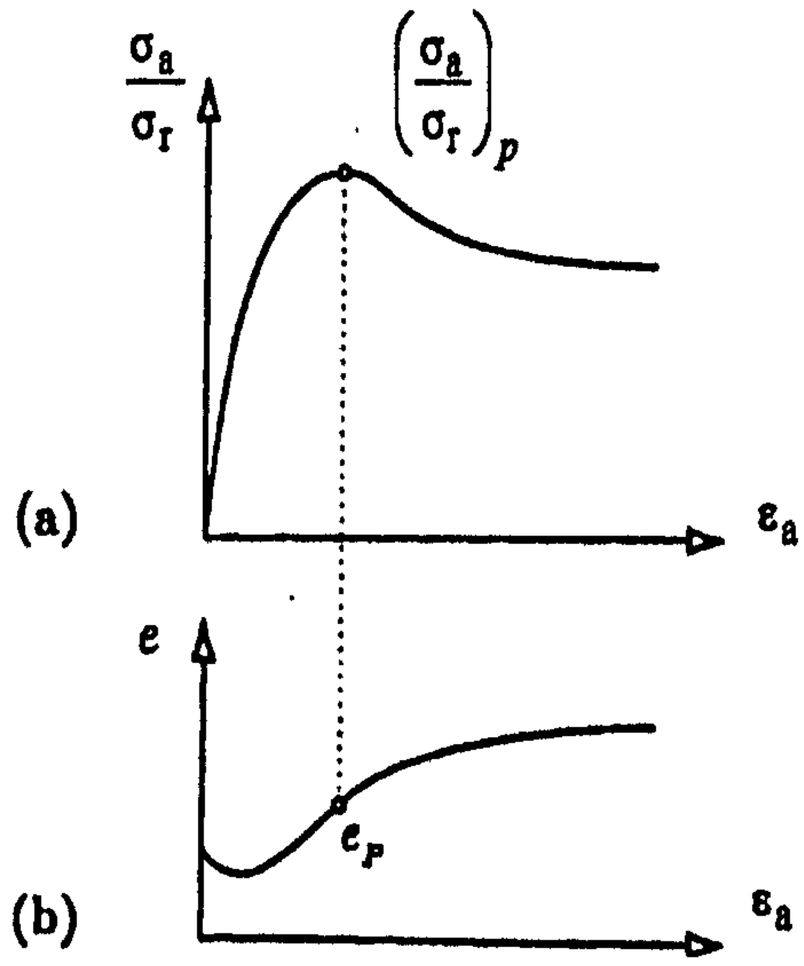

Figure (4.5) Stress ratio – void ratio relation, Herle and Gudehus (1999)

The relation of stress ratio and void ratio from a triaxial test at the peak shown in Figure (4.5a) can be expressed as

$$K_p = \left(\frac{\sigma_a}{\sigma_r}\right)_p$$

where subscript p stands for peak value as shown in Figure (4.5)

For a peak state characterized with vanish stress rate $\dot{\sigma}_a = 0$, α can be obtained from equation (4.17) as

$$\alpha = \frac{\ln\left[6\dfrac{(2+K_p)^2 + a^2 K_p(K_p - 1 - \tan\upsilon_p)}{a(2+K_p)(5K_p-2)\sqrt{4+2(1+\tan\upsilon_p)^2}}\right]}{\ln[(e-e_d)/(e_c-e_d)]} \tag{4.27}$$

where

$$a = \frac{\sqrt{3}(3-\sin\varphi_c)}{2\sqrt{2}\sin\varphi_c}$$

$$K_p = \frac{1+\sin\varphi_p}{1-\sin\varphi_p}$$

$$\tan\upsilon_p = 2\frac{K_p - 4 + 5AK_p^2 - 2AK_p}{(5K_p-2)(1+2A)} - 1$$

$$A = \frac{a^2}{(2+K_p)^2}\left[1 - \frac{K_p(4-K_p)}{5K_p-2}\right]$$

$$\sin\varphi_p = \left(\frac{\sigma_a - \sigma_r}{\sigma_a + \sigma_r}\right)_p$$

4.4.2.8 EXPONENT β

The factor f_s in equation (4.9) increases the calculated incremental stiffness modulus with increasing density and pressure. The exponent β plays an important role only if the current void ratio e is substantially lower than the maximum void ratio e_i. For a measured E corresponding to a particular pressure, density and direction of stretching, β can be calculated from the relation

$$\beta = \frac{\ln\left[E \dfrac{3 + a^2 - f_{do}\, a\sqrt{3}}{3 + a^2 - f_d\, a\sqrt{3}} \dfrac{e_i}{1 + e_i} \dfrac{n}{h_s} \left(\dfrac{3 p_s}{h_s} \right)^{n+1} \right]}{\ln(e_i / e)} \tag{4.28}$$

Where

$$f_{do} = \frac{e_{io} - e_{do}}{e_{co} - e_{do}}$$

$$f_d = \left(\frac{e - e_d}{e_c - e_d} \right)^{\alpha}$$

E is the incremental stiffness modulus (Young's modulus).

For any void ratio e, in the triaxial test, knowing a measured a value of $\dot{\sigma}_a$ and $\dot{\varepsilon}_a$ then E can be obtained from the relation $E = \dfrac{\dot{\sigma}_a}{\dot{\varepsilon}_a}$

Finally the hypoplastic model parameters for various different sand types are summarized in Table [A.1] after Herle and Gudehus (1999).

4.5 MODEL MODIFICATION FOR MONOTONIC LOADING

Some additional aspects should be taken into account when dealing with monotonic loading with high shear deformation and progressive failure required in situations like earth moving machinery or mechanical mine clearing equipment. These aspects are described below:

4.5.1 CRITICAL STATE

A critical state (subscript c) is defined by a vanishing stress rate under a constant rate of deformation, i.e. $\boldsymbol{\sigma}_c^\circ = \mathbf{0}$. It is characterized by a critical stress and critical void ratio. For the constitutive modeling of critical states the following assumptions should to be used, after Bauer (2000)

1. A critical state is characterized by an effective critical stress and an associated critical void ratio, which can be reached by sufficiently large monotonic shearing.
2. For the same deviator direction the ratios of the critical stress components are independent of the mean pressure.
3. The critical void ratio decreases with the mean effective pressure and is independent of the initial void ratio.

Based on these assumptions the set of all critical stress states can be represented by a single surface in the principal stress component space, which is called critical stress surface (CSS). It follows from the linear dependence of the critical stress components on the mean pressure that the CSS is a cone in a principal stress component space Figure (4.6a). In earlier hypoplastic relations the CSS could only be determined numerically, Wu and Bauer (1993), Gudehus (1996) and Bauer (1996), however it was shown that a special form enables an explicit analytical relation to describe the critical stress states by a separate factor. This factor allows the incorporation of any static limit condition with a conical CSS.

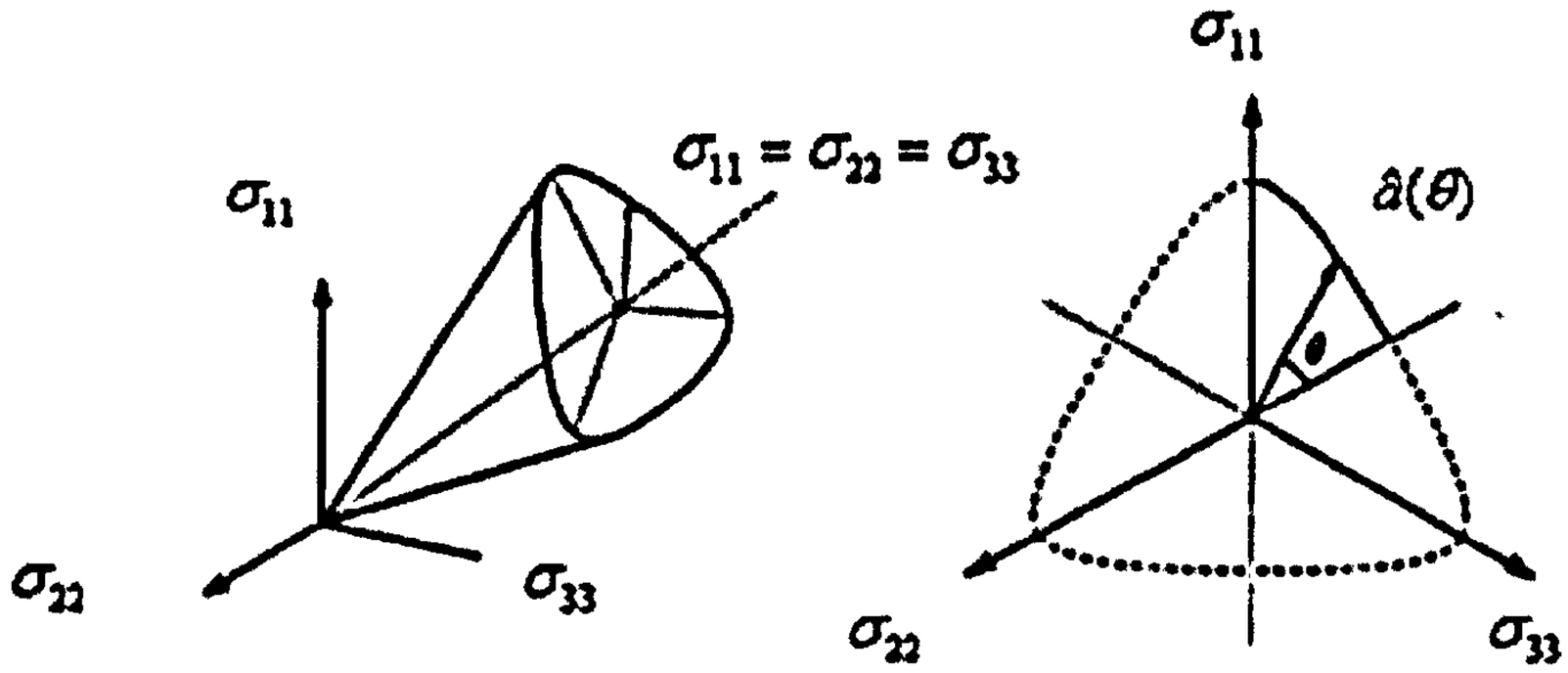

Figure (4.6) Critical stress surface, Bauer (2000): (a) in principle stresses space, (b) in π-plane

Hence, a function $\hat{a}(\theta)$ is embedded within the hypoplastic constitutive equation as follows, Bauer (2000):

Equation (4.9), (4.11) can be changed to

$$\boldsymbol{\sigma}^{\circ} = f_s \left\{ \hat{a}^2 \dot{\boldsymbol{\varepsilon}} + \hat{\boldsymbol{\sigma}}\, tr(\hat{\boldsymbol{\sigma}}\, \dot{\boldsymbol{\varepsilon}}) + f_d\, \hat{a} \left[\hat{\boldsymbol{\sigma}} + \hat{\boldsymbol{\sigma}}^* \right] \| \dot{\boldsymbol{\varepsilon}} \| \right\} \tag{4.29}$$

$$f_s = f_e f_b \frac{1}{tr(\hat{\boldsymbol{\sigma}}^2)} \tag{4.30}$$

where $\hat{a}(\theta)$ represents the radius of intersection between the CSS and the π-plane as shown in Figure (4.6b)

$$\hat{a} = \frac{\sin\varphi_c}{3 - \sin\varphi_c} \left[\sqrt{\frac{\frac{8}{3} - 3\left\|\hat{\boldsymbol{\sigma}}^*\right\|^2 + \sqrt{3/2}\left\|\hat{\boldsymbol{\sigma}}^*\right\|^2 \cos(3\theta)}{1 + \sqrt{3/2}\left\|\hat{\boldsymbol{\sigma}}^*\right\| \cos(3\theta)}} - \left\|\hat{\boldsymbol{\sigma}}^*\right\| \right] \tag{4.31}$$

$$f_b = \frac{h_s}{n} \left(\frac{1+e_i}{e_i} \right) \left(\frac{-tr\boldsymbol{\sigma}}{h_s} \right)^{1-n} \left[3\,\hat{a}^2 + 1 - \hat{a}\sqrt{3} \left(\frac{e_{io} - e_{do}}{e_{co} - e_{do}} \right)^{\alpha} \right]^{-1}$$

$$f_e = \left(\frac{e_i}{e} \right)^{\beta}$$

4.5.2 SELECTION OF THE OBJECTIVE STRESS RATE

Shearing of a material is accompanied by rotation of the principal stress axes, so that the use of a suitable objective stress rate is important to describe large deformations. The time derivative of the Cauchy stress, i.e. $\dot{\sigma} = d\sigma/dt$, does not only express the part of the stress rate resulting from stretching but it also expresses the part resulting from material rotation. In order to take into consideration stationary states with large amounts of shearing the objective stress rate and the time derivative of the Cauchy stress must vanish simultaneously with the volumetric strain rate. Bauer (2000) has proved that the Jaumann stress rate introduced in equation (4.6) is not suitable for large deformation. The Green and Naghdi stress rate has been shown to be more suitable for representation of the stress rate in large shear deformation. The Green and Naghdi stress rate can be described by the following equation

$$\sigma^{\circ} = \dot{\sigma} - \Omega\sigma + \sigma\Omega \tag{4.32}$$

where, Ω is the material angular velocity tensor.

$\Omega = \dot{\mathbf{R}}\,\mathbf{R}^{T}$, $\mathbf{R}$ is the rotation tensor

$$\dot{\mathbf{R}} = \frac{\mathbf{R} - \mathbf{R}_0}{dt}$$

$$\mathbf{R} = \mathbf{V}^{-1}\,\mathbf{F}$$

$$\mathbf{V} = \frac{I_1 I_3 [I] + (I_1^2 - I_2)[\mathbf{B}] - [\mathbf{B}^2]}{I_1 I_2 - I_3}$$

$$I_1 = \frac{\sqrt{\lambda_1} + \sqrt{\lambda_2} + \sqrt{\lambda_3}}{\sqrt{\lambda_1 + \lambda_2 + \lambda_3}} \sqrt{tr(\mathbf{B})}$$

where $\lambda_1, \lambda_2, \lambda_3$ Are the eigenvalues of the stress tensor

$$I_2 = \frac{1}{2}\left[I_1^2 - tr(\mathbf{B})\right]$$

$$I_3 = \sqrt{\det(\mathbf{B})}$$

$$\mathbf{B} = \mathbf{F}\,\mathbf{F}^{T}$$

$$\mathbf{R}_0 = \mathbf{V}_0^{-1}\,\mathbf{F}_o$$

$$\mathbf{V}_o = \frac{I_1 I_3 [I] + (I_1^2 - I_2)[\mathbf{B}_o] - [\mathbf{B}_o{}^2]}{I_1 I_2 - I_3}$$

$$\mathbf{B}_o = \mathbf{F}_o \, \mathbf{F}_o{}^{\mathrm{T}}$$

$\mathbf{F}_o$ is the deformation gradient at the beginning of the increment

$\mathbf{F}$ is the deformation gradient at the end of the increment.

4.5.3 EFFECT OF STRAIN RATE (RATE DEPENDENCY)

The hypoplastic equation is a rate type tensorial function but it is rate independent from the material behaviour point of view. In fact the mechanical behaviour of granular materials is commonly assumed to be time independent. However investigations have been done, Prisco and Imposimato (1996), to study the effect of strain rate using standard triaxial tests.

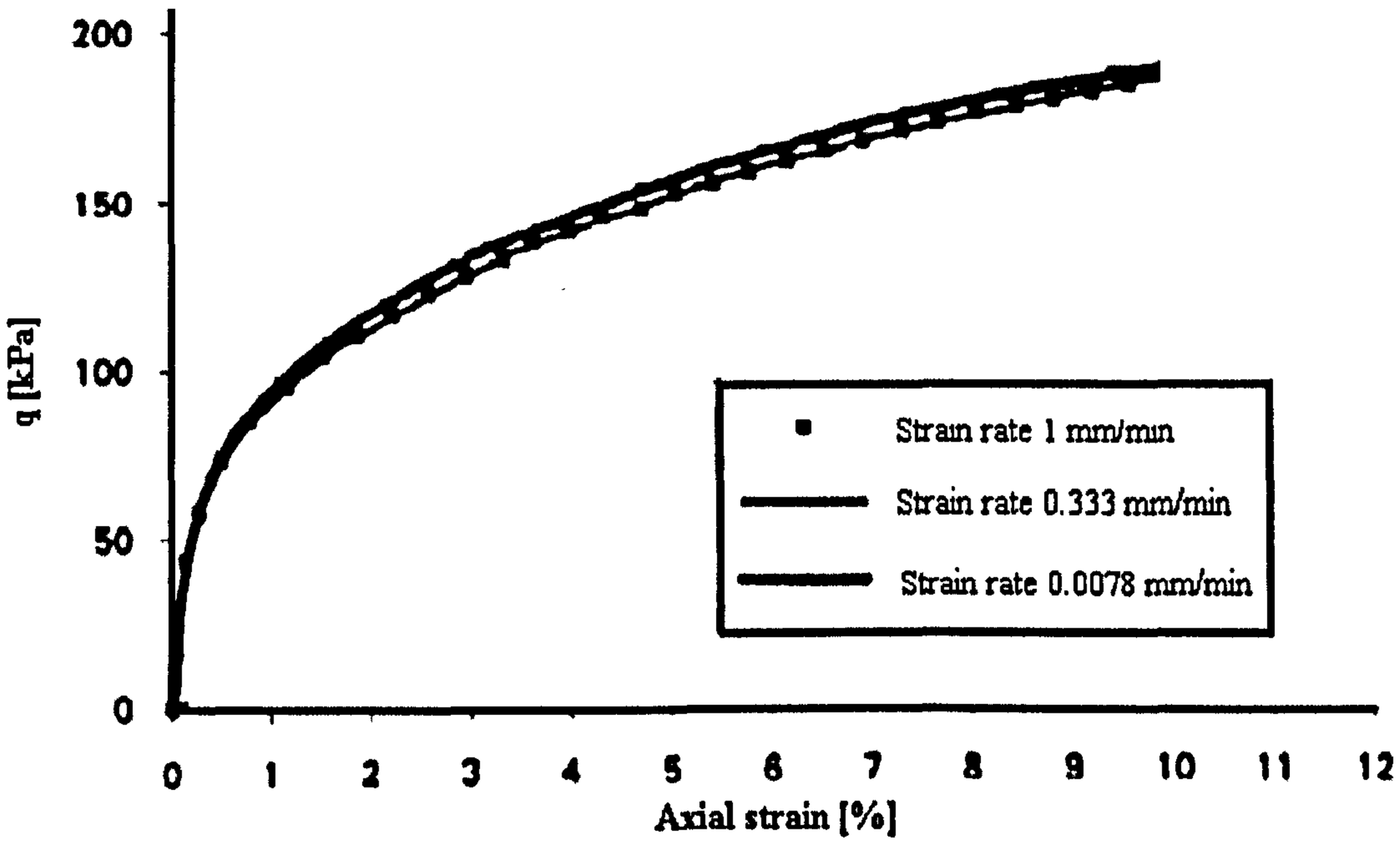

Figure (4.7) Rate effect on sand behaviour, Prisco and Imposimato (1996)

Figure (4.7) presents stress-strain relationship for a loose sand specimen at different strain rates. The figure reveals an insignificant effect of the strain rate on the stress. The strain rate effect may be significant in high speed cutting such as in rotary flails but its effect decreases with low cutting speed such as in mine clearing equipment.

4.6 NUMERICAL INTEGRATION OF THE PROPOSED MODEL

The implementation of the model for finite element analysis requires the development of appropriate algorithms to integrate the rate equation (4.6) over a finite strain increment. To begin with these algorithms, they need to be thoroughly tested and verified. The hypoplastic equation, (4.6), is a non linear ordinary differential equation in a tensorial form hence two different classes of integration schemes are considered in this study, Chapra and Canal (2002):

1. Implicit one-step algorithms
    - Euler forward
    - Generalized Mid-point
    - Euler backward
2. Explicit adaptive algorithms
    - RKF-56 (Runge-Kutta Fehlberg)

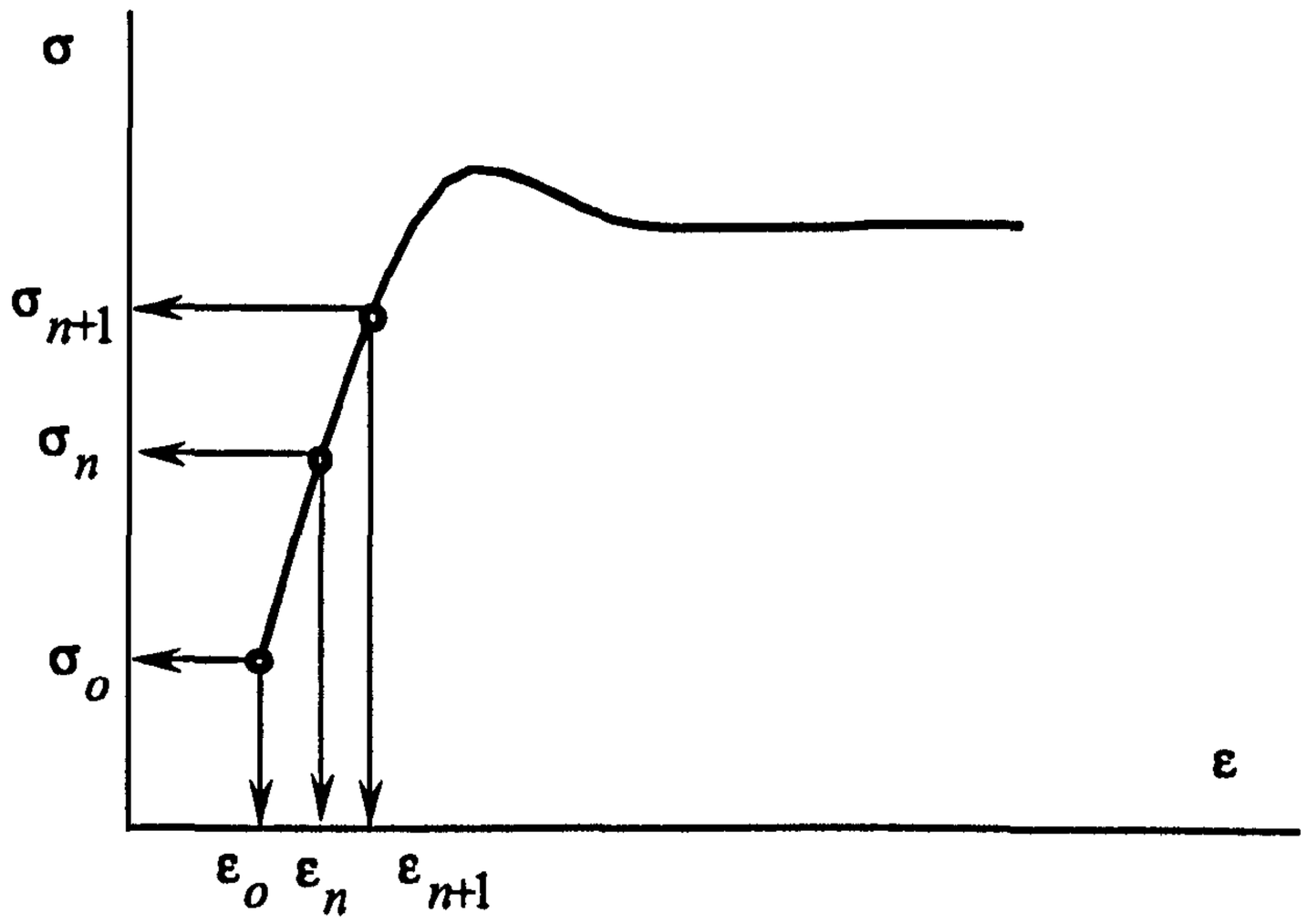

Figure (4.8) Incremental stress-strain relation

Firstly, the subscript '*n*' used in this section does not related to the hypoplastic material parameter *n*. Knowing the initial state $(\varepsilon_o, \sigma_o)$, starting from present increment *n* with state $(\varepsilon_n, \sigma_n)$ the problem to be solved is to obtain the stress at the

next increment $n+1$ ($\boldsymbol{\sigma}_{n+1}$) for a given strain increment $\Delta\boldsymbol{\varepsilon}_{n+1} = (\boldsymbol{\varepsilon}_{n+1} - \boldsymbol{\varepsilon}_n)$ over time increment $\Delta t = (t_{n+1} - t_n)$, should be known as shown in Figure (4.8).

The accuracy of the solution is strongly dependent on the increment size (or step size used to increment). In order to obtain reasonable results, care should be taken when selecting the step size. Many applications involve ordinary differential equations (ODEs) which solution exhibit some regions requiring a relatively small step-size for reasonable accuracy, Zill and Cullen (1997). A key is to develop adaptive algorithms that automatically vary the step size to accommodate local peculiarities in the solution.

4.6.1 IMPLICIT ONE-STEP ALGORITHMS

The first class of integration algorithms considered is based on the following implicit recurrence formula based on equation (4.6):

$$\boldsymbol{\sigma}_{n+1} = \boldsymbol{\sigma}_n + \mathbf{L}_{n+\alpha}\,\Delta\boldsymbol{\varepsilon}_{n+1} + \mathbf{N}_{n+\alpha}\,\|\,\Delta\boldsymbol{\varepsilon}_{n+1}\,\| \tag{4.33}$$

where

$$\mathbf{L}_{n+\alpha} = \mathbf{L}(\boldsymbol{\sigma}_{n+\alpha})$$

$$\mathbf{N}_{n+\alpha} = \mathbf{N}(\boldsymbol{\sigma}_{n+\alpha})$$

$$\boldsymbol{\sigma}_{n+\alpha} = (1-\alpha)\boldsymbol{\sigma}_n + \alpha\,\boldsymbol{\sigma}_{n+1}$$

α A factor, different from the hypoplastic material parameter, used to switch between the three integration schemes, Euler forward ($\alpha = 0$), Euler backward ($\alpha = 1$) and Mid-point ($\alpha = 0.5$), Tamagnini et al. (2000).

The flow chart in Figure (4.9) represents the main routine of the one-step algorithms. From the figure, the MAIN routine divides the strain increment into multiple sub-increments, adjusting the incremental time step and controls the solution during the step increment. Subroutine SIGMA, Figure (4.10) calculates the stress increment and the state variable using the hypoplastic equation.

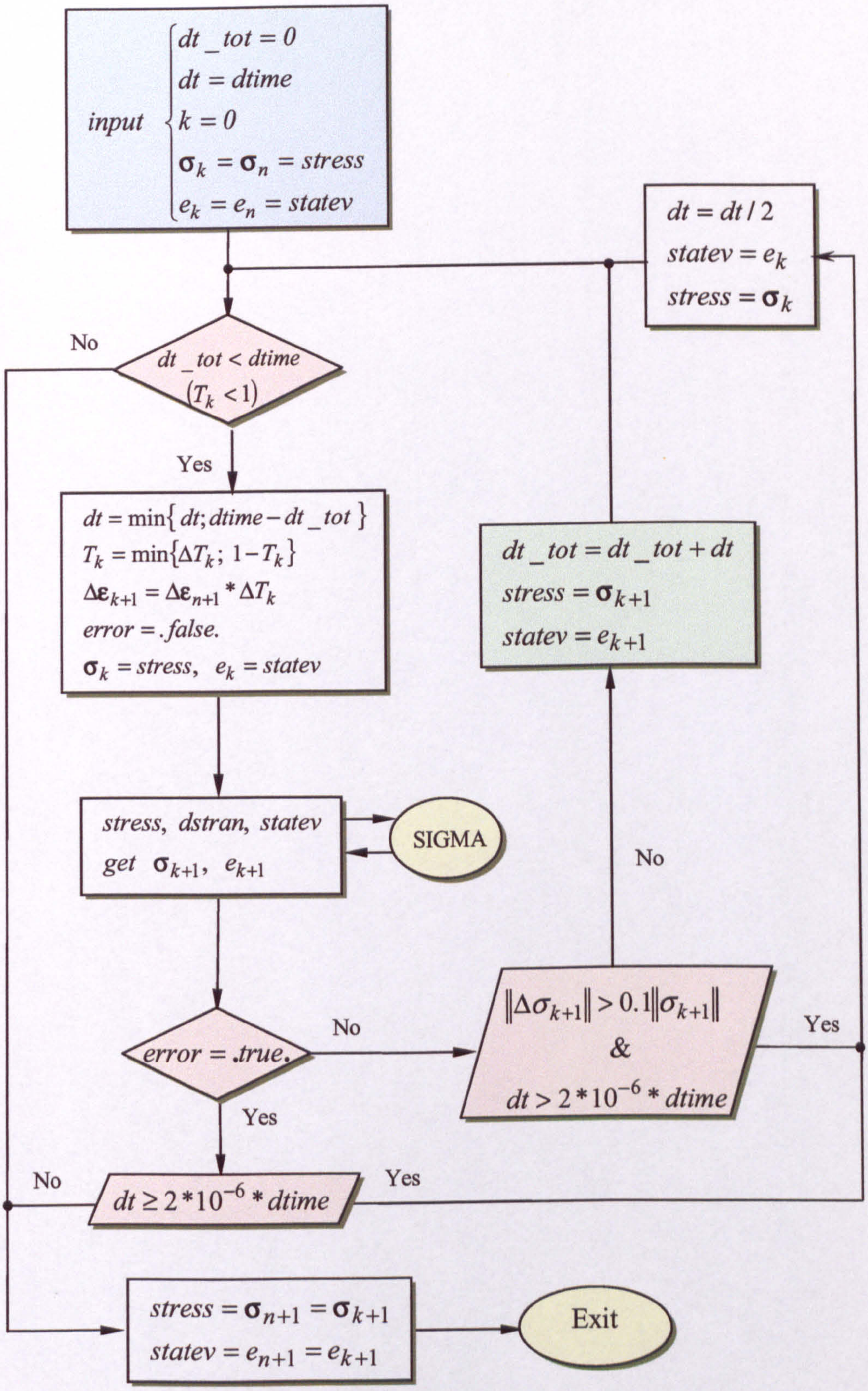

Figure (4.9) MAIN routine of one-step algorithm

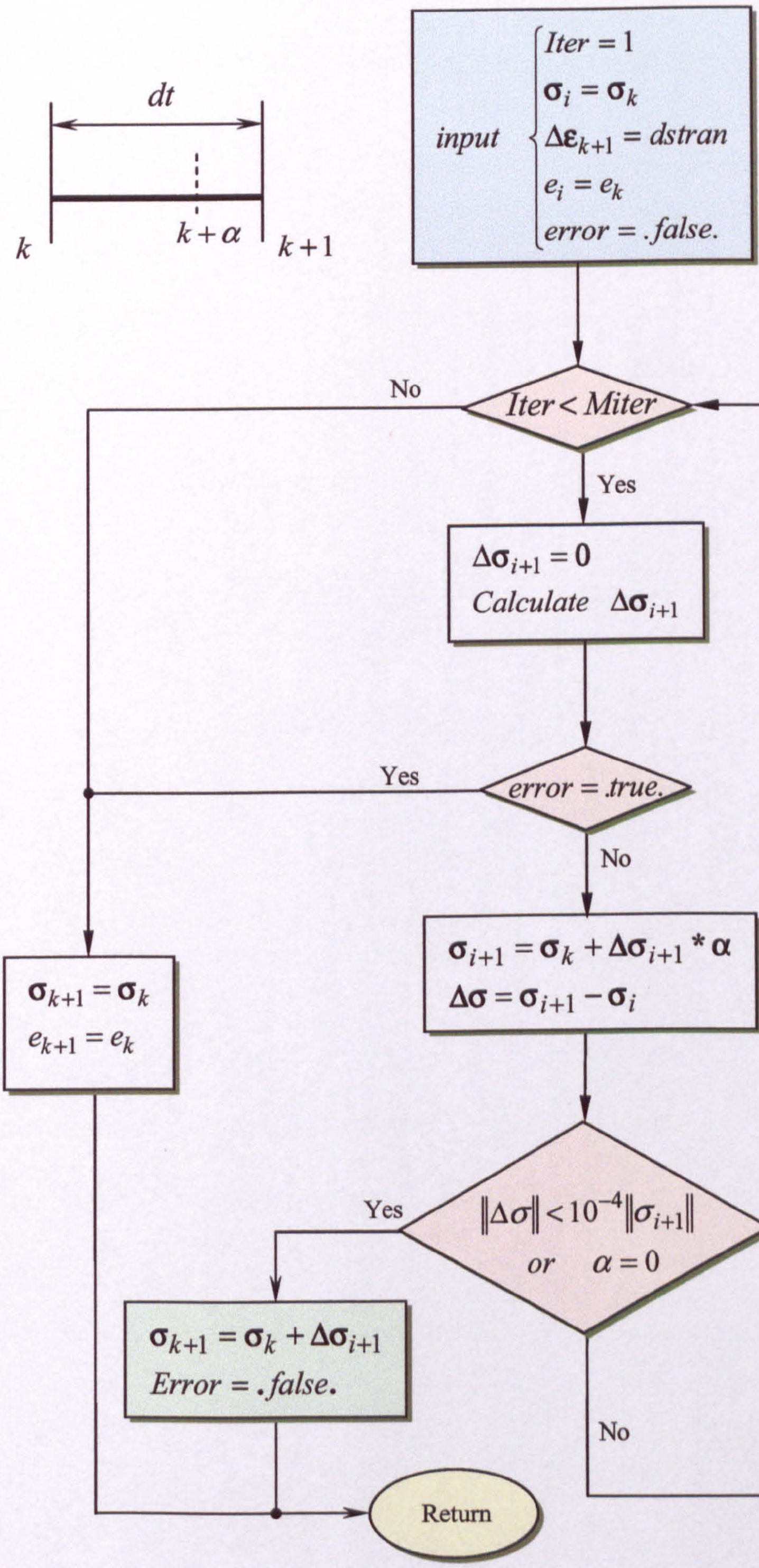

Figure (4.10) Subroutine SIGMA

4.6.2 EXPLICIT ADAPTIVE RUNGE-KUTTA-FEHLBERG ALGORITHM

The Runge-Kutta-Fehlberg algorithm is an explicit scheme with adaptive sub-stepping size control, in which the difference between the solutions obtained with two embedded Runge-Kutta algorithms of different order of accuracy (Runge-Kutta 5, Runge-Kutta 6) is used to extrapolate the substep size needed to achieve a prescribed accuracy of the solution, Tamagnini, Viggiani, et al. (2000).

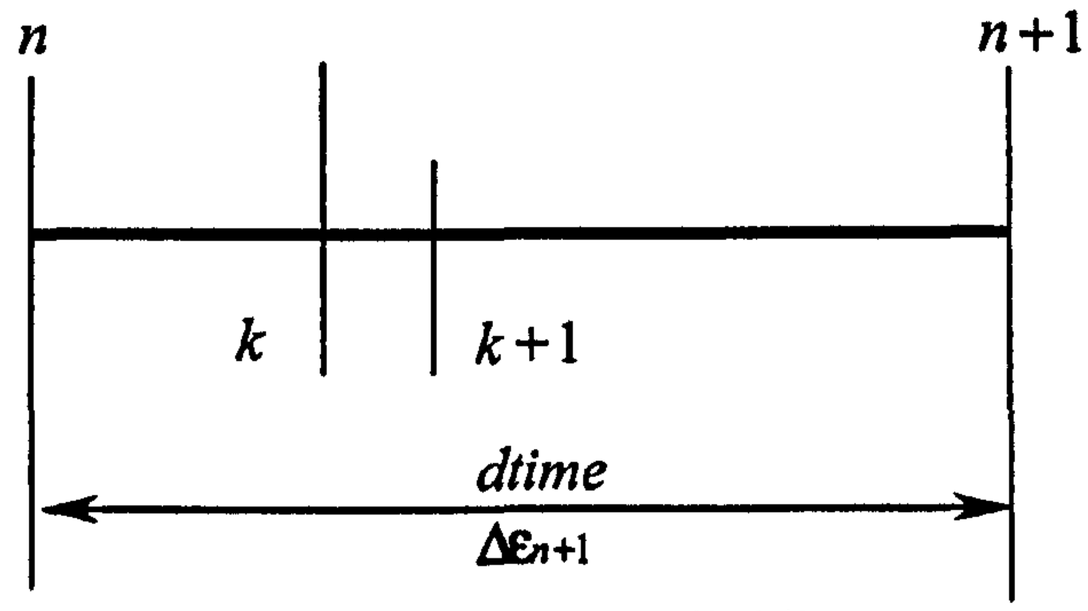

Figure (4.11) Step dividing

For a substep k in the time interval $(t_{n+1} - t_n)$, Figure (4.11), we use dimensionless size $\Delta T_k \in (0,1)$ given by the equation

$$\Delta T_k = \frac{t_{k+1} - t_k}{t_{n+1} - t_n} \tag{4.34}$$

Then two different numerical solutions of the hypoplastic differential equation (4.29) are obtained simultaneously

$$\tilde{\boldsymbol{\sigma}}_{k+1} = \boldsymbol{\sigma}_k + \boldsymbol{\Phi}_1 \Delta T_k \tag{4.35}$$

$$\hat{\boldsymbol{\sigma}}_{k+1} = \boldsymbol{\sigma}_k + \boldsymbol{\Phi}_2 \Delta T_k \tag{4.36}$$

where

$$\boldsymbol{\Phi}_1 = \sum_{J=0}^{5} \tilde{C}_J F_J(\boldsymbol{\sigma}_k, \Delta\boldsymbol{\varepsilon}_{n+1}, \Delta T_k) \tag{4.37}$$

$$\boldsymbol{\Phi}_2 = \sum_{J=0}^{6} \hat{C}_J F_J(\boldsymbol{\sigma}_k, \Delta\boldsymbol{\varepsilon}_{n+1}, \Delta T_k) \tag{4.38}$$

$$F_J = F\left(\boldsymbol{\sigma}_k + \Delta T_k \sum_{l=0}^{J-1} \beta_{Jl} F_l, \Delta\boldsymbol{\varepsilon}_{n+1}\right) \tag{4.39}$$

with $F_o = F(\boldsymbol{\varepsilon}_0, \boldsymbol{\sigma}_0)$

$\tilde{C}_J$, $\hat{C}_J$ and β_{Jl} are parameters for the Runge-Kutta-Fehlberg shown in table [A.2] after Store and Bulirch (1993).

Then the error is given by $r_k = \dfrac{||\hat{\boldsymbol{\sigma}}_{k+1} - \tilde{\boldsymbol{\sigma}}_{k+1}||}{||\hat{\boldsymbol{\sigma}}_{k+1}||}$ (4.40)

where

ΔT_{k+1}	Size of next sup-step
ΔT_k	Size of the present sup-step
T_k	Time of sub-step k / time at step n+1

The integration of the k^{th} sub-step is assumed to be successful if the error is within some acceptable tolerance TOL ($r_k \leq TOL$). When this tolerance is met; the stress will be equal to the solution obtained from the higher order Runge-Kutta i.e. $\boldsymbol{\sigma}_{k+1} = \hat{\boldsymbol{\sigma}}_{k+1}$. Subsequently the time of the next sub-step is adjusted as shown in the flow chart, Figure (4.12).

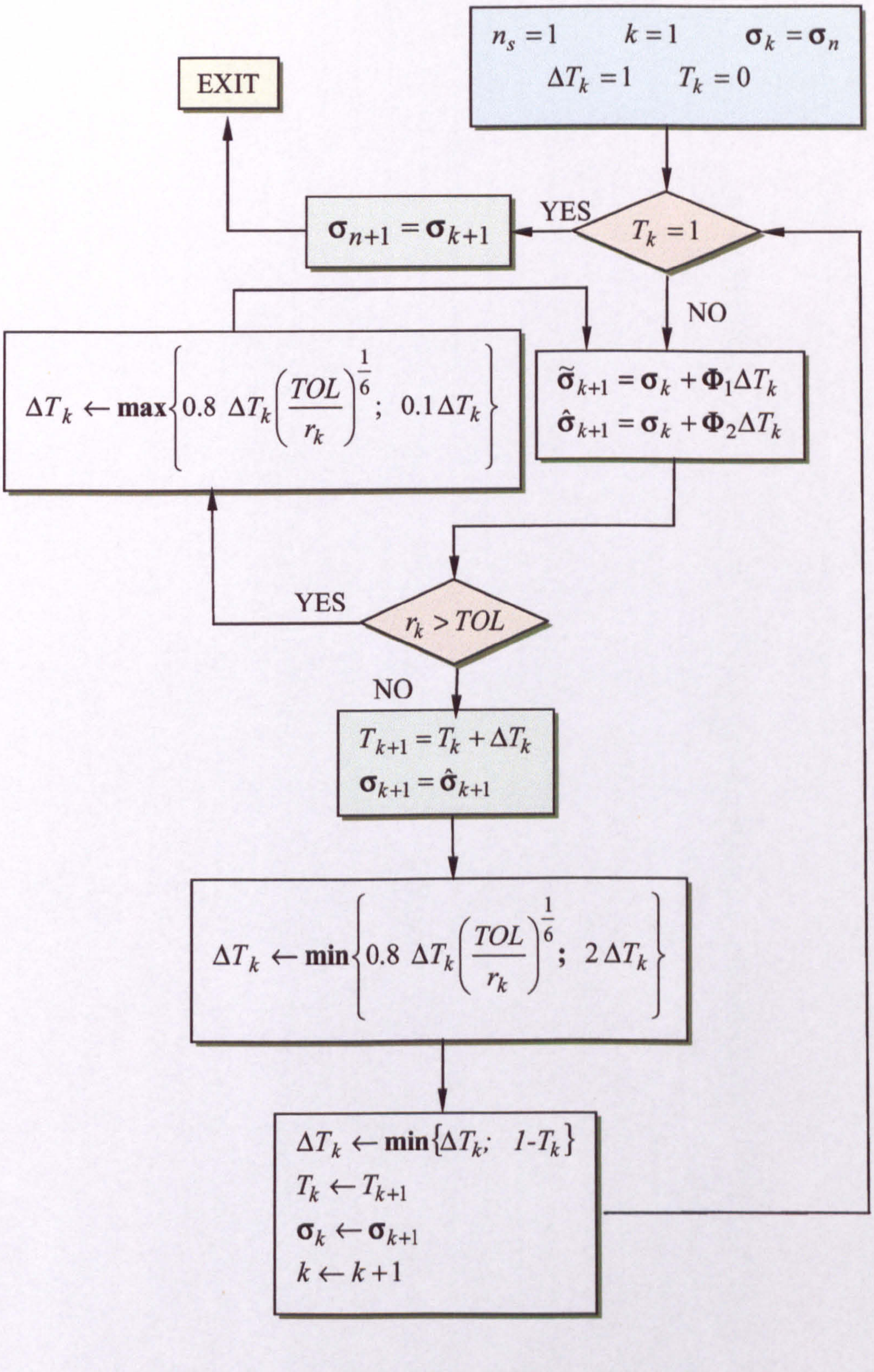

Figure (4.12) Flow chart of adaptive stress point algorithm

When the Runge-Kutta-Fehlberg algorithm was used, at its present state, to simulate the Oedometer test, using a FORTRAN program written especially for this, with a large step size it led to inaccurate solution hence the Runge-Kutta-Fehlberg algorithm should be applied to an infinite or a very small strain increment. To account for the change of the stress during these small strain increments, the 'one step algorithm' is developed in the following manner:

To get the stress σ for a given strain ε, the strain has to be divided first into small increments '*ns* steps' hence the strain increment for each step '$\Delta\varepsilon$' will be equal to ε/ns. Knowing the initial stress at the beginning of a step σ_n and the strain increment at the end of this step $\Delta\varepsilon_{n+1}$, the incremental stress σ_{n+1} due to an incremental strain $\Delta\varepsilon_{n+1}$ over a time interval $\Delta t = (t_{n+1} - t_n)$ through k sub-step can be obtained as shown in the flow chart, Figure (4.13).

The FORTRAN code of the adaptive Runge-Kutta-Fehlberg algorithm written using a FORTRAN 77 compiler, Koffman (1993), is listed in Appendix (D.1).

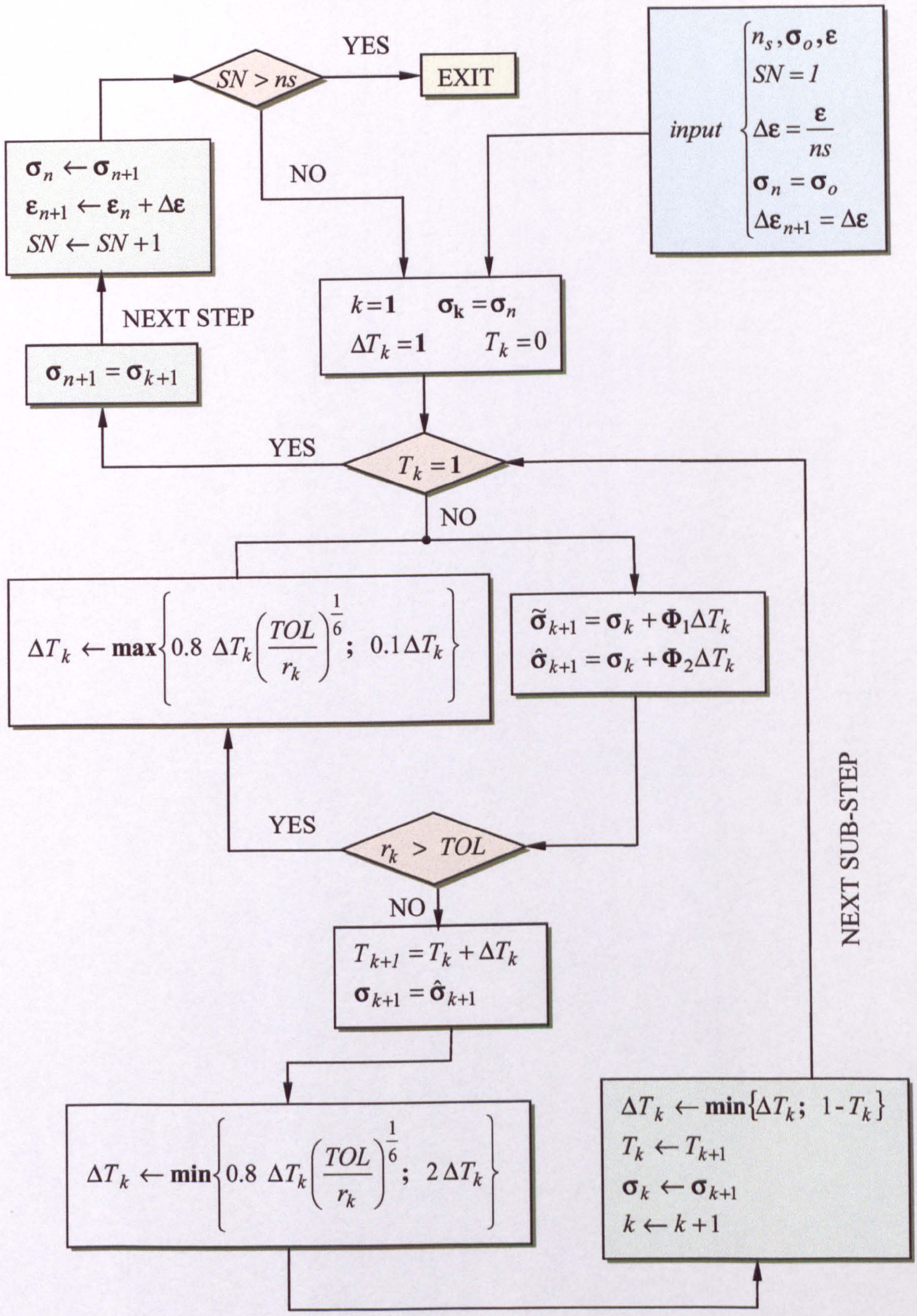

Figure (4.13) Flow chart of adaptive stress point algorithm with multi-steps

4.7 ALGORITHMS VERIFICATION

The capability of a constitutive model is checked by numerical element tests, which are the numerical equivalent of experimental tests. Results from these numerical tests can be verified by comparison with available experimental results. These element tests are:

1. Oedometer test
2. Plane strain (biaxial) test
3. Triaxial compression test
4. Simple shear test

Each of these tests has its own characteristics, as shown in Table [4.1].

Table [4.1] Stress, stress rate, stretching and spin tensors in elementary tests

Test parameters	Oedometer test	Triaxial test	Plane strain test	Simple shear test
$\boldsymbol{\sigma}$	$\begin{pmatrix}\sigma_1 & 0 & 0\\ 0 & \sigma_3 & 0\\ 0 & 0 & \sigma_3\end{pmatrix}$	$\begin{pmatrix}\sigma_1 & 0 & 0\\ 0 & \sigma_3 & 0\\ 0 & 0 & \sigma_3\end{pmatrix}$	$\begin{pmatrix}\sigma_1 & 0 & 0\\ 0 & \sigma_2 & 0\\ 0 & 0 & \sigma_3\end{pmatrix}$	$\begin{pmatrix}\sigma_{11} & \sigma_{12} & 0\\ \sigma_{12} & \sigma_{22} & 0\\ 0 & 0 & \sigma_{33}\end{pmatrix}$
$\dot{\varepsilon}$	$\begin{pmatrix}\dot{\varepsilon}_1 & 0 & 0\\ 0 & 0 & 0\\ 0 & 0 & 0\end{pmatrix}$	$\begin{pmatrix}\dot{\varepsilon}_1 & 0 & 0\\ 0 & \dot{\varepsilon}_3 & 0\\ 0 & 0 & \dot{\varepsilon}_3\end{pmatrix}$	$\begin{pmatrix}\dot{\varepsilon}_1 & 0 & 0\\ 0 & 0 & 0\\ 0 & 0 & \dot{\varepsilon}_3\end{pmatrix}$	$\begin{pmatrix}\dot{\varepsilon}_{11} & \dot{\varepsilon}_{12} & 0\\ \dot{\varepsilon}_{12} & \dot{\varepsilon}_{22} & 0\\ 0 & 0 & 0\end{pmatrix}$
$\boldsymbol{\sigma}^{\circ}$	$\begin{pmatrix}\sigma_1^{\circ} & 0 & 0\\ 0 & \sigma_3^{\circ} & 0\\ 0 & 0 & \sigma_3^{\circ}\end{pmatrix}$	$\begin{pmatrix}\sigma_1^{\circ} & 0 & 0\\ 0 & \sigma_3^{\circ} & 0\\ 0 & 0 & \sigma_3^{\circ}\end{pmatrix}$	$\begin{pmatrix}\sigma_1^{\circ} & 0 & 0\\ 0 & \sigma_2^{\circ} & 0\\ 0 & 0 & \sigma_3^{\circ}\end{pmatrix}$	$\begin{pmatrix}\sigma_{11}^{\circ} & \sigma_{12}^{\circ} & 0\\ \sigma_{12}^{\circ} & \sigma_{22}^{\circ} & 0\\ 0 & 0 & \sigma_{33}^{\circ}\end{pmatrix}$
$\mathbf{w}$	$\begin{pmatrix}0 & 0 & 0\\ 0 & 0 & 0\\ 0 & 0 & 0\end{pmatrix}$	$\begin{pmatrix}0 & 0 & 0\\ 0 & 0 & 0\\ 0 & 0 & 0\end{pmatrix}$	$\begin{pmatrix}0 & 0 & 0\\ 0 & 0 & 0\\ 0 & 0 & 0\end{pmatrix}$	$\begin{pmatrix}0 & w_{12} & 0\\ w_{12} & 0 & 0\\ 0 & 0 & 0\end{pmatrix}$

4.7.1 OEDOMETER TEST SIMULATION

One of the most important element tests shown in Figure (4.14) is the Oedometer test, which is characterized by zero radial deformation, i.e. $\varepsilon_{22} = \varepsilon_{33} = 0$.

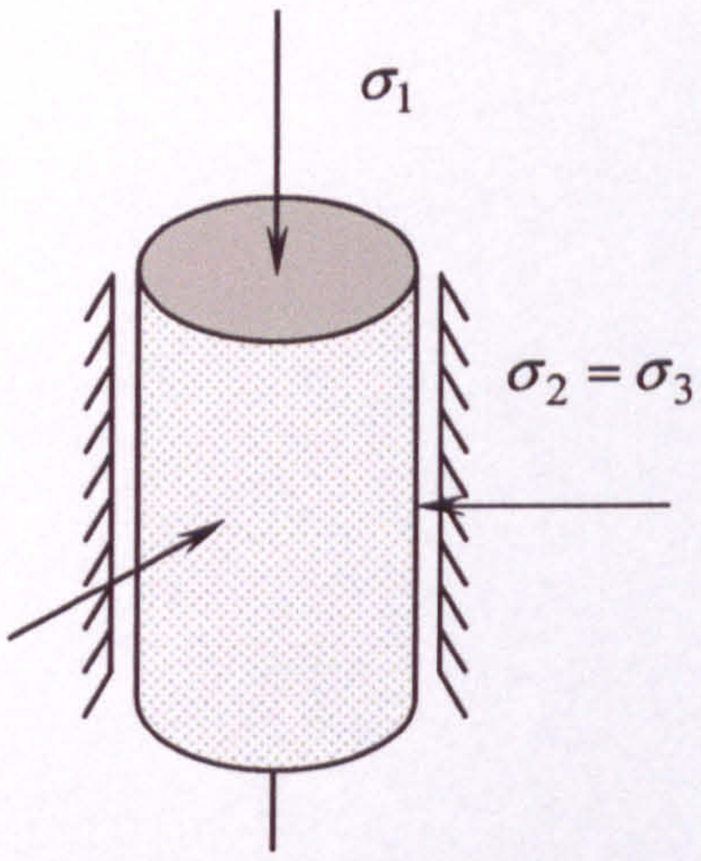

$$\boldsymbol{\sigma} = \begin{pmatrix} \sigma_1 & 0 & 0 \\ 0 & \sigma_3 & 0 \\ 0 & 0 & \sigma_3 \end{pmatrix}$$

Figure (4.14) Oedometer state of stress with corresponding stress tensor

The capability of the present hypoplastic integration algorithms discussed in the previous section, (4.6), was demonstrated with numerical simulation, using FORTRAN program, of the Oedometer test under drained condition, i.e. the effect of pore water pressure in the soil skeleton is not considered. The simulation was carried out on two samples of different initial void ratios (loose sample; $e_0 = 0.78$ and dense sample; $e_0 = 0.57$) of Karlsruhe sand. Experimental data for the Oedometer test on this sand type can be found in the literature, Bauer (1996). Numerical parameters of the hypoplastic model for the Karlsruhe sand are shown in Table [4.2]

Table [4.2] Parameters of the hypoplastic model for Karlsruhe sand

φ_c (deg)	h_s (MPa)	n	e_{d0}	e_{c0}	e_{i0}	α	β
30	5800	0.28	0.53	0.84	1.0	0.13	1.0

4.7.2 IMPLICIT ONE-STEP STRESS-POINT ALGORITHMS VERIFICATION

To examine the capability of the implicit one-step integration algorithms, the Oedometer test is simulated using Euler forward, Mid-point, and Euler backward. Numerical results are compared to experimental results in the plot shown in Figure (4.15). Results show that Euler forward has sufficient accuracy to simulate the Oedometer test.

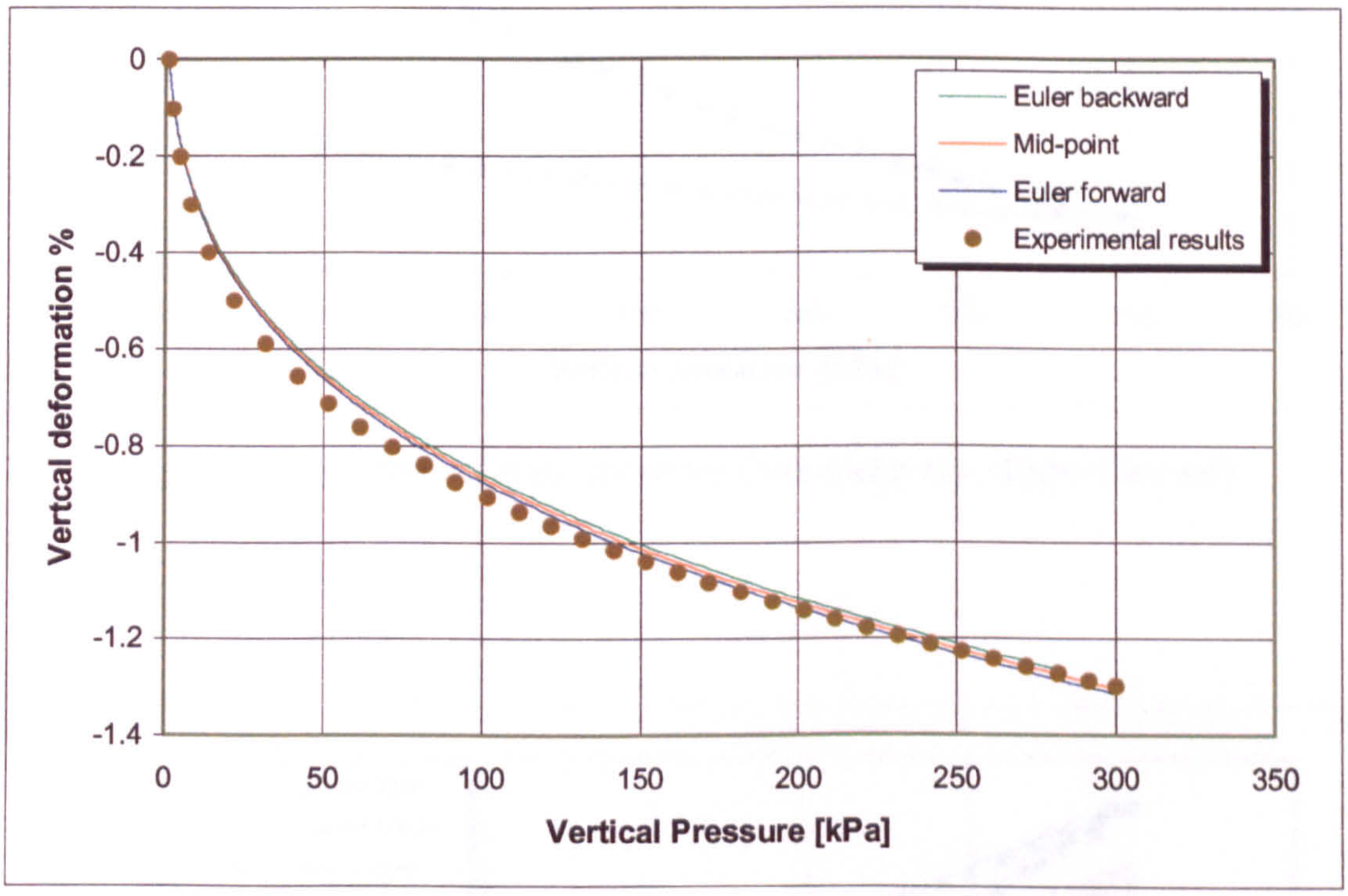

Figure (4.15) Loading simulation using different One-step stress-point algorithms

To check the validity of the Euler forward algorithm to simulate the Oedometer test numerically in both loading and unloading stress paths, loading and unloading responses of the present model for specimens with two different densities are represented together with the experimental results in Figure (4.16) and Figure (4.17)

Figure (4.16) shows the stress–strain relation of the two-test specimens (dense & loose) as simulated by the hypoplastic model. Dots represent the experimental data and straight lines represent the numerical results, the model is integrated using Euler-forward algoritms.

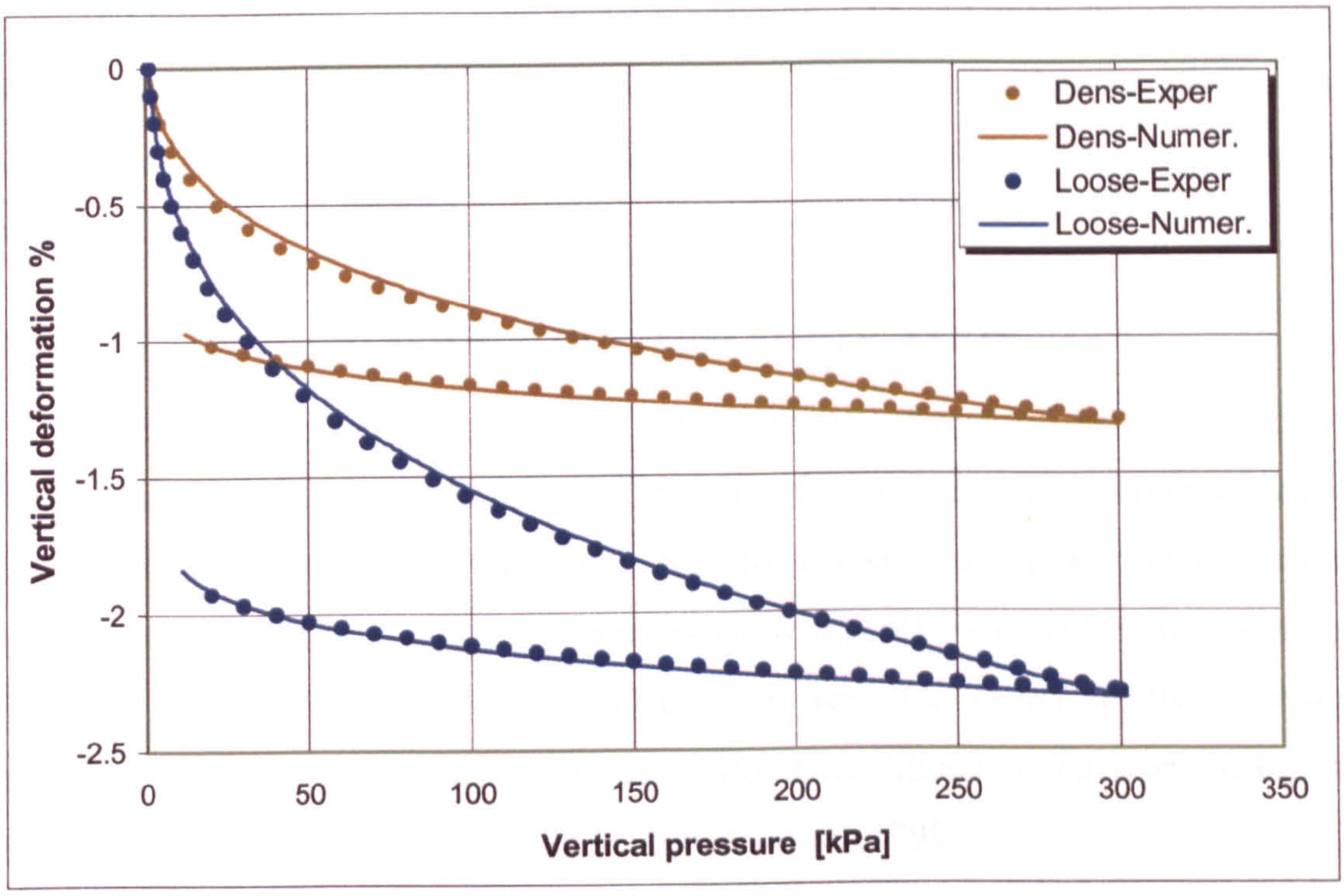

Figure (4.16) Stress – Strain curve for Oedometer test (Euler forward)

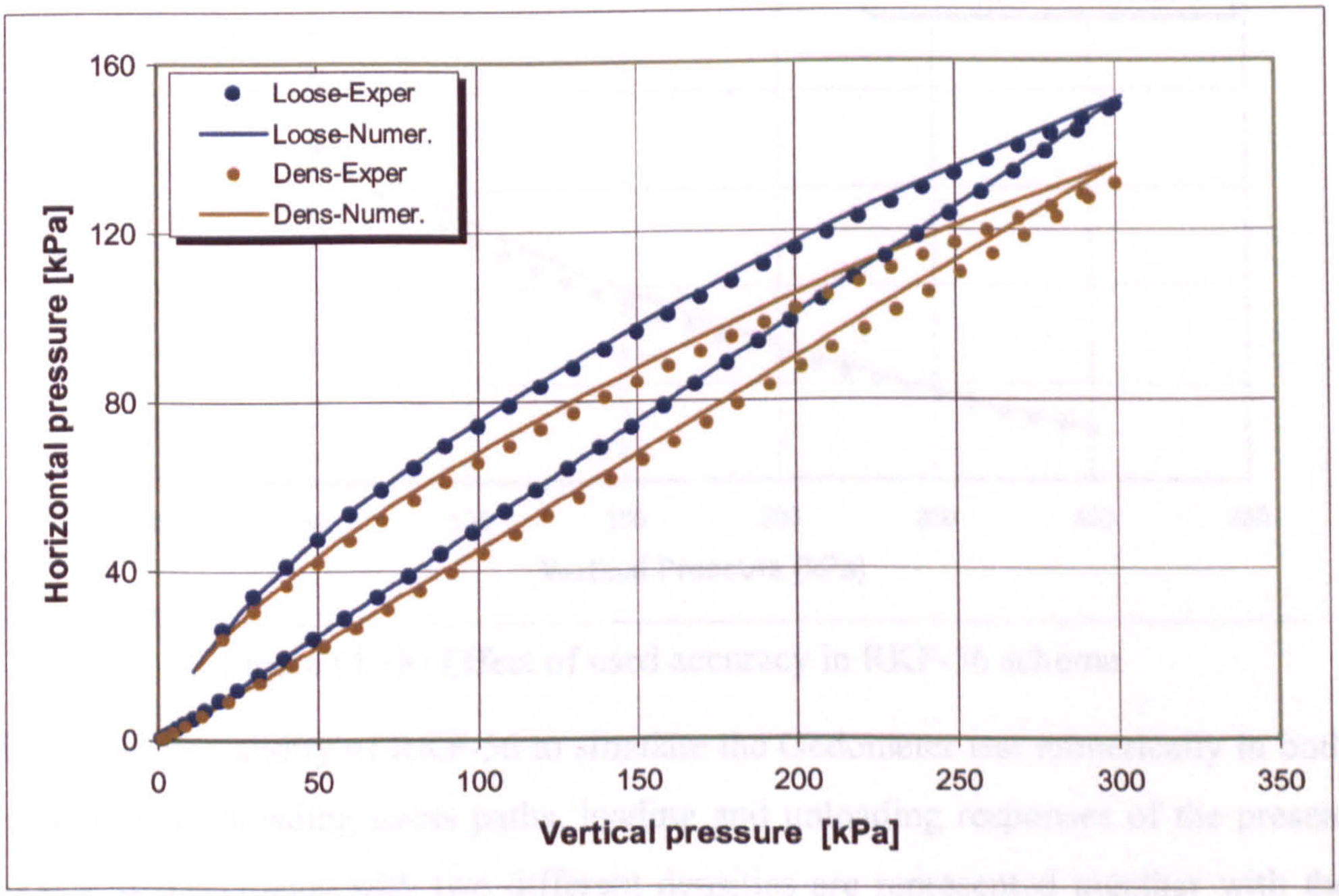

Figure (4.17) Stress path curve for Oedometer test (Euler forward)

Figure (4.17) shows the stress path curve for both loading and unloading stress paths. Results show the high performance of the present model to simulate sand behaviour and the capability of the Euler forward scheme to simulate the test over the stress paths.

4.7.3 EXPLICIT ADAPTIVE ALGORITHM VERIFICATION

To examine the capability of the previously discussed explicit adaptive Runge-Kutta-Fehlberg algorithms (RKF-56), the Oedometer test is simulated using RKF-56 with different error tolerances. Numerical results along with experimental results are plotted in Figure (4.18). Results show that RKF-56 with error tolerance 10e-5 is sufficient to simulate the Oedometer test due to its relative cheaper numerical cost and reasonable accuracy. Also it has found to be more stable in nonlinear problems by Tamagnini and Viggiani, et al. (1999).

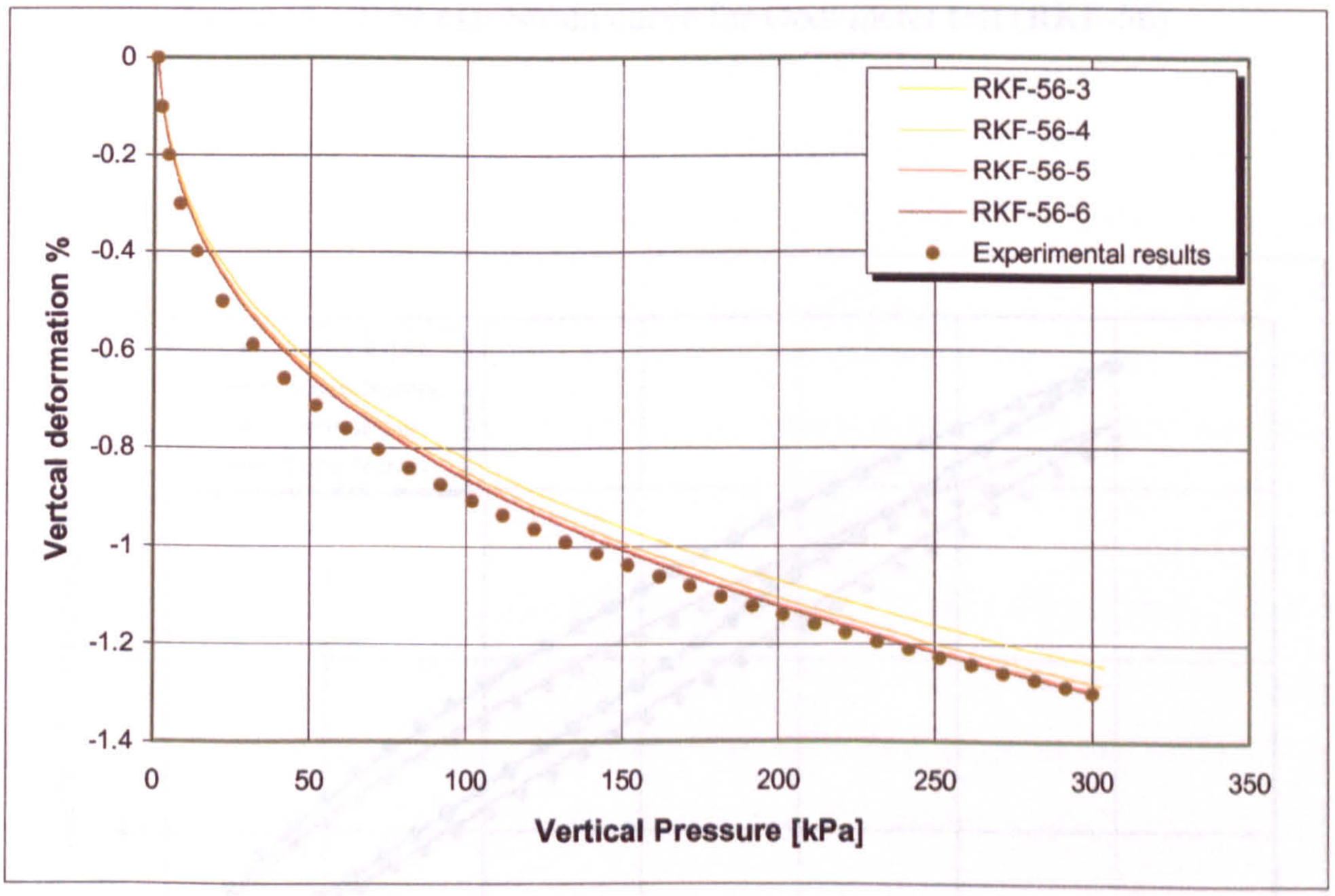

Figure (4.18) Effect of used accuracy in RKF-56 scheme

To check the validity of RKF-56 to simulate the Oedometer test numerically in both loading and unloading stress paths, loading and unloading responses of the present model for specimens with two different densities are represented together with the experimental results in Figure (4.19) and Figure (4.20).

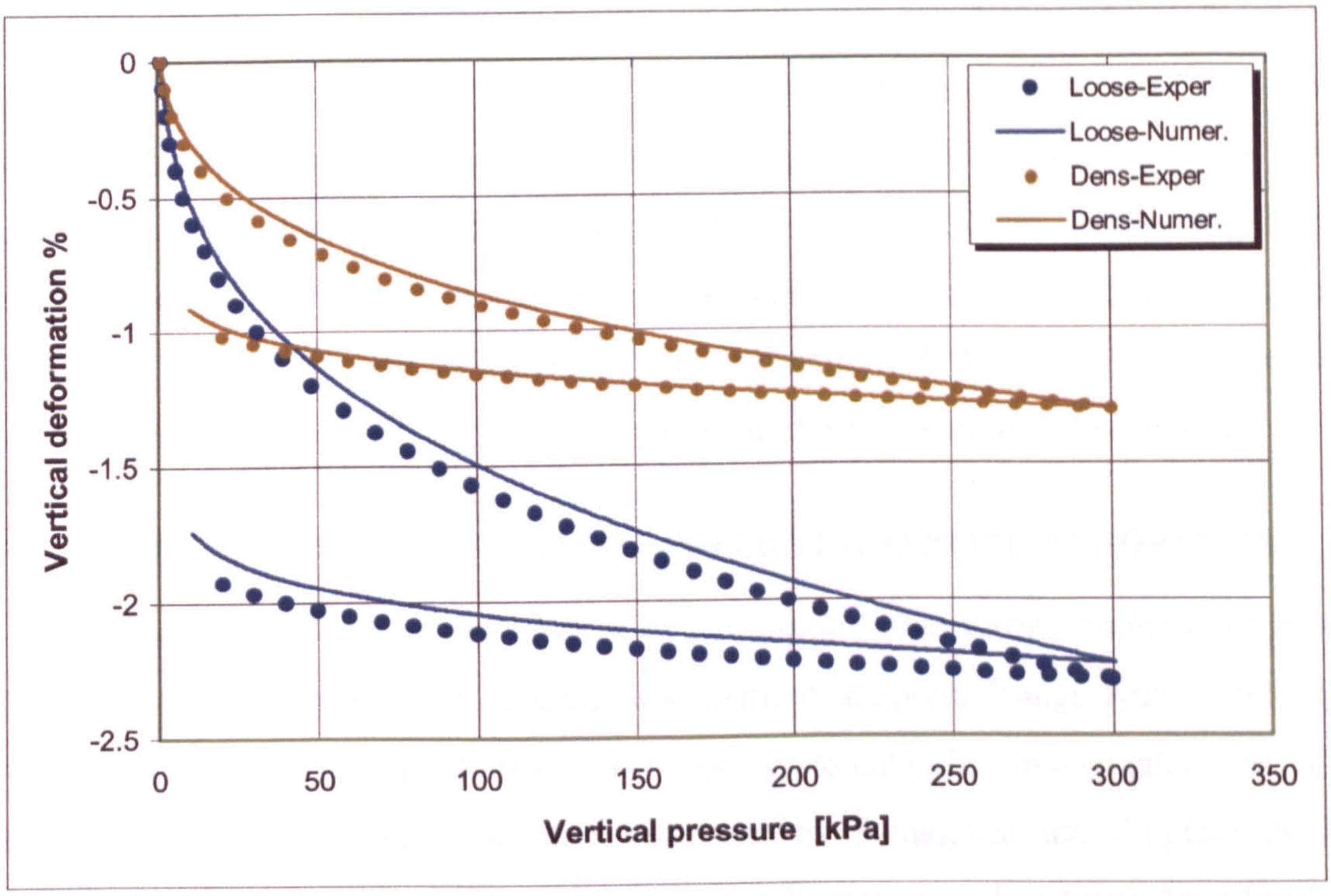

Figure (4.19) Stress–Strain curve for Oedometer test (RKF-56)

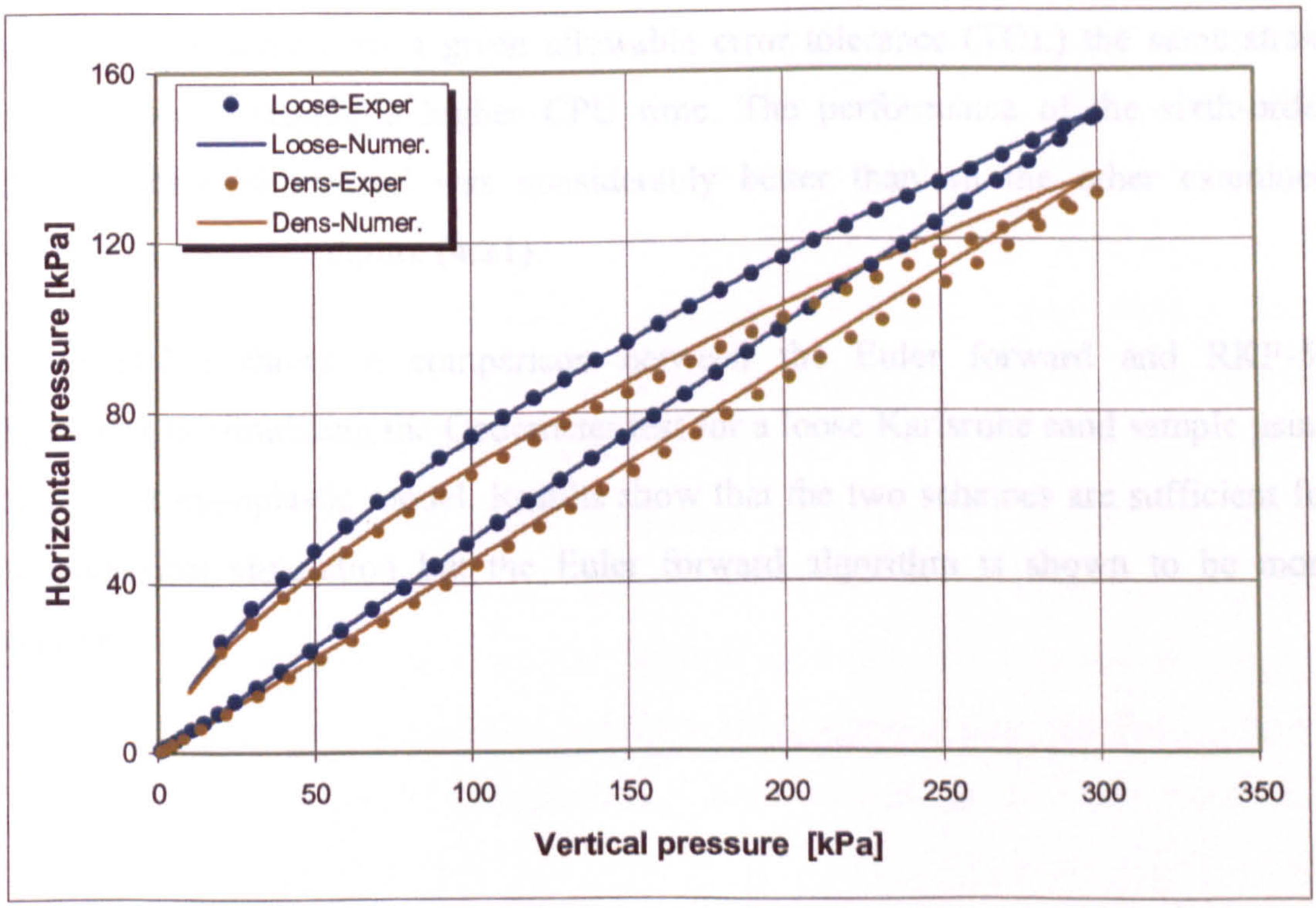

Figure (4.20) Stress path curve for Oedometer test (RKF-56)

Figure (4.19) shows the stress–strain relation of the two specimens (dense & loose) as simulated by the hypoplastic model. Dots represent the experimental data and straight lines represent the numerical results. Figure (4.20) shows the stress path curve for both loading and unloading stress paths. Results reveal the high performance of the present model to simulate sand behaviour. Results presented in Figure (4.19) and Figure (4.20) show the capability of the RKF-56 scheme to simulate the test over the required stress paths i.e. during loading and unloading.

4.7.4 IMPLICIT ONE-STEP VIRSOUS EXPLICIT ADAPTIVE ALGORITHMS

The performance of two classes of stress-point algorithms, implicit one-step generalized midpoint (GMT) methods and explicit adaptive Runge-Kutta-Fehlberg methods (RKF-12 and RKF-56) have been systematically investigated for the application to hypoplastic constitutive equations, by Tamagnini and Viggiani, et al. (1999). The performance of all the integration schemes considered was found to be greatly influenced by the direction of the applied strain increment. In fixed substepping schemes, for a given sub-step size (ΔT_k) the integration error was found to increase with the volumetric component of the applied strain path. In adaptive substepping schemes, for a given allowable error tolerance (TOL) the same strain paths generally require a higher CPU time. The performance of the sixth-order adaptive RKF-56 method was considerably better than all the other examined methods as shown in Figure (4.21).

Figure (4.21) shows a comparison between the Euler forward and RKF-56 algorithms in simulating the Oedometer test for a loose Karlsruhe sand sample using the present hypoplastic model. Results show that the two schemes are sufficient for the numerical simulation but the Euler forward algorithm is shown to be more accurate.

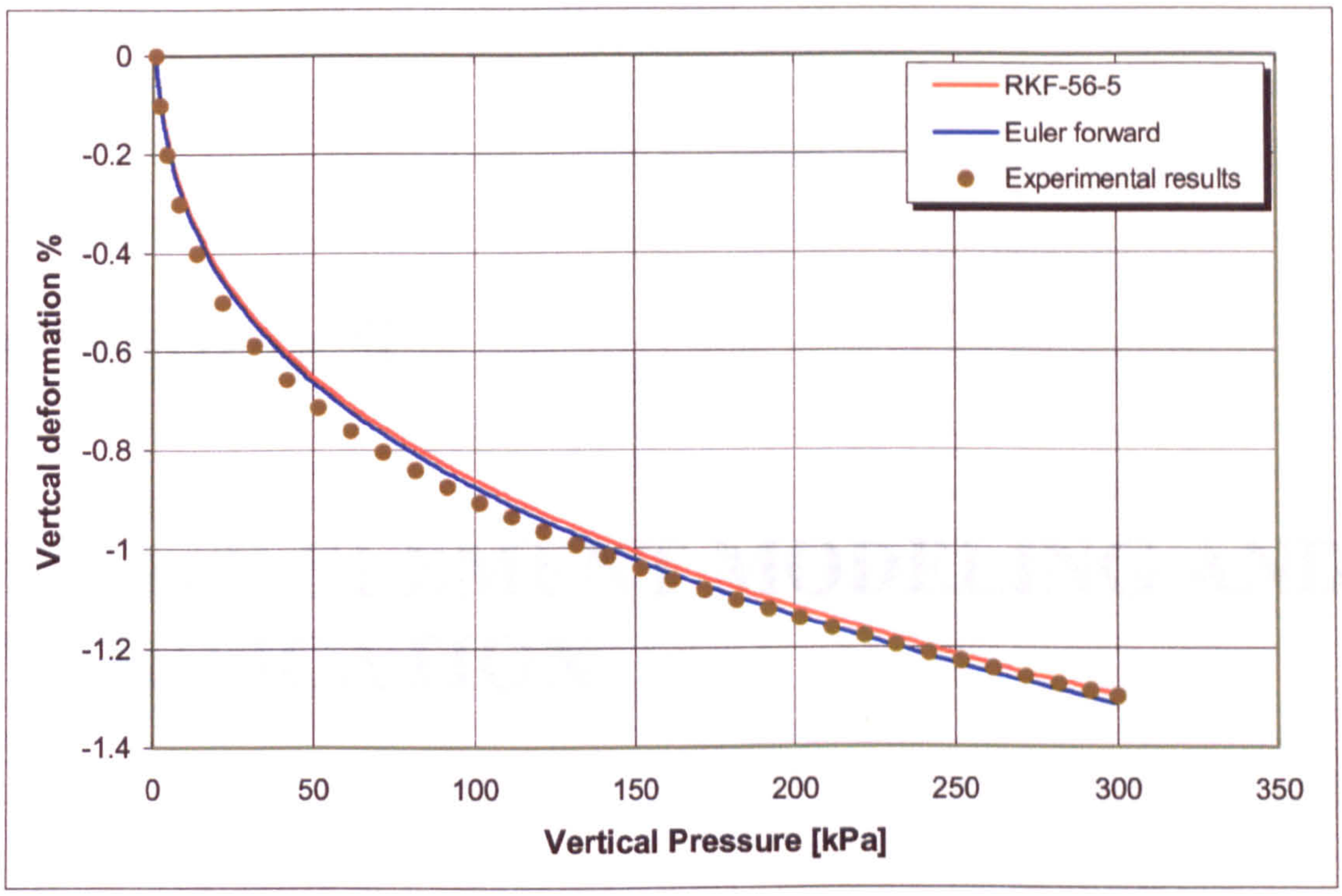

Figure (4.21) Comparison between present hypoplastic integration schemes

4.8 SUMMARY

In this chapter an outline of hypoplasticity is given along with a more detailed description of the Wolffersdorf hypoplastic model being the most appropriate model for our application. Methods of obtaining model parameters were discussed in detail based on some well known experimental tests. For the model to accommodate the simulation of soil under monotonic loading, with progressive failure, some modifications were applied to the original model, Bauer (2000). A verification study of several integration schemes required to integrate the modified model in finite element analysis was carried out by simulating the Oedometer test in both loading and unloading state. Numerical results compared well with the available experimental results and showed the validity of the modified model. In the next chapter this modified constitutive model will be implemented for finite element analysis along with a verification study through analysis of some benchmark problems.

Chapter 5

FINITE ELEMENT MODELING AND VERIFICATION

5.1 CHAPTER SYNOPSIS

The background theory and overall mathematical frame work of hypoplasticity has been given in Chapter 4. Numerical techniques available in integrating the non-linear tensorial hypoplastic equation were also introduced and verified. In this chapter the model is implemented for finite element analysis and verified using simple benchmark problems. Towards the end of this chapter a comparison is made between the hypoplastic model and other classical elastoplastic models. Finally a 2D soil-tool interaction problem is attempted and the ability of the hypoplastic model to simulate realistic sand behaviour is investigated and assessed.

5.2 SOFTWARE CAPABILITIES

Building up a finite element code from scratch is an exhaustive task that requires time and experience and should only be considered when the available commercial finite element codes fail to fulfill user requirements. An alternative approach is to program the constitutive model as an "external routine" which can then be linked to one of the available finite element codes to make use of solution and post processing capabilities of these available finite element codes. Hence a capability review of the available finite element codes was carried out to select the

most appropriate code for simulating sand using the hypoplastic model in soil-tool interaction problems. A comparison between some of the available finite element codes: commercial codes such as ABAQUS (HKS, Hibbit 2000), ANSYS, DYNA, and open codes such as TOCHNOG concluded that ABAQUS was the most appropriate for the following reasons:

1. A wide range of element types, including continuum elements (1d, 2d, 3d), beams, membranes and shells.
2. Element formulations are suitable for large displacements, rotations and strains; implemented within an updated Lagrangian framework.
3. Conventional material models for metals, soil, clay, concrete, jointed rock, plastics and rubber are available.
4. User-defined subroutine (UMAT) permits inclusion of additional material models, which is suitable for the hypoplastic model. This feature is not included in ANSYS and that's why ANSYS was excluded.
5. Surface-to-surface contact with frictional sliding.
6. Extensive documentation, including a Theory Manual, User's Manual (3 vols.), Example Problems Manual (2 vols.) and Verification Manual.

To this end, the hypoplastic model was implemented into ABAQUS via the user-defined subroutine UMAT, discussed later in section, (5.4), and listed in Appendix (D.2).

5.3 ABAQUS MODELING FEATURES

ABAQUS is a general-purpose finite element program designed specifically for advanced analysis applications. A wide variety of problems can be addressed with the available modeling tools. This section highlights features that are required for verifying the benchmark problems and analysis of soil-tool interaction in both two- and three-dimensions.

5.3.1 ANALYSIS TYPE

ABAQUS/Standard provides a variety of time- and frequency-domain analysis procedures. Two main analysis procedures were used in this study:

1. Static stress-displacement analysis; used for equilibrium problems and can include linear or nonlinear response. It is usually used when inertia effects and time-dependent material effects (creep, swelling, and viscoelasticity) can be neglected.
2. Dynamic stress-displacement analysis; in which inertia effects are important.

Each of the previously mentioned analysis types can be linear or non-linear according to the load type and/or the material behaviour. In this study of soil-tool interaction, non-linearity is to be considered. The effect of such non-linearity can be introduced in a general ABAQUS analysis step by including the NLGEOM parameter on the *STEP option, Hibbit, Karlsson and Sorensen (2000) (HKS).

Static stress-displacement analysis was first used to verify the implemented model and analyze some benchmark problems as discussed later in this chapter. It was also used to investigate the effect of blade geometry and operating conditions, except for the cutting speed, in the soil-tool interaction analysis in Chapter 6. The dynamic stress-displacement analysis was used in the 3-dimensional soil-tool interaction to study the effect of cutting speed on cutting forces as presented in Chapter 6.

5.3.2 SURFACE DEFINITION

Surfaces are considered part of the model definition; so all surfaces that may be needed in an analysis must be defined at the beginning of the simulation. Surface definitions are mainly needed to describe contact. ABAQUS has three classifications of contact surfaces:

1. Element-based surface
2. Node-based surface, and
3. Analytical rigid surface.

For two-dimensional analysis of soil-tool interaction, the blade is simulated as an analytical rigid surface using the *RIGID BODY, ANALYTICAL SURFACE option in ABAQUS; contact soil surface is simulated using an element-based surface for its ease of convergence and reliable results. In the three-dimensional analysis both the

contact surfaces are simulated as element-based surfaces, there is no control on the analytical rigid surface width i.e. it is extended through space.

A reference point can be assigned to a rigid surface or a body through which its motion can be described. This feature enables accounting for reaction forces acting on the blade in soil-tool interaction analysis.

5.3.3 CONTACT MODELING

There are two methods for modeling contact and interaction problems in ABAQUS: using surfaces or using contact elements. Most contact problems are modeled by using surface-based contact such as in contact between a rigid surface and a deformable body (as in our soil-tool interaction problem). The structures can be either two- or three-dimensional, and they can undergo either small sliding (sliding distance not exceed half of the element length) or finite sliding (no limit on the sliding distance so long as the two contact surfaces are facing each other).
There are three steps in defining a contact simulation:

1. Defining the surfaces of the bodies that could potentially be in contact,
2. Specifying which surfaces interact with one another (contact pairs), and
3. Defining the mechanical surface interaction model that governs the behavior of the surfaces when they are in contact.

ABAQUS defines contact between two bodies in terms of two surfaces that may interact; these surfaces are called a "contact pair". The order in which the two surfaces are specified on the *CONTACT PAIR option is critical because of the manner in which surface interactions are discretized. For each node on the first surface (the "slave" surface) ABAQUS attempts to find the closest point on the second surface (the "master" surface) of the contact pair where the master surface's normal passes through the node on the slave surface. The interaction is then discretized between the point on the master surface and the slave node.

5.3.4 MECHANICAL SURFACE INTERACTION MODELS

Some of the mechanical surface interaction models available in ABAQUS/Standard include:

1. **Friction** (Interaction tangential to the surface): when surfaces are in contact they usually transmit shear as well as normal forces across their interface, stick state discussed in section (2.2.3.2). There is generally a relationship between these two force components. The relationship, interpreted as the friction between the contacting bodies, is usually expressed in terms of the stresses at the interface of the bodies. An extended version of the classical isotropic Coulomb friction model is provided in ABAQUS for use with all contact analysis capabilities.
2. **Finite sliding** (Relative surface motions): where separation and sliding of finite amplitude and arbitrary rotation of the surfaces may arise. Slip state was discussed in section (2.2.3.2). The finite-sliding rigid contact capability is implemented by means of a family of contact elements that ABAQUS automatically generates based on the data associated with the *CONTACT PAIR option. At each integration point these elements construct a measure of overclosure (penetration of the point on the surface of the deforming body into the rigid surface) and measures of relative shear sliding.
3. **Softened contact** (Interaction normal to the surface): in which the contact pressure is an exponential function of the clearance between the surfaces.

To avoid convergence problems in the analysis of soil-tool interaction, mainly when the cut soil separated from the rest of soil bulk, an exponential pressure-overclosure relationship was included using the *SURFACE BEHAVIOR option.

5.3.5 ELEMENT TYPE

Choosing the appropriate element type for an analysis is one of the most important steps towards a correct simulation and analysis. Element choice is based on some well established factors:

1. Analysis type, static or dynamic.
2. Material behaviour, linear or non-linear.
3. Contact interaction status, whether there is a contact or not.
4. Is the structure thick or thin.
5. Will the mesh become severely distorted or not.
6. Which results are needed from the analysis.

7. Analysis dimension, 2D or 3D.

Considering these factors, an element has to be selected according to the following main element features:

5.3.5.1 Element family

One of the major distinctions between different element families is the geometry type that each family assumes. Different element family classification is listed below and can be shown in Figure (5.1)

a. Continuum solid elements
b. Shell elements
c. Beam elements
d. Rigid elements
e. Membrane elements
f. Infinite elements
g. Connector elements
h. Truss elements

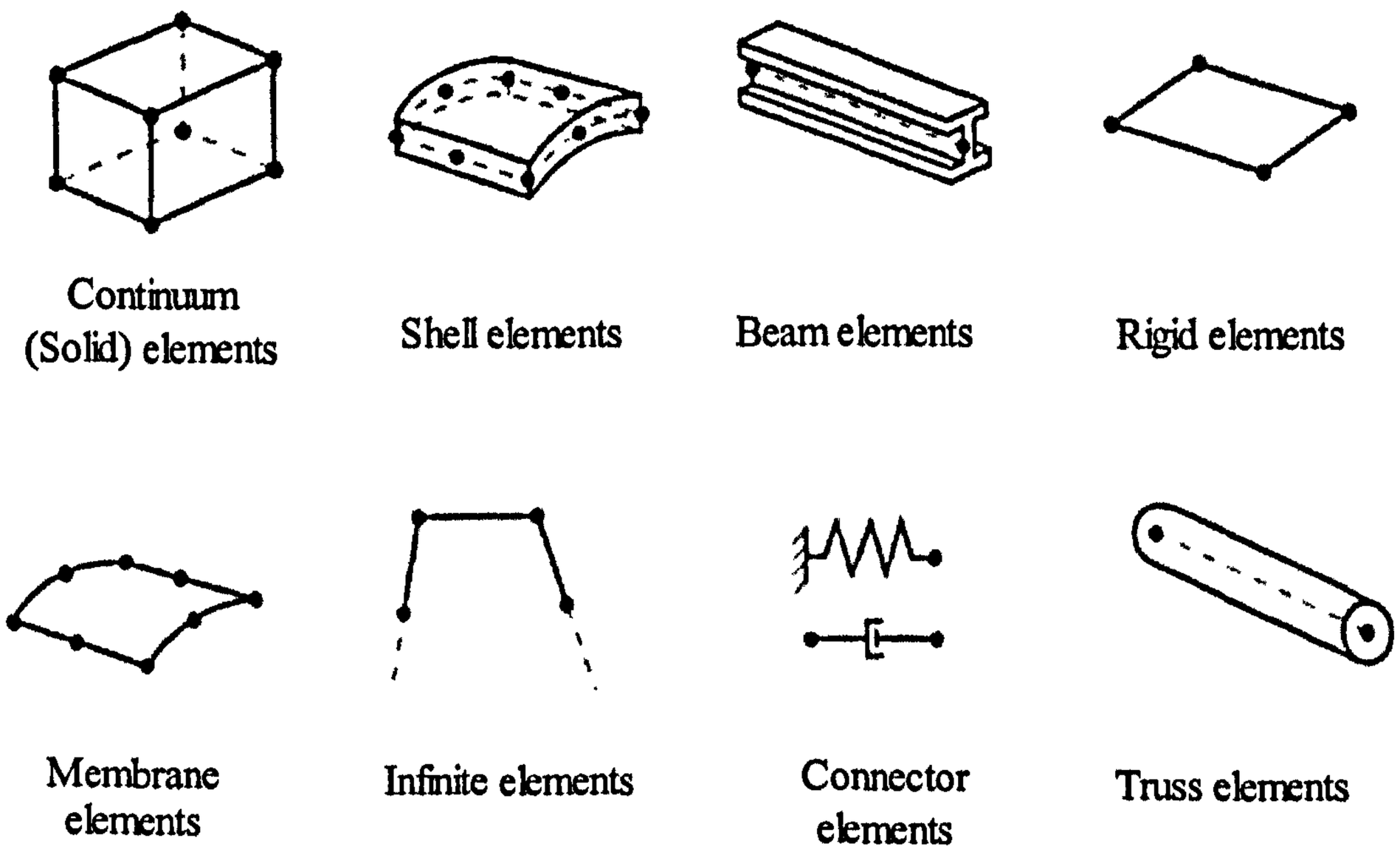

Figure (5.1) ABAQUS element families

The solid (or continuum) elements in ABAQUS can be used for linear analysis and for complex nonlinear analyses involving contact, plasticity, and large deformations and hence it will be used through the soil-tool interaction analysis.

5.3.5.2 Number of nodes and order of interpolation

Displacements and/or other degrees of freedom are calculated at the nodes of the element. At any other point in the element, the displacements are obtained by interpolating the nodal displacements. Usually the interpolation order is determined by the number of nodes used in the element.

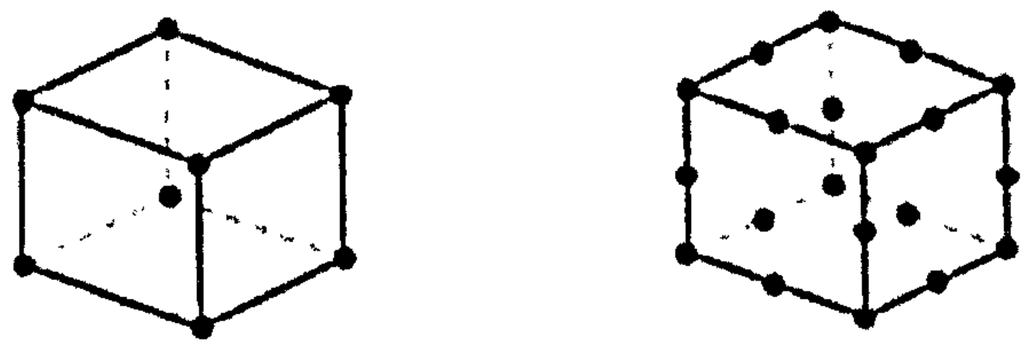

(a)Linear element (8-node brick, C3D8)

(b)Quadratic element (20-node brick, C3D20)

Figure (5.2) Number of nodes and order of interpolation

Elements that have nodes only at their corners, such as the 8-node brick shown in Figure (5.2a), use linear interpolation in each direction and are often called linear elements or first-order elements. Elements with midside nodes, such as the 20-node brick shown in Figure (5.2b), use quadratic interpolation and are often called quadratic elements or second-order elements.

First order brick elements, Figure (5.2a), are more suitable for analyzing problems where contact exists or nonlinearity and severe element distortion are expected during the analysis. They are also easier to be meshed using automatic mesh generation.

5.3.5.3 Element mode

An element may be compatible and incompatible according to its theoretical formulation. Incompatible mode elements are first-order elements that are enhanced by incompatible modes of deformation to improve their bending behavior. In

addition to the standard displacement degrees of freedom, incompatible deformation modes are added internally to the elements. The primary effect of these modes is to eliminate the parasitic shear stresses that cause the response of the regular first-order displacement elements to be too stiff in bending. Because of the added internal degrees of freedom due to the incompatible modes, these elements are somewhat more expensive computationally than the regular first-order displacement elements; however, they are significantly more economical than second-order elements.

5.3.5.4 Element integration

When forming element stiffness, the element may integrated in full mode or reduced mode. When a reduced integration element used, integration will not be carried out at all element nodes. Reduced integration reduces running time, especially in three dimensions. In addition, second-order reduced-integration elements generally yield more accurate results than the corresponding fully integrated elements.

5.3.5.5 Element dimension

The ABAQUS element library contains elements for modeling a wide range of spatial dimensionality. In this study of soil-tool interaction, the following element dimensions were used:

1. ***Plane strain element***

Plane strain elements can be used when it can be assumed that the strains in a loaded body or domain are functions of planar coordinates alone and the out-of-plane normal and shear strains are equal to zero. This modeling assumption is generally used for bodies that are very thick relative to their lateral dimensions, such as shafts, concrete dams, or walls. Plane strain theory can be applied for the analysis of soil-tool interaction in two-dimensions for fast parametric comparison study.

2. ***Three-dimensional elements***

Three-dimensional elements are defined in the global space. These elements are used when the geometry and/or the applied loading are too complex for any other element type with fewer spatial dimensions.

5.3.5.6 Summary of recommendations for element usage

The soil-tool interaction model contains contact between the tool and the soil and also expected element distortion due to the large deformation caused by monotonic loading during cutting. Hence an 8-node bilinear reduced integration plane strain continuum element (CPE8R) will be used in the two-dimensional analysis and the 8-node linear brick fully integration continuum element (C3D8) will be used in the three-dimensional analysis. ABAQUS will automatically generate the appropriate interface elements for the contact according to the contact topology.

5.3.6 PRESCRIBED CONDITIONS

The following types of external conditions can be prescribed in an ABAQUS model:

1. **Initial conditions**: Nonzero initial conditions can be defined for many variables. The initial void ratio of the simulated sand described by the hypoplastic model is specified as an initial condition using the *INITIAL CONDITION option.
2. **Boundary conditions**: Boundary conditions are used to prescribe values of basic solution variables: displacements and rotations in stress/displacement analysis. Various constrains of the model described using the *BOUNDARY option. During the analysis of the soil-tool interaction, tool displacement and velocity effect (in the dynamic analysis) are described using the *BOUNDARY option.
3. **Loads**: Many types of loading are available, depending on the analysis procedure such as concentrated force, distributed force, gravity force, etc. One of the most important factors that should be considered when describing sand using the hypoplastic model is the effect of gravity on the sand skeleton. As there is no cohesion force contracts sand particles to each other and as described before there is no elastic configuration in the hypoplastic model, ABAQUS will gives convergence problems at the beginning of the analysis if the gravity effect is neglected because this is the only force that forces sand grains to be in contact to each others.

5.3.7 ANALYSIS HISTORY AND CONTROL

An analysis history is defined in ABAQUS by dividing the problem history into steps, specifying an analysis procedure for each step; and prescribing loads, boundary conditions, and output requests for each step. A step starts with the *STEP option and ends with the *END STEP option.

5.3.7.1 Step Increments

ABAQUS offers a facility to constrain the upper limit of the incremental sub-step size. The total time is assumed to be one and the sub-step size is a fraction of one. Each step in an analysis is divided into multiple increments, each increment described through a sub-step of limited size. Describing sand behaviour using the hypoplastic constitutive model in soil-tool interaction analysis requires a small initial time increment, in the order of 1e-12 to avoid singularity and convergence problems may occur, and a proper selection of the sub-step size limit for reasonable results. For proper integration of the hypoplastic model strain increment which is controlled by the size of the time increment, it should be in the order of 1e-5, Roddeman (1997).

5.3.7.2 Linear and nonlinear analysis

A general analysis step is provided by ABAQUS which can be used to analyze linear or nonlinear response. Non-linearity can be introduced in the model during the step analysis as a consequence of material nonlinearity or/and geometrical nonlinearity. Material nonlinearity is accounted for by way of constitutive model integration, but geometry nonlinearity is accounted for by including the NLGEOM parameter in the *STEP option. For the expected large deformation of the cut soil in soil-tool interaction analysis, model nonlinearity was considered.

5.3.7.3 Matrix storage and solution scheme

ABAQUS generally uses Newton's method to solve nonlinear problems and the stiffness method to solve linear problems, Potts (1999). In both cases the stiffness matrix is needed. In some problems, such in Coulomb friction, contact interaction, and user-defined material, this matrix is not symmetric. Hence the UNSYMM=YES

parameter is to be used on the *STEP option to specify unsymmetric matrix storage and solution.

5.3.7.4 Stabilization of unstable problems

Some static problems can be naturally unstable, for a variety of reasons. Instability may occur because unconstrained rigid body motions exist. ABAQUS may be able to handle this type of problem with the *CONTACT CONTROLS, APPROACH option when rigid body motions exist during the approach of two bodies that will eventually come into contact.

Geometrically nonlinear static problems sometimes involve buckling or collapse behavior, where the load-displacement response shows a negative stiffness and the structure must release strain energy to remain in equilibrium. Several approaches are possible for modeling such behavior. One is to treat the buckling response dynamically, thus actually modeling the response with inertia effects included as the structure snaps. Another approach would be to use dashpots to stabilize the structure during a static analysis. ABAQUS offers an automated version of this approach by using the STABILIZE parameter on the static analysis procedures.

For soil-tool interaction analysis, where a geometric nonlinearity of the soil and the rigid body motion of the cutting tool are to be considered, the STABILIZE parameter was included into ABAQUS *STATIC option to avoid convergence problems.

5.4 UMAT IMPLEMENTATION

One of the main fields of constitutive models application is the implementation into finite element (FEM) codes. The FEM programme ABAQUS allows the user to implement particular constitutive equations within the subroutine UMAT. The initial model by Wolffersdorf (1996) was implemented by Roddeman (1997). In this study the modified model is implemented based on Roddeman, (1997).

The UMAT subroutine has to be programmed in such a way that knowing the stress $\boldsymbol{\sigma}(t)$ and the strain $\boldsymbol{\varepsilon}(t)$ at time 't' and for given strain increment $\Delta\boldsymbol{\varepsilon}$ over a time period Δt, it returns the stress $\boldsymbol{\sigma}(t+\Delta t)$ and calculates the Jacobian $\partial\dot{\boldsymbol{\sigma}}/\partial\dot{\boldsymbol{\varepsilon}}$ at time $t+\Delta t$ to evaluate the global stiffness matrix for the next increment. Depending on whether the given strain increment is small enough or not, it may be necessary to subdivide it into smaller steps (so called sub-stepping).

Referring to the hypoplastic equation, (4.9), in Chapter 4; an initial stress should be known or assumed in order to calculate the stress changes due to a given incremental of deformation, Kolymbas (1999). This initial stress could be an approximate value of the initial confining pressure of a sample or the gravity load acting on the soil particles in the real state.

5.5 VERIFICATION OF THE IMPLEMENTED MODEL

Verification of the implemented hypoplastic model was carried out through an extensive analysis of three benchmark problems: an Oedometer test, a strip footing and a soil-tool interface problem. This was to investigate the ability of the implemented model to describe the behaviour of sand in such problems. The effect of hypoplastic equation integration scheme, time step size and RKF error tolerance (TOL) on results accuracy are also investigated and discussed through the verification procedure.

5.5.1 OEDOMETER TEST SIMULATION

The Oedometer test, discussed previously in section (3.4.1), was simulated using ABAQUS in order to verify the implemented hypoplastic model. The simulated model dimension and boundary conditions are shown in Figure (5.3).

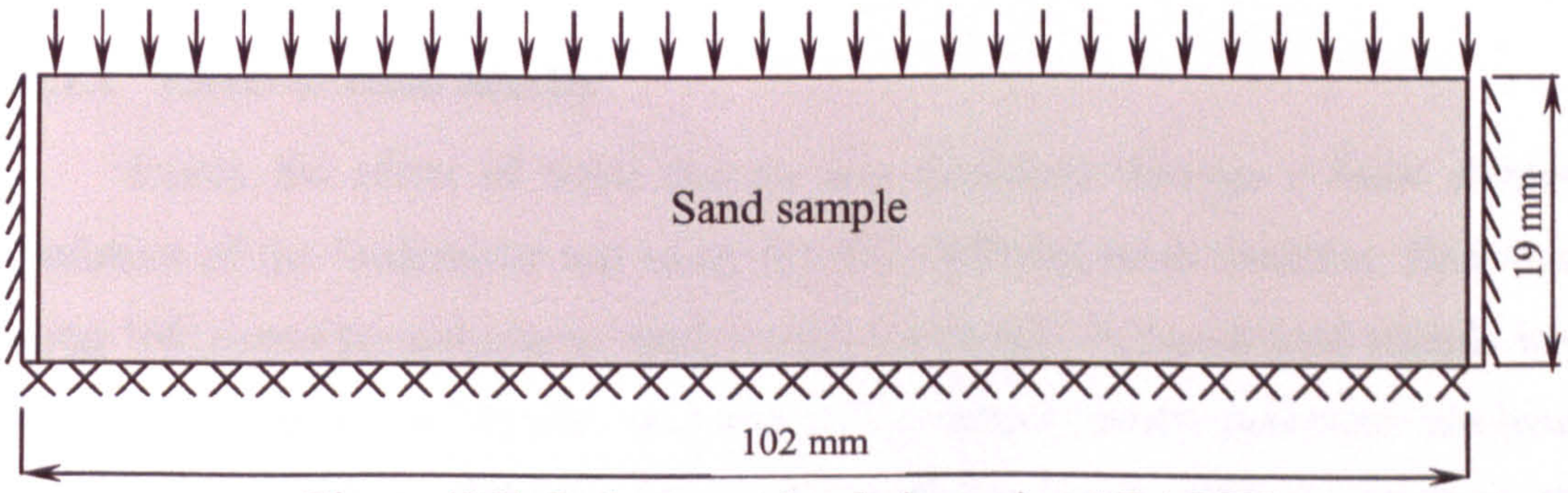

Figure (5.3) Oedometer simulation using ABAQUS

As shown in Figure (5.3), the right and left bounds of the sample are fixed horizontally and the bottom bound is fixed vertically and horizontally. Also the downward arrows at the top of the sample represent the displacement direction. Loose sand sample of initial void ration (e_o = 0.78) was used in simulating the Oedometer test. The sample was modeled using 8-node bi-quadratic plane strain element (CPE8). Two mesh densities were considered in this simulation, fine mesh (using 100 elements) and coarse mesh (using just one element). The finite element mesh is shown in Figure (5.4). The hypoplastic parameters of the simulated sand sample are listed in Table [5.1]. ABAQUS input file for the Oedometer test simulation is listed in Appendix (E.1).

Table [5.1] Parameters of the hypoplastic model for Karlsruhe sand

φ_c (deg)	h_s (MPa)	n	e_{d0}	e_{c0}	e_{i0}	α	β
30	5800	0.28	0.53	0.84	1.0	0.13	1.0

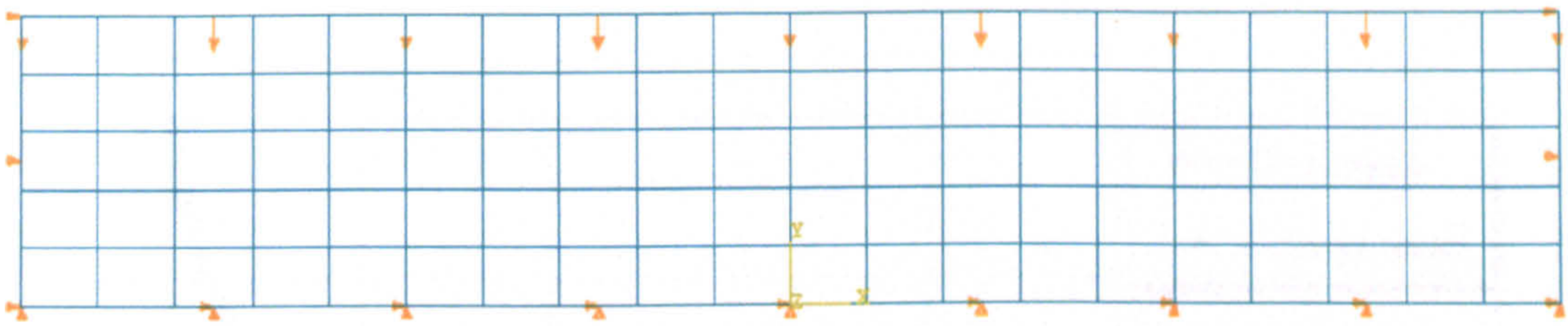

Figure (5.4) Finite element mesh of the simulated sample

The simulated sample was compressed vertically to about 2.3% of its original height. Comparison between the experimental results and the finite element model predicted results reveals a good corelation between the experimental and the predicted results as shown later in this chapter.

5.5.1.1 Effect of mesh density

Firstly the effect of mesh density was examined through a finite element simulation of the Oedometer test using the two different mesh densities, fine mesh (using 100 elements) and coarse mesh (using 1 element). A Loose sand sample with initial void ration (e_o=0.78) was used and its hypoplastic model parameter are listed in Table [5.1]. Three different integration schemes were used to integrate the hypoplastic equation, via ABAQUS user defined subroutine UMAT, which are Euler forward, Crank-Nicolson (Mid-point) and Runge-Kutta-Fehlberg (RKF) algorithms. The maximum sub-step time was 0.01 and the allowable error tolerance (TOL) for the RKF scheme was 1E-4. During the simulation of the Oedometer test the test samples were compressed vertically to about 2.3% of the total sample height which means monotonic compression only.

Figure (5.5) represents the relation between percentage of the vertical deformation $\left(\frac{Vertical\ displacement}{Total\ sample\ height}\%\right)$ and the corresponding pressure (vertical stress) in "kPa". Results obtained from the fine mesh simulation are represented by straight lines and

results obtained from the coarse mesh simulation are represented by hollow circles. Results shown in Figure (5.5) reveal the insignificant effect of the mesh density on simulating the Oedometer test whatever the integration scheme. This may be due to the non-rotating deformation of the material during the Oedometer test simulation according to its boundary and load state shown in Figure (5.3).

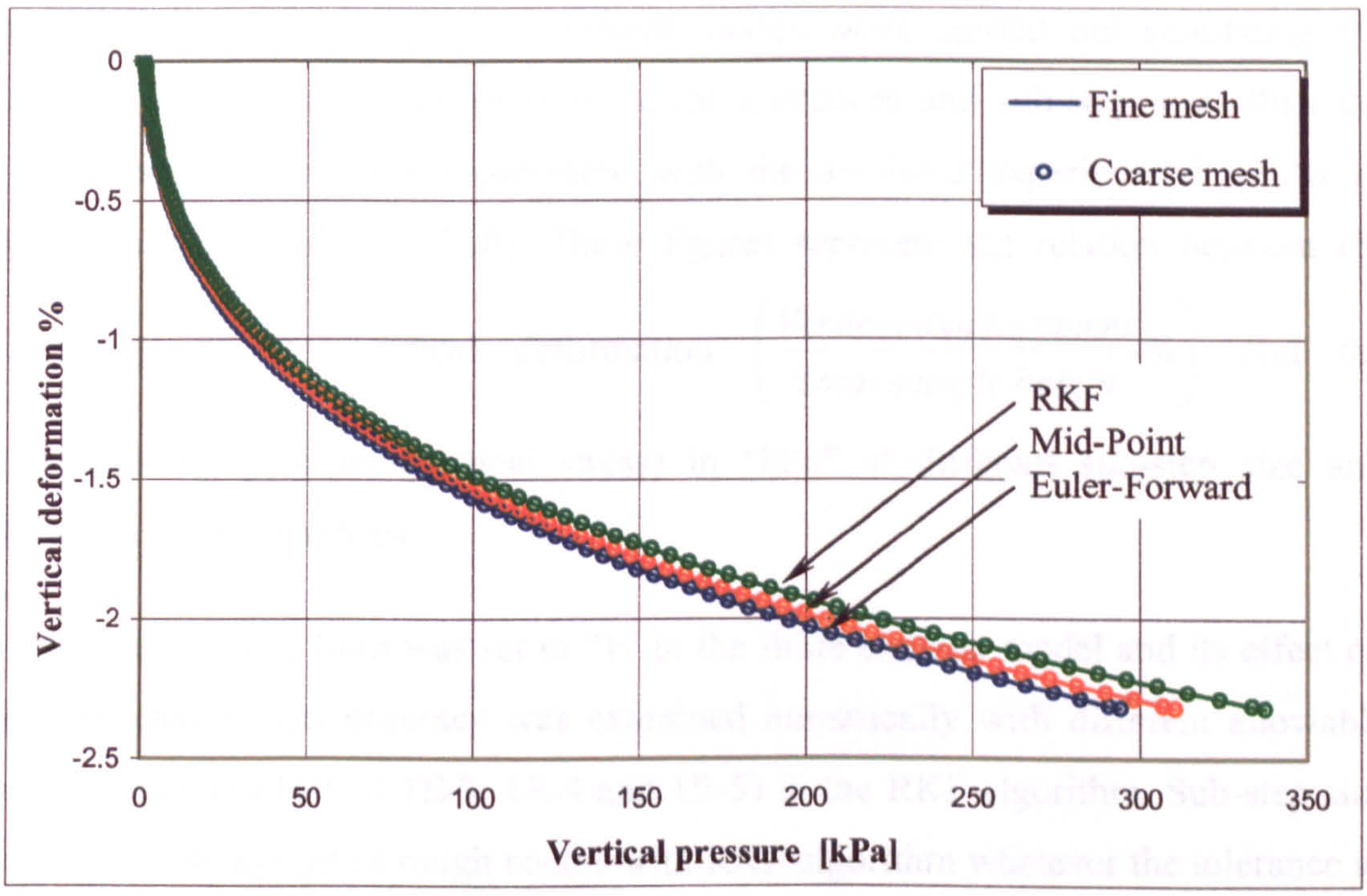

Figure (5.5) Effect of mesh density on Oedometer test simulation

5.5.1.2 Validation of different integration schemes

As mentioned previously, two kinds of integration schemes were used to integrate the hypoplastic constitutive equation, explicit adaptive algorithm (Runge-Kutta-Fehlberg (RKF)) and implicit one-step stress-point algorithms (Euler forward, Crank-Nicolson (Mid-Point)). Euler-backward was tested numerically using FORTRAN program as described previously in section (4.7.2) but it gave unreasonable results after being implemented into the finite element code ABAQUS. All the results were obtained through numerical simulation of the Oedometer test using sand sample described by hypoplastic model that implemented into the finite element code ABAQUS via the user defined material subroutine UMAT and were compared with experimental results of loose sand sample, properties in Table [5.1]. During this validation study, the test sample was compressed vertically to about

2.3% of the total sample height through the 'Loading' path and then expanded back through the 'Unloading' path.

Runge-Kutta-Fehlberg (RKF) algorithm

When implemented into ABAQUS, the RKF algorithm was shown to be dependant on both sub-step size and the allowable error tolerance (TOL). To study these effects, a series of finite element models were carried out simulating the Oedometer test at different allowable error tolerances and sub-step sizes then the finite element results were compared with the available experimental results as shown in figures (5.6 to 5.10). These figures represent the relation between the percentage of the vertical deformation $\left(\frac{Vertical\ displacement}{Total\ sample\ height}\%\right)$ and the corresponding pressure (vertical stress) in "kPa" at different sub-step size and allowable error tolerances.

Firstly the sub-step limit was set to "1" in the finite element model and its effect on the predicted results accuracy was examined numerically with different allowable error tolerances (TOL = 1E-3, 1E-4 and 1E-5) in the RKF algorithm. Sub-step size limit of '1' always gives rough results with RKF algorithm whatever the tolerance as shown in Figure (5.6). Then a series of finite element models were carried out to investigate the effect of sub-step size limit and the allowable error tolerance. In these models different values of the sub-step size limit was set (0.1, 0.01 and 0.001) along with different allowable error tolerances (TOL = 1E-3, 1E-4 and 1E-5). Relatively reasonable results were obtained using sub-step limit of '0.1' and error tolerance of 1E-5 as shown in Figure (5.7), or using sub-step limit of '0.01' and error tolerance of 1E-4 as shown in Figure (5.8). Figure (5.9) shows that the allowable error tolerance has insignificant effect when the sub-step limit is too small (0.001), but as the sub-step size increases error tolerance should be decreased to achieve reasonable results. As shown in Figure (5.10) using RKF with tolerance 1E-5 and sub-step size limit of '0.01' or '0.001' gave reasonable and similar results, but using sub-step size limit of '1' gave relatively bad results especially during the unloading process.

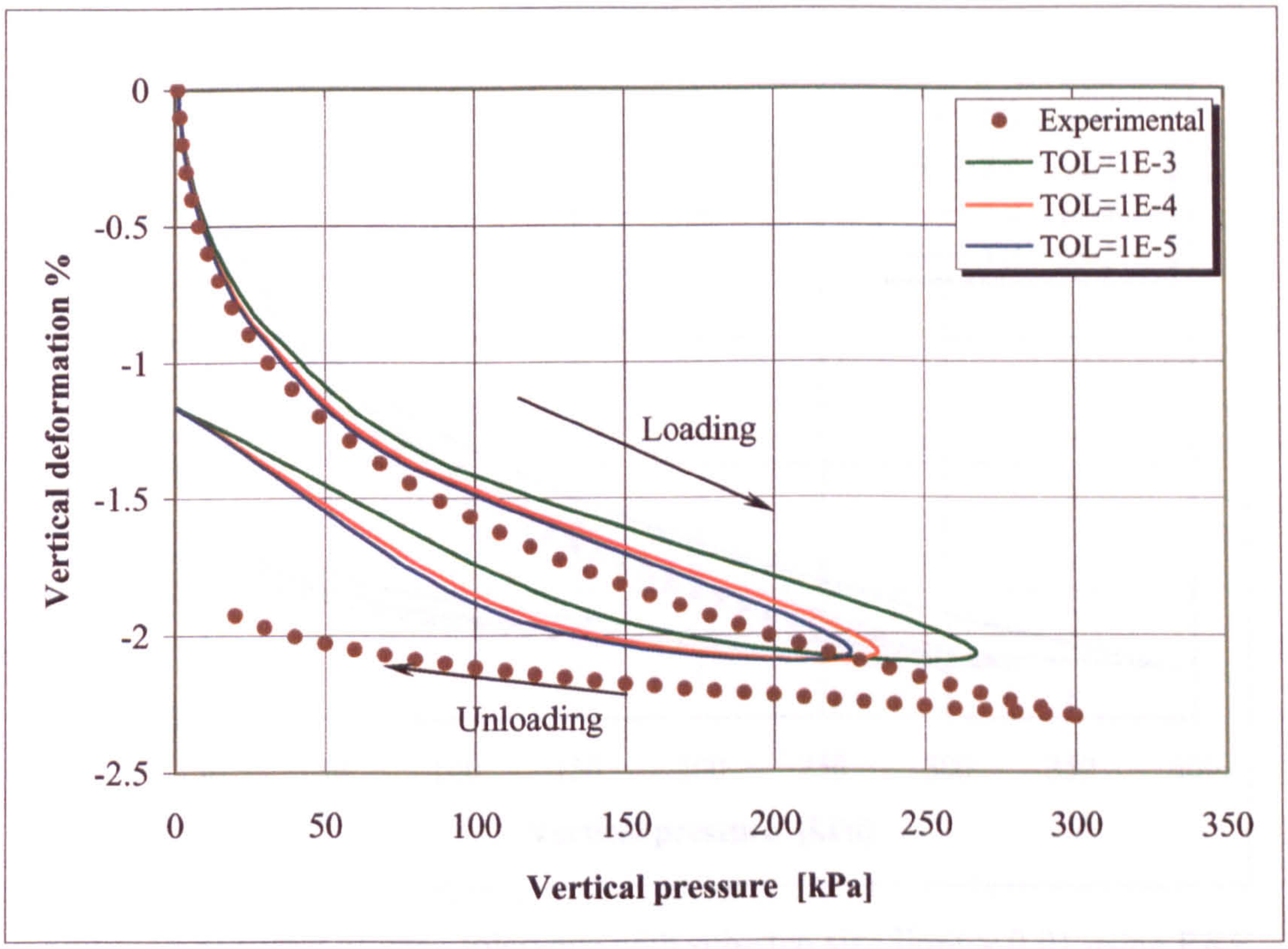

Figure (5.6) Effect of error tolerance with sub-step size limit =1 using RKF

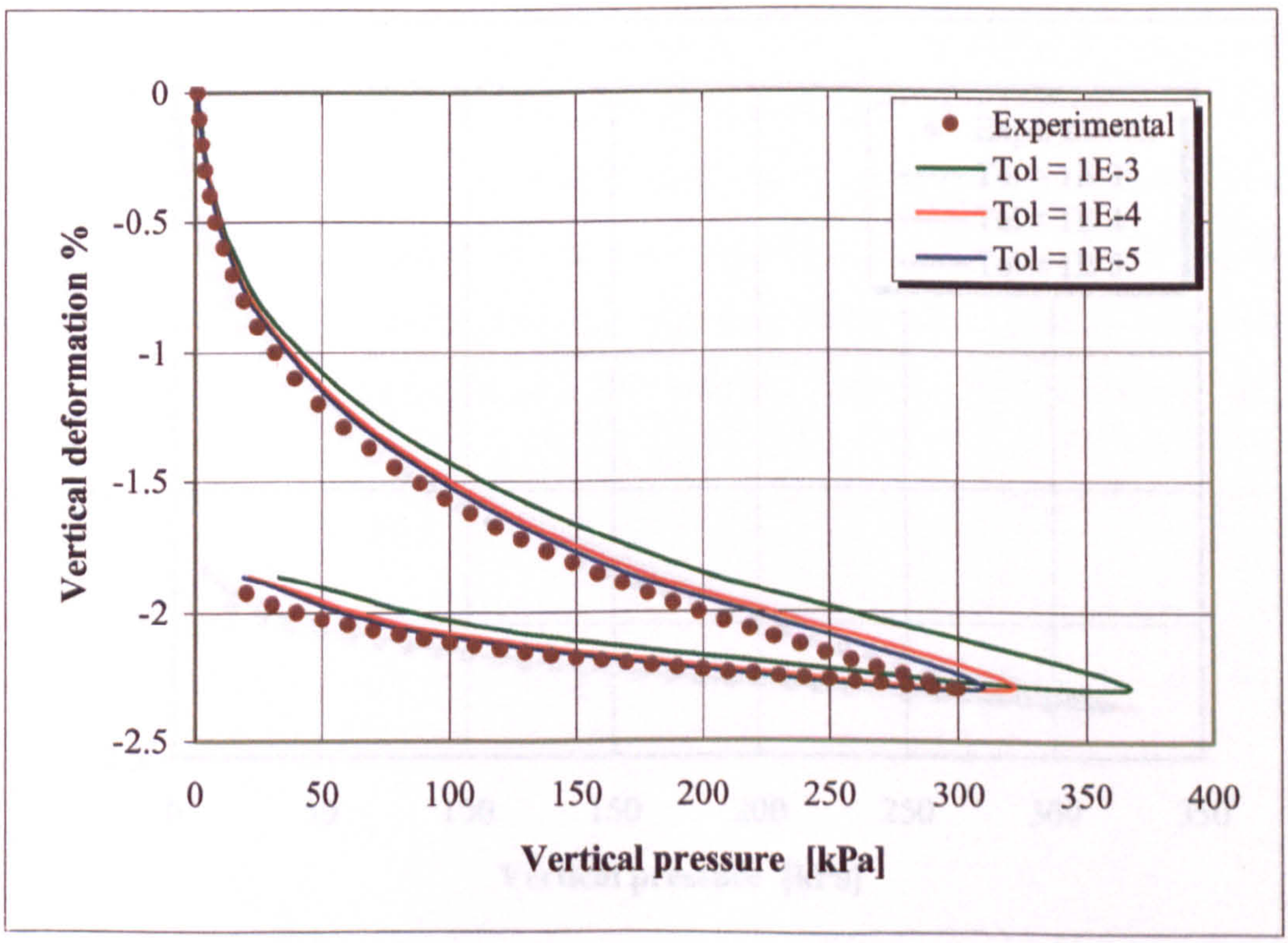

Figure (5.7) Effect of error tolerance with sub-step size limit = 0.1 using RKF

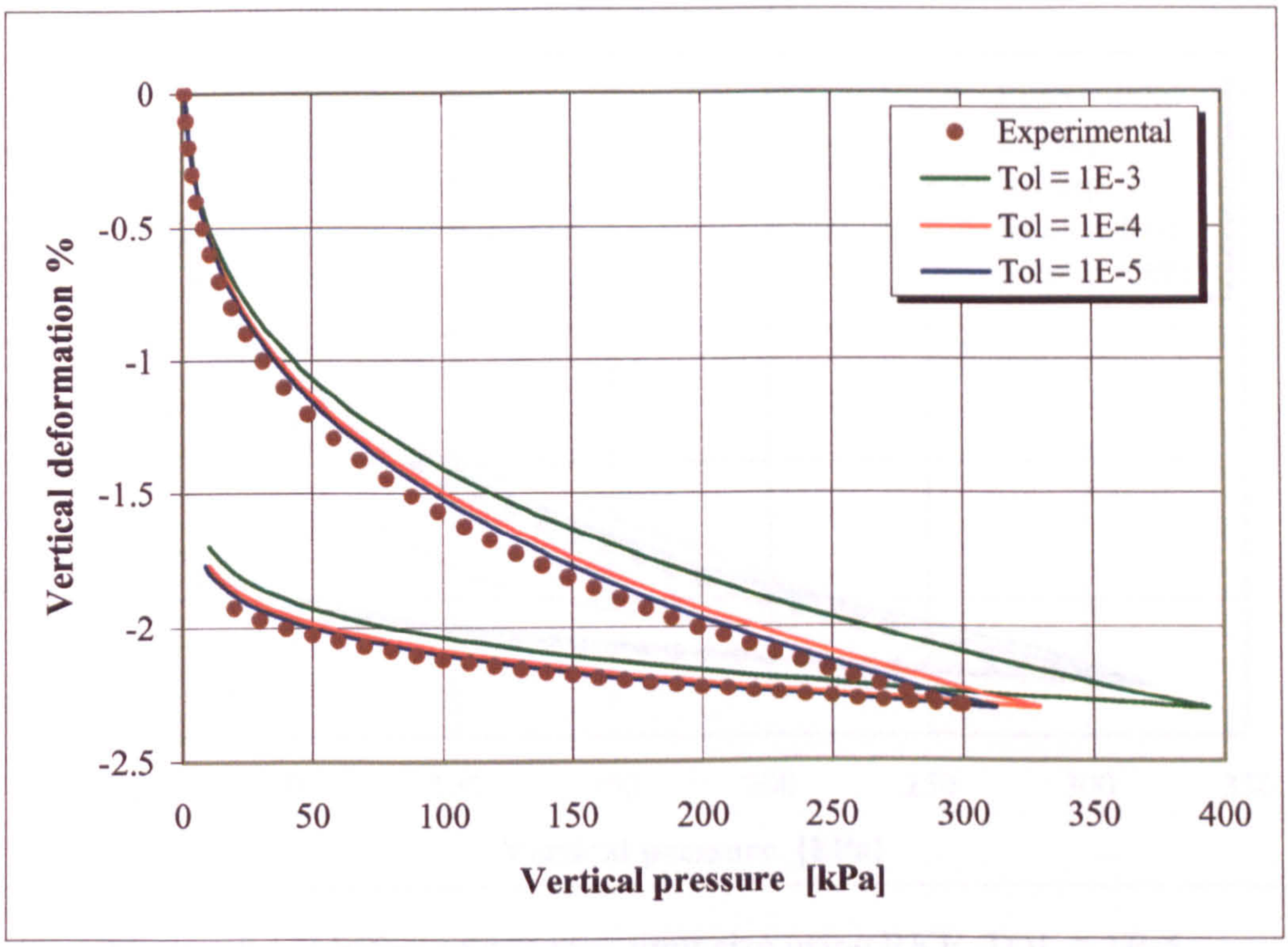

Figure (5.8) Effect of error tolerance with sub-step size limit = 0.01 using RKF

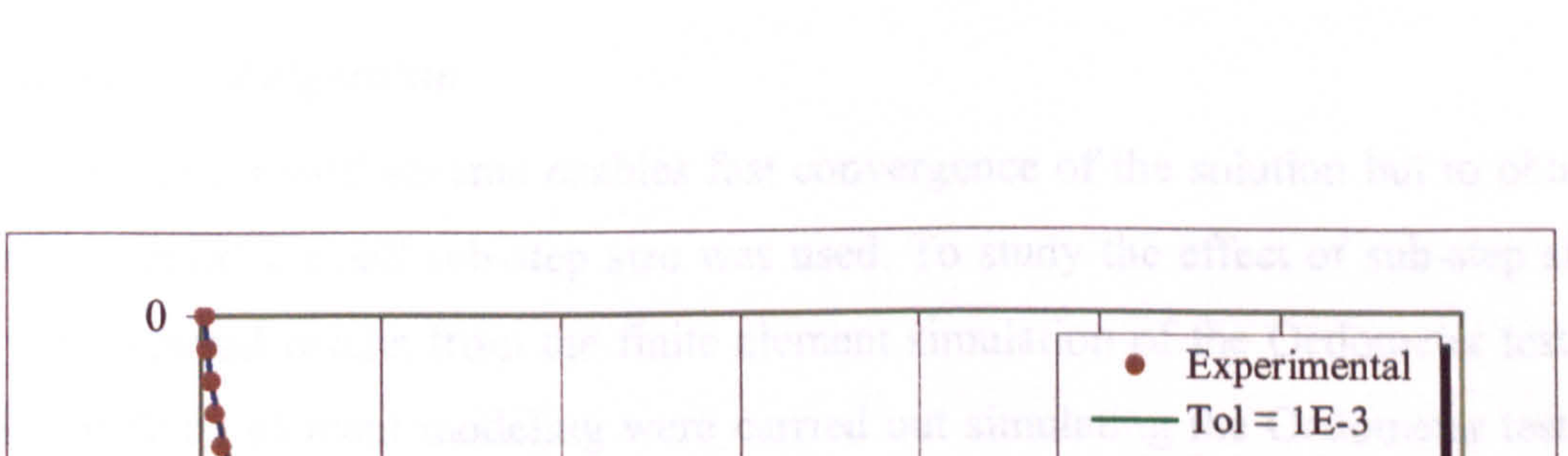

Figure (5.9) Effect of error tolerance with sub-step size limit = 0.001 using RKF

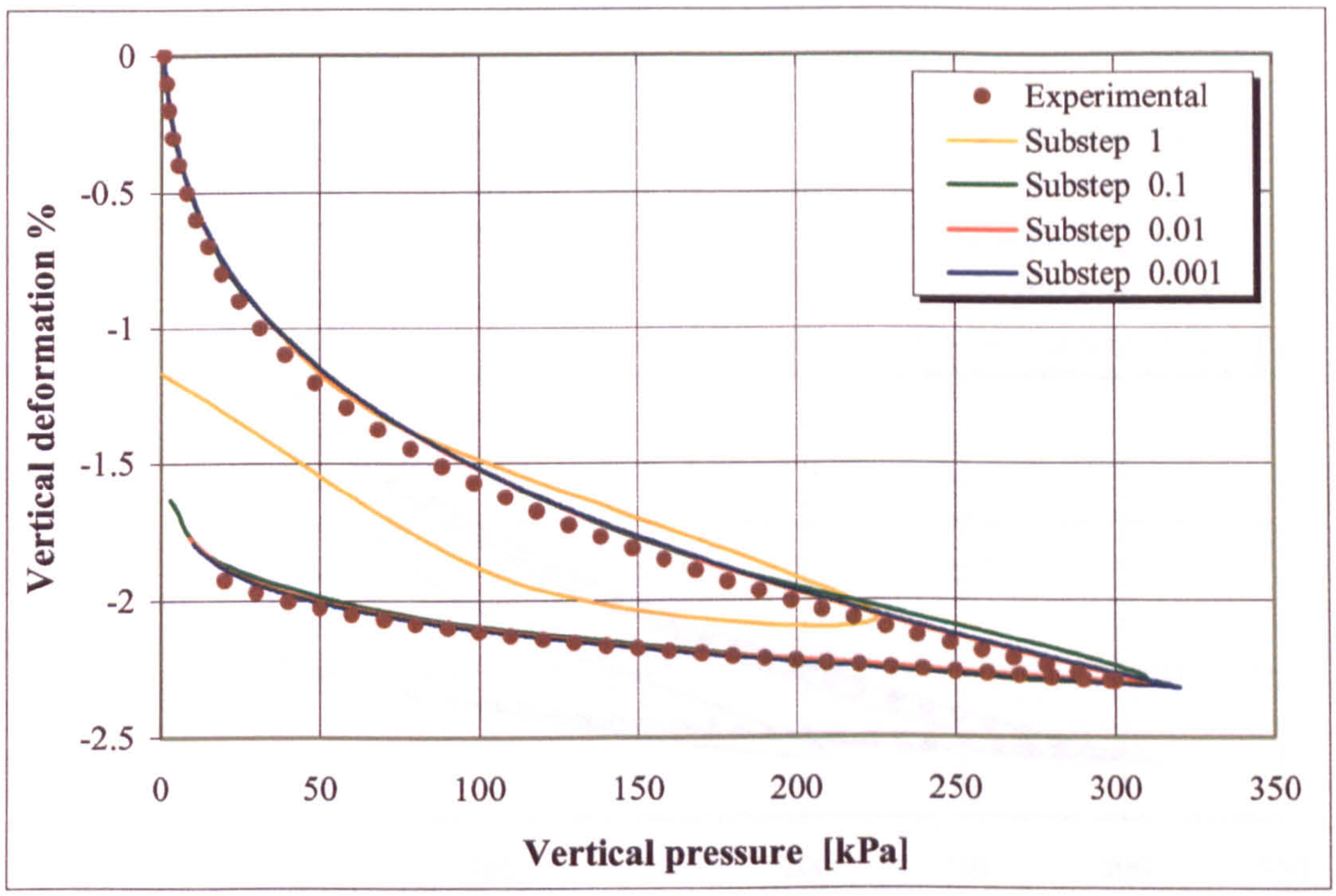

Figure (5.10) Effect of sub-step limit size using RKF, TOL = 1E-5

Euler-Forward algorithm

Euler-forward scheme enables fast convergence of the solution but to obtain accurate results a small sub-step size was used. To study the effect of sub-step size on the predicted results from the finite element simulation of the Oedometer test, a series of finite element modeling were carried out simulating the Oedometer test at different sub-step sizes during loading and unloading stress paths. Then the finite element results were compared with the available experimental results as shown in Figure (5.11). The figure represents the relation between the percentage of the vertical deformation $\left(\frac{Vertical\ displacement}{Total\ sample\ height}\%\right)$ and the corresponding pressure (vertical stress), in "kPa", at different sub-step sizes. The figure shows that accurate results can be obtained only with using a small sub-step size in the order of 0.001 or less.

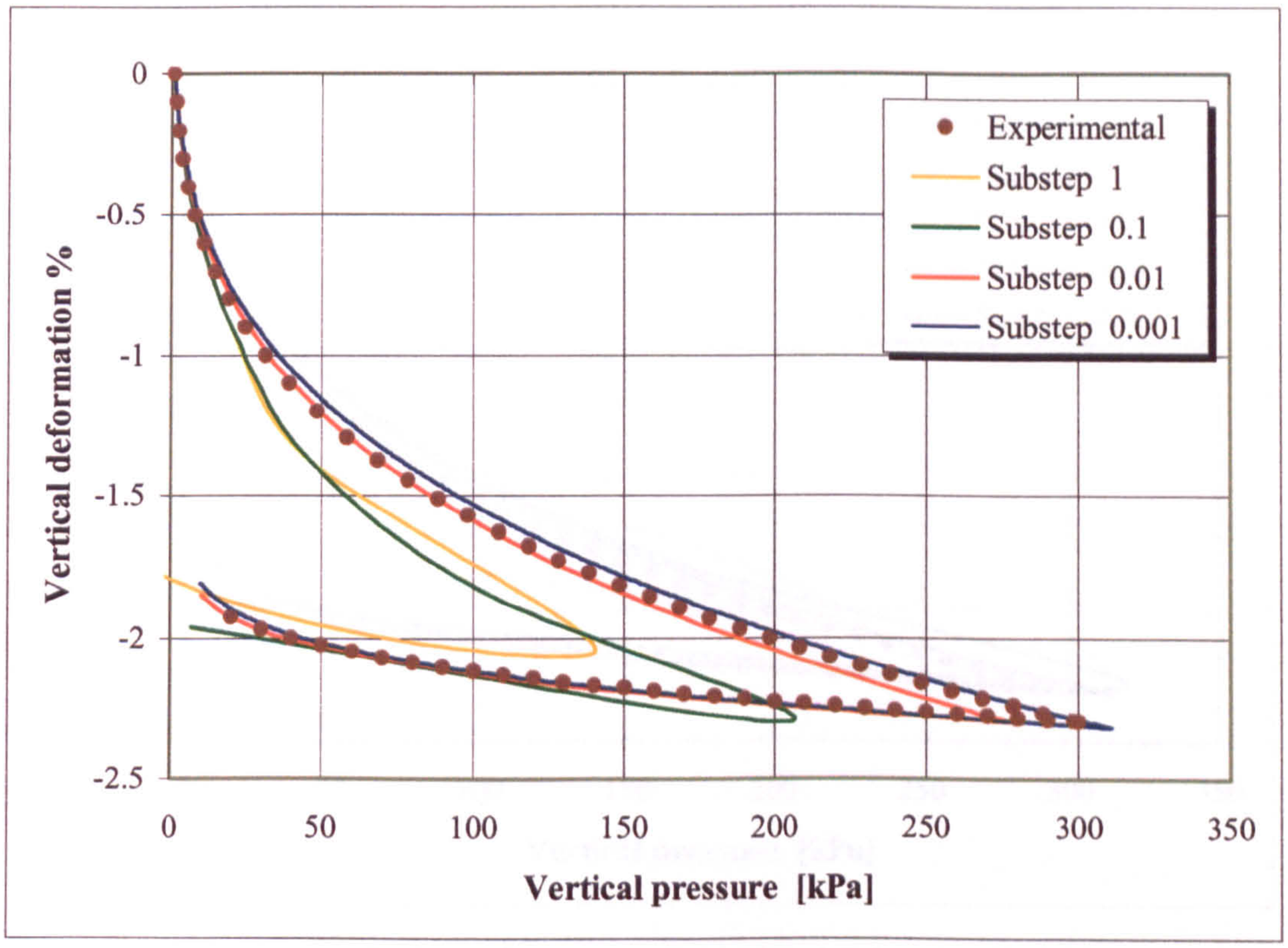

Figure (5.11) Effect of sub-step size using Euler-Forward algorithm

Crank-Nicolson (Mid-point) algorithm

The Crank-Nicolson algorithm has a known high performance, Tamagnini (1997). To study the effect of sub-step size on the predicted finite element results using the Crank-Nicolson algorithm a series of finite element simulations of the Oedometer test were carried out at different sub-step sizes (0.1, 0.01 and 0.001). Through the analysis of the Oedometer simulation the Crank-Nicolson scheme was shown to be more stable but slightly affected by sub-step size during loading. However during the unloading process using smaller sub-step size gave more accurate results. Figure (5.12) represents the relation between the percentage of the vertical deformation and the corresponding pressure (vertical stress), in "kPa", at different sub-step sizes. The figure shows that relatively computationally cheap results with reasonable accuracy can be obtained using a sub-step size limit in the order of '0.01'.

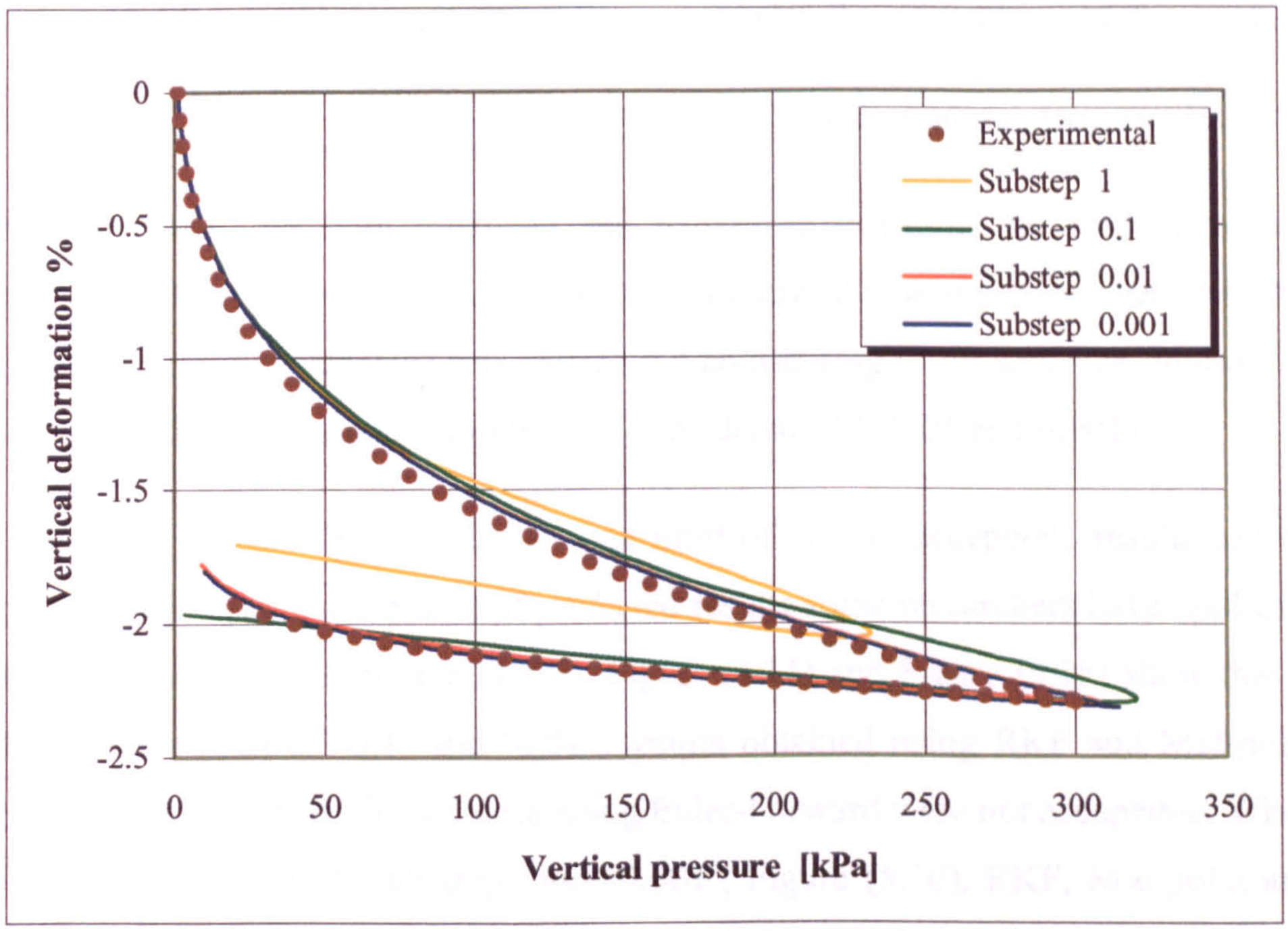

Figure (5.12) Effect of sub-step size using Mid-point algorithm

5.5.1.3 Effect of sub-step size

In the previous section a validation study of different integration schemes was discussed along with the effect of sub-step size on the performance of each integration scheme. In this section all the finite element results presented in the previous section were rearranged to make a comparison between these different integration schemes and to select the most appropriate one for integrating the hypoplastic model in a real finite element analysis. The overall run time for a simulation, with reasonable results, is strongly dependant on the sub-step size as shown in the previous section. As the upper limit of the sub-step size increases, ABAQUS will give results faster but increasing the upper limit may also affect result accuracy. Comparison between various different integration schemes at different sub-step sizes is presented in the following graphs, figures (5.13 – 5.16), in order to compare the performance of each integration scheme at different ABAQUS sub-step sizes.

Figures (5.13 – 5.16) present the relation between the percentage of the vertical deformation $\left(\frac{Vertical\ displacement}{Total\ sample\ height}\%\right)$ and the corresponding pressure (vertical stress) in "kPa" for both predicted and experimental results for Oedometer test simulation during loading and unloading. Firstly the comparison between the different integration schemes was carried out considering a sub-step size limit of '1' and then further sub-step size limits were considered (0.1, 0.01 and 0.001).

Figure (5.13) shows that at sub-step size limit of '1', no acceptable results can be achieved. To adjust for the drift of predicted results some researchers have applied a correction technique, Mattsson (1997). Figure (5.14) and Figure (5.15) show that at sub-step size limit of '0.1' and '0.01', results obtained using RKF and Mid-point were acceptable but results obtained using Euler-Forward were not acceptable. When using a relatively small sub-step limit '0.001', Figure (5.16), RKF, Mid-point and Euler-forward gave reasonable results that match the experimental results very well.

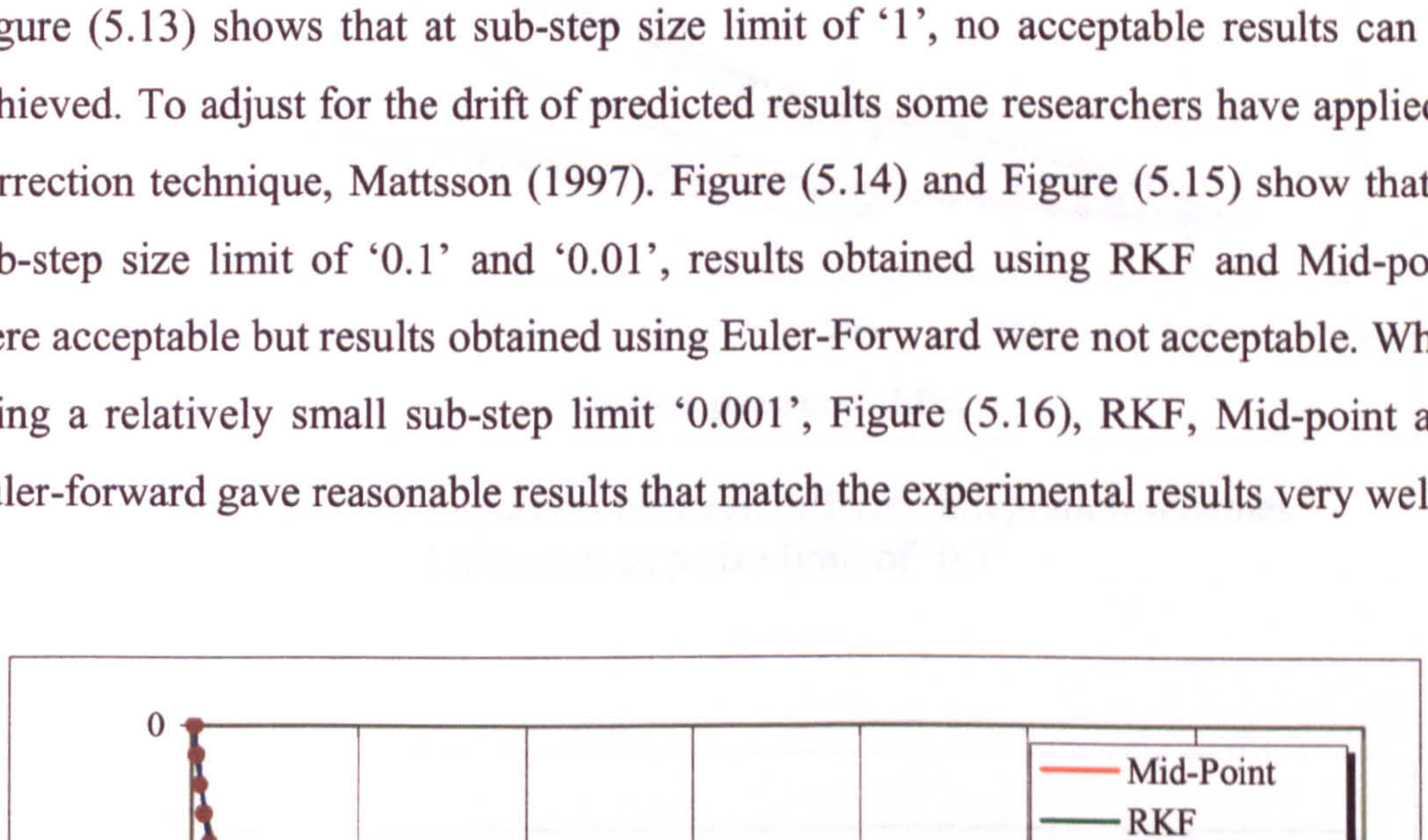

Figure (5.13) Comparison between different integration schemes
Using sub-step size limit of '1'

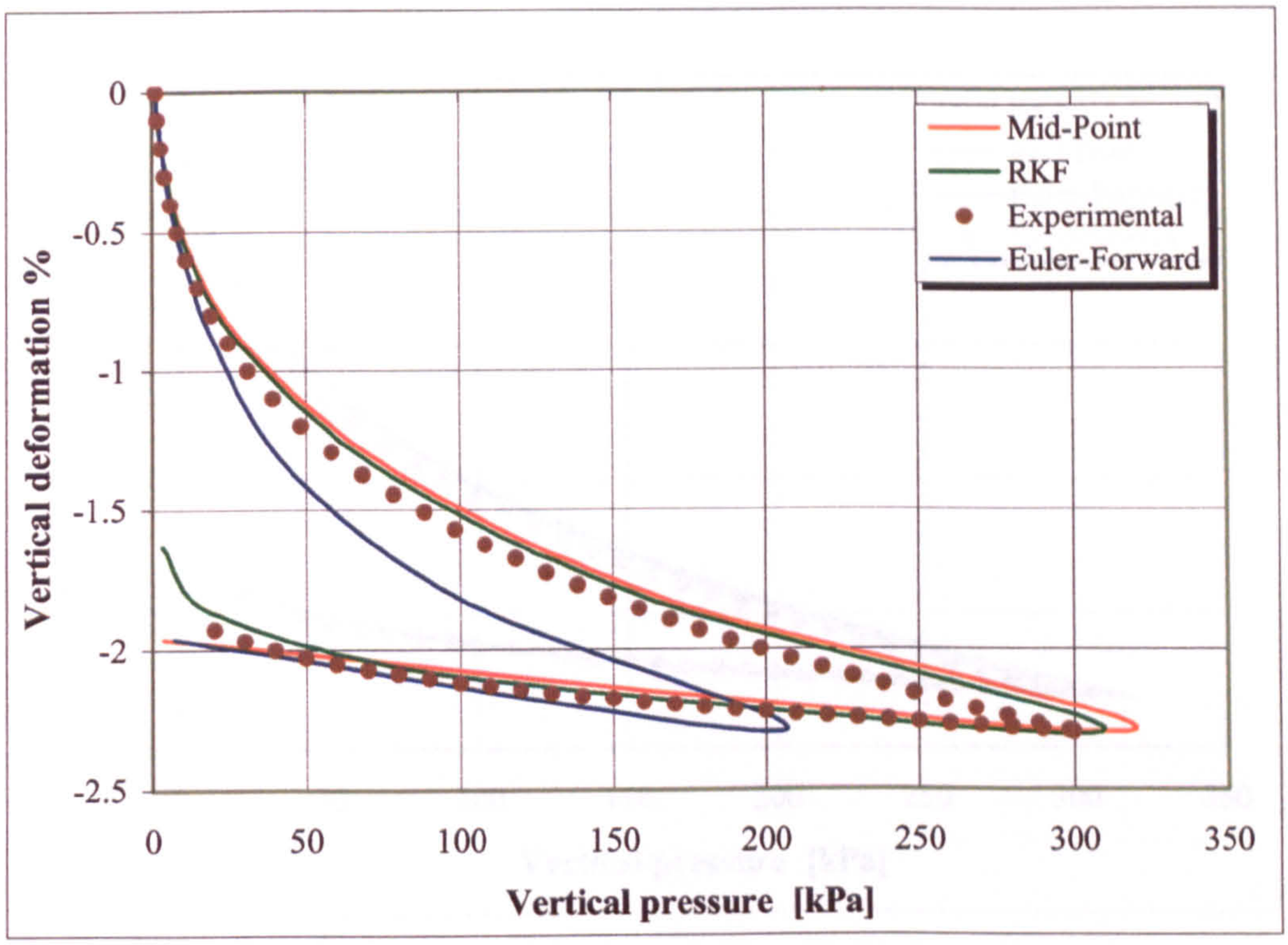

Figure (5.14) Comparison between different integration schemes
Using sub-step size limit of '0.1'

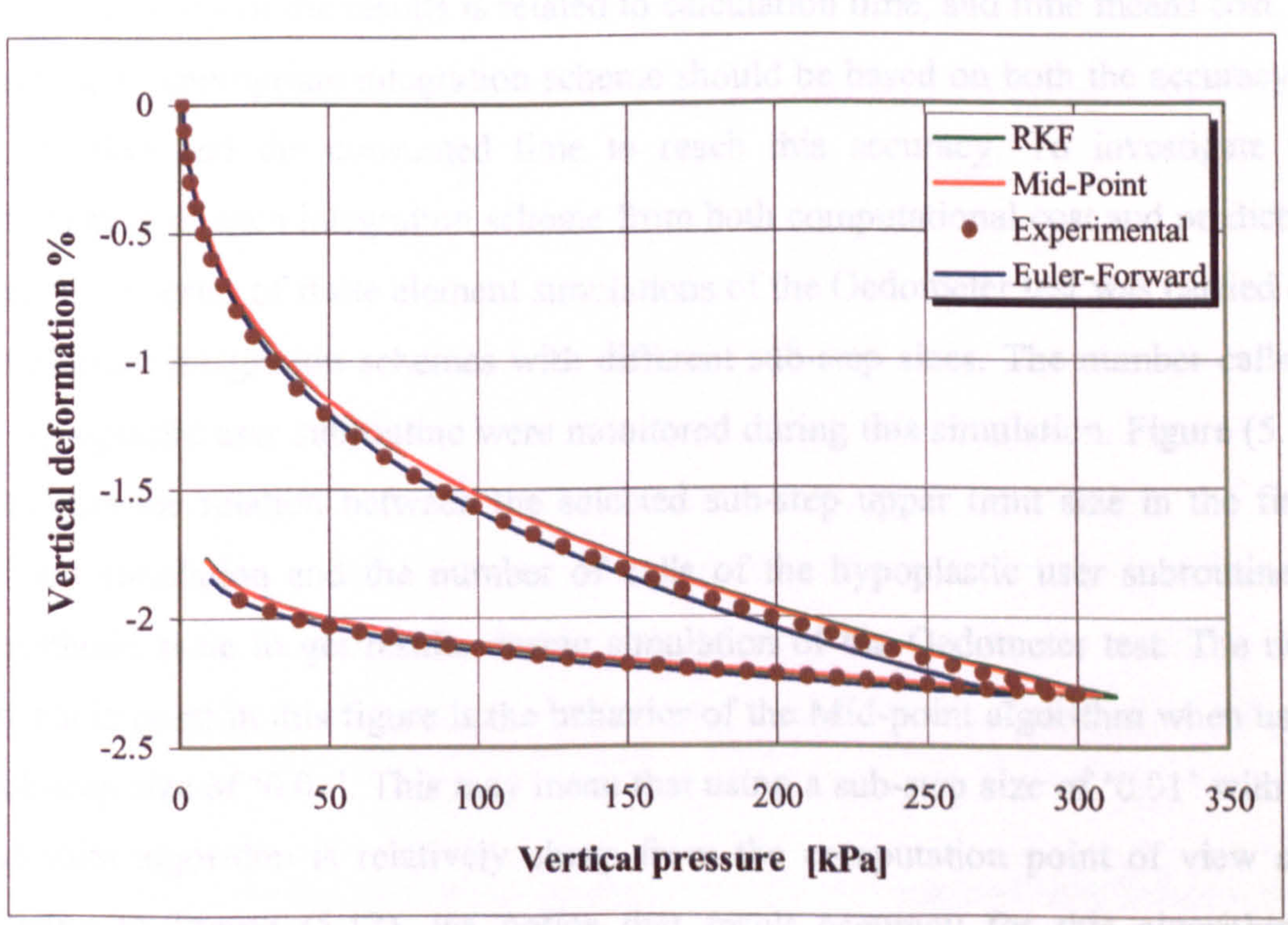

Figure (5.15) Comparison between different integration schemes
Using sub-step size limit of '0.01'

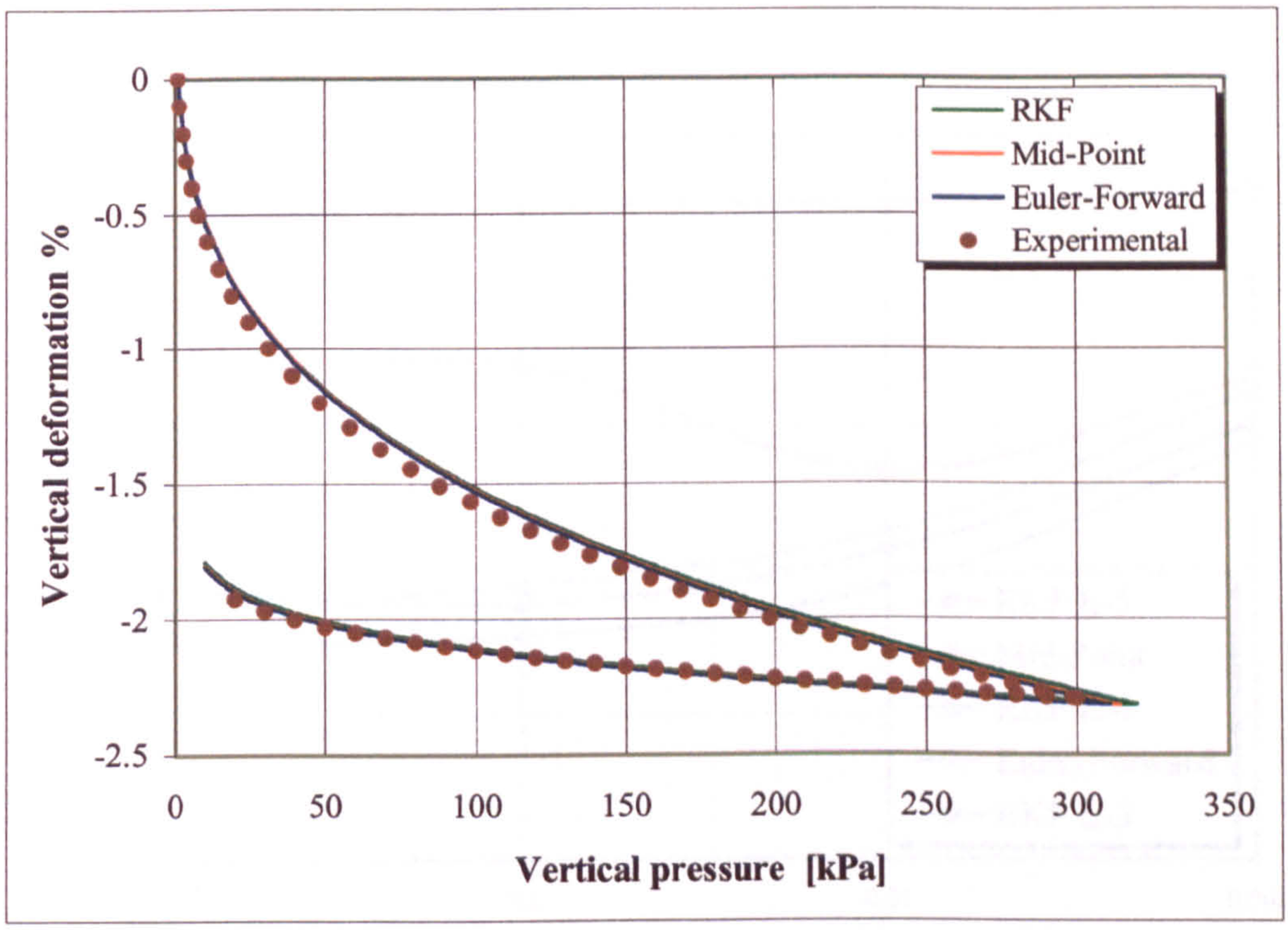

Figure (5.16) Comparison between different integration schemes
Using sub-step size limit of '0.001'

5.5.1.4 Computational time and result accuracy

Accuracy of the results is related to calculation time, and time means cost. So selecting an appropriate integration scheme should be based on both the accuracy of the solution and the consumed time to reach this accuracy. To investigate the performance of each integration scheme from both computational cost and prediction accuracy, a series of finite element simulations of the Oedometer test was carried out for different integration schemes with different sub-step sizes. The number calls of the hypoplastic user subroutine were monitored during this simulation. Figure (5.17) represents the relation between the selected sub-step upper limit size in the finite element simulation and the number of calls of the hypoplastic user subroutine in logarithmic scale to get results during simulation of the Oedometer test. The most noticeable point in this figure is the behavior of the Mid-point algorithm when using a sub-step size of '0.01'. This may mean that using a sub-step size of '0.01' with the Mid-point algorithm is relatively cheap from the computation point of view and, referring to Figure (5.12), we notice that result accuracy for this algorithm is reasonable.

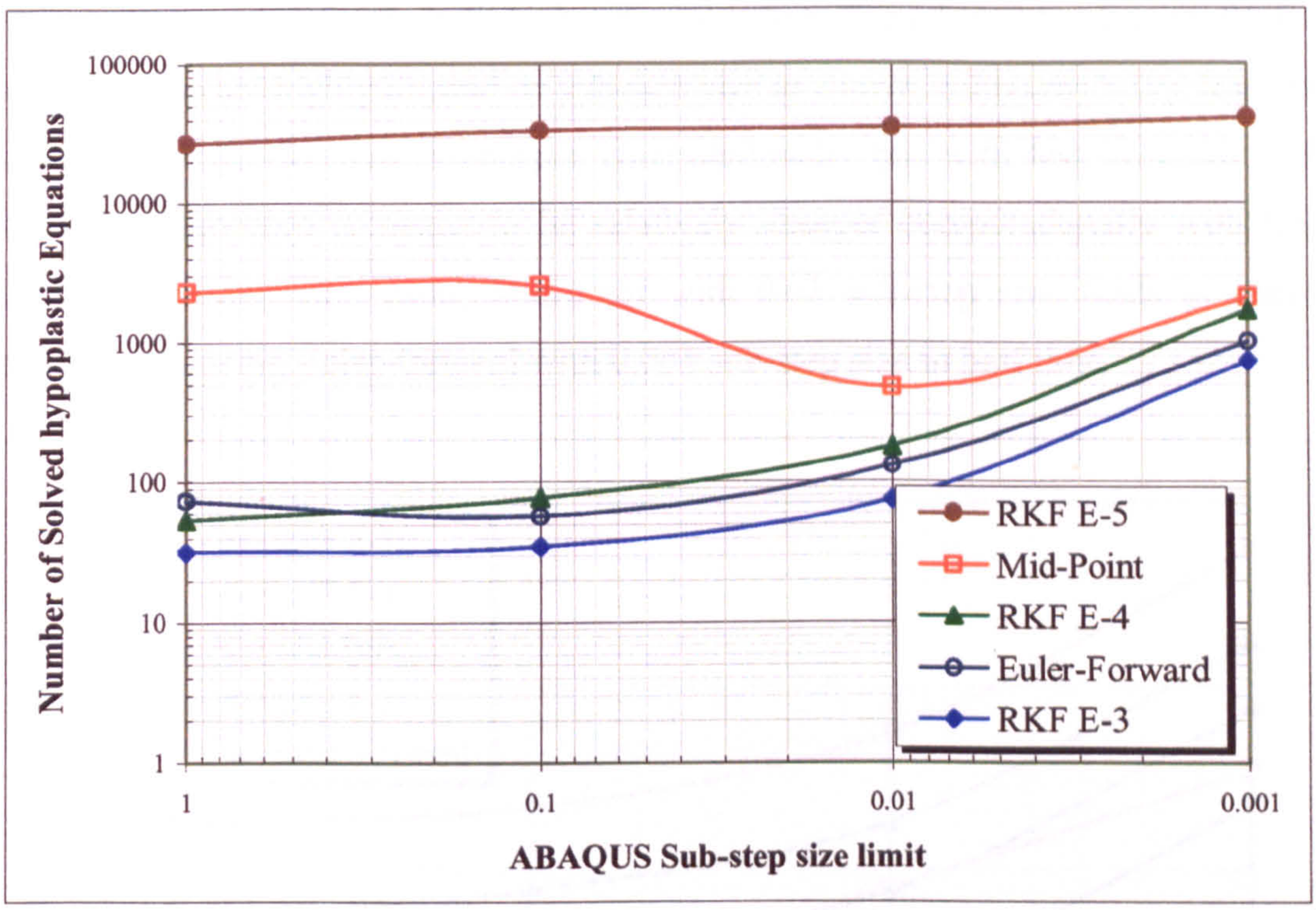

Figure (5.17) Computational comparison of different integration schemes

A clue to the computational behaviour of the Mid-point algorithm in Figure (5.17) was revealed when the solution procedure was monitored for each call of the user subroutine UMAT. Since occasionally the UMAT call does not return results, and it just modified the sub-step size for another call, the number of ABAQUS user subroutine calls may not be the best way to assess computational cost.

A more accurate way to compare the behavior of each integration scheme and to ascertain the most appropriate is to monitor time consumed to complete the simulation using different integration schemes and different sub-step limits. To this end, a comparison between different integration schemes was carried out at different sub-step sizes considering the time cost for each simulation to be done. This investigation was carried out using a single processor Pentium III 500 MHz with 120 MB ram computer.

Figure (5.18) represent the relation between the sub-step size and time consumed for different integration schemes in a logarithmic scale. From the Figure it is clear that

the RKF scheme was the most expensive method computationally for integration of the hypoplastic model even with high error tolerance. The advantage of using RKF is that results do not highly depend on sub-step size as shown in Figure (5.10). It is also shown that Euler-forward is cheaper computationally but with less accuracy. The Mid-point algorithm is seems to be relatively cheaper computationally with high accuracy; for example, using Mid-point with 0.01 sub-step size leads to results accurate than using Euler-forward with 0.001 sub-step size in half time.

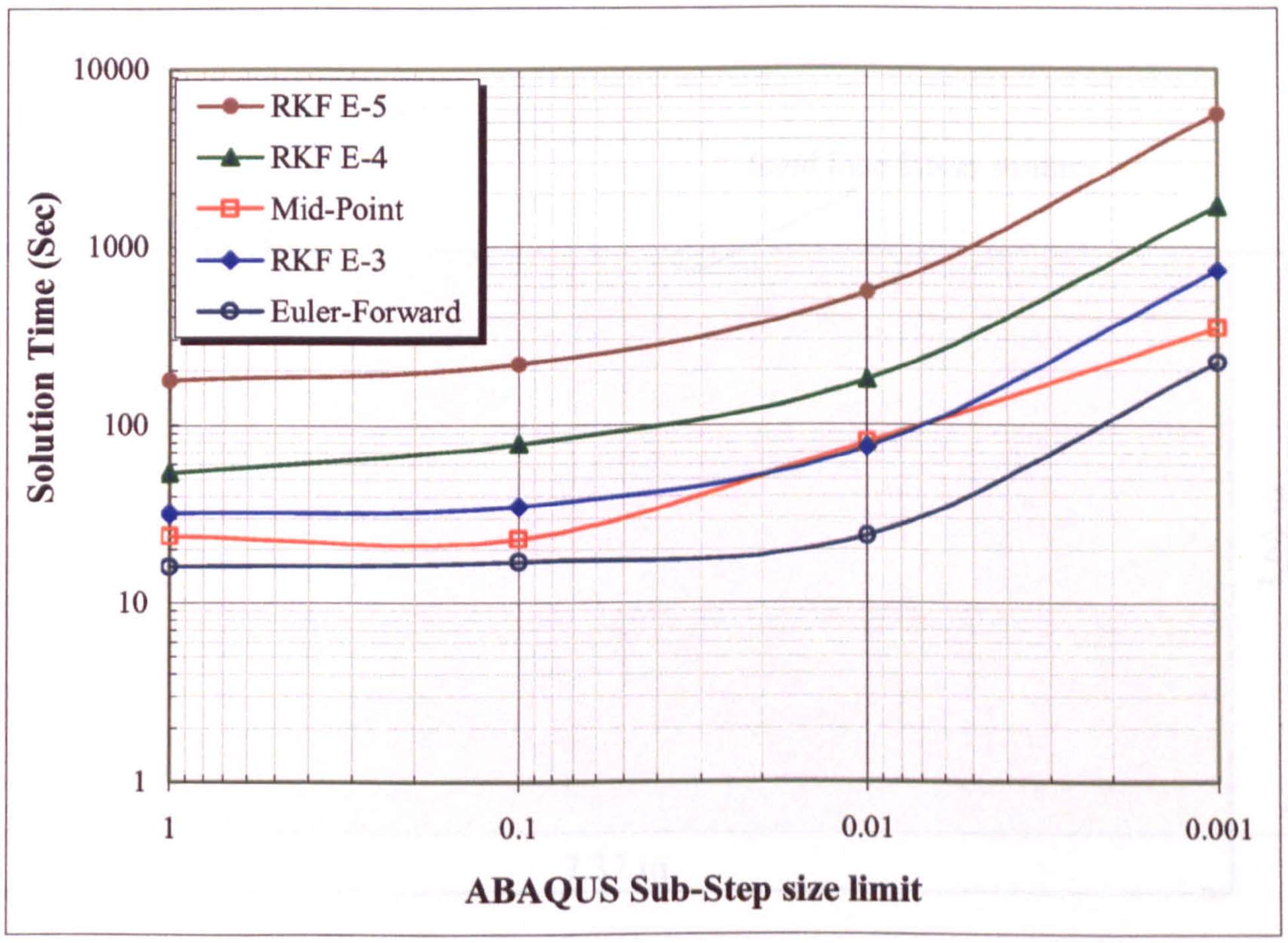

Figure (5.18) Time cost for different integration schemes – in Logarithmic scale

5.5.2 STRIP FOOTING SIMULATION

Before starting to use the hypoplastic model to simulate fully drained dry sandy soil in the soil-tool interface application, a more complex two-dimensional plane strain problem was simulated to check the performance of the hypoplastic model to describe sand behaviour.

5.5.2.1 Problem description

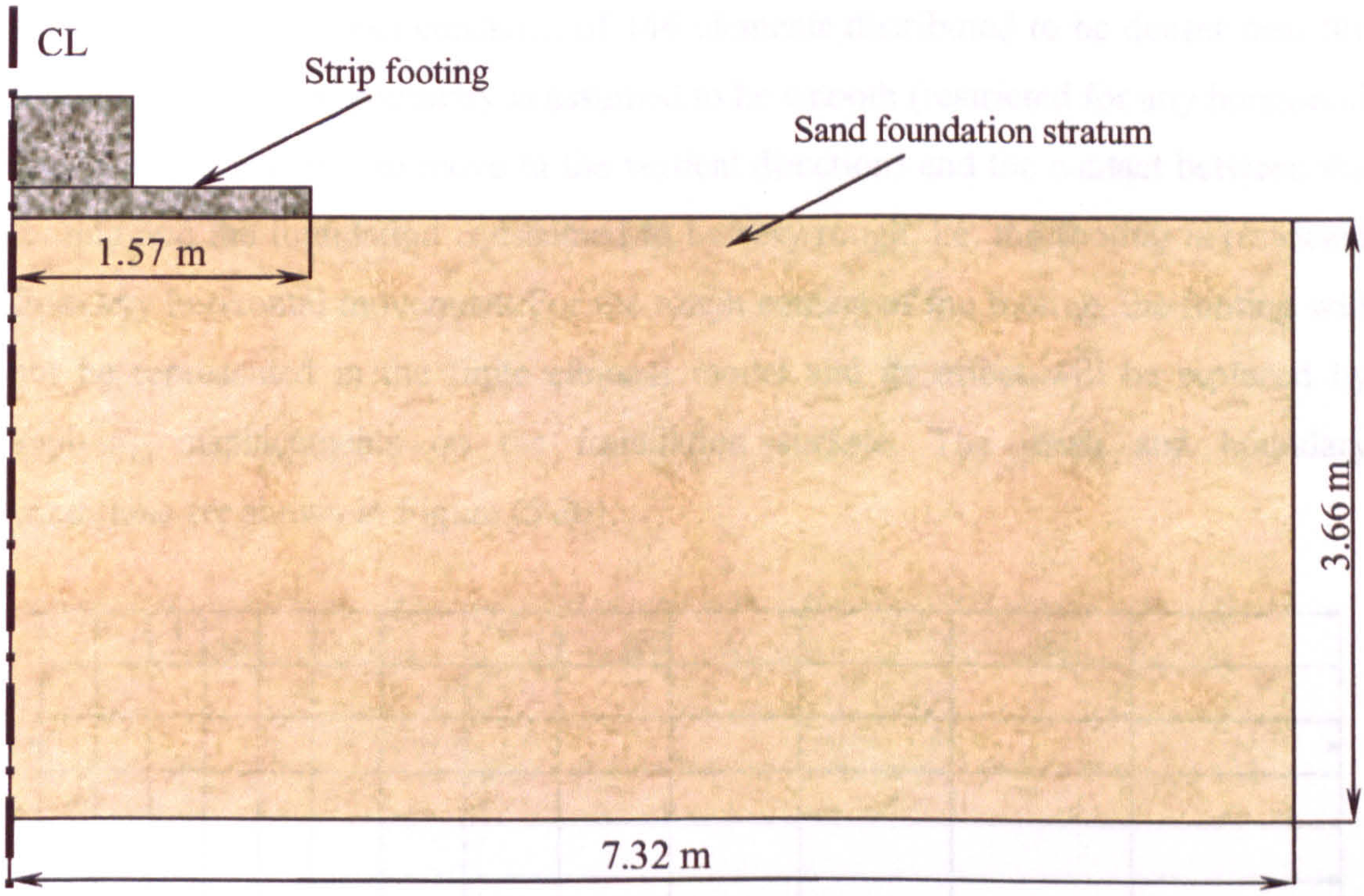

Figure (5.19) Footing and foundation stratum main features

A rough rigid strip footing subjected to vertical downward loading was analyzed. A strip footing of width 3.14 m is settled on a sandy foundation stratum extended to assumed bound located on a distance of 7.32 m from the footing center and having a depth of 3.66 m. The foundation was modeled using the hypoplastic parameters shown in Table [5.2] with initial void ratio $e_o = 0.69$. The vertical load of the footing was modeled by applying a displacement on the footing to allow settlement to about 10 % of the total modeled depth.

Table [5.2] Parameters of the hypoplastic model for strip-footing analysis

φ_c (deg)	h_s (MPa)	n	e_{d0}	e_{c0}	e_{i0}	α	β
33	1000	0.25	0.55	0.95	1.05	0.25	1.5

5.5.2.2 Finite element model

The problem is analyzed as a plane strain problem. The foundation was modeled using ABAQUS\Standard 2-Dimension continuum quadratic (8 node) reduced integration CPE8R elements. Due to symmetry, only one half of the footing was modeled. The mesh consisted of 144 elements distributed to be denser near the footing. The vertical boundary is assumed to be smooth (restricted for any horizontal displacement and free to move in the vertical direction) and the contact between the footing and the foundation is assumed to be very rough, i.e. the footing is restricted from any horizontal movement. For the rough contact of the footing, the footing will not be represented in the finite element model and its effect will be replaced by applying displacements on the foundation surface. The mesh and boundary conditions are shown in Figure (5.20).

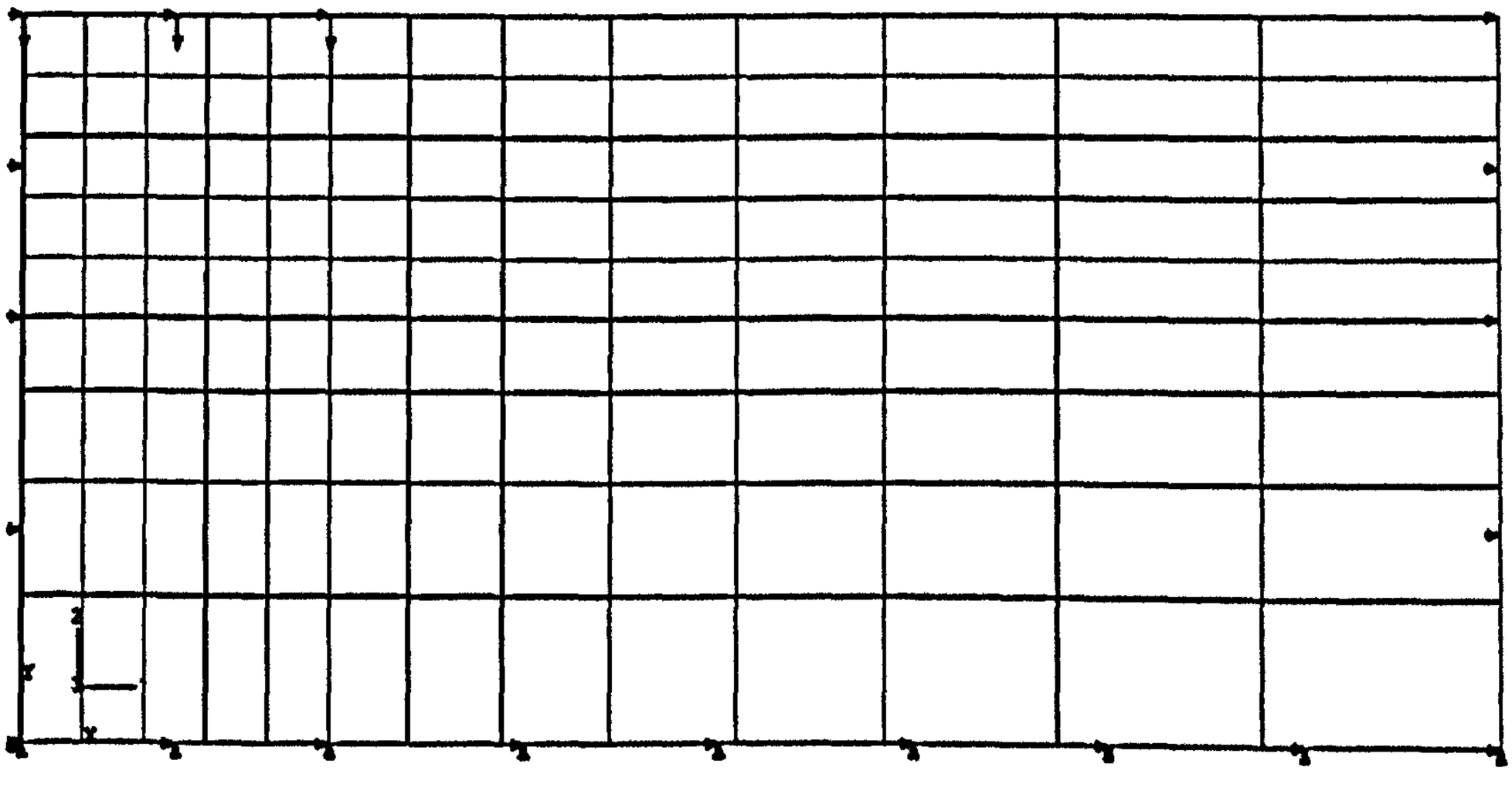

Figure (5.20) Finite element mesh and boundary conditions of a strip footing

As shown in this figure, the vertical and symmetric boundaries are restricted for any horizontal movement and the bottom horizontal boundary is restricted for both vertical and horizontal movement. The ABAQUS input file for the strip-footing simulation is listed in Appendix (E.2).

5.5.2.3 Effect of mesh density

First the effect of mesh density is examined by running a series of finite element simulations with different mesh densities, a coarse mesh (using 48 elements), a medium mesh (using 70 elements), a fine mesh (using 117 elements) and a very fine mesh (using 320 elements). The analysis was carried out using the Euler-forward algorithm to integrate the hypoplastic equation with a sub-step size limit of '0.001'. Figure (5.21) represents the relation between footing settlement, measured by the percentage of footing displacement to the total foundation simulated height, and the normal stress applied on the foundation measured at a node located just under the footing center for different mesh densities; the foundation settlement and its corresponding reaction normal stress are compressive sense. Results shown in Figure (5.21) reveal that using a coarse mesh may leads to inaccurate results and that as the mesh density increases this effect becomes insignificant. Hence the fine mesh (117 elements) was used in the finite element analysis of the strip footing problem. The same conclusion was drawn using the Mid-point algorithm to integrate the hypoplastic equation as shown in Figure (C.1).

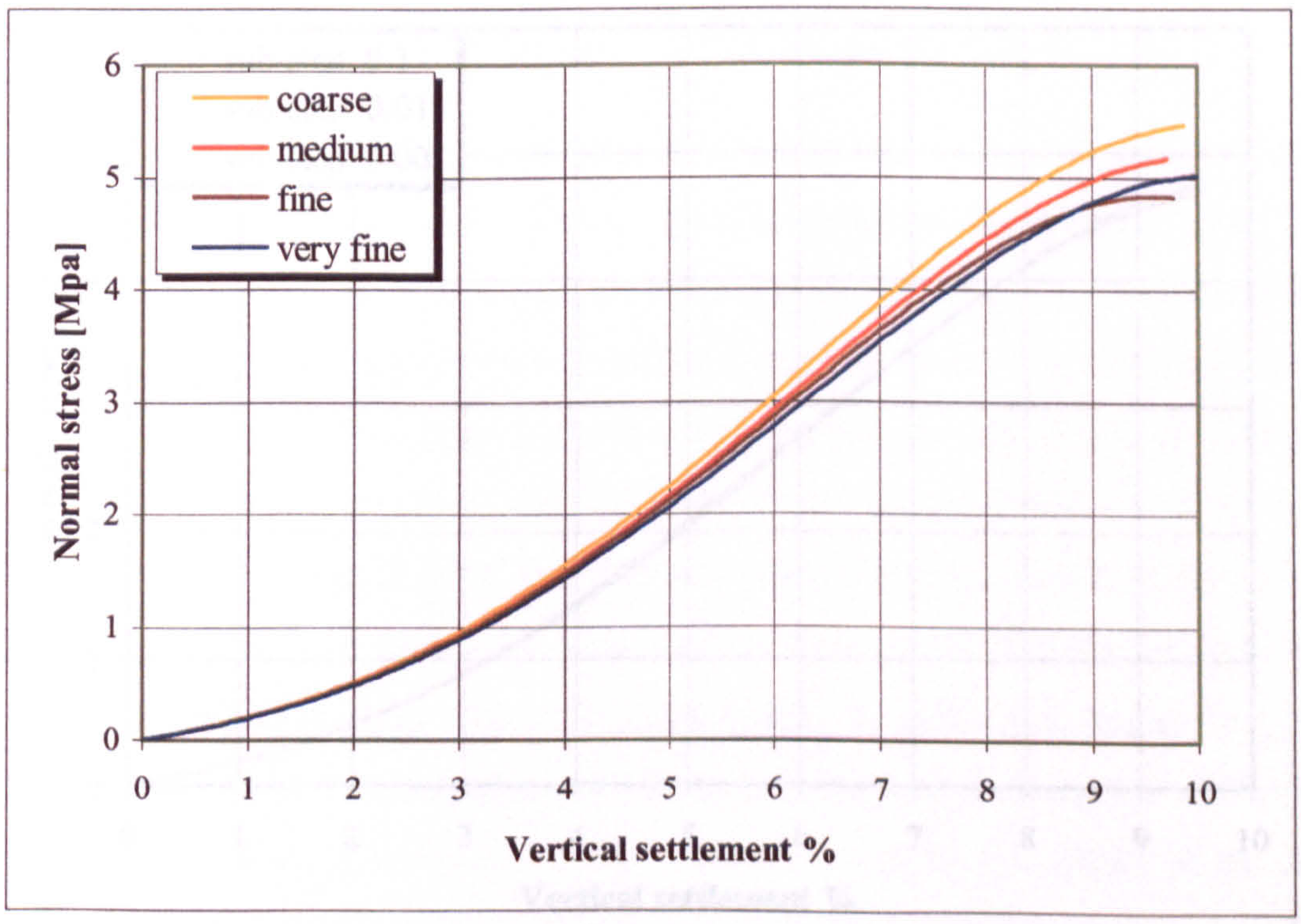

Figure (5.21) Effect of mesh density on simulating strip footing using Euler-forward

5.5.2.4 Validation of different integration schemes

To check the capability of the used algorithms, they were used again to integrate the hypoplastic model for simulating the strip footing on a foundation. The vertical settlement was plotted versus the reaction vertical compressive stress at a node just under the middle of the footing for different integration schemes and different sub-step size and different allowable error tolerances.

Runge-Kutta-Fehlberg (RKF) algorithm

The effect of substep size and allowable error tolerance, when using the RKF algorithm to integrate the hypoplastic model in the strip footing simulation, were examined. Figure (5.22) represents the relation between the percentage of the foundation settlement versus normal stress at a node just under the footing center using the RKF algorithm with different sub-step sizes (0.1, 0.01 and 0.001) and for an allowable error tolerance of '1E-3'. From the figure it is shown that results obtained by using the RKF are very close to each other for the examined range of sub-step size.

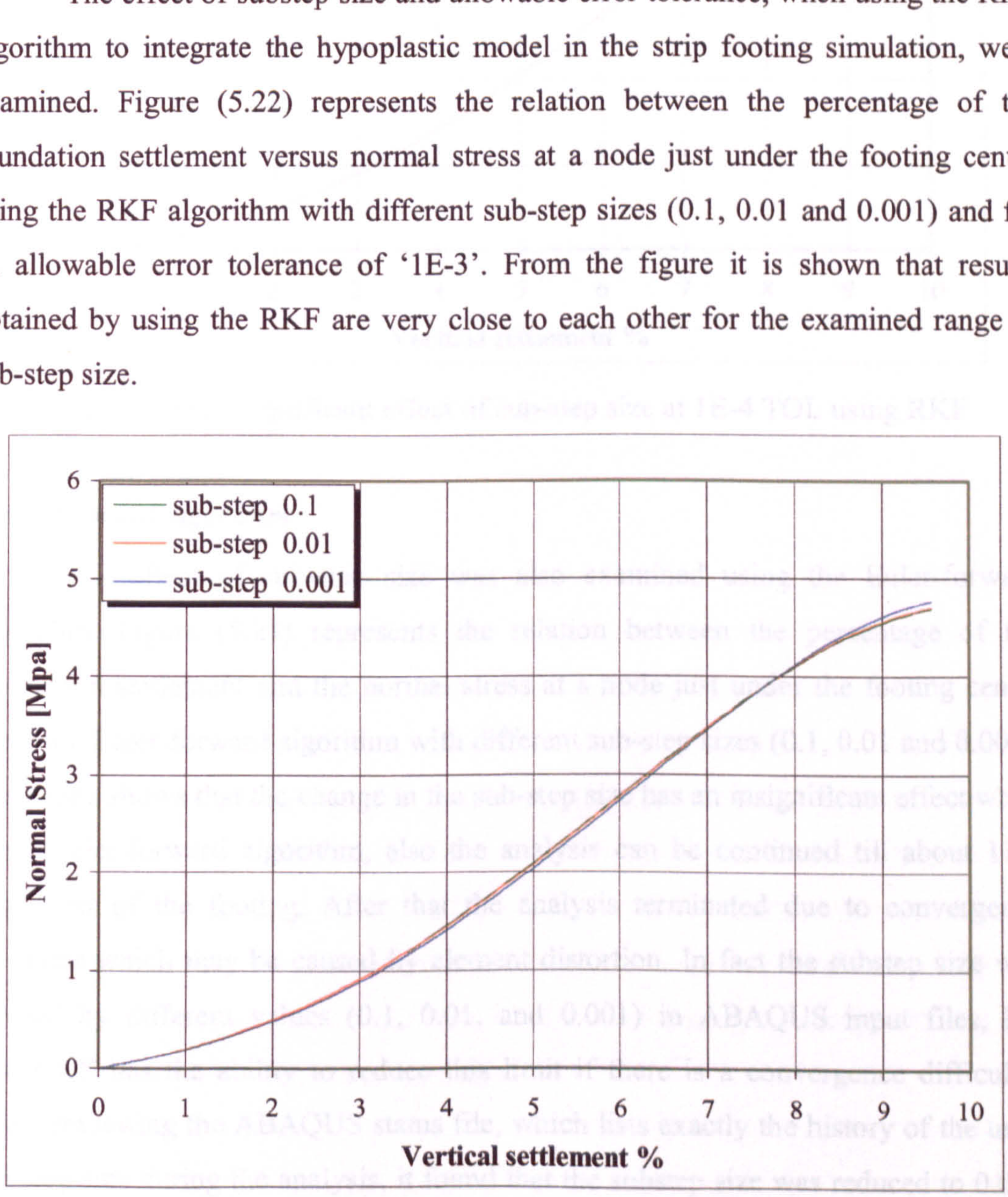

Figure (5.22) Effect of sub-step size at 1E-3 accuracy using RKF

An Insignificant effect of the sub-step size was obtained when allowable error tolerance was decreasing to (TOL = 1E-4) as shown in Figure (5.23).

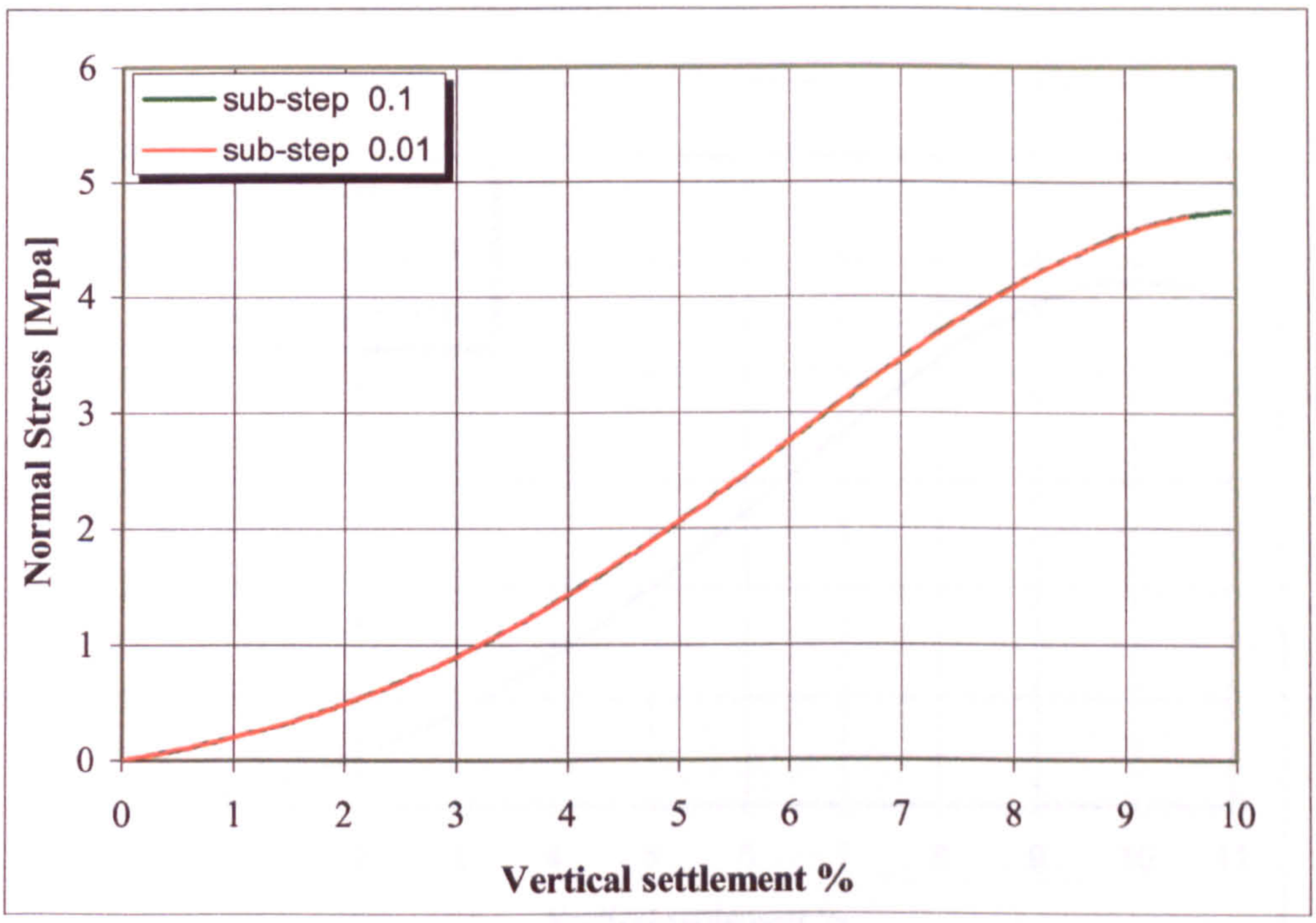

Figure (5.23) Insignificant effect of sub-step size at 1E-4 TOL using RKF

Euler-forward algorithm

The effect of sub-step size was also examined using the Euler-forward algorithm. Figure (5.24) represents the relation between the percentage of the foundation settlement and the normal stress at a node just under the footing center using the Euler-forward algorithm with different sub-step sizes (0.1, 0.01 and 0.001). The figure shows that the change in the sub-step size has an insignificant effect when using Euler-forward algorithm, also the analysis can be continued till about 11% settlement of the footing. After that the analysis terminated due to convergence problems which may be caused by element distortion. In fact the substep size was defined by different values (0.1, 0.01, and 0.001) in ABAQUS input files, but ABAQUS has the ability to reduce this limit if there is a convergence difficulty. When reviewing the ABAQUS status file, which lists exactly the history of the used sub-step size during the analysis, it found that the substep size was reduced to 0.001 (some times less than 0.001) to achieve convergence of the solution and hence the

substep sizes 0.1 and 0.01 in Figure (5.24) and were not considered by ABAQUS during the analysis and hence represents only results obtained using sub-step size of '0.001'.

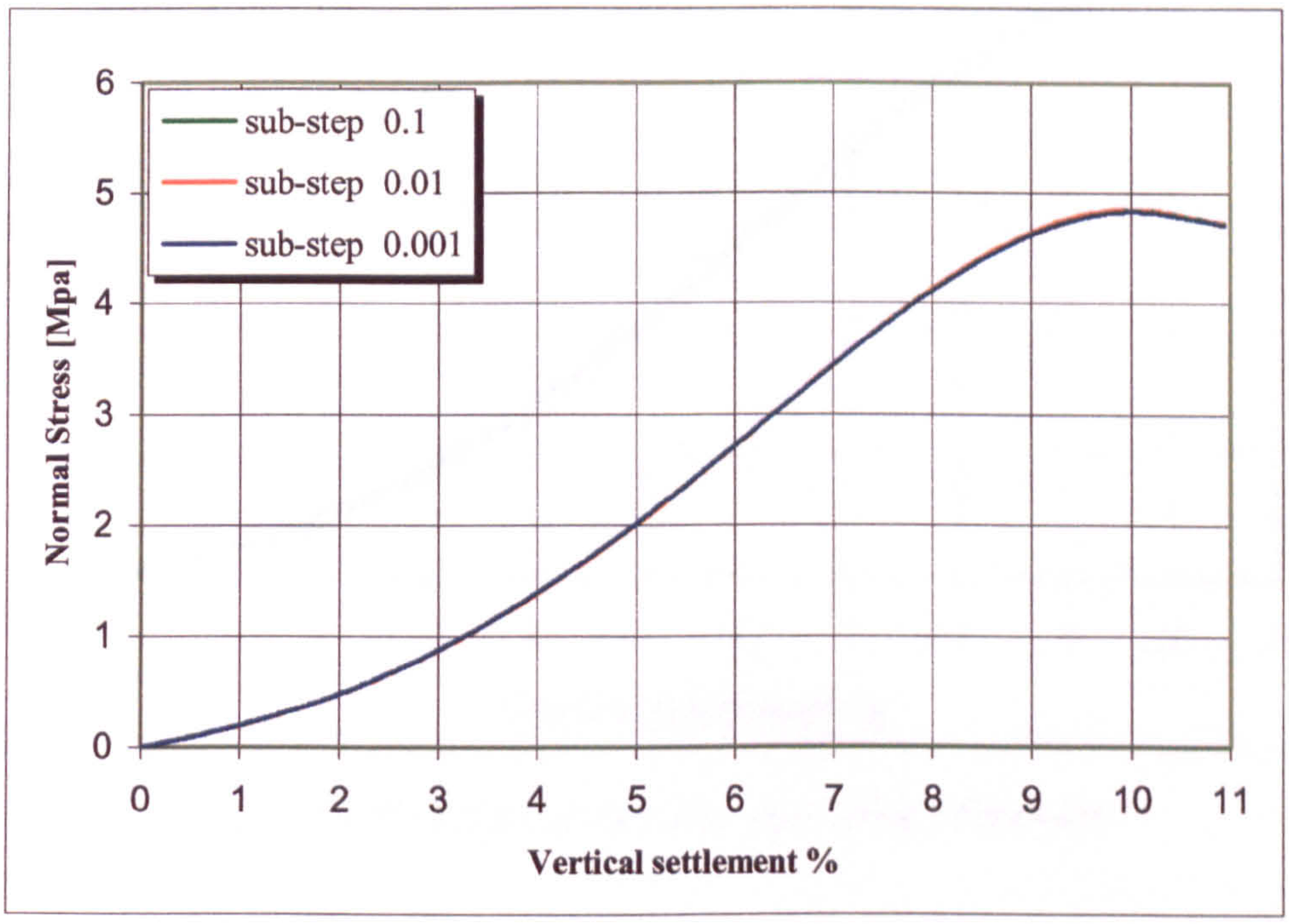

Figure (5.24) Effect of sub-step size using Euler-forward

Crank-Nicolson (Mid-point) algorithm

Similar conclusions of the effect of sub-step size on simulating the strip footing can be drawn by using the Mid-point algorithm. Figure (5.25) represents the relation of the percentage of the foundation settlement versus normal stress at a node just under the footing center using the Mid-point algorithm with different sub-step sizes (0.01 and 0.001). The figure shows insignificant effect of the sub-step size on result accuracy, but when using small sub-step size of '0.001' the analysis was carried on for about 11% foundation settlement. As mentioned before with Euler-forward, ABAQUS may also reduce the sub-step size during the analysis to achieve convergence using the Mid-point algorithm.

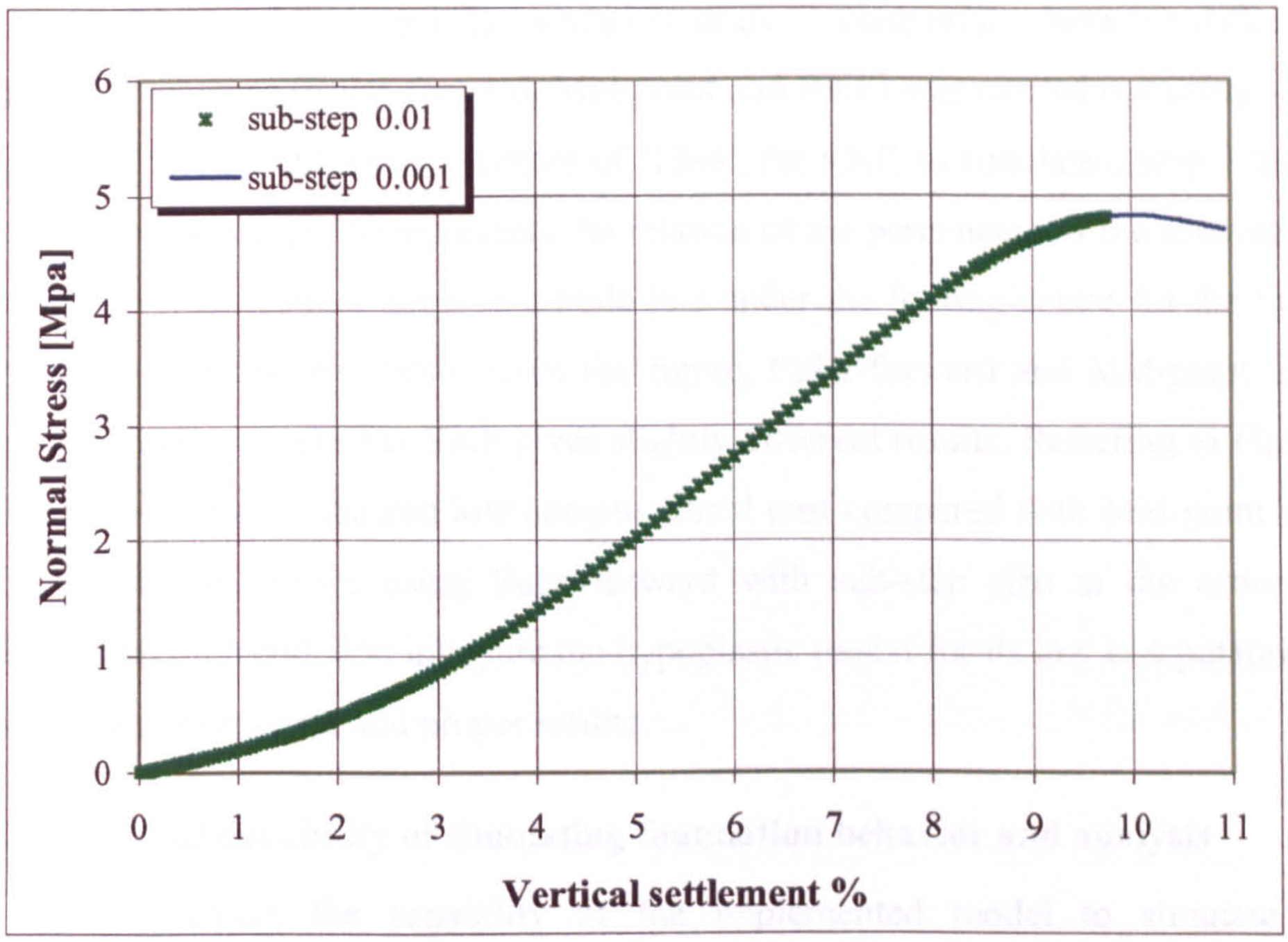

Figure (5.25) Effect of sub-step size using Mid-point

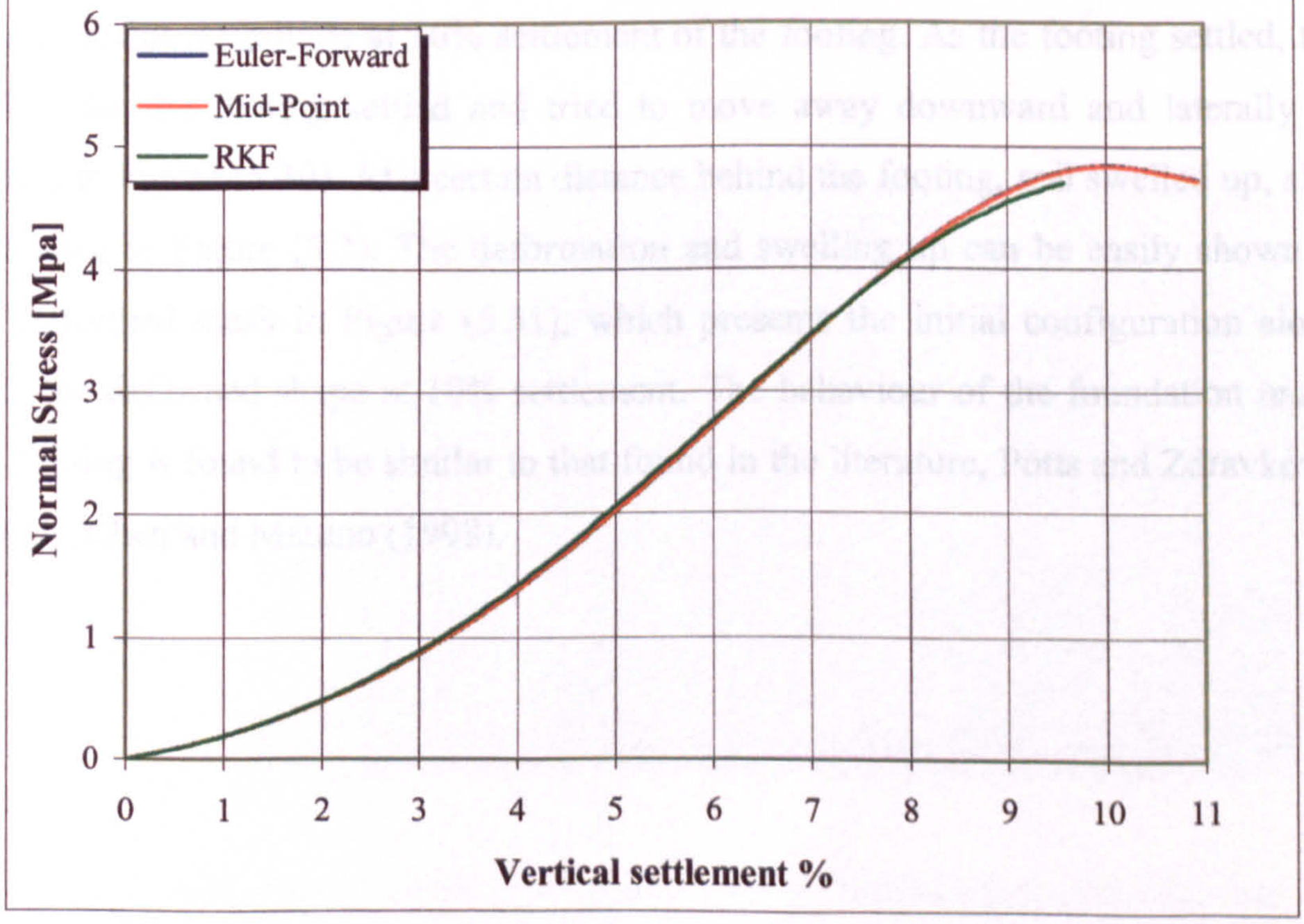

Figure (5.26) Comparison between different integration schemes

As a conclusion of the previous validation study, a comparison between different integration schemes (Euler-forward, Mid-point and RKF) was carried out using sub-step size of '0.001' and error tolerance of '1E-4', for RKF, to simulate a strip footing a fine mesh. Figure (5.26) represents the relation of the percentage of the foundation settlement versus normal stress at a node just under the footing center for the three integration schemes. As shown from the figure, Euler-forward and Mid-point give relatively similar results but RKF gives slightly different results. Referring to Figure (5.13), Euler-forward showed low computational cost compared with Mid-point and RKF algorithms. Hence using Euler-forward with sub-step size in the order of '0.001' is recommended to integrate the hypoplastic model for its low computational coast, ease convergence and proper results.

5.5.2.5 Model capability of simulating foundation behavior and analysis

To examine the capability of the implemented model to simulate 2-dimensional problems the displacement response of the foundation under the settled footing was monitored. Figure (5.27), Figure (5.28) and Figure (5.29) show contour plots of the displacement propagation of the foundation as the footing settled, for 1%, 5.5% and 10% settlement respectively. Figure (5.30) shows a vector plot of the displacement magnitude at 10% settlement of the footing. As the footing settled, the soil under the footing settled and tried to move away downward and laterally as shown in Figure (5.30). At a certain distance behind the footing, soil swelled up, also as shown in Figure (5.3). The deformation and swelling up can be easily shown in the deformed mesh in Figure (5.31), which presents the initial configuration along with the deformed shape at 10% settlement. The behaviour of the foundation under the footing is found to be similar to that found in the literature, Potts and Zdravkovic (1999), Chen and Mizuno (1998).

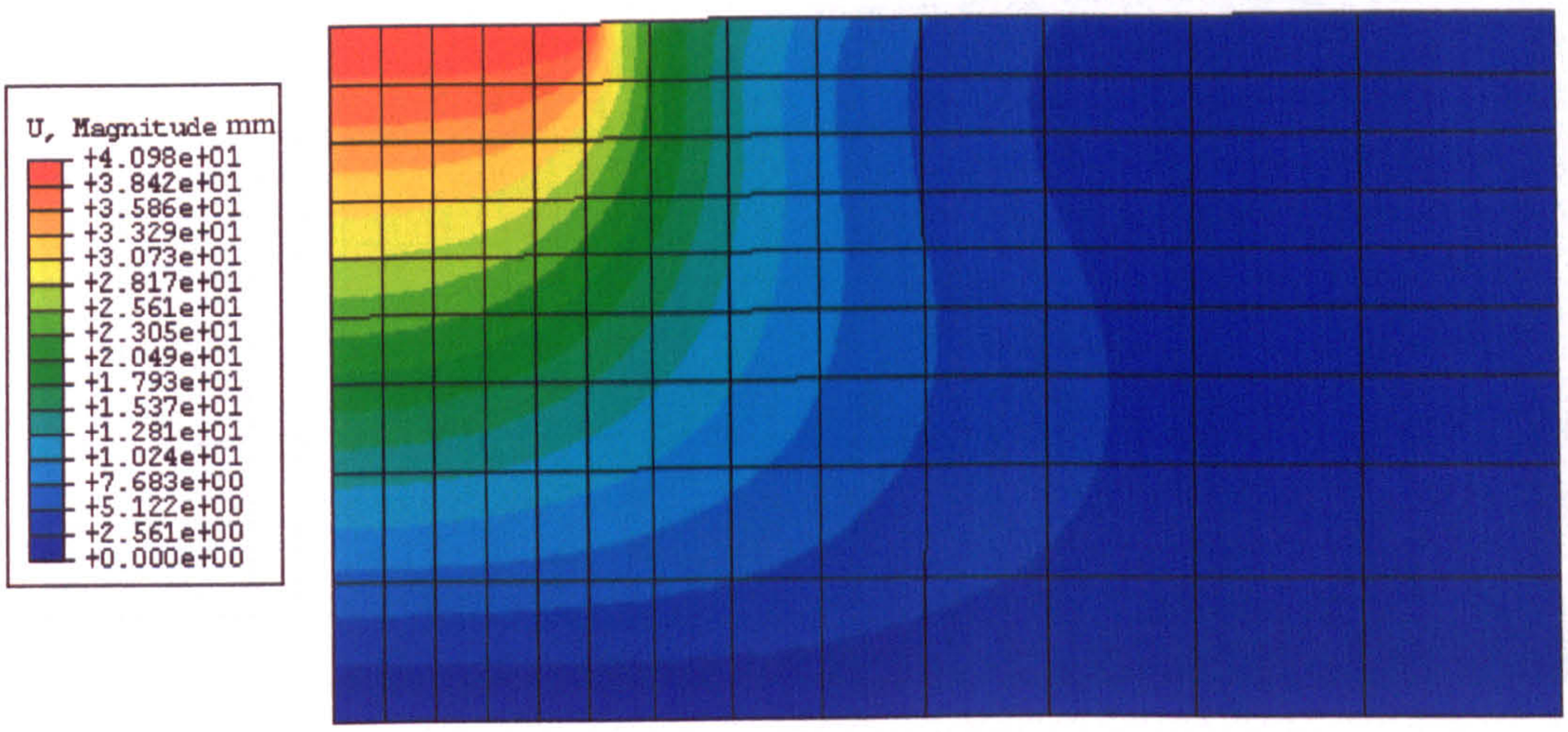

Figure (5.27) Displacement propagation after 1% settlement of the footing

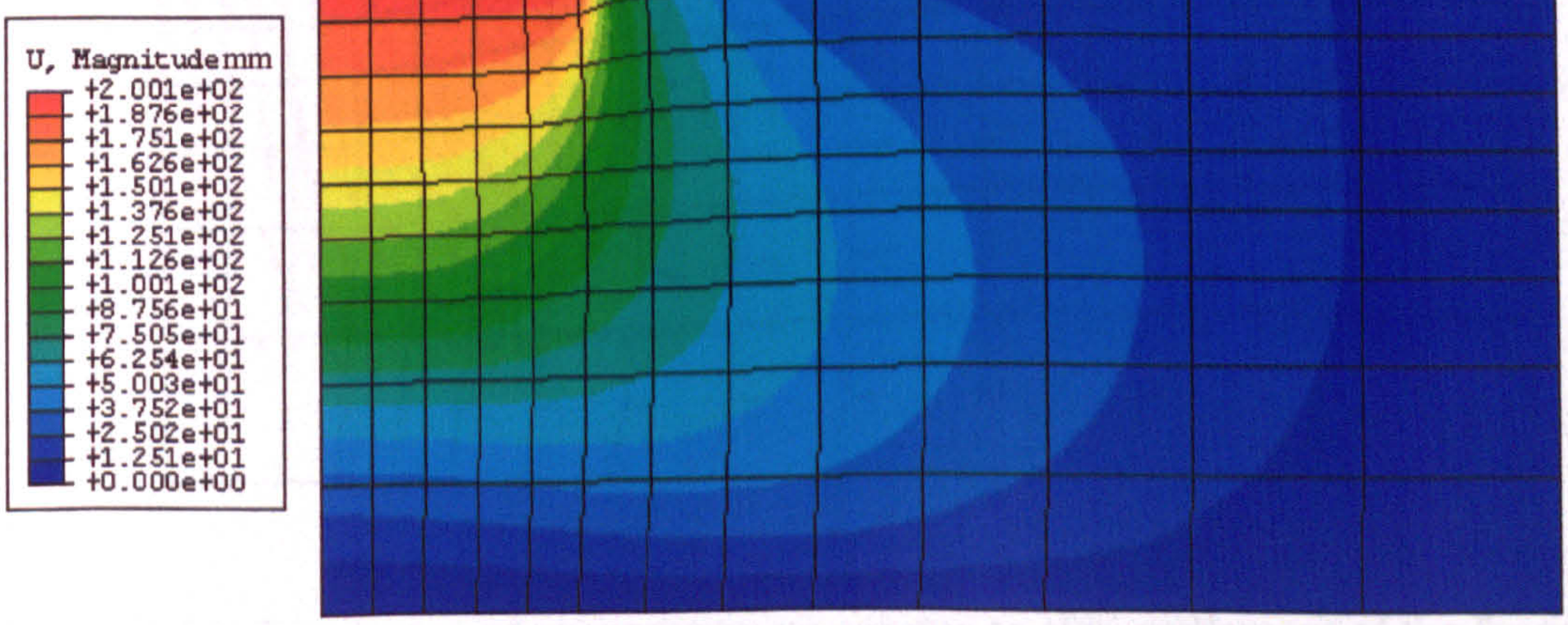

Figure (5.28) Displacement propagation after 5.5% settlement of the footing

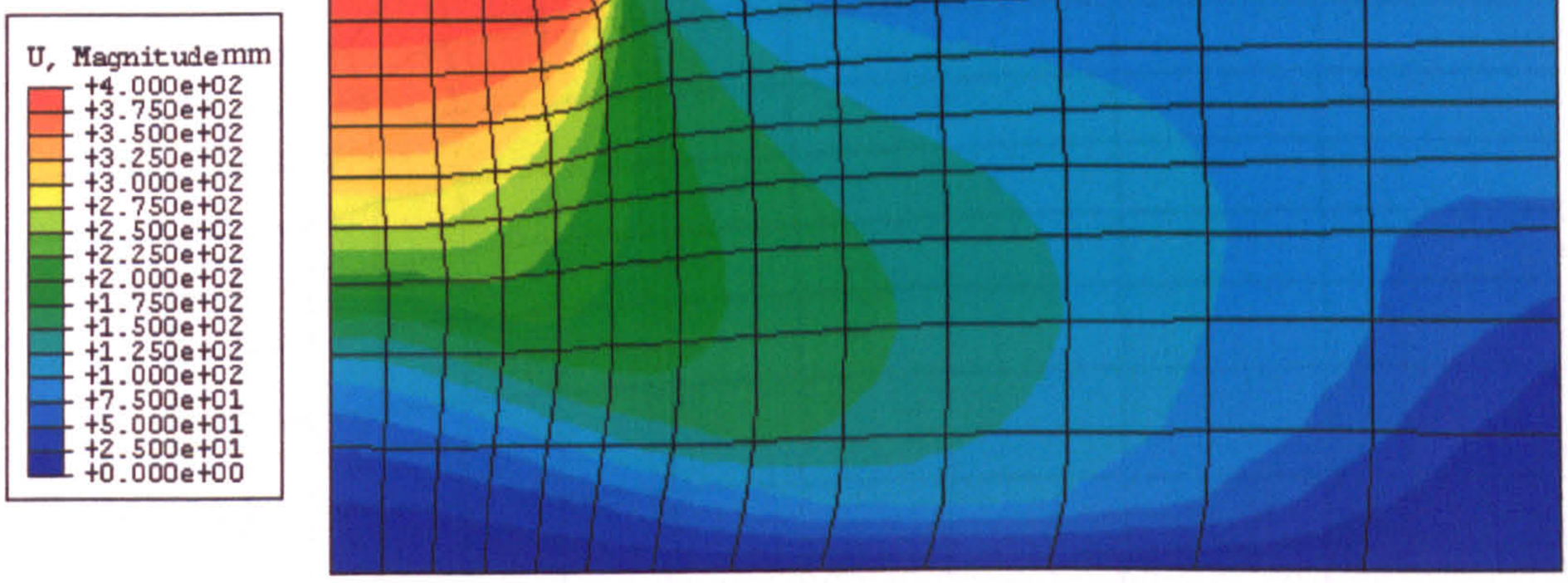

Figure (5.29) Displacement propagation after 10% settlement of the footing

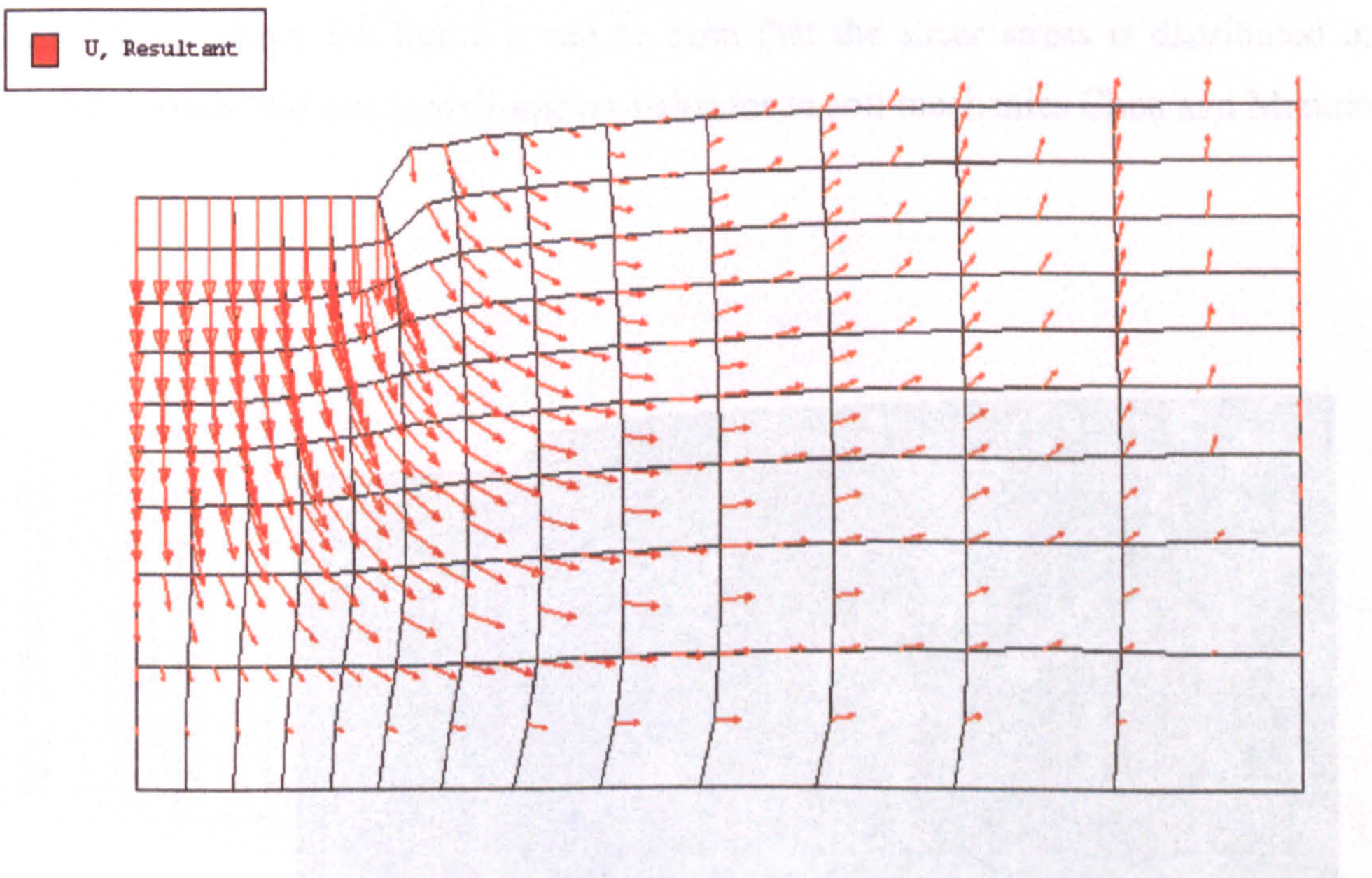

Figure (5.30) Displacement propagation vector due to 10% settlement of the footing

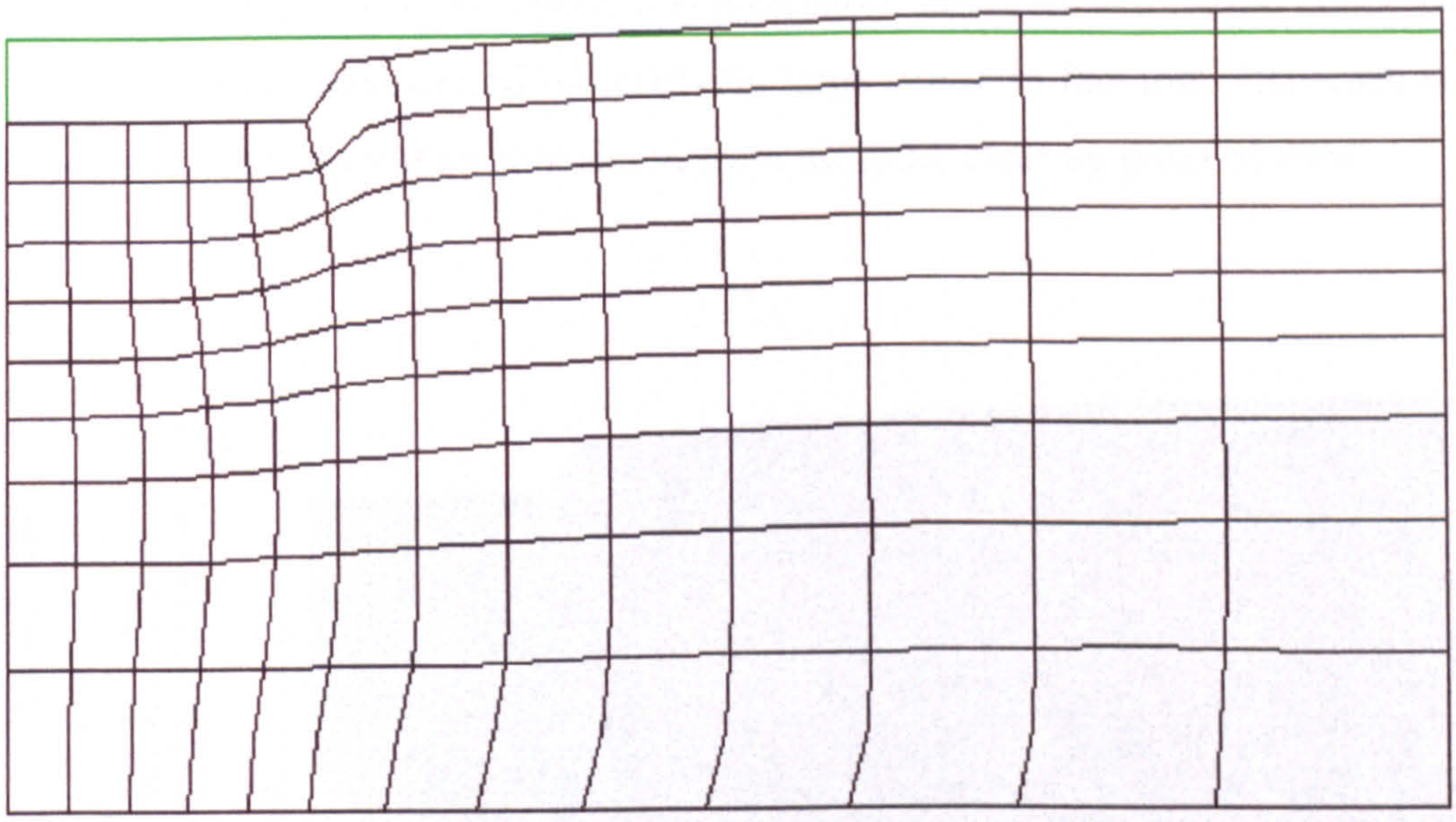

Figure (5.31) Deformed shape at 10% settlement of the footing

The shear stress distribution at 10% settlement of the footing is plotted in Figure (5.32). From the figure it can be seen that the shear stress is distributed in triangular bands and this is well-known behavior in soil mechanics Chen and Mizuno (1998).

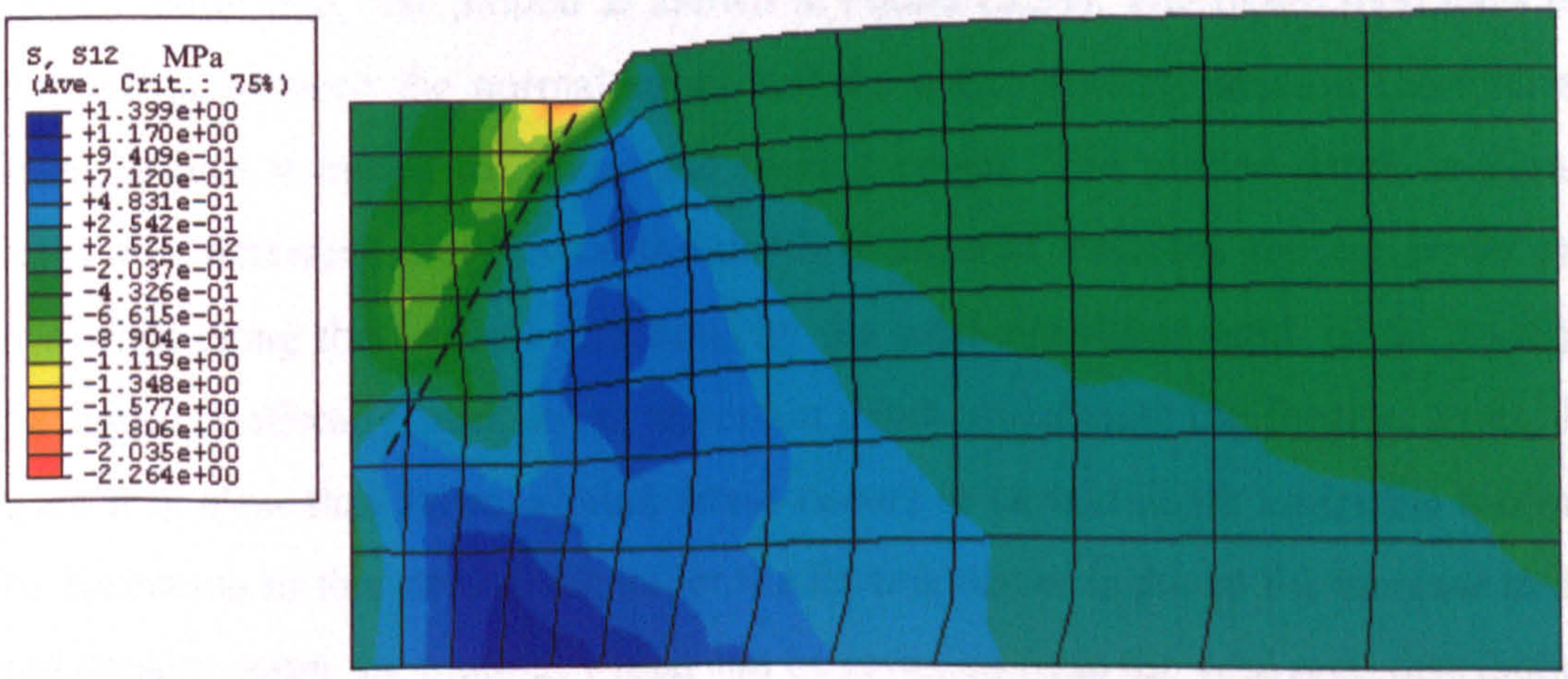

Figure (5.32) Shear stress distribution under the footing at 10% settlement

Contours of normal stress distribution under the footing are plotted in Figure (5.33) at 10% of footing settlement. The stresses are shown to be higher some distance beneath the footing. From the figure, it is noticeable that there is a region underneath the footing that is characterized by relatively large stress. In fact this phenomenon is so important that it should be considered from the mine clearing point of view.

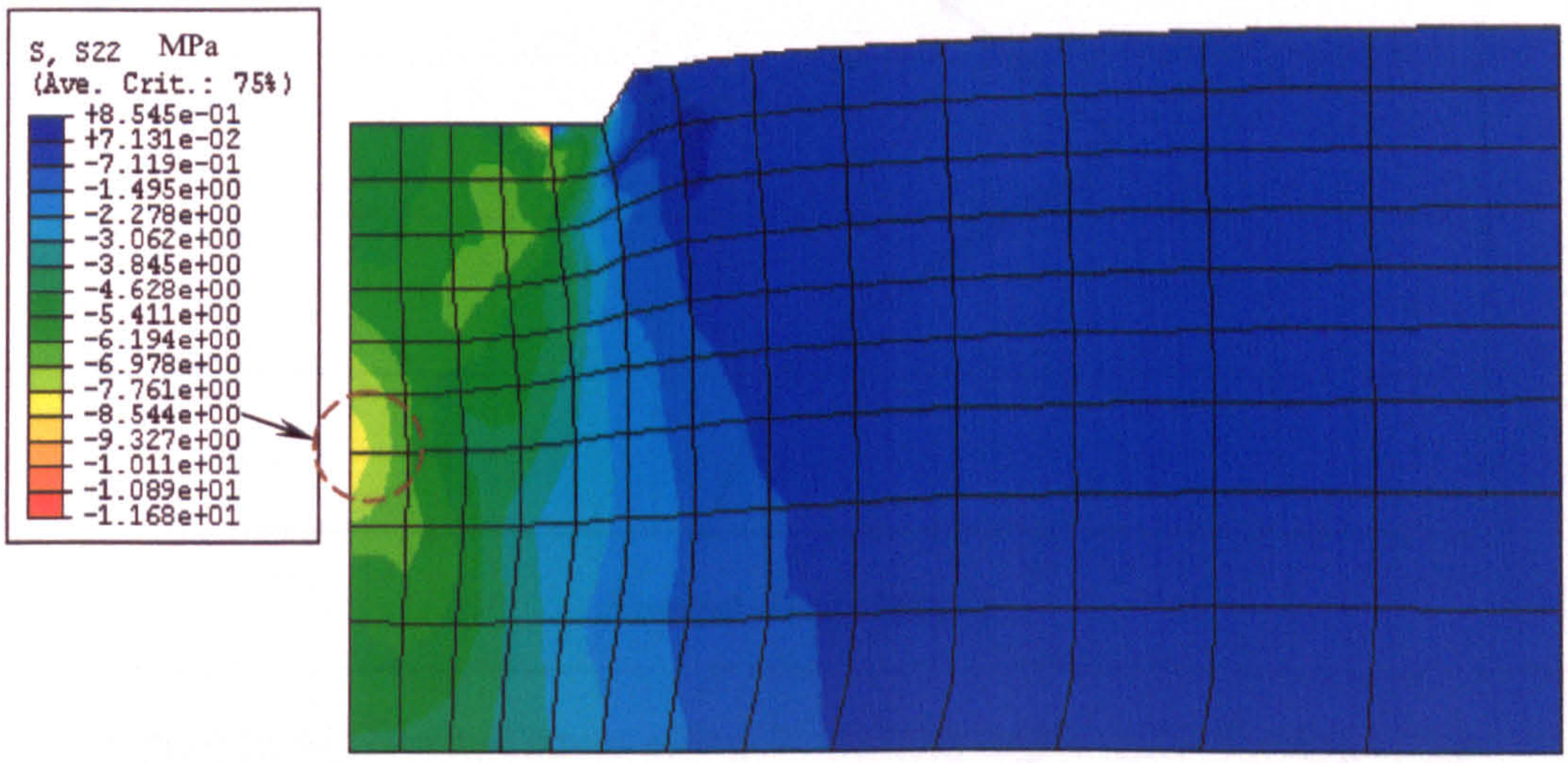

Figure (5.33) Normal stress distribution under the footing at 10% settlement

To interpret this increase in stress at a certain depth underneath the footing, a normal stress distribution along the foundation depth under footing center, i.e. along the vertical center line, was plotted as shown in Figure (5.34). The figure represents the relationship between the normal stress and the corresponding position (normalized depth), where it measured, under the footing center. The plotted depth in Figure (5.34) was normalized by divide the depth (measured from the footing center and downward along the vertical direction) by the total simulated depth of the footing. The figure confirms a peak stress at certain depth underneath the footing. From the figure it is clear that the maximum stress occurs at certain depth under the footing. The formation of this stress peak under the footing center is due to the increase in the sand density under the footing, which can be revealed from the void ratio distribution under the footing as shown in Figure (5.35). From the figure a wedge of dense sand can be seen (bounded by the dashed line); the same behaviour was found by Herle

and Tejchman (1997). This dense sand wedge concentrates the stress at its vertex as indicated by the dotted circle in Figure (5.33).

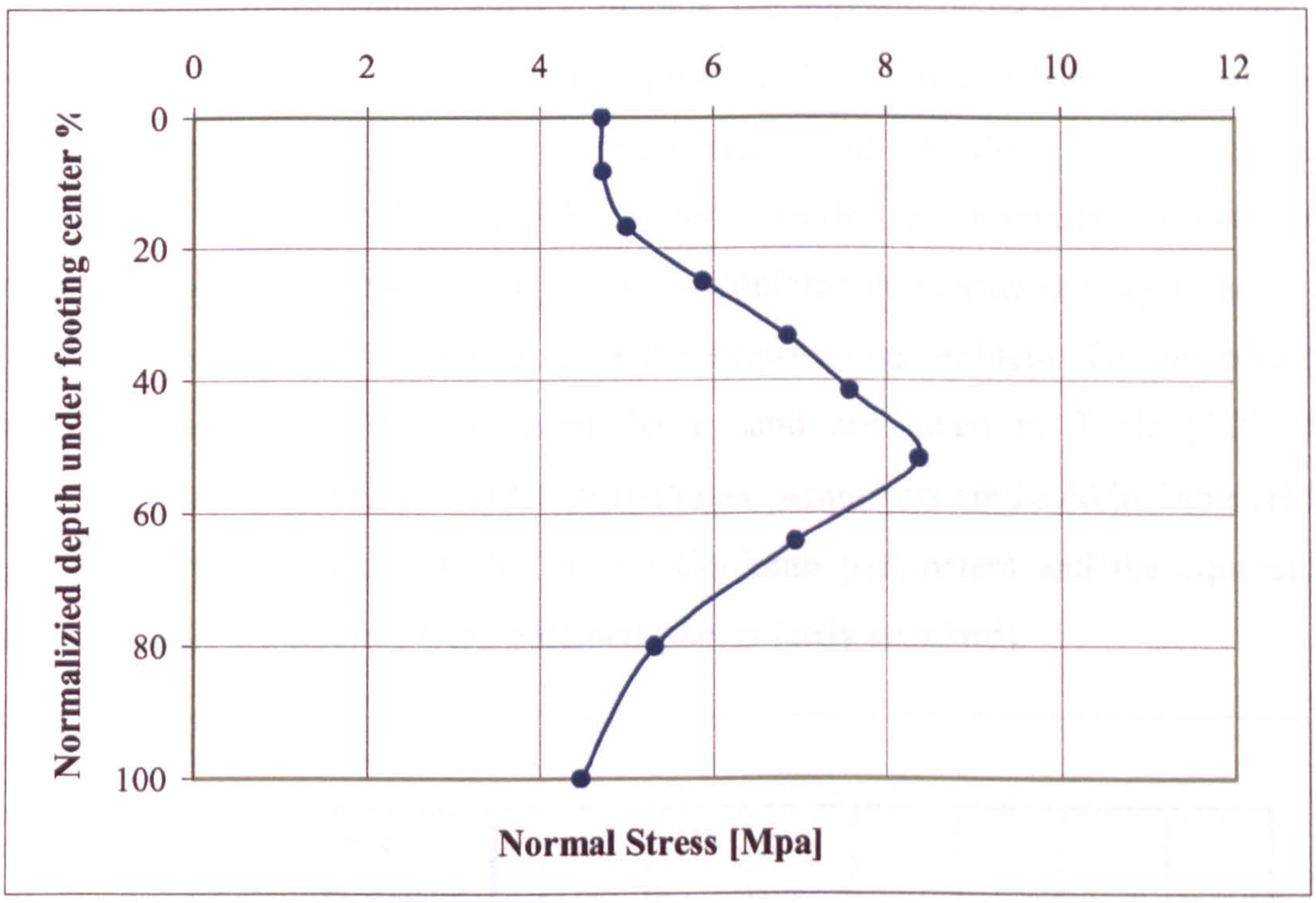

Figure (5.34) Normal stress along foundation depth under footing center

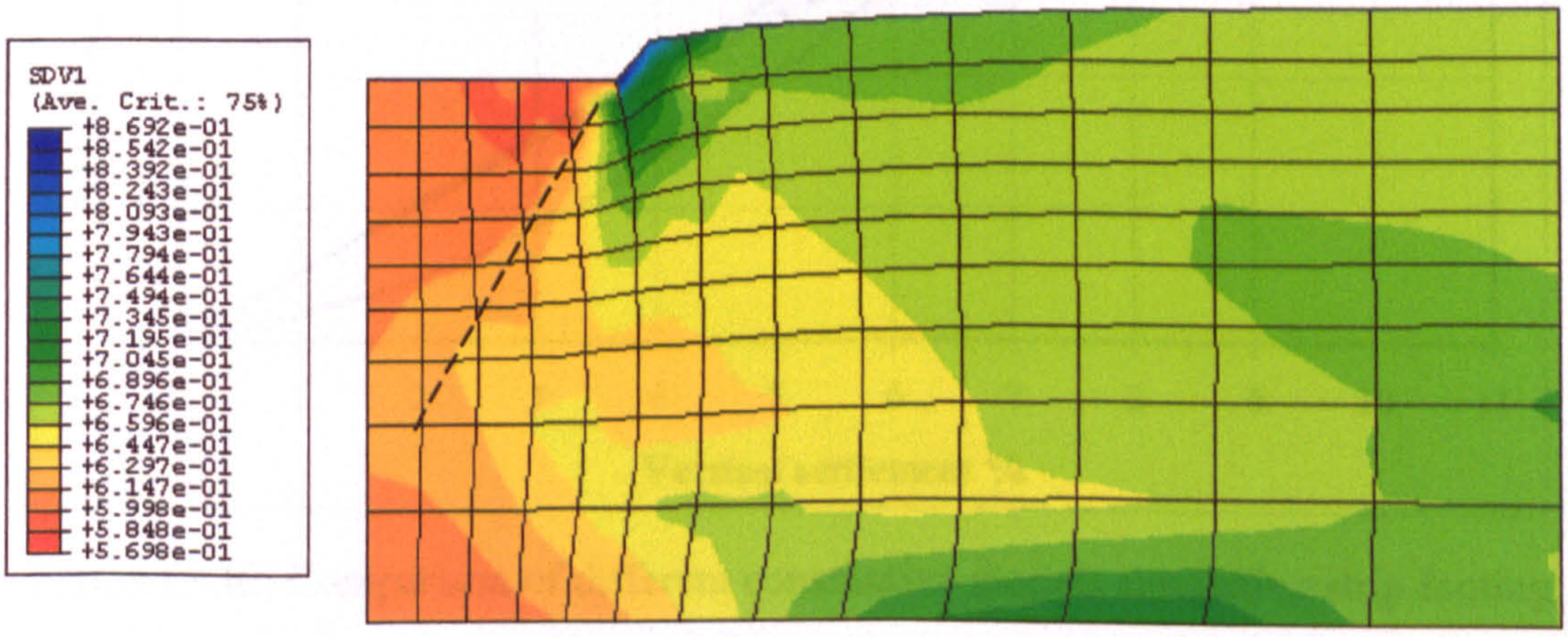

Figure (5.35) Void ratio distribution under the footing at 10% settlement

5.5.2.6 Hypoplastic and other materials models simulating strip footing

As discussed previously in Chapter 3, following a review of the most commonly available granular material models, the hypoplastic model was selected to simulate sand in the soil-tool interaction problem due to its capability of simulating its behaviour for a wide range of stress states and densities. To evaluate the performance of the implemented hypoplastic model as compared to two well established models in elastoplaticity, Mohr's-Coulomb and Drucker-Prager, the three constitutive models were again used in the strip-footing problem. The hypoplastic model parameters for the simulated dense sand are listed in Table [5.2], the equivalent Mohr's-Coulomb and Drucker-Prager parameters are listed in Table [B.1]. Appendix (B) describes how the Mohr's-Coulomb parameters and the equivalent Drucker-Prager parameters were obtained (this is fairly standard).

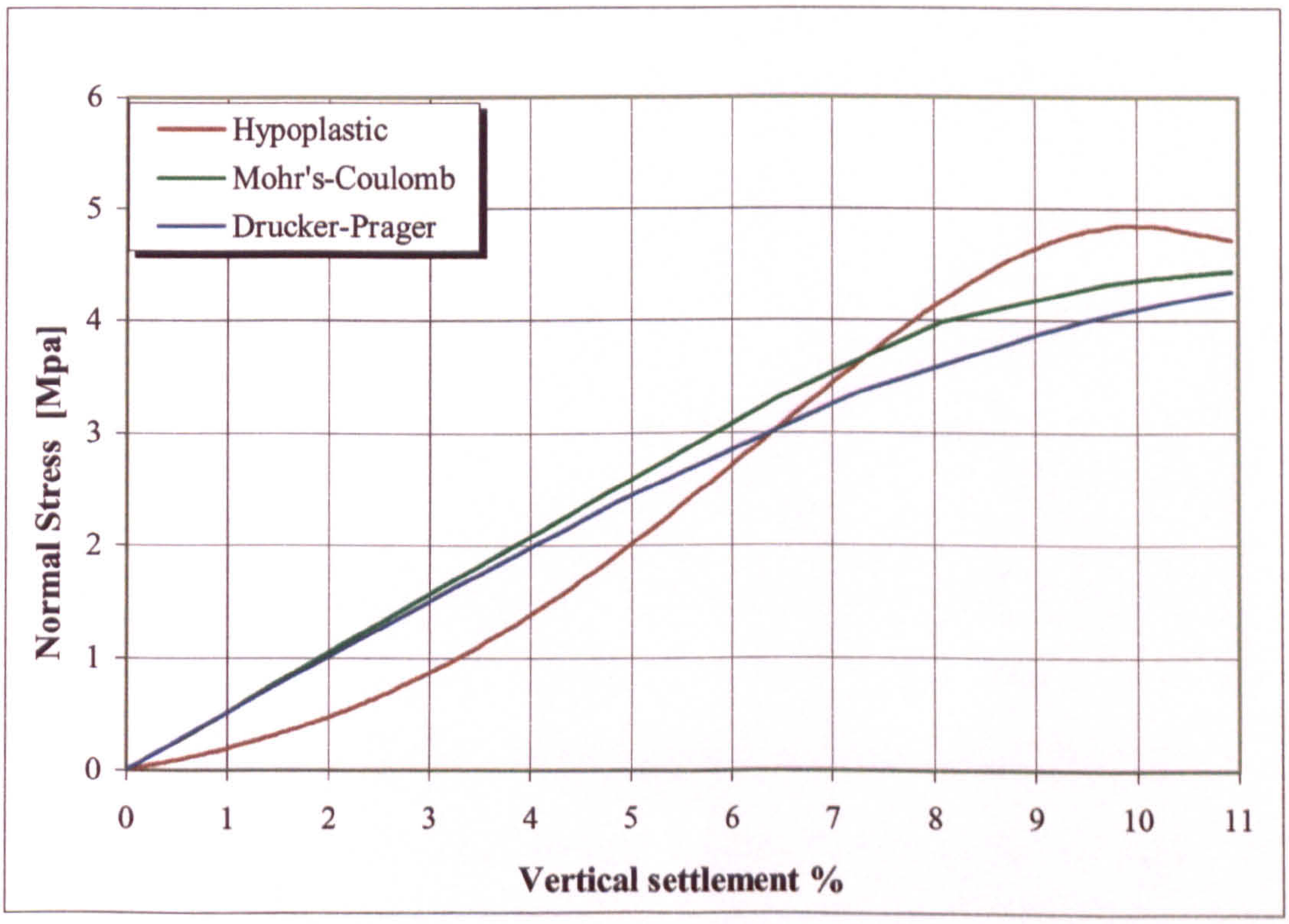

Figure (5.36) Comparison of different constitutive models simulating strip footing

A series of finite element models of strip footing were carried out using these constitutive models to investigate the capability of the hypoplastic model compared to conventional Elasto-plastic models for simulating sand behaviour. Figure (5.36) represents the relation of the percentage of foundation settlement versus normal

stress at a node just under the footing center for the three modeled constitutive models.

The figure reveals the ability of the hypoplastic model in simulating the salient behavior of the dense sand which is represented by a peak in the plotted relation followed by strain softening (as discussed in section (3.8)). Also, as shown in the figure, both Mohr's-Coulomb and Drucker-Prager describe the stress-strain behaviour by a linear relation (based on assumed parameters) and this contradicts the concept of stress level effect on sand behaviour discussed in section (3.7.13).

5.5.3 SOIL-TOOL INTERACTION

The final example employed to verify the implemented hypoplastic constitutive model and examine its capability was to directly simulate the soil-tool interaction process in a 2D situation using ABAQUS. The main aim of this study was to verify the ability of the implemented hypoplastic model of simulating shear band formation at a rupture plane, Tejchman and Wu (1996).

5.5.3.1 Problem description

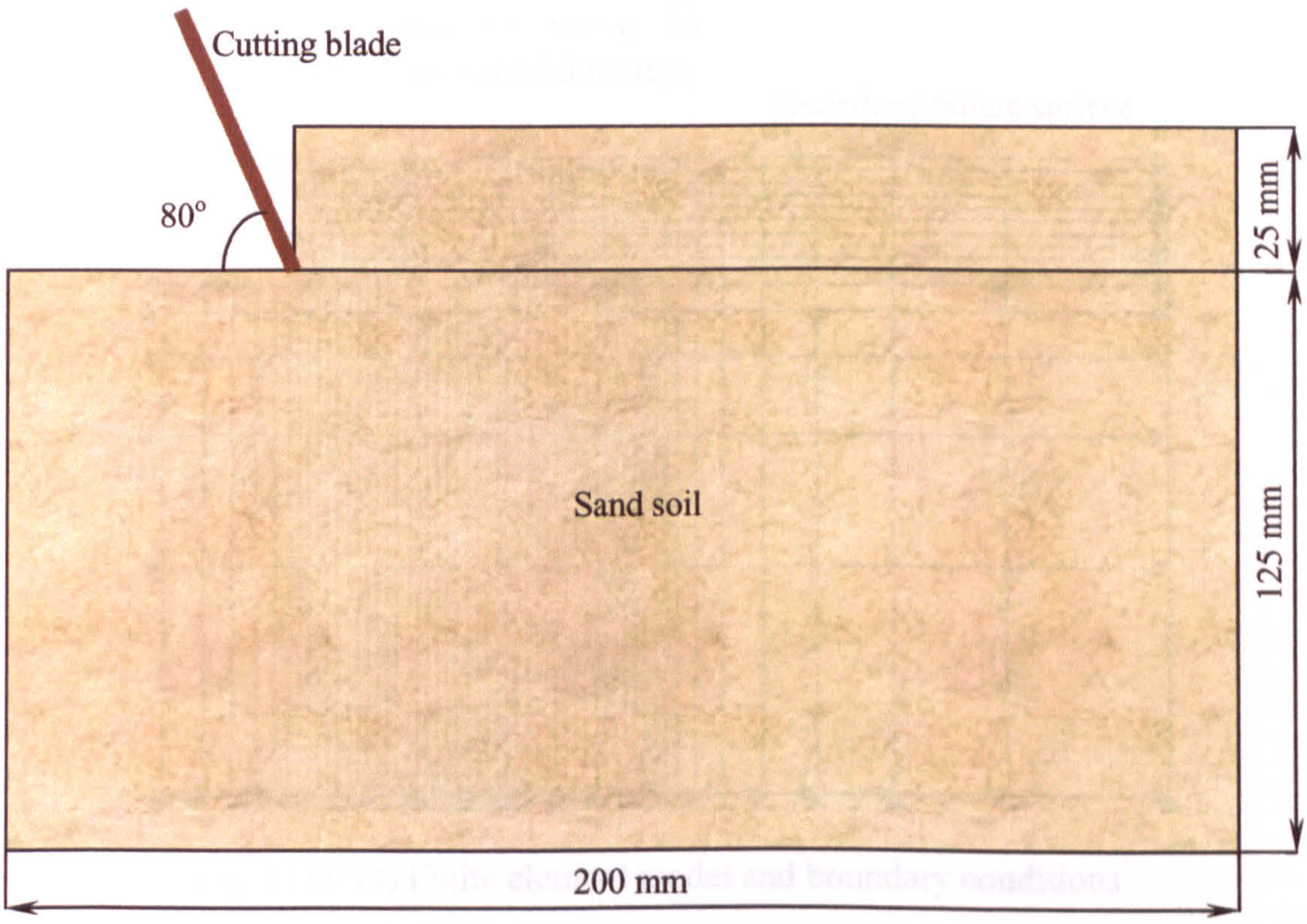

Figure (5.37) Main features of soil-tool interaction problem

The simulated sand block was of 200 mm width, 150 mm height; the blade cutting depth was selected to be 25 mm as shown in Figure (5.37). The blade was initially inclined by 80 degree over the ground level. A dense sand sample with initial void ratio of e_o=0.75 was considered; the hypoplastic parameters of the simulated sand are listed in Table [5.3], and soil-tool coefficient of friction was 0.2 (according to the soil angle of internal friction) to account for rough contact.

Table [5.3] Parameters of the hypoplastic model for Karlsruhe sand

φ_c (deg)	h_s (MPa)	n	e_{d0}	e_{c0}	e_{i0}	α	β
30	5800	0.28	0.53	0.84	1.0	0.13	1.0

5.5.3.2 Finite element modeling

The sand was modeled using 715 bilinear continuum plane strain elements, CPE4 (most suitable for the contact problems). The cutting blade is simulated as an analytical rigid surface with reference point, section (5.3.2), to control its motion.

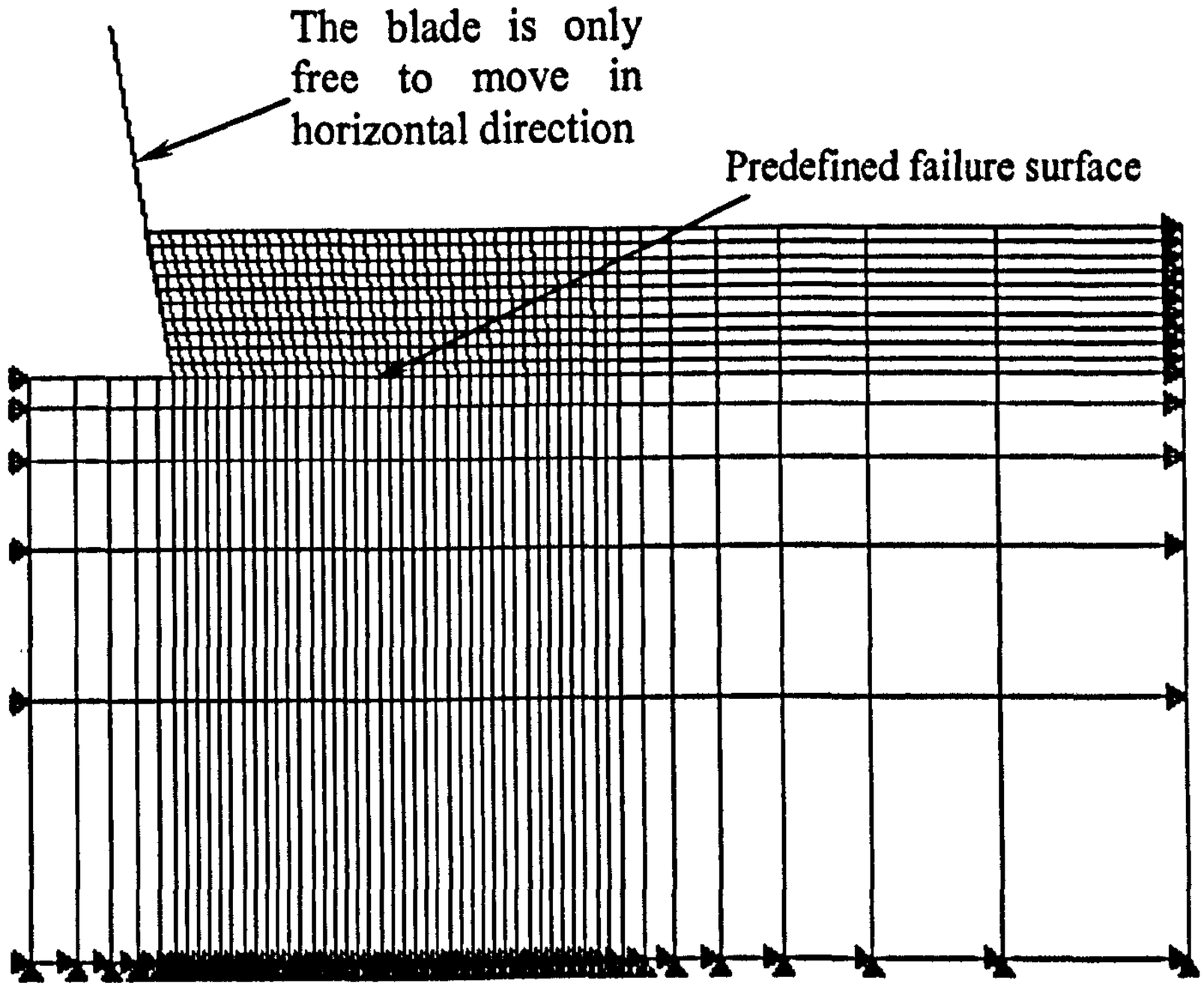

Figure (5.38) Finite element model and boundary conditions

As shown in Figure (5.38), the horizontal displacement was constrained at vertical boundaries, and both vertical and horizontal displacements were constrained at bottom boundary. A predefined failure surface was defined at the same level of the blade cutting tip, where failure is expected during cutting. By using a predefined failure surface, convergence problems due to element distortion are avoided especially when large deformation and relative motion are expected, Plouffe, Lague et al. (1999). The concept of so-called Master and Slave surfaces in ABAQUS was used to simulate the interaction at the predefined failure surface and at the soil-tool

interface. This blade geometry is just a flat dozer blade without curvature. The ABAQUS input file for the soil-tool interaction simulation is listed in Appendix (E.3).

5.5.3.3 Effect of mesh density

First the effect of mesh density was examined by running a series of finite element simulations with different mesh densities: a coarse mesh (using 174 elements), a medium mesh (using 715 elements) and a fine mesh (using 1285 elements). The analysis was carried out using the Euler-forward algorithm to integrate the hypoplastic equation with a sub-step size limit of '0.001'. Figure (5.39) represents the horizontal force (draft force) acting on the cutting blade through a horizontal displacement of 10mm for different mesh densities.

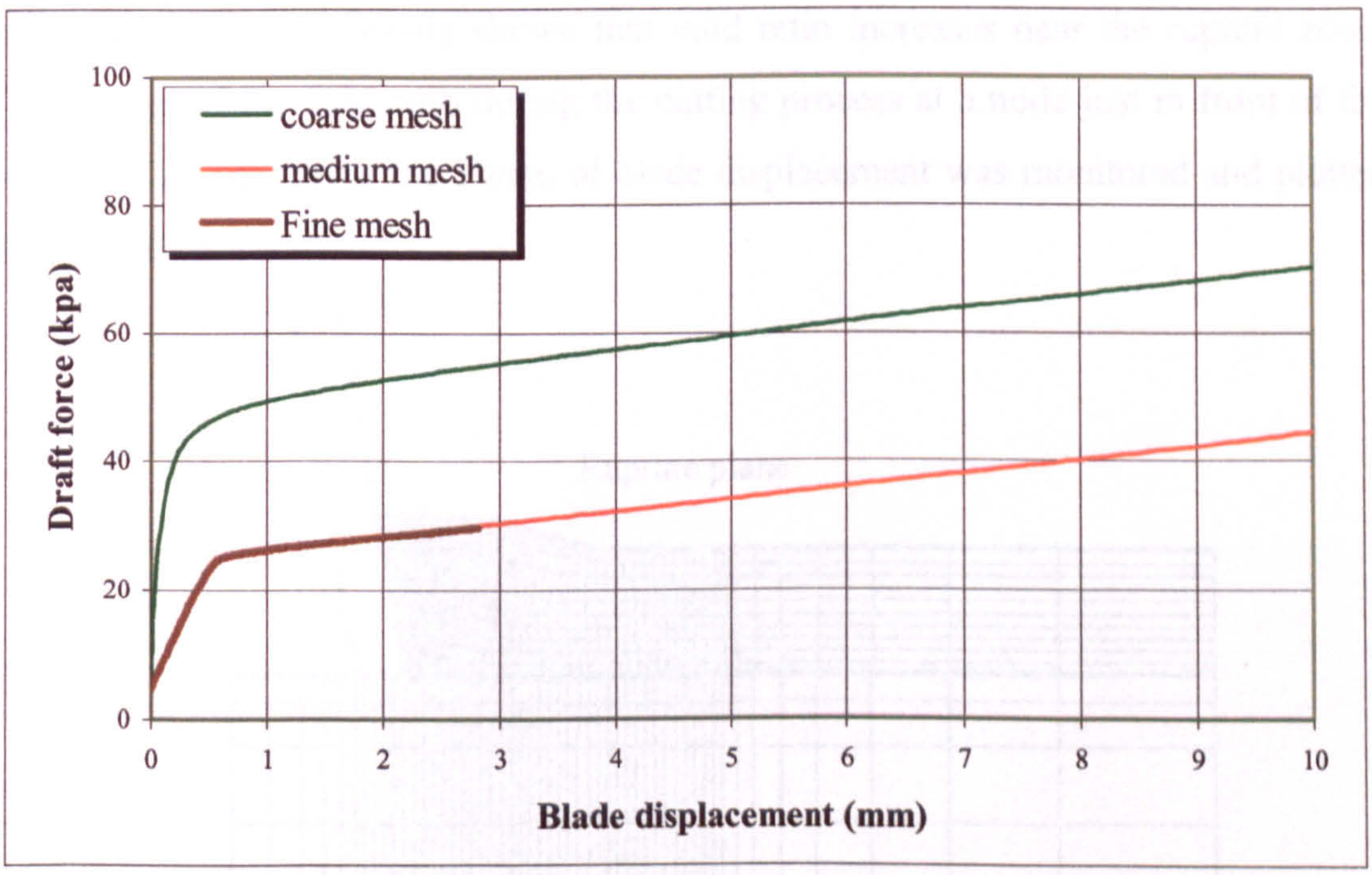

Figure (5.39) Effect of mesh density in simulating soil-tool interaction problem

Results shown in Figure (5.39) reveal that using a coarse mesh may lead to improper analysis and that as the mesh density increases its effect becomes insignificant in that both the medium and fine mesh gave the same results but for the case of fine mesh the analysis was quickly terminated due to element distortion. Hence the medium mesh (715 elements) was used in the finite element analysis of the soil-tool interaction problem.

5.5.3.4 Results and discussion

The analysis was carried out for a blade horizontal displacement of 10 mm. Figure (5.40) shows the deformed configuration of the analysis after 10 mm of blade movement. It is also seen from the figure that elements around the rupture plane, around the center line shown in Figure (5.40), were distorted and rotate. Figure (5.41) shows a maximum principal strain distribution from which a rupture surface can easily be identified as the maximum principal strain component and is located at a certain plane which indicate large shear and hence rupture. The rupture plane zone is characterized by a high void ratio which means a failure or shear located around the rupture plane. This can be easily seen from Figure (5.42) which presents the void ratio distribution contours in front of the cutting blade. Void ratio, as a state variable, represents the compaction state of the sand and changes during the cutting process, from which it can be easily shown that void ratio increases near the rupture zone. The change of the void ratio during the cutting process at a node just in front of the blade cutting tip during the 10mm of blade displacement was monitored and plotted in Figure (5.43).

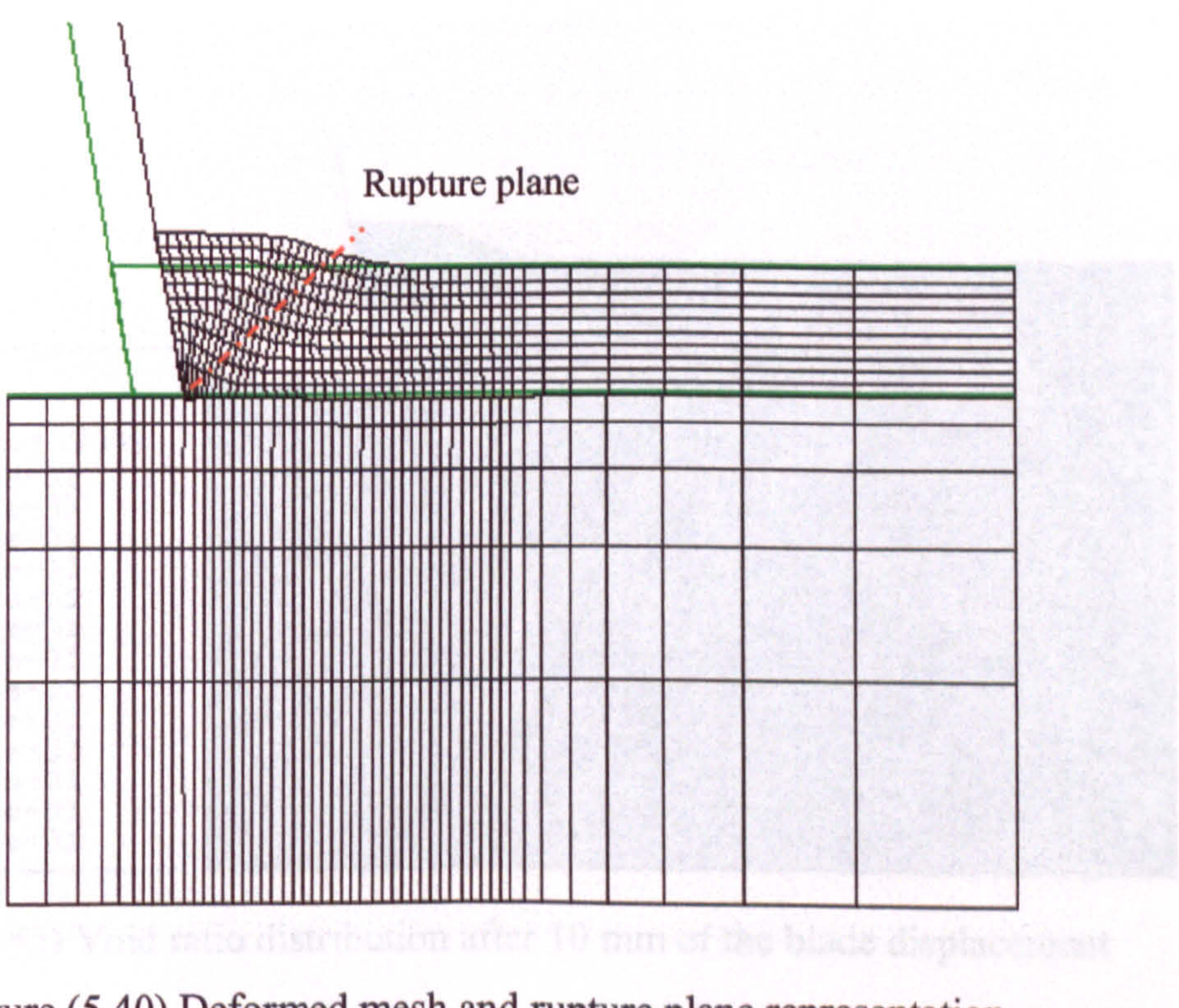

Figure (5.40) Deformed mesh and rupture plane representation

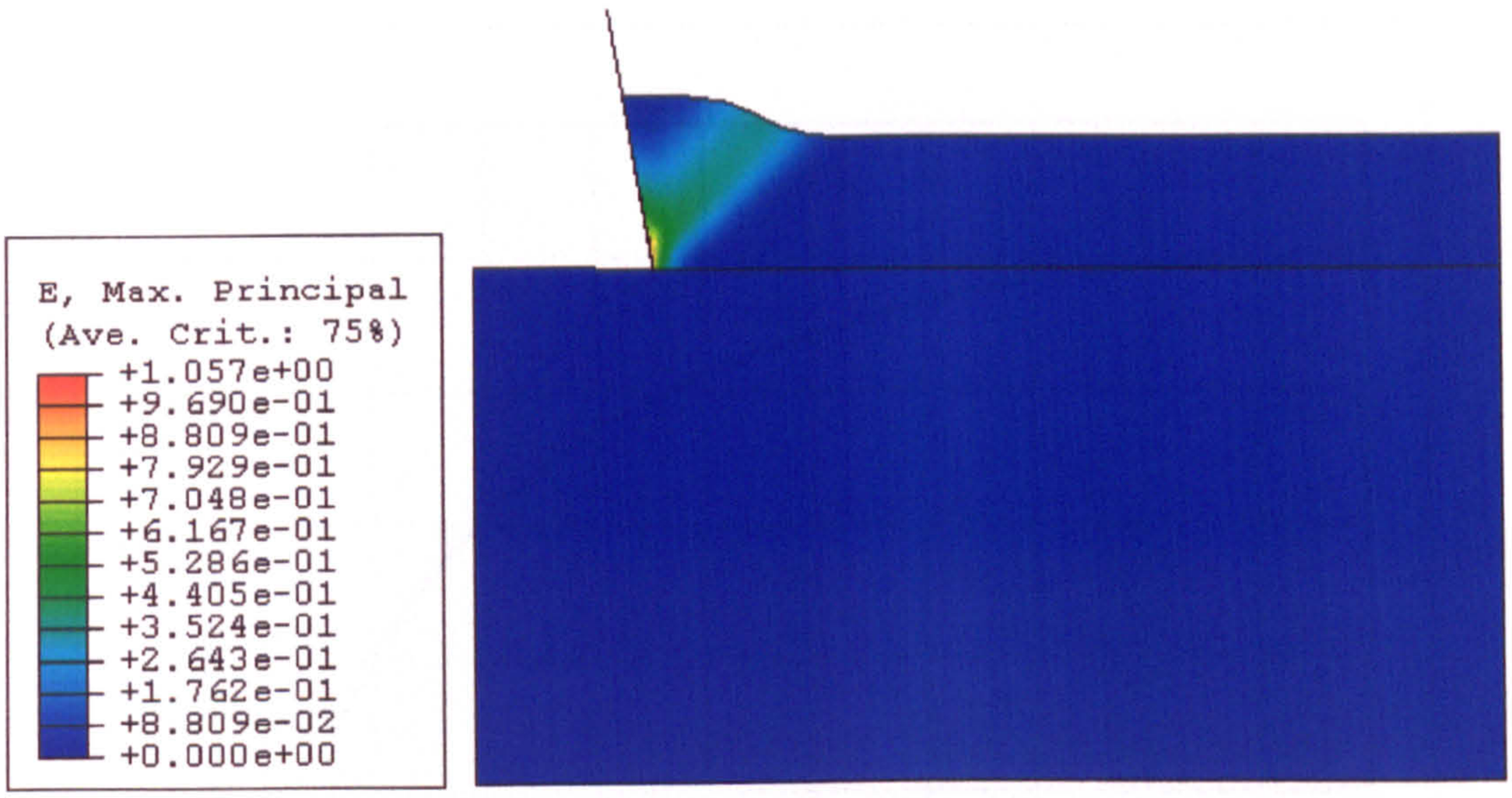

Figure (5.41) Maximum principal strain after 10 mm of the blade displacement

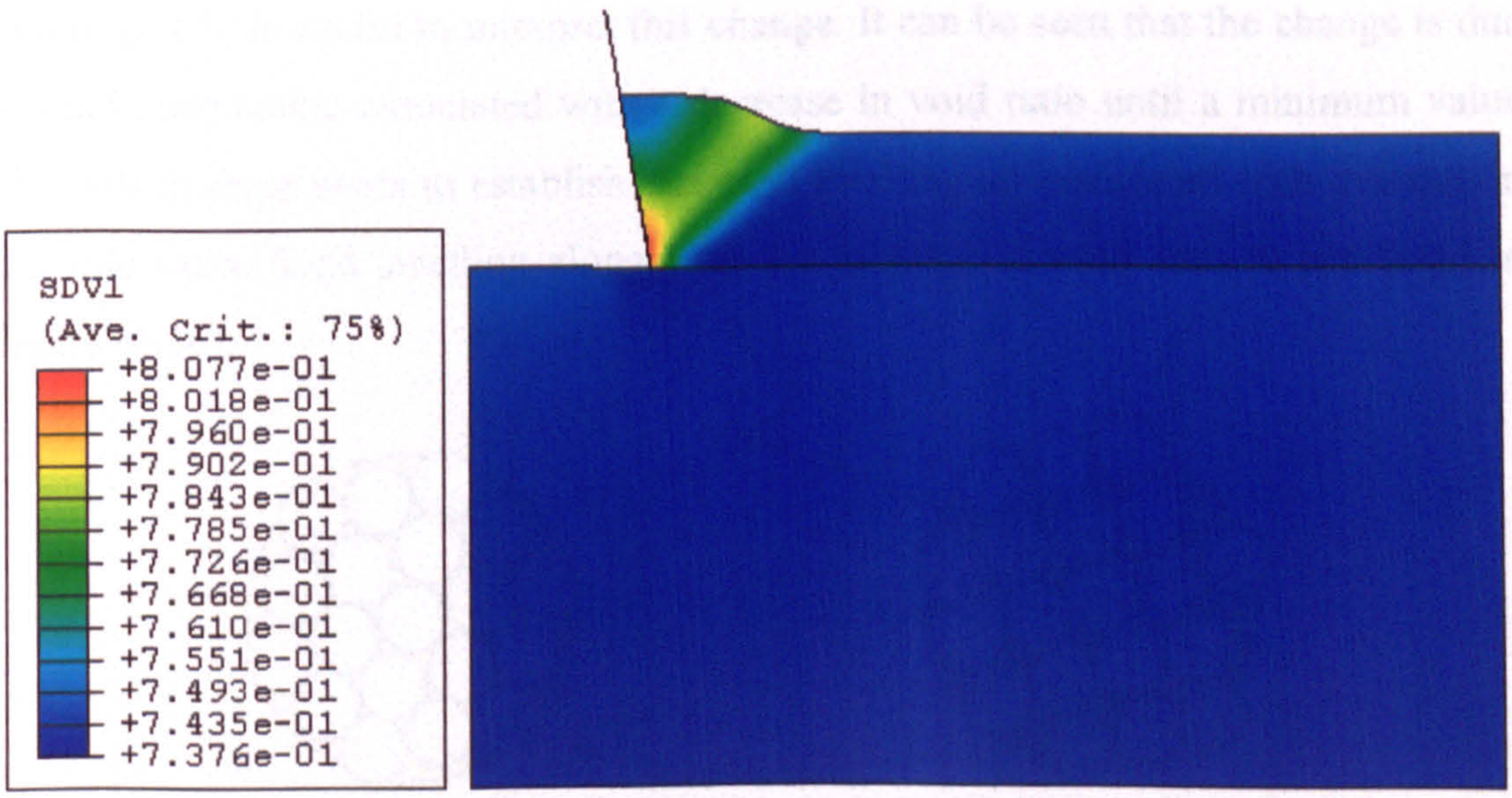

Figure (5.42) Void ratio distribution after 10 mm of the blade displacement

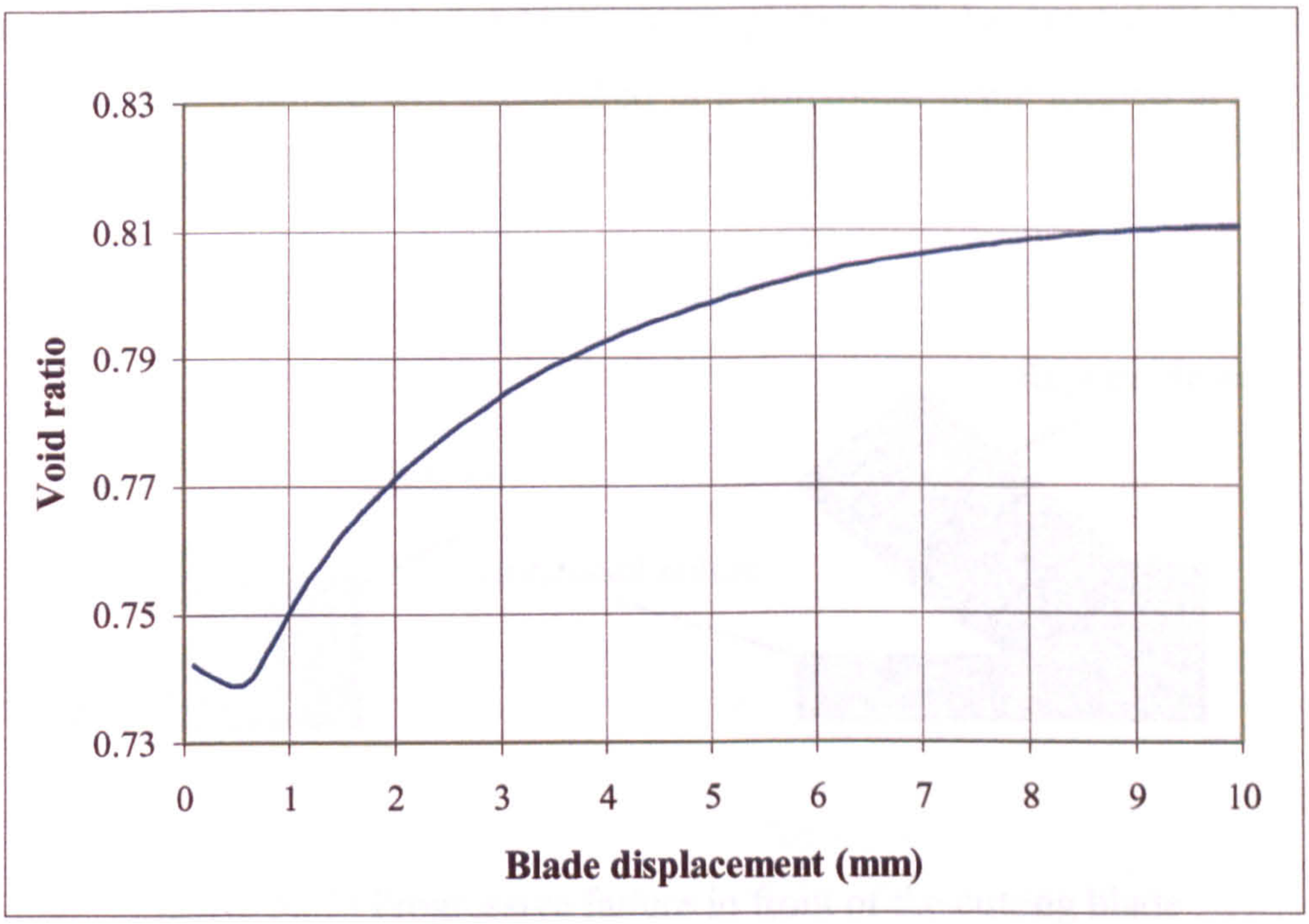

Figure (5.43) Change of Sand void ratio in front of blade cutting tip

A significant change in the void ratio at the beginning of the blade displacement is noticeable from Figure (5.43). The void ratio decreases to some minimum value during the first 0.5 mm and then increases toward the critical value listed in Table [5.3] which is 0.84. A close look at dense sand behaviour presented in Chapter 3, Figure (3.17), is useful to interpret this change. It can be seen that the change is due to sand compaction associated with a decrease in void ratio until a minimum value after which shear starts to establish and sand swelling up associated with increase in the void ratio. Sand swelling along with the increase in void ratio is presented in Figure (5.44).

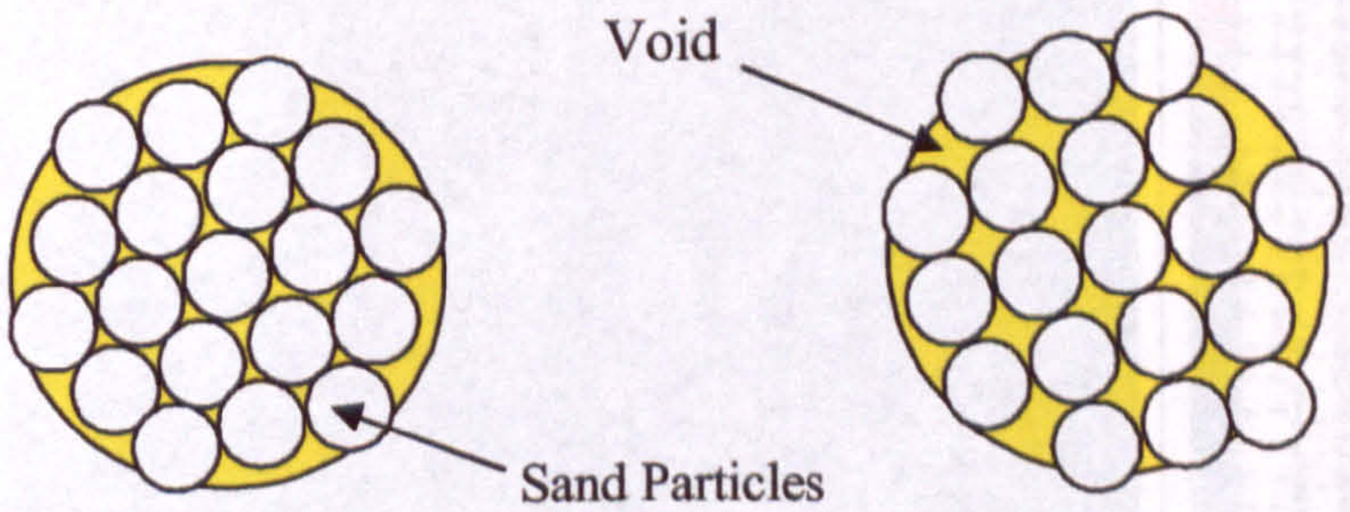

(a) Initial state (b) During shear

Figure (5.44) Sand voids increase and swelling up

During blade movement, progressive rupture planes will be created as shown in Figure (5.45), also failure will established in a horizontal plane located in the same level as the blade tip.

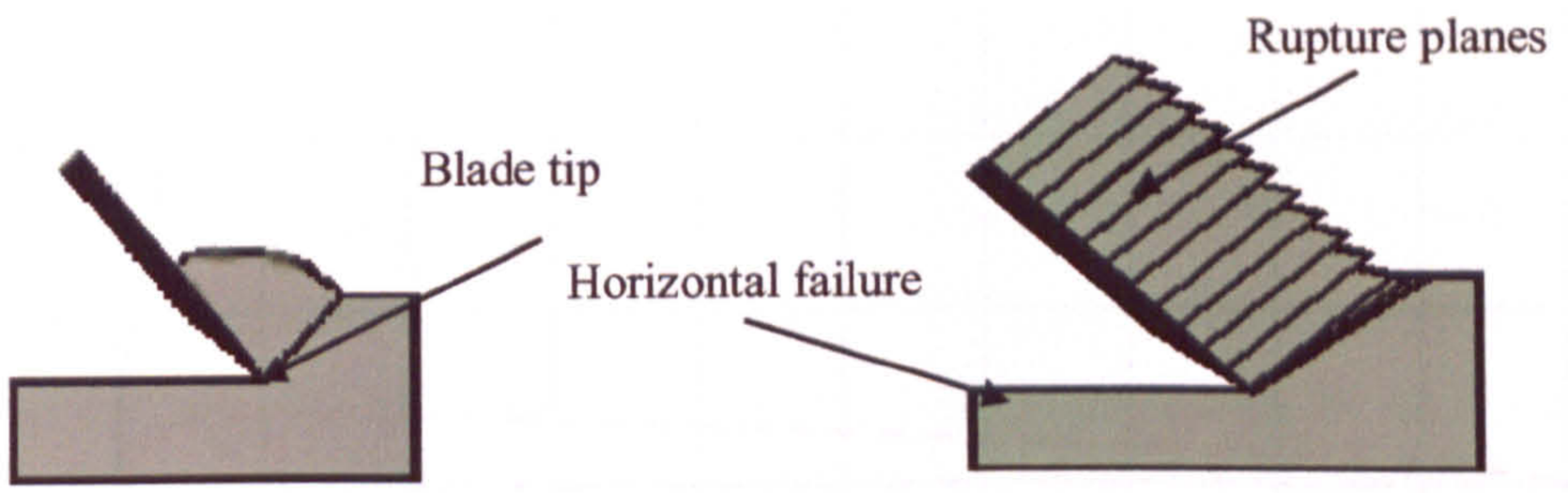

Figure (5.45) Progressive failure in front of the cutting blade

Figure (5.46) presents the shear stress distribution in front of the blade after 10 mm of the blade movement. From the figure two stress concentration zones can be identified; one of them located along the rupture plane and the other located in a horizontal plane along the predefined failure surface.

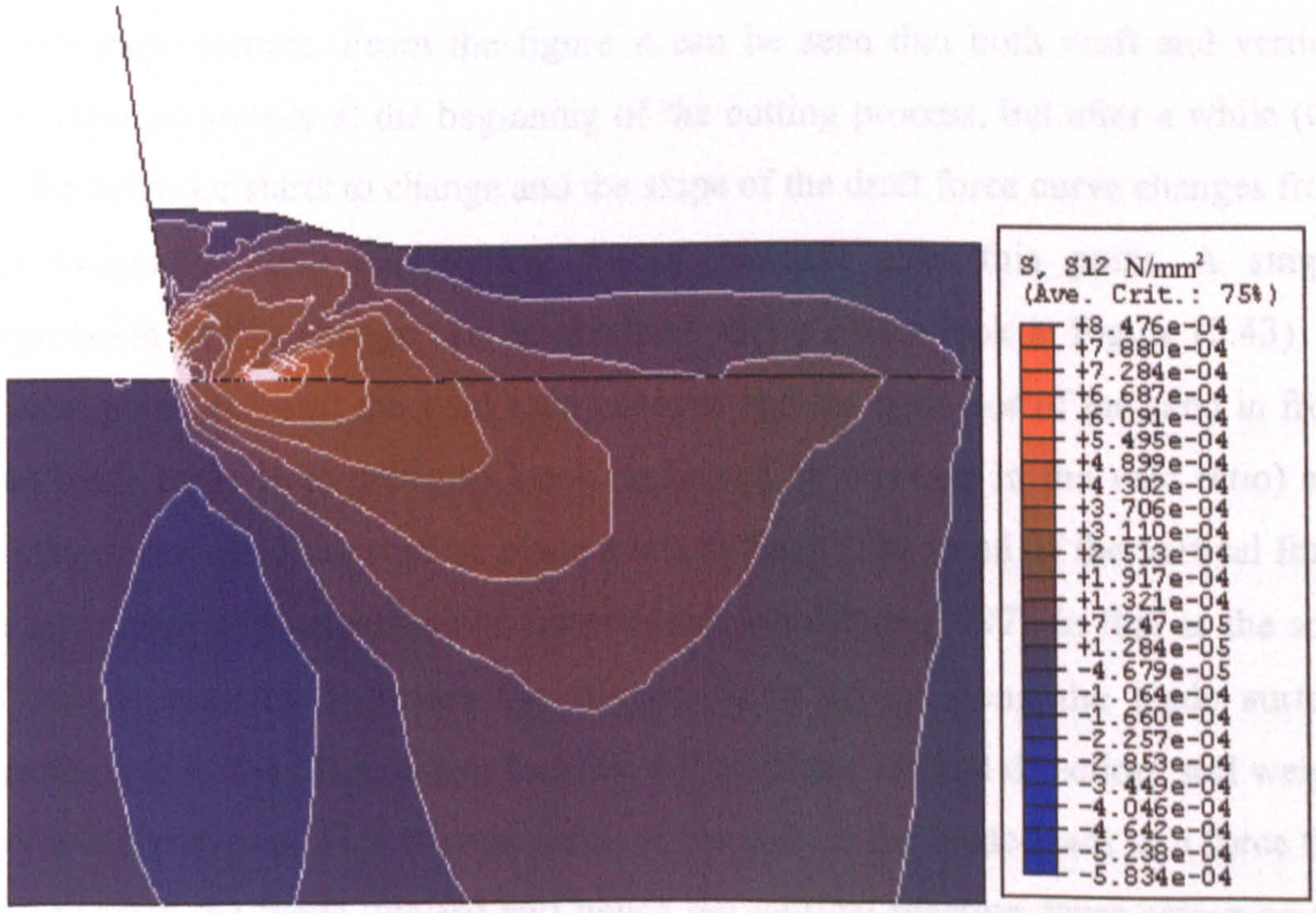

Figure (5.46) Shear stress distribution after 10mm of blade movement

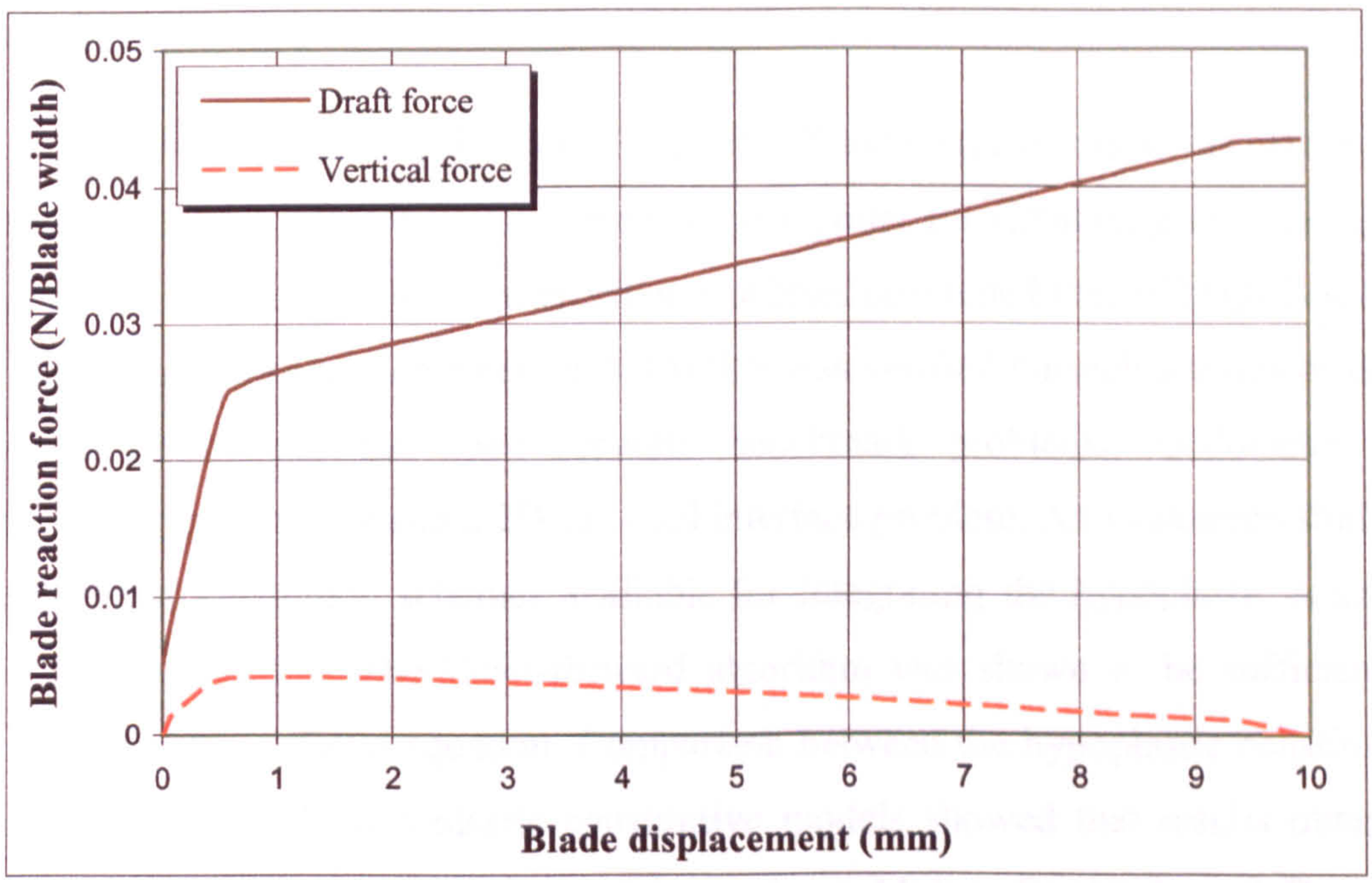

Figure (5.47) Reaction forces acting on cutting blade

The reaction forces - (1) draft force, acting on the blade in the horizontal direction after Shen and Kushwaha (1998), and (2) vertical force - were monitored and plotted in Figure (5.47) over 10mm of blade movement. The figure represents the total reaction forces acting on the blade in both draft and vertical directions through 10mm of blade displacement. From the figure it can be seen that both draft and vertical forces increase steeply at the beginning of the cutting process, but after a while (0.6 mm) the behavior starts to change and the slope of the draft force curve changes from steep to gentle. Also the vertical forces decrease after this point. A simple interpretation of this change can be obtained with a closer look at Figure (5.43). At the same point (0.6mm) the void ratio changes and the behavior of the sand in front of the blade turns from dense to loose (indicated by increase in the void ratio) and this may occur when the rupture plane starts to form. The trend of the vertical force is in agreement with experimental observation, AboElnor (1997), in that as the soil-tool contact pressure increases the friction force acting along the blade surface increases, and as the blade is just inclined 10^{o} from the vertical direction' soil weight effect is insignificant. This friction force of the soil on the blade leads to a force that trying to push the blade upward and hence the vertical reaction force acting on the blade decreases.

5.6 SUMMARY

A review of the capabilities of available finite element codes was carried out to select the most appropriate from the available codes for simulating sand using the hypoplastic model in soil-tool interaction problems concluded that ABAQUS should be used. The model implemented in ABAQUS was verified through a series of finite element simulations for three separate benchmark problems: Oedometer test simulation, strip footing and a 2D soil-tool interface problem. An evaluation study of the different integration schemes available for integrating the hypoplastic equation was also carried out. The Euler-forward algorithm was shown to be sufficient to integrate the hypoplastic equation. Comparison between the hypoplastic constitutive model and classical elastoplastic constitutive models showed that results obtained using conventional elastoplastic models, such as Mohr's-Coulomb and Drucker-Prager, were strongly dependant on material parameter selection. Throughout this chapter the hypoplastic model has been shown to be capable of the proper simulation of sand behaviour. An initial study of a 2D soil-tool interaction problem has shown the hypoplastic model capable of acceptable simulation of sand behaviour in terms of stresses, strains, void ratio and rupture plane formation. Hence more in depth analysis of the soil-tool interaction process will be carried out in the next chapter.

5.7 CONCLUSION

From the previous discussion some basic concluding remarks are drawn and listed as follows;

1. The implemented hypoplastic model is capable of simulating sand in monotonic loading and hence in the soil-tool interaction.
2. The Euler-forward algorithm is sufficient for integrating the hypoplastic model.
3. Using a time step of order 0.001 with Euler-forward leads to reasonable results, considering a strain of the order of 1E-5.
4. The user defined material feature in ABAQUS is quite robust for analysis via the implemented hypoplastic model.

Chapter 6

SOIL-TOOL INTERACTION

6.1 CHAPTER SYNOPSIS

In Chapter 5, a verification study of the chosen hypoplastic constitutive model was carried out. This study revealed the hypoplastic model's ability to describe sand behaviour under monotonic loading. Hence in this chapter a more extensive finite element analysis of soil-tool interaction in 2-dimensions (2D) is carried out to study the effect of various different geometry and operating conditions on cutting forces. Then the study is extended to 3-dimensions (3D), at the end of the chapter, to cover the limitations of the 2-dimensional analysis.

6.2 INTRODUCTION

When a blade penetrates soil during an excavation (earth moving) and/or mine clearing process resisting forces are applied on the tool as a reaction to the cutting process. These forces can be resolved into two main components: a draft force, which acts along the horizontal plane, and vertical force, which acts along the vertical plane. Indeed these forces are strongly affected by some governing conditions and blade geometrical parameters, as described in section (1.5). These parameters can be listed as follows:

1. Initial conditions
    a. Blade geometry, governed by blade radius of curvature

b. Blade surface roughness

c. Soil type

2. Operating conditions

a. Cutting angle (rake angle)

b. Cutting depth

2-D and 3-D soil-tool interface analyses were carried out to study the effect of such factors on cutting forces.

6.3 2D SOIL-TOOL INTERFACE ANALYSIS

A typical bulldozer blade was selected for its common use in earth moving and mine clearing equipment also since its width is probably wide enough to be considered as a plane strain problem in 2-dimensional analysis.

6.3.1 MODEL DESCRIPTION

The problem analyzed in this section was the soil-tool interaction of a bulldozer blade during digging and cutting processes. Soil selected was of the sand type that is the most common in the Egyptian desert infected with land mines and the target for development.

The modified hypoplastic model was implemented into the commercial finite element code "ABAQUS" via the user defined material subroutine "UMAT", HKS (2000), and is used to describe sand behaviour during digging and cutting processes. Table [6.1] represents the hypoplastic parameters of the simulated sand soil, the initial density was varied from relatively dense ($e_0 = 0.75$) to loose ($e_0 = 0.9$).

Table [6.1] Parameters of the hypoplastic model for Karlsruhe sand

φ_c (deg)	h_s (MPa)	n	e_{d0}	e_{c0}	e_{i0}	α	β
30	5800	0.28	0.53	0.84	1.0	0.13	1.0

6.3.1.1 Spatial dimension

As the width of a bulldozer blade is usually much greater than the cutting depth, the interaction problem of a bulldozer blade can be idealized to a two-dimensional plane strain problem. Figure (6.1) shows the main dimensions of the

simulated soil-tool interface problem and Figure (6.2) shows the main parameters of the cutting blade.

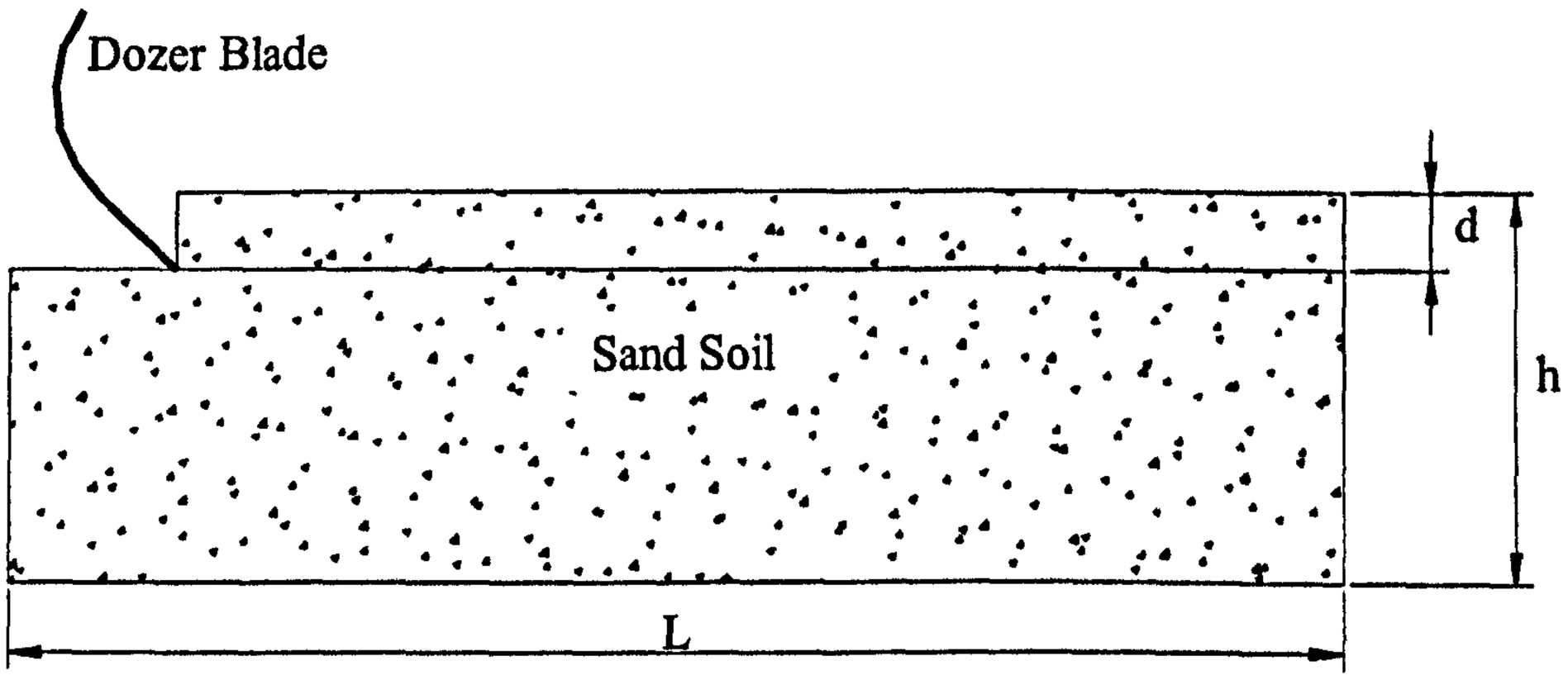

Figure (6.1) Soil-Tool interface model dimensions

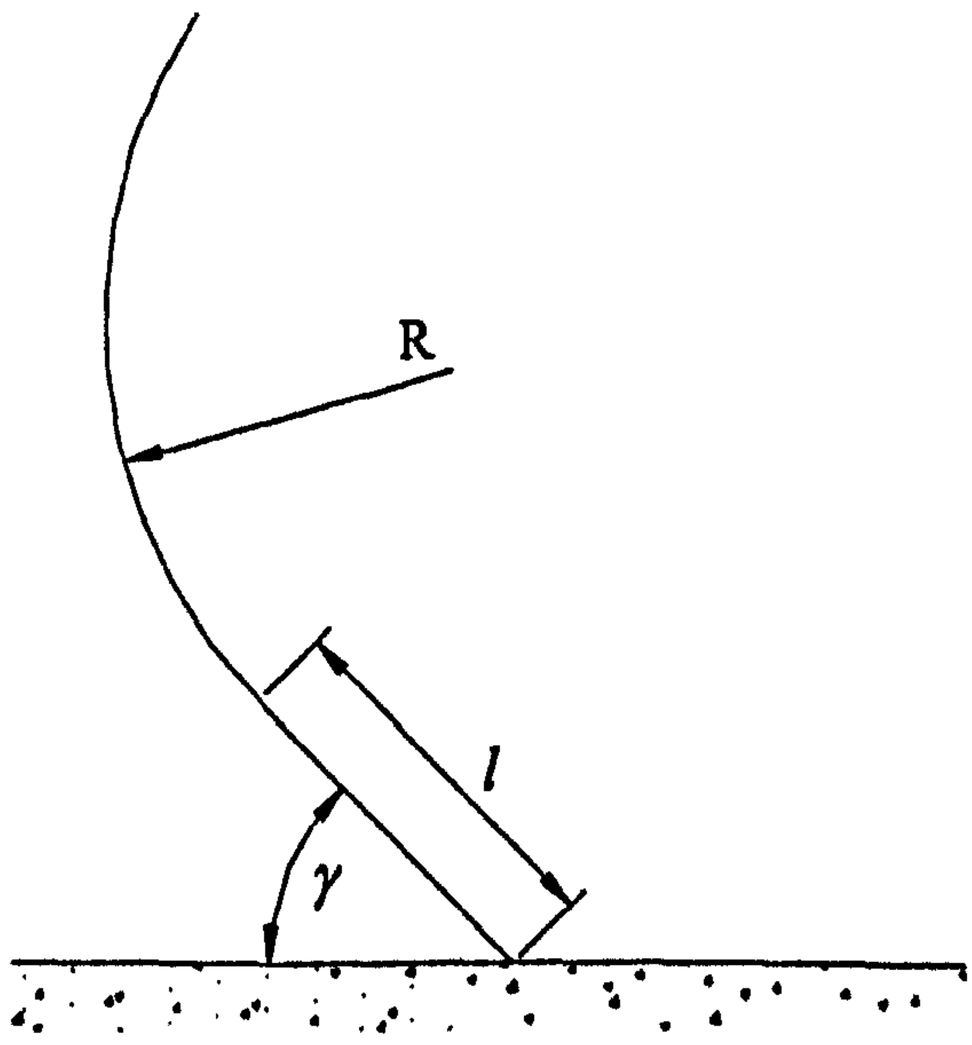

Figure (6.2) Blade main parameters

Where:

L	Sample length = 4500 mm
h	Sample height = 750 mm
d	Cutting depth = 150 ~ 350 mm
γ	Cutting angle = 15° ~ 75°

l Blade flat part length = 400 ~ 500 mm

R Blade radius of curvature = 600 ~ 1200 mm

μ Soil-Tool frictional coefficient = 0.05 ~ 0.2

6.3.1.2 Finite element mesh and boundary conditions

A plane strain two-dimensional bilinear continuum element CPE4 was used to represent both sand and blade in the finite element model as described in section (5.3.5).

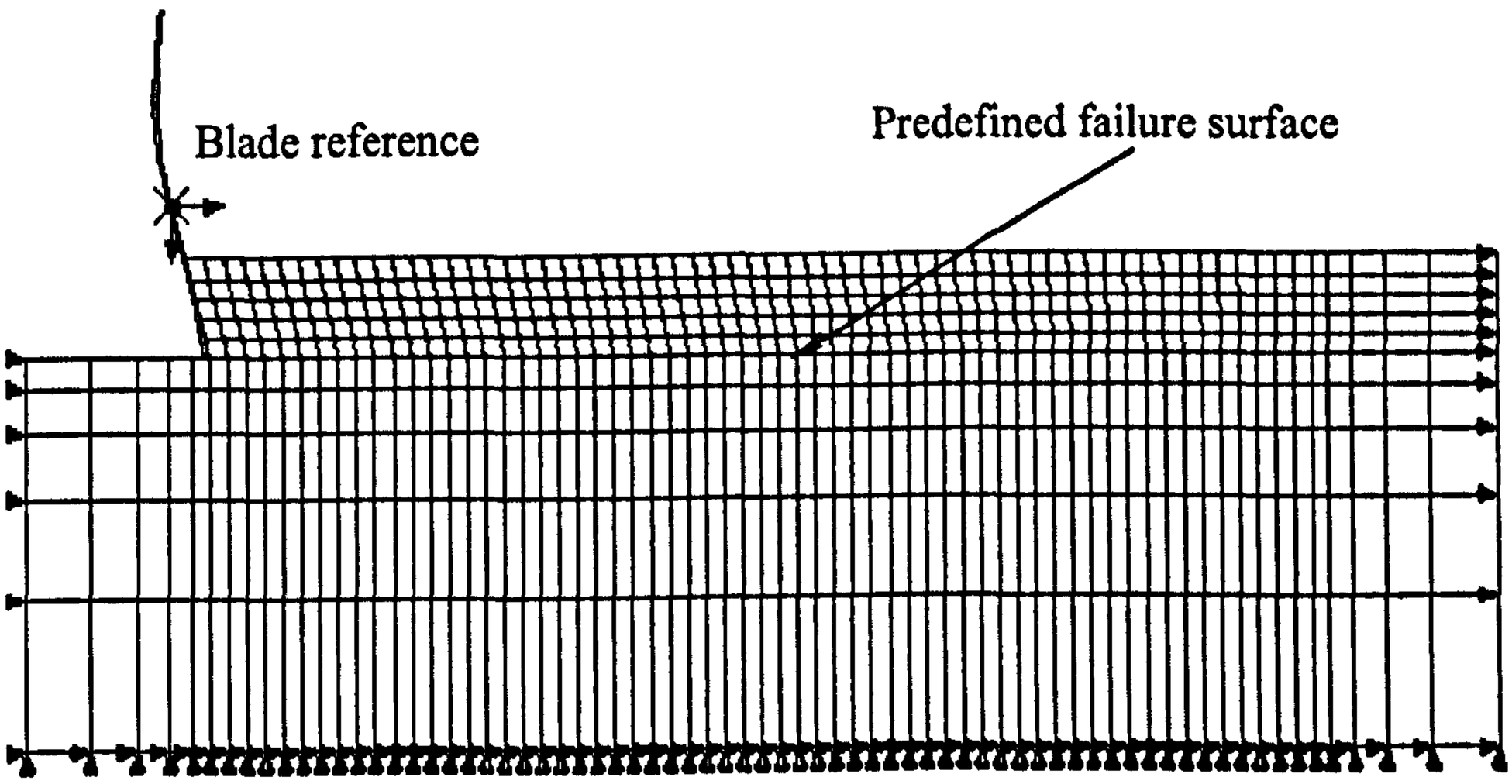

Figure (6.3) Finite element mesh and boundary conditions

675 elements were used (some times more or less) to simulate the sand, depending on cutting depth and mesh density, and 10 elements were used to simulate the blade which is defined as a rigid body with a reference node as shown in Figure (6.3). Simulating the blade using the *RIGID BODY feature in ABAQUS is important to monitor the reaction forces acting on it. A failure surface was predefined along a horizontal plane in front of the blade-cutting tip. The concept of master and slave contact in ABAQUS was used to simulate the interface between cutting blade and soil; and soil itself along the predefined failure surface. Relative motion was allowed with friction along the soil-tool interface. In two-dimensional cases, the common definitions for the boundary conditions of the soil body are as shown in Figure (6.3) and can be listed as follows:

1. Bottom base nodes are constrained on all degree of freedom
2. Nodes along both sides are just constrained in the horizontal direction.
3. All other nodes are free in both translation and rotation
4. The blade is constrained in vertical direction and rotation but it is free to displace in the horizontal direction.

The effect of gravity was taken into account by adding the gravitational acceleration on the sand weight for a single step to establish a real contact pressure along the predefined failure surface. As the analysis was carried out in plane strain, all the reaction forces will be of the dimension (N/blade width) and the width is taken as 1 unit in this analysis.

6.3.2 ANALYSIS AND DISCUSSION

When using earth moving equipment for digging and/or mine clearing there are some important issues which should be considered: first, safety precautions when dealing with mines in the case of mine clearing equipment and second productivity, which means maximum soil mass movement with lower power consumption. Whatever the desired issue is, experimental studies have shown that factors like geometry and operating conditions have effects on the blade cutting forces. Studying the effect of any particular factor requires that the rest have to be held constant. In the various graphs presented in this analysis, continuous lines will represent draft forces and dashed lines will represent vertical forces. The negative sign of the vertical forces means that the vertical forces try to push the blade downward and the positive sign of the draft forces means that the draft force resists the blade in the horizontal direction i.e. opposite to the blade displacement direction.

6.3.2.1 Effect of mesh density

The main concern of mesh density is how to make a good balance between running time cost and calculation accuracy. If a mesh is divided into a dense grid, the running time cost will be high. On the other hand, if a mesh is divided into a coarse grid, the accuracy of the prediction may not be sufficient. To investigate this balance between prediction accuracy and mesh density, a series of finite element models of

the soil-tool interaction problem were carried out for different mesh density: coarse (198 elements), medium (610 element), fine (675 elements) and very fine (740 elements). Figure (6.4) represents the progress in cutting forces as the blade moves horizontally using the various mesh densities. The measured forces dimension was taken as (N/Blade width). As the depth was considered to be one unit for the plane strain analysis, the dimension of the forces can be measured by (N). All the measured reaction forces were taken at the blade reference node, i.e. it represents the force acting on the all blade not just one node. Results of both draft and vertical forces are shown in Figure (6.4).

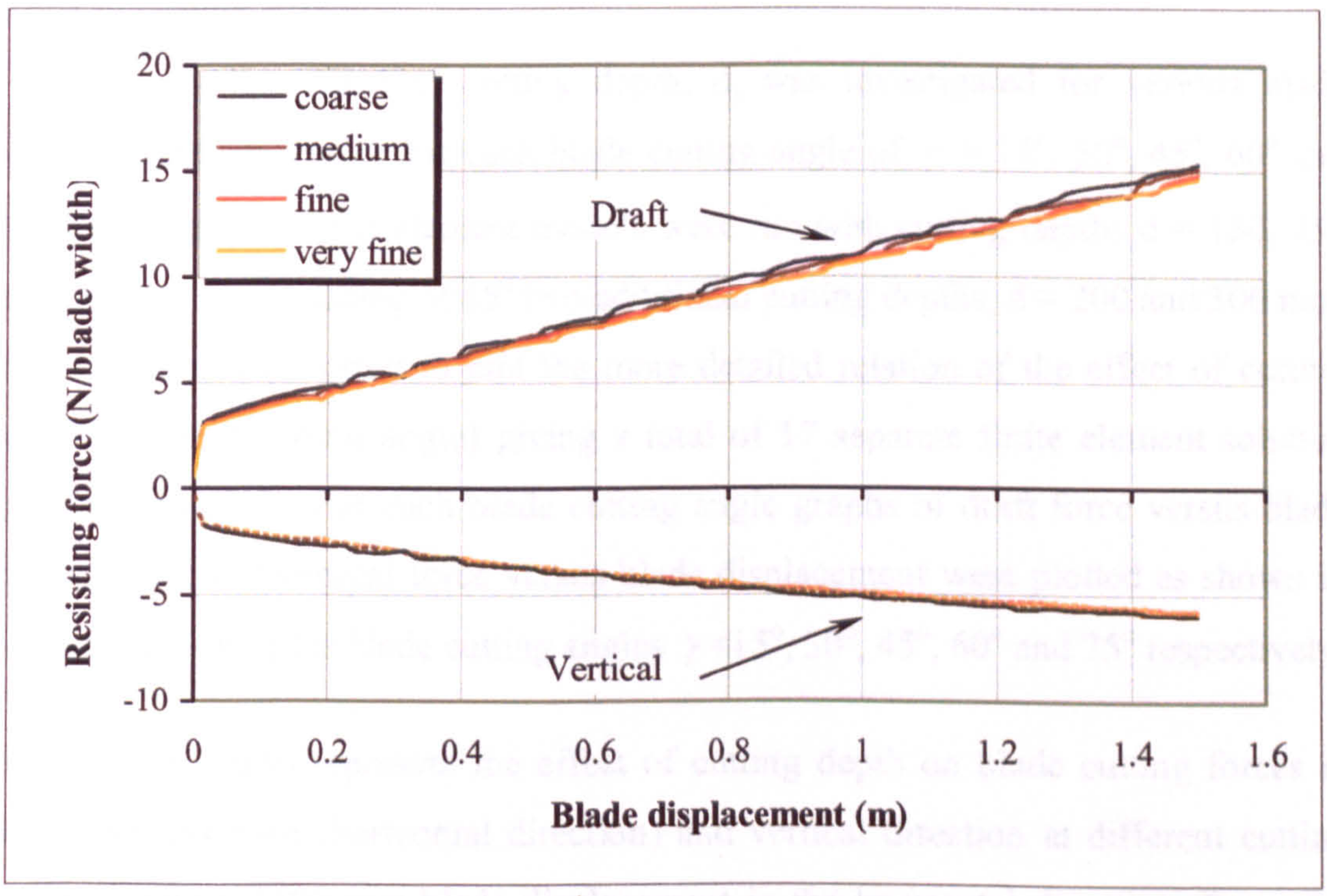

Figure (6.4) Effect of element mesh density

From Figure (6.4) it can be seen that the mesh density has a slight effect on the draft force and insignificant effect on the vertical force. Also it is noticeable that the difference of the predicted forces between medium mesh density and finer ones is insignificant and hence the medium mesh density, which contains 675 elements, was used in the remaining analysis.

6.3.2.2 Effect of operating conditions

A simple flat blade is used to study the effect of two operating conditions; cutting depth and cutting angle. Table [A.3] presents various different operating conditions used in simulating soil-tool interaction for a flat blade. Throughout the simulation the initial void ratio was ($e_0 = 0.75$), soil-metal friction coefficient ($\mu = 0.05$), blade radius ($R = \infty$) i.e. flat blade, and blade displacement (disp = 1500 mm). The two operating conditions studied through a series of analyses where the cutting depth and cutting angle were varied between special limits listed in table [A.3].

Effect of cutting depth

Firstly the effect of cutting depth, d, was investigated for various blade cutting angles, γ. Hence for each blade cutting angle of $\gamma = 15^\circ, 30^\circ, 45^\circ, 60^\circ$ and 75°, three separate finite element models were run with cutting depths d = 150, 250 and 350 mm. For a cutting of 45° two additional cutting depths, d = 200 and 300 mm, were considered (in order to plot the more detailed relation of the effect of cutting depth at certain cutting angle) giving a total of 17 separate finite element solution runs in ABAQUS. For each blade cutting angle graphs of draft force versus blade displacement and vertical force versus blade displacement were plotted as shown in Figures (6.5 ~ 6.9) for blade cutting angles γ=15°, 30°, 45°, 60° and 75° respectively.

Figures (6.5 ~ 6.9) represent the effect of cutting depth on blade cutting forces in both draft direction (horizontal direction) and vertical direction at different cutting angles during a 1500 mm blade displacement in the horizontal direction. From the figures it is clear that as the blade displacement increases both draft and vertical forces increase and also as the cutting depth increases both draft and vertical forces increase whatever the cutting angle. From these figures it is also noticeable that the effect of the cutting depth on draft force at small cutting angles ($\gamma < 45^\circ$) is less than its effect at large cutting angles ($\gamma > 45^\circ$) and vice versa for the vertical force i.e. the effect of the cutting depth on vertical force at small cutting angles ($\gamma < 45^\circ$) is higher than its effect at large cutting angles ($\gamma > 45^\circ$).

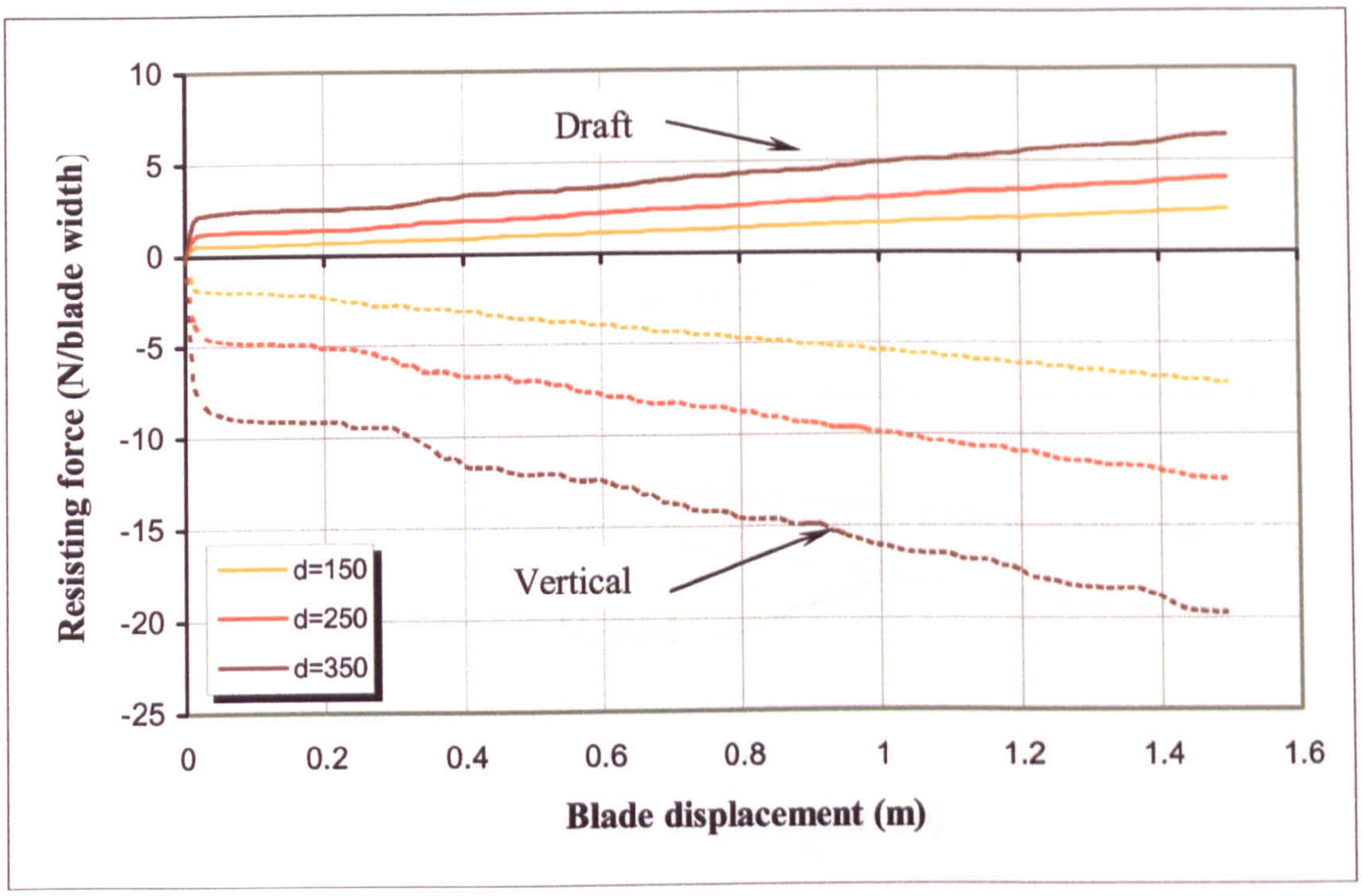

Figure (6.5) Effect of cutting depth at 15° cutting angle for flat blade

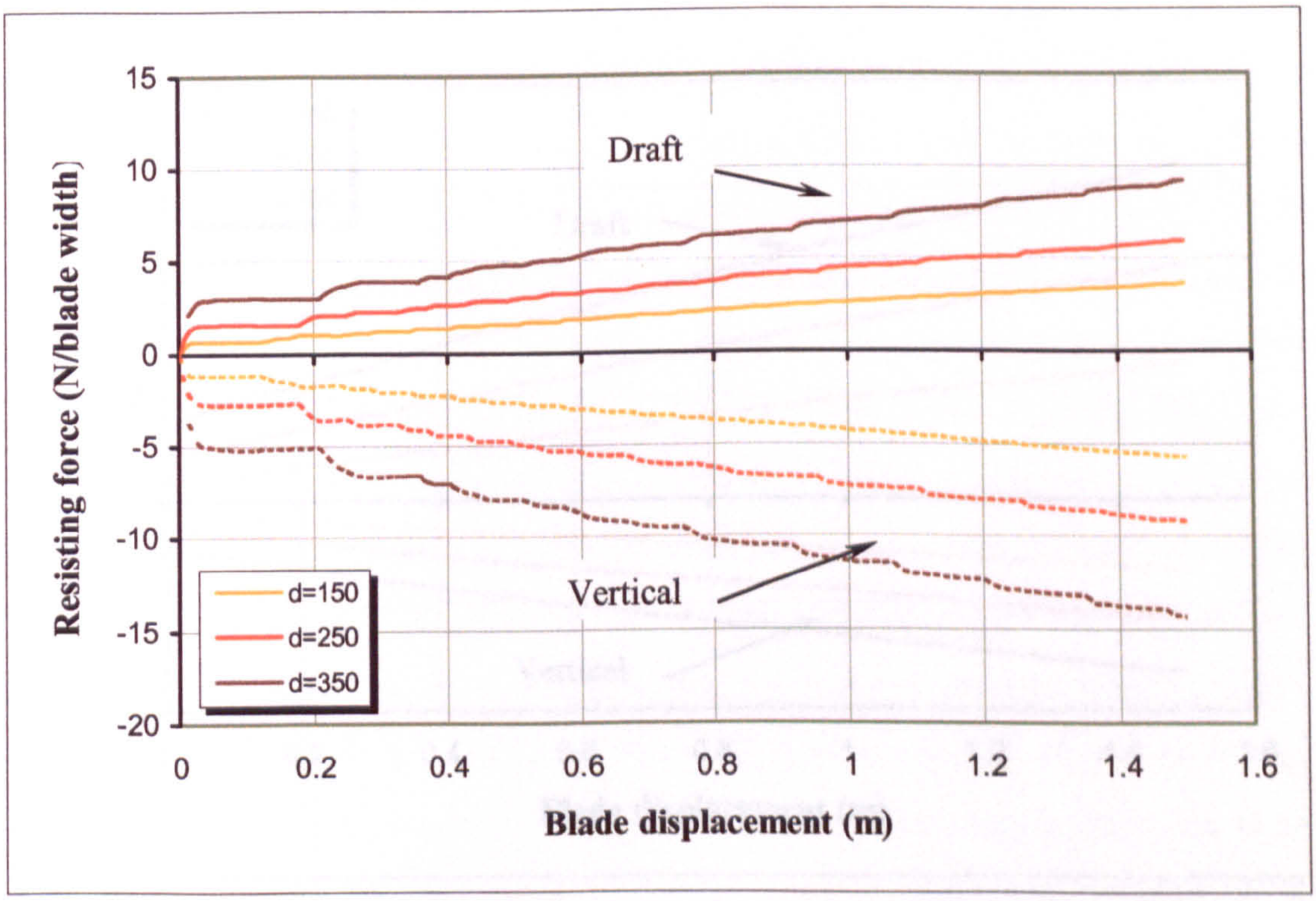

Figure (6.6) Effect of cutting depth at 30° cutting angle for flat blade

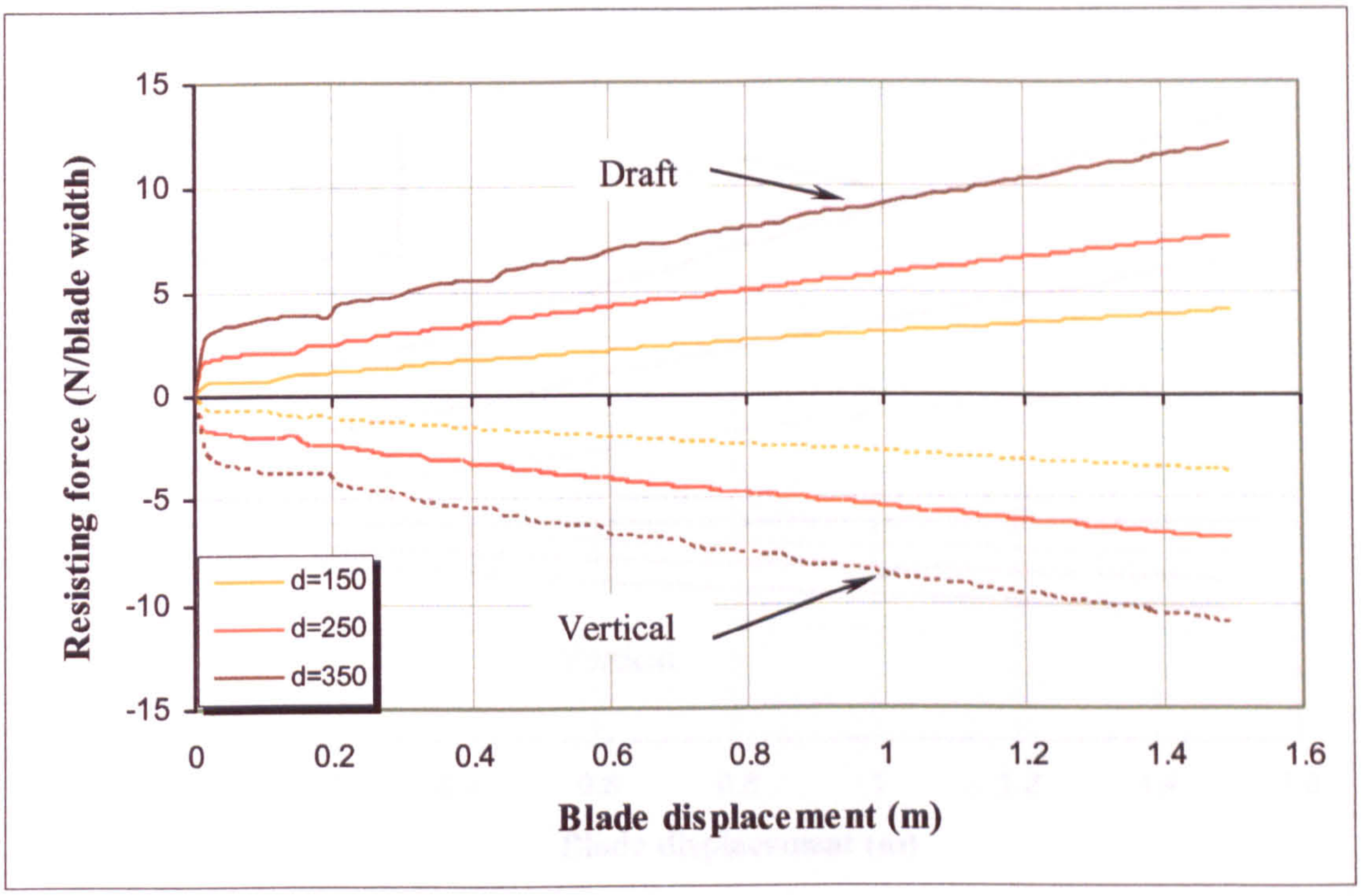

Figure (6.7) Effect of cutting depth at 45° cutting angle for flat blade

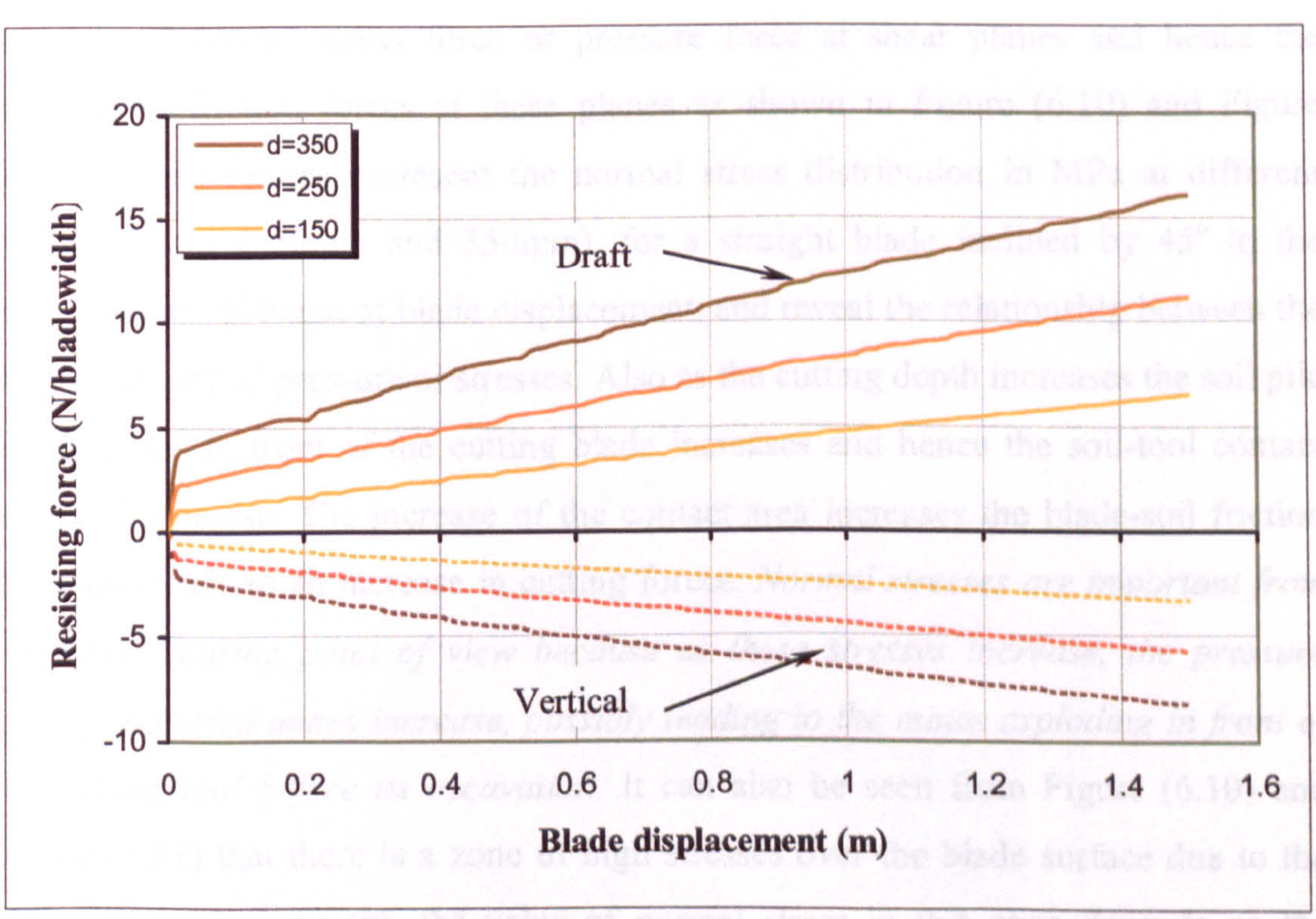

Figure (6.8) Effect of cutting depth at 60° cutting angle for flat blade

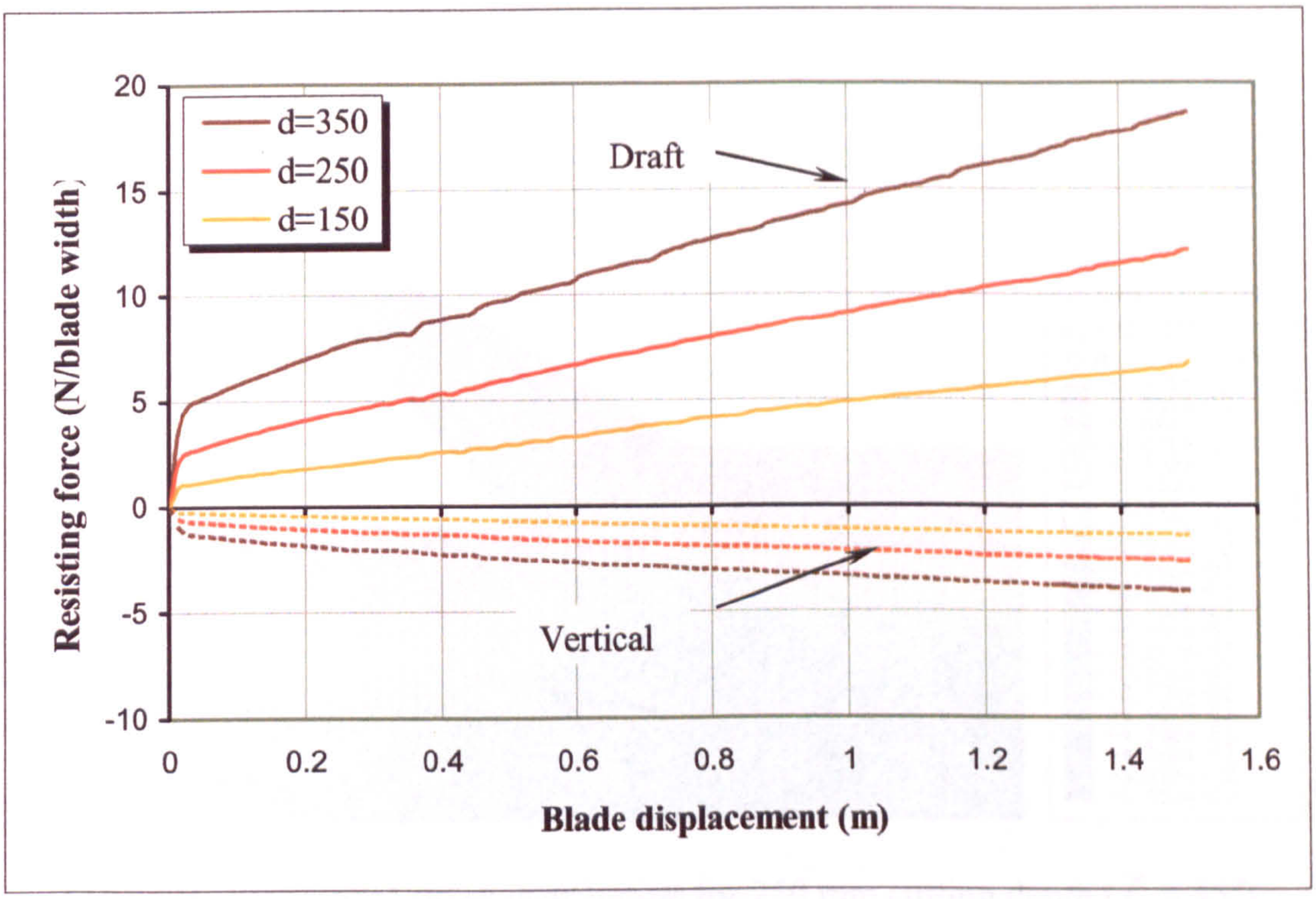

Figure (6.9) Effect of cutting depth at 75° cutting angle for flat blade

The increase in cutting forces with increasing cutting depth can be explained by the increase of normal stress force or pressure force at shear planes and hence the increase of friction forces at these planes as shown in Figure (6.10) and Figure (6.11). These figures represent the normal stress distribution in MPa at different cutting depths (250mm and 350mm), for a straight blade inclined by 45° to the horizontal at 1500 mm of blade displacement, and reveal the relationship between the depth and normal pressure or stresses. Also as the cutting depth increases the soil pile accumulated in front of the cutting blade increases and hence the soil-tool contact area will increase. The increase of the contact area increases the blade-soil friction force and leads to an increase in cutting forces. *Normal stresses are important from the mine clearing point of view because as these stresses increase, the pressure acting on buried mines increase, possibly leading to the mines exploding in front of the cutting tool before its excavation.* It can also be seen from Figure (6.10) and Figure (6.11) that there is a zone of high stresses over the blade surface due to the effect of cut soil weight, the value of normal stress in this zone depends on the cutting depth. This could explain the increase of the vertical force as the cutting depth increases.

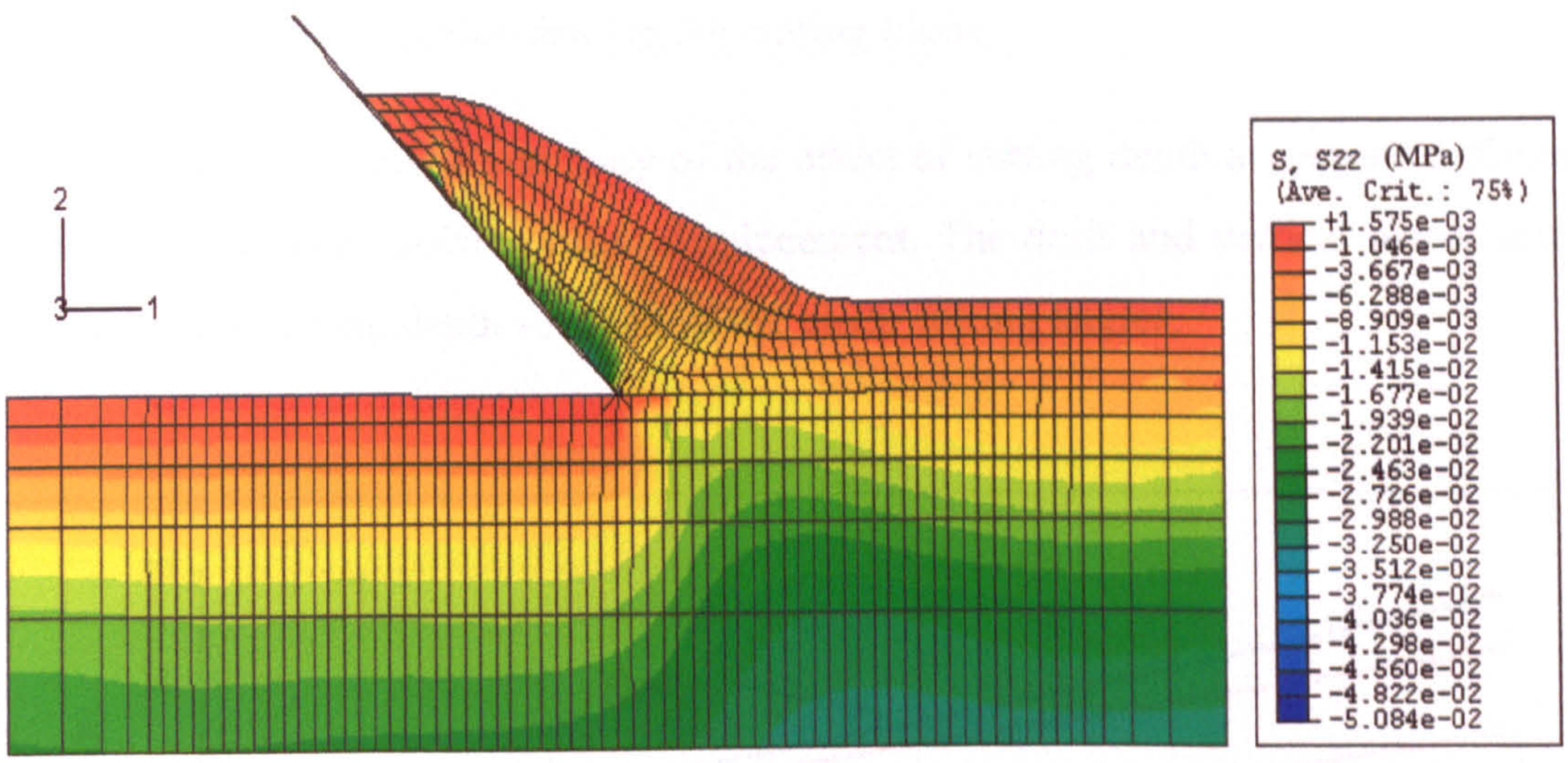

Figure (6.10) Normal stress distribution for 250 mm cutting depth ($\gamma = 45°$)

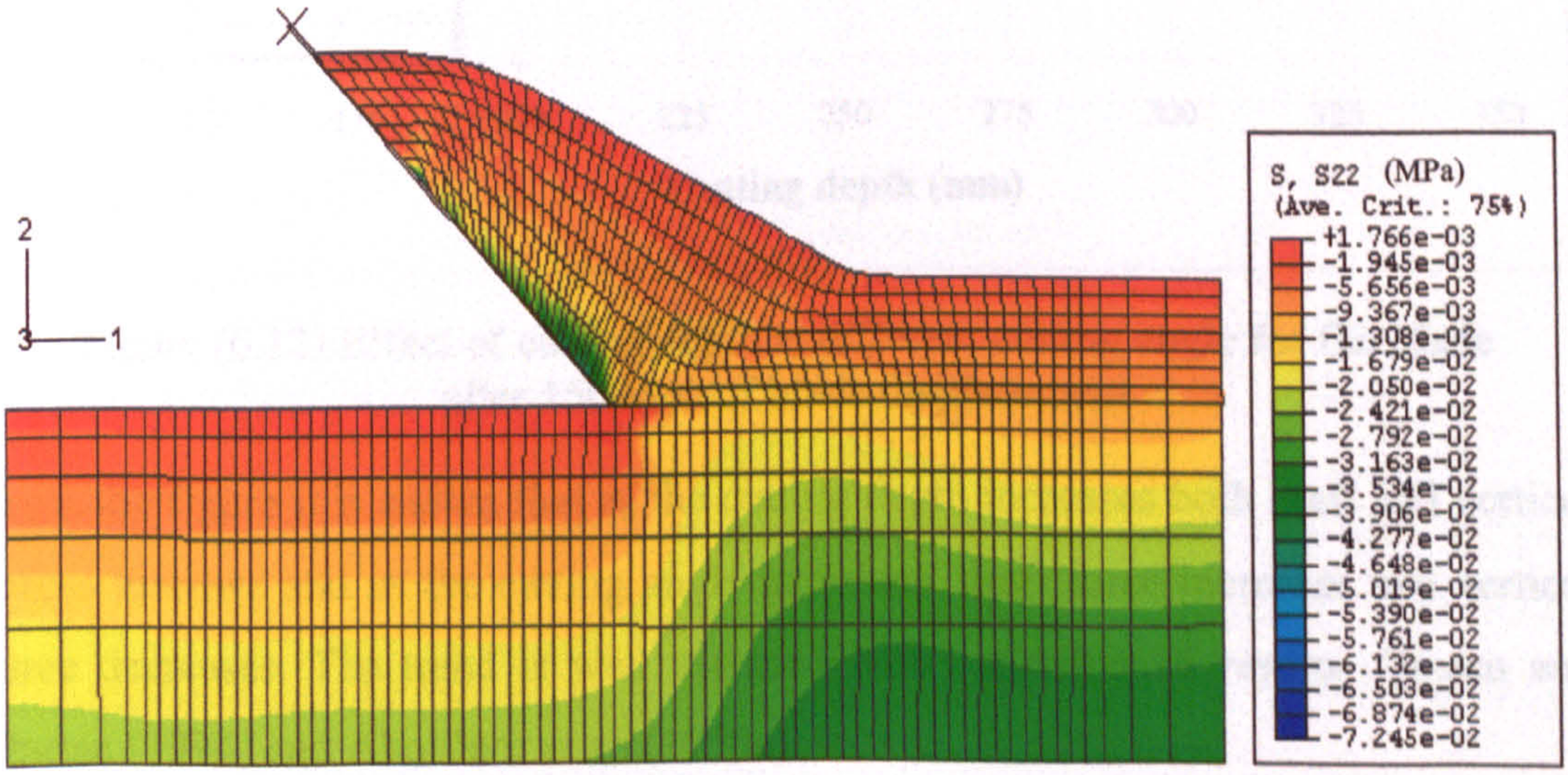

Figure (6.11) Normal stress distribution for 350 mm cutting depth ($\gamma = 45°$)

The draft force is often considered to be more important than the vertical force, Chi and Kushwaha (1990), but in fact the effect of the vertical force is also important as it affects the traction effort required for mobility and hence it affects the total power consumption of the machine driving the cutting blade.

Figure (6.12) represents a summary of the effect of cutting depth at various different cutting angles after 1500mm blade displacement. The draft and vertical forces were plotted versus cutting depth for each of the blade cutting angles.

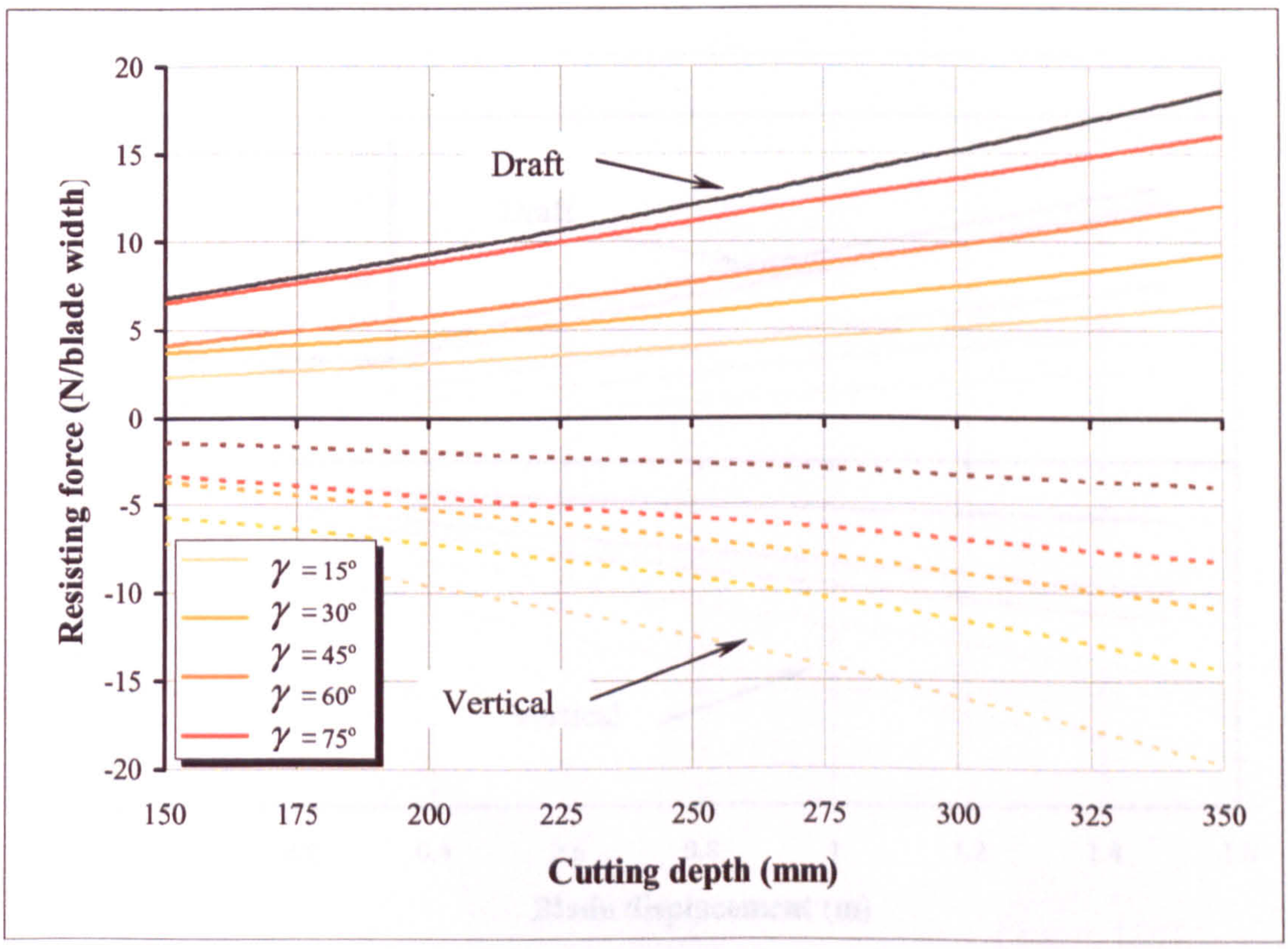

Figure (6.12) Effect of cutting depth at different cutting angle for flat blade after 1500mm of blade displacement

From the figure it is shown that as the cutting depth increases both draft and vertical forces increase and as the cutting angle increases, draft force increases and vertical force decreases. The trend is well matched with experimental results, Qinsen and Shuren (1994) and AboElnor et al. (1998a).

Effect of cutting angle

Experimental studies of the effect of cutting angle on blade cutting forces, AboElnor et al. (1998a), have shown a significant effect on both draft and vertical forces. To investigate the effect of cutting angle numerically, a series of finite element analyses was carried out at various different cutting angles and for a certain cutting depth (chosen as 250 mm). Figure (6.13) represents draft and vertical forces acting on the blade at different cutting angles, γ=15°, 30°, 45°, 60° and 75°, versus blade displacement. From the figure it can be seen that as the cutting angle increases, draft force increases and vertical force decreases.

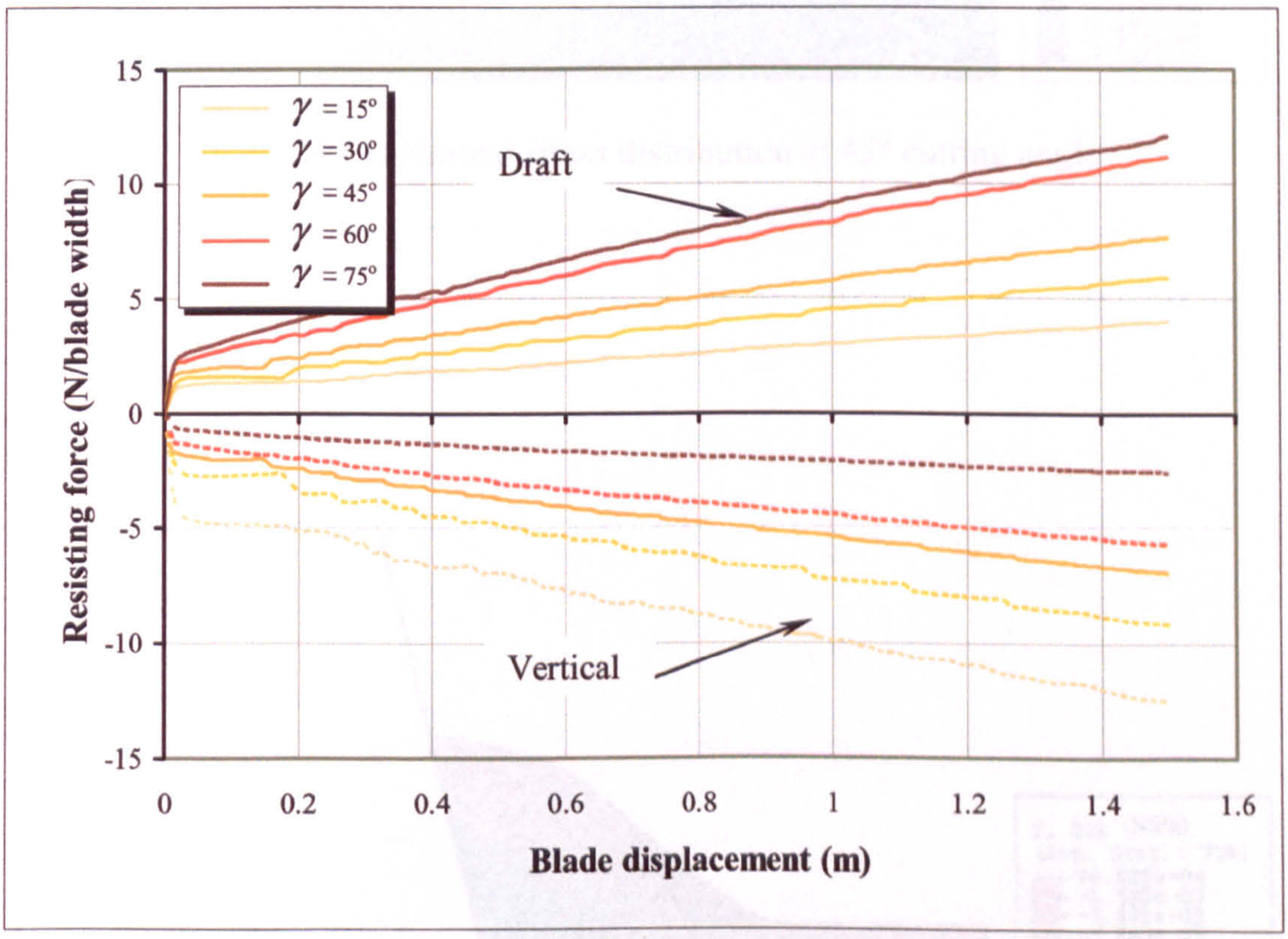

Figure (6.13) Effect of cutting angle at cutting depth of 250mm

To further interpret the effect of cutting angle on cutting forces, presented in Figure (6.13), the normal stress distribution at cutting angles, $\gamma = 45°$ and 75° were plotted as shown in Figure (6.14) and Figure (6.15) for a cutting depth of 350mm and blade displacement of 1500mm.

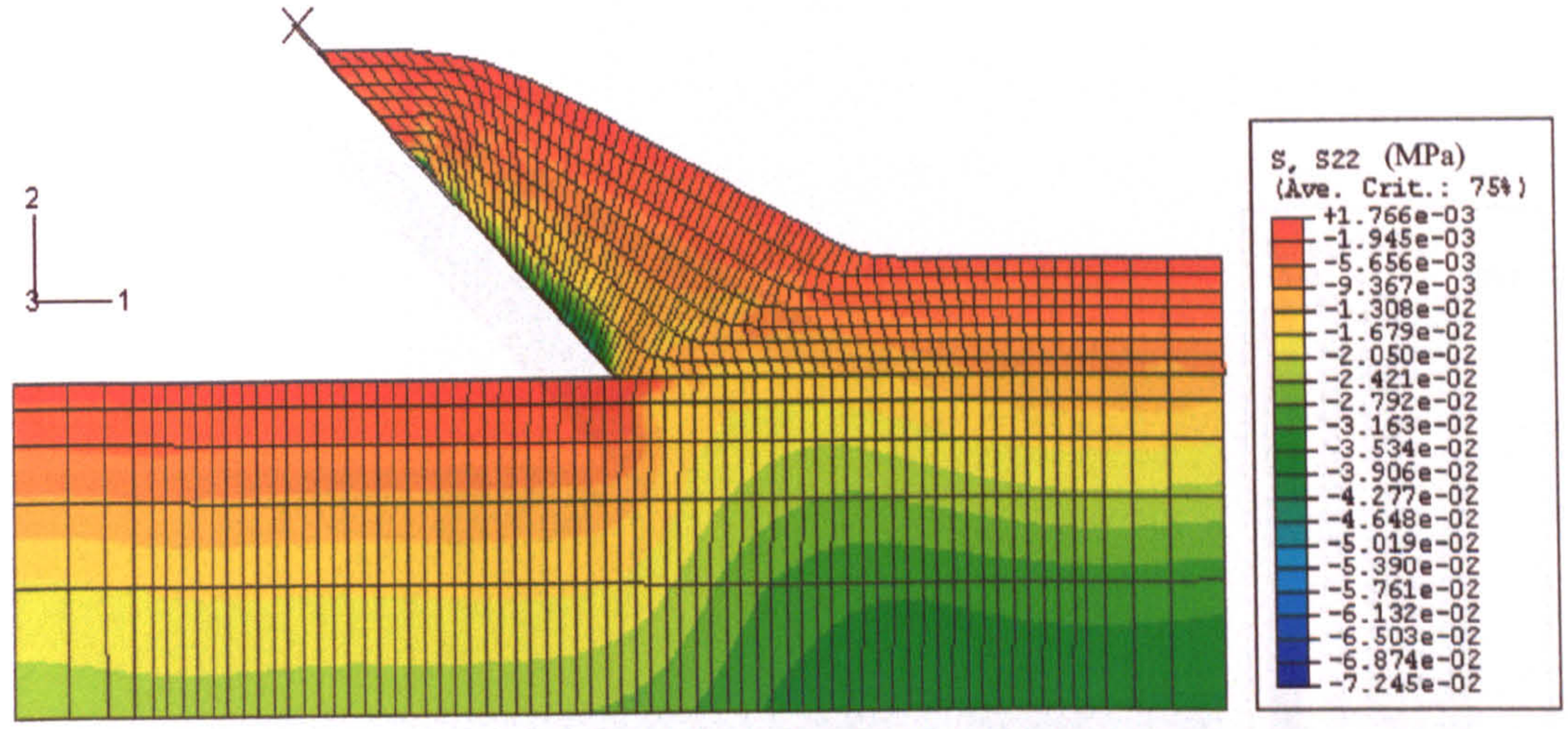

Figure (6.14) Normal stress distribution at 45° cutting angle

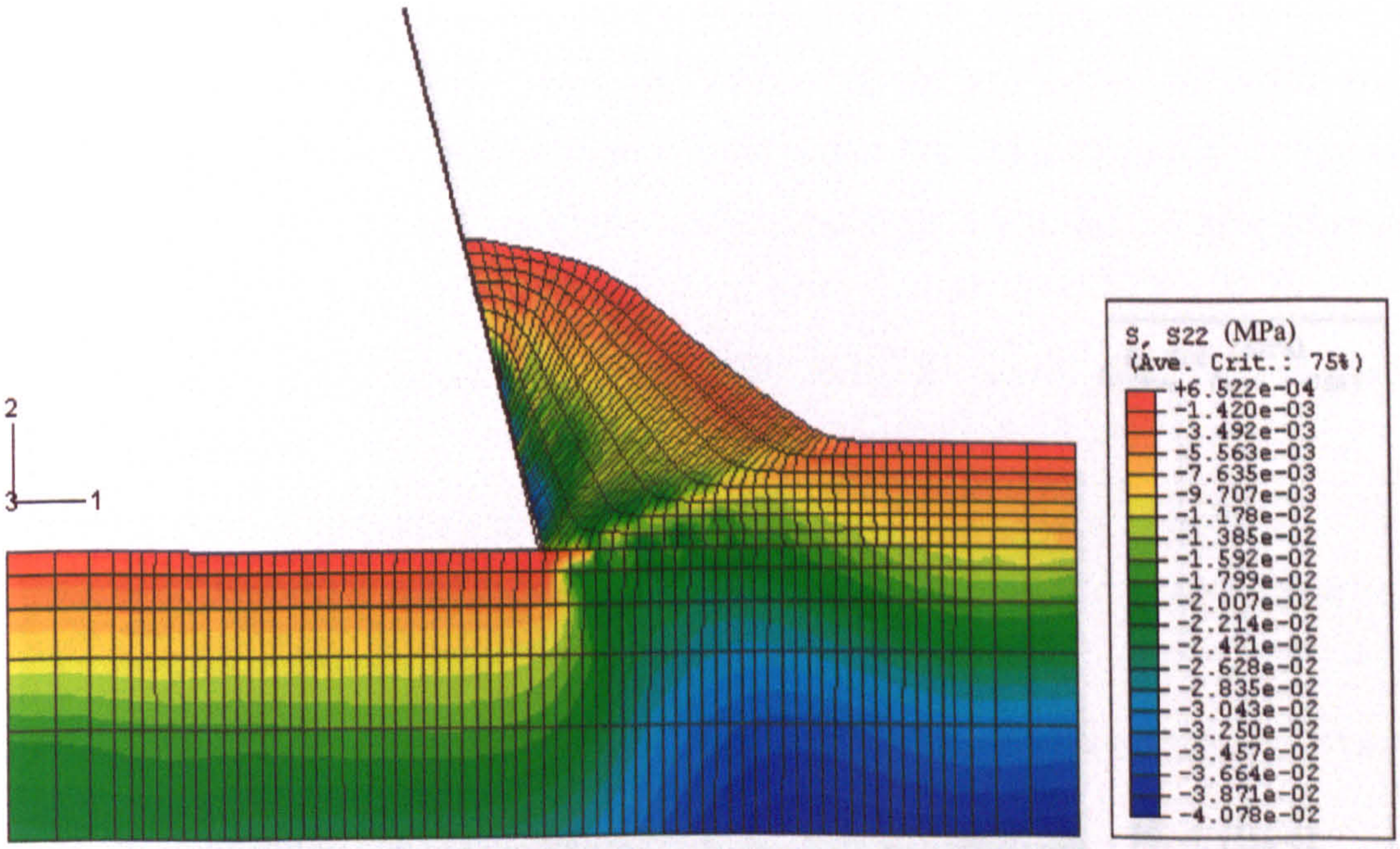

Figure (6.15) Normal stress distribution at 75° cutting angle

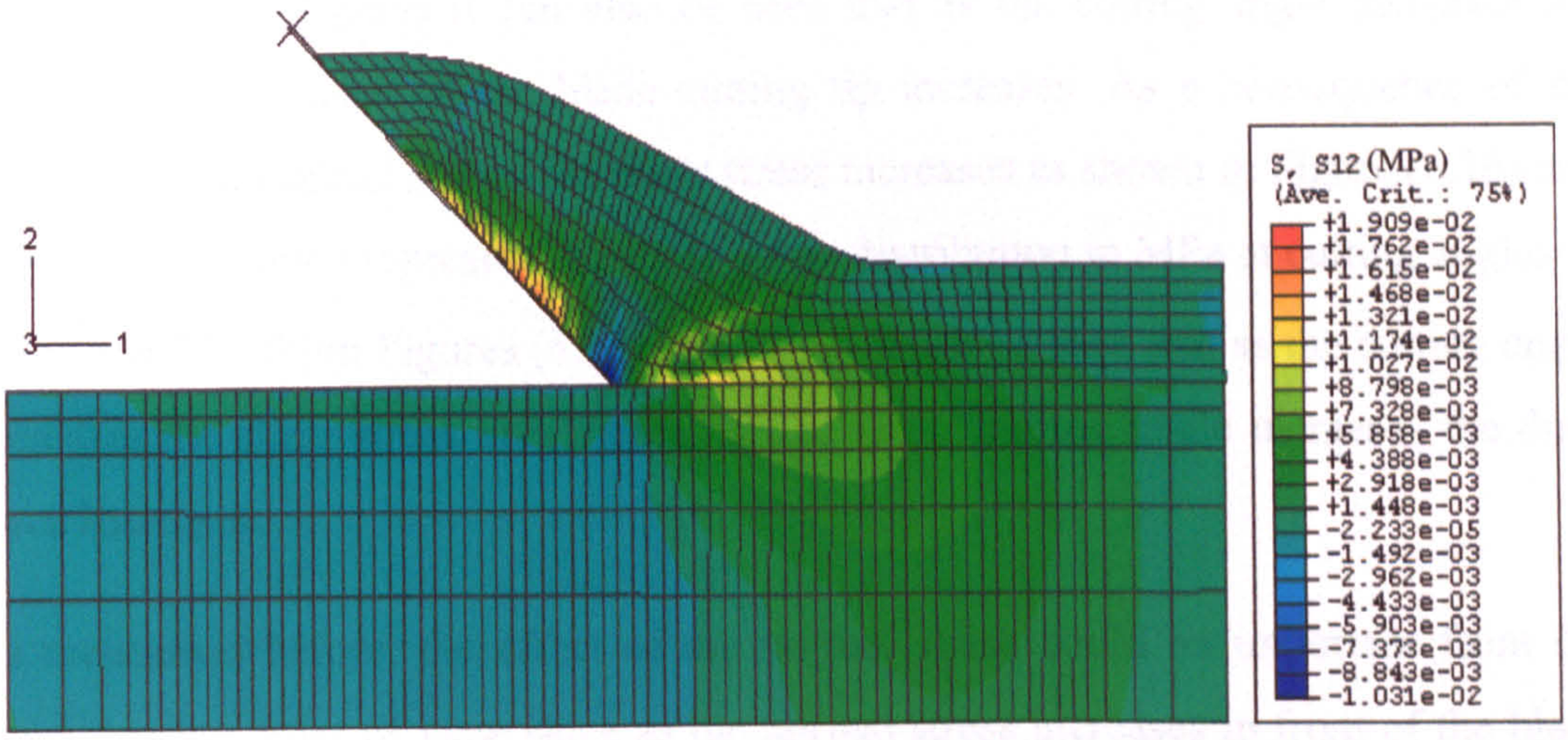

Figure (6.16) Shear stress distribution at 45° cutting angle

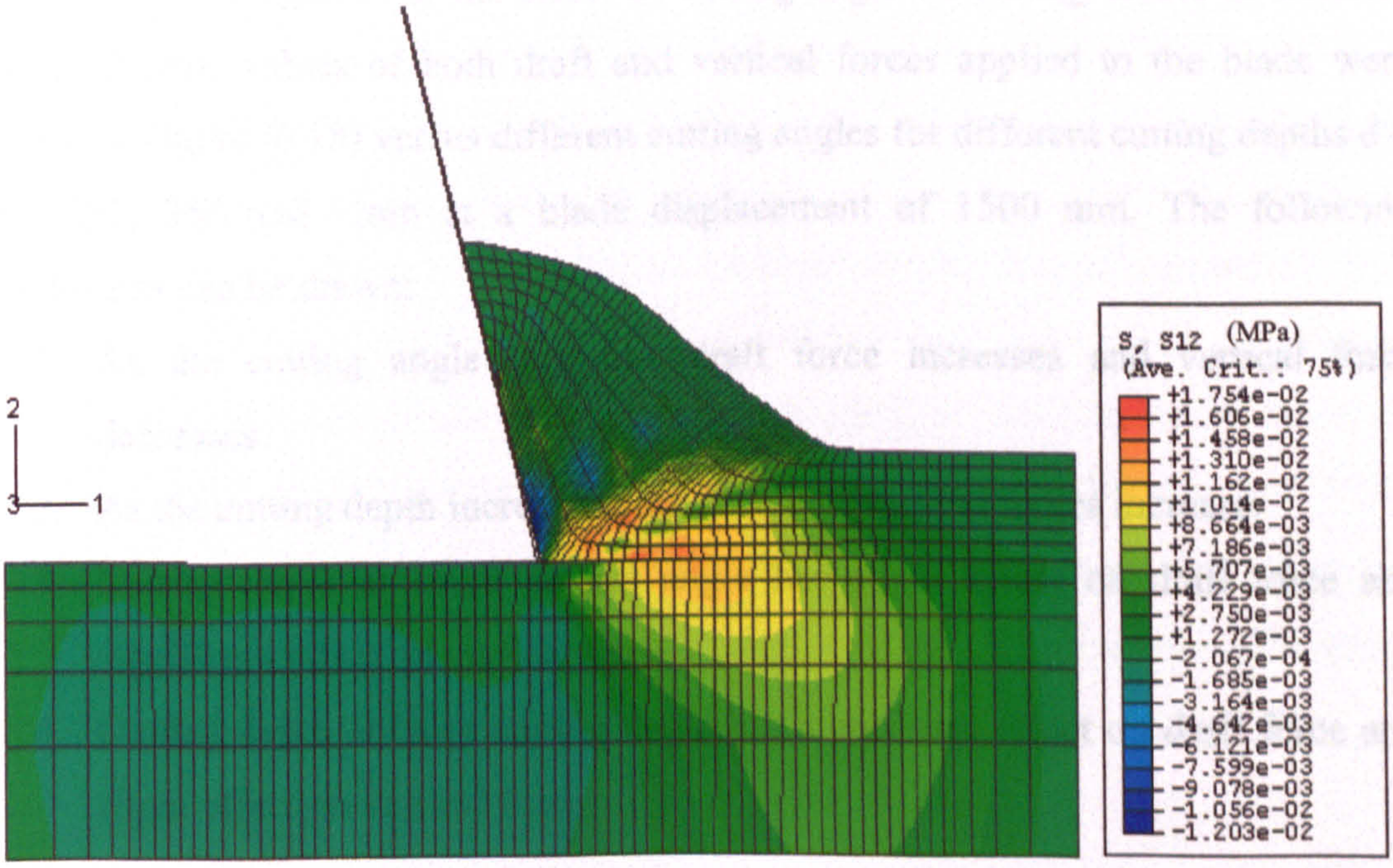

Figure (6.17) Shear stress distribution at 75° cutting angle

From figures (6.14 and 6.15) it can be easily seen that as the cutting angle increases the weight component of the cut soil acting on the blade, presented by normal stress, decreases and hence the vertical force decreases with increasing the cutting angle. From these two figures it can also be seen that as the cutting angle increases the normal stress in front of the blade cutting tip increases. As a consequence of the increase in the normal stress, the shear stress increases as shown in Figure (6.16) and Figure (6.17) which represent the shear stress distribution in MPa at cutting angles γ = 45° and 75°. From Figures (6.16) and (6.17) it can be seen that as the cutting angle increases the shear stress also increases, i.e. as the cutting angle increases the draft force increases.

As mentioned before, the effect of the normal stress could be important from the mine clearing point of view since as the normal stress increases in front of the blade the chance of mine explosion increases. Removal of the accumulated soil in front of the blade during mine clearing process could be safer but at the same time it means lower productivity and this may be why "V type" blades in mine clearing equipment are very often preferable than a straight blade.

For further investigation of the effect of cutting angle on cutting forces at different cutting depths, values of both draft and vertical forces applied to the blade were plotted in Figure (6.18) versus different cutting angles for different cutting depths d = 150, 250, 350 and mm at a blade displacement of 1500 mm. The following conclusions can be drawn:

1. As the cutting angle increases draft force increases and vertical force decreases
2. As the cutting depth increases both draft and vertical forces increase.
3. Cutting depth at small cutting angle has slight effect on draft force and significant effect on vertical force
4. Cutting depth at large cutting angle has significant effect on draft force and slight effect on vertical force.

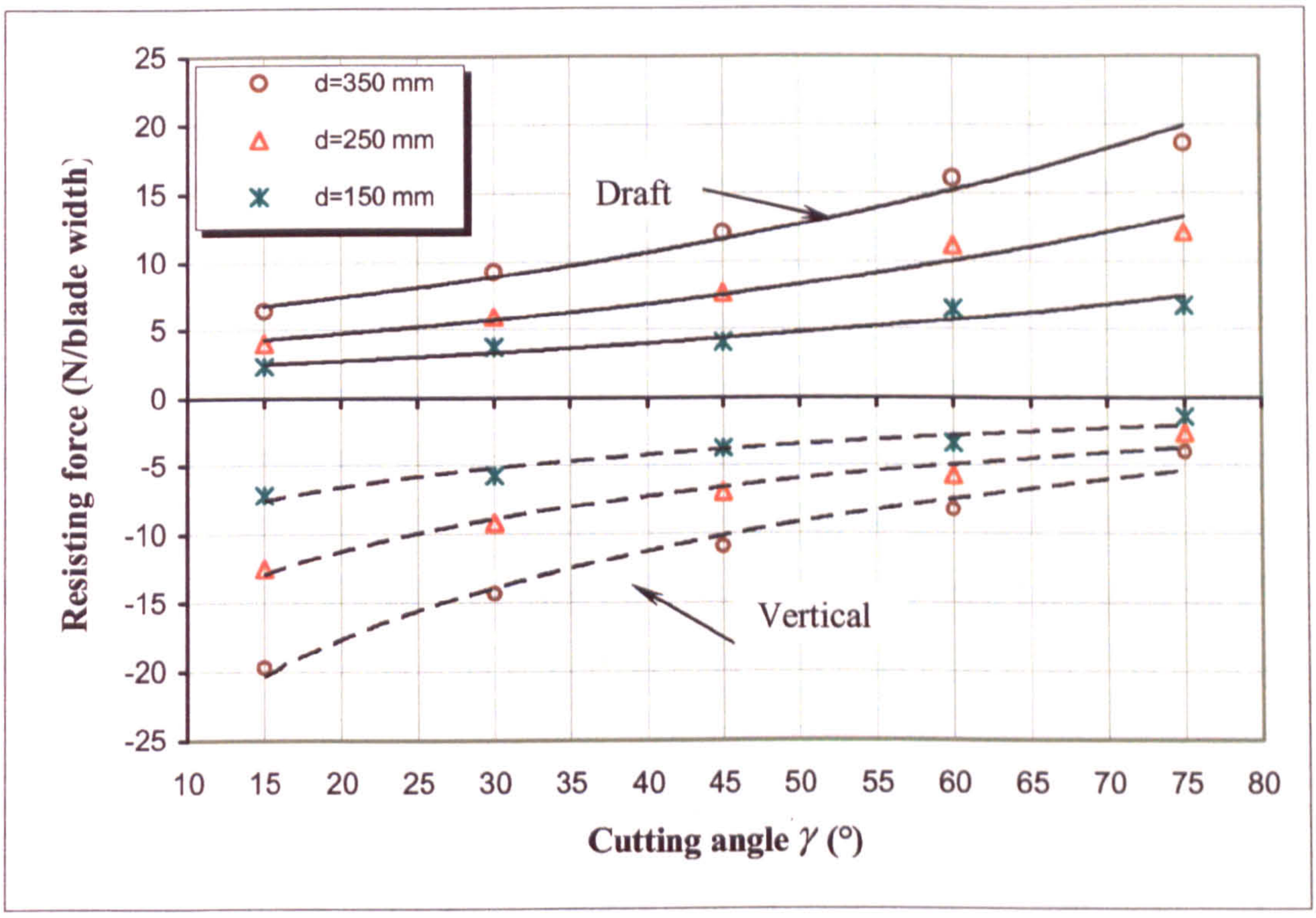

Figure (6.18) Effect of cutting angle at different cutting depth for flat blade at 1500mm of blade displacement

6.3.2.3 Effect of initial conditions

Initial condition means a condition that may relates to: (1) a design parameter such as blade geometry and soil-metal coefficient of friction which dependant on the blade surface roughness or (2) natural parameters such as soil type and density. To study the effect of the initial conditions on blade cutting forces a series of finite element simulations of soil-tool interaction at different initial conditions were carried out. The simulated conditions are listed in table [A.4] at blade radius of curvature (R=800), blade cutting angle (γ=45°), cutting depth (d=250mm), and blade displacement of 1500 mm. These blade geometry parameters and operating conditions were selected as values between the extremes of all the simulated values used through the soil-tool interaction analysis.

Effect of sand density

Soil properties depend on many factors such as grain size, degree of saturation, grains hardness and cohesion. Particularly for sand, the key factor that describes the state of the sand is the void ratio (*e*). If this value is higher than a critical value it means that sand is in loose state and if it is lower that means sand is in dense state. To investigate the effect of soil density a series of finite element analyses was carried out for different initial sand densities, e_o = 0.6, 0.75 and 0.9. Figure (6.19) represents various different forces acting on the blade through a cutting distance of 1500mm for different states of sand density according to the value of the initial void ratio.

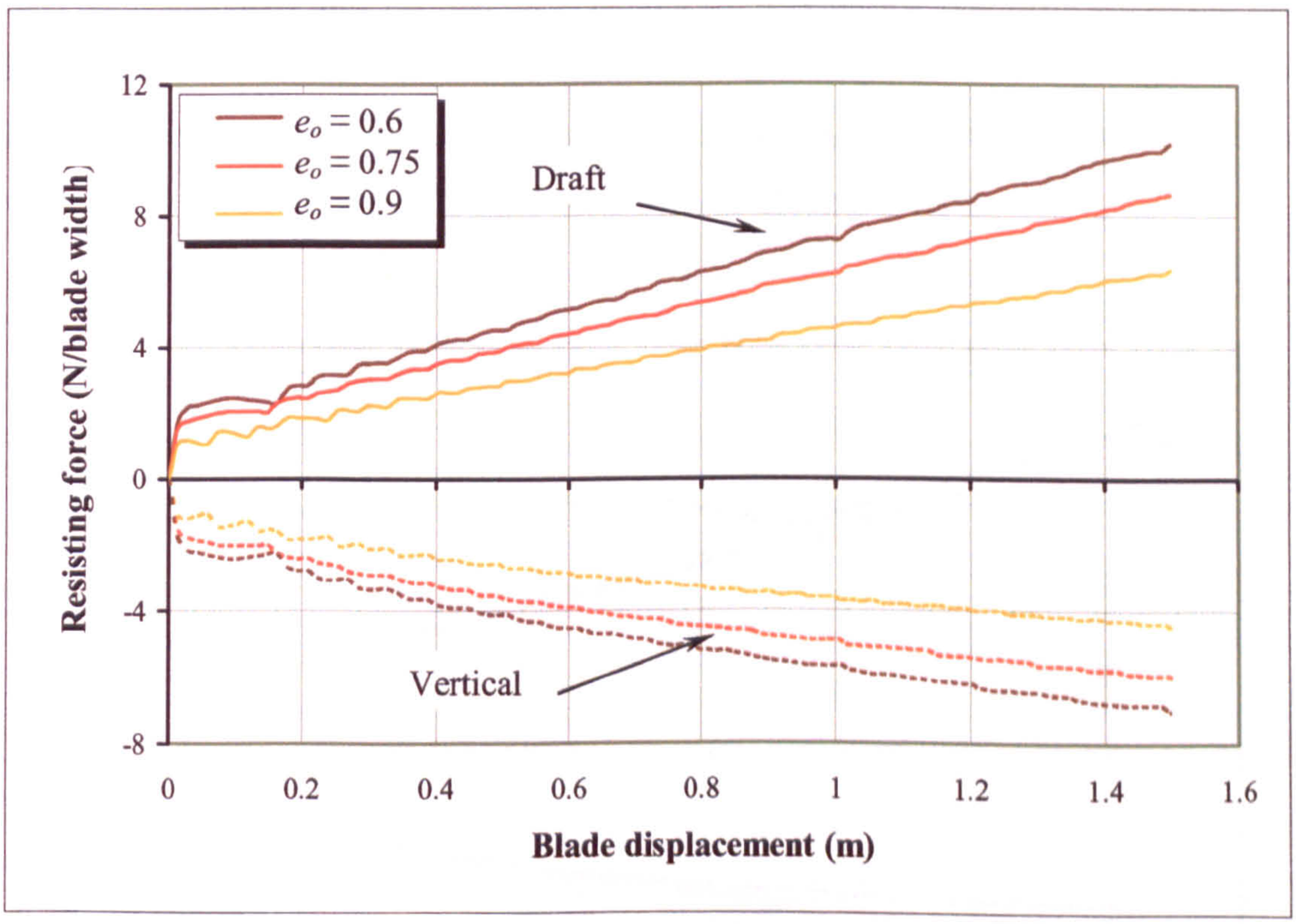

Figure (6.19) Effect of sand density on blade cutting forces ($\gamma = 45°$, d = 250 mm)

The figure reveals the significant effect of void ratio on blade cutting forces that as the void ratio decreases (i.e. density increases) both draft and vertical forces increase and as the void ration increases (i.e. density decreases) both draft and vertical forces decrease.

Effect of blade surface roughness

Blade surface roughness is a design factor, which can be adjusted during the blade manufacture; the value of the soil-metal friction coefficient μ is dependant on soil type as well. To study the effect of blade roughness on blade cutting forces a series of finite element analyses was carried out on a blades of various soil-tool friction coefficient μ=0.05, 0.1 and 0.2. These analyses were carried at cutting angle (γ= 45°) and cutting depth (d = 250) mm. for each finite element simulation the cutting forces in both draft and vertical directions were plotted through blade displacement of 1500 mm. Figure (6.20) represents the effect of friction coefficient on blade cutting forces, the figure reveals that as the friction coefficient increases draft force increases and vertical force decreases. It is shown also from the figure that the effect of the soil-metal friction coefficient was insignificant at the beginning of the blade displacement and then became significant later as soil accumulate in front of the blade i.e. as the normal stress acting on the blade increases.

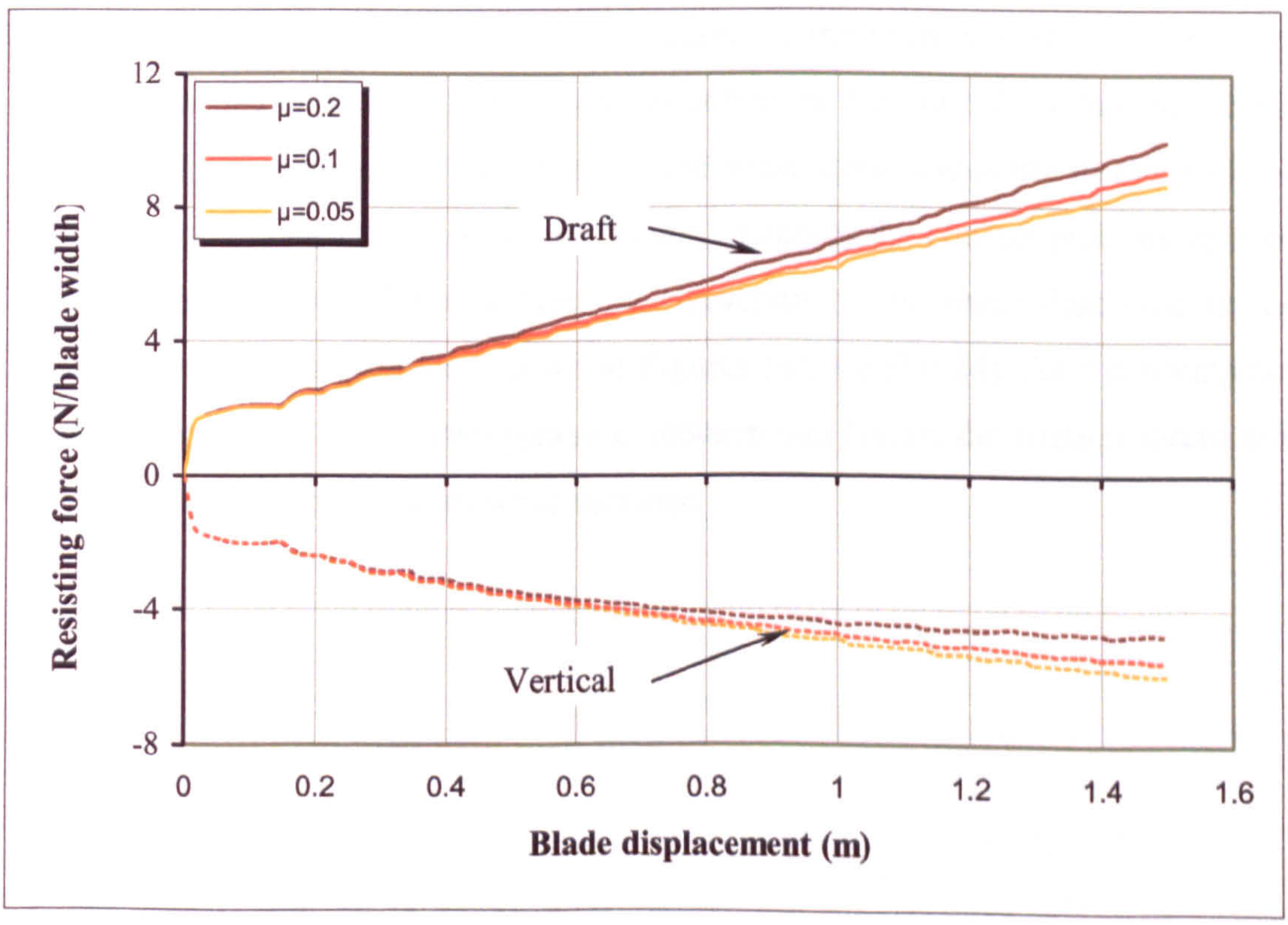

Figure (6.20) Effect of blade roughness on cutting forces (γ= 45°, d = 250 mm)

To interpret the behaviour shown in Figure (6.20), surface results feature in ABAQUS is used to plot both the friction shear stresses distribution at the soil-tool interface and the contact pressure distribution along the predefined failure surface for two finite element analyses of blades with different roughness (μ=0.05 and 0.2). Figures (6.21 and 6.22) represent the friction shear stress distribution along the soil-tool interface for different blade roughness (μ=0.05 and 0.2) respectively. Figures (6.23 and 6.24) represent the contact pressure distribution along the predefined failure surface for different blade roughness (μ=0.05 and 0.2) respectively. The behaviour shown in Figure (6.21) was interpreted using Figures (6.21 to 6.24) as follows:

1. For the vertical force, as the friction coefficient increases the soil-blade contact shear (frictional shear) stress increases as shown in Figures (6.21 and 6.22). This increase in the contact shear stress creates a reaction force that is trying to push the blade upward in a direction tangent to the blade along the contact line and hence the magnitude of the vertical force decreases.
2. For the draft force, the reaction force caused by the frictional shear stress in the horizontal plane will act in the same direction as the draft force and hence the draft force increases. Not only the friction shear stress cause the increase of the draft force but also as the soil-tool friction increases the contact pressure applied on the predefined failure surface, as a reaction of the force described in the previous point, increases as shown in Figures (6.23 and 6.24). As a consequence of the increase in the contact pressure between soil layers, the friction forces will increase and hence the draft force increase.

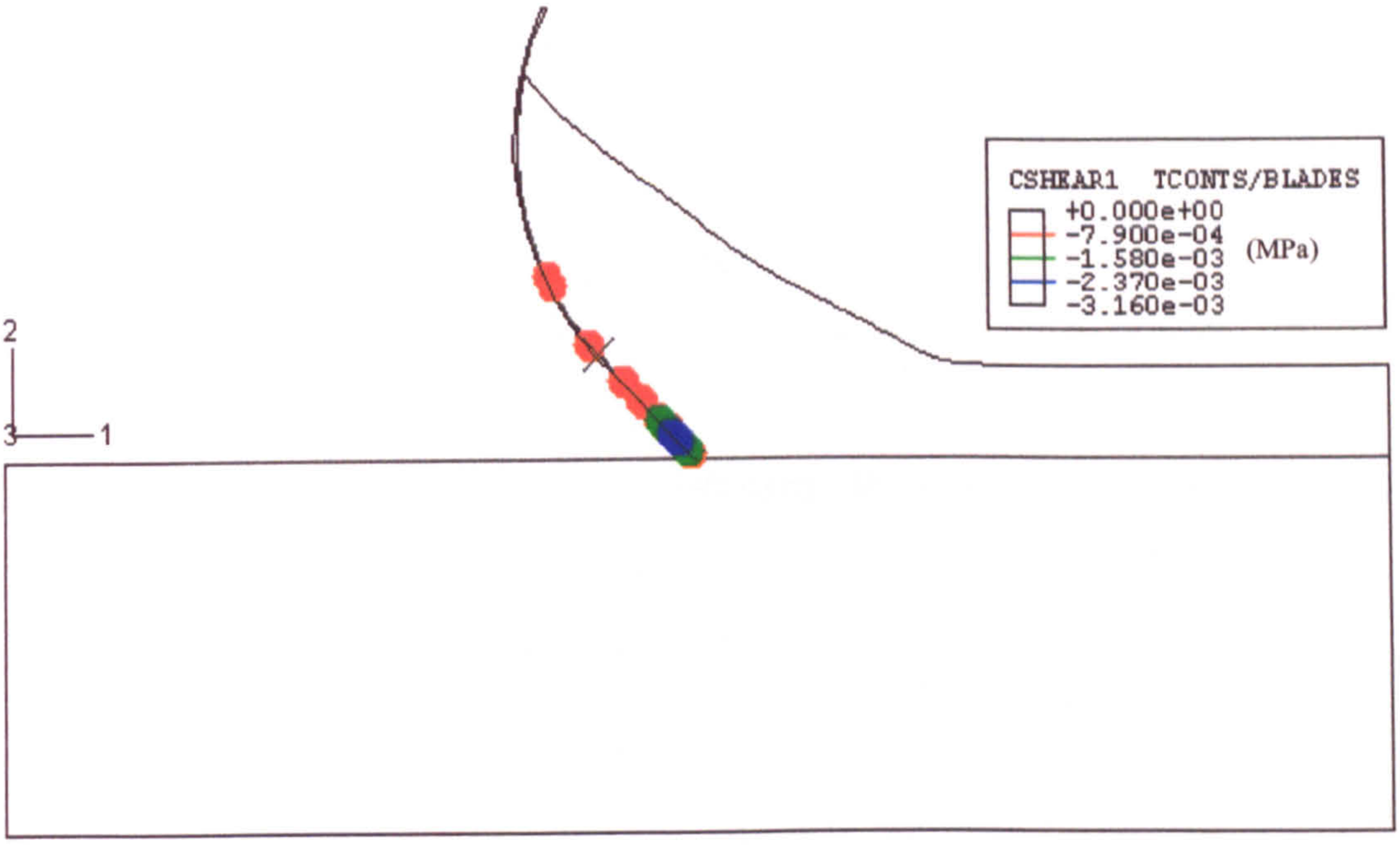

Figure (6.21) Frictional shear stress along blade surface for μ=0.05

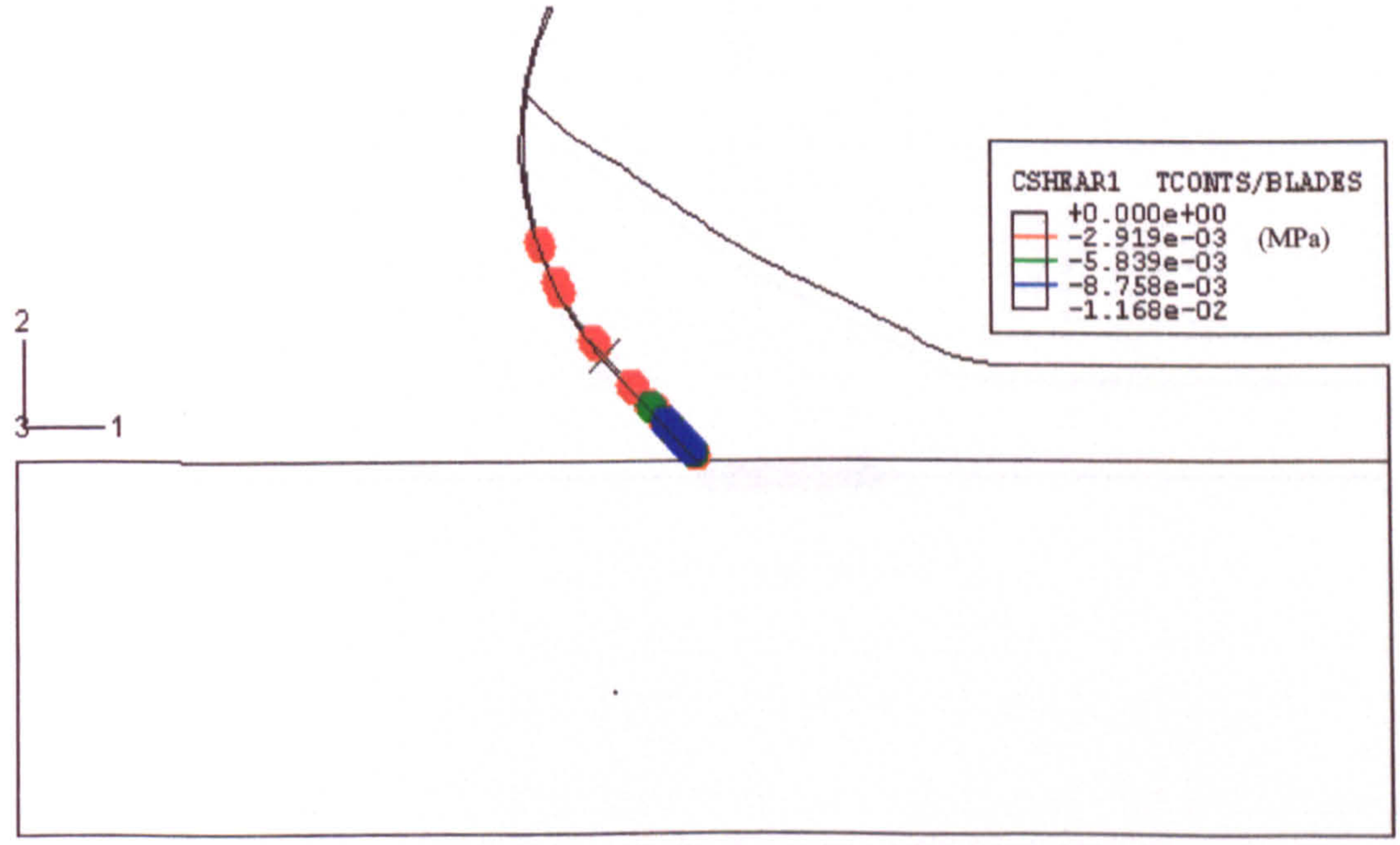

Figure (6.22) Frictional shear stress along blade surface for μ=0.2

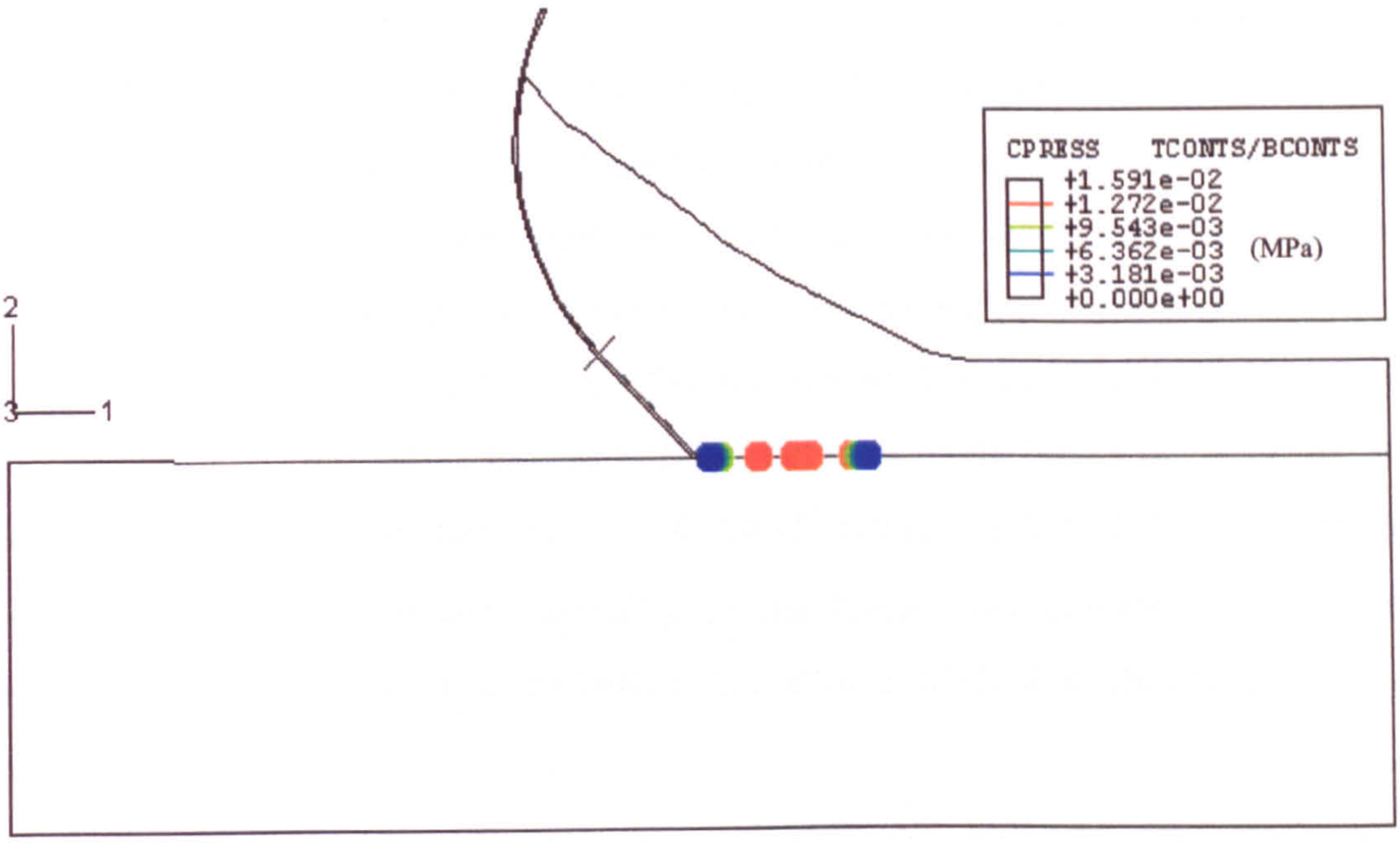

Figure (6.23) Contact pressure along failure surface for μ=0.05

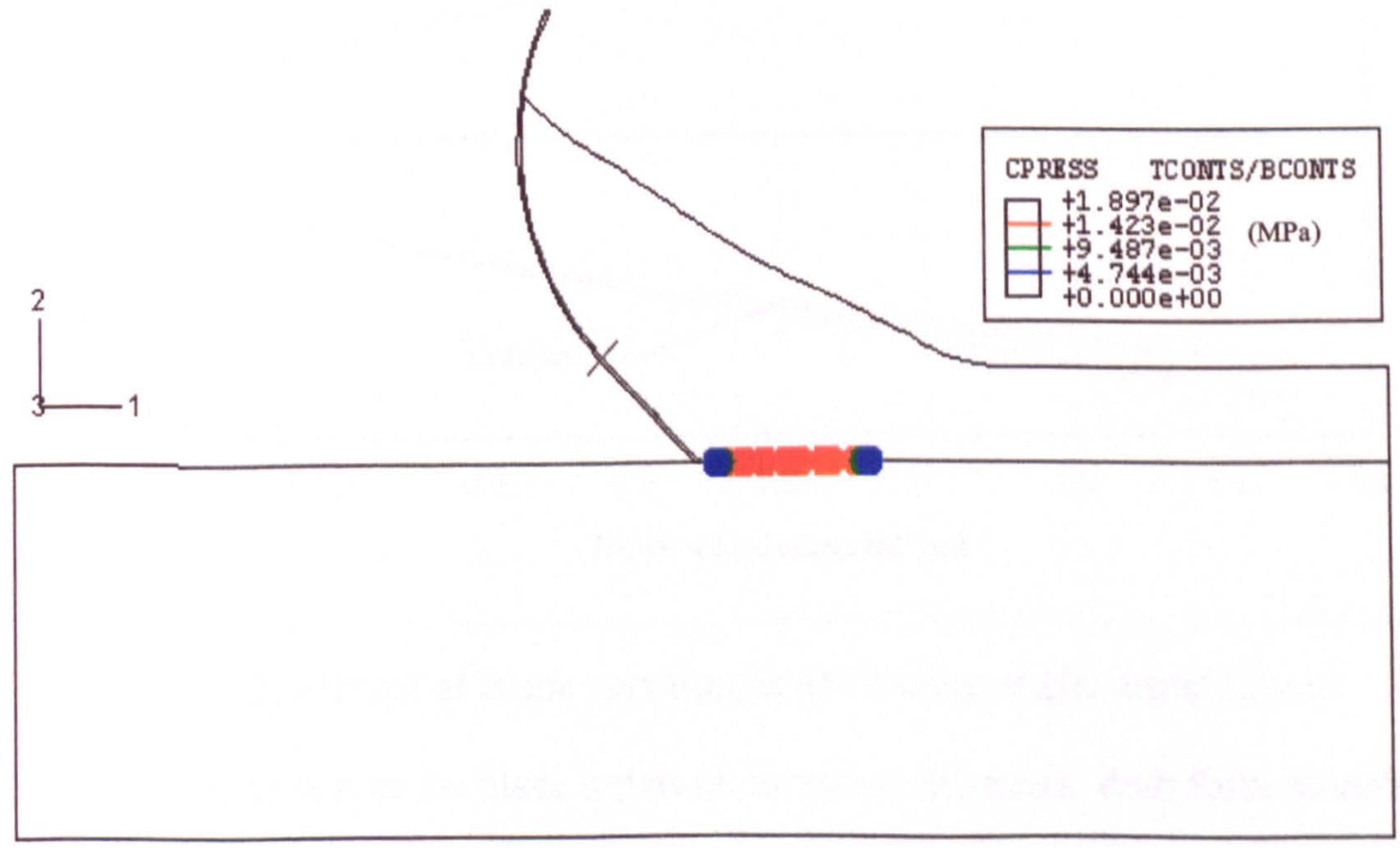

Figure (6.24) Contact pressure along failure surface for μ=0.2

Effect of blade radius of curvature

An experimental study previously carried out by AboElnor et al. (1998a) to study the effect of blade geometry on cutting forces concluded that the blade radius of curvature had a slight effect if compared with other factors, particularly in the case of sand soil. A finite element study was therefore undertaken here to verify this result. A series of finite element simulations of soil-tool interaction for blades of various curvature R=600, 800, 1000, 1200 mm and straight dozer as well was carried out. Figure (6.25) represents the relationship between blade radius of curvature and cutting forces at cutting angle of $\gamma = 45°$ and cutting depth d=250mm. From the figure it is clear that at the beginning of the blade displacement there was no significant effect of the blade curvature, but after a while a slight effect starts to establish.

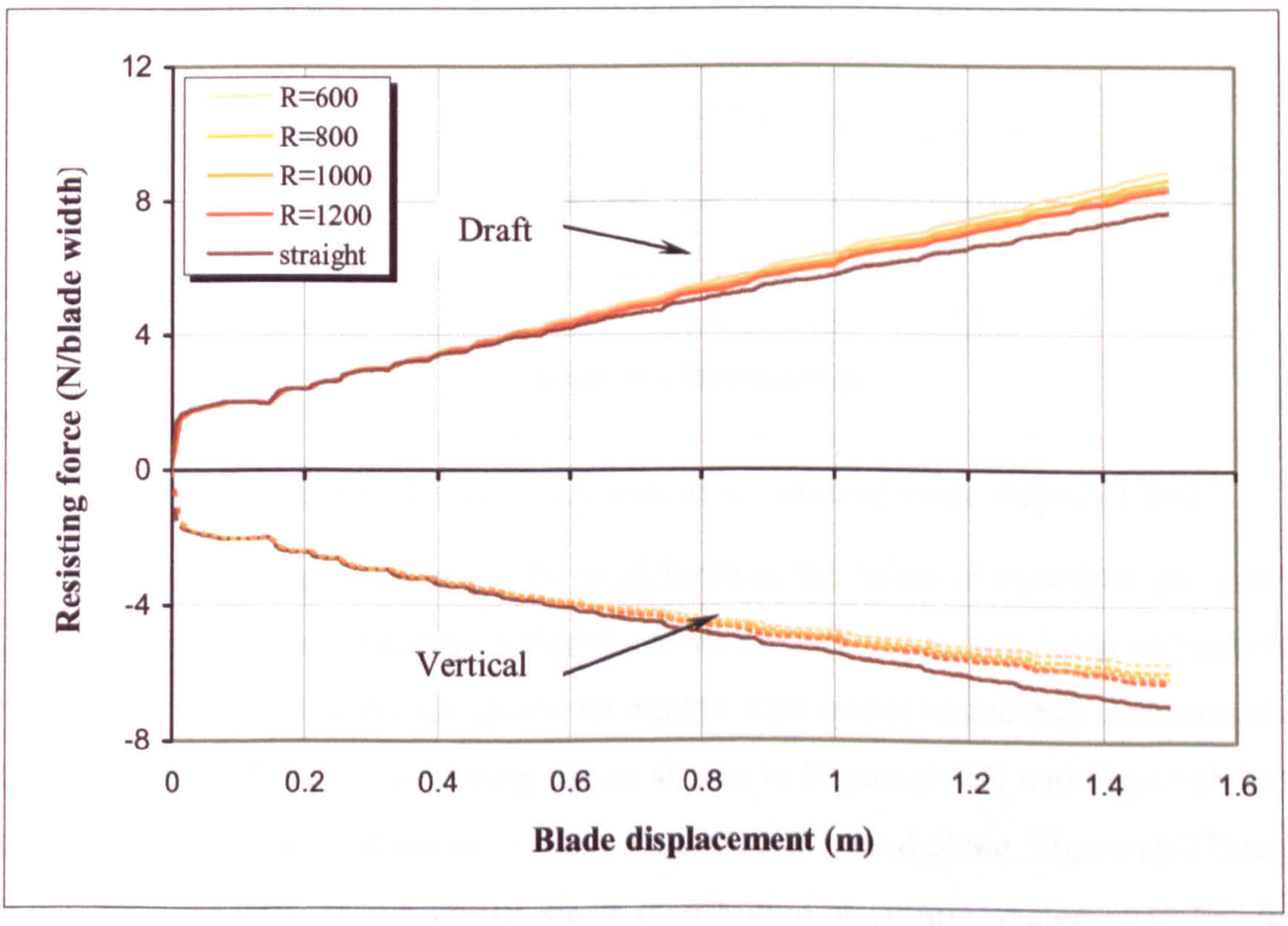

Figure (6.25) Effect of Blade curvature at 45° cutting angle, depth 250mm

The figure shows that as the blade radius of curvature decreases, draft force increases and vertical force decreases. It is shown also from the figure that the effect of the blade curvature was insignificant at the beginning of the blade displacement since the

interaction was acting along the blade flat part and then the effect of the blade curvature started to be accounted for as the blade displaced. The same conclusion can be drawn at different cutting angles as shown in Figure (6.26) which represents the relationship between blade radius of curvature and cutting forces at cutting angle of $\gamma = 60°$ and cutting depth d=250mm.

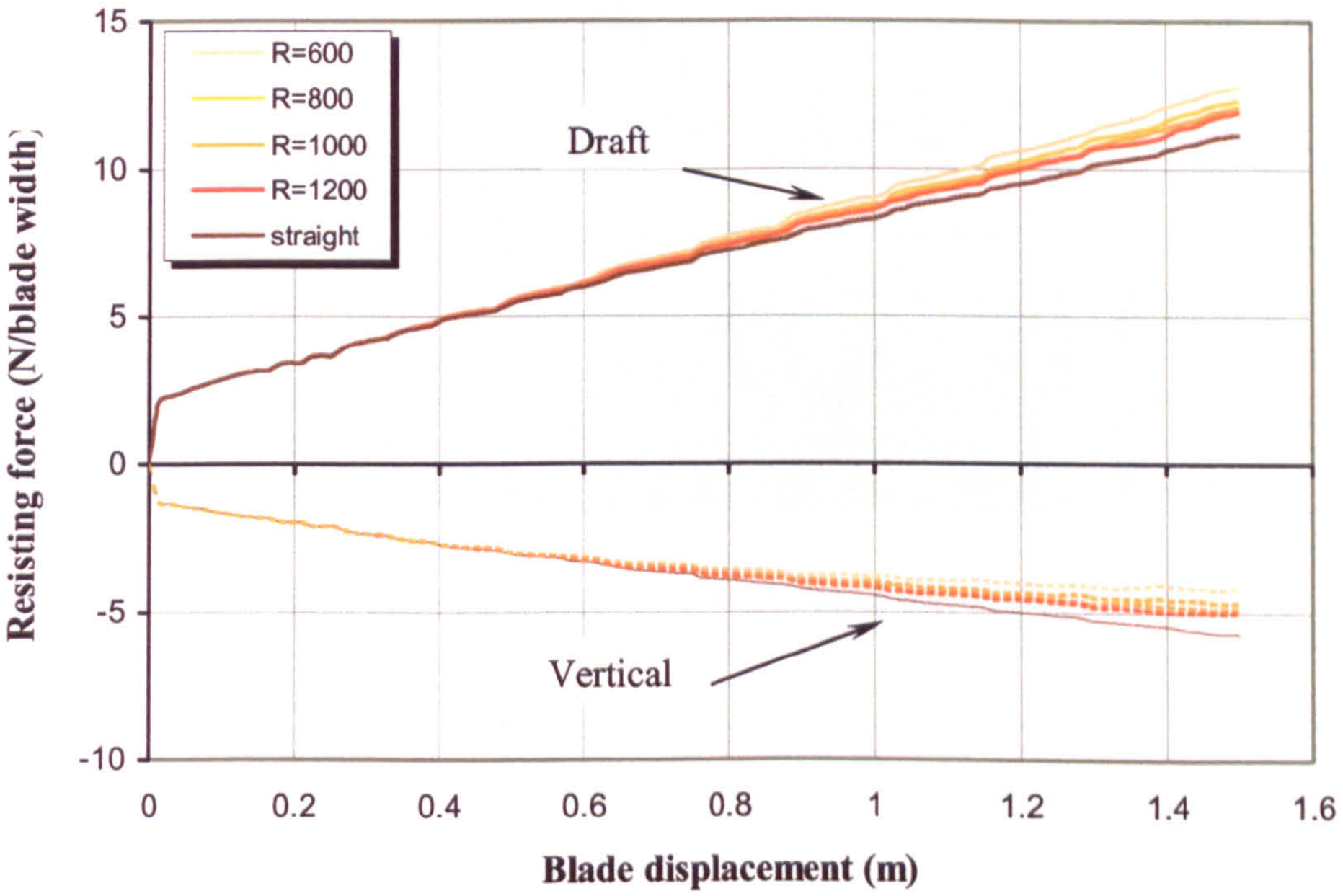

Figure (6.26) Effect of Blade curvature at 60° cutting angle, depth 250mm

The cause of the slight increase in the draft force as the radius of curvature decreases (i.e. as the curvature increases) is due to an increase of the accumulated soil pile in front of the cutting blade (not above the blade). This accumulated pile increases the normal stress in front of the cutting tip, as shown in Figure (6.27) and Figure (6.28), and hence increases the shear resistance along the horizontal plane. Figure (6.27) and Figure (6.28) represent the normal stress distribution at cutting angles, $\gamma = 45°$ for different blade curvature straight and curved (R=1200 mm) respectively.

The formation of the accumulated pile slightly away from the blade leads to a decrease in the vertical forces acting on the blade as the gravity effect of most of this pile acts away from the blade.

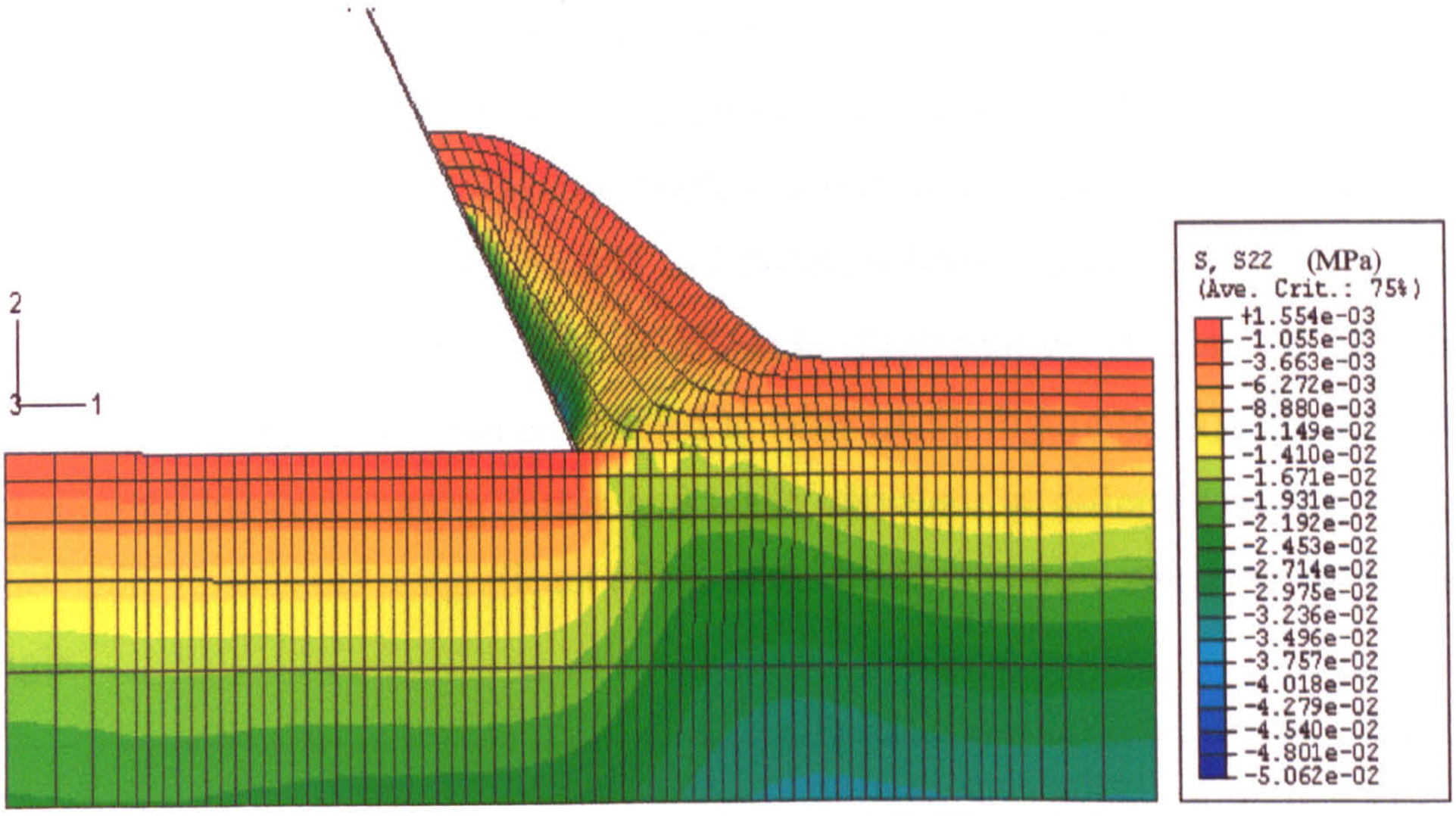

Figure (6.27) Normal stress due to an accumulated soil in front of flat bade

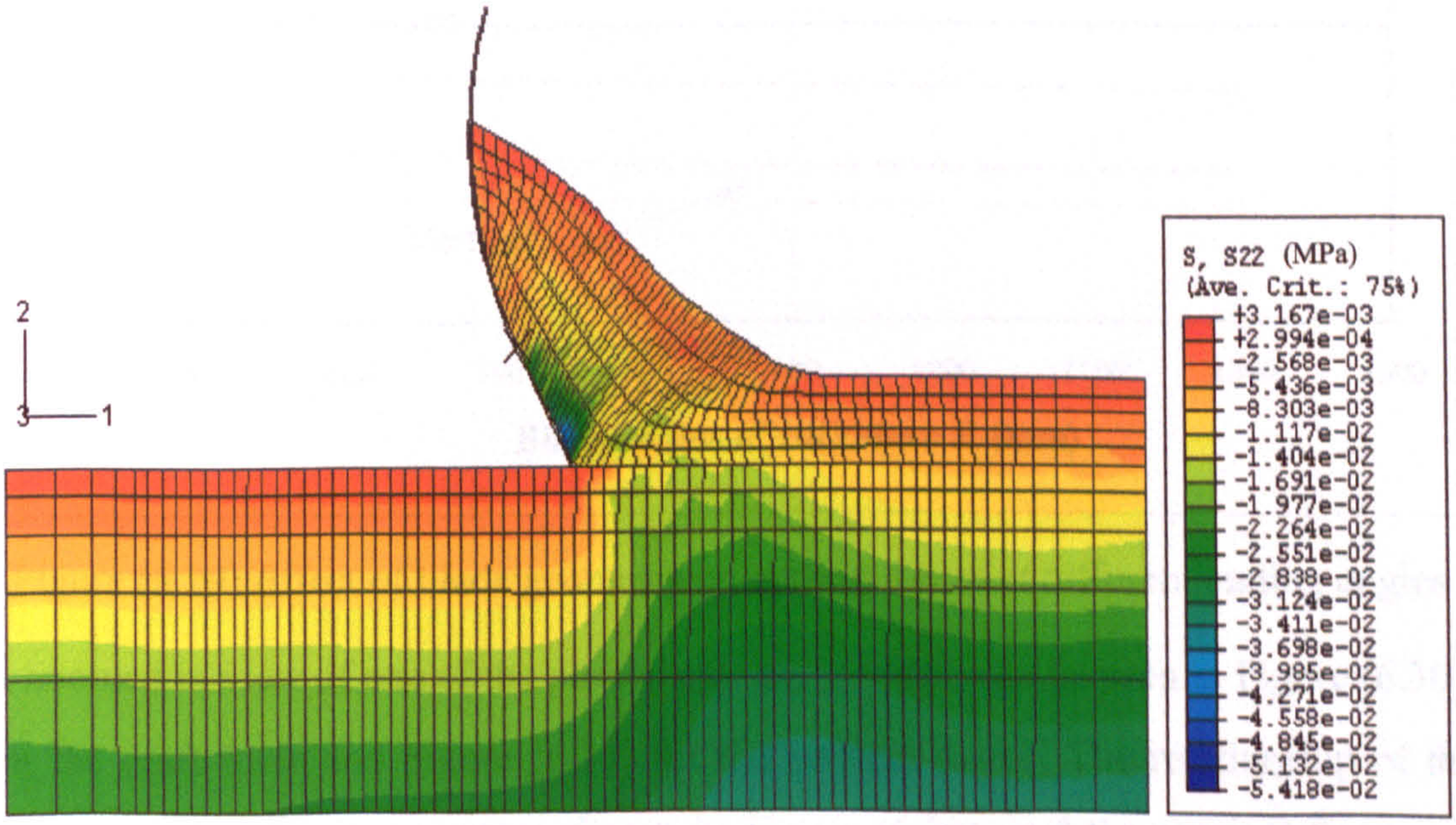

Figure (6.28) Normal stress due to an accumulated soil in front of curved blade

For further investigation of the effect of blade curvature on cutting forces at various different cutting angles, another series of finite element simulation was carried out. Parameters of these simulations are listed in table [A.5] where cutting depth (d=250mm), initial void ratio (e_0 =0.75), soil-metal friction coefficient (μ=0.05) and blade displacement (disp=1500mm). Draft and vertical forces are plotted at different cutting angles γ = 45°, 60° and 75° and different blade curvatures R = 600, 800, 1000 and 1200 mm after 1500 mm of blade displacement. A total of 12 finite element simulations were run as detailed in table [A.5]. Figure (6.29) represents the relationship between cutting forces and blade curvature at different cutting angles. The figure reveals the insignificant effect of the blade curvature whatever the cutting angle.

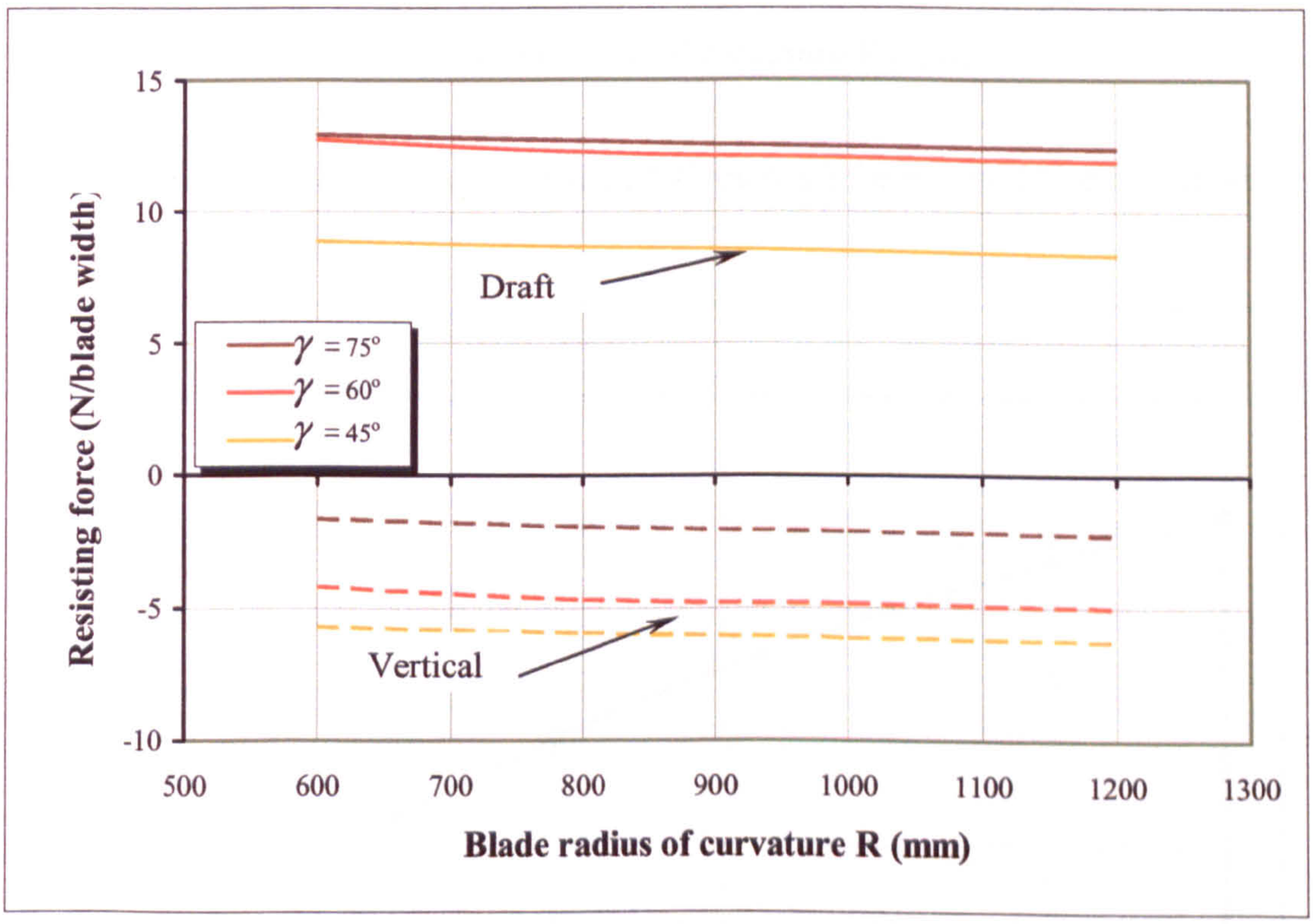

Figure (6.29) Effect of blade geometry on cutting forces at different cutting angles

A zoomed in view of one of the plotted curves, $\gamma = 45°$, can be seen in Figure (6.30), for the draft force and Figure (6.31) for the vertical force. The relationship of the draft force and blade curvature shown in Figure (6.30), and the vertical force and blade curvature shown in Figure (6.31) could be described by an exponential

function but indeed the difference between the curvature extremes in this simulation is nearly in the range of 6% of the draft force and 9% of the vertical force.

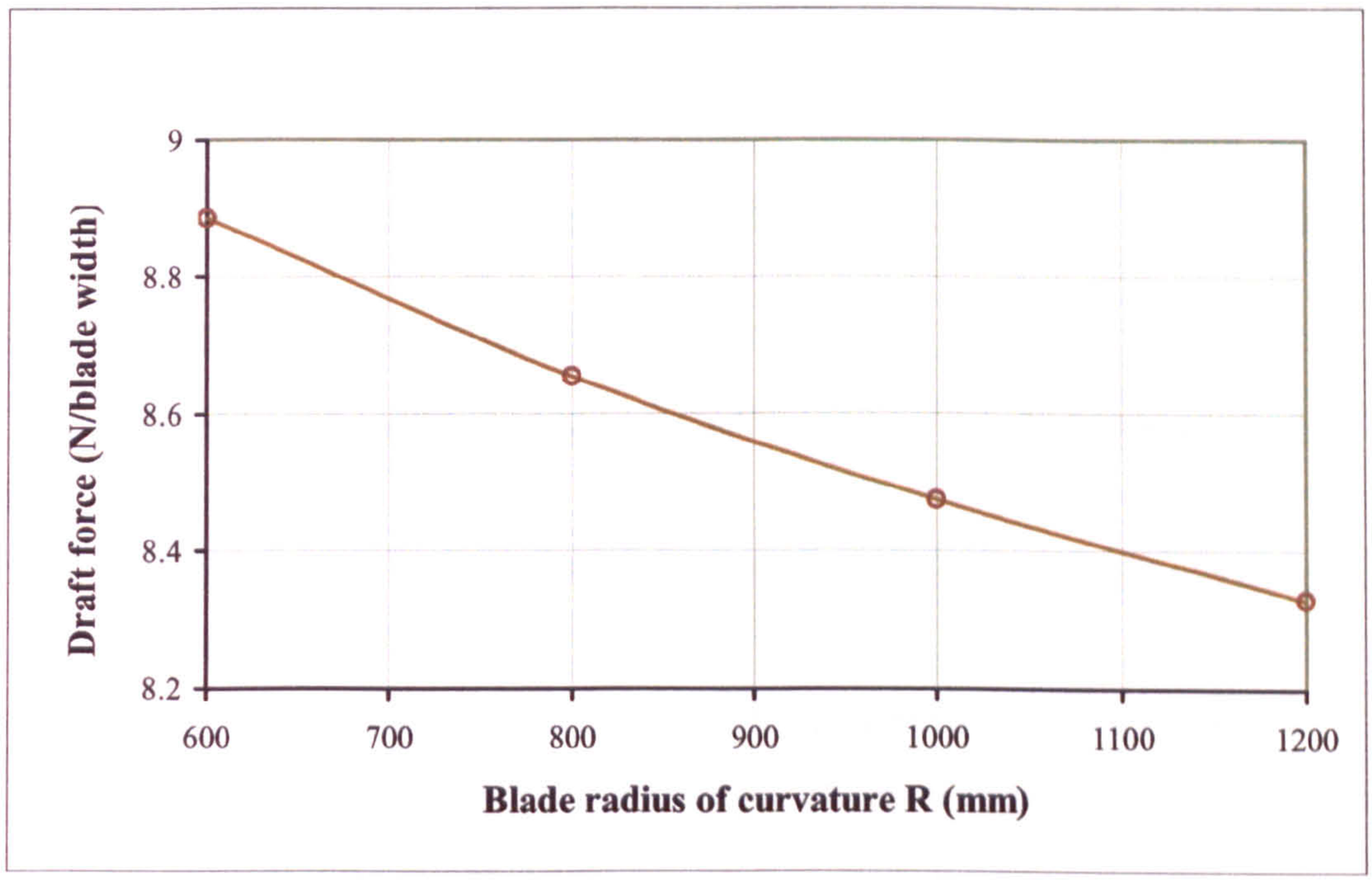

Figure (6.30) Effect of blade curvature "R" on draft force, $\gamma = 45°$, d = 250 mm

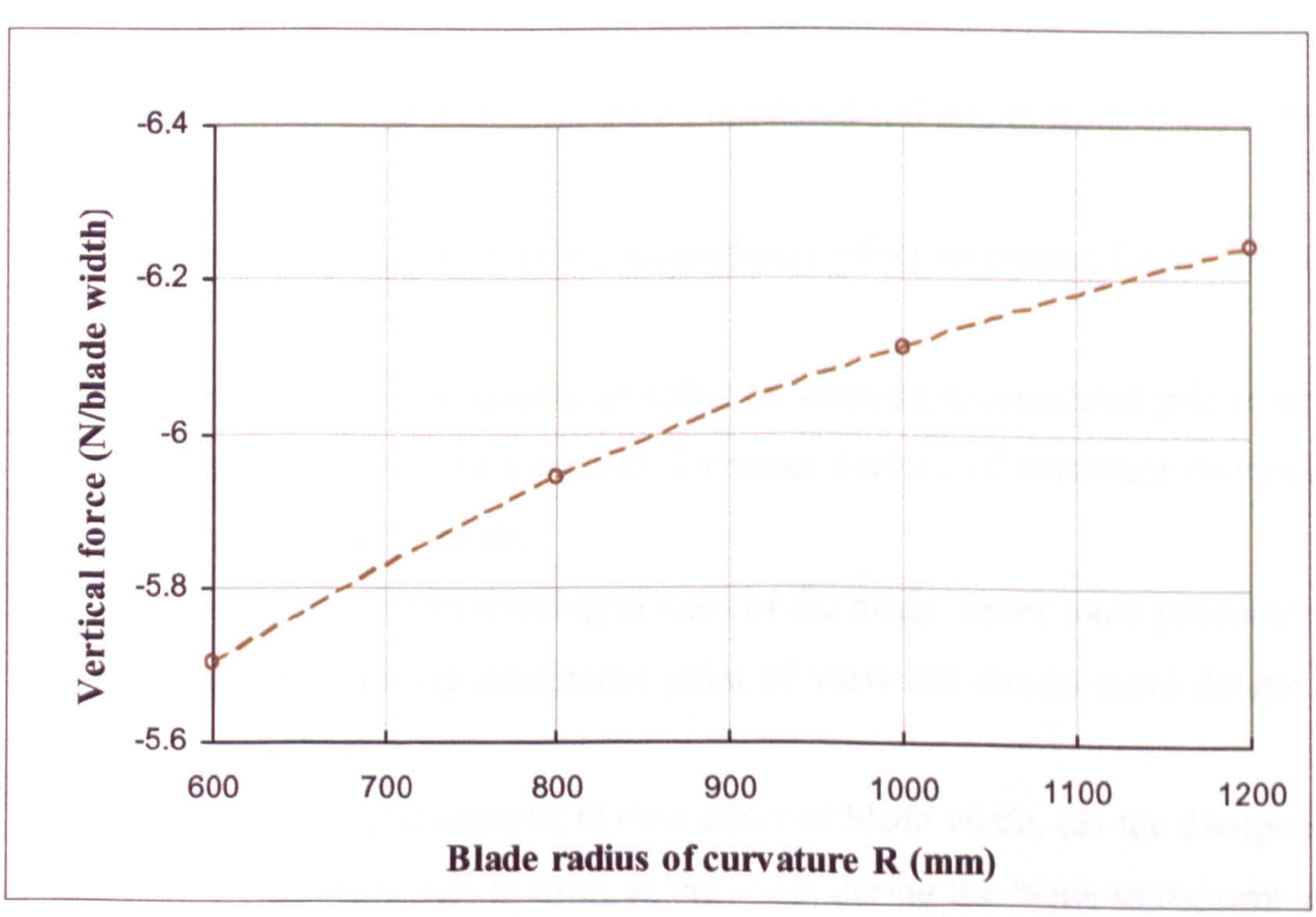

Figure (6.31) Effect of blade curvature "R" on vertical force, $\gamma = 45°$, d = 250 mm

Accumulated soil pile formation in front of the blade is an important issue from the point of view of the earth moving process as the main aim is to move as much as possible soil and hence the use of curved blades is required. But from the mine clearing point of view getting ride of the accumulated soil is an important issue to reduce the effect of this pile on the normal stresses and hence earth pressure underneath the ground which reduces the possibility of exploding of existing mines.

6.3.3 Conclusion of the 2D analysis

From the various 2D analyses carried out, some concluding remarks can be drawn as follows:

1. Soil state (dense or loose) has a significant effect on cutting forces in both draft and vertical force components.
2. As the cutting depth increases both draft and vertical forces increase
3. Blade surface roughness has a significant effect on cutting forces in both draft and vertical force components.
4. As the cutting angle increases, draft force increases and vertical force decreases and as the cutting angle decreases, draft force decreases and vertical force increases.
5. As the cutting angle increases, the accumulated soil pile in front of the cutting blade increases.
6. Blade curvature has a relatively insignificant effect on cutting forces for sand soil.
7. Blade curvature has a significant effect on forming accumulated pile in front of the blade that as the curvature increases (radius of curvature decreases) accumulated soil increases.
8. More accumulated soil forming in front of the blade means more productivity from an earth moving equipment point of view but means more danger of mines exploding.
9. Plane strain analysis ignores; (1) the effect of blade width, (2) the dissipation of the accumulated soil in front of the blade during the blade movement and (3) the effect of frictional shear of both vertical cutting wedge sides.

6.4 3D SOIL-TOOL INTERACTION

Although the 2D analysis gave some very valuable results, investigation of the effect of cutting speed, blade width, boundary proximity, the dissipation of the accumulated soil in front of the blade during the blade movement and the effect of frictional shear of both vertical cutting wedge sides was not possible under the 2D soil-tool interface analysis. Hence a 3D (three-dimensional) finite element analysis of the soil-tool interaction was carried out to investigate the effect of these factors. Additionally dynamic analyses were carried out to investigate the effect of cutting speed and acceleration. During the analysis some additional factors were shown to have a significant effect on the overall reliability of the 3D analysis such as mesh density and model dimensions as shown later in this section.

6.4.1 MODEL DESCRIPTION

The problem analyzed in this section is the three dimensional soil-tool interaction of the blade cutting process in a sand soil. The hypoplastic model, implemented in ABAQUS as a user defined material using the UMAT user subroutine, was used to describe sand behaviour. Table [6.1] represents the hypoplastic model parameters of the simulated sand soil with initial void ratio of $e_0 = 0.75$.

6.4.1.1 Spatial dimensions

The 3D model main dimensions are presented in Figure (6.32) and listed in table [6.2], where 'W1' is the lateral bound width, 'W2' is the blade cutting width,'L1' is the distance between the blade and the left boundary, 'L' is the soil bin length, 'h' is the soil bin high, 'd' is the cutting depth and 'γ' is the cutting angle. W1 and W2 were varied to study the effect of blade width and lateral bound width of the simulated sample respectively as shown later, the remaining dimensions were held constant. A total of 30 separate finite element models were run.

Most of the analyses were carried out through 50 mm of blade displacement in the horizontal plane along the X axis direction shown in Figure (6.32). A blade

displacement of 50 mm was chosen as a compromise to cut down solution times, which for a typical 3D model were about 50 hours to account for 200 mm of blade displacement using a dual Xenon 1 GHz processor PC with 500 MB of memory. To verify the behaviour of the cut soil in front of the cutting blade, one analysis was run for a blade displacement of 200 mm and took about 50 hrs to complete.

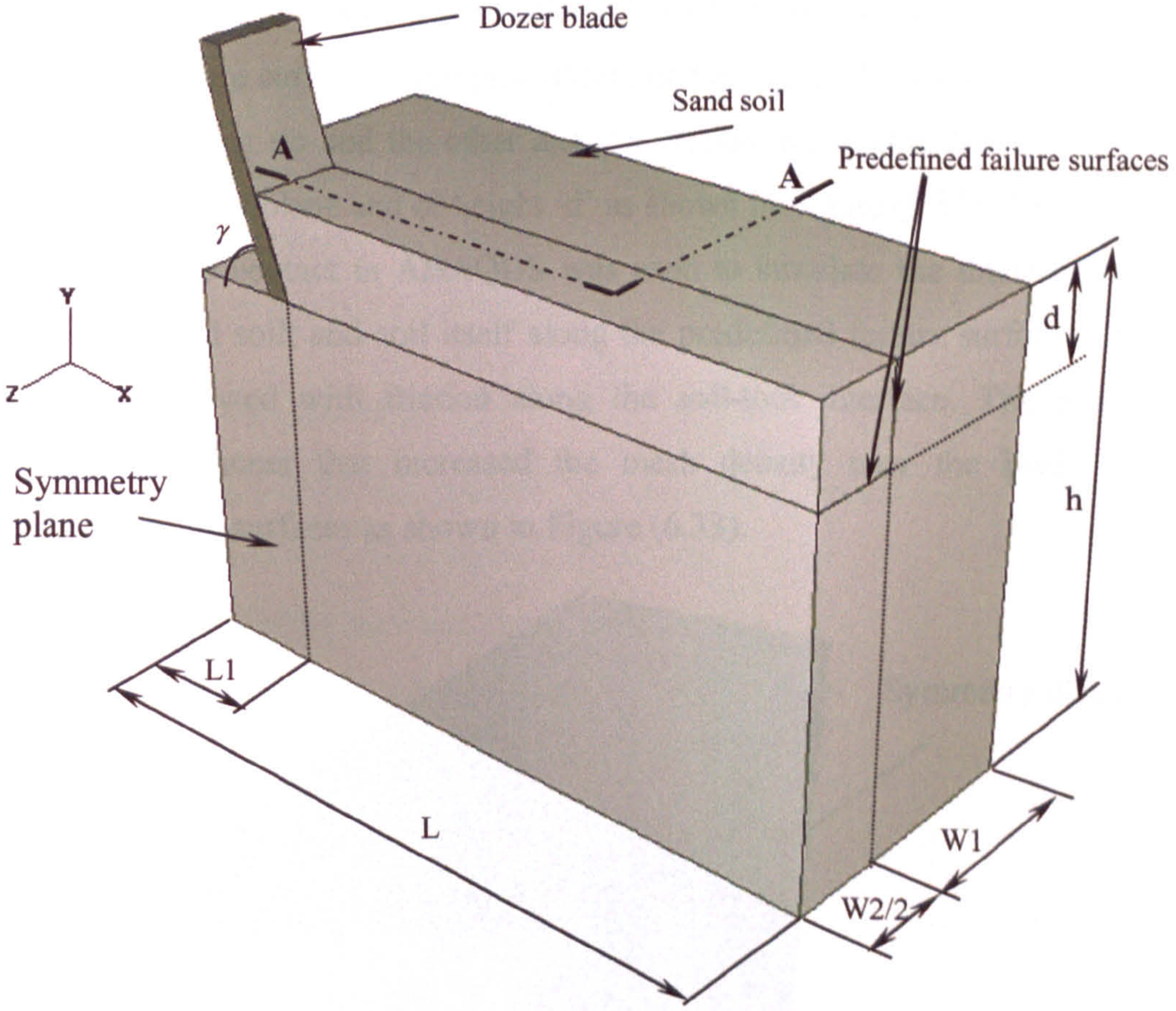

Figure (6.32) Soil-Tool interface model dimensions

Table [6.2] Main dimensions of the 3D soil-tool interaction model

L1 (mm)	L (mm)	h (mm)	d (mm)	W1 (mm)	W2 (mm)	γ (°)
200	900	700	200	200 ~ 600	300 ~ 700	75

6.4.1.2 Finite element mesh and boundary conditions

A Three dimensional 8-node linear brick continuum element (C3D8) was selected, as described in section (5.3.5), to represent both sand and blade in the finite

element model. 1082 elements were used to simulate the sand, this number is varied depending on blade width and mesh density, and 288 elements were used to simulate the blade which is defined as a rigid body with a reference node. Simulating the blade using the *RIGID BODY feature in ABAQUS enables the calculation of the resultant reaction forces acting on the entire blade at a single node which is called "the reference node for the rigid body". Due to the symmetric geometry of the model, one half of the model was simulated but all the results consider the complete model. Two failure surfaces were predefined, one along the horizontal plane in front of the blade-cutting tip and the other along a vertical plane at a distance of 'W2/2' from the symmetric plane and of height 'd' as shown in Figure (6.32). The concept of master and slave contact in ABAQUS was used to simulate the interface between cutting blade and soil; and soil itself along the predefined failure surfaces. Relative motion was allowed with friction along the soil-tool interface. The model was meshed in a manner that increased the mesh density near the blade and the predefined failure surfaces as shown in Figure (6.33).

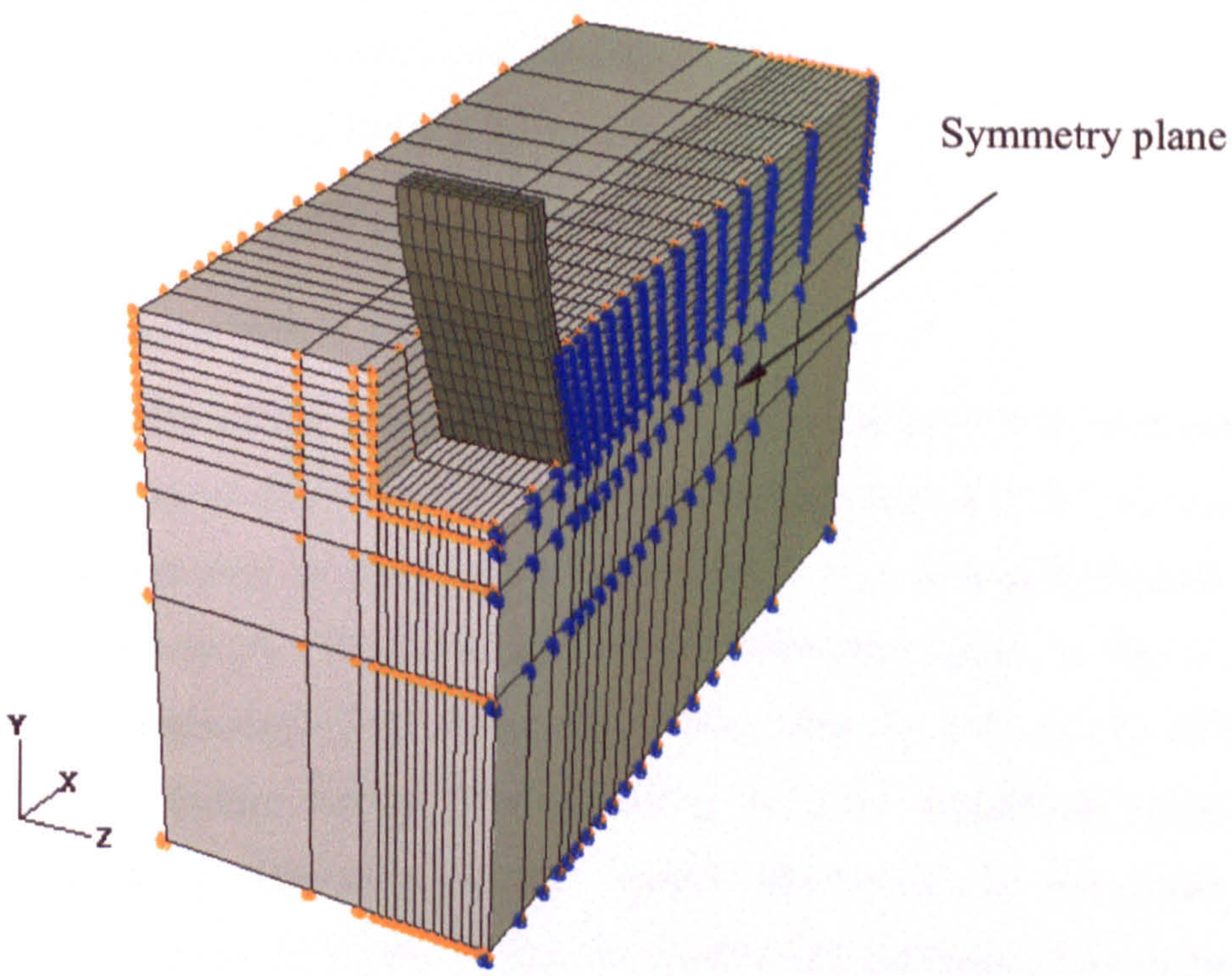

Figure (6.33) Finite element mesh and boundary conditions

Boundary conditions of the model are also shown in Figure (6.33) and can be listed as follows:

1. Bottom base nodes, at Y=0, are constrained in the vertical direction, Y axis.
2. Nodes on vertical boundaries parallel to the Y-Z plane, at X=0 and X=L, are constrained in the horizontal direction along X axis.
3. Nodes on vertical boundaries parallel to the X-Y plane, at Z=0 and Z=(W2/2)+W1 (Symmetry plane), are constrained in the lateral direction along Z axis.
4. The blade is constrained in the vertical direction and any rotation but it is free to displace in the horizontal direction.

To establish a physical contact between the blade and the soil and along the predefined failure surfaces, the gravity effect was taken into account by applying the gravity acceleration as a body load to simulate the sand weight for a single step.

6.4.2 MODEL VALIDATION

The validation of the present 3D soil-tool interface model was verified through investigation of various aspects as follows:

- Predefined failure surfaces validation
- Sand failure and shear band formation
- Sand swelling up and accumulation

6.4.2.1 Predefined failure surfaces validity

The validity of the assumed predefined failure surfaces was examined first. The Von Mises stress distribution at zero blade displacement and the vertical (X-Y) shear stress distribution at 50mm blade displacement were plotted in Figures (6.34) and (6.35) respectively. The continuity of the contours plotted in Figure (6.34) reveals the homogeneity of the stress distribution after the soil gravity effect was applied and just before cutting. During cutting the most significant variable that could judge the performance of the contact mechanism is the shear stress distribution. As shown in Figure (6.35), the continuous contours of the shear stress distribution along the predefined failure surfaces reveals the validity of predefined failure surfaces assumption under the condition that the gravity effect has to be considered.

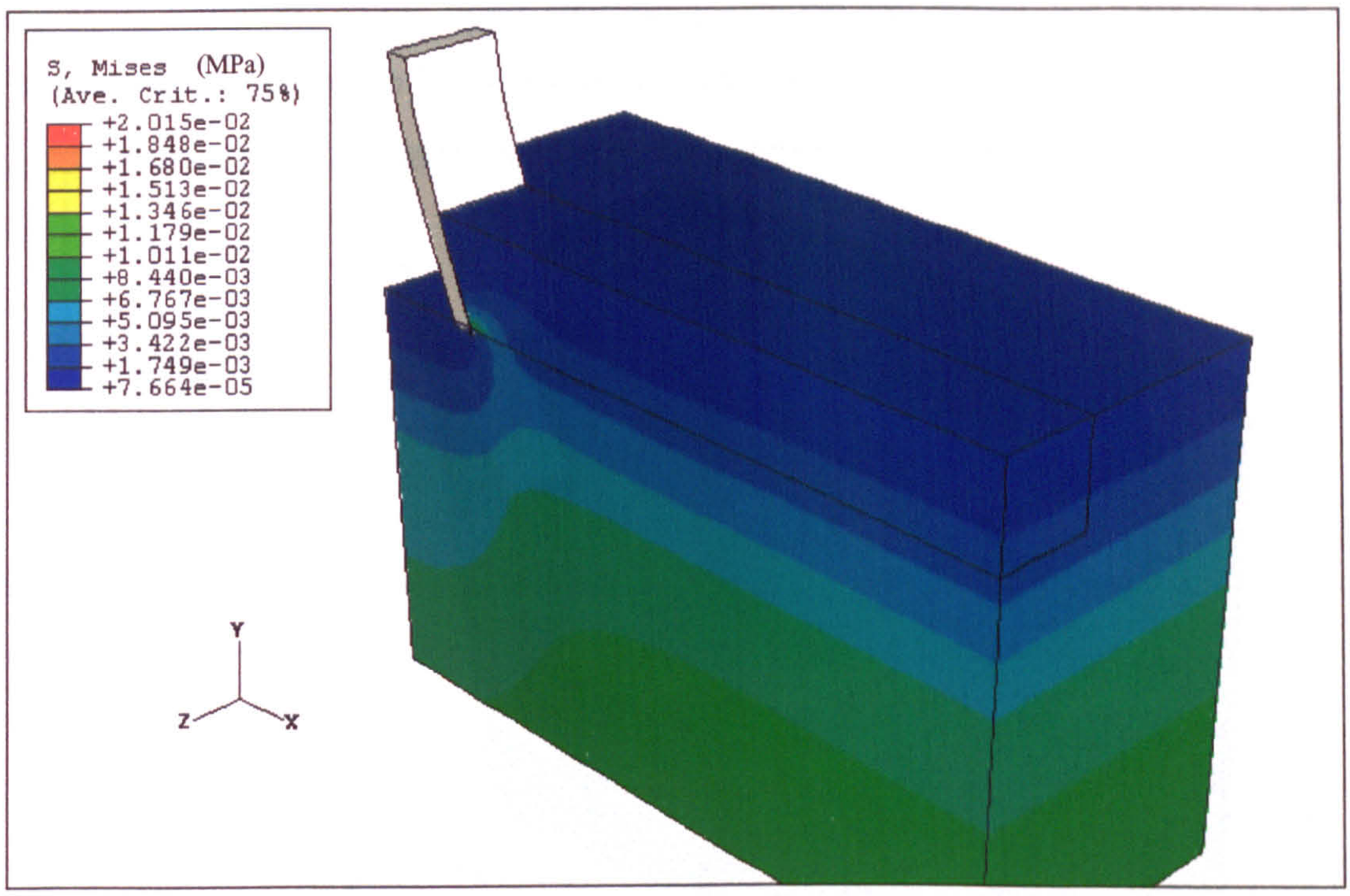

Figure (6.34) Von Mises stress distribution at zero blade displacement

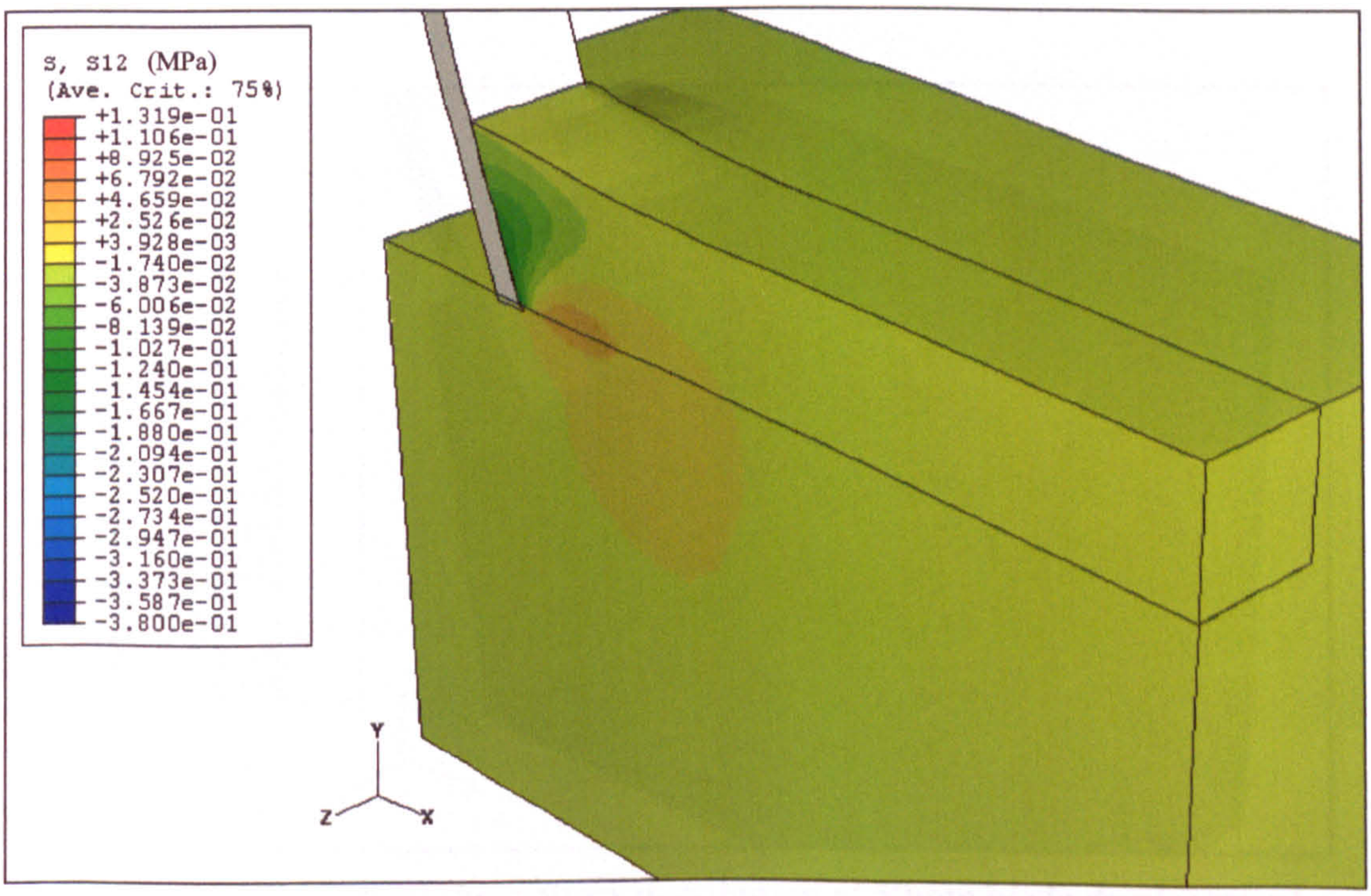

Figure (6.35) Vertical shear stress distribution at 50mm blade displacement

The same continuity of the stress contours inside the soil model, for Section A-A in Figure (6.32), is shown in Figure (6.36) and (6.37).

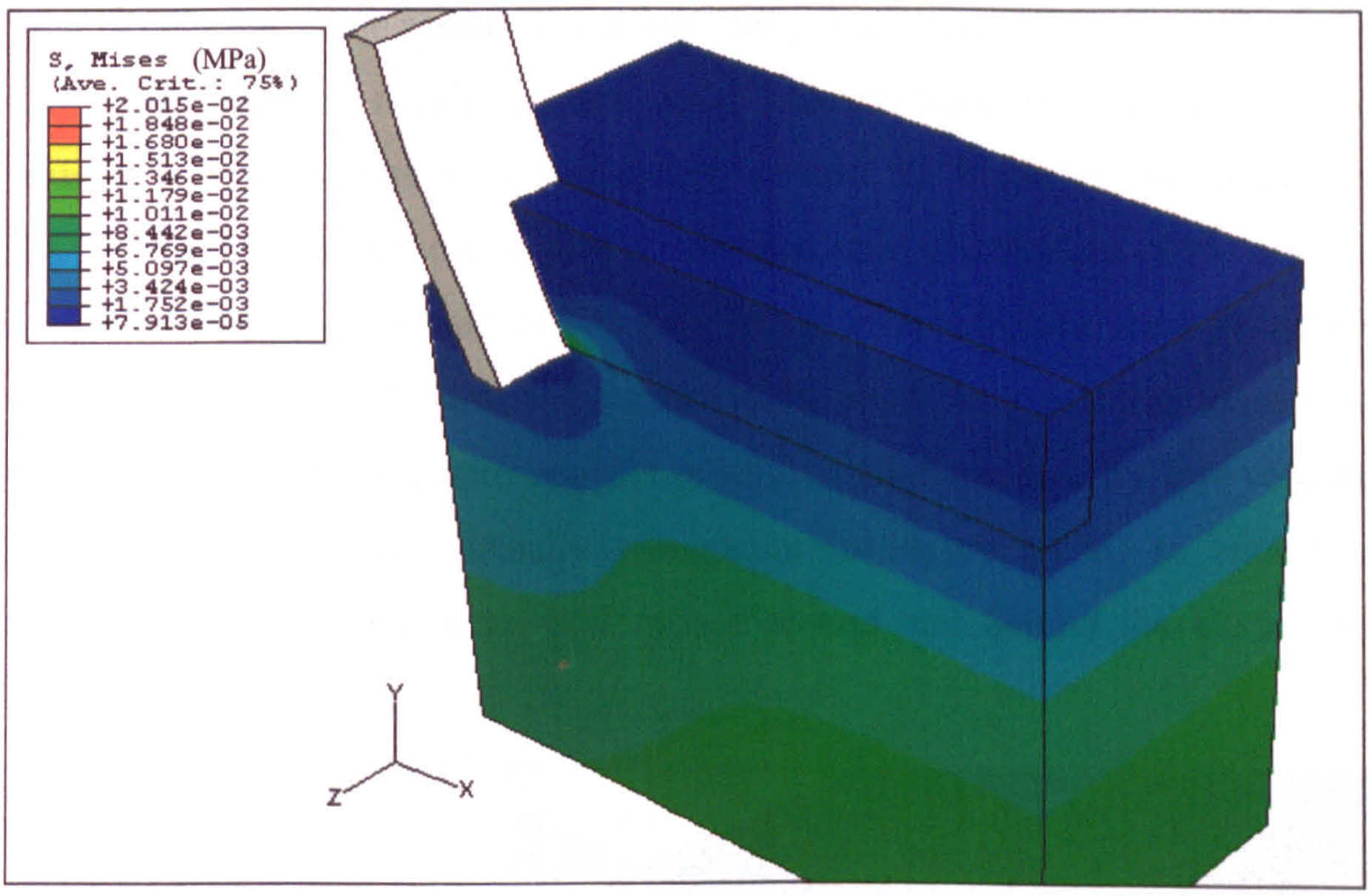

Figure (6.36)Von Mises stress distribution at zero blade displacement for Section A-A

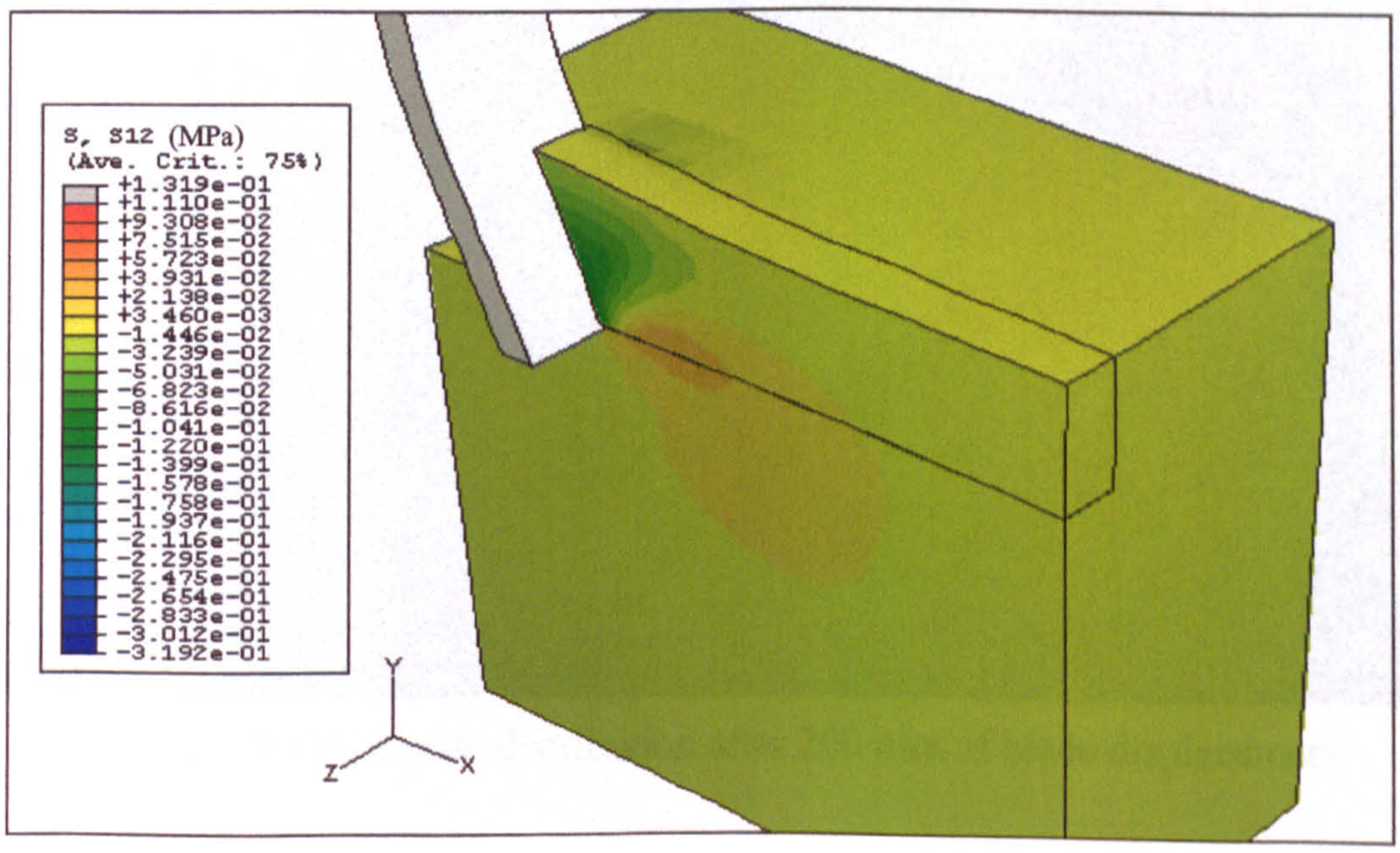

Figure (6.37) Vertical shear stress distribution at 50mm blade displacement for Section A-A

6.4.2.2 Sand failure and shear band formation

The formation of a shear band during cutting was observed in the 2D finite element simulation of the soil-tool interface analysis discussed in section (5.4.3.4). In the 3D finite element simulation this band, characterized by high void ratio, is obvious as a conical zone or a hemisphere around the blade as shown in Figure (6.38). Figure (6.38) represents a plot of the void ratio distribution of the simulated sand after a blade displacement of 200 mm. As mentioned before, the void ratio is a parameter that indicates the soil compaction state (dense or loose) that loose sand is characterized by high void ratio and dense sand is characterized by low void ratio. The blade was set to be virtually transparent in Figure (6.38) to enable ease identification of the shear zone. Soil failure around and behind the blade can be easily seen from the figure.

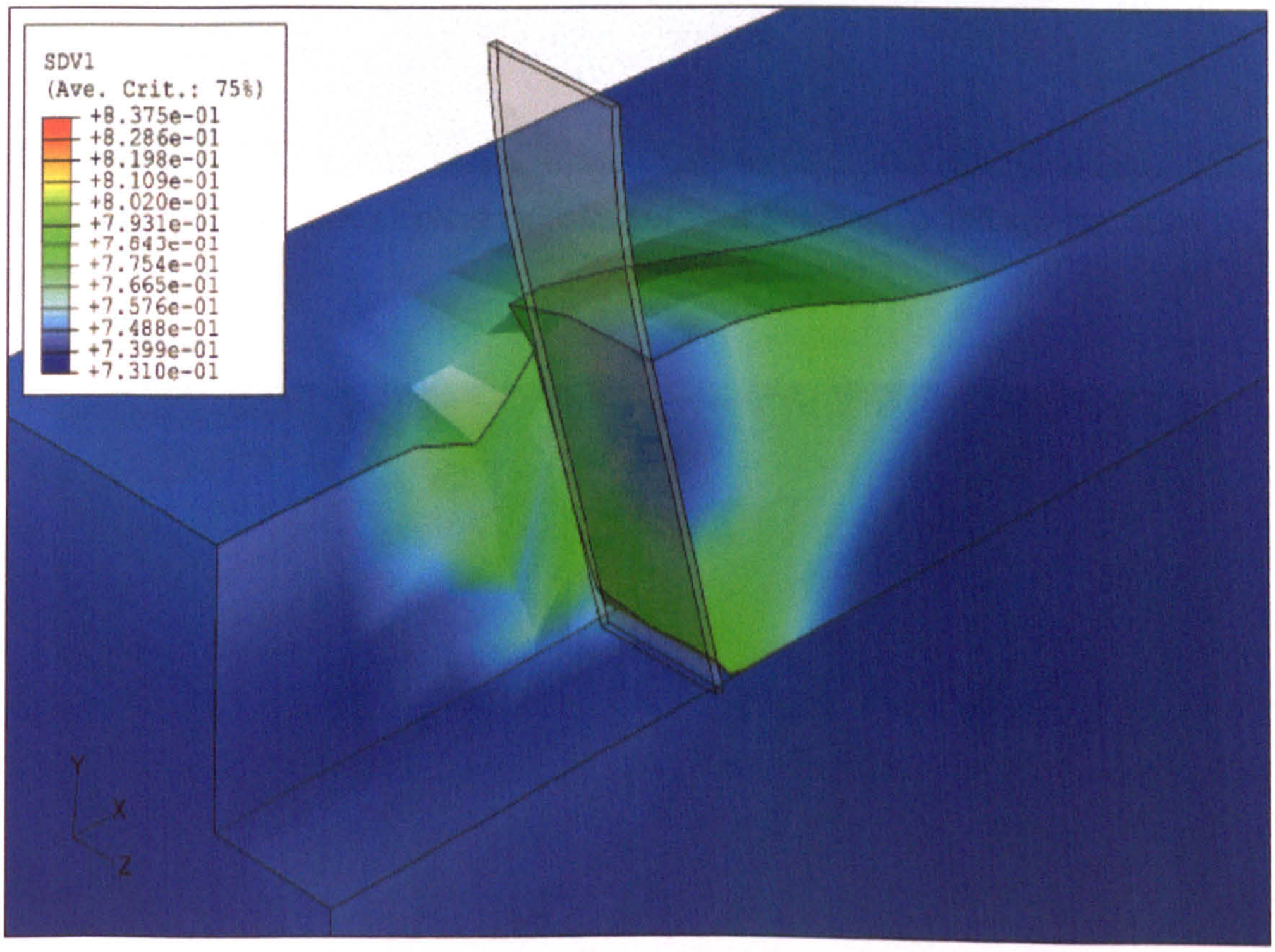

Figure (6.38) Void ratio distribution after 200 mm of blade displacement

6.4.2.3 Sand swelling up and accumulation

Sand swelling up and accumulation in front of the blade during cutting was observed experimentally by AboElnor (1997). The swelling up and accumulation behaviour of the sand obtained from the present finite element model is found to match well the behaviour previously obtained experimentally using an indoor soil bin as shown in Figure (6.39) and Figure (6.40) respectively.

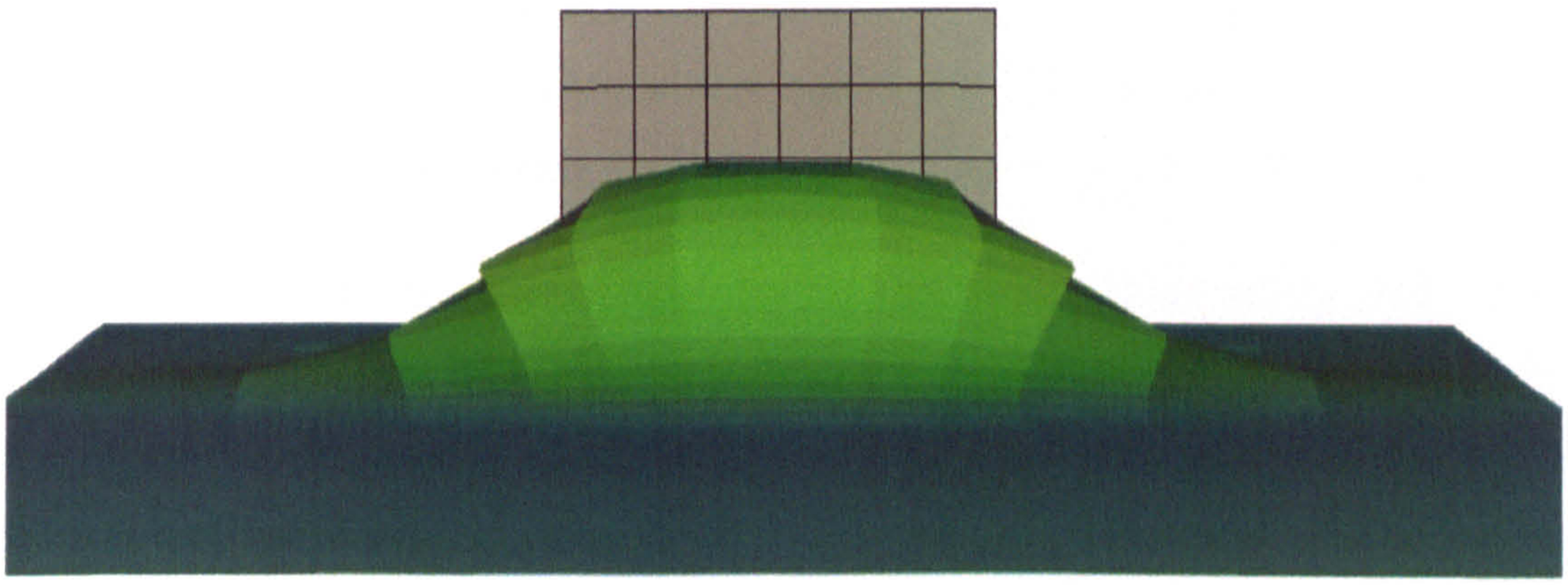

Figure (6.39) Finite element modeling of sand swelling up and accumulation

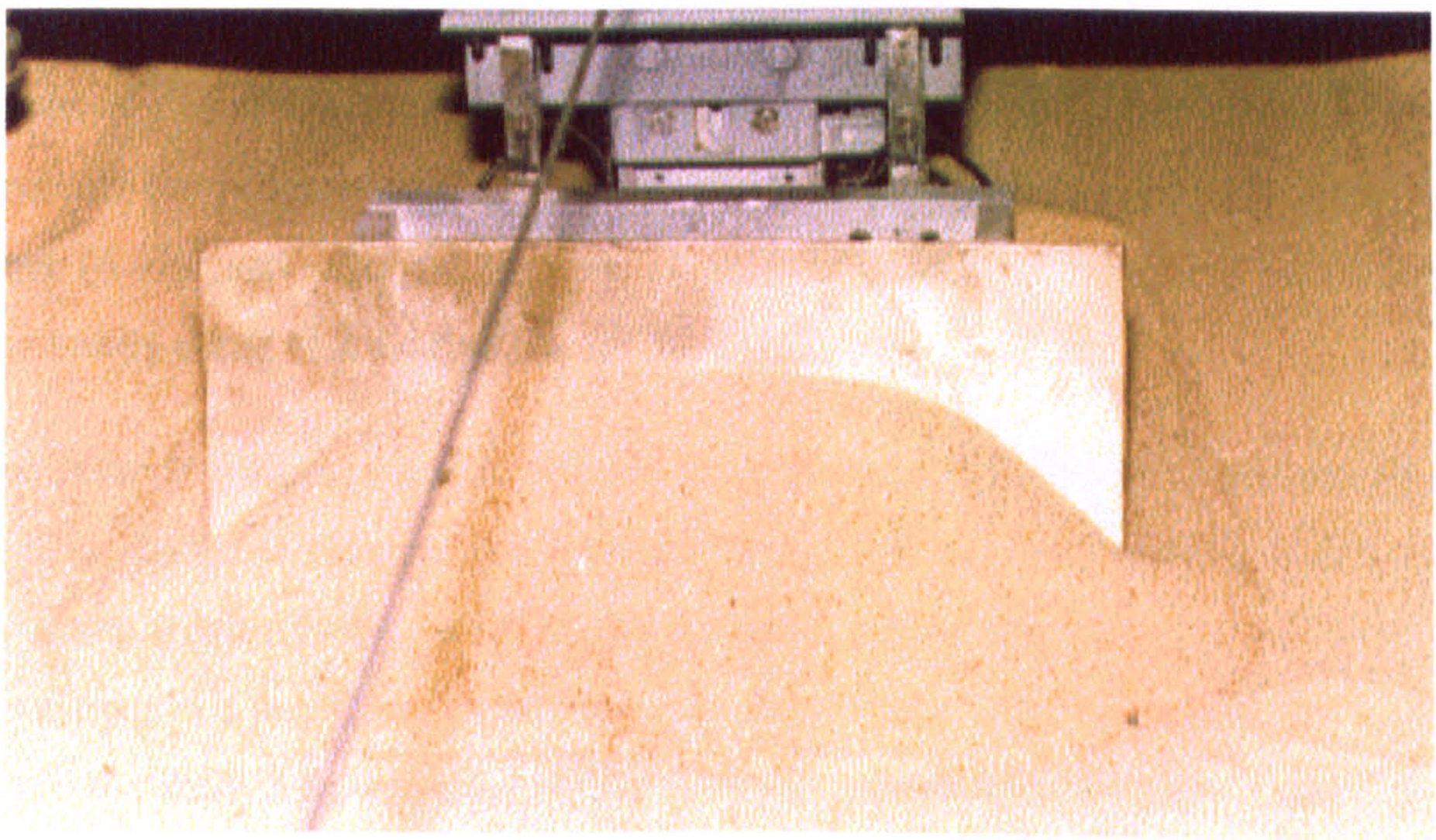

Figure (6.40) Experimental presentation of sand swelling up and accumulation, AboElnor (1997)

6.4.3 ANALYSIS AND DISCUSSION

The validation study of the present finite element model reveals the model capability of simulating soil-tool interaction and hence some further analyses were carried out as follows.

6.4.3.1 Effect of mesh density

The effect of mesh density on the reliability of the 3D finite element simulation of soil-tool interaction was investigated by Shen and Kushwaha (1998). Mesh density was found to have a very significant effect on the predicted results when using elastoplastic models to simulate sand in a soil-tool interface problem.

In the present study the effect of mesh density was found to have a very slight effect on the predicted results of a 2D soil-tool interaction as shown in section (6.4.1). To investigate the effect of the mesh density on the predicted finite element results of a 3D soil-tool interaction, a series of 3D finite element models was carried out for different various mesh densities and for 50 mm of blade displacement. The mesh density distribution of each model is listed in table [A.6] in Appendix (A). Predicted cutting forces acting on the blade in both draft and vertical directions were monitored during each finite element analysis and presented in Figure (6.41) and Figure (6.42) respectively through 50mm of horizontal blade displacement. Figure (6.41) represents the progress in draft cutting forces as the blade moves horizontally and Figure (6.42) represents the progress in vertical cutting forces as the blade moves horizontally using various mesh densities.

From these two figures it is noticeable that the mesh density has a very significant effect on the finite element predicted forces in both draft and vertical directions in that as the mesh density increases the predicted forces decreases. For example, the reduction of the predicted forces can be in the order of 200% with slight increase in the mesh density. To obtain a highly accurate quantitative analysis, a very dense mesh should be considered with expected 10 day run time using a dual Xenon 1 GHz processor PC with 500 MB of memory. Hence a more qualitative analysis was

considered in this study using medium mesh density (1082 elements) in order to obtain a compromise between solution time and accuracy.

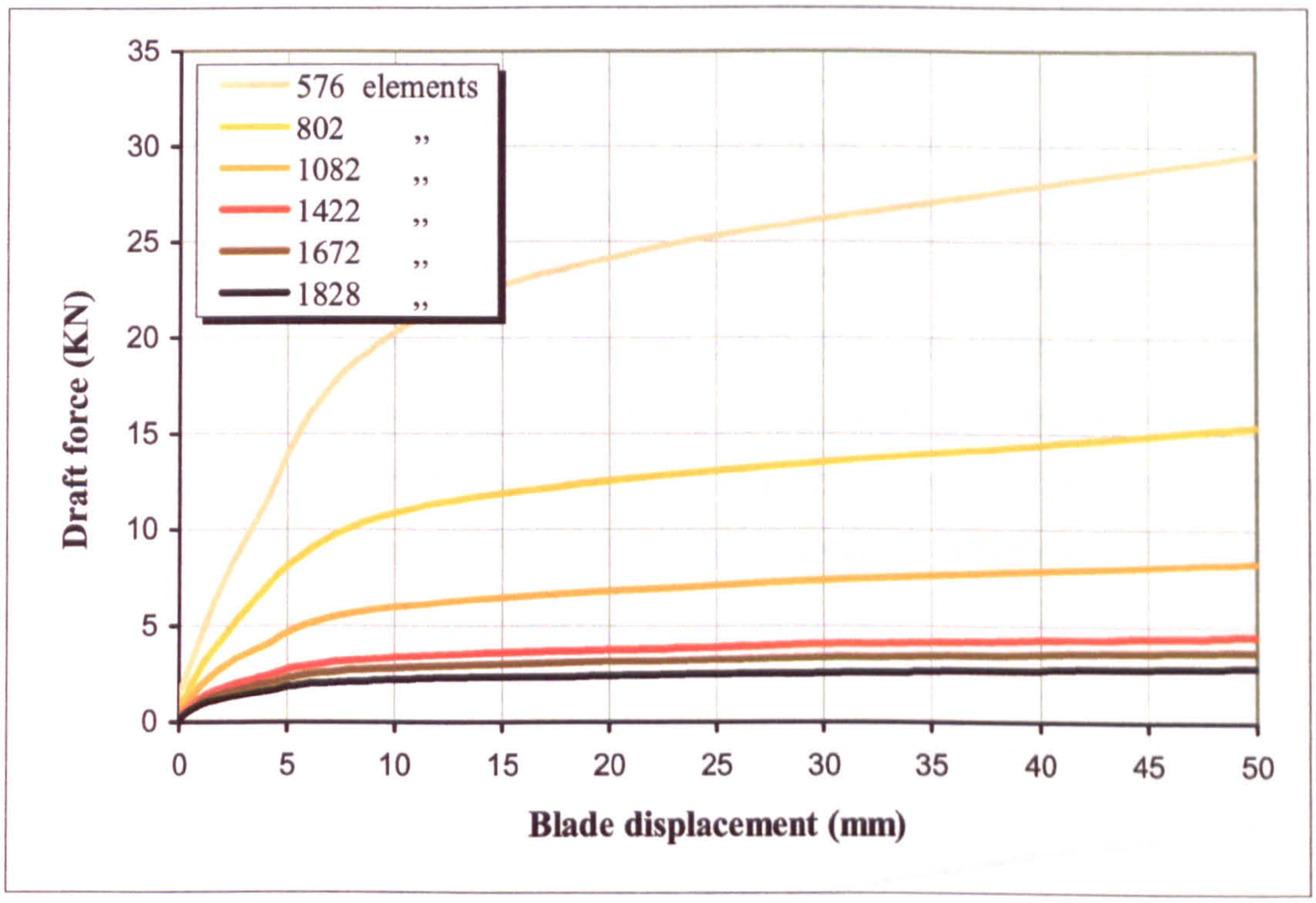

Figure (6.41) Effect of mesh density on predicted Draft forces

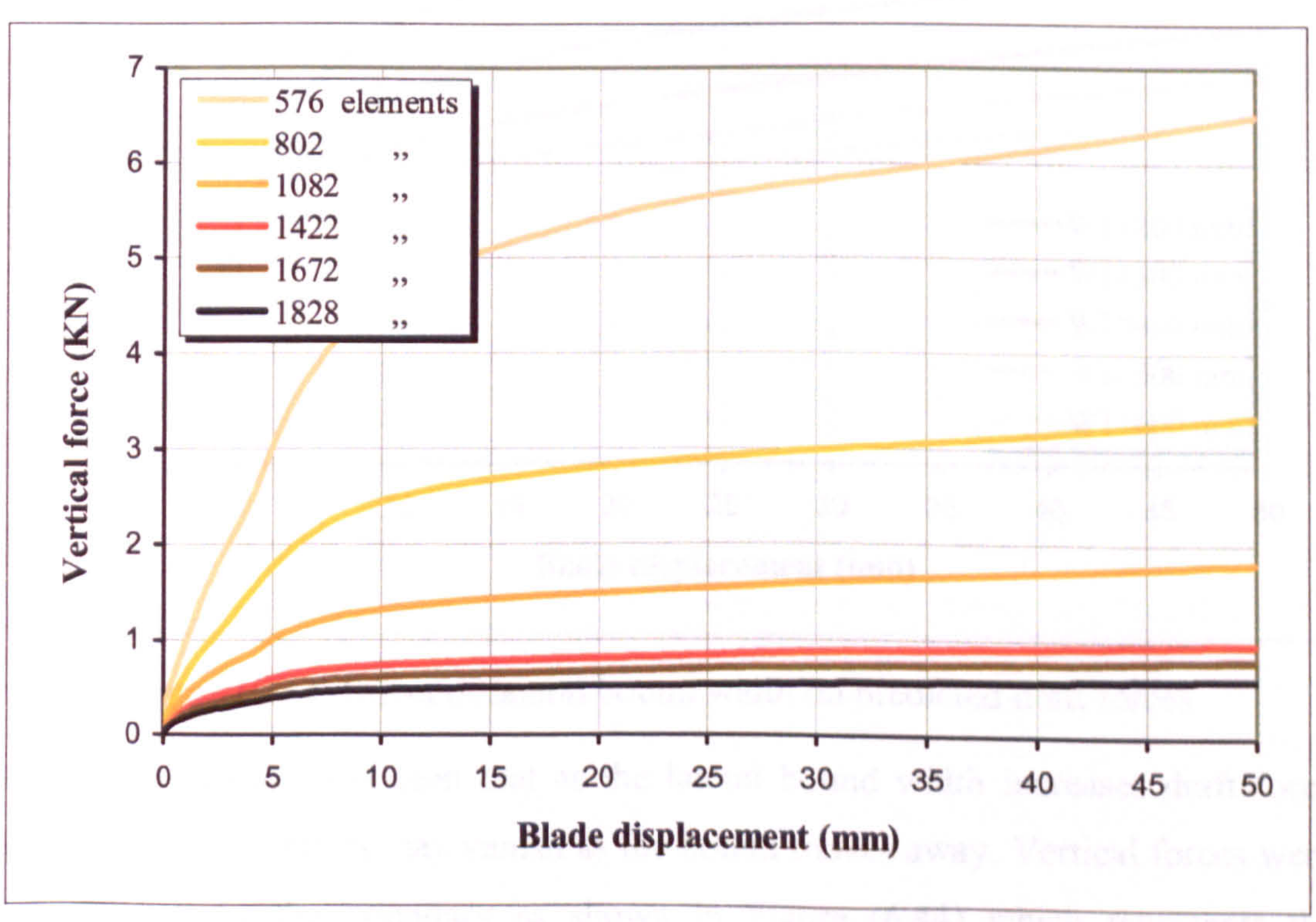

Figure (6.42) Effect of mesh density on predicted vertical forces

6.4.3.2 Effect of model boundary

One of the main critical factors that should be considered for a 3D model of soil-tool interaction is the effect of the boundary. The lateral bound width (parallel to the symmetric plane and of distance W1 from the vertical cutting edge) was considered in this study. To investigate the effect of the lateral bound width (W1) on blade cutting forces a series of finite element models were carried out for different lateral bound widths, W1=200, 300, 400, 500 and 600 mm. Model dimensions according to Figure (6.32) for the boundary effect study are listed in table [A.8] in Appendix (A). Predicted cutting forces acting on the blade in both draft and vertical directions were monitored during each finite element analysis through a 50 mm of horizontal blade displacement. Figure (6.43) represents the progress in draft cutting forces as the blade moves horizontally.

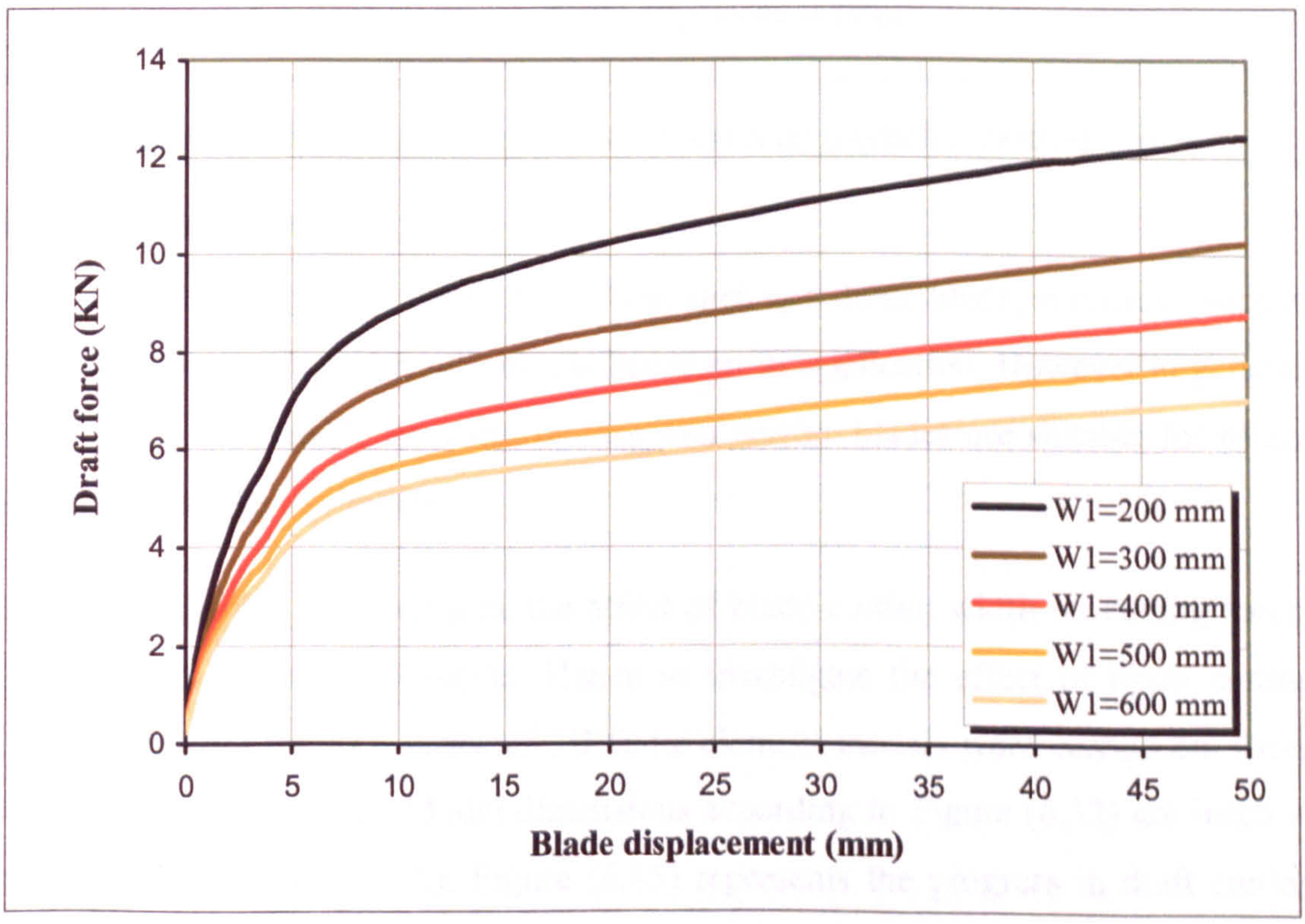

Figure (6.43) Effect of lateral bound width on predicted draft forces

From Figure (6.43) it is seen that as the lateral bound width increases draft force decreases and this effect may vanish as the bound moves away. Vertical forces were also affected by the boundary as shown in Figure (6.44) which represents the progress in vertical cutting forces as the blade moves horizontally.

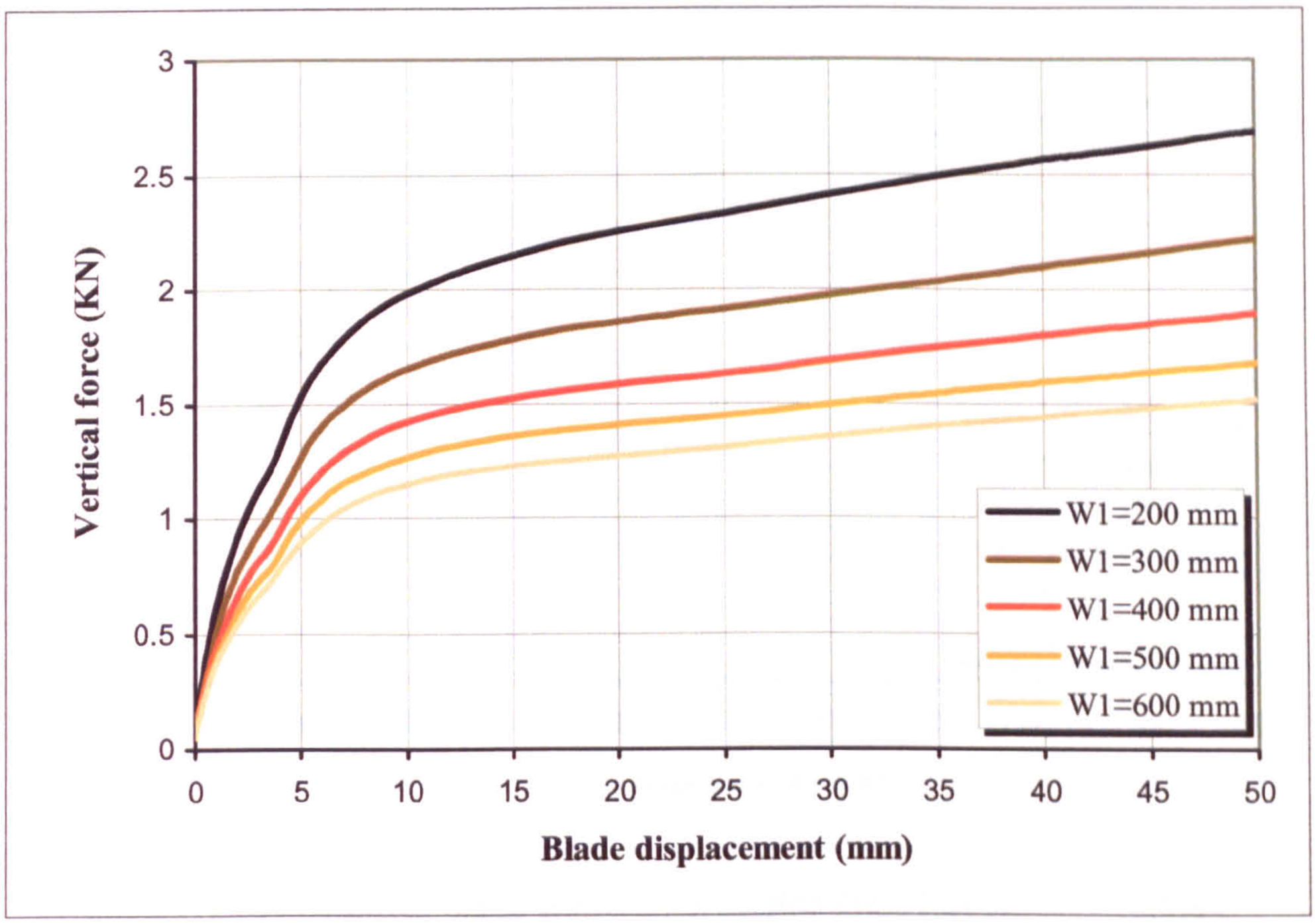

Figure (6.44) Effect of lateral bound width on predicted vertical forces

6.4.3.3 Effect of cutting width

Cutting blades are varied from wide, such as a dozer blade, to narrow, such as tillage blades. Blade width selection is based on its application. However in general, wide blades are suitable for earth moving and narrow blades are suitable for tillage and mine clearing equipment.

It was not possible to investigate the effect of blade cutting width on cutting forces using the plane strain 2D model. Hence to investigate the effect of blade cutting width on cutting forces a series of 3D finite element models were carried out using blades of different width. Model dimensions according to Figure (6.32) are listed in table [A.7] in Appendix (A). Figure (6.45) represents the progress in draft cutting forces as the blade moves horizontally though 50 mm for different blade widths of W2 = 200, 300, 400, 500, 600 and 700 mm, the lateral bound width was kept constant (W1 = 400mm). From the figure it is noticeable that as the cutting width increases draft force, acting on the blade, increases.

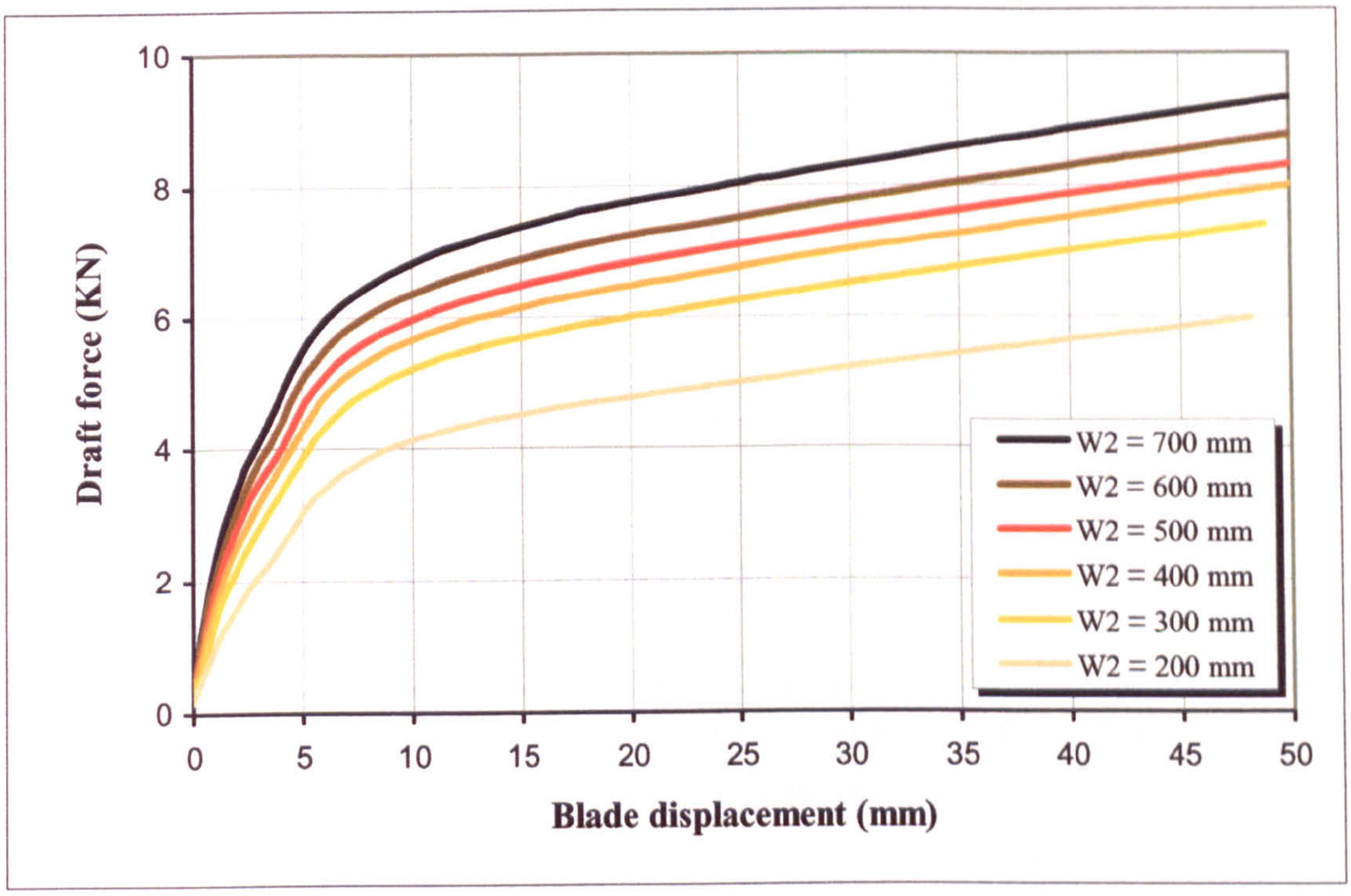

Figure (6.45) Effect of blade width on predicted draft forces, W1=400mm

The behaviour shown in Figure (6.45) seems logical, but a closer comparative look at the results highlights the existence of a cutting force component that does not depend on the cutting width. For example; the draft force acting on a blade of width W2=600 mm is about 120% of that acting on a blade of width W2=300mm and not about 200%. This observation reveals that there is a force that acts on the blade and not depends on the cutting width only, and this force is high compared with the total forces acting on the blade as shown in Figure (6.46) which represents draft cutting forces for different cutting widths at 5, 20 and 40 mm of blade displacement. The relation between cutting forces and the cutting width is shown to be nonlinear which indicates the existence of a cutting force component that does not depend only on the cutting width. This force component could be related to the shear resistance along the vertical bounds of the cutting wedge as a result of the lateral earth pressure of the cutting wedge and sand swelling up during the cutting process as discussed later in section (6.4.3.4).

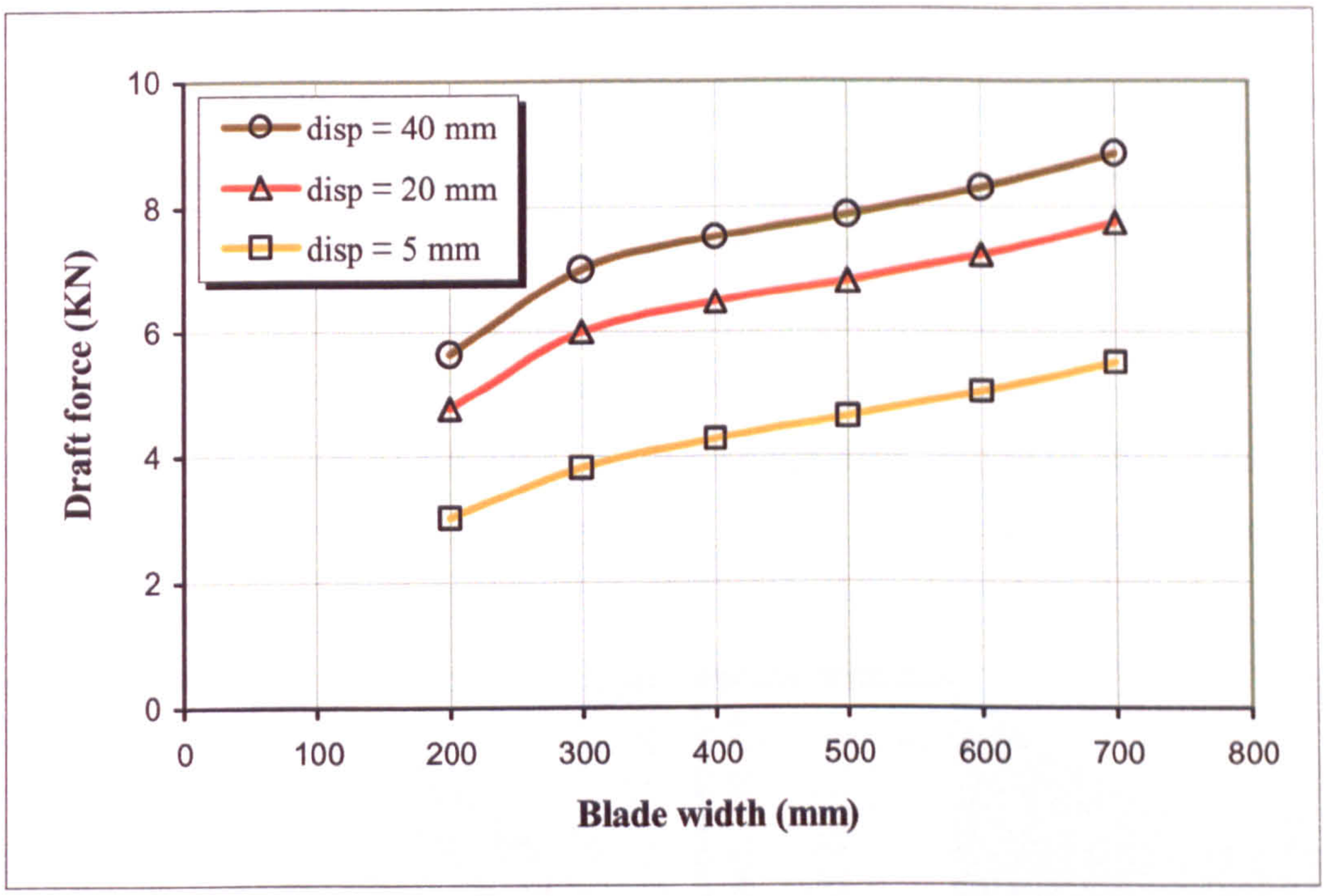

Figure (6.46) Draft forces measured for different blade widths

Vertical forces were also affected by the cutting width as shown in Figure (6.47) which represents the progress in vertical cutting forces as the blade moves horizontally for different cutting widths.

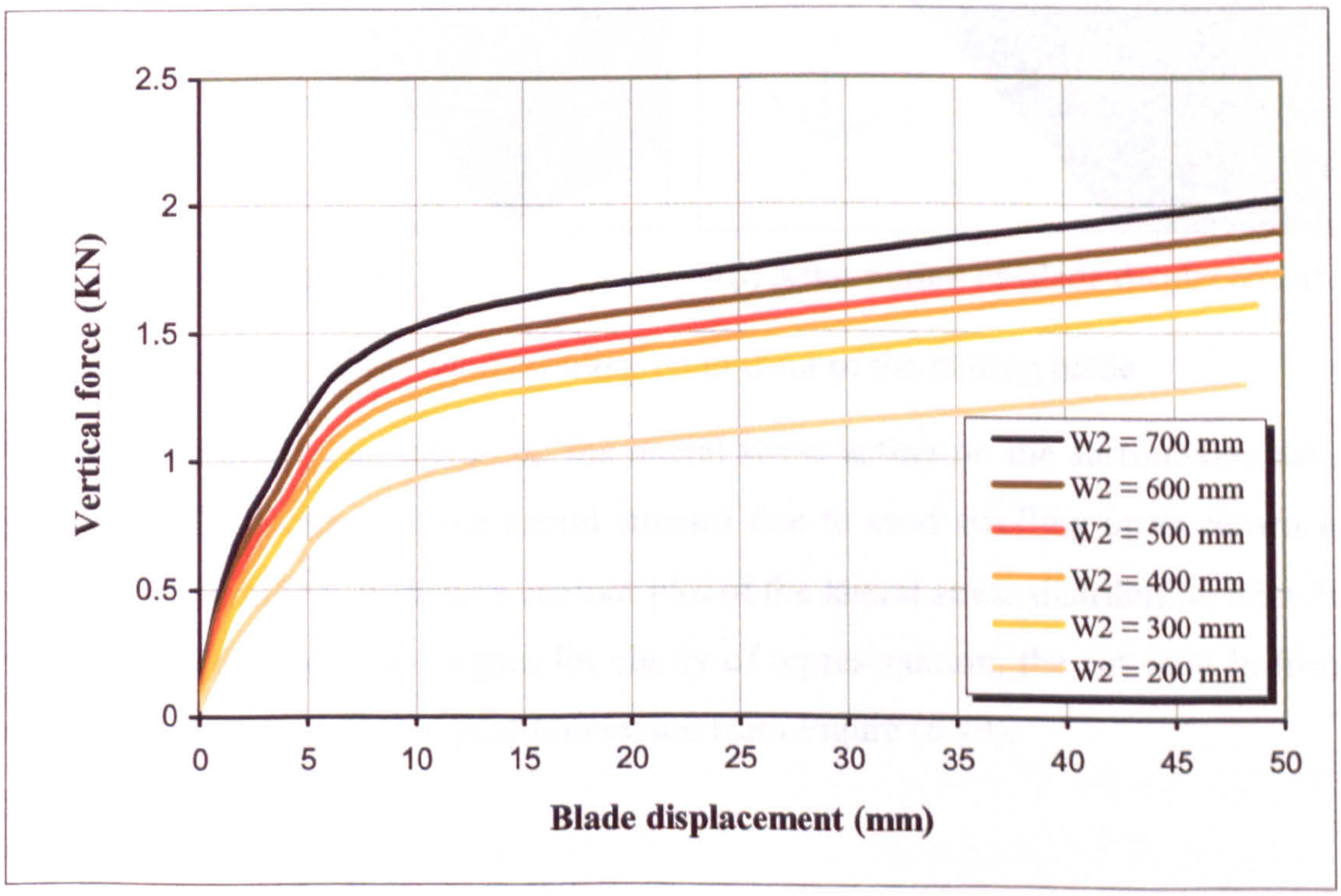

Figure (6.47) Effect of blade cutting width on predicted vertical forces

6.4.3.4 Effect of sand swelling up

As the blade moves in the horizontal direction, the cut soil (sand) accumulates in front of the blade and the soil being cut tends to swell up. Sand swelling up is found to occur not only upward, but in the lateral direction as well. This can easily be seen from Figure (6.48) which represents a contour plot of the cut soil void ratio distribution in front of the cutting blade before movement, Figure (6.48a), and after 50mm of horizontal blade displacement, Figure (6.48b). The rest of the simulated sand was excluded in post-processing for clarity of representation of the swelling up.

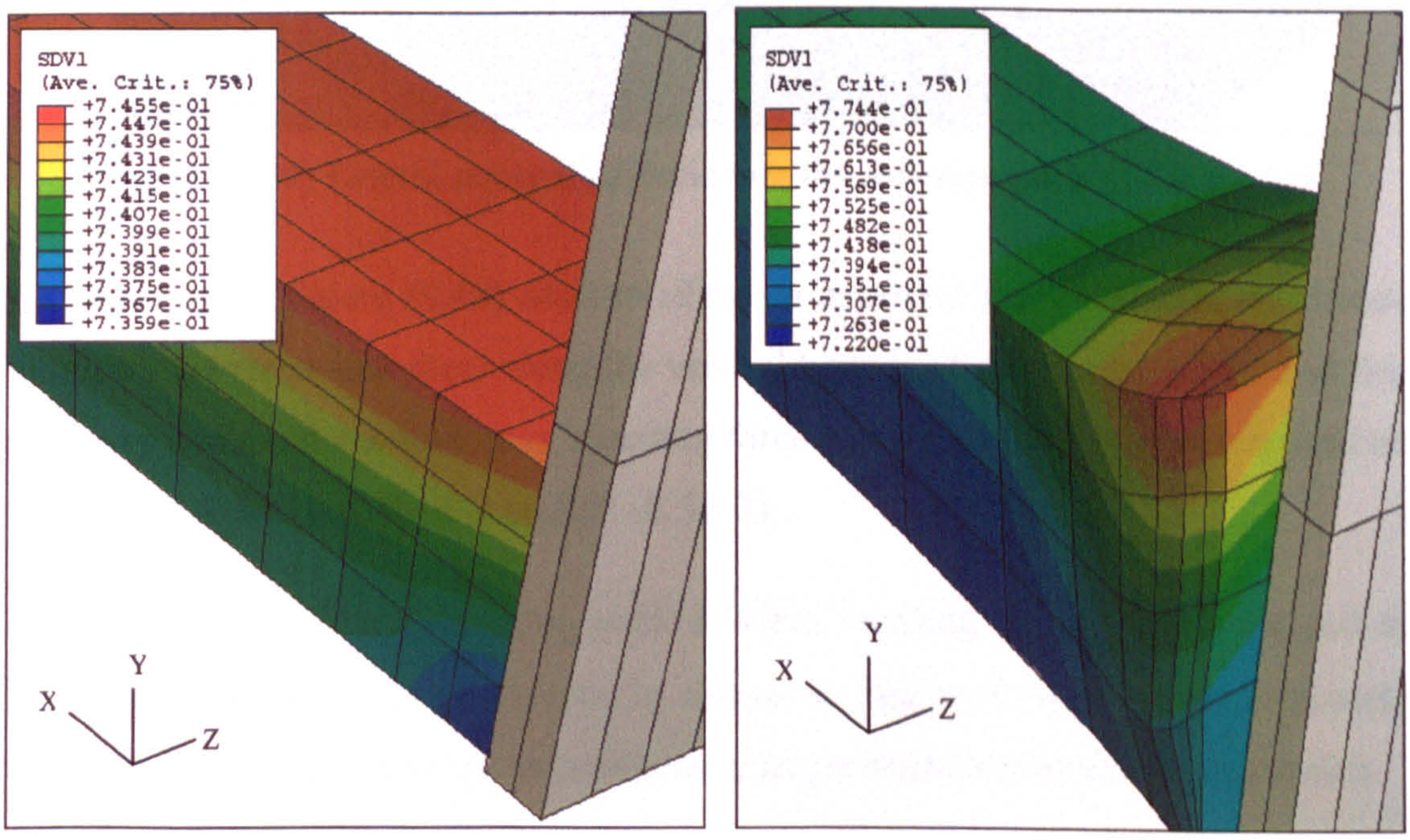

(a) At rest (b) After 50mm of blade displacement

Figure (6.48) Sand swelling up in front of the cutting blade

As the sand swelling up increases, the lateral stress acting on the surrounding sand increases. The increase in the lateral stresses due to sand swelling up is shown in Figure (6.49) which represents a contour plot of the lateral stress distribution after 50 mm of blade displacement. Again for clarity of representation, the cut sand in front of the blade was excluded in post-processing from Figure (6.49).

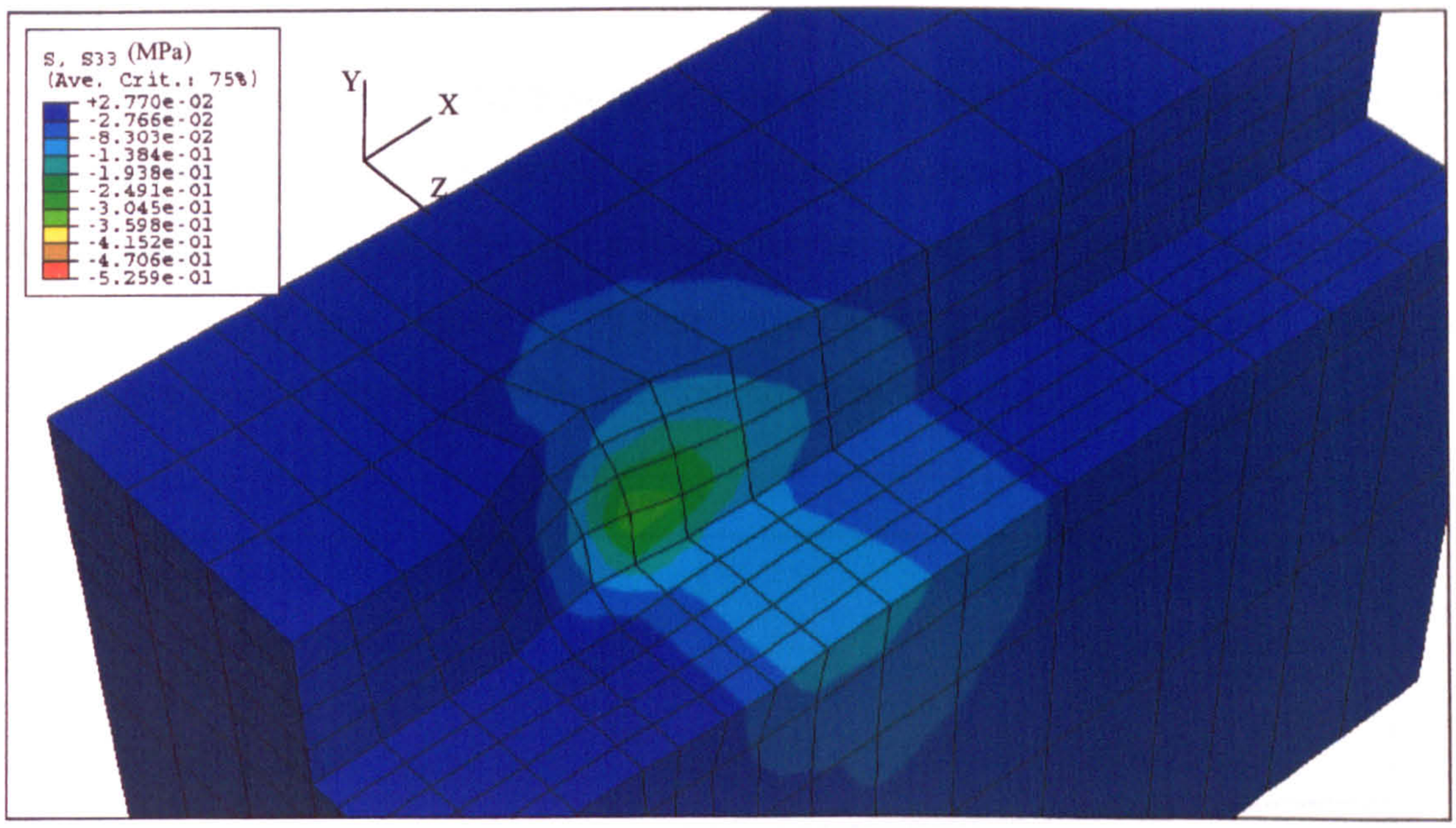

Figure (6.49) Lateral stress distribution on the soil surrounding the cut soil

As shown from Figure (6.49) sand swelling up increases lateral stresses and hence increases the resistance shear along the vertical bounds of the cutting wedge and this also may explain the existence of a cutting force component that does not depend on the cutting width described in section (6.5.3.3).

From the finite element modeling point of view, swelling up causes the cut soil to lose contact with the cutting blade, as shown in Figure (6.48b), which ultimately results in numerical convergence problems at larger blade horizontal displacements.

6.4.3.5 Dynamic analysis

As mentioned before in Chapter 4, the hypoplastic model described sand behaviour through a rate independent constitutive relation, i.e. the cutting speed should not show any significant effect on the cutting forces. However from the kinetics point of view, the inertia of the cutting blade and the inertia of the sand should affect the reaction forces. Hence moving the blade with a constant velocity (zero acceleration) should not affect the cutting forces but accelerating it should affect the cutting forces. Based on model dimensions of model 'Width 250' in Table [A.7] and mesh distribution of model 'Mesh 1082' in Table [A.6], all the parameters of the dynamic analysis are listed in Table [A.9] in Appendix (A).

Effect of cutting speed

To investigate the effect of cutting speed on blade cutting forces, a series of finite element models were carried out at different constant cutting speeds (V =10, 30, 50, 100, 200 mm/sec) through a blade displacement of 50 mm in the horizontal direction along X axis. Figure (6.50) represents the progress in draft cutting forces as the blade moves horizontally with different constant velocities.

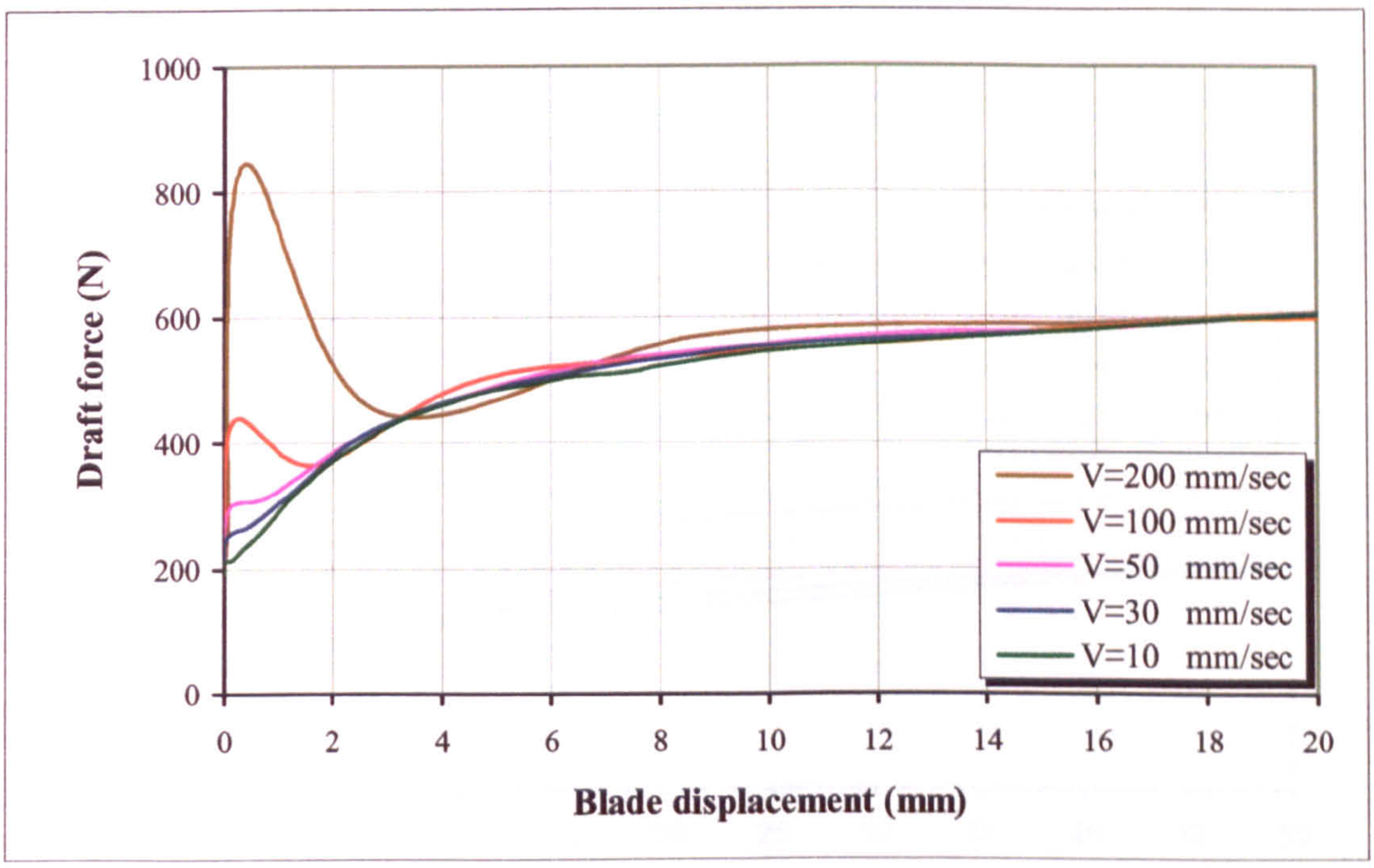

Figure (6.50) Effect of cutting speed on draft forces

As shown in Figure (6.50), the cutting forces increase rapidly at the beginning of blade displacement and are then "damped out" after a while and then increase linearly as the blade moves further. Hence at the beginning of the motion the cutting speed showed a very significant effect on the cutting forces and then this effect vanishes as the blade displaced. The rapid change of the cutting forces with cutting speed at the beginning of the motion may be due to the momentum change between the two contacting bodies, the blade with an initial velocity and the soil at rest. This rapid change in momentum is dependent on the cutting speed and increases as the speed increases. However in general, the cutting speed seems to have no effect on the blade cutting forces.

Effect of cutting acceleration

To investigate the effect of cutting acceleration on blade cutting forces, a series of finite element models were carried out at different cutting accelerations (a = 1, 9, 25, 100, 400 mm/s^2) through a blade displacement of 50mm in the horizontal direction along X axis. The blade was assumed initially to be initially at rest. Figure (6.51) represents the progress in draft cutting forces as the blade moves horizontally with different accelerations.

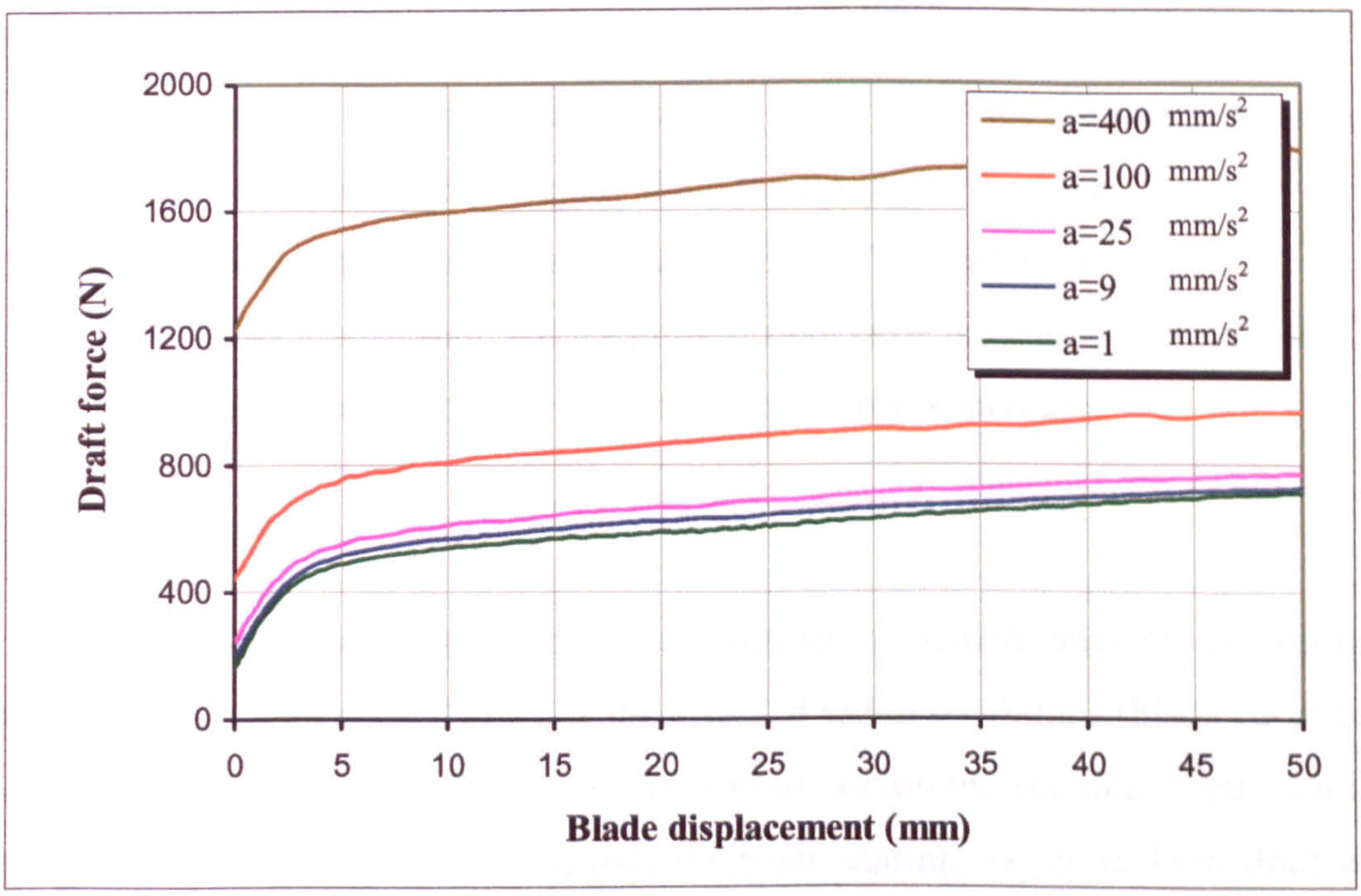

Figure (6.51) Effect of cutting acceleration on draft forces

As shown from the figure, the cutting acceleration has a significant effect on blade cutting forces and that as the cutting acceleration increases the cutting forces increase.

6.4.4 CONCLUSION OF THE 3D ANALYSIS

From the various 3D analyses carried out, some concluding remarks can be made as follows:

1. The concept of predefined failure surfaces has shown to be suitable for modeling the 3D soil-tool interaction problem.

2. The mesh density has a very significant effect on the predicted results in both draft and vertical directions in that as the mesh increases the predicted forces decreases.
3. Simulated lateral bound width distances have a significant effect on the predicted results.
4. Blade cutting width has a significant effect on cutting forces in both draft and vertical direction.
5. The effect of vertical shear stresses along the cutting wedge sides has a noticeable effect on the total cutting forces.
6. Sand swelling up in front of the cutting blade increases the lateral stress and hence the vertical shear stresses along the cutting wedge sides.
7. The cutting speed has an insignificant effect of the cutting forces.
8. The cutting acceleration has a significant effect on the cutting forces in that as the cutting acceleration increases the cutting forces increase.

6.5 SUMMARY

Two-dimensional and three-dimensional finite element analyses of soil-tool interaction have been carried to study the effect of initial conditions (blade curvature, soil density and blade roughness) and operating conditions (cutting depth, cutting angle, cutting width and cutting speed) on blade cutting forces in both draft and vertical directions. A plane strain analysis was considered in the 2D analysis due to the large width of the bulldozer blade compared with its cutting depth. The modified hypoplastic constitutive model was used to describe the behaviour of the simulated sand in monotonic loading. The mesh density was found to have insignificant effect on the 2D analysis predicted results but has a very significant effect on the 3D analysis predicted results. A series of models were analyzed with various different initial and operating conditions using both two-dimensional and three-dimensional models. Results showed the significant effect of cutting depth, cutting width, cutting acceleration, sand density, blade roughness on cutting forces and the insignificant effect of the cutting angle and cutting speed.

Chapter 7

CONCLUSION AND FUTURE WORK

7.1 GENERAL

Numerical simulation of the soil-tool interaction process has been investigated in this thesis in order to research an alternative method to expensive and time consuming experimental studies of soil-tool interaction which also require accurate measuring devices to obtain reasonable results. In fact the numerical simulation of soil-tool interaction was an overall aim, beyond that a more specific aim was to investigate several factors affecting cutting forces required for earth cutting and moving in both civilian and military applications of soil-tool interaction. Through this work some skills have been learned and enhanced, these skills can be summarized as:

- using electronic databases
- understanding new concepts such as constitutive models and their implementation
- learning about numerical methods of solving non-linear differential equations
- using programming languages such as FORTRAN
- interaction with different platforms (computer system) such as UNIX and WinNT
- interaction with several finite element packages such as ABAQUS, ANSYS and TOCHNOG

In this study various concluding remarks have been made based on:

- Experience of more than 70 journal and conference papers.
- Knowledge from more than 15 text books.
- Previous personal experience of soil-tool interaction.
- About 40 numerical simulations using FORTRAN programming.
- About 130 separate finite element analysis using ABAQUS/Standard.
- Experimental validation study of the effect of cutting speed

In the following sections a list of the various concluding remarks will be presented based on the chapter from which it was drawn.

7.2 LITERATURE REVIEW

Chapter 2 reviewed various different approaches (experimental, analytical and numerical) used to study soil-tool interaction along with available numerical models of simulating soil-tool interaction. The most significant findings in the literature review were:

- The significant effect of the cutting angle and cutting depth on blade cutting forces whatever the blade width.
- Draft and vertical forces are linearly related to the tool width and cutting depth and non-linearly to the cutting angle.
- The significant effect of cutting speed on blade cutting forces in draft and vertical directions, this effect decreases as the speed increases over certain limit (0.1 mm/s).
- Finite element method is more reliable compared with analytical methods.
- For reasonable simulation of soil-tool interaction, an accurate constitutive model of the soil behaviour is more important than simulating the interface between the blade and soil.

7.3 SOIL PROPERTIES & MODELING

Comparison review of the available constitutive models for simulating sand was carried out in Chapter 3 based on well understood of soil properties and behaviour. The main aim of this chapter was selection of the most appropriate model for simulating sand in soil-tool interaction analysis.

The major findings from this chapter were:

- Most elastoplastic models parameters are based on some assumptions such as a linear stress-strain relationship for sand. These assumptions may lead to inaccurate results.
- Hypoplastic model features described in the literature and outlined in Chapter 3 (particularly the Wolffersdorf model) appeared to have more promise in simulating sand in soil-tool interaction analysis.

7.4 NUMERICAL INTEGRATION AND VERIFICATION OF THE HYPOPLASTIC MODEL

In Chapter 4, a verification study of various different numerical methods used to integrate the rate type hypoplastic equation was carried out. Two different classes of integration schemes were considered; implicit one-step stress-point algorithms and explicit adaptive algorithm. Simulating the Oedometer test numerically was the benchmark problem for verification of the different integration schemes. The most significant findings in Chapter 4 were:

- Results obtained by using the explicit adaptive Runge-Kutta-Fehlberg algorithm were strongly dependent on the allowable error tolerance prescribed in the algorithm.
- Euler-forward integration scheme was most suitable to integrate the hypoplastic equation at small sub-step size i.e. at small strain increment.
- Comparison with available experimental data from the Oedometer test revealed the capability and accuracy of the hypoplastic model of simulating sand behaviour during loading and unloading.

7.5 FINITE ELEMENT MODELING

In Chapter 5 a verification study of the implemented hypoplastic model was carried out through finite element analysis of some benchmark problems related to soil-tool interaction. Through the finite element analysis, some concluding remarks were drawn and listed as follows:

- The ABAQUS User defined material feature was adequate for implementing the hypoplastic model.
- The implemented hypoplastic model was capable of proper simulation of sand behaviour in various different soil-tool interaction applications.
- The Euler-Forward integration scheme was sufficient for integrating the hypoplastic model.

7.6 SOIL-TOOL INTERACTION

Extensive finite element analysis of soil-tool interaction was carried out in Chapter 6 to study the effect of various different geometry and operating conditions on blade cutting forces. The major findings from this chapter were:

- Soil state (dense or loose) has a significant effect on cutting forces in both draft and vertical force components.
- Blade surface roughness has a significant effect on cutting forces in both draft and vertical force components.
- As the cutting depth increases both draft and vertical forces increase.
- As the cutting width increases both draft and vertical forces increase.
- As the cutting angle increases, draft force increases and vertical force decreases and as the cutting angle decreases, draft force decreases and vertical force increases.
- As the cutting angle increases, the accumulated soil pile in front of the cutting blade increases.
- Blade curvature has relatively insignificant effect on cutting forces for sand soil.
- Blade curvature has a significant effect on forming of an accumulated pile in front of the blade in that as the curvature increases (radius of curvature decreases) accumulated soil increases.

- More accumulated soil forming in front of the blade means more productivity from the earth moving equipment point of view but means more danger of mines exploding from mine clearing point of view.
- Plane strain analysis ignores (1) the effect of blade width, (2) the dissipation of the accumulated soil around the blade during the blade movement and (3) the effect of frictional shear of vertical cutting wedge sides. Hence the effect of these factors can not be studied through two-dimensional analysis.
- Constant cutting speed has an insignificant effect of the cutting forces.
- Cutting acceleration has a significant effect on the cutting forces in that as the cutting acceleration increases the cutting forces increase.
- The mesh density has a very significant effect on the 3D predicted results in both draft and vertical directions in that as the mesh increases the predicted forces decreases.
- Simulated lateral bound width distances have a significant effect on the predicted results.

The present soil-tool interface analysis technique is reliable for prediction of blade cutting forces provided the existence of a high speed computing processor to solve a very dense mesh model and avoid the effect of the mesh density on the predicted results. Also the concept of the predefined failure surface may be limited to a relatively simple blade geometry but for a complex tool geometry, using an adaptive mesh technique may be more applicable. In general, the present technique can be used in comparison study of soil-tool interaction at different operating conditions.

7.7 SUGGESTIONS FOR FURTHER STUDY

The work conducted in this thesis has identified several areas where further research may be required:

- Incorporation of the rate effect on the global behaviour of sand into the hypoplastic model.
- Implementing the hypoplastic model into ABAQUS/Explicit or LSDYNA/3D to enable the use of the adaptive mesh feature of these packages in simulating soil-tool interaction which enables account for failure without using a predefined failure surfaces in the model.
- Studying the effect of using a vibratory blade to reduce the cutting forces.
- Analyze the performance of different types of cutting tools such as tillage and ploughs.
- Studying the effect of mine explosion on the cutting tool and the effect of the tool geometry on the damage that may occur on mine clearing machinery.

REFERENCES

AboElnor, M. (1997). "The use of scale model tests and FEM to study soil-tool interaction for bulldozer blades.", *MSc. Thesis, Military Tech. College, CAIRO.*

AboElnor, M., S. M. A. El-Aziz, et al. (1998a). "Experimental Study of Blade-Soil Interaction Forces". *8th Int. Applied Mechanics and Mechanical Engineering Conference, CAIRO.*

AboElnor, M., S. M. A. El-Aziz, et al. (1998b). "Development of a Mathematical Model for Predicting Blade-Soil Interaction Forces". *8th Int. Applied Mechanics and Mechanical Engineering Conference, CAIRO.*

Atkinson, J. (1993). An Intoduction to the mechanics of soils and foundations, McGraw-Hill Book Company Europe.

Baladi, G. Y. and B. Rohani (1979). "Elastic-Plastic model for saturated sand.", *Journal of Geotechnical Engineering Division,* **105**(GT4), 465-480.

Bardet, J. P. (1986). "Bounding surface plasticity model for sands.", *Journal of Engineering Mechanics,* **112**(11), 1198-1217.

Bardet, J. P. (1990). "Hypoplastic model for sands.", *Journal of Engineering Mechanics,* **116**(9), 1973-1994.

Bauer, E. (1996). "Calibration of a comprehensive hypoplastic model for granular materials.", *Soils and Foundations,* **36**(1), 13-26.

Bauer, E. (2000). "Conditions for embedding Casagrande's critical states into hypoplasticity.", *Mechanics Of Cohesive-Frictional Materials,* **5**, 125-148.

Bauer, E. and W. Huang (1999). "Effect of initial anisotropy on shear banding in granular materials". *Numerical Models in Geomechanics - NUMOG, Balkema, Rotterdam,* VII, 121-126.

Been, K. and M. G. Jefferies (1985). "A State parameter for sands.", *Geotechnique,* **35**(2), 99-112.

Budhu, M. and M. Budhu (1999). Soil mechanics and foundations, Wiley, John & Sons.

Chambon, R., D. Caillerie, et al. (1999). "A Comparison of incremental behaviour of Elastoplastic and CLoE models.", *International Journal For Numerical and Analytical Methods in Geomechanics,* **23**, 295-316.

Chambon, R., J. Desrues, et al. (1994). "CLoE, A New Rate-Type Constitutive Model for Geomaterials Theoretical Basis and Implementation.", *International Journal For Numerical and Analytical Methods in Geomechanics,* **18**, 253-278.

Chazallon, C. and P. Y. Hicher (1998). "A Constitutive model coupling elastoplasticity and damage for cohesive-frictional materials.", *Mechanics Of Cohesive-Frictional Materials,* **3**, 41-63.

Chen, W. F. and E. Mizuno (1998). Nonlinear analysis in soil mechanics. Amsterdam 1990, Elsevier.

Chi, L. and R. L. Kushwaha (1990). "A Non-linear 3 D finite element analysis of soil failure with tillage tool.", *Journal of Terramechanics,* **27**(4), 343-366.

Dechao, Z. and Y. Yusu (1991). "Investigation on the relationship between soil shear strength and shear rate.", *Journal of Terramechanics,* **28**(1), 1-10.

Dechao, Z. and Y. Yusu (1992). "A Dynamic model for soil cutting by blade and tine.", *Journal of Terramechanics,* **29**(3), 317-327.

Desai, C. S. and H. J. Siriwardane (1984). Constitutive laws for engineering materials, Prentice-Hall, Inc.

Fakharian, K. and E. Evgin (2000). "Elasto-Plastic modelling of stress-path-dependent behaviour of interfaces.", *International Journal For Numerical and Analytical Methods in Geomechanics,* **24**, 183-199.

Fukushima, S. and F. Tatsuoka (1982). "Deformation and strength of sand in torsional simple shear". *IUTAM Conference on Deformation and Failure of Granular Materials, Deflt.*

Gajo, A. and D. M. Wood (1999). "A Kinematic hardening constitutive model for sands: The multiaxial formulation.", *International Journal For Numerical and Analytical Methods in Geomechanics,* **23**, 925-965.

Ghaboussi, J. and H. Momen (1984). "Plasticity model for inherently anisotropic behaviour of sands.", *International Journal For Numerical and Analytical Methods in Geomechanics,* **8**, 1-17.

Goodbody, A. M. (1982). Cartesian tensors with applications to mechanics, fluid mechanics and elasticity, Chichester Horwood.

Gudehus, G. (1979). "A Comparison of some constitutive laws for soils under radially symmetric loading and unloading". *Third International Conference on Numerical Methods in Geomechanics, Aachen,* 1309-1323.

Gudehus, G. (1996). "A Comprehensive constitutive equation for granular materials.", *Soils and Foundations,* **36**(1), 1-12.

Herle, I. (1997). "On parameters for geotechnical calculations". *25th Conference Foundations, Brno,* 16-19.

Herle, I. (1998). "Drawbacks of oversimplified soil models in the numerical modelling of soil-structure interaction.". *Int. Sci. Conf. 60th Anniversary of the Faculty of Civil Eng.,* 223-228.

Herle, I. and G. Gudehus (1999). "Determination of parameters of a hypoplastic constitutive model from properties of grain assemblies.", *Mechanics Of Cohesive-Frictional Materials,* **4**, 461-486.

Herle, I. and K. Nubel (1999). "Hypoplastic description of the interface behaviour". *Numerical Models in Geomechanics - NUMOG, Balkema, Rotterdam,* VII, 53-58

Herle, I. and J. Tejchman (1997). "Effect of Grain Size and Pressure Level on Bearing Capacity of Footings on Sand". *Deformation and Progressive Failure in Geomechanics, Pergamon, Rotterdam, Nagoya (JP),* 781-786.

Hibbit, Karlsson, et al. (2000). ABAQUS/Standard User's Manual, Version 6.1. Pawtucket, RI, USA.

Ignatieff, Y. A. (1996). The mathematical world of Walter Noll, Springer.

Jori, L. J. and G. Kerenyi (1998). "Simulation of wide blade performance in different soils". *Proceedongs of the 1998 1st Conference on Mechanical Engineering, Gepeszet, Technical Univ of Budapest,* 1, 382-386.

Koffman, E. B. and F. L. Friedman (1993). Fortran with engineering applications, Addison-Wesley.

Kolymbas, D. (1991). "An Outline of hypoplasticity.", *Archive of Applied Mechanics,* **61**, 143-151.

Kolymbas, D. (1995). "Hypoplastic constitutive equation with internal variables.", *International Journal For Numerical and Analytical Methods in Geomechanics,* **19**, 415-436.

Kolymbas, D. (1999). Intorduction to Hypoplasticity, Balkem, A. A.

Kolymbas, D. (2000). Constitutive Modelling of Granular Materials. New York, Springer-Verlag.

Kolymbas, D. and E. Bauer (1993). "Soft oedometer. A new testing device and its application for the calibration of hypoplastic constitutive laws.", *Geotechnical Testing Journal,* **16**(2), 263-270.

Kolymbas, D. and W. Wu (1990). "Recent results of triaxial tests with granular materials.", *Powder Technology,* **60**, 99-119.

Kushwaha, R. L. and J. Shen (1995a). "Numeric Simulation of Friction Phenomenon at Soil-Tool Interface.", *Tribology Transactions,* **38**(2), 424-430.

Kushwaha, R. L. and J. Shen (1995b). "Finite element analysis of the dynamic interaction between soil and tillage tool.", *Transactions of the ASAE,* **37**(5), 1315-1319.

Kushwaha, R. L. and J. Shen (1996). "Investigation on contact mechanism between soil and metal.", *American Society of Agricultural Engineers,* **39**(1), 187-193.

Lade, P. V. and R. B. Nelson (1984). "Incrementalization procedure for Elasto-Plastic constitutive model with multiple, intersecting yield surfaces.", *International Journal For Numerical and Analytical Methods in Geomechanics,* **8**, 311-323.

Lancellotta, R. (1995). Geotechnical Engineering. Rotterdam ; Brookfield, A.A. Balkema.

Li, X.-S., Y. F. Dafalias, et al. (1999). "State-dependent dilatancy in critical-state constitutive modelling of sand.", *Can. Geotech.,* **36**, 599-611.

Liu, J. (1995). "Investigation of the stress-strain relatioship of sand.", *Journal of Terramechanics,* **32**(5), 221-230.

Luengo, O. and S. Singh (1998). "Modeling and identification of Soil-Tool interaction in automated excavation". *IEEE/RSJ International Conferenec on Intelligent Robotic Systems, Canada, Victoria, B.C.*

Manzari, M. T. and Y. F. Dafalias (1997). "A Critical state two-surfaces plasticity model for sands.", *Geotechnique,* **47**(2), 255-272.

Matsuko, H. and T. Nakai (1977). "Stress-strain relatioship of soil based on tle 'SMP'". *Constitutive Equations of Soils. Proc. of Specialty Session 9, IX Int. Conf. Soil Mech. Found. Eng., Tokyo,* 153-162.

Mattsson, H., K. Axelsson, et al. (1997). "A Method to correct yield surface drift in soil plasticity under mixed control and explicit integration.", *International Journal For Numerical and Analytical Methods in Geomechanics,* **21**, 175-197.

Mouazen, A. M. and M. Nemenyi (1999). "Finite element analysis of subsoiler cutting in non-homogeneous sandy loam soil.", *Soil & Tillage Research,* **51**, 1-15.

Niemunis, A. and I. Herle (1997). "Hypoplastic model for cohesionless soils with elastic strain range.", *Mechanics Of Cohesive-Frictional Materials,* **2**, 279-299.

Oda, M. and K. Iwashita (1999). Mechanics of Granular Materials: An Introduction, Balkema.

Parry, R. H. G. (1995). Mohr Circles, Stress Paths and Geotechnics, E & FN Spon.

Pestana, J. M. and a. j. Whittle (1999). "Formulation of a unified constitutive model for clays and sands.", *International Journal For Numerical and Analytical Methods in Geomechanics,* **23**, 1215-1243.

Plouffe, C., C. Lague, et al. (1999). "Moldboard plow performane in a clay soil: simulation and experiment.", *Transactions of the ASAE,* **42**(6), 1531-1539.

Potts, D. M. and L. Zdravkovic (1999). Finite element analysis in geotechnical engineering. London, Thomas Telford.

Prisco, C. d. and S. Imposimato (1996). "Time dependent mechanical behaviour of loose sands.", *Mechanics Of Cohesive-Frictional Materials,* **1**, 45-73.

Qinsen, Y. and S. Shuren (1994). "A soil-tool interaction model for bulldozer blades.", *Journal of Terramechanics,* **31**(2), 55-65.

Rao, S. S. (1999). The Finite Element Method in Engineering, Butterworth-Heinemann.

Richey, S. B., A. K. Srivastava, et al. (1989). "The Use of three dimensional computer graphics to design Mouldboard plough surfaces.", *Journal of Agricultural Engineering research,* **43**, 245-258.

Roddeman, D. (1997). "FEM-Implementation of Hypoplasticity". *European Union Projekt.*

Rosa, U. A. and D. Wulfsohn (1999). "Constitutive model for high speed tillage using narrow tools.", *Journal of Terramechanics,* **36**, 221-234.

Royis, P. and T. Doanh (1998). "Theoretical analysis of strain response envelopes using incrementally non-linear constititutive equations.", *International Journal For Numerical and Analytical Methods in Geomechanics,* **22**, 97-132.

Shames, I. H. and F. A. Cozzarelli (1992). Elastic and inelastic stress analysis. New Jersey, A Simon & Schuster Company.

Shen, J. and R. L. Kushwaha (1998). Soil-Machine Interaction: A Finite Element Perspective, MARCEL DEKKER, INC.

Smith, I. M. and D. F. Griffiths (1997). Programming the Finite Element Method, John Wiley & Sons.

Somerville, S. H. and M. A. Paul (1983). Dictionary of Geotechnics, Butterworths.

Spektor, M. and M. Katz (1985). "Experimental study of frontal resistance force in soil cutting.", *Journal of Terramechanics,* **22**(3), 127-133.

Store, j. and R. Bulirch (1993). Introduction to numerical analysis, Springer-Verlag.

Swick, W. C. and J.V.Perumpral (1988). "A model for predicting soil-tool interaction.", *Journal of Terramechanics,* **25**(1), 43-56.

Tamagnini, C., G. Viggiani, et al. (1999). "Performance of different stress-point algorithms for the integration of hypoplastic constitutive equations for geomaterials". *Numerical Models in Geomechanics - NUMOG, Balkema, Rotterdam,* VII, 189-194.

Tamagnini, C., G. Viggiani, et al. (1997). "Evaluation of a stress point algorithm for a hypoplastic constitutive model for granular materials". *Numerical Models in Geomechanics, Balkema, Rotterdam,* 387-392.

Tamagnini, C., G. Viggiani, et al. (2000). "Evaluation of different strategies for the integration of hypoplastic constitutiveequations: Application to the CLoE model.", *Mechanics Of Cohesive-Frictional Materials,* **5**, 263-289.

Tejchman, J. and E. Bauer (1996). "Numerical simulation of shear band formation with a polar hypoplastic constitutive model.", *Computers and Geotechnics,* **19**(3), 221-244.

Tejchman, J. and G. Gudehus (2001). "Shearing of a narrow granular layer with polar quantities.", *International Journal For Numerical and Analytical Methods in Geomechanics,* **25**, 1-28.

Tejchman, J., I. Herle, et al. (1999). "FE-Studies on the influence of initial void ratio, pressure level and mean grain diameter on shear localization.", *International Journal For Numerical and Analytical Methods in Geomechanics,* **23**, 2045-2074.

Tejchman, J. and W. Wu (1995). "Experimental and Numerical Study of Sand-Steel Interfaces.", *International Journal For Numerical and Analytical Methods in Geomechanics,* **19**, 513-536.

Tejchman, J. and W. Wu (1996). "Numerical simulation of shear band formation with a Hypoplastic constitutive model.", *Computers and Geotechnics,* **18**(1), 71-84.

Terzaghi, K. (1959). Theoretical Soil-Tool Mechanics, J. Wiley & Sons Inc., N. Y.

Vardoulakis, I. and B. Graf (1985). "Calibration of constitutive models for granular materials using data from biaxial experiments.", *Geotechnique,* **35**(3), 299-317.

Viggiani, G. and C. Tamagnini (2000). "Ground movements around excavations in granular soils: a few remarks on the influence of the constitutive assumptions on FE predictions.", *Mechanics Of Cohesive-Frictional Materials,* **5**, 399-423.

Wan, R. G. and P. J. Guo (1998). "A Simple constitutive model for granular soils: Modified Stress-Dilatancy approach.", *Computers and Geotechnics,* **22**(2), 109-133.

Wan, R. G. and P. J. Guo (1999). "A consistent framework with embedded microstructural considerations for stress-dilatancy behaviour of sands". *Numerical Models in Geomechanics - NUMOG, Balkema, Rotterdam,* VII, 41-46.

Wang, Z.-L., Y. F. Dafalias, et al. (1990). "Bounding surface hypoplasticity model for sand.", *Journal of Engineering Mechanics,* **116**(5), 983-1001.

Wang, Z.-L. and F. I. Makdisi (1999). "Implementing a bounding surface hypoplasticity model for sand into the FLAC program". *The International Symposium on Numerical Modeling in Geomechanics, Minnesota, USA,* 483-490.

Wolffersdorf, P.-A. v. (1996). "A hypoplastic relation for granular materials with a predefined limit state surface.", *Mechanics Of Cohesive-Frictional Materials,* **1**, 251-271.

Wood, D. M., K. Belkheir, et al. (1994). "Strain softening and state parameter for sand modelling.", *Geotechnique,* **44**(2), 335-339.

Woodward, P. K. and F. Molenkamp (1999). "Application of an advanced Multi-Surface kinematic constitutive soil model.", *International Journal For Numerical and Analytical Methods in Geomechanics,* **23**, 1995-2043.

Wu, W. (1998). "Rational approach to anisotropy of sand.", *International Journal For Numerical and Analytical Methods in Geomechanics,* **22**, 921-940.

Wu, W. (1999). "On a simple critical state modl for sand". *Numerical Models in Geomechanics - NUMOG, Balkema, Rotterdam, Rotterdam,* VII, 47-52.

Wu, W. (2000). "Non-linear analysis of shear band formation in sand.", *International Journal For Numerical and Analytical Methods in Geomechanics,* **24**, 245-263.

Wu, W. and E. Bauer (1993). A Hypoplastic model for Baratropy and Pyknotropy of granular soils. Modern Approaches to Plasticity. D. Kolymbas, Elsevier Science Publishers B. V.

Wu, W. and E. Bauer (1994). "A Simple hypoplastic constitutive model for sand.", *International Journal For Numerical and Analytical Methods in Geomechanics,* **18,** 833-862.

Wu, W., E. Bauer, et al. (1996). "Hypoplastic constitutive model with critical state for granular materials.", *Mechanics of Materials,* **23,** 45-69.

Wu, W. and D. Kolymbas (1990). "Numerical testing of the stability criterion for hypoplastic constitutive equations.", *Mechanics of Materials,* **9,** 245-253.

Wu, W. and A. Niemunis (1996). "Failure criterion, flow rule and dissipation function derived from hypoplasticity.", *Mechanics Of Cohesive-Frictional Materials,* **1,** 145-163.

Wu, W. and A. Niemunis (1997). "Beyond failure in granular materials.", *International Journal For Numerical and Analytical Methods in Geomechanics,* **21,** 153-174.

Wu, W., J. Tejchman, et al. (1994). "Modelling progressive failure with hypoplastic constitutive model". *International Conference on Computational Methods in Structural and Geotechnical Engineering, Homg Kong,* 819-823.

Yong, R. N. and A. W. Hanna (1977). "Finite Element analysis of plane soil cutting.", *Journal of Terramechanics,* **14**(3), 103-125.

Yu, H. S. (1998). "CASM: A Unified state parameter model for clay and sand.", *International Journal For Numerical and Analytical Methods in Geomechanics,* **22,** 621-653.

Yusu, Y. and Z. Dechao (1990). "Investigation of the relationship between soil-metal friction and sliding speed.", *Journal of Terramechanics,* **27**(4), 283-290.

Zervos, A., I. Vardoulakis, et al. (2000). "Numerical investigation of granular interfaces kinematics.", *Mechanics Of Cohesive-Frictional Materials,* **5,** 305-324.

Zill, D. G. and M. R. Cullen (1997). Differential Equations with boundary-value problems. England, Brooks/Cloe.

APPENDICES

Appendix A

A.1 HYPOPLASTIC MODEL PARAMETERS

Table [A.1] Hypoplastic parameters for different sand soil and other granular materials after Herle and Gudehus (1999)

Material	φ_c [°]	h_s [MPa]	n	e_{d0}	e_{c0}	e_{i0}	α	β
Toyoura sand	30	2600	0,27	0,61	0,98	1,10	0,18	1,00
Hochstetten sand	33	1500	0,28	0,55	0,95	1,05	0,25	1,50
Schlabendorf sand	33	1600	0,19	0,44	0,85	1,00	0,25	1,00
Hostun sand	31	1000	0,29	0,61	0,91	1,09	0,13	2,00
Karlsruhe sand	30	5800	0,28	0,53	0,84	1,00	0,13	1,05
Zbraslav sand	31	5700	0,25	0,52	0,82	0,95	0,23	1,00
Ottawa sand	30	4900	0,29	0,49	0,76	0,88	0,10	1,00
Ticino sand	31	5800	0,31	0,60	0,93	1,05	0,20	1,00
SLB sand	30	8900	0,33	0,49	0,79	0,90	0,14	1,00
Hochstetten gravel	36	32000	0,18	0,26	0,45	0,50	0,10	1,80
plastics	32	110	0,33	0,53	0,73	0,80	0,08	1,00
wheat	39	20	0,37	0,57	0,84	0,95	0,02	1,00

A.2 RUNGE-KUTTA-FEHLBERG PARAMETERS

Table [A.2] Runge-Kutta-Fehlberg parameters

J	$\tilde{C}_J$	$\hat{C}_J$	β_{J0}	β_{J1}	β_{J2}	β_{J3}	β_{J4}	β_{J5}
0	$\frac{35}{384}$	$\frac{5179}{57600}$						
1	0	0	$\frac{1}{5}$					
2	$\frac{500}{1113}$	$\frac{7571}{16695}$	$\frac{3}{40}$	$\frac{9}{40}$				
3	$\frac{125}{192}$	$\frac{393}{640}$	$\frac{44}{45}$	$\frac{-56}{15}$	$\frac{32}{9}$			
4	$\frac{-2187}{6784}$	$\frac{-92097}{339200}$	$\frac{19372}{6561}$	$\frac{-25360}{2187}$	$\frac{64448}{6561}$	$\frac{-212}{729}$		
5	$\frac{11}{84}$	$\frac{187}{2100}$	$\frac{9017}{3168}$	$\frac{355}{33}$	$\frac{46732}{5247}$	$\frac{49}{176}$	$\frac{-5103}{18656}$	
6	0	$\frac{1}{40}$	$\frac{35}{384}$	0	$\frac{500}{1113}$	$\frac{125}{192}$	$\frac{-2187}{6784}$	$\frac{11}{84}$

A.3 SOIL-TOOL INTERACTION PARAMETERS

Table [A.3] Parameters for operating conditions analysis

Object name	Cutting angle (γ) °	Cutting depth (d) mm
St-R0a15d150	15	150
St-R0a15d250	15	250
St-R0a15d350	15	350
St-R0a30d150	30	150
St-R0a30d250	30	250
St-R0a30d350	30	350
St-R0a45d150	45	150
St-R0a45d200	45	200
St-R0a45d250	45	250
St-R0a45d300	45	300
St-R0a45d350	45	350
St-R0a60d150	60	150
St-R0a60d250	60	250
St-R0a60d350	60	350
St-R0a75d150	75	150
St-R0a75d250	75	250
St-R0a75d350	75	350

Table [A.4] Parameters for Initial conditions effect analysis

Object name	Friction coefficient μ	Initial void ratio e_o
St-R800a45d250	0.05	0.75
St-R800a45d250f2	0.1	0.75
St-R800a45d250f	0.2	0.75
St-R800a45d250e	0.05	0.9
St-R800a45d250e2	0.05	0.6

Table [A.5] Parameters for Blade geometry analysis

Object name	Blade radius (R) mm	Cutting angle (γ) °
St-R800a30d250	800	30
St-R600a45d250	600	45
St-R800a45d250	800	45
St-R1000a45d250	1000	45
St-R1200a45d250	1200	45
St-R600a60d250	600	60
St-R800a60d250	800	60
St-R1000a60d250	1000	60
St-R1200a60d250	1200	60
St-R600a75d250	600	75
St-R800a75d250	800	75
St-R1000a75d250	1000	75
St-R1200a75d250	1200	75

Table [A.6] Mesh distribution for 3D soil-tool interface models

Object name	EL1	EL	Eh	Ed	EW1	EW2/2	Total elements
Mesh 576	2	9	9	6	2	6	576
Mesh 802	2	10	10	7	2	7	802
Mesh 1082	2	11	11	8	2	8	1082
Mesh 1422	2	12	12	9	2	9	1422
Mesh 1672	2	12	13	10	2	10	1672
Mesh 1828	2	13	13	10	2	10	1828

Table [A.7] 3D soil-tool interface models parameters for different cutting widths

Object name	L1	L	h	d	W1	W2
Width300	200	900	700	200	400	300
Width 400	200	900	700	200	400	400
Width 500	200	900	700	200	400	500
Width 600	200	900	700	200	400	600
Width 700	200	900	700	200	400	700

Table [A.8] 3D soil-tool interface models parameters for different bound widths

Object name	L1	L	h	d	W1	W2
Bound 200	200	900	700	200	200	600
Bound 300	200	900	700	200	300	600
Bound 400	200	900	700	200	400	600
Bound 500	200	900	700	200	500	600
Bound 600	200	900	700	200	600	600

Table [A.9] 3D soil-tool interface models parameters for dynamic analysis

Object name	Cutting velocity mm/sec	Object name	Cutting acceleration mm/sec^2
Vel 10	10	Acc 1	1
Vel 30	30	Acc 9	9
Vel 50	50	Acc 25	25
Vel 100	100	Acc 100	100
Vel 200	200	Acc 400	400

Appendix B

DETERMINATION OF ELASTO-PLASTIC MODEL PARAMETERS

In order to get comparable results between Hypoplastic and Elasto-plastic calculations for both Mohr's-Coulomb and Drucker-Prager, the equivalent material parameters for each of these models have to be calculated. In the following section numerical simulation of both Triaxial test and Oedometer test were carried out using the hypoplastic model to simulate sand in these two element tests in order to obtain Elasto-plastic material parameters equivalent to the hypoplastic model parameters.

B.1 ELASTIC PARAMETERS

As known the Elasto-plastic models describe sand behaviour in two main stages; Elastic and yield. The material parameters for describing the elastic stage such as ν and E can be calculated through a numerical simulation of triaxial and Oedometer tests, respectively, using the Hypoplastic parameters given in table [5.2]

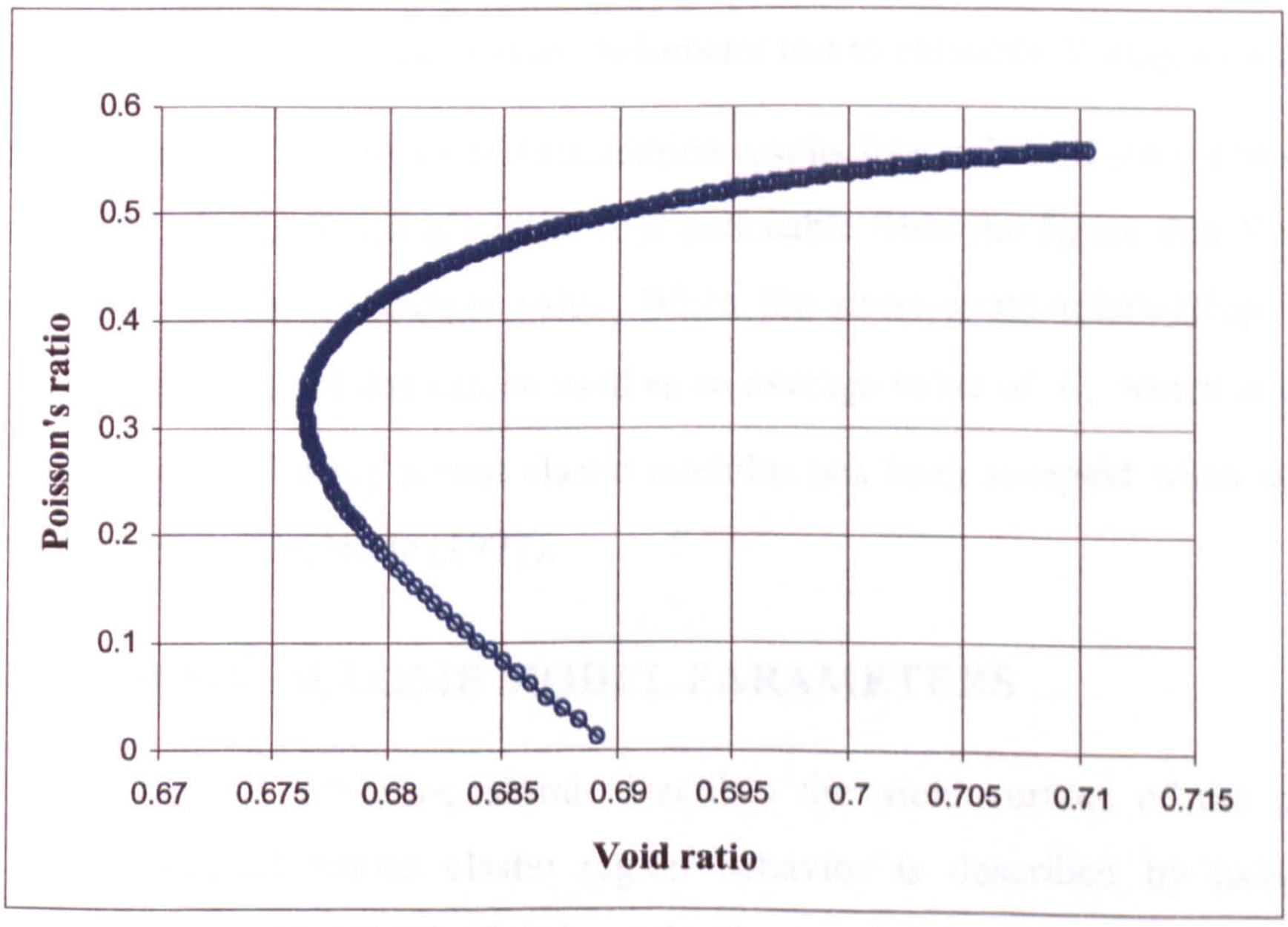

Figure (B.1) Numerical simulation of Triaxial test to calculate Poisson's ratio

Figure (B.1) present triaxial test simulation results from which Poisson's ratio was calculated. It is noticeable from the figure that Poisson's ratio does not have unique value but it depends on the sand state represented by the void ratio. Referring to the literature, Herle (1998), an average value of 0.3 was selected.

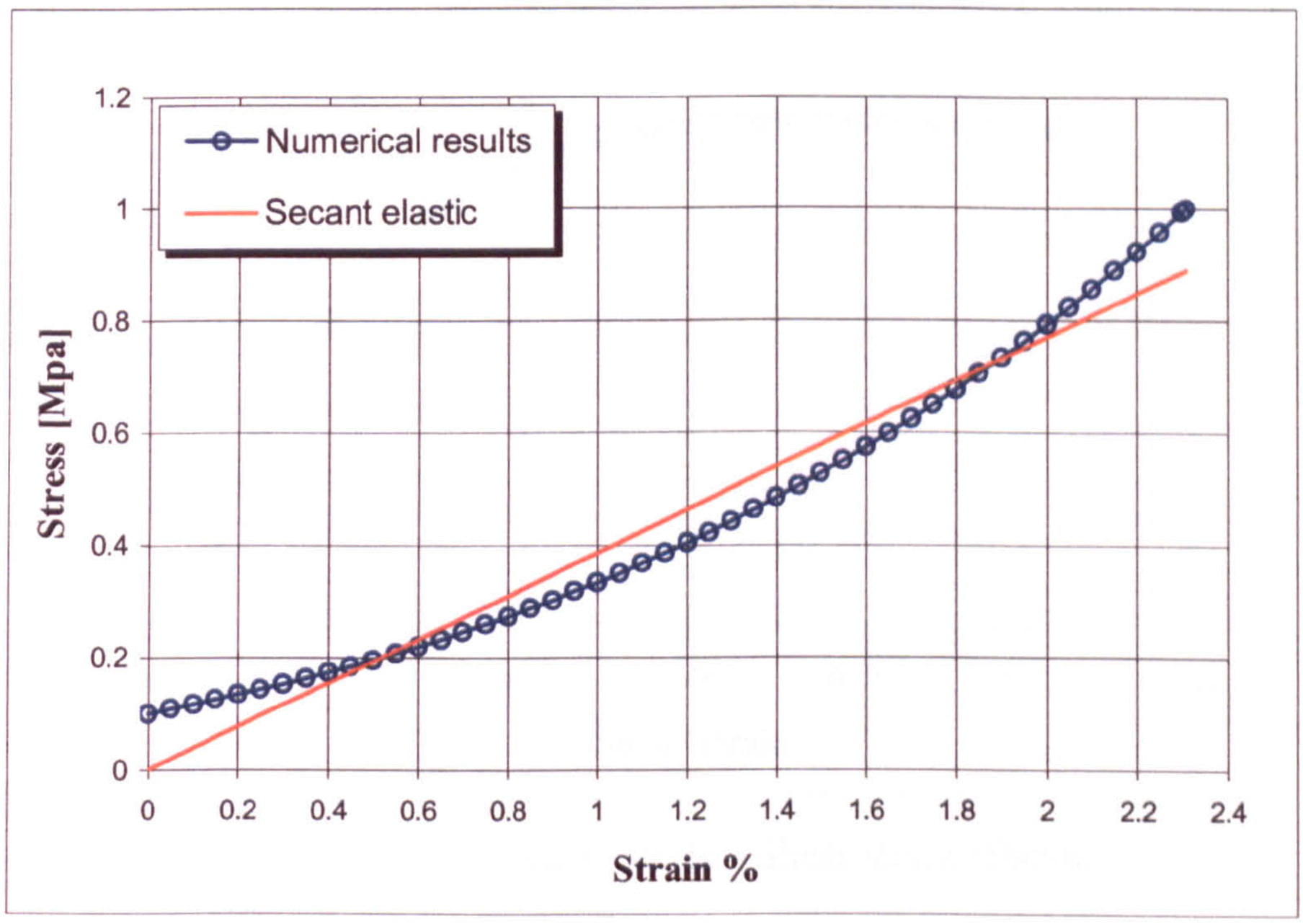

Figure (B.2) Numerical simulation of Oedometer test to calculate Young's modulus

Figure (B.2) present Oedometer test simulation results from which Young's modulus was calculated. As for Poisson's ratio, it is noticeable from the figure that Young's modulus does not have a unique value. When the stress-strain relationship is not linear, secant elastic modulus can be used as an average value of E_s which equal 40 MPa. The concept of using secant elastic modulus has been accepted when dealing with granular materials, Herle (1997).

B.2 MOHR'S-COULOMB MODEL PARAMETERS

In ABAQUS, Mohr's-coulomb describes the yield surface of the plastic region of a material whose elastic region behavior is described by using the *ELASTIC option. ABAQUS Mohr's-coulomb parameters are; angle of internal

friction "φ" and angle of dilatancy "ψ_{mc}". The angle of internal friction "φ" is already defined from the Hypoplastic model parameters, table [5.2].

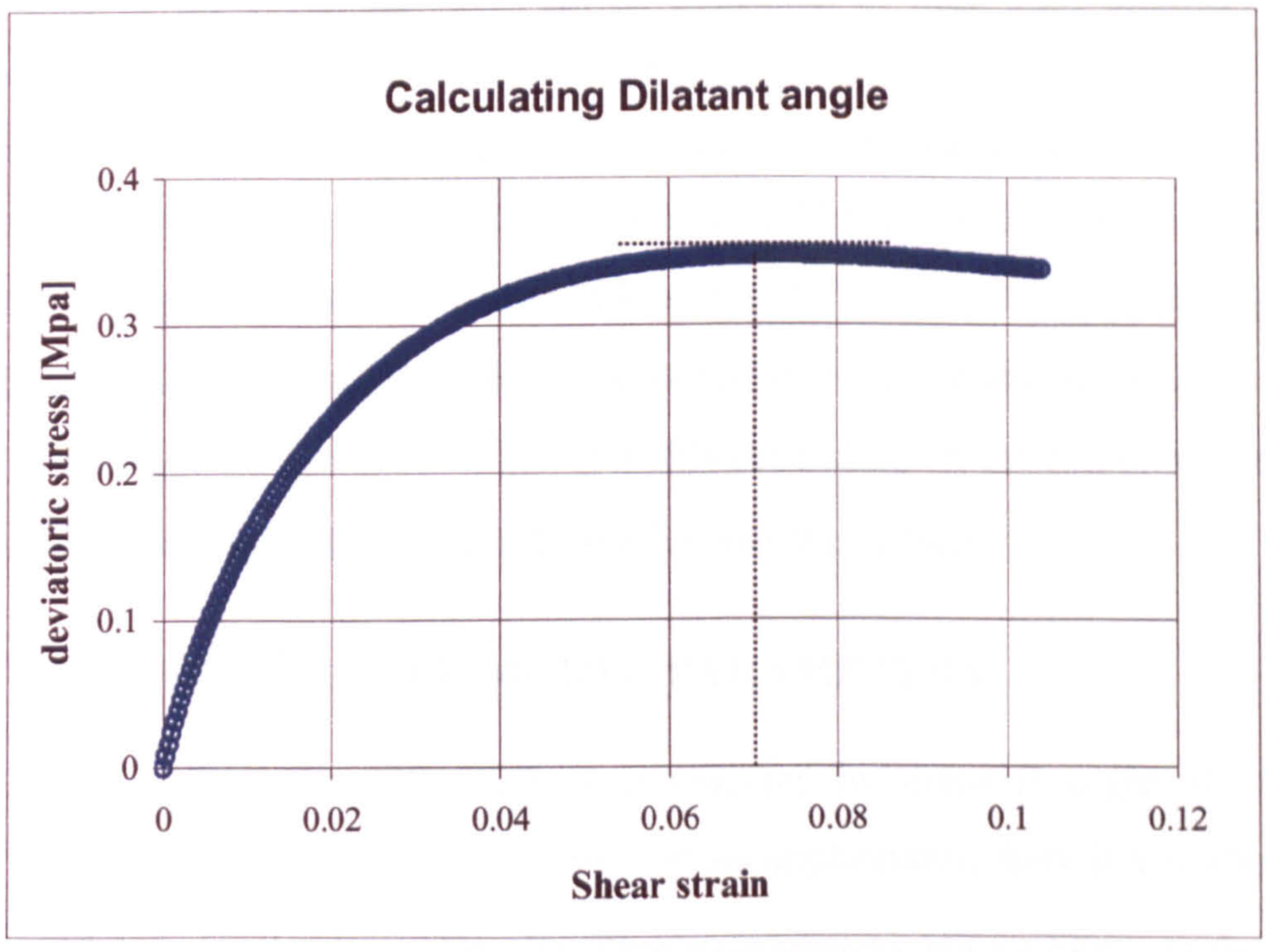

Figure (B.3) Deviatoric stress – Shear strain relation

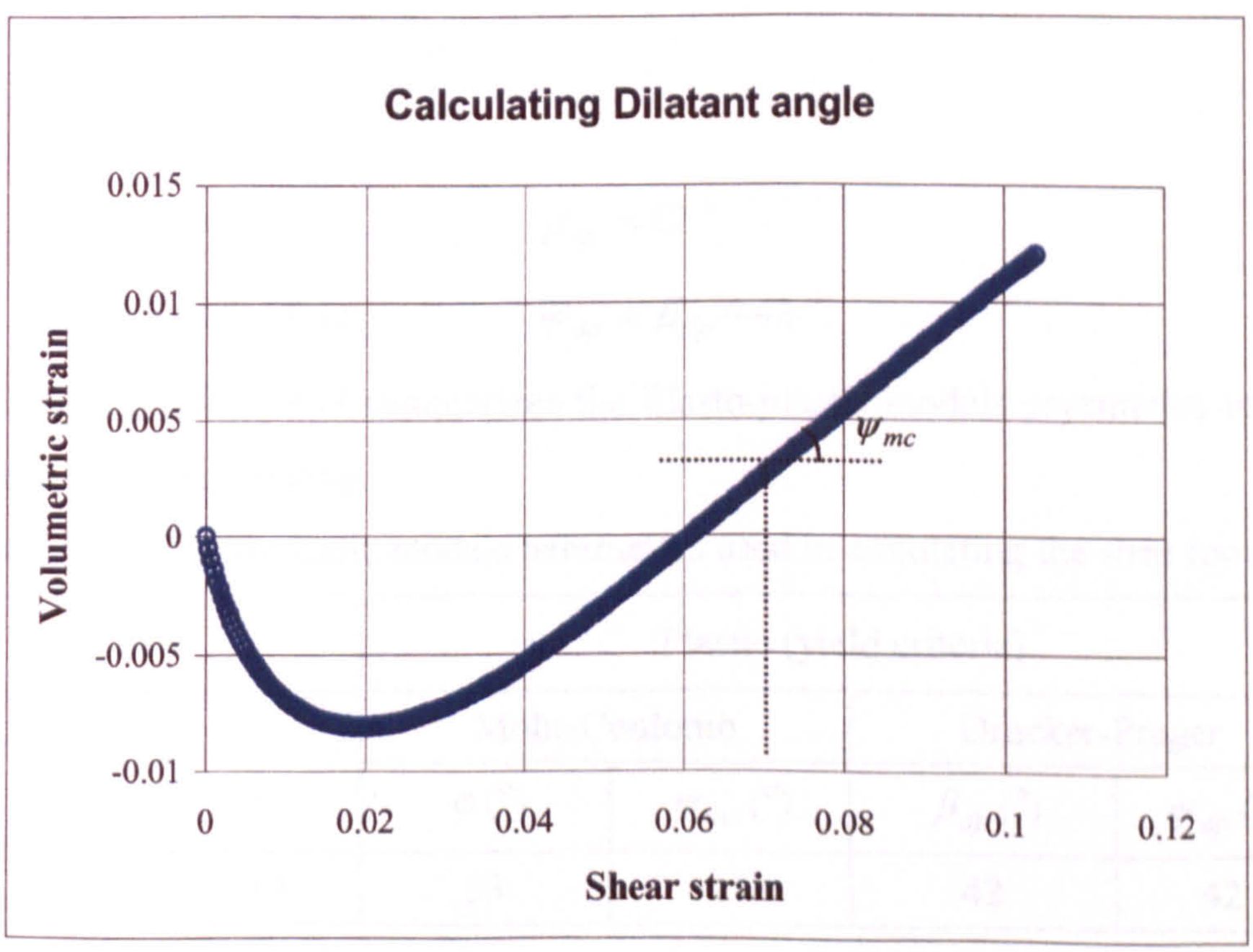

Figure (B.4) Volumetric strain – Shear strain relation

To determine ψ_{mc}, a numerical simulation of the triaxial test was carried out. The deviatoric stress - shear strain relationship was plotted in figure (B.3) from which a peak value of the deviatoric stress (as an indication of high sand dilatancy) was observed at 0.07 shear strain. Then the slope of the volumetric strain – shear strain diagram, shown in figure (B.4), was measured at the same shear strain value correspond to the peak deviatoric stress (i.e at 0.07 shear strain). This slope will present the angle of dilatancy "ψ_{mc}", Atkinson (1993), which found to be equal to 15°. Results from the triaxial test should be obtained at high confining pressure as the value of the angle of dilatancy "ψ_{mc}" is highly depending on the confining pressure or in other words on the stress level, Kolymbas and Wu (1990).

B.3 DRUCKER-PRAGER MODEL PARAMETERS

Drucker-Prager in ABAQUS is represented by material angle of friction "β_{dp}" and Dilation angle "ψ_{dp}". For plane strain applications, there is a relationship between Mohr's-Coulomb and Drucker-Prager parameters, HKS (2000), as shown in the following equations.

$$\tan(\beta_{dp}) = \frac{\sqrt{3}\sin\varphi}{\sqrt{1+\frac{1}{3}\sin^2\varphi}}$$

For $\varphi = 33$, $\beta_{dp} = 42^\circ$

For associated flow $\psi_{dp} = \beta_{dp} = 42^\circ$

The following table [B.1] summarizes the Elasto-plastic models parameters used in simulating the strip footing.

Table [B.1] Elasto-plastic models parameters used in simulating the strip footing

Elastic		Plastic (yield criteria)			
		Mohr-Coulomb		Drucker-Prager	
E (MPa)	ν	$\varphi(^\circ)$	$\psi_{mc}(^\circ)$	$\beta_{dp}(^\circ)$	$\psi_{dp}(^\circ)$
40	0.3	33	15	42	42

Appendix C

C.1 MESH DENSITY EFFECT ON STRIP-FOOTING SIMULATION

The following figure represents the relation between footing settlement, measured by the percentage of footing displacement to the total foundation simulated height, and the normal stress applied on the foundation measured at a node located just under the footing center for different mesh densities using the Mid-Point integration scheme to integrate the hypoplastic equation with sub-step size limit of '0.001'.

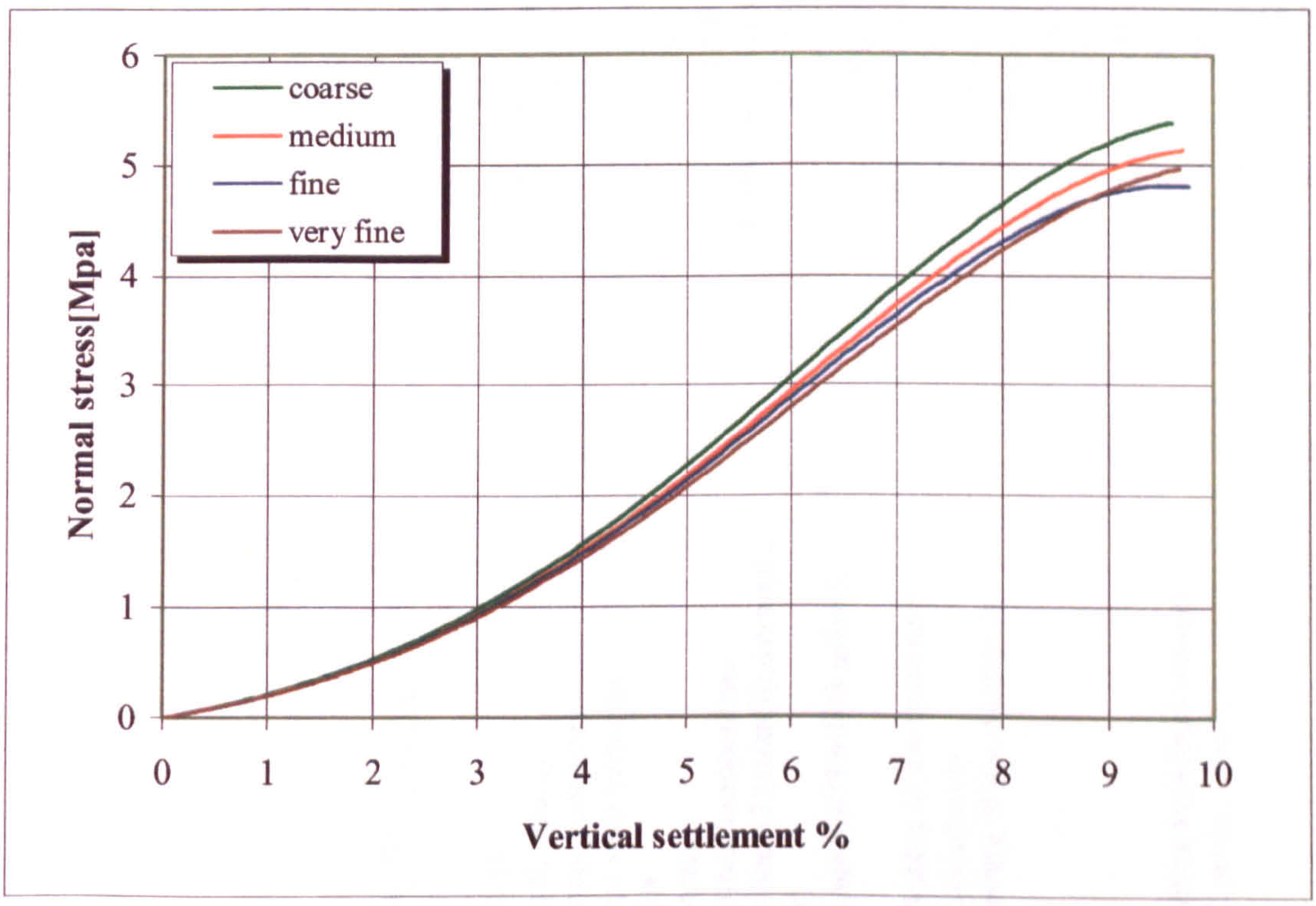

Figure (C.1) Effect of mesh density on simulating strip-footing using Mid-point

APPENDIX D

FORTRAN 77 CODES

D.1 RKF-65 FORTRAN 77 CODE

```
C   Hypoplastic integration using RKF-65
      INTEGER ntens, nstatv, nprops, ndi, nshr,i,j
C ntens:  Size of the stress or strain component array
C nstatv: Number of solution-dependent state variables
C nprops: Number of material constants
C ndi: Number of direct stress components
C nshr: Number of engineering shear stress components
      DOUBLE PRECISION stress(6),statev(2),stran(6),dstran(6),
     & pi, dtime, dat(8,10000), props(9)
      PARAMETER (ntens=6,nstatv=2,nprops=9,ndi=3,nshr=3,
     & pi=3.1415927d0)
C stress: Stress tensor array at the beginning of the increment
C statev: Solution-dependent state variables array
C stran: Total strains array at the beginning of the increment
C dstran: Array of strain increments
C dtime: Time increment
C dat: Data output array
C props: Array of material constants
C Opening data file 'stress' which contains the initial stresses
          OPEN (unit = 1, file = 'stress', status = 'old')
          DO 54 m=1, ntens
             READ *, stress(m)
 54    CONTINUE
          CLOSE (unit = 1)
C Opening data file 'stran' which contains the initial strain
          OPEN (unit = 1, file = 'stran', status = 'old')
          DO 55 m=1, ntens
             READ *, stran(m)
 55    CONTINUE
          CLOSE (unit = 1)
C Opening data file 'dstran' which contains strain increment
          OPEN (unit = 1, file = 'dstran', status = 'old')
          DO 56 m=1, ntens
             READ *, dstran(m)
 56    CONTINUE
          CLOSE (unit = 1)
C Opening data file 'props' which contains material properties
          OPEN (unit = 1, file = 'props', status = 'old')
          DO 57 j=1, nprops
            READ *, props(j)
 57       CONTINUE
          CLOSE (unit = 1)
C Opening data file 'stat' which contains solution dependant vaiables
          OPEN (unit = 1, file = 'stat', status = 'old')
          DO 58 j=1, nstatv
            READ *, statev(j)
 58       CONTINUE
          CLOSE (unit = 1)
          dtime = statev(2)
          props(1) = props(1)*( 2.d0 * pi / 360.d0 )
             dat(1,1)=stress(1)
             dat(2,1)=stress(2)
             dat(3,1)=stress(3)
             dat(7,1)=stran(1)
             dat(8,1)=statev(1)
C Calculating the stress increment using the Hypoplastic equations
       CALL sigma(stress,statev,stran,
     &     ndi,nshr,ntens,nstatv,props,dat,dstran)
```

```
      CLOSE (unit = 3)
C Opening data file 'dataplot.txt' and write output results
          OPEN (unit = 3, file = 'dataplot.txt', status = 'old')
                        i=1
                  WRITE (3,*) -dat(1,i),-dat(2,i),dat(7,i)*100,dat(8,i)
                        i=2
                  DO WHILE (abs(dat(1,i)).lt.0.32d3)
                        write (3,*) -dat(1,i),-dat(2,i),dat(7,i)*100,dat(8,i)
                        i=i+1
                  END DO
          CLOSE (unit = 3)
          STOP
          END
c ---------------------------------------------------------------------
      SUBROUTINE sigma(stress,statev,stran,ndi,
     & nshr,ntens,nstatv,props,dat,dstran)
c ---------------------------------------------------------------------
      INCLUDE 'ABA_PARAM.INC'
      INTEGER mdim, mprops,i
      DOUBLE PRECISION tol
      PARAMETER ( mdim=3, tol=1.0d-5,mprops=9 )
      LOGICAL error,null
      DOUBLE PRECISION stress(ntens),statev(nstatv),dstran(ntens),
     & stran(ntens), props(mprops), eold, edot, e, dtk, tk,
     & d(mdim,mdim), fj(7,3,3), bjl(7,6), dsegmj(3,3), dstr(3,3),
     & segmj(3,3), usk1(3,3), usk2(3,3), c1j(7), sub(3,3), rk, c2j(7),
     & told(3,3), normmat, dtime, dat(8,10000)

          dtime = statev(2)
          error = .false.
C Arrays initializing
      CALL zero(bjl,7*6)
      CALL zero(c1j,7)
      CALL zero(c2j,7)
      CALL zero(dsegmj,3*3)
      CALL zero(fj,7*3*3)
C Extract one column format to matrix format
      CALL extract( ndi, nshr, ntens, stress, dstran, dtime, told, d )
C Parameters of RKF-65 used in equation (4.32)
          bjl(2,1) = 0.2d0
          bjl(3,1) = 0.075d0
          bjl(4,1) = 0.97777777d0
          bjl(5,1) = 2.952598689d0
          bjl(6,1) = 2.846275252d0
          bjl(7,1) = 0.091145833d0
          bjl(3,2) = 0.225d0
          bjl(4,2) = -3.73333333d0
          bjl(5,2) = -11.5957933d0
          bjl(6,2) = 10.757575757d0
          bjl(7,2) = 0.d0
          bjl(4,3) = 3.555555555d0
          bjl(5,3) = 9.8228928516d0
          bjl(6,3) = 8.90642271d0
          bjl(7,3) = 0.449236298d0
          bjl(5,4) = -0.2908093278d0
          bjl(6,4) = 0.2784090909d0
          bjl(7,4) = 0.65104166666d0
          bjl(6,5) = -0.2735313036d0
          bjl(7,5) = -0.322376179245d0
          bjl(7,6) = 0.13095238095d0
C Parameters of RKF-65 used in equation (4.30)
          c1j(1) = 0.09114583333d0
          c1j(2) = 0.d0
          c1j(3) = 0.44923629829d0
          c1j(4) = 0.65104166666d0
          c1j(5) = -0.3223761792d0
          c1j(6) = 0.13095238095d0
          c1j(7) = 0.d0
C Parameters of RKF-65 used in equation (4.31)
          c2j(1) = 0.0902256944d0
          c2j(2) = 0.d0
```

```
      c2j(3) = 0.4534890685d0
      c2j(4) = 0.6140625d0
      c2j(5) = -0.27151238207d0
      c2j(6) = 0.089047619047d0
      c2j(7) = 0.025d0

      tk = 0.d0
      dtk = 1.d0
      rk=0.d0
      i = 2

    DO WHILE (tk.lt.1)
C Initial conditions
      eold = statev(1)
C New void ratio using equation (4.22)
      edot = ( 1.d0 + eold ) * tra( d )
 40   e = eold + edot *dtk*dtime
      statev(1) = e
      CALL mmult(dstr,d,dtime)
      CALL zero (dsegmj,3*3)
      CALL zero (fj,7*3*3)
          DO 53 j=1, 7
          DO 52 m=1, 3
            DO 51 n=1, 3
              DO 50 l=1, j-1
               dsegmj(m,n)=dsegmj(m,n)+bjl(j,l)*fj(l,m,n)
50            CONTINUE
              segmj(m,n) = told(m,n) + dtk*dsegmj(m,n)
51          CONTINUE
52          CONTINUE
            CALL getfj(error,segmj,dstr,e, fj, j, props)
            IF (error) THEN
            error = .false.
            IF (0.8d0*dtk*(tol/rk)**(1.d0/6.d0) .LT. 0.1d0*dtk) THEN
               dtk = 0.8d0*dtk*(tol/rk)**(1.d0/6.d0)
              ELSE
                dtk =0.1d0*dtk
              END IF
              GO TO 40
              END IF
53          CONTINUE
            CALL getusk(fj, usk1, c1j, told, dtk,6)
            CALL getusk(fj, usk2, c2j, told, dtk,7)
            CALL minus(usk2, usk1, sub,9)
            rk = normmat(sub)/normmat(usk2)
            IF (rk.EQ.0d0) THEN
              dtk=0.1d0*dtk
              GO TO 40
            END IF
           IF (rk.GT.tol) THEN
              IF (0.8d0*dtk*(tol/rk)**(1.d0/6.d0) .GT. 0.1d0*dtk) THEN
                 dtk = 0.8d0*dtk*(tol/rk)**(1.d0/6.d0)
              ELSE
                 dtk =0.1d0*dtk
              END IF
              GOTO 40
            END IF
            tk = tk + dtk
      CALL copy( usk2,told, mdim*mdim )
            IF (0.8d0*dtk*(tol/rk)**(1.d0/6.d0).LT. 2.d0*dtk) THEN
                dtk = 0.8d0*dtk*(tol/rk)**(1.d0/6.d0)
            ELSE
                dtk =2.d0*dtk
            END IF
            IF ( dtk .LT. (1.d0-tk)) THEN
            dtk =dtk
            else
            dtk = 1.d0-tk
            END IF
c     new stress in abaqus vector format
```

```
      CALL matvec( 3, 3, 6, told, stress )
            dat(7,i)=dat(7,i-1)+dstr(1,1)*dtk
            dat(8,i)=statev(1)
            j=1
            DO WHILE (j.le.6)
            dat(j,i)=stress(j)
            j=j+1
            END DO
             i = i+1
            END DO
      END
c -------------------------------------------------------------------
        SUBROUTINE getfj(error,ttheta,dstran,e, fj, j, props)
c -------------------------------------------------------------------
      LOGICAL error
      INTEGER mdim,mprops,j
      PARAMETER ( mdim=3, mprops=9 )
      DOUBLE PRECISION normmat, tra, power, tmp, fac,
     & a, f, tanpsi, cos3th, e, ei, ei0, ec, ec0, ed, ed0,
     & fe, fd, fb, hs, n, alfa, beta, phic,
     & ttheta(mdim,mdim), work2(mdim,mdim),fj(7,mdim,mdim),
     & that(mdim,mdim), thatdev(mdim,mdim),props(mprops),
     & inct(mdim,mdim), dstran(mdim,mdim), work1(mdim,mdim)
      LOGICAL null, negativ

c     von wolffersdorff, karlsruher sand, dimensions: [m], [n]
      phic = props(1)
      hs   = props(2)
      ec0  = props(3)
      ed0  = props(4)
      ei0  = props(5)
      n    = props(6)
      alfa = props(7)
      beta = props(8)

      CALL zero( inct, mdim*mdim )
      IF ( null( tra(ttheta) ) ) THEN
       error = .true.
       GOTO 100
      END IF
      CALL copy( ttheta, that, mdim*mdim )
      CALL mul( that, 1.d0/tra(ttheta), mdim*mdim )
      CALL dev( that, thatdev )
           tanpsi = sqrt(3.d0) * normmat( thatdev )
      CALL abc( thatdev, thatdev, work1 )
      CALL abc( thatdev, work1, work2 )
      IF ( tra(work1).lt.1.d-10  ) THEN
           cos3th = 1.d0
      else
       cos3th = -sqrt(6.d0)*tra(work2)/power(tra(work1),3.d0/2.d0)
           IF ( cos3th.lt.-1.d0 ) cos3th = -1.0d0
           IF ( cos3th.gt.+1.d0 ) cos3th = +1.0d0
      END IF
       a = ( sqrt(3.d0) * ( 3.d0 - sin(phic) ) ) /
     &   ( 2.d0 * sqrt(2.d0) * sin(phic) )
       tmp = tanpsi*tanpsi/8.d0 +
     &   (2.d0-tanpsi*tanpsi)/(2.d0+sqrt(2.d0)*tanpsi*cos3th)
       IF ( negativ( tmp ) ) THEN
        error = .true.
        GOTO 100
       END IF
       f = sqrt( tmp ) - tanpsi/(2.d0*sqrt(2.d0))
       IF ( negativ( -tra(ttheta) ) ) THEN
        error = .true.
        GOTO 100
       END IF
       tmp = exp(-power(-tra(ttheta)/hs,n) )
       ei = tmp * ei0
       ec = tmp * ec0
       ed = tmp * ed0
```

```
IF ( negativ( ec/e ) ) THEN
 error = .true.
 GOTO 100
END IF
fe = power( ec/e, beta )
IF ( null( ec-ed ) ) THEN
 error = .true.
 GOTO 100
END IF
tmp = (e-ed)/(ec-ed)
if ( tmp.gt.0.d0 ) then
  if (tmp.eq.1.d0) then
    fd = 1
  ELSE
  fd = power( (e-ed)/(ec-ed), alfa )
  END IF
ELSE
 fd = 0.d0
END IF
IF ( null( ei ) ) THEN
 error = .true.
 GOTO 100
END IF
IF ( negativ( ei0 ) ) THEN
 error = .true.
 GOTO 100
END IF
IF ( negativ( ec0 ) ) THEN
 error = .true.
 GOTO 100
END IF
IF ( null( ec0-ed0 ) ) THEN
 error = .true.
 GOTO 100
END IF
IF ( negativ( (ei0-ed0)/(ec0-ed0) ) ) THEN
 error = .true.
 GOTO 100
END IF
fb = ( hs/n ) * ( (1.d0+ei)/ei ) *
&   power(ei0/ec0,beta) * power(-tra(ttheta)/hs,1.d0-n) /
&   ( 3.d0 + a*a -
&     sqrt(3.d0)*a*power((ei0-ed0)/(ec0-ed0),alfa) )
CALL abc( that, that, work1 )
IF ( null( tra(work1) ) ) THEN
 error = .true.
 GOTO 100
END IF
fac = fb * fe / tra(work1)
tmp = fac * f * f
CALL addfac( inct, dstran, tmp, mdim*mdim )
CALL abc( that, dstran, work1 )
tmp = fac * a * a * tra( work1 )
CALL addfac( inct, that, tmp, mdim*mdim )
tmp = fac * fd * a * f * normmat( dstran )
CALL add( that, thatdev, work1, mdim*mdim )
CALL addfac( inct, work1, tmp, mdim*mdim )
      DO 16 m=1,3
       DO 17 l=1,3
       fj(j,m,l)=inct(m,l)
17      CONTINUE
16     CONTINUE
100 CONTINUE
      RETURN
      END
c ------------------------------------------------------------------
      SUBROUTINE getusk(fj, usk, cj, segmk, dtk,limit)
c ------------------------------------------------------------------
      INTEGER limit
c     to get the matrix fi using the values of the matrix fj
```

```
      DOUBLE PRECISION fj(7,3,3), usk(3,3), cj(7), segmk(3,3), dtk
       DO 18 m=1 ,3
         DO 19 n=1, 3
              usk(m,n) = 0
           DO 20 j=1, limit
             usk(m,n) = usk(m,n) + cj(j) * fj(j,m,n)
20             CONTINUE
           usk(m,n) = usk(m,n)*dtk + segmk(m,n)
19       CONTINUE
18     CONTINUE
       RETURN
       END
c ---------------------------------------------------------------
       SUBROUTINE mmult(a,b,c)
c ---------------------------------------------------------------
       DOUBLE PRECISION a(3,3), b(3,3),c
       DO 10 m=1 ,3
         DO 20 n=1 ,3
           a(m,n)=b(m,n)*c
20       CONTINUE
10     CONTINUE
       RETURN
       END
c ---------------------------------------------------------------
   SUBROUTINE abc( a, b, c )
c ---------------------------------------------------------------
   INTEGER mdim
   PARAMETER ( mdim=3 )
   INTEGER idi, jdi, kdi
   DOUBLE PRECISION a(mdim,mdim), b(mdim,mdim), c(mdim,mdim)
   DO 30, idi=1,3
    DO 20, jdi=1,3
     c(idi,jdi) = 0.0d0
     DO 10, kdi=1,3
      c(idi,jdi) = c(idi,jdi) + a(idi,kdi)*b(kdi,jdi)
10     CONTINUE
20   CONTINUE
30 CONTINUE
   END
c ---------------------------------------------------------------
   subroutine add( a, b, c, n )
c ---------------------------------------------------------------
   INTEGER i, n
   DOUBLE PRECISION a(n), b(n), c(n)
   DO 10, i = 1, n
    c(i) = a(i) + b(i)
10 CONTINUE
   end
c ---------------------------------------------------------------
   SUBROUTINE addfac( tot, inc, factor, n )
c ---------------------------------------------------------------
   INTEGER i, n
   DOUBLE PRECISION factor, tot(n), inc(n)
   DO 10, i = 1, n
    tot(i) = tot(i) + factor * inc(i)
10 CONTINUE
   END
c ---------------------------------------------------------------
   SUBROUTINE copy( a, b, n )
c ---------------------------------------------------------------
   INTEGER i, n
   DOUBLE PRECISION a(n), b(n)
   DO 10, i = 1, n
    b(i) = a(i)
10 CONTINUE
   END
c ---------------------------------------------------------------
   SUBROUTINE dev( a, adev )
c ---------------------------------------------------------------
   INTEGER mdim
```

```
      PARAMETER ( mdim=3 )
      INTEGER idi, jdi
      DOUBLE PRECISION tmp, tra, a(mdim,mdim), adev(mdim,mdim)
      tmp = tra( a )
      DO 20, idi = 1, mdim
       DO 10, jdi = 1, mdim
        adev(idi,jdi) = a(idi,jdi)
   10  CONTINUE
       adev(idi,idi) = adev(idi,idi)-tra(a)/3.0d0
   20 CONTINUE
      END
c ------------------------------------------------------------------
      SUBROUTINE extract( ndi, nshr, ntens, stress, dstr, dt,
     & told, d )
c ------------------------------------------------------------------
      INTEGER mdim
      PARAMETER ( mdim=3 )
      INTEGER idi, ndi, nshr, ntens
      DOUBLE PRECISION dt, stress(ntens), dstr(ntens),
     & told(mdim,mdim), d(mdim,mdim)
      CALL vecmat( ndi, nshr, ntens, stress, told )
      CALL zero( d, mdim*mdim )
      DO 10, idi=1,ndi
       d(idi,idi) = dstr(idi)/dt
   10 CONTINUE
          d(2,2)=0.d0
          d(3,3)=0.d0
      IF ( nshr.GE.1 ) THEN
       d(1,2) = 0.5d0*dstr(ndi+1)/dt
       d(2,1) = d(1,2)
      END IF
      IF ( nshr.GE.2 ) THEN
       d(1,3) = 0.5d0*dstr(ndi+2)/dt
       d(3,1) = d(1,3)
      END IF
      IF ( nshr.GE.3 ) then
       d(2,3) = 0.5d0*dstr(ndi+3)/dt
       d(3,2) = d(2,3)
      END IF
      END
c ------------------------------------------------------------------
      SUBROUTINE matvec( ndi, nshr, ntens, mat, vec )
c ------------------------------------------------------------------
      INTEGER mdim
      PARAMETER ( mdim=3 )
      INTEGER idi, ndi, nshr, ntens
      DOUBLE PRECISION vec(ntens), mat(mdim,mdim)
      DO 10, idi = 1, ndi
       vec(idi) = mat(idi,idi)
   10 CONTINUE
      IF ( nshr.GE.1 ) vec(ndi+1) = mat(1,2)
      IF ( nshr.GE.2 ) vec(ndi+2) = mat(1,3)
      IF ( nshr.GE.3 ) vec(ndi+3) = mat(2,3)
      END
c ------------------------------------------------------------------
      SUBROUTINE minus( a, b, c, n )
c ------------------------------------------------------------------
      INTEGER i, n
      DOUBLE PRECISION a(n), b(n), c(n)
      DO 10, i = 1, n
       c(i) = a(i) - b(i)
   10 CONTINUE
      END
c ------------------------------------------------------------------
      SUBROUTINE mul( a, scal, n )
c ------------------------------------------------------------------
      INTEGER n
      DOUBLE PRECISION scal, a(n)
      DO 10, i = 1, n
       a(i) = scal * a(i)
```

```
 10 CONTINUE
    END


c ---------------------------------------------------------------------
    LOGICAL FUNCTION negativ( x )
c ---------------------------------------------------------------------
    DOUBLE PRECISION x
    IF ( x.LT.1.e-8 ) THEN
     negativ = .true.
    ELSE
     negativ = .false.
    END IF
    END
c ---------------------------------------------------------------------
    DOUBLE PRECISION FUNCTION normmat( a )
c ---------------------------------------------------------------------
    INTEGER mdim
    PARAMETER ( mdim=3 )
    DOUBLE PRECISION tra, a(mdim,mdim), work(mdim,mdim)
    CALL abc( a, a, work )
    normmat = sqrt( tra(work) )
    END
c ---------------------------------------------------------------------
    DOUBLE PRECISION FUNCTION normvec( a, n )
c ---------------------------------------------------------------------
    INTEGER i, n
    DOUBLE PRECISION a(n)
    normvec = 0.d0
    DO 10, i = 1, n
     normvec = normvec + a(i) * a(i)
  10 CONTINUE
    normvec = sqrt( normvec )
    END
c ---------------------------------------------------------------------
    LOGICAL FUNCTION null( x )
c ---------------------------------------------------------------------
    DOUBLE PRECISION x
    IF ( abs(x).lt.1.e-8 ) THEN
     null = .true.
    ELSE
     null = .false.
    END IF
    END
c ---------------------------------------------------------------------
    DOUBLE PRECISION FUNCTION power( x, y )
c ---------------------------------------------------------------------
    DOUBLE PRECISION x, y
    power = x ** y
    END
c ---------------------------------------------------------------------
    DOUBLE PRECISION FUNCTION tra( a )
c ---------------------------------------------------------------------
    INTEGER mdim
    PARAMETER ( mdim=3 )
    DOUBLE PRECISION a(mdim,mdim)
    tra = a(1,1) + a(2,2) + a(3,3)
    END
c ---------------------------------------------------------------------
    SUBROUTINE vecmat( ndi, nshr, ntens, vec, mat )
c ---------------------------------------------------------------------
    INTEGER mdim
    PARAMETER( mdim=3 )
    INTEGER idi, ndi, nshr, ntens
    DOUBLE PRECISION vec(ntens), mat(mdim,mdim)
    CALL zero( mat, mdim*mdim )
    DO 10, idi = 1, ndi
     mat(idi,idi) = vec(idi)
  10 CONTINUE
```

```
      IF (nshr.ge.1) THEN
        mat(1,2) = vec(ndi+1)
        mat(2,1) = mat(1,2)
      END IF
      IF (nshr.ge.2) THEN
        mat(1,3) = vec(ndi+2)
        mat(3,1) = mat(1,3)
      END IF
      IF (nshr.ge.3) THEN
        mat(2,3) = vec(ndi+3)
        mat(3,2) = mat(2,3)
      END IF
      END
c ------------------------------------------------------------------
      SUBROUTINE zero( a, n )
c ------------------------------------------------------------------
      INTEGER i, n
      DOUBLE PRECISION a(n)
      DO 10, i = 1, n
        a(i) = 0.0d0
   10 CONTINUE
      END
c ------------------------------------------------------------------
      SUBROUTINE eigen( sigmat, eigval )
c ------------------------------------------------------------------
      INTEGER mdim
      DOUBLE PRECISION pi
      PARAMETER ( mdim=3, pi=3.14159297943115 23d0 )
      DOUBLE PRECISION sigmat(mdim,mdim), eigval(mdim)
      DOUBLE PRECISION i1, i2, i3, r, s, t, p, q,
     $ bigr, phi, y0, y1, y2, tmp, inv(mdim)
      CALL invar( sigmat, inv )
      i1 = inv(1)
      i2 = inv(2)
      i3 = inv(3)
      r = -i1
      s = +i2
      t = -i3
      p = (3.d0*s-r*r)/3.d0
      q = 2.d0*r*r*r/27.d0 - r*s/3.d0 + t
      IF ( abs(q).LT.1.d-10 ) THEN
        y0 = -sqrt(abs(p))
        y1 = +sqrt(abs(p))
        y2 = 0.d0
      ELSE
        bigr = sqrt(abs(p)/3.d0)
        IF ( q.LT.0.d0 ) bigr = -bigr
        tmp = q/(2.d0*bigr*bigr*bigr)
        IF ( tmp.LT.-1.d0 ) tmp = -1.d0
        IF ( tmp.GT.+1.d0 ) tmp = +1.d0
        phi = acos(tmp)
        y0 = -2.d0*bigr*cos(phi/3.d0)
        y1 = -2.d0*bigr*cos(phi/3.d0+2.d0*pi/3.d0)
        y2 = -2.d0*bigr*cos(phi/3.d0+4.d0*pi/3.d0)
      END IF
      eigval(1) = y0 - r/3.d0
      eigval(2) = y1 - r/3.d0
      eigval(3) = y2 - r/3.d0
      END
c ------------------------------------------------------------------
      SUBROUTINE invar( sigmat, inv )
c ------------------------------------------------------------------
      INTEGER mdim
      PARAMETER ( mdim=3 )
      DOUBLE PRECISION sigmat(mdim,mdim), inv(mdim)
      inv(1) = sigmat(1,1) + sigmat(2,2) + sigmat(3,3)
      inv(2) = sigmat(1,1)*sigmat(2,2) + sigmat(2,2)*sigmat(3,3) +
     &         sigmat(3,3)*sigmat(1,1) - sigmat(1,2)*sigmat(2,1) -
     &         sigmat(2,3)*sigmat(3,2) - sigmat(3,1)*sigmat(1,3)
      CALL determ( sigmat, inv(3) )
```

```
      END
c -----------------------------------------------------------------------
      SUBROUTINE determ( a, det )
c -----------------------------------------------------------------------
      INTEGER mdim
      PARAMETER ( mdim=3 )
      DOUBLE PRECISION a(mdim,mdim), det
      det = a(1,1)*(a(2,2)*a(3,3)-a(3,2)*a(2,3)) -
     &      a(1,2)*(a(2,1)*a(3,3)-a(3,1)*a(2,3)) +
     &      a(1,3)*(a(2,1)*a(3,2)-a(3,1)*a(2,2))
      END
```

D.2 UMAT SUBROUTINE

UMAT is a powerful user defined subroutine tool provided by ABAQUS. Using this subroutine enables ease implementation of a constitutive model to describe material laws that may not included in the main ABAQUS package.

The following steps are required to write up a UMAT subroutine:

1. Explicit definition of stress
2. Definition of internal state variables
3. Transformation of the constitutive rate equation into an incremental equation using a suitable integration procedure such as Euler forward or RKF
4. Calculation of the Jacobian
5. Coding the UMAT in FORTRAN or C programming languages

In the following section, a UMAT subroutine used to implement the hypoplastic model is described. This subroutine was programmed by Dennis Roddeman, Roddeman (1997) and modified to be suitable for describing monotonic loading of soil-tool interaction.

```
c ------------------------------------------------------------------
      SUBROUTINE UMAT(STRESS,STATEV,DDSDDE,SSE,SPD,SCD,
     & RPL,DDSDDT,DRPLDE,DRPLDT, STRAN,DSTRAN,TIME,
     & DTIME,TEMP,DTEMP,PREDEF,DPRED,CMNAME, NDI,NSHR,
     & NTENS,NSTATV,PROPNNS,NPROPS,COORDS,DROT,PNEWDT,
     & LENT,DFGRD0,DFGRD1,NOEL,NPT,LAYER,KSPT,KSTEP,KINC)
c ------------------------------------------------------------------
      INCLUDE 'ABA_PARAM.INC'

      INTEGER MTENS, MSTATV
      DOUBLE PRECISION DELTA, EPS_SUB
      PARAMETER( MTENS=6, MSTATV=100, DELTA=-1.D-3,
     & EPS_SUB=0.1D0, EPS_SIG=1.D-1, EPS_DT=1.D-6)

      CHARACTER*80 CMNAME
      DOUBLE PRECISION STRESS(NTENS),STATEV(NSTATV),
     & DDSDDE(NTENS,NTENS),DDSDDT(NTENS),DRPLDE(NTENS),
     & STRAN(NTENS),DSTRAN(NTENS),TIME(2),PREDEF(1),
     & DPRED(1), PROPS(NPROPS),COORDS(3),DROT(3,3),
     & DFGRD0(3,3), DFGRD1(3,3)

      INTEGER ITENS, JTENS
      DOUBLE PRECISION NORMVEC, DT, DT_TOT,DTIME,
     & EOLD, DSTRAN0(MTENS), STRESS0(MTENS),
     & STATEV0(MSTATV), WORK1(MTENS), DSTR(MTENS),
     & WORK2(MTENS)
      LOGICAL ERROR
```

Printing current increment number and the corresponding total time taken from the first increment to the current increment.

```
      PRINT *, KINC, TIME(2)
```

Define initial value of the principle stresses to start hypoplastic calculations

```
      IF (KINC .LT. 1) THEN
      GOTO 211
      END IF
      IF (KINC .LT. 2 .AND. KSTEP .EQ. 1) THEN
            STRESS(1) = -5.D-8
            STRESS(2) = -1.D-7
            STRESS(3) = -5.D-8
      END IF
```

Initiate the loop control of the MAIN routine, figure (4.10)

```
    DT = DTIME
    DT_TOT = 0.D0
    DO WHILE (DT_TOT .LT. DTIME)
adjust, if required, last sub-step size
     IF (DT .GT. (DTIME-DT_TOT)) DT = DTIME - DT_TOT
adjust strain for sub-stepping
      CALL COPY(DSTRAN, DSTR, NTENS )
      CALL MUL(DSTR, DT/DTIME, NTENS )
remember from last sub-step
       EOLD = STATEV(1)
       IF ( EOLD.LE.0.D0 ) THEN
        PRINT *, 'ILLEGAL POROSITY DETECTED IN UMAT'
       END IF
       CALL COPY( STRESS, WORK1, NTENS )
```

Calculate new stress using subroutine SIGMA, figure (4.11)

```
       ERROR = .FALSE.
       CALL SIGMA(ERROR, STRESS,STATEV,DDSDDE,SSE,SPD, SCD,
     & RPL,DDSDDT,DRPLDE,DRPLDT, STRAN,DSTR,TIME, DT,TEMP,
     & DTEMP,PREDEF,DPRED,CMNAME, NDI,NSHR,NTENS,NSTATV,
     & PROPS,NPROPS,COORDS,DROT,PNEWDT, CELENT,
     & DFGRD0,DFGRD1,NOEL,NPT,LAYER,KSPT,KSTEP,KINC)
       IF ( ERROR ) THEN
        IF ( DT.GE.2.D0*EPS_DT*DTIME ) THEN
         DT = DT / 2.D0
         STATEV(1) = EOLD
         CALL COPY( WORK1, STRESS, NTENS )
        ELSE
         GOTO 210
        END IF
       ELSE
        CALL MINUS( STRESS, WORK1, WORK2, NTENS )
        IF  NORMVEC(WORK2,NTENS).GT.EPS_SUB*
     &       NORMVEC(STRESS,NTENS)
     &      .AND. NORMVEC(STRESS,NTENS).GT.EPS_SIG
     &      .AND. DT.GE.2.D0*EPS_DT*DTIME ) THEN
         DT = DT / 2.D0
         STATEV(1) = EOLD
         CALL COPY( WORK1, STRESS, NTENS )
        ELSE
         DT_TOT = DT_TOT + DT
        END IF
       END IF
      END DO
 210   CONTINUE
store stuff
 211  CALL COPY( DSTRAN, DSTRAN0, NTENS )
      CALL COPY( STRESS, STRESS0, NTENS )
      CALL COPY( STATEV, STATEV0, NSTATV )
```

Calculating the Jacobian matrix with central differences

```
    DO 100, JTENS = 1, NTENS
first differentiation point
      CALL COPY( STRESS0, STRESS, NTENS )
      CALL COPY( STATEV0, STATEV, NSTATV )
      CALL ZERO( DSTRAN, NTENS )
```

```
      DSTRAN(JTENS) = DSTRAN(JTENS) - DELTA
      CALL SIGMA(ERROR,
     &   STRESS,STATEV,DDSDDE,SSE,SPD,SCD, RPL,DDSDDT,
     &   DRPLDE,DRPLDT, STRAN,DSTRAN,TIME,DTIME,TEMP,
     &   DTEMP,PREDEF,DPRED,CMNAME, NDI,NSHR,NTENS,
     &   NSTATV,PROPS,NPROPS,COORDS,DROT,PNEWDT, CELENT,
     &   DFGRD0,DFGRD1,NOEL,NPT,LAYER,KSPT,KSTEP,KINC)
      CALL COPY( STRESS, WORK1, NTENS )
```
second differentiation point
```
      CALL COPY( STRESS0, STRESS, NTENS )
      CALL COPY( STATEV0, STATEV, NSTATV )
      DSTRAN(JTENS) = DSTRAN(JTENS) + 2.D0 * DELTA
      CALL SIGMA(ERROR,
     &   STRESS,STATEV,DDSDDE,SSE,SPD,SCD, RPL,DDSDDT,
     &   DRPLDE,DRPLDT, STRAN,DSTRAN,TIME,DTIME,TEMP,
     &   DTEMP,PREDEF,DPRED,CMNAME, NDI,NSHR,NTENS,
     &   NSTATV,PROPS,NPROPS,COORDS,DROT,PNEWDT, CELENT,
     &   DFGRD0,DFGRD1,NOEL,NPT,LAYER,KSPT,KSTEP,KINC)
      CALL COPY( STRESS, WORK1, NTENS )
      CALL COPY( STRESS, WORK2, NTENS )
```
Calculate the Jacobian matrix
```
      DO 90, ITENS = 1, NTENS
       DDSDDE(ITENS,JTENS) = ( WORK2(ITENS) - WORK1(ITENS) ) /
     &    ( 2.D0 * DELTA )
  90  CONTINUE
 100  CONTINUE
```
restore stuff
```
      CALL COPY( DSTRAN0, DSTRAN, NTENS )
      CALL COPY( STRESS0, STRESS, NTENS )
      CALL COPY( STATEV0, STATEV, NSTATV )
      END
```

Subroutine SIGMA for integration the hypoplastic equation using Euler integration schemes

```
c -----------------------------------------------------------------
      SUBROUTINE SIGMA(ERROR,STRESS,STATEV,DDSDDE,SSE,
     & SPD,SCD, RPL,DDSDDT,DRPLDE,DRPLDT,STRAN,DSTR,
     & TIME,DT,TEMP,DTEMP,PREDEF,DPRED,CMNAME, NDI,NSHR,
     & NTENS,NSTATV,PROPS,NPROPS,COORDS,DROT,PNEWDT,
     & CELENT,DFGRD0,DFGRD1,NOEL,NPT,LAYER,KSPT,KSTEP,
     & KINC)
c -----------------------------------------------------------------
```
time integration:
THETA=0 is euler explicit
THETA=0.5 is the midpoint rule
THETA=1 is euler implicit

```
      INTEGER MDIM, MITER
      DOUBLE PRECISION PI, EPS_ITER, THETA
      PARAMETER (MDIM=3, MITER=1000, PI=3.1415927D0,
     & EPS_ITER=1.0D-4,THETA=0.D0, EPS_SIG=1.D-4)

      CHARACTER*80 CMNAME
      LOGICAL ERROR
      DOUBLE PRECISION STRESS(NTENS),STATEV(NSTATV),
     & DDSDDE(NTENS,NTENS),DDSDDT(NTENS),DRPLDE(NTENS),
     & STRAN(NTENS),DSTR(NTENS),TIME(2),DT,PREDEF(1),
     & DPRED(1), PROPS(NPROPS),COORDS(3),DROT(3,3),
     & DFGRD0(3,3),DFGRD1(3,3)

      INTEGER ITER, ITENS
      DOUBLE PRECISION NORMMAT, TRA, POWER, TMP, FAC,
     & EOLD, EDOT,A, COS3TH, E, EI, EI0, EC, EC0, ED, ED0,
     & FE, FD, FB, HS, N, ALFA, BETA, PHIC, COHESION,
     & TMIN, TMAX, PHIMOB, EIGVAL(MDIM), TNEW(MDIM,MDIM),
     & TOLD(MDIM,MDIM), TTHETA(MDIM,MDIM),
     & THAT(MDIM,MDIM), THATDEV(MDIM,MDIM),
     & INCT(MDIM,MDIM), D(MDIM,MDIM), WORK1(MDIM,MDIM),
     & WORK2(MDIM,MDIM)
```

```
      LOGICAL MYNULL, NEGATIV

         COHESION = 0.D0
         PHIC = PROPS(1)
         HS   = PROPS(2)
         EC0  = PROPS(3)
         ED0  = PROPS(4)
         EI0  = PROPS(5)
         N    = PROPS(6)
         ALFA = PROPS(7)
         BETA = PROPS(8)
*add the cohesion for cohesive soils
         IF (NPROPS.GT. 8) THEN
         COHESION = PROPS(9)
         END IF
*initial conditions
      EOLD = STATEV(1)
      CALL EXTRACT( NDI, NSHR, NTENS, STRESS, DSTR, DT, TOLD,
     & D )
*new void ratio using equation (4.22)
      EDOT = (1.D0 + EOLD) * TRA( D )
      E = EOLD + EDOT * DT
      STATEV(1) = E
      CALL COPY( TOLD, TTHETA, MDIM*MDIM )
      DO 100, ITER = 1, MITER
*subtract the cohesion (if any) to get hypoplastic law for cohesion
       DO ITENS = 1, NDI
        TTHETA(ITENS,ITENS) = TTHETA(ITENS,ITENS) - COHESION
       ENDDO
       CALL ZERO( INCT, MDIM*MDIM )
       IF ( MYNULL( TRA(TTHETA) ) ) THEN
        ERROR = .TRUE.
        GOTO 200
       END IF
*Calculating the stress increment using the hypoplastic equation (4.9)
      CALL COPY( TTHETA, THAT, MDIM*MDIM )
      CALL MUL( THAT, 1.D0/TRA(TTHETA), MDIM*MDIM )
      CALL DEV( THAT, THATDEV )
      TANPSI = SQRT(3.D0) * NORMMAT( THATDEV )
      CALL ABC( THATDEV, THATDEV, WORK1 )
      CALL ABC( THATDEV, WORK1, WORK2 )
      IF ( TRA(WORK1).LT.1.D-10 ) THEN
       COS3TH = 1.D0
      ELSE
       COS3TH = - SQRT(6.D0)*TRA(WORK2)/
     &              POWER(TRA(WORK1),3.D0/2.D0)
        IF ( COS3TH.LT.-1.D0 ) COS3TH = -1.0D0
        IF ( COS3TH.GT.+1.D0 ) COS3TH = +1.0D0
      END IF

       TMP = ((8.D0/3.D0)- 3.D0*NORMMAT(WORK1)+
     &   (SQRT(3.D0/2.D0)*
     &   NORMMAT(WORK2)*COS3TH))/(1.D0+SQRT(3.D0/2.D0)*
     &   NORMMAT(THATDEV)*COS3TH)
       IF ( NEGATIV( TMP ) ) THEN
        ERROR = .TRUE.
        GOTO 200
       END IF
       A = ( SQRT(TMP) -NORMMAT(THATDEV))*SIN(PHIC)/
     &   ( 3.D0 - SIN(PHIC) )
       IF ( NEGATIV( -TRA(TTHETA) ) ) THEN
        ERROR = .TRUE.
        GOTO 200
       END IF
       TMP = EXP(-POWER(-TRA(TTHETA)/HS,N) )
       EI = TMP * EI0
       EC = TMP * EC0
       ED = TMP * ED0
```

```
IF ( NEGATIV( EC/E ) ) THEN
 ERROR = .TRUE.
 GOTO 200
END IF
FE = POWER( EI/E, BETA )
IF ( MYNULL( EC-ED ) ) THEN
 ERROR = .TRUE.
 GOTO 200
END IF
TMP = (E-ED)/(EC-ED)
IF ( TMP.GT.0.D0 ) THEN
            IF ( TMP .EQ. 1.D0 ) THEN
                  FD = 1.D0
            ELSE
 FD = POWER( (E-ED)/(EC-ED), ALFA )
            END IF
ELSE
 FD = 0.D0
END IF
IF ( MYNULL( EI ) ) THEN
 ERROR = .TRUE.
 GOTO 200
END IF
IF ( NEGATIV( EI0 ) ) THEN
 ERROR = .TRUE.
 GOTO 200
END IF
IF ( NEGATIV( EC0 ) ) THEN
 ERROR = .TRUE.
 GOTO 200
END IF
IF ( MYNULL( EC0-ED0 ) ) THEN
 ERROR = .TRUE.
 GOTO 200
END IF
 IF ( NEGATIV( (EI0-ED0)/(EC0-ED0) ) ) THEN
  ERROR = .TRUE.
  GOTO 200
 END IF
 FB = ( HS/N ) * ( (1.D0+EI)/EI ) *
&   POWER(-TRA(TTHETA)/HS,1.D0-N) /
&   ( 3.D0 *A*A +1-
&    SQRT(3.D0)*A*POWER((EI0-ED0)/(EC0-ED0),ALFA) )

  CALL ABC( THAT, THAT, WORK1 )
 IF ( MYNULL( TRA(WORK1) ) ) THEN
  ERROR = .TRUE.
  GOTO 200
 END IF
 FAC = FB * FE / TRA(WORK1)

 TMP = FAC * A * A * DT
 CALL ADDFAC( INCT, D, TMP, MDIM*MDIM )

    CALL ABC( THAT, D, WORK1 )
    TMP = FAC * TRA( WORK1 ) * DT
    CALL ADDFAC( INCT, THAT, TMP, MDIM*MDIM )

    TMP = FAC * FD * A * NORMMAT( D ) * DT
    CALL ADD( THAT, THATDEV, WORK1, MDIM*MDIM )
    CALL ADDFAC( INCT, WORK1, TMP, MDIM*MDIM )
```

Green-Nagadi deformation tensor for large shear as stated in section (4.5.2)

```
    CALL GETW(DFGRD0,DFGRD1,DT,WW)
    CALL NEWINCT(INCT,TTHETA,WW)
```

add cohesion to restore real stresses

```
    DO ITENS = 1, NDI
```

```
      TTHETA(ITENS,ITENS) = TTHETA(ITENS,ITENS) + COHESION
     ENDDO

store old ttheta (stress increment)
     CALL COPY( TTHETA, WORK1, MDIM*MDIM )

calculate new ttheta
     CALL COPY( TOLD, TTHETA, MDIM*MDIM )
     CALL ADDFAC( TTHETA, INCT, THETA, MDIM*MDIM )

calculate change in ttheta
     CALL MINUS( TTHETA, WORK1, WORK2, MDIM*MDIM )

stop iterating if change in ttheta is small
     IF ( NORMMAT(WORK2) .LT. EPS_ITER*NORMMAT(TTHETA) )
GOTO 110

stop iterating if ttheta is small
     IF ( NORMMAT(TTHETA) .LT. EPS_SIG ) GOTO 110

 also stop iterating if euler explicit
     IF ( THETA.EQ.0.D0 ) GOTO 110

 100  CONTINUE
 110  CONTINUE

    IF ( ITER.GE.MITER ) THEN
     ERROR = .TRUE.
     GOTO 200
    END IF

Calculate new stress
    CALL COPY( TOLD, TNEW, MDIM*MDIM )
    CALL ADD( INCT, TNEW, TNEW, MDIM*MDIM )

new stress in abaqus vector format
    CALL MATVEC( NDI, NSHR, NTENS, TNEW, STRESS )
 200 CONTINUE
    END
```

Utilities subroutines used through the MAIN subroutine and SIGMA subroutine

```
c ------------------------------------------------------------------
Multiplying two matrixes A and B, the result goes to C
    SUBROUTINE ABC( A, B, C )
c ------------------------------------------------------------------
    INTEGER MDIM
    PARAMETER ( MDIM=3 )
    INTEGER IDI, JDI, KDI
    DOUBLE PRECISION A(MDIM,MDIM), B(MDIM,MDIM),
C(MDIM,MDIM)
    DO 30, IDI=1,3
     DO 20, JDI=1,3
      C(IDI,JDI) = 0.0D0
      DO 10, KDI=1,3
       C(IDI,JDI) = C(IDI,JDI) + A(IDI,KDI)*B(KDI,JDI)
 10    CONTINUE
 20   CONTINUE
 30  CONTINUE
    END
c ------------------------------------------------------------------
Add one column matrix A and B, result goes to C
    SUBROUTINE ADD( A, B, C, N )
c ------------------------------------------------------------------
    INTEGER I, N
    DOUBLE PRECISION A(N), B(N), C(N)
    DO 10, I = 1, N
     C(I) = A(I) + B(I)
```

```
 10 CONTINUE
    END
c -------------------------------------------------------------
    SUBROUTINE ADDFAC( TOT, INC, FACTOR, N )
c -------------------------------------------------------------
    INTEGER I, N
    DOUBLE PRECISION FACTOR, TOT(N), INC(N)
    DO 10, I = 1, N
     TOT(I) = TOT(I) + FACTOR * INC(I)
 10 CONTINUE
    END
c -------------------------------------------------------------
    SUBROUTINE COPY( A, B, N )
c -------------------------------------------------------------
    INTEGER I, N
    DOUBLE PRECISION A(N), B(N)
    DO 10, I = 1, N
     B(I) = A(I)
 10 CONTINUE
    END
c -------------------------------------------------------------
Calculating a matrix deviatoric
    SUBROUTINE DEV( A, ADEV )
c -------------------------------------------------------------
    INTEGER MDIM
    PARAMETER ( MDIM=3 )
    INTEGER IDI, JDI
    DOUBLE PRECISION TMP, TRA, A(MDIM,MDIM),
ADEV(MDIM,MDIM)
    TMP = TRA( A )
    DO 20, IDI = 1, MDIM
     DO 10, JDI = 1, MDIM
      ADEV(IDI,JDI) = A(IDI,JDI)
 10   CONTINUE
     ADEV(IDI,IDI) = ADEV(IDI,IDI)-TRA(A)/3.0D0
 20 CONTINUE
    END
c -------------------------------------------------------------
Change matrix order from ABAQUS one column format into regular
one
    SUBROUTINE EXTRACT( NDI, NSHR, NTENS, STRESS, DSTR,
   & DT, TOLD, D )
c -------------------------------------------------------------
    INTEGER MDIM
    PARAMETER ( MDIM=3 )
    INTEGER IDI, NDI, NSHR, NTENS
    DOUBLE PRECISION DT, STRESS(NTENS), DSTR(NTENS),
   & TOLD(MDIM,MDIM), D(MDIM,MDIM)
    CALL VECMAT( NDI, NSHR, NTENS, STRESS, TOLD )
    CALL ZERO( D, MDIM*MDIM )
    DO 10, IDI=1,NDI
     D(IDI,IDI) = DSTR(IDI)/DT
 10 CONTINUE
    IF ( NSHR.GE.1 ) THEN
     D(1,2) = 0.5D0*DSTR(NDI+1)/DT
     D(2,1) = D(1,2)
    ENDIF
    IF ( NSHR.GE.2 ) THEN
     D(1,3) = 0.5D0*DSTR(NDI+2)/DT
     D(3,1) = D(1,3)
    ENDIF
    IF ( NSHR.GE.3 ) THEN
     D(2,3) = 0.5D0*DSTR(NDI+3)/DT
     D(3,2) = D(2,3)
    ENDIF
    END
c -------------------------------------------------------------
    SUBROUTINE MATVEC( NDI, NSHR, NTENS, MAT, VEC )
c -------------------------------------------------------------
    INTEGER MDIM
```

```
      PARAMETER ( MDIM=3 )
      INTEGER IDI, NDI, NSHR, NTENS
      DOUBLE PRECISION VEC(NTENS), MAT(MDIM,MDIM)
      DO 10, IDI = 1, NDI
       VEC(IDI) = MAT(IDI,IDI)
   10 CONTINUE
      IF ( NSHR.GE.1 ) VEC(NDI+1) = MAT(1,2)
      IF ( NSHR.GE.2 ) VEC(NDI+2) = MAT(1,3)
      IF ( NSHR.GE.3 ) VEC(NDI+3) = MAT(2,3)
      END
c ------------------------------------------------------------------
      SUBROUTINE MINUS( A, B, C, N )
c ------------------------------------------------------------------
      INTEGER I, N
      DOUBLE PRECISION A(N), B(N), C(N)
      DO 10, I = 1, N
       C(I) = A(I) - B(I)
   10 CONTINUE
      END
c ------------------------------------------------------------------
      SUBROUTINE MUL( A, SCAL, N )
c ------------------------------------------------------------------
      INTEGER N
      DOUBLE PRECISION SCAL, A(N)
      DO 10, I = 1, N
       A(I) = SCAL * A(I)
   10 CONTINUE
      END
c ------------------------------------------------------------------
      LOGICAL FUNCTION NEGATIV( X )
c ------------------------------------------------------------------
      DOUBLE PRECISION X
      IF ( X.LT.1.E-8 ) THEN
       NEGATIV = .TRUE.
      ELSE
       NEGATIV = .FALSE.
      END IF
      END
c ------------------------------------------------------------------
      DOUBLE PRECISION FUNCTION NORMMAT( A )
c ------------------------------------------------------------------
      INTEGER MDIM
      PARAMETER ( MDIM=3 )
      DOUBLE PRECISION TRA, A(MDIM,MDIM),WORK(MDIM,MDIM)

      CALL ABC( A, A, WORK )
      NORMMAT = SQRT( TRA(WORK) )
      END
c ------------------------------------------------------------------
      DOUBLE PRECISION FUNCTION NORMVEC( A, N )
c ------------------------------------------------------------------
      INTEGER I, N
      DOUBLE PRECISION A(N)
      NORMVEC = 0.D0
      DO 10, I = 1, N
       NORMVEC = NORMVEC + A(I) * A(I)
   10 CONTINUE
      NORMVEC = SQRT( NORMVEC )
      END
c ------------------------------------------------------------------
      LOGICAL FUNCTION MYNULL( X )
c ------------------------------------------------------------------
      DOUBLE PRECISION X
      IF ( ABS(X).LT.1.E-8 ) THEN
       MYNULL = .TRUE.
      ELSE
       MYNULL = .FALSE.
      END IF
      END
```

```
c ------------------------------------------------------------------
      DOUBLE PRECISION FUNCTION POWER( X, Y )
c ------------------------------------------------------------------
      DOUBLE PRECISION X, Y
      POWER = X ** Y
      END
c ------------------------------------------------------------------
      SUBROUTINE PRIDBL( LABEL, A )
c ------------------------------------------------------------------
      CHARACTER*6 LABEL
      DOUBLE PRECISION A
      WRITE(6,*) LABEL, A
      END
c ------------------------------------------------------------------
      SUBROUTINE PRITXT( LABEL )
c ------------------------------------------------------------------
      CHARACTER*6 LABEL
      WRITE(6,*) LABEL
      END
c ------------------------------------------------------------------
      SUBROUTINE PRIVEC( LABEL, A, N )
c ------------------------------------------------------------------
      CHARACTER*6 LABEL
      INTEGER I, N
      DOUBLE PRECISION A(N)
      WRITE(6,*) LABEL
      DO 10, I = 1, N
        WRITE(6,*) A(I)
   10 CONTINUE
      END
c ------------------------------------------------------------------
      DOUBLE PRECISION FUNCTION TRA( A )
c ------------------------------------------------------------------
      INTEGER MDIM
      PARAMETER ( MDIM=3 )
      DOUBLE PRECISION A(MDIM,MDIM)
      TRA = A(1,1) + A(2,2) + A(3,3)
      END
c ------------------------------------------------------------------
      SUBROUTINE VECMAT( NDI, NSHR, NTENS, VEC, MAT )
c ------------------------------------------------------------------
      INTEGER MDIM
      PARAMETER( MDIM=3 )
      INTEGER IDI, NDI, NSHR, NTENS
      DOUBLE PRECISION VEC(NTENS), MAT(MDIM,MDIM)
      CALL ZERO( MAT, MDIM*MDIM )
      DO 10, IDI = 1, NDI
        MAT(IDI,IDI) = VEC(IDI)
   10 CONTINUE
      IF (NSHR.GE.1) THEN
        MAT(1,2) = VEC(NDI+1)
        MAT(2,1) = MAT(1,2)
      END IF
      IF (NSHR.GE.2) THEN
        MAT(1,3) = VEC(NDI+2)
        MAT(3,1) = MAT(1,3)
      END IF
      IF (NSHR.GE.3) THEN
        MAT(2,3) = VEC(NDI+3)
        MAT(3,2) = MAT(2,3)
      END IF
      END
c ------------------------------------------------------------------
      SUBROUTINE ZERO( A, N )
c ------------------------------------------------------------------
      INTEGER I, N
      DOUBLE PRECISION A(N)
      DO 10, I = 1, N
        A(I) = 0.0D0
   10 CONTINUE
```

```
      END
c ------------------------------------------------------------------
      SUBROUTINE EIGEN( SIGMAT, EIGVAL )
c ------------------------------------------------------------------
      INTEGER MDIM
      DOUBLE PRECISION PI
      PARAMETER ( MDIM=3, PI=3.1415929794311523D0 )
      DOUBLE PRECISION SIGMAT(MDIM,MDIM), EIGVAL(MDIM)
      DOUBLE PRECISION I1, I2, I3, R, S, T, P, Q,
     $  BIGR, PHI, Y0, Y1, Y2, TMP, INV(MDIM)
      CALL INVAR( SIGMAT, INV )
      I1 = INV(1)
      I2 = INV(2)
      I3 = INV(3)
      R = -I1
      S = +I2
      T = -I3
      P = (3.D0*S-R*R)/3.D0
      Q = 2.D0*R*R*R/27.D0 - R*S/3.D0 + T
      IF ( ABS(Q).LT.1.D-10 ) THEN
       Y0 = -SQRT(ABS(P))
       Y1 = +SQRT(ABS(P))
       Y2 = 0.D0
      ELSE
       BIGR = SQRT(ABS(P)/3.D0)
       IF ( Q.LT.0.D0 ) BIGR = -BIGR
       TMP = Q/(2.D0*BIGR*BIGR*BIGR)
       IF ( TMP.LT.-1.D0 ) TMP = -1.D0
       IF ( TMP.GT.+1.D0 ) TMP = +1.D0
       PHI = ACOS(TMP)
       Y0 = -2.D0*BIGR*COS(PHI/3.D0)
       Y1 = -2.D0*BIGR*COS(PHI/3.D0+2.D0*PI/3.D0)
       Y2 = -2.D0*BIGR*COS(PHI/3.D0+4.D0*PI/3.D0)
      END IF
      EIGVAL(1) = Y0 - R/3.D0
      EIGVAL(2) = Y1 - R/3.D0
      EIGVAL(3) = Y2 - R/3.D0
      END
c ------------------------------------------------------------------
      SUBROUTINE INVAR( SIGMAT, INV )
c ------------------------------------------------------------------
      INTEGER MDIM
      PARAMETER ( MDIM=3 )
      DOUBLE PRECISION SIGMAT(MDIM,MDIM), INV(MDIM)
      INV(1) = SIGMAT(1,1) + SIGMAT(2,2) + SIGMAT(3,3)
      INV(2) = SIGMAT(1,1)*SIGMAT(2,2) + SIGMAT(2,2)*SIGMAT(3,3)
     &       + SIGMAT(3,3)*SIGMAT(1,1) - SIGMAT(1,2)*SIGMAT(2,1) -
     &       SIGMAT(2,3)*SIGMAT(3,2) - SIGMAT(3,1)*SIGMAT(1,3)
      CALL DETERM( SIGMAT, INV(3) )
      END
c ------------------------------------------------------------------
      SUBROUTINE DETERM( A, DET )
c ------------------------------------------------------------------
      INTEGER MDIM
      PARAMETER ( MDIM=3 )
      DOUBLE PRECISION A(MDIM,MDIM), DET
      DET = A(1,1)*(A(2,2)*A(3,3)-A(3,2)*A(2,3)) -
     &     A(1,2)*(A(2,1)*A(3,3)-A(3,1)*A(2,3)) +
     &     A(1,3)*(A(2,1)*A(3,2)-A(3,1)*A(2,2))
      END
c ------------------------------------------------------------------
      SUBROUTINE TRANS(A,B)
c ------------------------------------------------------------------
      INTEGER MDIM
      PARAMETER ( MDIM=3 )
      INTEGER IDI, JDI
      DOUBLE PRECISION A(MDIM,MDIM),B(MDIM,MDIM)
      DO 20, IDI=1,3
       DO 10, JDI=1,3
       B(IDI,JDI)= A(JDI,IDI)
```

```
 10   CONTINUE
 20  CONTINUE
     END
c ------------------------------------------------------------------
     DOUBLE PRECISION FUNCTION DELTA(I,J)
c ------------------------------------------------------------------
     INTEGER I,J
     IF (I.EQ.J) THEN
     DELTA = 1.D0
     ELSE
     DELTA = 0.D0
     END IF
     END
c ------------------------------------------------------------------
     SUBROUTINE INVMAT(MAT,INV)
c ------------------------------------------------------------------
     INTEGER MDIM
     PARAMETER ( MDIM=3 )
     DOUBLE PRECISION MAT(MDIM,MDIM), INV(MDIM,MDIM),
    & DET , MATT(MDIM,MDIM),
     CALL TRANS(MAT,MATT)
     CALL DETERM (MAT,DET)
     DO 20, IDI=1,3
      DO 10, JDI=1,3
       INV(IDI,JDI)=MATT(IDI,JDI)/DET
 10   CONTINUE
 20  CONTINUE
     END
c ------------------------------------------------------------------
     SUBROUTINE GETR(F,R)
c ------------------------------------------------------------------
     INTEGER MDIM, IDI, JDI
     PARAMETER ( MDIM=3 )
     DOUBLE PRECISION F(MDIM,MDIM), FT(MDIM,MDIM),
    & R(MDIM,MDIM),BEIGEN(MDIM),I1,I2,I3,DET, V(MDIM,MDIM),
    & B(MDIM,MDIM), SB(MDIM,MDIM), VINV(MDIM,MDIM)
     CALL TRANS(F,FT)
     CALL ABC(F,FT,B)
     CALL ABC(B,B,SB)
     CALL EIGEN(B,BEIGEN)
     I1=((SQRT(BEIGEN(1))+SQRT(BEIGEN(2))+SQRT(BEIGEN(3)))/
    & SQRT(BEIGEN(1)+BEIGEN(2)+BEIGEN(3)))*SQRT(TRA(B))
     I2=(I1*I1-TRA(B))/2.D0
     CALL DETERM(B,DET)
     I3=SQRT(DET)
     DO 20, IDI=1,3
      DO 10, JDI=1,3
      V(IDI,JDI)= (I1*I3+(I1*I1-I2)*B(IDI,JDI)-
     &   SB(IDI,JDI))/(I1*I2-I3)
 10   CONTINUE
 20  CONTINUE
     CALL INVMAT(V,VINV)
     CALL ABC(VINV,F,R)
     END
c ------------------------------------------------------------------
     SUBROUTINE GETW(F0,F1,DT,W)
c ------------------------------------------------------------------
     INTEGER MDIM, IDI, JDI
     PARAMETER ( MDIM=3 )
     DOUBLE      PRECISION      F0(MDIM,MDIM),F1(MDIM,MDIM),
W(MDIM,
    &  MDIM),DT,R0(MDIM,MDIM), R1(MDIM,MDIM),RDOT(MDIM,
    &  MDIM),RT(MDIM,MDIM)
     CALL GETR(F0,R0)
     CALL GETR(F1,R1)
     CALL TRANS(R1,RT)
     DO 20, IDI=1,3
      DO 10, JDI=1,3
       RDOT(IDI,JDI)=(R1(IDI,JDI)-R0(IDI,JDI))/DT
 10   CONTINUE
```

```
 20 CONTINUE
    CALL ABC(RDOT,RT,W)
    END
c ---------------------------------------------------------------------
    SUBROUTINE NEWINCT(INCT,S,W)
c ---------------------------------------------------------------------
    INTEGER MDIM, IDI, JDI
    PARAMETER ( MDIM=3 )
    DOUBLE PRECISION INCT(MDIM,MDIM),S(MDIM,MDIM),
   & W(MDIM,MDIM),WS(MDIM,MDIM),SW(MDIM,MDIM)
    CALL ABC(W,S,WS)
CALL ABC(S,W,SW)
    DO 20, IDI=1,3
     DO 10, JDI=1,3
      INCT(IDI,JDI)=INCT(IDI,JDI) + WS(IDI,JDI) - SW(IDI,JDI)
 10   CONTINUE
 20 CONTINUE
END
```

APPENDIX E

ABAQUS INPUT FILES

E.1 OEDOMETER TEST SIMULATION

```
*Heading
** Job name: OED-2D-1 Model name: Model-1
*Preprint, model=YES
**
** PARTS
**
*Part, name=SOIL-BLOCK
*End Part
**
** ASSEMBLY
**
*Assembly, name=Assembly
**
*Instance, name=SOIL-BLOCK-1, part=SOIL-BLOCK
*Node
      1,      -51.,       0.
      2,       51.,       0.
      3,      -51.,      19.
      4,       51.,      19.
      5,       0.,        0.
      6,       51.,       9.5
      7,       0.,       19.
      8,      -51.,       9.5
*Element, type=CPE8
1, 1, 2, 4, 3, 5, 6, 7, 8
** Region: (Section-1:Picked)
*Elset, elset=_I1, internal
 1,
** Section: Section-1
*Solid Section, elset=_I1, material=SOIL-HYPO
1.,
*End Instance
*Nset, nset=ALL, instance=SOIL-BLOCK-1, generate
 1,  8,  1
*Elset, elset=ALL, instance=SOIL-BLOCK-1
 1,
*Nset, nset=TOP, instance=SOIL-BLOCK-1
 3, 4, 7
*Elset, elset=TOP, instance=SOIL-BLOCK-1
 1,
*Nset, nset=_G6, internal, instance=SOIL-BLOCK-1
 1, 2, 5
*Elset, elset=_G6, internal, instance=SOIL-BLOCK-1
 1,
*Nset, nset=_G7, internal, instance=SOIL-BLOCK-1
 1, 2, 3, 4, 6, 8
*Elset, elset=_G7, internal, instance=SOIL-BLOCK-1
 1,
*Nset, nset=_G8, internal, instance=SOIL-BLOCK-1
 3, 4, 7
*Elset, elset=_G8, internal, instance=SOIL-BLOCK-1
 1,
*End Assembly
*Amplitude, name=Disp, smooth=0
```

```
0., 0., 0.5, 1., 1., 0.5
**
** MATERIALS
**
*Material, name=SOIL-HYPO
*Depvar
    1,
*User Material, constants=9
 0.576,1000., 0.95, 0.55, 1.05, 0.25, 0.25,  1.5
 1.
**
*INITIAL CONDITIONS, TYPE=SOLUTION
ALL,  0.78
**
** BOUNDARY CONDITIONS
**
** Name: BASE Type: Displacement/Rotation
*Boundary
_G6, 1, 1
_G6, 2, 2
** Name: ROUND Type: Displacement/Rotation
*Boundary
_G7, 1, 1
** ----------------------------------------------------------------
**
** STEP: DISP
**
*Step, inc=10000
DISP: TOP DISPLACEMENT
*Static
0.0001, 1., 1e-08, 0.001
**
** BOUNDARY CONDITIONS
**
** Name: TOP-DISP Type: Displacement/Rotation
*Boundary, amplitude=Disp
_G8, 2, 2, -0.231
**
** OUTPUT REQUESTS
**
*Restart, write, frequency=1
*Output, field, frequency=1
*Node Output
U,
*Element Output
S,
*Output, history, frequency=1
*Element Output, elset=ALL
SDV,
*El Print, freq=999999
*Node Print, freq=999999
*End Step
```

E.2 STRIP-FOOTING SIMULATION

```
*Heading
** Job name: Strip-footing Model name: Model-
1
**
** PARTS
**
*Part, name=Part-1
*End Part
**
** ASSEMBLY
**
*Assembly, name=Assembly
**
*Instance, name=Part-1-1, part=Part-1
*Node
     1,      1524.,      2133.6
     2,      1524.,          0.
     3,     7315.2,          0.
     4,     7315.2,      2133.6
     5,     7315.2,      3657.6
     6,      1524.,      3657.6
     7,         0.,      2133.6
     8,         0.,          0.
     9,         0.,      3657.6
    10,      1524.,      1942.06
    11,      1524.,      1703.44
    12,      1524.,       1406.2
    13,      1524.,      1035.91
    14,      1524.,      574.631
    15,      1524.,      2037.83
    16,      1524.,      1822.75
    17,      1524.,      1554.82
    18,      1524.,      1221.05
    19,      1524.,       805.271
    20,      1524.,       287.315
    21,     1838.66,          0.
    22,     2194.17,          0.
    23,     2595.84,          0.
    24,     3049.66,          0.
    25,      3562.4,          0.
    26,      4141.7,          0.
    27,     4796.22,          0.
    28,     5535.72,          0.
    29,     6371.22,          0.
    30,      7315.2,      574.631
    31,      7315.2,      1035.91
    32,      7315.2,       1406.2
    33,      7315.2,      1703.44
    34,      7315.2,      1942.06
    35,     6371.22,      2133.6
    36,     5535.72,      2133.6
    37,     4796.22,      2133.6
    38,      4141.7,      2133.6
    39,      3562.4,      2133.6
    40,     3049.66,      2133.6
    41,     2595.84,      2133.6
    42,     2194.17,      2133.6
    43,     1838.66,      2133.6
    44,     6843.21,      2133.6
    45,     5953.47,      2133.6
    46,     5165.97,      2133.6
    47,     4468.96,      2133.6
    48,     3852.05,      2133.6
    49,     3306.03,      2133.6
    50,     2822.75,      2133.6
    51,     2395.01,      2133.6
    52,     2016.42,      2133.6
    53,     1681.33,      2133.6
    54,      7315.2,       2286.
    55,      7315.2,      2438.4
    56,      7315.2,      2590.8
    57,      7315.2,      2743.2
    58,      7315.2,      2895.6
    59,      7315.2,       3048.
    60,      7315.2,      3200.4
    61,      7315.2,      3352.8
    62,      7315.2,      3505.2
    63,      7315.2,      2209.8
    64,      7315.2,      2362.2
    65,      7315.2,      2514.6
    66,      7315.2,       2667.
    67,      7315.2,      2819.4
    68,      7315.2,      2971.8
    69,      7315.2,      3124.2
    70,      7315.2,      3276.6
    71,      7315.2,       3429.
    72,      7315.2,      3581.4
    73,     6371.22,      3657.6
    74,     5535.72,      3657.6
    75,     4796.22,      3657.6
    76,      4141.7,      3657.6
    77,      3562.4,      3657.6
    78,     3049.66,      3657.6
```

79, 2595.84, 3657.6
80, 2194.17, 3657.6
81, 1838.66, 3657.6
82, 6843.21, 3657.6
83, 5953.47, 3657.6
84, 5165.97, 3657.6
85, 4468.96, 3657.6
86, 3852.05, 3657.6
87, 3306.03, 3657.6
88, 2822.75, 3657.6
89, 2395.01, 3657.6
90, 2016.42, 3657.6
91, 1681.33, 3657.6
92, 1524., 3505.2
93, 1524., 3352.8
94, 1524., 3200.4
95, 1524., 3048.
96, 1524., 2895.6
97, 1524., 2743.2
98, 1524., 2590.8
99, 1524., 2438.4
100, 1524., 2286.
101, 1524., 3581.4
102, 1524., 3429.
103, 1524., 3276.6
104, 1524., 3124.2
105, 1524., 2971.8
106, 1524., 2819.4
107, 1524., 2667.
108, 1524., 2514.6
109, 1524., 2362.2
110, 1524., 2209.8
111, 1371.6, 2133.6
112, 1219.2, 2133.6
113, 1066.8, 2133.6
114, 914.4, 2133.6
115, 762., 2133.6
116, 609.6, 2133.6
117, 457.2, 2133.6
118, 304.8, 2133.6
119, 152.4, 2133.6
120, 1447.8, 2133.6
121, 1295.4, 2133.6
122, 1143., 2133.6
123, 990.6, 2133.6
124, 838.2, 2133.6
125, 685.8, 2133.6
126, 533.4, 2133.6
127, 381., 2133.6
128, 228.6, 2133.6
129, 76.2, 2133.6
130, 0., 1942.06
131, 0., 1703.44
132, 0., 1406.2
133, 0., 1035.91
134, 0., 574.631
135, 0., 2037.83
136, 0., 1822.75
137, 0., 1554.82
138, 0., 1221.05
139, 0., 805.271
140, 0., 287.315
141, 152.4, 0.
142, 304.8, 0.
143, 457.2, 0.
144, 609.6, 0.
145, 762., 0.
146, 914.4, 0.
147, 1066.8, 0.
148, 1219.2, 0.
149, 1371.6, 0.
150, 76.2, 0.
151, 228.6, 0.
152, 381., 0.
153, 533.4, 0.
154, 685.8, 0.
155, 838.2, 0.
156, 990.6, 0.
157, 1143., 0.
158, 1295.4, 0.
159, 1447.8, 0.
160, 1371.6, 3657.6
161, 1219.2, 3657.6
162, 1066.8, 3657.6
163, 914.4, 3657.6
164, 762., 3657.6
165, 609.6, 3657.6
166, 457.2, 3657.6
167, 304.8, 3657.6
168, 152.4, 3657.6
169, 1447.8, 3657.6
170, 1295.4, 3657.6
171, 1143., 3657.6
172, 990.6, 3657.6
173, 838.2, 3657.6
174, 685.8, 3657.6
175, 533.4, 3657.6
176, 381., 3657.6
177, 228.6, 3657.6
178, 76.2, 3657.6
179, 0., 3505.2
180, 0., 3352.8
181, 0., 3200.4
182, 0., 3048.
183, 0., 2895.6

184, 0., 2743.2
185, 0., 2590.8
186, 0., 2438.4
187, 0., 2286.
188, 0., 3581.4
189, 0., 3429.
190, 0., 3276.6
191, 0., 3124.2
192, 0., 2971.8
193, 0., 2819.4
194, 0., 2667.
195, 0., 2514.6
196, 0., 2362.2
197, 0., 2209.8
198, 1838.66, 1942.06
199, 1838.66, 1703.44
200, 1838.66, 1406.2
201, 1838.66, 1035.91
202, 1838.66, 574.631
203, 2194.17, 1942.06
204, 2194.17, 1703.44
205, 2194.17, 1406.2
206, 2194.17, 1035.91
207, 2194.17, 574.631
208, 2595.84, 1942.06
209, 2595.84, 1703.44
210, 2595.84, 1406.2
211, 2595.84, 1035.91
212, 2595.84, 574.631
213, 3049.66, 1942.06
214, 3049.66, 1703.44
215, 3049.66, 1406.2
216, 3049.66, 1035.91
217, 3049.66, 574.631
218, 3562.4, 1942.06
219, 3562.4, 1703.44
220, 3562.4, 1406.2
221, 3562.4, 1035.91
222, 3562.4, 574.631
223, 4141.7, 1942.06
224, 4141.7, 1703.44
225, 4141.7, 1406.2
226, 4141.7, 1035.91
227, 4141.7, 574.631
228, 4796.22, 1942.06
229, 4796.22, 1703.44
230, 4796.22, 1406.2
231, 4796.22, 1035.91
232, 4796.22, 574.631
233, 5535.72, 1942.06
234, 5535.72, 1703.44
235, 5535.72, 1406.2
236, 5535.72, 1035.91
237, 5535.72, 574.631
238, 6371.22, 1942.06
239, 6371.22, 1703.44
240, 6371.22, 1406.2
241, 6371.22, 1035.91
242, 6371.22, 574.631
243, 1838.66, 2286.
244, 1838.66, 2209.8
245, 1681.33, 2286.
246, 2194.17, 2286.
247, 2194.17, 2209.8
248, 2016.42, 2286.
249, 2595.84, 2286.
250, 2595.84, 2209.8
251, 2395.01, 2286.
252, 3049.66, 2286.
253, 3049.66, 2209.8
254, 2822.75, 2286.
255, 3562.4, 2286.
256, 3562.4, 2209.8
257, 3306.03, 2286.
258, 4141.7, 2286.
259, 4141.7, 2209.8
260, 3852.05, 2286.
261, 4796.22, 2286.
262, 4796.22, 2209.8
263, 4468.96, 2286.
264, 5535.72, 2286.
265, 5535.72, 2209.8
266, 5165.97, 2286.
267, 6371.22, 2286.
268, 6371.22, 2209.8
269, 5953.47, 2286.
270, 6843.21, 2286.
271, 1838.66, 2438.4
272, 1838.66, 2362.2
273, 1681.33, 2438.4
274, 2194.17, 2438.4
275, 2194.17, 2362.2
276, 2016.42, 2438.4
277, 2595.84, 2438.4
278, 2595.84, 2362.2
279, 2395.01, 2438.4
280, 3049.66, 2438.4
281, 3049.66, 2362.2
282, 2822.75, 2438.4
283, 3562.4, 2438.4
284, 3562.4, 2362.2
285, 3306.03, 2438.4
286, 4141.7, 2438.4
287, 4141.7, 2362.2
288, 3852.05, 2438.4

289, 4796.22, 2438.4
290, 4796.22, 2362.2
291, 4468.96, 2438.4
292, 5535.72, 2438.4
293, 5535.72, 2362.2
294, 5165.97, 2438.4
295, 6371.22, 2438.4
296, 6371.22, 2362.2
297, 5953.47, 2438.4
298, 6843.21, 2438.4
299, 1838.66, 2590.8
300, 1838.66, 2514.6
301, 1681.33, 2590.8
302, 2194.17, 2590.8
303, 2194.17, 2514.6
304, 2016.42, 2590.8
305, 2595.84, 2590.8
306, 2595.84, 2514.6
307, 2395.01, 2590.8
308, 3049.66, 2590.8
309, 3049.66, 2514.6
310, 2822.75, 2590.8
311, 3562.4, 2590.8
312, 3562.4, 2514.6
313, 3306.03, 2590.8
314, 4141.7, 2590.8
315, 4141.7, 2514.6
316, 3852.05, 2590.8
317, 4796.22, 2590.8
318, 4796.22, 2514.6
319, 4468.96, 2590.8
320, 5535.72, 2590.8
321, 5535.72, 2514.6
322, 5165.97, 2590.8
323, 6371.22, 2590.8
324, 6371.22, 2514.6
325, 5953.47, 2590.8
326, 6843.21, 2590.8
327, 1838.66, 2743.2
328, 1838.66, 2667.
329, 1681.33, 2743.2
330, 2194.17, 2743.2
331, 2194.17, 2667.
332, 2016.42, 2743.2
333, 2595.84, 2743.2
334, 2595.84, 2667.
335, 2395.01, 2743.2
336, 3049.66, 2743.2
337, 3049.66, 2667.
338, 2822.75, 2743.2
339, 3562.4, 2743.2
340, 3562.4, 2667.
341, 3306.03, 2743.2
342, 4141.7, 2743.2
343, 4141.7, 2667.
344, 3852.05, 2743.2
345, 4796.22, 2743.2
346, 4796.22, 2667.
347, 4468.96, 2743.2
348, 5535.72, 2743.2
349, 5535.72, 2667.
350, 5165.97, 2743.2
351, 6371.22, 2743.2
352, 6371.22, 2667.
353, 5953.47, 2743.2
354, 6843.21, 2743.2
355, 1838.66, 2895.6
356, 1838.66, 2819.4
357, 1681.33, 2895.6
358, 2194.17, 2895.6
359, 2194.17, 2819.4
360, 2016.42, 2895.6
361, 2595.84, 2895.6
362, 2595.84, 2819.4
363, 2395.01, 2895.6
364, 3049.66, 2895.6
365, 3049.66, 2819.4
366, 2822.75, 2895.6
367, 3562.4, 2895.6
368, 3562.4, 2819.4
369, 3306.03, 2895.6
370, 4141.7, 2895.6
371, 4141.7, 2819.4
372, 3852.05, 2895.6
373, 4796.22, 2895.6
374, 4796.22, 2819.4
375, 4468.96, 2895.6
376, 5535.72, 2895.6
377, 5535.72, 2819.4
378, 5165.97, 2895.6
379, 6371.22, 2895.6
380, 6371.22, 2819.4
381, 5953.47, 2895.6
382, 6843.21, 2895.6
383, 1838.66, 3048.
384, 1838.66, 2971.8
385, 1681.33, 3048.
386, 2194.17, 3048.
387, 2194.17, 2971.8
388, 2016.42, 3048.
389, 2595.84, 3048.
390, 2595.84, 2971.8
391, 2395.01, 3048.
392, 3049.66, 3048.
393, 3049.66, 2971.8

394, 2822.75, 3048.
395, 3562.4, 3048.
396, 3562.4, 2971.8
397, 3306.03, 3048.
398, 4141.7, 3048.
399, 4141.7, 2971.8
400, 3852.05, 3048.
401, 4796.22, 3048.
402, 4796.22, 2971.8
403, 4468.96, 3048.
404, 5535.72, 3048.
405, 5535.72, 2971.8
406, 5165.97, 3048.
407, 6371.22, 3048.
408, 6371.22, 2971.8
409, 5953.47, 3048.
410, 6843.21, 3048.
411, 1838.66, 3200.4
412, 1838.66, 3124.2
413, 1681.33, 3200.4
414, 2194.17, 3200.4
415, 2194.17, 3124.2
416, 2016.42, 3200.4
417, 2595.84, 3200.4
418, 2595.84, 3124.2
419, 2395.01, 3200.4
420, 3049.66, 3200.4
421, 3049.66, 3124.2
422, 2822.75, 3200.4
423, 3562.4, 3200.4
424, 3562.4, 3124.2
425, 3306.03, 3200.4
426, 4141.7, 3200.4
427, 4141.7, 3124.2
428, 3852.05, 3200.4
429, 4796.22, 3200.4
430, 4796.22, 3124.2
431, 4468.96, 3200.4
432, 5535.72, 3200.4
433, 5535.72, 3124.2
434, 5165.97, 3200.4
435, 6371.22, 3200.4
436, 6371.22, 3124.2
437, 5953.47, 3200.4
438, 6843.21, 3200.4
439, 1838.66, 3352.8
440, 1838.66, 3276.6
441, 1681.33, 3352.8
442, 2194.17, 3352.8
443, 2194.17, 3276.6
444, 2016.42, 3352.8
445, 2595.84, 3352.8
446, 2595.84, 3276.6
447, 2395.01, 3352.8
448, 3049.66, 3352.8
449, 3049.66, 3276.6
450, 2822.75, 3352.8
451, 3562.4, 3352.8
452, 3562.4, 3276.6
453, 3306.03, 3352.8
454, 4141.7, 3352.8
455, 4141.7, 3276.6
456, 3852.05, 3352.8
457, 4796.22, 3352.8
458, 4796.22, 3276.6
459, 4468.96, 3352.8
460, 5535.72, 3352.8
461, 5535.72, 3276.6
462, 5165.97, 3352.8
463, 6371.22, 3352.8
464, 6371.22, 3276.6
465, 5953.47, 3352.8
466, 6843.21, 3352.8
467, 1838.66, 3505.2
468, 1838.66, 3429.
469, 1681.33, 3505.2
470, 2194.17, 3505.2
471, 2194.17, 3429.
472, 2016.42, 3505.2
473, 2595.84, 3505.2
474, 2595.84, 3429.
475, 2395.01, 3505.2
476, 3049.66, 3505.2
477, 3049.66, 3429.
478, 2822.75, 3505.2
479, 3562.4, 3505.2
480, 3562.4, 3429.
481, 3306.03, 3505.2
482, 4141.7, 3505.2
483, 4141.7, 3429.
484, 3852.05, 3505.2
485, 4796.22, 3505.2
486, 4796.22, 3429.
487, 4468.96, 3505.2
488, 5535.72, 3505.2
489, 5535.72, 3429.
490, 5165.97, 3505.2
491, 6371.22, 3505.2
492, 6371.22, 3429.
493, 5953.47, 3505.2
494, 6843.21, 3505.2
495, 1838.66, 3581.4
496, 2194.17, 3581.4
497, 2595.84, 3581.4
498, 3049.66, 3581.4

499,	3562.4,	3581.4
500,	4141.7,	3581.4
501,	4796.22,	3581.4
502,	5535.72,	3581.4
503,	6371.22,	3581.4
504,	1371.6,	1942.06
505,	1371.6,	2037.83
506,	1447.8,	1942.06
507,	1219.2,	1942.06
508,	1219.2,	2037.83
509,	1295.4,	1942.06
510,	1066.8,	1942.06
511,	1066.8,	2037.83
512,	1143.,	1942.06
513,	914.4,	1942.06
514,	914.4,	2037.83
515,	990.6,	1942.06
516,	762.,	1942.06
517,	762.,	2037.83
518,	838.2,	1942.06
519,	609.6,	1942.06
520,	609.6,	2037.83
521,	685.8,	1942.06
522,	457.2,	1942.06
523,	457.2,	2037.83
524,	533.4,	1942.06
525,	304.8,	1942.06
526,	304.8,	2037.83
527,	381.,	1942.06
528,	152.4,	1942.06
529,	152.4,	2037.83
530,	228.6,	1942.06
531,	76.2,	1942.06
532,	1371.6,	1703.44
533,	1371.6,	1822.75
534,	1447.8,	1703.44
535,	1219.2,	1703.44
536,	1219.2,	1822.75
537,	1295.4,	1703.44
538,	1066.8,	1703.44
539,	1066.8,	1822.75
540,	1143.,	1703.44
541,	914.4,	1703.44
542,	914.4,	1822.75
543,	990.6,	1703.44
544,	762.,	1703.44
545,	762.,	1822.75
546,	838.2,	1703.44
547,	609.6,	1703.44
548,	609.6,	1822.75
549,	685.8,	1703.44
550,	457.2,	1703.44
551,	457.2,	1822.75
552,	533.4,	1703.44
553,	304.8,	1703.44
554,	304.8,	1822.75
555,	381.,	1703.44
556,	152.4,	1703.44
557,	152.4,	1822.75
558,	228.6,	1703.44
559,	76.2,	1703.44
560,	1371.6,	1406.2
561,	1371.6,	1554.82
562,	1447.8,	1406.2
563,	1219.2,	1406.2
564,	1219.2,	1554.82
565,	1295.4,	1406.2
566,	1066.8,	1406.2
567,	1066.8,	1554.82
568,	1143.,	1406.2
569,	914.4,	1406.2
570,	914.4,	1554.82
571,	990.6,	1406.2
572,	762.,	1406.2
573,	762.,	1554.82
574,	838.2,	1406.2
575,	609.6,	1406.2
576,	609.6,	1554.82
577,	685.8,	1406.2
578,	457.2,	1406.2
579,	457.2,	1554.82
580,	533.4,	1406.2
581,	304.8,	1406.2
582,	304.8,	1554.82
583,	381.,	1406.2
584,	152.4,	1406.2
585,	152.4,	1554.82
586,	228.6,	1406.2
587,	76.2,	1406.2
588,	1371.6,	1035.91
589,	1371.6,	1221.05
590,	1447.8,	1035.91
591,	1219.2,	1035.91
592,	1219.2,	1221.05
593,	1295.4,	1035.91
594,	1066.8,	1035.91
595,	1066.8,	1221.05
596,	1143.,	1035.91
597,	914.4,	1035.91
598,	914.4,	1221.05
599,	990.6,	1035.91
600,	762.,	1035.91
601,	762.,	1221.05
602,	838.2,	1035.91
603,	609.6,	1035.91

604,	609.6,	1221.05
605,	685.8,	1035.91
606,	457.2,	1035.91
607,	457.2,	1221.05
608,	533.4,	1035.91
609,	304.8,	1035.91
610,	304.8,	1221.05
611,	381.,	1035.91
612,	152.4,	1035.91
613,	152.4,	1221.05
614,	228.6,	1035.91
615,	76.2,	1035.91
616,	1371.6,	574.631
617,	1371.6,	805.271
618,	1447.8,	574.631
619,	1219.2,	574.631
620,	1219.2,	805.271
621,	1295.4,	574.631
622,	1066.8,	574.631
623,	1066.8,	805.271
624,	1143.,	574.631
625,	914.4,	574.631
626,	914.4,	805.271
627,	990.6,	574.631
628,	762.,	574.631
629,	762.,	805.271
630,	838.2,	574.631
631,	609.6,	574.631
632,	609.6,	805.271
633,	685.8,	574.631
634,	457.2,	574.631
635,	457.2,	805.271
636,	533.4,	574.631
637,	304.8,	574.631
638,	304.8,	805.271
639,	381.,	574.631
640,	152.4,	574.631
641,	152.4,	805.271
642,	228.6,	574.631
643,	76.2,	574.631
644,	1371.6,	287.315
645,	1219.2,	287.315
646,	1066.8,	287.315
647,	914.4,	287.315
648,	762.,	287.315
649,	609.6,	287.315
650,	457.2,	287.315
651,	304.8,	287.315
652,	152.4,	287.315
653,	152.4,	2286.
654,	152.4,	2209.8
655,	76.2,	2286.
656,	304.8,	2286.
657,	304.8,	2209.8
658,	228.6,	2286.
659,	457.2,	2286.
660,	457.2,	2209.8
661,	381.,	2286.
662,	609.6,	2286.
663,	609.6,	2209.8
664,	533.4,	2286.
665,	762.,	2286.
666,	762.,	2209.8
667,	685.8,	2286.
668,	914.4,	2286.
669,	914.4,	2209.8
670,	838.2,	2286.
671,	1066.8,	2286.
672,	1066.8,	2209.8
673,	990.6,	2286.
674,	1219.2,	2286.
675,	1219.2,	2209.8
676,	1143.,	2286.
677,	1371.6,	2286.
678,	1371.6,	2209.8
679,	1295.4,	2286.
680,	1447.8,	2286.
681,	152.4,	2438.4
682,	152.4,	2362.2
683,	76.2,	2438.4
684,	304.8,	2438.4
685,	304.8,	2362.2
686,	228.6,	2438.4
687,	457.2,	2438.4
688,	457.2,	2362.2
689,	381.,	2438.4
690,	609.6,	2438.4
691,	609.6,	2362.2
692,	533.4,	2438.4
693,	762.,	2438.4
694,	762.,	2362.2
695,	685.8,	2438.4
696,	914.4,	2438.4
697,	914.4,	2362.2
698,	838.2,	2438.4
699,	1066.8,	2438.4
700,	1066.8,	2362.2
701,	990.6,	2438.4
702,	1219.2,	2438.4
703,	1219.2,	2362.2
704,	1143.,	2438.4
705,	1371.6,	2438.4
706,	1371.6,	2362.2
707,	1295.4,	2438.4
708,	1447.8,	2438.4

709, 152.4, 2590.8
710, 152.4, 2514.6
711, 76.2, 2590.8
712, 304.8, 2590.8
713, 304.8, 2514.6
714, 228.6, 2590.8
715, 457.2, 2590.8
716, 457.2, 2514.6
717, 381., 2590.8
718, 609.6, 2590.8
719, 609.6, 2514.6
720, 533.4, 2590.8
721, 762., 2590.8
722, 762., 2514.6
723, 685.8, 2590.8
724, 914.4, 2590.8
725, 914.4, 2514.6
726, 838.2, 2590.8
727, 1066.8, 2590.8
728, 1066.8, 2514.6
729, 990.6, 2590.8
730, 1219.2, 2590.8
731, 1219.2, 2514.6
732, 1143., 2590.8
733, 1371.6, 2590.8
734, 1371.6, 2514.6
735, 1295.4, 2590.8
736, 1447.8, 2590.8
737, 152.4, 2743.2
738, 152.4, 2667.
739, 76.2, 2743.2
740, 304.8, 2743.2
741, 304.8, 2667.
742, 228.6, 2743.2
743, 457.2, 2743.2
744, 457.2, 2667.
745, 381., 2743.2
746, 609.6, 2743.2
747, 609.6, 2667.
748, 533.4, 2743.2
749, 762., 2743.2
750, 762., 2667.
751, 685.8, 2743.2
752, 914.4, 2743.2
753, 914.4, 2667.
754, 838.2, 2743.2
755, 1066.8, 2743.2
756, 1066.8, 2667.
757, 990.6, 2743.2
758, 1219.2, 2743.2
759, 1219.2, 2667.
760, 1143., 2743.2
761, 1371.6, 2743.2
762, 1371.6, 2667.
763, 1295.4, 2743.2
764, 1447.8, 2743.2
765, 152.4, 2895.6
766, 152.4, 2819.4
767, 76.2, 2895.6
768, 304.8, 2895.6
769, 304.8, 2819.4
770, 228.6, 2895.6
771, 457.2, 2895.6
772, 457.2, 2819.4
773, 381., 2895.6
774, 609.6, 2895.6
775, 609.6, 2819.4
776, 533.4, 2895.6
777, 762., 2895.6
778, 762., 2819.4
779, 685.8, 2895.6
780, 914.4, 2895.6
781, 914.4, 2819.4
782, 838.2, 2895.6
783, 1066.8, 2895.6
784, 1066.8, 2819.4
785, 990.6, 2895.6
786, 1219.2, 2895.6
787, 1219.2, 2819.4
788, 1143., 2895.6
789, 1371.6, 2895.6
790, 1371.6, 2819.4
791, 1295.4, 2895.6
792, 1447.8, 2895.6
793, 152.4, 3048.
794, 152.4, 2971.8
795, 76.2, 3048.
796, 304.8, 3048.
797, 304.8, 2971.8
798, 228.6, 3048.
799, 457.2, 3048.
800, 457.2, 2971.8
801, 381., 3048.
802, 609.6, 3048.
803, 609.6, 2971.8
804, 533.4, 3048.
805, 762., 3048.
806, 762., 2971.8
807, 685.8, 3048.
808, 914.4, 3048.
809, 914.4, 2971.8
810, 838.2, 3048.
811, 1066.8, 3048.
812, 1066.8, 2971.8
813, 990.6, 3048.

814, 1219.2, 3048.
815, 1219.2, 2971.8
816, 1143., 3048.
817, 1371.6, 3048.
818, 1371.6, 2971.8
819, 1295.4, 3048.
820, 1447.8, 3048.
821, 152.4, 3200.4
822, 152.4, 3124.2
823, 76.2, 3200.4
824, 304.8, 3200.4
825, 304.8, 3124.2
826, 228.6, 3200.4
827, 457.2, 3200.4
828, 457.2, 3124.2
829, 381., 3200.4
830, 609.6, 3200.4
831, 609.6, 3124.2
832, 533.4, 3200.4
833, 762., 3200.4
834, 762., 3124.2
835, 685.8, 3200.4
836, 914.4, 3200.4
837, 914.4, 3124.2
838, 838.2, 3200.4
839, 1066.8, 3200.4
840, 1066.8, 3124.2
841, 990.6, 3200.4
842, 1219.2, 3200.4
843, 1219.2, 3124.2
844, 1143., 3200.4
845, 1371.6, 3200.4
846, 1371.6, 3124.2
847, 1295.4, 3200.4
848, 1447.8, 3200.4
849, 152.4, 3352.8
850, 152.4, 3276.6
851, 76.2, 3352.8
852, 304.8, 3352.8
853, 304.8, 3276.6
854, 228.6, 3352.8
855, 457.2, 3352.8
856, 457.2, 3276.6
857, 381., 3352.8
858, 609.6, 3352.8
859, 609.6, 3276.6
860, 533.4, 3352.8
861, 762., 3352.8
862, 762., 3276.6
863, 685.8, 3352.8
864, 914.4, 3352.8
865, 914.4, 3276.6
866, 838.2, 3352.8
867, 1066.8, 3352.8
868, 1066.8, 3276.6
869, 990.6, 3352.8
870, 1219.2, 3352.8
871, 1219.2, 3276.6
872, 1143., 3352.8
873, 1371.6, 3352.8
874, 1371.6, 3276.6
875, 1295.4, 3352.8
876, 1447.8, 3352.8
877, 152.4, 3505.2
878, 152.4, 3429.
879, 76.2, 3505.2
880, 304.8, 3505.2
881, 304.8, 3429.
882, 228.6, 3505.2
883, 457.2, 3505.2
884, 457.2, 3429.
885, 381., 3505.2
886, 609.6, 3505.2
887, 609.6, 3429.
888, 533.4, 3505.2
889, 762., 3505.2
890, 762., 3429.
891, 685.8, 3505.2
892, 914.4, 3505.2
893, 914.4, 3429.
894, 838.2, 3505.2
895, 1066.8, 3505.2
896, 1066.8, 3429.
897, 990.6, 3505.2
898, 1219.2, 3505.2
899, 1219.2, 3429.
900, 1143., 3505.2
901, 1371.6, 3505.2
902, 1371.6, 3429.
903, 1295.4, 3505.2
904, 1447.8, 3505.2
905, 152.4, 3581.4
906, 304.8, 3581.4
907, 457.2, 3581.4
908, 609.6, 3581.4
909, 762., 3581.4
910, 914.4, 3581.4
911, 1066.8, 3581.4
912, 1219.2, 3581.4
913, 1371.6, 3581.4
914, 1681.33, 1942.06
915, 1838.66, 2037.83
916, 1681.33, 1703.44
917, 1838.66, 1822.75
918, 1681.33, 1406.2

919,	1838.66,	1554.82
920,	1681.33,	1035.91
921,	1838.66,	1221.05
922,	1681.33,	574.631
923,	1838.66,	805.271
924,	1681.33,	0.
925,	1838.66,	287.315
926,	2016.42,	1942.06
927,	2194.17,	2037.83
928,	2016.42,	1703.44
929,	2194.17,	1822.75
930,	2016.42,	1406.2
931,	2194.17,	1554.82
932,	2016.42,	1035.91
933,	2194.17,	1221.05
934,	2016.42,	574.631
935,	2194.17,	805.271
936,	2016.42,	0.
937,	2194.17,	287.315
938,	2395.01,	1942.06
939,	2595.84,	2037.83
940,	2395.01,	1703.44
941,	2595.84,	1822.75
942,	2395.01,	1406.2
943,	2595.84,	1554.82
944,	2395.01,	1035.91
945,	2595.84,	1221.05
946,	2395.01,	574.631
947,	2595.84,	805.271
948,	2395.01,	0.
949,	2595.84,	287.315
950,	2822.75,	1942.06
951,	3049.66,	2037.83
952,	2822.75,	1703.44
953,	3049.66,	1822.75
954,	2822.75,	1406.2
955,	3049.66,	1554.82
956,	2822.75,	1035.91
957,	3049.66,	1221.05
958,	2822.75,	574.631
959,	3049.66,	805.271
960,	2822.75,	0.
961,	3049.66,	287.315
962,	3306.03,	1942.06
963,	3562.4,	2037.83
964,	3306.03,	1703.44
965,	3562.4,	1822.75
966,	3306.03,	1406.2
967,	3562.4,	1554.82
968,	3306.03,	1035.91
969,	3562.4,	1221.05
970,	3306.03,	574.631
971,	3562.4,	805.271
972,	3306.03,	0.
973,	3562.4,	287.315
974,	3852.05,	1942.06
975,	4141.7,	2037.83
976,	3852.05,	1703.44
977,	4141.7,	1822.75
978,	3852.05,	1406.2
979,	4141.7,	1554.82
980,	3852.05,	1035.91
981,	4141.7,	1221.05
982,	3852.05,	574.631
983,	4141.7,	805.271
984,	3852.05,	0.
985,	4141.7,	287.315
986,	4468.96,	1942.06
987,	4796.22,	2037.83
988,	4468.96,	1703.44
989,	4796.22,	1822.75
990,	4468.96,	1406.2
991,	4796.22,	1554.82
992,	4468.96,	1035.91
993,	4796.22,	1221.05
994,	4468.96,	574.631
995,	4796.22,	805.271
996,	4468.96,	0.
997,	4796.22,	287.315
998,	5165.97,	1942.06
999,	5535.72,	2037.83
1000,	5165.97,	1703.44
1001,	5535.72,	1822.75
1002,	5165.97,	1406.2
1003,	5535.72,	1554.82
1004,	5165.97,	1035.91
1005,	5535.72,	1221.05
1006,	5165.97,	574.631
1007,	5535.72,	805.271
1008,	5165.97,	0.
1009,	5535.72,	287.315
1010,	5953.47,	1942.06
1011,	6371.22,	2037.83
1012,	5953.47,	1703.44
1013,	6371.22,	1822.75
1014,	5953.47,	1406.2
1015,	6371.22,	1554.82
1016,	5953.47,	1035.91
1017,	6371.22,	1221.05
1018,	5953.47,	574.631
1019,	6371.22,	805.271
1020,	5953.47,	0.
1021,	6371.22,	287.315
1022,	6843.21,	1942.06
1023,	7315.2,	2037.83

```
 1024,    6843.21,    1703.44
 1025,     7315.2,    1822.75
 1026,    6843.21,     1406.2
 1027,     7315.2,    1554.82
 1028,    6843.21,    1035.91
 1029,     7315.2,    1221.05
 1030,    6843.21,     574.631
 1031,     7315.2,    805.271
 1032,    6843.21,         0.
 1033,     7315.2,    287.315
*Element, type=CPE8
1,  1,  10, 198,  43,  15, 914, 915,  53
2,  10,  11, 199, 198,  16, 916, 917, 914
3,  11,  12, 200, 199,  17, 918, 919, 916
4,  12,  13, 201, 200,  18, 920, 921, 918
5,  13,  14, 202, 201,  19, 922, 923, 920
6,  14,  2,  21, 202,  20, 924, 925, 922
7,  43, 198, 203,  42, 915, 926, 927,  52
8, 198, 199, 204, 203, 917, 928, 929, 926
9, 199, 200, 205, 204, 919, 930, 931, 928
10, 200, 201, 206, 205, 921, 932, 933, 930
11, 201, 202, 207, 206, 923, 934, 935, 932
12, 202,  21,  22, 207, 925, 936, 937, 934
13,  42, 203, 208,  41, 927, 938, 939,  51
14, 203, 204, 209, 208, 929, 940, 941, 938
15, 204, 205, 210, 209, 931, 942, 943, 940
16, 205, 206, 211, 210, 933, 944, 945, 942
17, 206, 207, 212, 211, 935, 946, 947, 944
18, 207,  22,  23, 212, 937, 948, 949, 946
19,  41, 208, 213,  40, 939, 950, 951,  50
20, 208, 209, 214, 213, 941, 952, 953, 950
21, 209, 210, 215, 214, 943, 954, 955, 952
22, 210, 211, 216, 215, 945, 956, 957, 954
23, 211, 212, 217, 216, 947, 958, 959, 956
24, 212,  23,  24, 217, 949, 960, 961, 958
25,  40, 213, 218,  39, 951, 962, 963,  49
26, 213, 214, 219, 218, 953, 964, 965, 962
27, 214, 215, 220, 219, 955, 966, 967, 964
28, 215, 216, 221, 220, 957, 968, 969, 966
29, 216, 217, 222, 221, 959, 970, 971, 968
30, 217,  24,  25, 222, 961, 972, 973, 970
31,  39, 218, 223,  38, 963, 974, 975,  48
32, 218, 219, 224, 223, 965, 976, 977, 974
33, 219, 220, 225, 224, 967, 978, 979, 976
34, 220, 221, 226, 225, 969, 980, 981, 978
35, 221, 222, 227, 226, 971, 982, 983, 980
36, 222,  25,  26, 227, 973, 984, 985, 982
37,  38, 223, 228,  37, 975, 986, 987,  47
38, 223, 224, 229, 228, 977, 988, 989, 986
39, 224, 225, 230, 229, 979, 990, 991, 988
40, 225, 226, 231, 230, 981, 992, 993, 990
41, 226, 227, 232, 231, 983, 994, 995, 992
42, 227,  26,  27, 232, 985, 996, 997, 994
43,  37, 228, 233,  36, 987, 998, 999,  46
44, 228, 229, 234, 233, 989, 1000, 1001, 998
45, 229, 230, 235, 234, 991, 1002, 1003,
1000
46, 230, 231, 236, 235, 993, 1004, 1005,
1002
47, 231, 232, 237, 236, 995, 1006, 1007,
1004
48, 232,  27,  28, 237, 997, 1008, 1009, 1006
49,  36, 233, 238,  35, 999, 1010, 1011,  45
50, 233, 234, 239, 238, 1001, 1012, 1013,
1010
51, 234, 235, 240, 239, 1003, 1014, 1015,
1012
52, 235, 236, 241, 240, 1005, 1016, 1017,
1014
53, 236, 237, 242, 241, 1007, 1018, 1019,
1016
54, 237,  28,  29, 242, 1009, 1020, 1021, 1018
55,  35, 238,  34,   4, 1011, 1022, 1023,  44
56, 238, 239,  33,  34, 1013, 1024, 1025, 1022
57, 239, 240,  32,  33, 1015, 1026, 1027, 1024
58, 240, 241,  31,  32, 1017, 1028, 1029, 1026
59, 241, 242,  30,  31, 1019, 1030, 1031, 1028
60, 242,  29,   3,  30, 1021, 1032, 1033, 1030
*Element, type=CPE8
 61,  1,  43, 243, 100,  53, 244, 245, 110
 62,  43,  42, 246, 243,  52, 247, 248, 244
 63,  42,  41, 249, 246,  51, 250, 251, 247
 64,  41,  40, 252, 249,  50, 253, 254, 250
 65,  40,  39, 255, 252,  49, 256, 257, 253
 66,  39,  38, 258, 255,  48, 259, 260, 256
 67,  38,  37, 261, 258,  47, 262, 263, 259
 68,  37,  36, 264, 261,  46, 265, 266, 262
 69,  36,  35, 267, 264,  45, 268, 269, 265
 70,  35,   4,  54, 267,  44,  63, 270, 268
 71, 100, 243, 271,  99, 245, 272, 273, 109
 72, 243, 246, 274, 271, 248, 275, 276, 272
 73, 246, 249, 277, 274, 251, 278, 279, 275
 74, 249, 252, 280, 277, 254, 281, 282, 278
 75, 252, 255, 283, 280, 257, 284, 285, 281
 76, 255, 258, 286, 283, 260, 287, 288, 284
 77, 258, 261, 289, 286, 263, 290, 291, 287
 78, 261, 264, 292, 289, 266, 293, 294, 290
 79, 264, 267, 295, 292, 269, 296, 297, 293
 80, 267,  54,  55, 295, 270,  64, 298, 296
 81,  99, 271, 299,  98, 273, 300, 301, 108
 82, 271, 274, 302, 299, 276, 303, 304, 300
 83, 274, 277, 305, 302, 279, 306, 307, 303
 84, 277, 280, 308, 305, 282, 309, 310, 306
 85, 280, 283, 311, 308, 285, 312, 313, 309
```

86, 283, 286, 314, 311, 288, 315, 316, 312
87, 286, 289, 317, 314, 291, 318, 319, 315
88, 289, 292, 320, 317, 294, 321, 322, 318
89, 292, 295, 323, 320, 297, 324, 325, 321
90, 295, 55, 56, 323, 298, 65, 326, 324
91, 98, 299, 327, 97, 301, 328, 329, 107
92, 299, 302, 330, 327, 304, 331, 332, 328
93, 302, 305, 333, 330, 307, 334, 335, 331
94, 305, 308, 336, 333, 310, 337, 338, 334
95, 308, 311, 339, 336, 313, 340, 341, 337
96, 311, 314, 342, 339, 316, 343, 344, 340
97, 314, 317, 345, 342, 319, 346, 347, 343
98, 317, 320, 348, 345, 322, 349, 350, 346
99, 320, 323, 351, 348, 325, 352, 353, 349
100, 323, 56, 57, 351, 326, 66, 354, 352
101, 97, 327, 355, 96, 329, 356, 357, 106
102, 327, 330, 358, 355, 332, 359, 360, 356
103, 330, 333, 361, 358, 335, 362, 363, 359
104, 333, 336, 364, 361, 338, 365, 366, 362
105, 336, 339, 367, 364, 341, 368, 369, 365
106, 339, 342, 370, 367, 344, 371, 372, 368
107, 342, 345, 373, 370, 347, 374, 375, 371
108, 345, 348, 376, 373, 350, 377, 378, 374
109, 348, 351, 379, 376, 353, 380, 381, 377
110, 351, 57, 58, 379, 354, 67, 382, 380
111, 96, 355, 383, 95, 357, 384, 385, 105
112, 355, 358, 386, 383, 360, 387, 388, 384
113, 358, 361, 389, 386, 363, 390, 391, 387
114, 361, 364, 392, 389, 366, 393, 394, 390
115, 364, 367, 395, 392, 369, 396, 397, 393
116, 367, 370, 398, 395, 372, 399, 400, 396
117, 370, 373, 401, 398, 375, 402, 403, 399
118, 373, 376, 404, 401, 378, 405, 406, 402
119, 376, 379, 407, 404, 381, 408, 409, 405
120, 379, 58, 59, 407, 382, 68, 410, 408
121, 95, 383, 411, 94, 385, 412, 413, 104
122, 383, 386, 414, 411, 388, 415, 416, 412
123, 386, 389, 417, 414, 391, 418, 419, 415
124, 389, 392, 420, 417, 394, 421, 422, 418
125, 392, 395, 423, 420, 397, 424, 425, 421
126, 395, 398, 426, 423, 400, 427, 428, 424
127, 398, 401, 429, 426, 403, 430, 431, 427
128, 401, 404, 432, 429, 406, 433, 434, 430
129, 404, 407, 435, 432, 409, 436, 437, 433
130, 407, 59, 60, 435, 410, 69, 438, 436
131, 94, 411, 439, 93, 413, 440, 441, 103
132, 411, 414, 442, 439, 416, 443, 444, 440
133, 414, 417, 445, 442, 419, 446, 447, 443
134, 417, 420, 448, 445, 422, 449, 450, 446
135, 420, 423, 451, 448, 425, 452, 453, 449
136, 423, 426, 454, 451, 428, 455, 456, 452
137, 426, 429, 457, 454, 431, 458, 459, 455
138, 429, 432, 460, 457, 434, 461, 462, 458
139, 432, 435, 463, 460, 437, 464, 465, 461
140, 435, 60, 61, 463, 438, 70, 466, 464
141, 93, 439, 467, 92, 441, 468, 469, 102
142, 439, 442, 470, 467, 444, 471, 472, 468
143, 442, 445, 473, 470, 447, 474, 475, 471
144, 445, 448, 476, 473, 450, 477, 478, 474
145, 448, 451, 479, 476, 453, 480, 481, 477
146, 451, 454, 482, 479, 456, 483, 484, 480
147, 454, 457, 485, 482, 459, 486, 487, 483
148, 457, 460, 488, 485, 462, 489, 490, 486
149, 460, 463, 491, 488, 465, 492, 493, 489
150, 463, 61, 62, 491, 466, 71, 494, 492
151, 92, 467, 81, 6, 469, 495, 91, 101
152, 467, 470, 80, 81, 472, 496, 90, 495
153, 470, 473, 79, 80, 475, 497, 89, 496
154, 473, 476, 78, 79, 478, 498, 88, 497
155, 476, 479, 77, 78, 481, 499, 87, 498
156, 479, 482, 76, 77, 484, 500, 86, 499
157, 482, 485, 75, 76, 487, 501, 85, 500
158, 485, 488, 74, 75, 490, 502, 84, 501
159, 488, 491, 73, 74, 493, 503, 83, 502
160, 491, 62, 5, 73, 494, 72, 82, 503
*Element, type=CPE8
161, 1, 111, 504, 10, 120, 505, 506, 15
162, 111, 112, 507, 504, 121, 508, 509, 505
163, 112, 113, 510, 507, 122, 511, 512, 508
164, 113, 114, 513, 510, 123, 514, 515, 511
165, 114, 115, 516, 513, 124, 517, 518, 514
166, 115, 116, 519, 516, 125, 520, 521, 517
167, 116, 117, 522, 519, 126, 523, 524, 520
168, 117, 118, 525, 522, 127, 526, 527, 523
169, 118, 119, 528, 525, 128, 529, 530, 526
170, 119, 7, 130, 528, 129, 135, 531, 529
171, 10, 504, 532, 11, 506, 533, 534, 16
172, 504, 507, 535, 532, 509, 536, 537, 533
173, 507, 510, 538, 535, 512, 539, 540, 536
174, 510, 513, 541, 538, 515, 542, 543, 539
175, 513, 516, 544, 541, 518, 545, 546, 542
176, 516, 519, 547, 544, 521, 548, 549, 545
177, 519, 522, 550, 547, 524, 551, 552, 548
178, 522, 525, 553, 550, 527, 554, 555, 551
179, 525, 528, 556, 553, 530, 557, 558, 554
180, 528, 130, 131, 556, 531, 136, 559, 557
181, 11, 532, 560, 12, 534, 561, 562, 17
182, 532, 535, 563, 560, 537, 564, 565, 561
183, 535, 538, 566, 563, 540, 567, 568, 564
184, 538, 541, 569, 566, 543, 570, 571, 567
185, 541, 544, 572, 569, 546, 573, 574, 570
186, 544, 547, 575, 572, 549, 576, 577, 573
187, 547, 550, 578, 575, 552, 579, 580, 576
188, 550, 553, 581, 578, 555, 582, 583, 579
189, 553, 556, 584, 581, 558, 585, 586, 582

190, 556, 131, 132, 584, 559, 137, 587, 585
191, 12, 560, 588, 13, 562, 589, 590, 18
192, 560, 563, 591, 588, 565, 592, 593, 589
193, 563, 566, 594, 591, 568, 595, 596, 592
194, 566, 569, 597, 594, 571, 598, 599, 595
195, 569, 572, 600, 597, 574, 601, 602, 598
196, 572, 575, 603, 600, 577, 604, 605, 601
197, 575, 578, 606, 603, 580, 607, 608, 604
198, 578, 581, 609, 606, 583, 610, 611, 607
199, 581, 584, 612, 609, 586, 613, 614, 610
200, 584, 132, 133, 612, 587, 138, 615, 613
201, 13, 588, 616, 14, 590, 617, 618, 19
202, 588, 591, 619, 616, 593, 620, 621, 617
203, 591, 594, 622, 619, 596, 623, 624, 620
204, 594, 597, 625, 622, 599, 626, 627, 623
205, 597, 600, 628, 625, 602, 629, 630, 626
206, 600, 603, 631, 628, 605, 632, 633, 629
207, 603, 606, 634, 631, 608, 635, 636, 632
208, 606, 609, 637, 634, 611, 638, 639, 635
209, 609, 612, 640, 637, 614, 641, 642, 638
210, 612, 133, 134, 640, 615, 139, 643, 641
211, 14, 616, 149, 2, 618, 644, 159, 20
212, 616, 619, 148, 149, 621, 645, 158, 644
213, 619, 622, 147, 148, 624, 646, 157, 645
214, 622, 625, 146, 147, 627, 647, 156, 646
215, 625, 628, 145, 146, 630, 648, 155, 647
216, 628, 631, 144, 145, 633, 649, 154, 648
217, 631, 634, 143, 144, 636, 650, 153, 649
218, 634, 637, 142, 143, 639, 651, 152, 650
219, 637, 640, 141, 142, 642, 652, 151, 651
220, 640, 134, 8, 141, 643, 140, 150, 652
*Element, type=CPE8
221, 7, 119, 653, 187, 129, 654, 655, 197
222, 119, 118, 656, 653, 128, 657, 658, 654
223, 118, 117, 659, 656, 127, 660, 661, 657
224, 117, 116, 662, 659, 126, 663, 664, 660
225, 116, 115, 665, 662, 125, 666, 667, 663
226, 115, 114, 668, 665, 124, 669, 670, 666
227, 114, 113, 671, 668, 123, 672, 673, 669
228, 113, 112, 674, 671, 122, 675, 676, 672
229, 112, 111, 677, 674, 121, 678, 679, 675
230, 111, 1, 100, 677, 120, 110, 680, 678
231, 187, 653, 681, 186, 655, 682, 683, 196
232, 653, 656, 684, 681, 658, 685, 686, 682
233, 656, 659, 687, 684, 661, 688, 689, 685
234, 659, 662, 690, 687, 664, 691, 692, 688
235, 662, 665, 693, 690, 667, 694, 695, 691
236, 665, 668, 696, 693, 670, 697, 698, 694
237, 668, 671, 699, 696, 673, 700, 701, 697
238, 671, 674, 702, 699, 676, 703, 704, 700
239, 674, 677, 705, 702, 679, 706, 707, 703
240, 677, 100, 99, 705, 680, 109, 708, 706
241, 186, 681, 709, 185, 683, 710, 711, 195
242, 681, 684, 712, 709, 686, 713, 714, 710
243, 684, 687, 715, 712, 689, 716, 717, 713
244, 687, 690, 718, 715, 692, 719, 720, 716
245, 690, 693, 721, 718, 695, 722, 723, 719
246, 693, 696, 724, 721, 698, 725, 726, 722
247, 696, 699, 727, 724, 701, 728, 729, 725
248, 699, 702, 730, 727, 704, 731, 732, 728
249, 702, 705, 733, 730, 707, 734, 735, 731
250, 705, 99, 98, 733, 708, 108, 736, 734
251, 185, 709, 737, 184, 711, 738, 739, 194
252, 709, 712, 740, 737, 714, 741, 742, 738
253, 712, 715, 743, 740, 717, 744, 745, 741
254, 715, 718, 746, 743, 720, 747, 748, 744
255, 718, 721, 749, 746, 723, 750, 751, 747
256, 721, 724, 752, 749, 726, 753, 754, 750
257, 724, 727, 755, 752, 729, 756, 757, 753
258, 727, 730, 758, 755, 732, 759, 760, 756
259, 730, 733, 761, 758, 735, 762, 763, 759
260, 733, 98, 97, 761, 736, 107, 764, 762
261, 184, 737, 765, 183, 739, 766, 767, 193
262, 737, 740, 768, 765, 742, 769, 770, 766
263, 740, 743, 771, 768, 745, 772, 773, 769
264, 743, 746, 774, 771, 748, 775, 776, 772
265, 746, 749, 777, 774, 751, 778, 779, 775
266, 749, 752, 780, 777, 754, 781, 782, 778
267, 752, 755, 783, 780, 757, 784, 785, 781
268, 755, 758, 786, 783, 760, 787, 788, 784
269, 758, 761, 789, 786, 763, 790, 791, 787
270, 761, 97, 96, 789, 764, 106, 792, 790
271, 183, 765, 793, 182, 767, 794, 795, 192
272, 765, 768, 796, 793, 770, 797, 798, 794
273, 768, 771, 799, 796, 773, 800, 801, 797
274, 771, 774, 802, 799, 776, 803, 804, 800
275, 774, 777, 805, 802, 779, 806, 807, 803
276, 777, 780, 808, 805, 782, 809, 810, 806
277, 780, 783, 811, 808, 785, 812, 813, 809
278, 783, 786, 814, 811, 788, 815, 816, 812
279, 786, 789, 817, 814, 791, 818, 819, 815
280, 789, 96, 95, 817, 792, 105, 820, 818
281, 182, 793, 821, 181, 795, 822, 823, 191
282, 793, 796, 824, 821, 798, 825, 826, 822
283, 796, 799, 827, 824, 801, 828, 829, 825
284, 799, 802, 830, 827, 804, 831, 832, 828
285, 802, 805, 833, 830, 807, 834, 835, 831
286, 805, 808, 836, 833, 810, 837, 838, 834
287, 808, 811, 839, 836, 813, 840, 841, 837
288, 811, 814, 842, 839, 816, 843, 844, 840
289, 814, 817, 845, 842, 819, 846, 847, 843
290, 817, 95, 94, 845, 820, 104, 848, 846
291, 181, 821, 849, 180, 823, 850, 851, 190
292, 821, 824, 852, 849, 826, 853, 854, 850
293, 824, 827, 855, 852, 829, 856, 857, 853

294, 827, 830, 858, 855, 832, 859, 860, 856
295, 830, 833, 861, 858, 835, 862, 863, 859
296, 833, 836, 864, 861, 838, 865, 866, 862
297, 836, 839, 867, 864, 841, 868, 869, 865
298, 839, 842, 870, 867, 844, 871, 872, 868
299, 842, 845, 873, 870, 847, 874, 875, 871
300, 845, 94, 93, 873, 848, 103, 876, 874
301, 180, 849, 877, 179, 851, 878, 879, 189
302, 849, 852, 880, 877, 854, 881, 882, 878
303, 852, 855, 883, 880, 857, 884, 885, 881
304, 855, 858, 886, 883, 860, 887, 888, 884
305, 858, 861, 889, 886, 863, 890, 891, 887
306, 861, 864, 892, 889, 866, 893, 894, 890
307, 864, 867, 895, 892, 869, 896, 897, 893
308, 867, 870, 898, 895, 872, 899, 900, 896
309, 870, 873, 901, 898, 875, 902, 903, 899
310, 873, 93, 92, 901, 876, 102, 904, 902
311, 179, 877, 168, 9, 879, 905, 178, 188
312, 877, 880, 167, 168, 882, 906, 177, 905
313, 880, 883, 166, 167, 885, 907, 176, 906
314, 883, 886, 165, 166, 888, 908, 175, 907
315, 886, 889, 164, 165, 891, 909, 174, 908
316, 889, 892, 163, 164, 894, 910, 173, 909
317, 892, 895, 162, 163, 897, 911, 172, 910
318, 895, 898, 161, 162, 900, 912, 171, 911
319, 898, 901, 160, 161, 903, 913, 170, 912
320, 901, 92, 6, 160, 904, 101, 169, 913

** Region: (Section-1:Picked)
*Elset, elset=_I1, internal, generate
1, 320, 1
** Section: Section-1
*Solid Section, elset=_I1, material=Soil-block
1.,
*End Instance
*Nset, nset=_G4, internal, instance=Part-1-1
2, 3, 8, 21, 22, 23, 24, 25, 26, 27, 28, 29, 141, 142, 143,
144
145, 146, 147, 148, 149, 150, 151, 152, 153, 154, 155, 156, 157,
158, 159, 924
936, 948, 960, 972, 984, 996, 1008, 1020, 1032
*Elset, elset=_G4, internal, instance=Part-1-1
6, 12, 18, 24, 30, 36, 42, 48, 54, 60, 211, 212, 213, 214, 215, 216
217, 218, 219, 220
*Nset, nset=_G5, internal, instance=Part-1-1
3, 4, 5, 7, 8, 9, 30, 31, 32, 33, 34, 54, 55, 56, 57, 58
59, 60, 61, 62, 63, 64, 65, 66, 67, 68, 69, 70, 71, 72, 130,
131
132, 133, 134, 135, 136, 137, 138, 139, 140, 179, 180, 181, 182,
183, 184, 185
186, 187, 188, 189, 190, 191, 192, 193, 194, 195, 196, 197, 1023,
1025, 1027, 1029
1031, 1033
*Elset, elset=_G5, internal, instance=Part-1-1
55, 56, 57, 58, 59, 60, 70, 80, 90, 100, 110, 120, 130, 140, 150, 160
170, 180, 190, 200, 210, 220, 221, 231, 241, 251, 261, 271, 281, 291, 301,
311
*Nset, nset=_G6, internal, instance=Part-1-1
6, 9, 160, 161, 162, 163, 164, 165, 166, 167, 168, 169, 170, 171, 172, 173
174, 175, 176, 177, 178
*Elset, elset=_G6, internal, instance=Part-1-1, generate
311, 320, 1
*Nset, nset=Soilregion, instance=Part-1-1, generate
1, 1033, 1
*Elset, elset=Soilregion, instance=Part-1-1, generate
1, 320, 1
*Nset, nset=allsoil, instance=Part-1-1, generate
1, 1033, 1
*Elset, elset=allsoil, instance=Part-1-1, generate
1, 320, 1
*End Assembly
**
** Using the Hypoplastic material

```
** MATERIALS
**
*Material, name=Soil-block
*Depvar
     1,
*User Material, constants=9
 0.576, 1000., 0.95, 0.55, 1.05, 0.25, 0.25,   1.5
  0.1,
*INITIAL CONDITIONS, TYPE=SOLUTION
allsoil,  0.69
**
**

** Using MOHR COULOMB material
** *Material, name=Soil-block
** *Elastic
** 40., 0.3
** *MOHR COULOMB
**  33. , 15.
** *MOHR COULOMB HARDENING
**  0.1,
**

** Using DRUCKER PRAGER material
** *Material, name=Soil-block
** *Elastic
** 40., 0.3
** *DRUCKER PRAGER HARDENING
**  0.197 , 0.
** *DRUCKER PRAGER, SHEAR CRITERION=LINEAR
 ** 42, 1., 42
**
```

```
** BOUNDARY CONDITIONS
**
** Name: BC-1 Type: Displacement/Rotation
*Boundary
_G4, 1, 1
_G4, 2, 2
** Name: Sides Type: Displacement/Rotation
*Boundary
_G5, 1, 1
** ----------------------------------------------------------------
**
** STEP: Disp
**
*Step, inc=100000
Disp
*Static
0.0001, 1., 1e-12, 1.
**
** BOUNDARY CONDITIONS
**
** Name: Strip Type: Displacement/Rotation
*Boundary
_G6, 1, 1
_G6, 2, 2, -375.
**
** OUTPUT REQUESTS
**
*Restart, write, frequency=1
*Output, field, frequency=1
*Node Output
U,
*Element Output
S,
*Output, history, frequency=1
```

```
*El Print, freq=999999
*Node Print, freq=999999
*End Step
```

E.3 2-D SOIL-TOOL INTERACTION

```
*HEADING
Soil-Tool interface ; Depth=250mm , Angle=45, Blade Radius=800
*RESTART, WRITE, OVERLAY
*PARAMETER
D = 250
A = 45
R = 800
DISP = 1500
L = 400
LT = 1000
W = 10
Y0 = 0
X0 = 0
YG = -10
XG = 0
T = LT*180/(pi*R)
X = T-90+A
BX = X0-L*cos(A*pi/180)
BY = Y0+L*sin(A*pi/180)
SX = -D/tan(A*pi/180)
SY = D
XC = BX+R*sin(A*pi/180)
YC = BY+R*cos(A*pi/180)
XE = XC - R*cos(X*pi/180)
YE = YC + R*sin(X*pi/180)
X0W = X0 - W
BXW = BX - W
XEW = XE - W
N = D/50
NL0 = 606
NM0 = 666
NR0 = 671
NL = NL0 + 100*N
NM = NM0 + 100*N
NR = NR0 + 100*N
LE = 351 + 65*(N-1)
**
**
**
*NODE, NSET=CENTER
9998,<XC>,<YC>
*NODE, NSET=BLADEREF
9999,<BX>,<BY>
*NODE
1,-500,-1000
6,0,-1000
66,3000,-1000
71,3500,-1000
501,-500,0
506,0,0
566,3000,0
571,3500,0
<NL0>,0,0
<NM0>,3000,0
<NR0>,3500,0
<NL>,<SX>,<SY>
<NM>,3000,<SY>
<NR>,3500,<SY>
** for the blade :
2002,<X0>,<Y0>
2502,<BX>,<BY>
3502,<XE>,<YE>
2001,<X0W>,<Y0>
2501,<BXW>,<BY>
```

```
3501,<XEW>,<YE>
**
*NGEN, NSET=BLADE
2001,2501,100
2002,2502,100
*NGEN, LINE=C,NSET=BLADE
2501,3501,100,9998
2502,3502,100,9998
**
**
*NGEN, NSET=TM1
<NL0>,<NL>,100
*NGEN, NSET=TM2
<NM0>,<NM>,100
*NGEN, NSET=TR
<NR0>,<NR>,100
*NSET, NSET=BLD
1
*NSET, NSET=BLU
501
*NSET, NSET=BM1D
6
*NSET, NSET=BM1U
506
*NSET, NSET=BM2D
66
*NSET, NSET=BM2U
566
*NSET, NSET=BRD
71
*NSET, NSET=BRU
571
**
** Node generation by filling inbetween existing nodes
*NFILL, BIASE=1.5,NSET=BL
BLD,BLU,5,100
*NFILL, BIASE=1.5,NSET=BM1
BM1D,BM1U,5,100
*NFILL, BIASE=1.5,NSET=BM2
BM2D,BM2U,5,100
*NFILL, BIASE=1.5,NSET=BR
BRD,BRU,5,100
*NFILL,BIAS=1
TM1,TM2,60,1
*NFILL,BIAS=1
BM1,BM2,60,1
*NFILL,BIAS=1.4
BL,BM1,5,1
*NFILL,BIAS=0.7
TM2,TR,5,1
*NFILL,BIAS=0.7
BM2,BR,5,1
**
** Element generation for the soil
**
*ELEMENT,TYPE=CPE4
1,1,2,102,101
351,606,607,707,706
*ELGEN,ELSET=SOIL
1,70,1,1,5,100,70
351,65,1,1,<N>,100,65
**
*ELSET,ELSET=FRONT,GENERATE
351,<LE>,65
*ELSET,ELSET=TCONT, GENERATE
351,390,1
*ELSET,ELSET=BCONT, GENERATE
286,325,1
```

```
*ELSET,ELSET=TTIE, GENERATE
391,415,1
*ELSET,ELSET=BTIE, GENERATE
326,350,1
**
** Element generation for the Blade
**
*ELEMENT,TYPE=CPE4
2000,2001,2002,2102,2101
*ELGEN,ELSET=BLADE
2000,1,1,1,15,100,1
*RIGID BODY, REF NODE=BLADEREF, ELSET=blade
** boundary nodes
*NSET, NSET=BASE, GENERATE
1,71,1
*NSET, NSET=BOUND, GENERATE
101,501,100
171,571,100
771,<NR>,100
**
** Surfaces generation
**
*SURFACE, TYPE=ELEMENT, NAME=FRONTS
FRONT, S4
*SURFACE, TYPE=ELEMENT, NAME=TCONTS
TCONT, S1
*SURFACE, TYPE=ELEMENT, NAME=BCONTS
BCONT, S3
*SURFACE, TYPE=ELEMENT, NAME=TTIES
TTIE, S1
*SURFACE, TYPE=element, NAME=BTIES
BTIE,S3
*SURFACE, TYPE=ELEMENT, NAME=BLADES
BLADE, S2
*NORMAL, TYPE=CONTACT SURFACE
BLADES,2002,1.0,0.0,0.0
**
** MATERIALS
**
*SOLID SECTION, ELSET=blade, MATERIAL=bladmat
*MATERIAL, NAME=bladmat
*ELASTIC
 3.0e20,0.3
*SOLID SECTION, ELSET=SOIL, MATERIAL=SOILM
*MATERIAL, NAME=SOILM
*DENSITY
265.E-11,
*DEPVAR
1,
*USER MATERIAL, CONSTANTS=9
0.52,5800., 0.84, 0.53,   1., 0.28, 0.13,   1.
1E-4
*INITIAL CONDITIONS, TYPE=SOLUTION
SOIL,  0.75
**
** INTERACTIONS
**
*CONTACT PAIR,INTERACTION=BLADE-SOIL,HCRIT=1.0,
EXTENSION ZONE=0.2, adjust=1
FRONTS, BLADES
TCONTS, BLADES
*CONTACT PAIR, INTERACTION=SOIL-SOIL
TCONTS, BCONTS
*CONTACT PAIR, INTERACTION=SOIL-FAR,SMALL SLIDING
TTIES,BTIES
**
*SURFACE INTERACTION, NAME=BLADE-SOIL
1.
```

```
*FRICTION
0.000001
*SURFACE INTERACTION, NAME=SOIL-SOIL
1.
*FRICTION
0.000001
*SURFACE INTERACTION, NAME=SOIL-far
1.
*FRICTION
0.000001
*AMPLITUDE,NAME=RAMP1,VALUE=RELATIVE,TIME=TOTAL
TIME
0.,0., 1,1., 2.,1.
**
**BOUNDARY CONDITIONS
**
*BOUNDARY
BASE, 1,2
BOUND,1,
** BLADEREF,2,
BLADEREF,6,
** ----------------------------------------------------------------
**
** STEP: Gravity
*STEP, INC=10000, AMPLITUDE=RAMP
Gravity Effect
*STATIC, ,STABILIZE
1E-5,1.0,1E-20,0.01
*DLOAD,AMPLITUDE=RAMP1
soil,GRAV,9810.,0.,-1.,0.
*BOUNDARY
BLADEREF,1,,<XG>
BLADEREF,2,,<YG>
*Output, history, frequency=100
*Element Output, elset=soil
SDV,
*Output, field, frequency=100
*Node Output, VARIABLE=ALL
*Element Output, VARIABLE=ALL
*Contact Output, VARIABLE=ALL
*END STEP
**
*STEP, INC=1000000, AMPLITUDE=RAMP, Nlgeom
Displacement
*STATIC,STABILIZE
1E-5,1.0,1E-30, 0.0001
*CHANGE FRICTION, INTERACTION=BLADE-SOIL
*FRICTION
0.05
*CHANGE FRICTION, INTERACTION=SOIL-SOIL
*FRICTION
0.9
*CHANGE FRICTION, INTERACTION=SOIL-far
*FRICTION
2
*BOUNDARY
BLADEREF,1,,<DISP>
*Output, history, frequency=100
*Element Output, elset=soil
SDV,
*Output, field, frequency=100
*Node Output, VARIABLE=ALL
*Element Output, VARIABLE=ALL
*Contact Output, VARIABLE=ALL
*END STEP
```